PF23
SA43/ L. Wear

TWR-17272

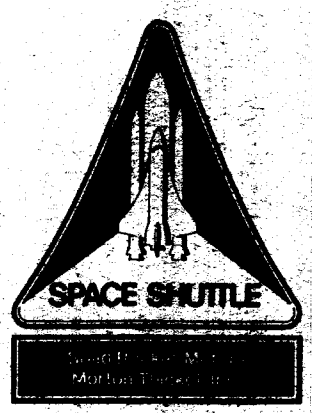

Flight Motor Set 360L001 (STS-26R) Final Report

Volume 1

December 1988

Prepared for

National Aeronautics and Space Administration
George C. Marshall Space Flight Center
Marshall Space Flight Center, Alabama 35812

Contract No. NAS8-30490
DR No. 3-5
WBS No. 4B601-03-08
ECS No. 956

MORTON THIOKOL, INC.
Aerospace Group
Space Operations
P.O. Box 707, Brigham City, Utah 84302-0707 (801) 863-3511

Publications No. 89435

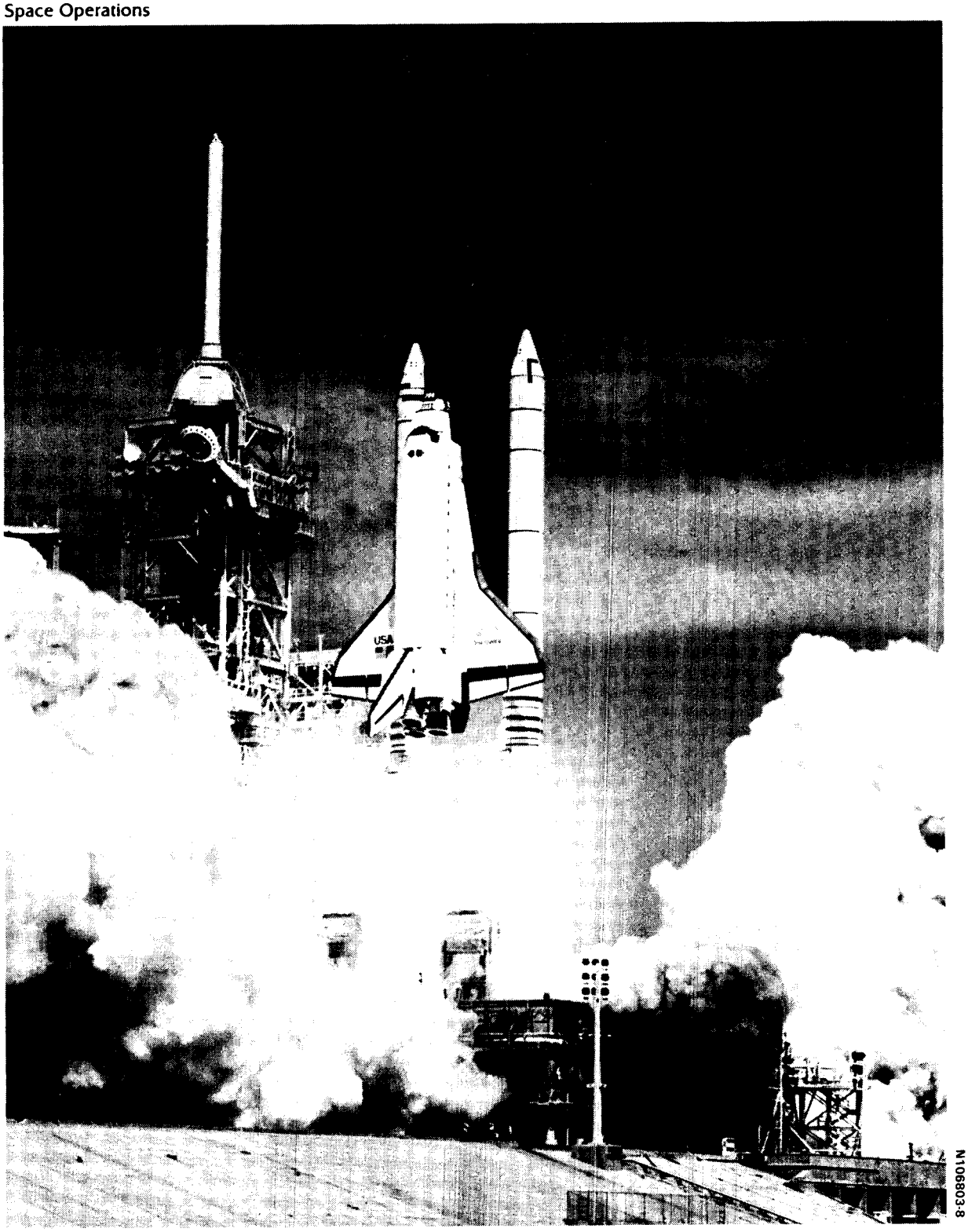

Morton Thiokol solid rocket motor set 360L001 thunders off the pad during ascent of the space shuttle Discovery, launched 29 Sep 1988. During this historic manned return to space flight, both solid rocket motors performed in a near-flawless manner throughout the approximate 2-min burn time.

MORTON THIOKOL, INC.
Space Operations

Flight Motor Set 360L001 (STS-26R)
Final Report

Prepared by:

Glen A Rich
Test Planning and Reporting

Approved by:

Neal Black
Test Planning and Reporting
Supervisor

Space Systems Engineering
Manager

Systems Test and Support
Manager

Jack R. Kapp
Space Engineering Design
Manager

Project Engineer

C. A. Saderholm
Program Manager

Certification Planning

System Safety

Richard Adams
Reliability

P C Tydeck 1-11-89
Data Management
ECS No. 956

The following are contributors to the major sections of this report, with an acceptance signature from a section representative.

Craig Richards
Mass Properties
C. Richards

B Laubacher
Ballistics
K. Speas
B. Hutchinson
B. Laubacher

Hal M Huppi
Aero/Thermal
H. Huppi
J. Maw
R. Buttars

David Gurney
Structural Applications
(Ascent Loads and Seals)
D. Gurney
J. Durtschi

Russell J. George
Nozzles
R. George
S. Meyer

Bryan L Baugh
Instrumentation
B. Baugh
J. Wright

Vicki L. Call
Dynamics
V. Call
C. Chang

Virginia Chandler
Insulation Design
V. Chandler

Rex Mackley
Case Component
R. Mackley

ABSTRACT

The NASA space shuttle flight STS-26R, launched at 11:37.00.009 a.m. EDT on 29 Sep 1988, used the redesigned solid rocket motors (RSRM) 360L001A and 360L001B.

Evaluation of the ground environment instrumentation (GEI) data recorded prior to flight showed 1) no launch commit criteria violations, 2) that the field joint heater and aft skirt thermal conditioning systems performed adequately, and 3) that the GEI data showed good agreement with thermal model predictions.

Evaluation of the developmental flight instrumentation (DFI) revealed excellent agreement with both the predicted and required ballistic specifications. All parameters were well within the CEI specification requirements including propellant burn rates, specific impulse values, and thrust imbalance. Recorded strain values also indicated satisfactory radial growth and stress levels, as well as verification of adequate safety factors.

Postflight inspection of the insulation, seals, case, and nozzles showed overall excellent performance. Some thermal DFI protective cork was missing, and inoperative field joint vent valves on the thermal protection cork allowed water entry into the field joints upon splashdown. Evaluation of these anomalies, as well as complete evaluation of all RSRM components, is contained in this report.

CONTENTS

CONTENTS (Cont)

FIGURES

FIGURES (Cont)

FIGURES (Cont)

FIGURES (Cont)

FIGURES (Cont)

FIGURES (Cont)

TABLES

TABLES (Cont)

TABLES (Cont)

ACRONYMS

CEI	contract end item
CCP	carbon-cloth phenolic
CF/EPDM . .	carbon fiber/ethylene propylene diene monomer
DFI	development flight instrumentation
DOP	detailed operating procedures
D&V	development and verification
EPDM . . .	ethylene propylene diene monomer
ET	external tank
ETA	external tank attach
FEWG . . .	Flight Evaluation Working Group
FMEA . . .	failure mode effects analysis
FRF	flight readiness firing
GEI	ground environment instrumentation
GCP	glass-cloth phenolic
HOSC . . .	Huntsville Operations Support Center
HPM	high-performance motor
ID	inside diameter
IFA	in-flight anomalies
IR	infrared
JPS	joint protection system
KSC	Kennedy Space Center
LCC	launch control center
LSC	linear-shaped charge
MLP	mobile launch platform
MSFC . . .	Marshall Space Flight Center
NBR	nitrile butadiene rubber
OBR	outer boot ring
OD	outside diameter
OFI	operational flight instrumentation
OMRSD . . .	operations and maintenance requirements and specification document
OPT	operational pressure transducer
PMBT . . .	propellant mean bulk temperature
RSRM . . .	redesigned solid rocket motor
RTV	room temperature vulcanization
S&A	safety and arming device
SF	safety factor
SPS	samples per second
SRB	solid rocket booster
SRM	solid rocket motor
SSME . . .	Space Shuttle main engine
TCDDT . . .	terminal countdown demonstration test
TPS	thermal protection system
TVC	thrust vector control
USBI . . .	United Space Boosters Inc.
WCDDT . . .	wet countdown demonstration test
2-D	two-dimensional
3-D	three-dimensional

1

INTRODUCTION

The redesigned solid rocket motor (RSRM) flight set used for the 26th space shuttle mission (STS-26R) was designated as motors 360L001A (left) and 360L001B (right). Actual launch time was 11:37.00.009 a.m. EDT on 29 Sep 1988, from pad 39B at Kennedy Space Center (KSC), Florida. This volume (Volume I) of this report contains the Morton Thiokol Flight Evaluation Working Group (FEWG) input submitted to United Space Boosters Inc. (USBI) for incorporation into the shuttle prime contractors' FEWG report (Document MSFC-RPT-1573). An executive summary overview of the entire RSRM flight set performance is also included. The volumes of this report containing detailed component information are as follows:

Volume	Component
I	System Overview
II	Case
III	Insulation
IV	Seals
V	Nozzle
VI	Igniter
VII	Joint Heater
VIII	Systems Tunnel
IX	Instrumentation
X	Performance and Mass Properties
XI	Dynamics (Reconstructed Loads Evaluation)

As explained previously, this volume (Volume I) primarily contains the input provided to USBI for incorporation into the FEWG contractors' report. Subsections submitted to USBI as part of the FEWG report are so designated with the FEWG report paragraph number.

2

OBJECTIVES

This section corresponds to FEWG report Section 2.1.1.

The objectives of this flight, as applicable to the solid rocket motors (SRMs), were derived from test summary sheet TGX-12.0 of the Development and Verification (D&V) plan (TWR-17523) and were included in the engineering requirements document for flight set 360L001 (TWR-17535). The applicable contract end item (CEI) specification paragraphs are listed in parentheses. All objectives and CEI paragraphs are also listed and correlated with flight results on a one-to-one basis in Section 3.2 of this report.

Qualification Objectives

A. Certify that the ignition interval meets specification requirements. (3.2.1.1.1.1, Morton Thiokol proposed)

B. Certify that the pressure rise rate meets specification requirements. (3.2.1.1.1.2, Morton Thiokol proposed)

C. Certify that the thrust time performance falls within the nominal thrust time curve (3.2.1.1.2.1)

D. Certify that the measured motor performance parameters, when corrected to a 60°F propellant mean bulk temperature (PMBT), meet specification requirements. (3.2.1.1.2.2)

E. Certify that the thrust time curve complies with impulse requirements. (3.2.1.1.2.4)

F. Certify that ICD 2-0A002 specified temperature constraints are maintained in the nozzle-to-case joint region. (3.2.1.2.1.f)

G. Verify the structural integrity of the case. (3.2.1.3.b)

H. Certify proper monitoring of the motor and igniter chamber pressure during flight. (3.2.1.6.2.1)

I. Certify that the field joint external heater and sensor assembly maintain the case field joint at 75°F minimum and 120°F maximum. (3.2.1.11.a)

J. Certify that each field joint heater assembly meets all performance requirements when the power supply furnished meets characteristics as defined in ICD 3-44005. (3.2.1.11.1.2)

K. Demonstrate the flex bearing system reusability. (3.2.1.9.c)

L. Demonstrate the thermal protection of the systems tunnel floor plates. (3.2.1.10.1)

M. Demonstrate the isolation of subsystem anomalies if required on first flight hardware. (3.2.3.3)

N. Demonstrate the assembly/disassembly in both the vertical and horizontal positions. (3.2.5.1)

O. Demonstrate the assembly and verification of the SRB prior to external tank (ET) mating. (3.2.5.4)

P. Demonstrate that the RSRM and its components are capable of being transported to and from fabrication, test, operational launch, recovery/retrieval, and refurbishment sites. (3.2.8)

Q. Demonstrate the remove and replace capability to the functional line replaceable unit. (3.4.1)

Qualification Test Objectives by Inspection

Perform the required pre- and postflight phase inspections:

R. Inspection of all RSRM seals to verify seal performance. (3.2.1.2)

S. Inspect seals for satisfactory operation within the temperature range resulting from natural and induced environments. (3.2.1.2.1.b, 3.2.1.2.3.b, 3.2.1.2.4.b, 3.2.1.2.5.b)

T. Inspect the factory joint insulation for accommodation to structural deflection and erosion. (3.2.1.2.2.a)

U. Inspect the factory joint insulation for operation within a temperature range. (3.2.1.2.2.b)

V. Inspection to verify at least one virgin ply of insulation over the factory joint. (3.2.1.2.2.d)

W. Inspection to verify that there was no leakage through the insulation. (3.2.1.2.2.e)

X. Inspection of flex bearing to determine sealing performance in the flight environment. (3.2.1.2.3.b)

Y. Inspection to verify that no gas leaks occurred between the flex bearing internal components. (3.2.1.2.3.d)

Z. Inspect risers for damage or cracks that would degrade the pressure-holding capability of the case. (3.2.1.3.c)

AA. Inspect case for proper tang alignment slots. (3.2.1.3.f)

AB. Inspect case segment mating joints for pin retention device. (3.2.1.3.g)

AC. Inspection for flex bearing damage due to water impact. (3.2.1.4.6.a)

AD. Inspection to verify nozzle liner performance. (3.2.1.4.13)

AE. Inspect ignition system seals for evidence of hot gas leakage. (3.2.1.5.a)

AF. Inspect igniter for evidence of debris formation or damage. (3.2.1.5.2)

AG. Inspect seal for protection of degradation from motor combustion gas. (3.2.1.8.1.1.d)

AH. Inspect insulation for required performance. (3.2.1.8.1.1.e)

AI. Inspect for shedding insulation material. (3.2.1.8.1.1.f)

AJ. Inspect joint insulation for evidence of slag damage. (3.2.1.8.1.1.g)

AK. Inspect for thermal protection system (TPS) allowance of any environmental damage to the RSRM. (3.2.1.8.2)

AL. Inspect for thermal damage to igniter chamber or adapter metal parts. (3.2.1.8.3)

AM. Postflight inspection of case, igniter, safe and arm (S&A), operational pressure transducer (OPT), and igniter chamber pressure transducers for reusability. (3.2.1.9.a, 3.2.1.9.d, 3.2.1.9.e, 3.2.1.9.f)

AN. Postflight inspection of the case factory joint external seal for moisture. (3.2.1.12)

AO. Inspect hardware for damage or anomalies identified by failure mode effects analyses (FMEAs). (3.2.3)

AP. Perform inspections to determine the adequacy of design safety factors, relief provisions, fracture control, and safe-life and/or fail-safe characteristics. (3.2.3.1)

AQ. Inspect to determine the adequacy of subsystem redundancy and fail-safe requirements. (3.2.3.2)

AR. Inspection of identification numbers for traceability. (3.3.1.5)

AS. Inspect structural safety factor for case/insulation bonds. (3.3.6.1.1.2.a)

AT. Inspect case insulation to verify remaining insulation thickness. (3.3.6.1.2.2, 3.3.6.1.2.3, 3.3.6.1.2.4, 3.3.6.1.2.6)

AU. Inspect to verify remaining nozzle ablative thicknesses. (3.3.6.1.2.7)

AV. Inspect to verify nozzle safety factors. (3.3.6.1.2.8)

AW. Inspect the design of functional and physical interfaces between solid rocket booster (SRBs) and retrieval station. (3.6.2.e)

AX. Demonstrate that recovery procedures meet interface control drawing (ICD) specifications. (3.6.2.e)

AY. Postflight inspection for the presence of stress corrosion. (3.3.8.2.b)

3

RESULTS SUMMARY, CONCLUSIONS, AND RECOMMENDATIONS

3.1 RESULTS SUMMARY

This section contains an executive summary of the key results from the flight data evaluation and postflight inspection. Additional information and details can be found in the referenced report sections or in the separate component volumes of this report.

3.1.1 In-Flight Anomalies

There were three designated In-Flight Anomalies (IFAs) relating to the SRMs, which are listed as follows.

Marshall Space Flight Center IFA No.	Problem Title/ Description	Corrective Action/ Closure
STS-26-M-1	DFI TPS cork debris - breakup and loss of some TPS cork DFI covering.	Tap testing and repair of cork on subsequent motors ensures adequate future TPS cork bond.
STS-26-M-2	Leaking field joint TPS vent valves - allowed sea water to enter joint upon splashdown.	Verification of vent valve closure prior to rollout precludes threat of ascent with water in JPS weatherseals.
STS-26-M-3	"Fretting" in field joints - small gouges, pits, or scratches on capture feature hardware (on non-sealing surface).	Specific cause under investigation - no flight safety effect due to minute size of scratches.

All IFAs are considered closed and none were considered flight constraints. The complete disposition of all IFAs, as well as additional information, is found in Section 4.1.

3.1.2. Mass Properties

Evaluation of the mass properties for flight motors 360L001A and 360L001B showed the sequential weight and center of gravity (cg) data in excellent agreement with predicted values, as all values (predicted versus measured) were within 1 percent. All SRM weight values were within all required CEI specification limits. Complete mass property values are listed in Section 4.3 and Volume X of this report.

3.1.3 Propulsion Performance (Ballistics)

Propellant Burn Rates/Specific Impulse

Overall propulsion performance was excellent. The delivered burn rates for both motors (360L001A and 360L001B) was 0.366 in./sec at 625 psia and 60°F, exactly as predicted for motor 360L001A (left) and 0.001 in./sec lower for motor 360L001B (right). Reconstructed specific impulse values were 267.53 and 268.81 lbf-sec/lbm for the left and right motors, respectively, and were very close to the predicted value of 268.82 lbf-sec/lbm. The left motor had a lower specific impulse (than predicted) due to a pressure transducer error, or to a slightly different erosion pattern in the nozzle.

CEI Specification Values

All data were within the expected ranges and met all CEI specification requirements. Thrust imbalance was very minimal compared to the allowable values. Complete ballistic evaluation is found in Section 4.4 and Volume X of this report.

3.1.4 Ascent Loads

Girth Gages

The girth gage measurements from field and nozzle-to-case joints compare closely to pretest predictions. The predictions used a typical load case rather than actual loads, so they were only expected to be within an order of magnitude. The highest percentage difference (between predicted and actual) was -17.1 percent on the forward field joint, 17.1 percent on the nozzle-to-case joint, and -5.6 percent on case membrane.

Biaxial Gages

The biaxial gage line/load measurements also compared closely with predicted values. The maximum measured axial and hoop stresses were 78.8 and 140.2 ksi, respectively. (The yield strength of D6AC steel is 180 ksi, so no local yielding was measured). These stresses also indicate minimum safety factors of 2.72 and 1.53 in the axial and hoop directions, respectively.

Bending Moment and Shear Forces

The bending moment general trends in the Y (My) and Z (Mz) directions were as expected, and correlation was very good with past flights. Some differences were noted in the trends of the axial forces in the x direction (Vx); however, the discrepancies are explainable.

Flight Envelopes and Strut Forces

Some discrepancies in the comparison of the bending moments and axial forces as compared to the predicted flight envelopes were noted. The data compared favorably with previous flights. All strut forces were within the design limit loads. Complete evaluation of all ascent loads is given in Section 4.6.

3.1.5 Structural Dynamics

Accelerometer data evaluation indicated no anomalous vibration levels or frequencies. Comparison of predicted and measured values was limited due to the ranging of the gages and the analysis model bounds. Complete evaluation of the modal frequencies and vibrational amplitudes is found in Section 4.7.

3.1.6 TPS/External Evaluation

Postflight inspection revealed no thermal anomalies or unexpected problems. The vent valves allowed water into the field joints upon splashdown as discussed as IFA STS-26-M-2 in Section 4.1. The condition of both SRMs was similar to previous flights. All DFI thermal trajectory data was within the design estimates, with the exception of the nozzle fixed housing flange within the SRB aft skirt base region. This high measured temperature value was attributed to possible adhesive failure, causing gage detachment from the hardware. Refer to Section 4.9 for additional information.

3.1.7 Aero/Thermal Evaluation

On-Pad Local Environment Effects

No apparent evidence of temperature depression due to ET cooling was observed. Predictions indicated a decrease of up to 2°F was possible. The ambient environment was in good agreement with historical September data.

Launch Commit Criteria (LCC)/Infrared (IR) Readings

No LCC violations were encountered, and the field joint heaters and aft skirt conditioning systems performed adequately. Some heater sensor misconnections did occur; however, this was considered and presented no problem. IR measurements were also comparable to the GEI readings. Complete Aero/Thermal evaluation, including GEI data, is found in Section 4.9.

Thermal Model Verification

Only limited access of near real-time on-pad GEI and environmental data was available to Morton Thiokol after pad validation. These data are used to forecast the local SRM environment and PMBT predictions.

GEI data were in relatively good agreement with on-pad thermal model predictions for both September historical and pre-T-6 hour real-time assessments. Actual flow model verification in the aft skirt region was not possible due to lack of sufficient instrumentation on the hardware (SRM, aft skirt, thermal curtain, and adjacent to the hardware in the gas stream and at the orifice).

3.1.8 Instrumentation

A total of 310 developmental flight instrumentation (DFI) measurements were installed on flight set 360L001, of which 264 (80 percent) performed properly. Thirty-two of thirty-seven (97 percent) of the GEI performed properly. A complete listing of all instrumentation is found in Sections 4.10, 4.11, and Volume IX.

3.1.9 Postflight Hardware Assessment

Insulation

No evidence of pressure past the J-joint was evident in all field joints on both SRMs. Char and heat effects were nominal. No polysulfide blowholes in either nozzle-to-case joint were identified. All factory joints had a safety factor of at least 2, and a minimum of three virgin plies remained over all factory joints. All internal insulation was comparable to past flight and static motors. Complete insulation evaluation is found in Section 4.12.1 and Volume III of this report.

Case

The hardware performed as expected during flight. All case joints, including the newly redesigned field joints and nozzle-to-case joints, performed as expected. Only during splashdown, and possibly during disassembly did any structural damage occur. Cracking of the stiffener stubs on 360L001B (right) was observed. Small gouges, or "fretting," were also observed upon disassembly (IFA STS-26-M-3 in Section 4.1). A complete evaluation of the case component can be found in Section 4.12.2 and Volume II of this report.

Seals

Postflight inspection of both motors showed all seals to be in excellent condition. There was no hot gas or soot past the J-leg on the six field joints or past the polysulfide adhesive on the two nozzle-to-case joints. The igniter joints had no hot gas or soot past the primary seals. There was no soot to the nozzle aft exit cone primary seals. Inspection of all O-rings and gasket seals revealed no damage, heat effects, or erosion. Complete seals evaluation is found in Section 4.12.3 and Volume IV of this report.

Nozzle/Thrust Vector Control (TVC) Performance

Overall nozzle performance was good, and similar to past fired nozzles. The carbon-cloth phenolic (CCP) on the exit cone was either fractured or completely missing from linear-shaped charge (LSC) use and water impact, exposing the glass-cloth phenolic (GCP) insulator. The GCP was delaminated

from water impact, but showed no signs of heat effect. The internal parts of the nozzle had the appearance of previously postflight hardware. There were intermittent impact marks located circumferentially around both of the nozzles. There were a few instances of charred CCP popping up and postfire wedgeouts, which also have been observed on previously postfired nozzles. A complete evaluation of both nozzles can be found in Section 4.12.4 and Volume V of this report.

3.2 CONCLUSIONS

The conclusions as they relate specifically to the objectives and CEI paragraphs are as follows. Included with the conclusion is the report section where the applicable information can be found.

Objective	CEI Paragraph	Conclusions
Certify that the ignition interval is between 202 and 262 ms with a 40 ms environmental delay after ignition command.	3.2.1.1.1.1, Ignition Interval. The ignition interval shall be between 202 and 262 ms...	Certified. The ignition intervals for RSRMs 360L001A and 3600L001B were 0.230 and 0.231 sec, respectively. (Table 4.4-1)
Certify that the pressure rise rate meets specification requirements.	3.2.1.1.1.2, Pressure Rise Rate. The maximum rate of pressure buildup shall be 115.9 psi for any 10 ms interval.	Certified. The maximum pressure rise rate for RSRMs 360L001A and 360L001B was 99.0 and 80.5* psi/10 ms, respectively. (Table 4.4-1)
Certify that the thrust time performance falls within the nominal thrust time curve.	3.2.1.1.2.1. (Refer to Nominal Thrust Time Curve)	Certified. The thrust time performance was within the nominal thrust time curve. (Figure 2.3.1-8)
Certify that the measured motor performance parameters, when corrected to a 60°F PMBT, fall within the specification limits.	3.2.1.1.2.2. The delivered performance values for each individual motor when corrected to a 60°F PMBT shall not exceed the limits specified...	Certified. All motor performance values were well within the specification requirements. (Tables 4.4-3 and 4.4-4)

*Value is questionable due to data dropout.

Objective	CEI Paragraph	Conclusions
Certify that the thrust time curve complies with impulse requirements.	3.2.1.1.2.4, Impulse Gates. Time (sec) / Tot Impulse (10E6 lb-sec) 20 — 63.1 min 60 — 172.9 -1% +3% Action time (AT) 293.8 min	Certified. The nominal thrust time curve values are: Time (sec) / Value 20 — 64.7 60 — 172.8 AT — 296.7 (Section 4.4)
Verify that ICD 2-0A002 specified temperatures are maintained constraints in the nozzle-to-case joint region.	3.2.1.2.1.f. Nozzle-to-case joint O-rings shall be maintained within the temperature range as specified in ICD 2-0A002. (75° to 120°F)	Verified. Temperature ranges in the nozzle-to-case joint region were: RH 83 to 94°F LH 86 to 94°F (Table 4.9-4)
Verify the structural integrity of the case.	3.2.1.3.b. The structural integrity of the pressurized portion of the case segments shall be demonstrated and verified prior to each use...	Verified. Proof testing of all case segments was performed in accordance with the following specifications: STW7-3306 Std wt STW7-3307 Lt wt STW7-3438 Aft dome STW7-2888 Fxd hsg STW7-2744 Refurb
Certify proper monitoring of motor and igniter chamber pressure during flight.	3.2.1.6.2.1. The OPT shall monitor the chamber pressure of the RSRMs over the range from 0 to 1,050 ±/15 psi. They shall operate in accordance with ICD 3-44005...	Certified. The OPTs properly monitored the chamber pressure and operated in accordance with ICD 3-44005. Recorded pressure data and values are discussed in Section 4.4.
	3.2.1.6.2.3 (Addendum G). Development flight instrumentation (DFI) shall monitor in-flight SRM chamber and igniter pressure...	Certified. DFI chamber pressure was monitored and recorded at 320 samples/sec. Data results are discussed in Section 4.4.

Objective	CEI Paragraph	Conclusions
Certify that the field joint external heater and sensor assembly maintain the case field joint at 75°F minimum and 120°F maximum.	3.2.1.11.a. The case field joint external heater and sensor assembly shall maintain the case field joint O-ring seals between 75° and 120°F at launch...	Certified. The joint heaters maintained all field joints between 94 and 109°F during the prelaunch period. (Section 4.9).
Certify that each field joint heater assembly meets all performance requirements when the power supply furnished meets characteristics as defined in ICD 3-44005.	3.2.1.11.1.2, Power Supply. Each field joint external heater assembly shall meet all performance requirements... as defined in ICD 3-44005.	Certified. The field joint heaters met all performance requirements (Section 4.9). The power supply was in accordance with ICD 3-44005. Details are in Volume VII of this report.
Demonstrate flex bearing system reusability.	3.2.1.9.c. Flex bearing system reinforced shims, end rings, and elastomer materials.	Evaluation indicates no condition which would adversely affect the reusability of the flex bearing system. Detailed analysis to be completed during flex bearing acceptance testing.
Demonstrate thermal protection of the cables and systems tunnel floor plates.	3.2.1.10.1. The tunnel floor plates and tunnel cables will be maintained at a temperature at or below that specified in ICD 3-44002.	Postflight inspection showed no adverse thermal effects to the system tunnel floor plates. No means of direct thermal measurement is possible during flight. Thermal analysis indicated all temperatures are within the design limits (TWR-16517). Details are in Volume VIII of this report.

Objective	CEI Paragraph	Conclusions
Demonstrate isolation of subsystem anomalies if required on first flight hardware.	3.2.3.3. Isolation of anomalies of time-critical functions shall be provided so that a faulty subsystem element can be deactivated without disrupting its own or other subsystems.	No anomalies were detected, therefore isolation of subsystems could and need not have been demonstrated. (Test Summary Sheet DGX-14, TWR-15723)
Demonstrate assembly/ disassembly in both vertical and horizontal positions.	3.2.5.1. The RSRM shall be capable of assembly/ disassembly in both vertical and horizontal positions. The RSRM shall be capable of vertical assembly in a manner to meet the alignment criteria of USBI-10183-0022 without a requirement for optical equipment.	RSRM vertical assembly in accordance with USBI-10183-0022 was demonstrated in the vehicle assembly building (VAB) prior to pad rollout. No vertical disassembly was required. Postflight horizontal disassembly was accomplished at the hangar AF facilities.
Demonstrate assembly and verification of the SRB prior to ET mating.	3.2.5.4. The RSRM assembly and verification on the mobile launch platform (MLP) shall be required prior to mating to the external tank.	The RSRMs were successfully assembled on the MLP and mated to the ET.
Demonstrate that the RSRM and its components are capable of being transported to and from fabrication, test, operational launch recovery/retrieval, and refurbishment sites.	3.2.8. The RSRM and its component parts... shall be capable of being handled and transported by rail or other suitable means to and from fabrication, test, operational launch, recovery/retrieval, and refurbishment sites.	The RSRM and its associated components demonstrated transportability from fabrication in Utah to launch in Florida, and were recovered, retrieved, and transported back to the refurbishment sites in Utah.

Objective	CEI Paragraph	Conclusions
Demonstrate remove and replace capability to the functional line replaceable unit.	3.4.1. The maintenance concept shall be to "remove and replace"... in a manner which will... prevent deterioration of inherent design levels of reliability and operating safety at minimum practical costs.	All of the OPTs (6), igniter pressure transducers (2), special bolts (4), and inner bolts were changed on flight set 360L001A and -B, in accordance with TWA-1903 and TWA-1904, demonstrating the remove and replace concept required.
Inspect all RSRM seals to verify seal performance.	3.2.1.2. Redundant, verifiable seals shall be provided for each pressure vessel leak path. Both the primary and secondary seals shall provide independent sealing capability through the entire ignition transient and motor burn without evidence of blowby or erosion.	No evidence of hot gas, heat effect, erosion, or blowby was evident on any of the seals. (Section 4.12.3)
Inspect seals for capability of operating within temperature range resulting from natural and induced environments.	3.2.1.2.1.b. Field and Nozzle/Case Joint Seals... 3.2.1.2.3.b, Flex Bearing Seals... 3.2.1.2.4.b, Ignition System Seals... 3.2.1.2.5.b, Nozzle Internal Seals... ...shall be capable of operating within a temperature range resulting from all natural and induced environments...all manufacturing processes, and any motor-induced environments.	All field joint seals, nozzle-to-case joint seals, and ignition system seals operated within all induced environments and showed no evidence of heat effects, erosion, or blowby (Section 4.12.3). Preliminary evaluation indicates no anomalies with the flex bearing and nozzle internal seals. Details are in Volume V of this report.

Objective	CEI Paragraph	Conclusions
Inspect factory joint insulation for accommodation to structural deflection and erosion.	3.2.1.2.2.a. Sealing shall accommodate any structural deflections or erosion which may occur.	The factory joint insulation remained sealed and accommodated all deflection and erosion. (Section 4.12.1)
Inspect factory joint insulation for operation within a temperature range.	3.2.1.2.2.b. Factory joint seals shall be capable of operating within a temperature range resulting from all natural and induced environments, all manufacturing processes, and any motor-induced environments.	Preliminary observations indicate the factory joint seal (insulation) operated within all induced environments (Section 4.12.1). Details are in Volume III of this report.
Inspect to verify at least one virgin ply of insulation over factory joint.	3.2.1.2.2.d. The insulation shall provide one or more virgin ply coverages at end of motor operation. The design shall perform the seal function throughout SRM operation.	Preliminary measurements indicated that three virgin insulation plies remained over the factory joint at the end of motor operation. (Section 4.12.1). Final evaluation results are in Volume III of this report.
Inspect to verify no leakage through insulation.	3.2.1.2.2.e. The insulation used as a primary seal shall be adequate to preclude leaking through the insulation.	No evidence of leakage through the factory joint insulation was detected. (Section 4.12.1)

Objective	CEI Paragraph	Conclusions
Inspection of flex bearing to determine and verify sealing performance in the flight environment.	3.2.1.2.3.b. Seals shall be capable of operating within a temperature range resulting from all natural and induced environments, all manufacturing processes, and any motor-induced environments.	Preliminary inspection indicates the flex bearing remained sealed throughout all motor-induced environments. Final evaluation to be completed during acceptance testing.
Inspect to verify no gas leaks occurred between the flex bearing internal components.	3.2.1.2.3.d. The flex bearing shall maintain a positive gas seal between its internal components.	Preliminary inspection indicates the flex bearing maintained positive seal within its internal components. Detailed inspection to be completed during acceptance testing.
Inspect risers for damage or cracks that would degrade the pressure holding capability of the case.	3.2.1.3.c. The case shall contain risers for attaching the ET/SRB aft attach ring as defined in ICD 3-44004. The risers shall be part of the pressurized section of the case and shall not degrade the integrity of the case.	No damage or adverse effects to the external tank attach (ETA) risers was noted during post-test inspection. Cracking was observed on the stiffener stubs, however. (Section 4.12.2). Complete case evaluation is in Volume II of this report.
Inspect case for tang alignment slots.	3.2.1.3.f. The case segment mating joints shall incorp-ate provision to ensure proper segment orienta-tion and alignment to facilitate joining, stacking, disassembly, and refurbishment for reuse.	Post-test case inspec-tion revealed no damage, indicating that the segment tang slots provided proper orienta-tion and alignment. (Section 4.12.2)

Objectives	CEI Paragraph	Conclusions
Inspect case segment mating joints for pin retention device.	3.2.1.3.g. The case segment mating joints shall contain a pin retention device.	Post-test inspection verified the pin retainer bands functioned properly and were in place on all joints. Detailed results are in Volume II of this report.
Inspect for flex bearing damage due to water impact.	3.2.1.4.6.a The nozzle assembly shall incorporate a nozzle snubbing device suitable for preventing flex bearing damage resulting from water impact...	Preliminary inspection indicates no damage occurred. Final evaluation to be included during flex bearing acceptance testing.
Inspect to verify nozzle liner performance. Note: SCN 49 proposes to change the CEI paragraph wedgeout requirement from "greater than 0.250 inches deep" to "yield a positive margin of safety."	3.2.1.4.13. The nozzle flame front liners shall prevent the formation of 1) pockets greater than 0.250 in. deep (as measured from the adjacent nonpocketed areas), 2) wedgeouts greater than 0.250 in. deep, and 3) prefire anomalies except as allowed by TWR-16340.	Evaluation of both nozzle liners revealed erosion profiles similar to what has been observed in the past. No pockets greater than 0.25 in. were observed. The 360L001B nozzle showed wedgeouts of CCP material in the nose cap and cowl aft ends that may have occurred during motor burn. (Sectioning will positively determine the time of occurrence, and be evaluated in Volume V) All other 360L001 wedge-outs occurred postburn. No prefire anomalies were observed. (Section 4.12.4)
Inspect ignition system seals for evidence of hot gas leakage.	3.2.1.5.a. The ignition system shall preclude hot gas leakage during and subsequent to motor ignition.	All ignition system seals showed no evidence of heat effects, erosion, or blowby. (Section 4.12.3)

Objective	CEI Paragraph	Conclusions
Inspect igniter for evidence of debris formation or damage.	3.2.1.5.2. ...the igniter hardware and materials shall not form any debris...	Preliminary indications show no evidence of any igniter debris formation. Complete evaluation is in Volume VI of this report.
Inspect seals for protection of degradation from motor combustion gas.	3.2.1.8.1.1.d. Insulation shall protect primary and secondary seals from visible degradation from motor combustion gas.	There was no evidence of hot gas or soot past the J-leg on the six field joints or past the polysulfide adhesive on the two nozzle-to-case joints. (Section 4.12.3)
Inspect insulation for required performance.	3.2.1.8.1.1.e. The insulation shall ...meet all performance requirements under worst manufacturing tolerances and geometry changes during and after assembly and throughout motor operation.	Preliminary inspection indicates the insulation met all the performance requirements. (Section 4.12.1) Detailed results are in Volume III of this report.
Inspect shedding insulation material.	3.2.1.8.1.1.f. Insulation materials shall not shed fibrous or particulate matter during assembly which could prevent sealing.	No shedding of fibrous or particulate matter during assembly was detected. (Section 4.12.1 and Volume III)
Inspect joint insulation for evidence of slag damage.	3.2.1.8.1.1.g. The joint insulation shall withstand slag accumulation during motor operation.	The insulation withstood all slag accumulation during motor operation. (Section 4.12.1 and Volume III)
Inspect for TPS allowance of any environmental damage to the RSRM.	3.2.1.8.2. TPS shall ensure that the mechanical properties of the RSRM components are not degraded when exposed to the environments...	All cork on all field joints was in place with no pieces or parts of pieces missing. No ablative compound was missing, and no debonds were found. The TPS vent values did allow water into the field joints upon splashdown, recorded

Objective	CEI Paragraph	Conclusions
		as IFA STS-26-M-2. (IFA discussed in Section 4.1, TPS performance discussed in Section 4.9)
Inspect for thermal damage to igniter chamber or adapter metal parts.	3.2.1.8.3. The igniter insulation shall provide thermal protection for the main igniter chamber and adapter metal parts to ensure that RSRM operation does not degrade their functional integrity or make them unsuitable for refurbishment.	Preliminary investigation revealed no thermal damage to the igniter due lack of insulation functionality. (Section 4.12.1) Igniter details are in Volume VI of this report.
Postflight inspection of case, igniter, S&A, OPT and igniter chamber pressure transducers for reusability.	3.2.1.9.a. Case - cylindrical segments, stiffener segments, attach segments, forward and aft segments, stiffener rings, clevis joint pins.	Preliminary postflight inspection revealed nothing that would adversely affect reuse of any case part. Detailed inspection results are in Volume II of this report.
	3.2.1.9.d. Igniter - chamber, adapter, igniter port, special bolts. 3.2.1.9.e, Safe and Arm Device.	Preliminary postflight inspection revealed nothing that would adversely affect reuse of any igniter and/or S&A part. Detailed inspection results are in Volume VI of this report.
	3.2.1.9.f, Transducers.	Post-test inspection revealed no issues that would adversely affect any transducer reuse. Details are in Volume IX of this report.

Objective	CEI Paragraph	Conclusions
Postflight inspection of the case factory joint external seal for moisture.	3.2.1.12. The factory joint external seal shall prevent the prelaunch intrusion of rain into the factory joints from the time of assembly of the segment until launch... The factory joint seal shall remain intact through flight and, as a goal, through recovery.	Visual examination of the factory joint external seal revealed no anomalous conditions. The aft factory joint on RSRM 360L001B (right) was penetrated during postflight evaluation. No evidence of moisture was present. Detailed evaluation is in Volume VII of this report.
Inspect hardware for damage or anomalies identified by FMEAs.	3.2.3 The design shall minimize the probability of failure taking into consideration the potential failure modes identified and defined by FMEAs.	No hardware damage or anomalies were found that were identified by FMEAs. Specific inspection results are in the individual component volumes of this report.
Perform inspections to determine adequacy of design safety factors, relief provisions, fracture control, and safe-life and/or fail-safe characteristics.	3.2.3.1. The primary structure, thermal protection, thermal protection, and pressure vessel subsystems shall be designed to preclude failure by use of adequate design safety factors, relief provisions, fracture control, and safe-life and/or fail-safe characteristics.	Postflight inspections verified adequate design safety factors, relief provisions, fracture control, and safe-life and/or fail-safe characteristics for the thermal protection and pressure vessel subsystems. Stiffener ring stub cracking may affect fracture control of the primary structure, and is being evaluated per refurbishment specification STW7-2744.
Inspect to determine adequacy of subsystem redundancy and fail-safe requirements.	3.2.3.2. The redundancy requirements for subsystems... shall be established on an individual subsystem basis, but shall not be less than fail-safe...	Inspection revealed no primary subsystem failure; thus subsystem redundancy cannot be evaluated.

Objective	CEI Paragraph	Conclusions
Inspect identification numbers for traceability.	3.3.1.5. Traceability shall be provided by assigning a traceability identification to each RSRM part and material and providing a means of correlating each to its historical records...	Inspection numbers for traceability of each RSRM part and material are provided, and are maintained in the Automatic Data Collection and Retrieval (ADCAR) computer system. The past history of all RSRM parts is in Section 4.2.
Inspect structural safety factor for case/insulation bonds.	3.3.6.1.1.2.a. The structural safety factor for the case/insulation bonds shall be 2.0 minimum during the life of the RSRM.	Verification of a 2.0 safety factor cannot be done by inspection; however, flight performance verified a bond safety factor of at least 1.0. Case/insulation bond safety factors of 2.0 are verified by analysis (TWR-16961).
Inspect case insulation to verify remaining insulation thickness.	3.3.6.1.2.2. The case insulation shall have a minimum design safety factor of 1.5, assuming normal motor operation, and 1.2, assuming loss of a castable inhibitor.	All preliminary insulation thickness measurements indicate an insulation safety factor of at least 2.0. (Section 4.12.1) Detailed results are in Volume III of this report.
	3.3.6.1.2.3. Case insulation adjacent to metal part field joints, nozzle/case joints, and extending over factory joints shall have a minimum safety factor of 2.0.	All preliminary insulation thickness measurements indicate an insulation safety factor of at least 2.0. (Section 4.12.1. and Volume III)

Objective	CEI Paragraph	Conclusions
	3.3.6.1.2.4. Case insulation in sandwich construction regions (aft dome and center segment aft end) shall have a minimum safety factor of 1.5.	All preliminary insulation thickness measurements indicate an insulation safety factor of at least 2.0. (Section 4.12.1 and Volume III)
	3.3.6.1.2.6. Insulation performance shall be calculated using actual pre- and post-motor operation insulation thickness measurements.	Preliminary insulation thickness measurements were made using a "Fletcher" needle depth gage. (Section 4.12.1) Standard measurement techniques were used for final evaluation. (Volume III)
Inspect to verify remaining nozzle ablative thicknesses.	3.3.6.1.2.7. The minimum design safety factors for the nozzle assembly primary ablative materials shall be as listed below... (Values not included here as detailed results are not available at this writing.)	Preliminary inspections indicate nozzle ablative thicknesses were within design safety factors. (Section 4.12.4) Detailed results are in Volume V of this report.
Inspect to verify nozzle safety factors.	3.3.6.1.2.8. The nozzle performance margins of safety shall be zero or greater...	The nozzle performance margins are discussed in Volume V of this report.
Inspect design of functional and physical interfaces between SRBs and retrieval station. Demonstrate that recovery procedures meet ICD specifications.	3.6.2.e, ICD 2-4A002 Solid Rocket Booster Retrieval Station.	Both RSRMs were successfully recovered and returned to Clearfield, Utah for refurbishment without significant problems. However, problem reports are being reviewed for ICD 2-4A002 requirements.

Objective	CEI Paragraph	Conclusions
Postflight inspection for presence of stress corrosion.	3.3.8.2.b. The criteria for material selection in the design to prevent stress corrosion failure of fabricated components shall be in accordance with MSFC-SPEC-522 and SE-019-094-2H.	No evidence of stress corrosion was found during post-test case inspection. Details are in Volume II of this report.

3.3 RECOMMENDATIONS

A summary of the recommendations made pertaining to flight motor set 360L001 is as follows.

3.3.1 Aerothermal Recommendations

Cork Debris Problem

The problem of missing regions of TPS from the cork caps covering the instrumentation cables could be alleviated by one of two avenues. These are:

a. Ensure better cork bonds by requiring that adhesive be applied to both adherents. This should also include the use of a vacuum bag cure on all bonds.

b. Remove the cork cap completely and rely on the K5NA filler to insulate the instrumentation cables.

(A thermal analysis was conducted to determine the K5NA thickness required to keep the temperature of the instrumentation cables below the required 500°F. The analysis results indicated that the required minimum thickness of K5NA over the cable jacket was 0.1 in. for the forward and center segments, and 0.15 in. for the aft segment.)

It should also be mentioned, that from a thermal perspective, the side strips of cork are unnecessary along these runs of cable. One inch of K5NA on both sides of the cables would suffice. However, removing the side strips would possibly create other problems from a structural and installation point of view.

DFI Measurement Problem

No insulation was used to cover the DFI thermal gages in the nozzle-to-case region, which experienced high temperature readings. These high readings are explainable, assuming slight gage detachment, as a result of direct gage exposure to the hot reentry nozzle flame and aerodynamic heating environment following thermal curtain breakup.

This assessment will be confirmed with data from flight set 360L002 (STS-27) and subsequent development flight sets, where the gages will be directly insulated from the environment with a minimal amount of K5NA. If the assessment is not confirmed, the SRB reentry environments and/or SRM aft end thermal modeling should be considered and appropriately modified.

GEI Prediction Problem

Data correlations, predictions versus actual, suggest relatively good agreement. However, it is recommended that modeling considerations (environment and detail) need to be looked at closely. Future modeling should check the observations and suggested modeling improvements discussed in Section 4.9 and incorporate updates as solutions are found.

Field Joint Heater Sensor Placement Problem

It is recommended that sensor strip installation and jiffy connection procedures be reviewed and possibly changed to avoid the reoccurrence of sensor misconnection.

Aft Skirt Conditioning Problem

It is not possible for any practical model extrapolation to be made of a worst-case cold environment due to lack of instrumentation in the aft skirt area. It is recommended that the on-pad system be tested in a worst-case, on-pad cold environment prior to a cold weather launch.

If the actual on-pad system cannot be tested, a suitable alternative should be found, such as a fully instrumented mock-up and/or QM-8 testing. Testing of the conditioning system in a cold environment should include simulated convective cooling on the aft skirt and exit cone due to wind

effects. Aft skirt and conditioning system hardware should be as close to flight configuration as possible.

GEI Accuracy Problem

It is recommended that the GEI data collection accuracy be increased by reducing the gage range and increasing the digital word length.

Infrared Measurement Problem

It is recommended that future infrared field joint measurements be taken at locations corresponding to joint heater sensor angular locations so that better correlations with GEI data can be made. Also, it is recommended that additional measurements be taken prior to joint heater activation.

Real-Time Data Acquisition Problem

It is recommended that aft skirt conditioning system data (GN2 temperature and pressure) be built into and be accessible from the Huntsville Operations Support Center (HOSC) data network system. (These data are necessary for aft end data correlations and postflight flex bearing predictions.)

It is also recommended that near real-time, on-pad GEI and environmental data be available to Morton Thiokol after pad validation. These data, collected hourly, need to be transmitted electronically at weekly intervals until two weeks prior to scheduled launch dates. From this point until launch, daily transmittals are necessary. These data are necessary to help meet the requirement of PMBT updates prior to launch and to aid in predicting the local SRM environment by building a variable conditions data base.

3.3.2 Seals Recommendations

Field Joints

In some areas the grease application was light, but overall the grease was nominal. In some of the corroded areas of the joint it was evident that the grease had not been rubbed into the metal thoroughly. It is recommended that the KSC grease application personnel be more consistent in applying the grease to the joints.

4

FLIGHT EVALUATION RESULTS AND DISCUSSION

4.1 SRM IN-FLIGHT ANOMALIES

This section corresponds to FEWG report Section 2.1.2.

Tables 4.1-1, 4.1-2, and 4.1-3 are the summary sheets for the three IFAs identified as pertaining to motor set 360L001.

4.2 SRM CONFIGURATION

This section corresponds with FEWG report Section 2.1.3.2.

SRM Hardware Changes

Due to the extensive rework and numerous design changes between the 360L001 RSRMs (STS-26R) and the SRMs used on STS-51L, design change specifics are not included here. A complete description of all hardware changes are documented in Morton Thiokol documents TWR-18414 (RSRM Design Certification Review Board Overview), and TWR-18654, Revision A (Redesign Solid Rocket Motor Flight Readiness Review, Level III).

SRM Reuse Hardware

Figures 4.2-1 through 4.2-11 detail the reuse hardware for RSRMs 360L001A and 360L001B.

4.3 SRB MASS PROPERTIES

This section corresponds to FEWG report Section 2.2.0.

Sequential Mass Properties

Tables 4.3-1 and 4.3-2 provide STS-26 left- and right-hand reconstructed sequential mass properties.

Predicted Data Versus Postflight Reconstructed Data

Tables 4.3-3 and 4.3-4 compare RSRM predicted sequential weight and center of gravity data with postflight reconstructed data. Prefire mass properties data are based on average actual data presented in the 5 Mar 1988 Mass

Table 4.1-1. In-Flight Anomaly Summary, STS-26-M-1

1. MSFC IFA No.: STS-26-M-1
2. PAS Tracking No.: A11767
3. Contractor No.: DR4-5/114
4. Element/System: TPS
5. Subsystem: Cap Cork
6. Criticality: 1

7. Problem Title: RSRM-1 (STS-26) DFI TPS Debris

8. Description of Problem:

   Should be: no debris from RSRMs during boost phase

   Is: Postflight inspections identify breakup and loss of cork debris (STS-42200) on both RSRMs. The cap cork is part of the thermal protection system (TPS) for the development flight instrumentation (DFI).

9. Effectivity: STS-27 and subsequent flights

10. Consequence of Recurrence:

    Contributes to debris problem during boost phase

11. Design Engineer: Mark Allison/William Gerhart

12. Prime Contractor: Morton Thiokol, Inc.

13. Resolution Summary:

    Only TPS cap cork is missing (cork-to-cork bondline)
    No TPS base cork is missing (cork-to-case bondline)
    Apparent failure mode is insufficient or ineffective cork-to-cork bondline.

    Note: Paint was observed under some bondlines
    Bondline voids in many areas

14. Investigation/Resolution:

    Tap testing has been performed on most of STS-27 cork, and has revealed over 100 voids so far. Most are edge unbonds. Where there are center voids bonded on both edges, the cork will be vented by drilling 0.125-in. holes into the void area. Edge unbonds are being removed and replaced with K5NA. To prevent this problem from occurring in the future, the possibility of removing the cap cork completely is being evaluated. Flat patterns of the cork runs are being generated to show where cork was lost on STS-26, where voids have been found on STS-27, and to document the postflight condition of STS-27 and STS-28.

Table 4.1-2. In-Flight Anomaly Summary, STS-26-M-2

1. MSFC IFA No.: STS-26-M-2
2. PAS Tracking No.: A11 85L
3. Contractor No.: DR4-5/118
4. Element/System: JPS
5. Subsystem: Vent Valve (Moisture Seal)
6. Criticality: 3

7. Problem Title: RSRM-1 (STS-26) Vent Valve Anomaly

8. Description of Problem:

Seawater found in all six field joint weatherseals, resulting from leaking SRB joint protection system (JPS) vent valves.

9. Effectivity: STS-27 and subsequent flights

10. Consequence of Recurrence:

Verification of vent valve closure prior to rollout precludes threat of ascent flight with water in JPS weatherseals.

11. Design Engineer: Charles Greatwood, Jim Seiler

12. Prime Contractor: Morton Thiokol, Inc.

13. Resolution Summary:

The outward flow function of each vent valve is verified during the joint assembly "close-out" at KSC. Reverse direction vent valve closure was not verified for STS-26. Analysis of weatherseal bulge contents and vent valve assessment produced the following conclusions:

a. STS-26 field joint weatherseals ingested seawater.
b. Structural damage was found in some recovered STS-26 valves.
c. Aluminum oxide and cork were identified as trapped debris.

Closure of the STS-27 and subsequent flight vent valves will be verified prior to rollout.

14. Investigation/Resolution:

Postflight visual inspection detected bulged TPS near field joints. Dissected bulges found to contain seawater and access paths near vent valve location near each field joint. No seawater access route was determined other than the vent valves. Vent valve examination showed cause of leaking/malfunction to be trapped debris, structural damage, or function failure prior to launch. Sample valves were given to KSC Malfunction Analysis Branch for assessment.

Table 4.1-3. In-Flight Anomaly Summary, STS-26-M-3

1. MSFC IFA No.: STS-26-M-3
2. PAS Tracking No: A11871
3. Contractor No: DR4-5/123
4. Element/System: Field Joints
5. Subsystem: Capture Feature
6. Criticality: 3

7. Problem Title: Fretting in the field joints of STS-26 (RSRM-1)

8. Description of Problem:

   Gouges, pits, and/or scratches on case field joint capture feature.

9. Effectivity: STS-27 and subsequent flights

10. Consequence of Recurrence:

    Fracture mechanics calculations indicate scratches on this magnitude would allow approximately 310 hardware uses before achieving a critical size; therefore, even if the "fretting" is assumed to occur preflight, no flight safety effect is predicted.

11. Design Engineer: Dave Campbell, Don Mason

12. Prime Contractor: Morton Thiokol, Inc.

13. Resolution Summary:

    Cause of this condition is concluded to be "fretting".

    Include in the postflight refurbishment activity the hand removal of all burrs and smoothing of all raised metal on both capture feature component surfaces. Initiate a subscale study to identify mechanism of the metal surface "fretting" phenomena and evaluate any metal fatigue concerns.

14. Investigation/Resolution:

    Postflight hardware inspections have identified small gouges, pits, and/or scratches located on recovered segment field joint capture feature surfaces. The cause is considered to be "fretting" or formation of many localized cold, welded spots on the tightly-fitted capture feature surfaces. This has not been seen on any HPM flight or RSRM static test hardware. Classical "fretting" occurs on mating metallic surfaces which can "vibrate" during system operation. Timing/cause of the STS-26 "fretting" is unknown, but considered to be associated with specific RSRM flight hardware/activities, including rollout, flight readiness firing (FRF), flight, and towback.

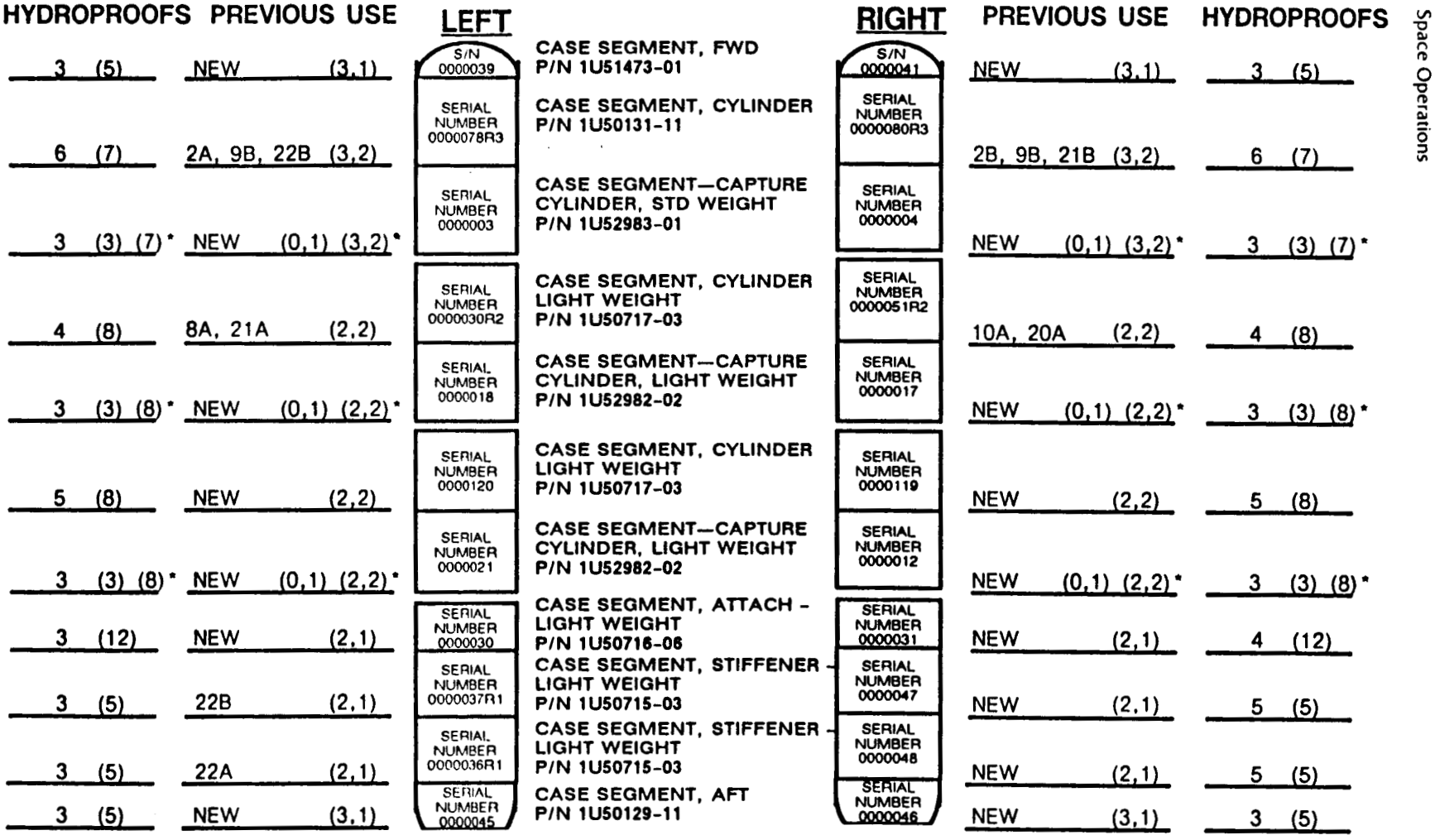

(Flight,Test) Denotes Fleet Leader Status
(Flight,Test)* Denotes Fleet Leader Status of Part Prior to Redesign

Figure 4.2-1. Reuse Hardware, Case Segments

001-FRRa-18

Motor	Joint	Raw PMD	Adjusted for Bias	TF (Raw)	Confidence (%)
Flight-1A	Fwd	1.2	4.8	2.0+	98.42
	Ctr	-0.3	3.3	2.0+	93.02
	Aft	2.1	5.7	2.0+	99.47
Flight-1B	Fwd	3.0	6.6	2.0+	99.84
	Ctr	-0.6	3.0	2.0+	91.04
	Aft	2.1	5.7	2.0+	99.47
Flight-2A	Fwd	2.3	5.9	2.0+	99.59
	Ctr	1.7	5.3	2.0+	99.12
	Aft	2.8	6.4	2.0+	99.97
Flight-2B	Fwd	0.1	3.7	2.0+	95.12
	Ctr	-1.6	2.0	2.0+	81.47
	Aft	2.4	6.0	2.0+	99.63

Note: The column labeled "Confidence (%)" is the confidence level for verifying (assuring) that the joint will be at least line-to-line

Figure 4.2-2. Reuse Hardware, Field Joint Interference Fit

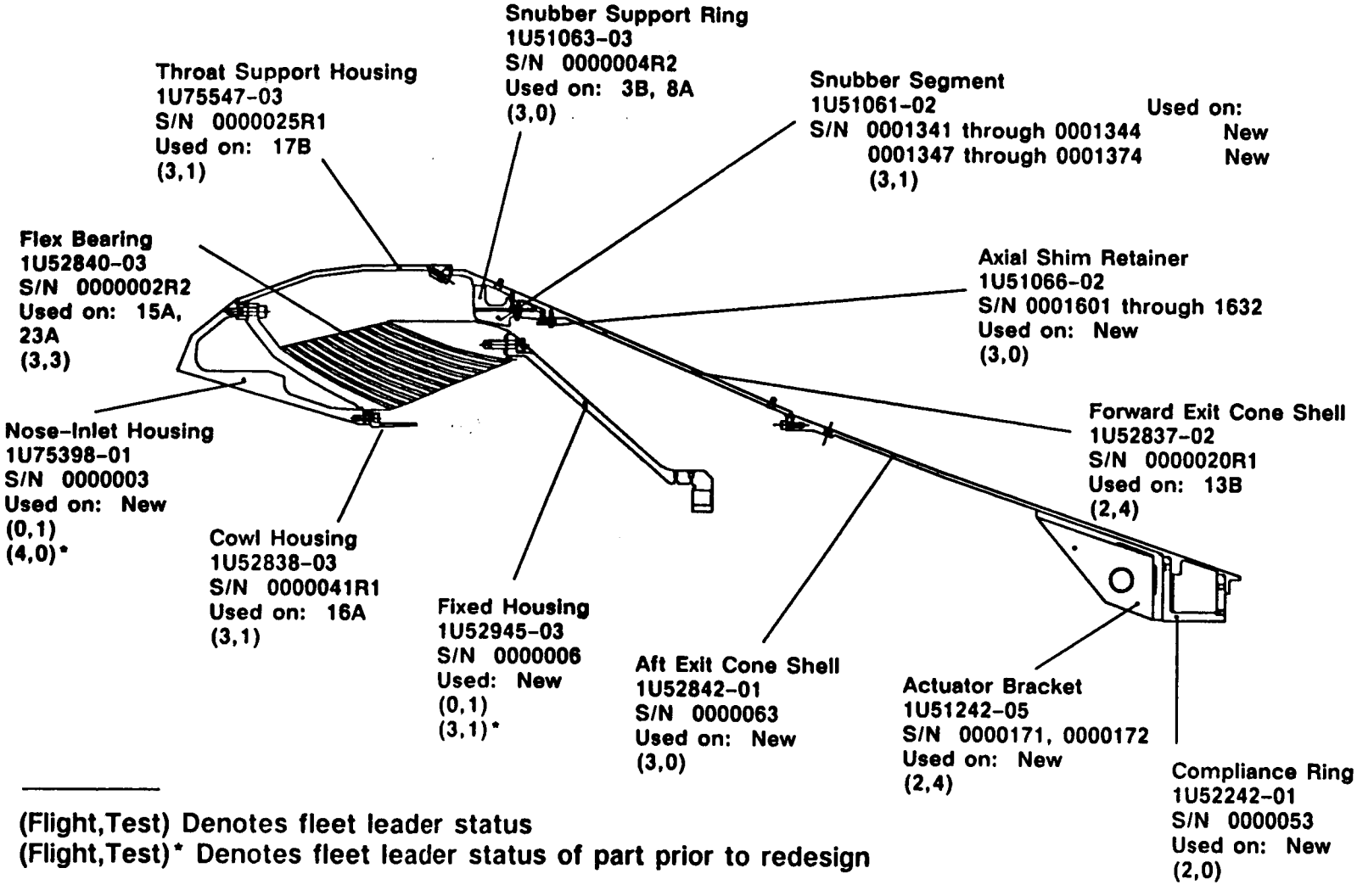

(Flight,Test) Denotes fleet leader status
(Flight,Test)* Denotes fleet leader status of part prior to redesign

Figure 4.2-3. Previous Use History, Left-Hand Nozzle

001-FRRa-20

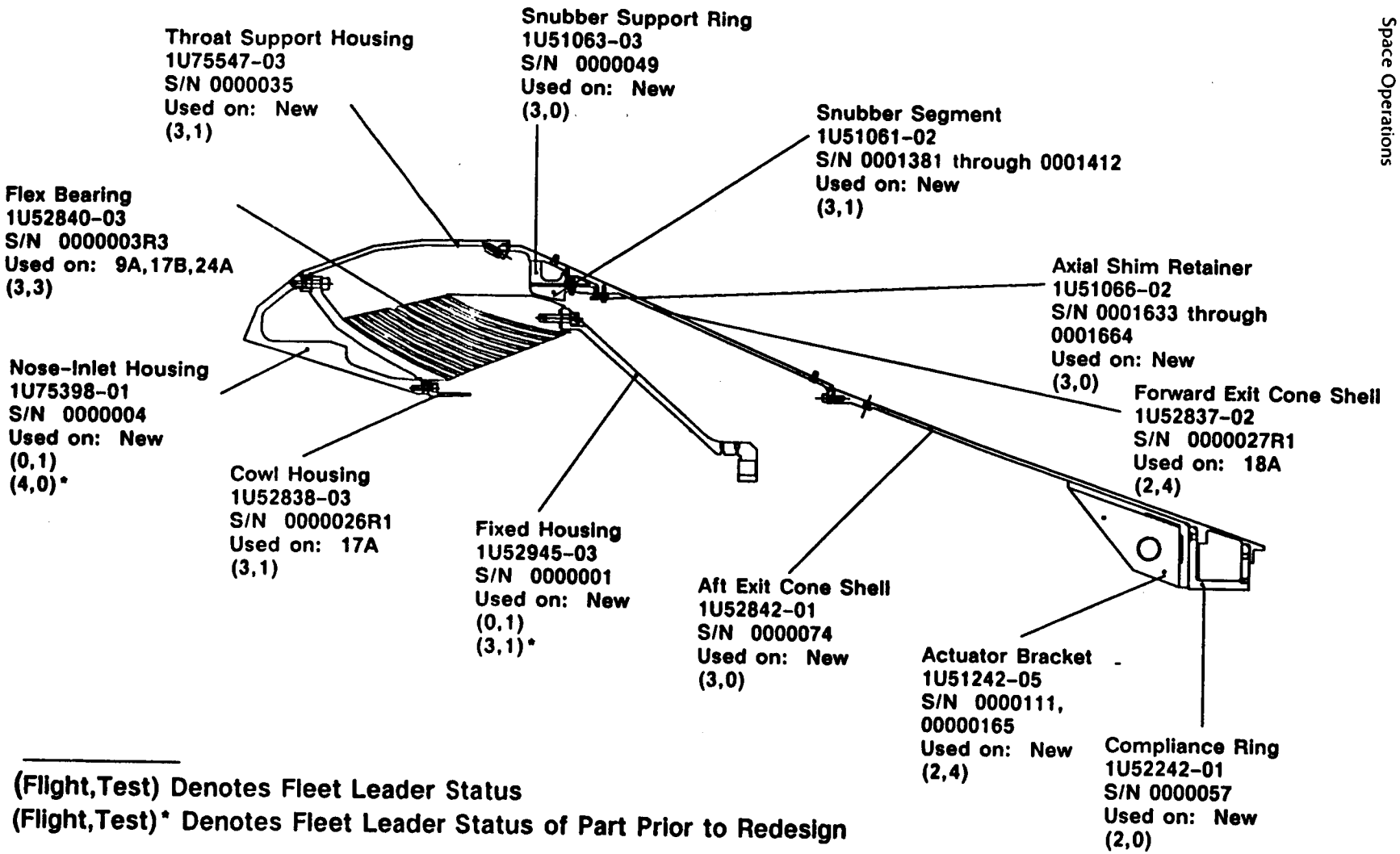

(Flight,Test) Denotes Fleet Leader Status
(Flight,Test)* Denotes Fleet Leader Status of Part Prior to Redesign

Figure 4.2-4. Previous Use History, Right-Hand Nozzle

001-FRRa-21

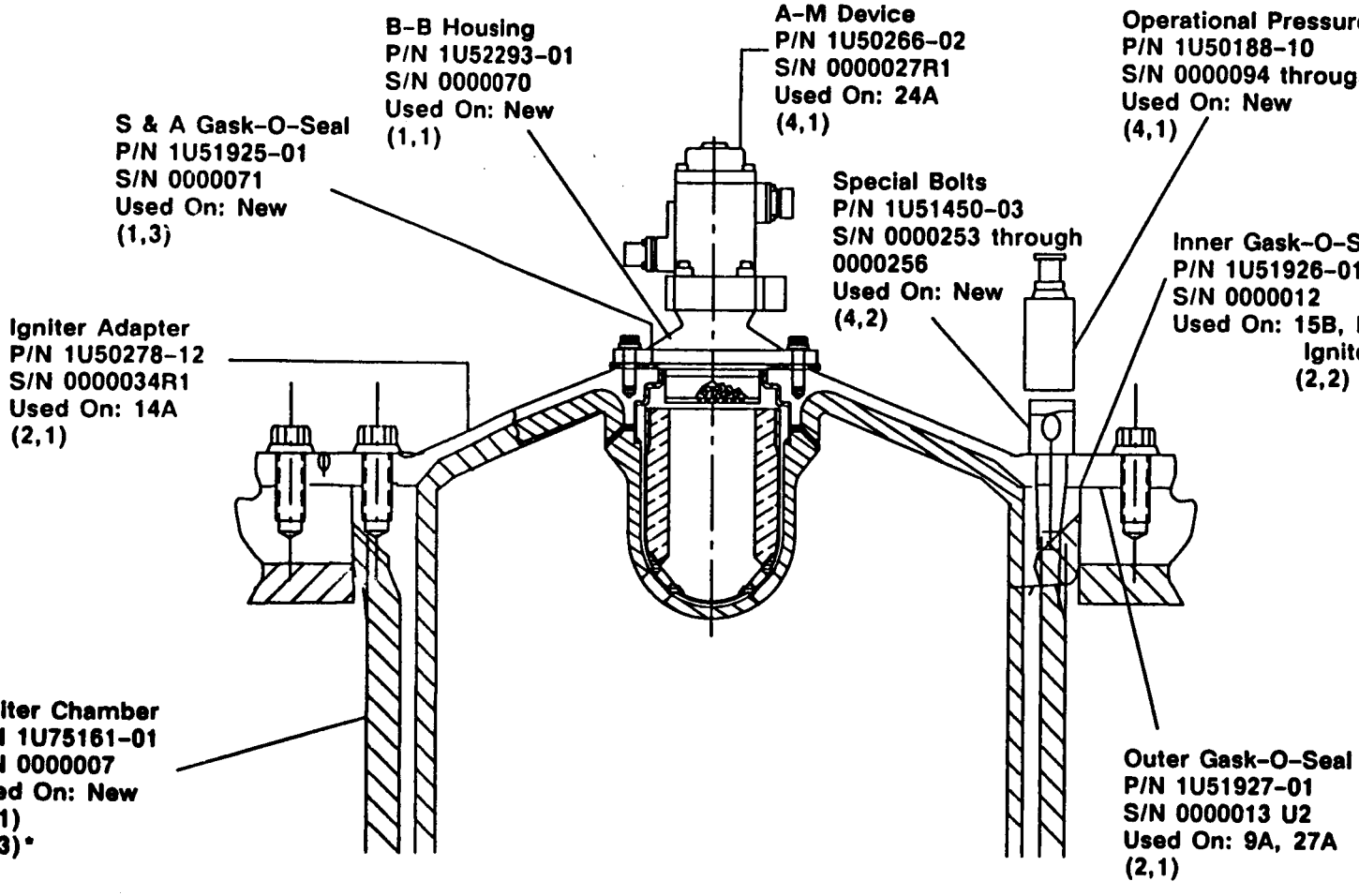

(Flight,Test) Denotes Fleet Leader Status
(Flight,Test)* Denotes Fleet Leader Status of Part Prior to Redesign

Figure 4.2-5. Previous Use History, Left Igniter

001-FRRa-22

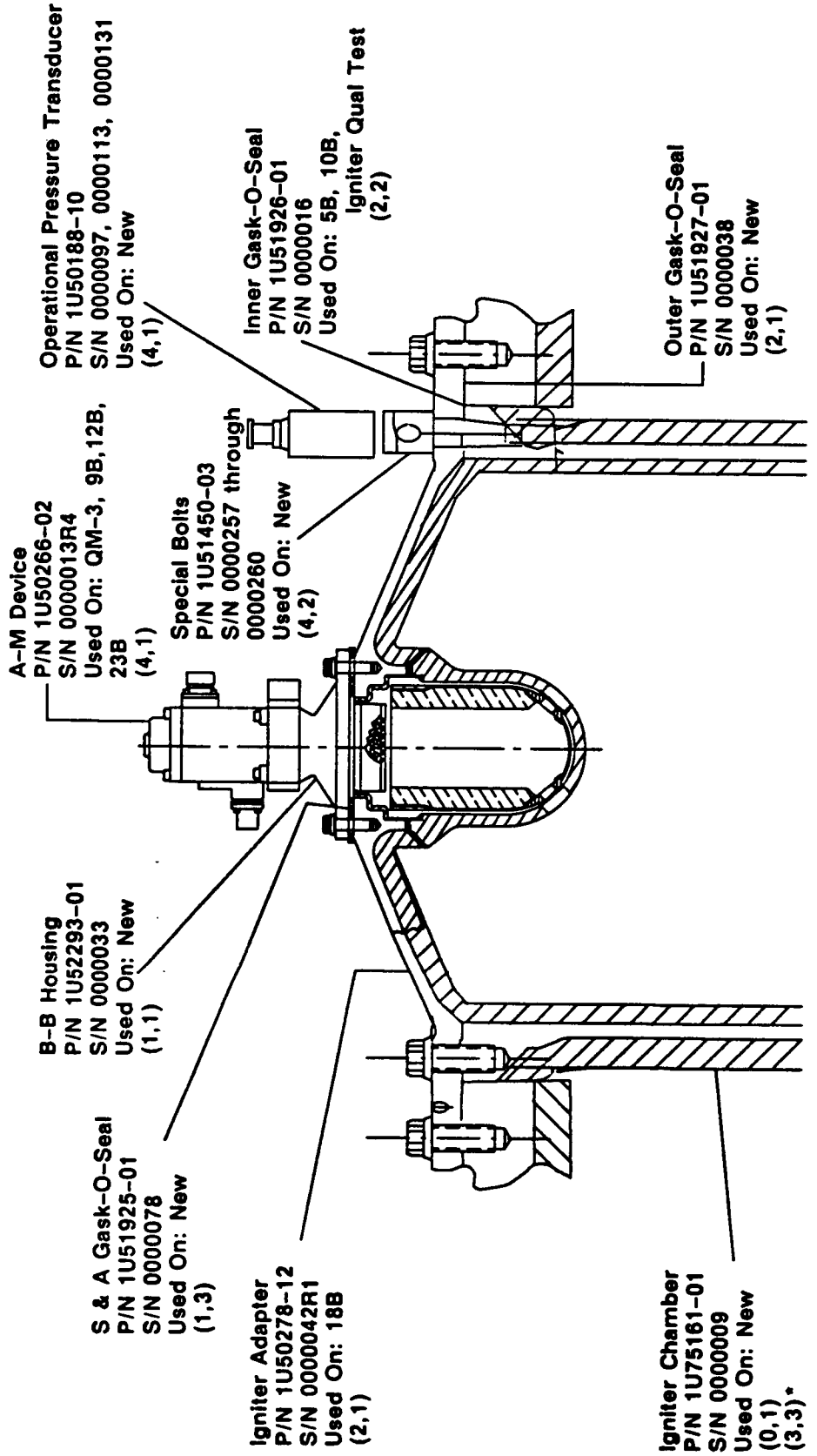

Figure 4.2-6. Previous Use History, Right Igniter

001-FRRa-23

Part No.	Serial No.	Previous Use	Fleet Leader
1U52502-04	0000049R1	19	(2,0)
Stiffener Ring,	0000050R1	18	
	0000061R1	22	
	0000062	NEW	
	0000063	NEW	
	0000064	NEW	
1U52502-07	0000006R2	15, 23	(2,0)
Stiffener Ring	0000060R1	22	
	0000061R1	22	
	0000063	NEW	
	0000064	NEW	
	0000084	NEW	
1U52502-08	0000007R2	14, 23	(2,0)
Stiffener Ring	0000041R1	19	
	0000050R1	21	
	0000051R1	21	
	0000062	NEW	
	0000063	NEW	
1U52503-02	0000003R3	8, 13, 19	(3,0)
Splice Plate	0000004R3	8, 13, 19	
1U52503-04	0000075R1	18	(3,0)
Splice Plate	0000076R1	18	
	0000077R1	18	
	0000078R1	18	
	0000079R1	18	
	0000080R1	18	
	0000081R1	18	
	0000082R1	18	
	0000083R1	19	
	0000084R1	19	

[ ] Fleet Leader

(Flight,Test) Denotes fleet leader status

(Flight,Test)* Denotes fleet leader status of part prior to redesign

Figure 4.2-7. Previous Use History, Stiffener Rings

001-FRRa-24

Part No.	Serial No.	Previous Use	Fleet Leader
1U52503-05	0000006	New	(0,1)
Splice Plate	0000011	New	(3,0)*
	0000012	New	
	0000017	New	
	0000019	New	
	0000024	New	
1U52504-05	0000005R2	14, 21	(2,1)
Adapter Assembly,	0000017R2	15, 23	
Stiffener Ring	0000020R2	15, 23	
	0000083R1	18	
	0000085R1	18	
	0000088R1	19	
	0000091R1	19	
	0000092R1	19	
	0000093R1	19	
	0000095R1	20	
	0000096R1	20	
	0000097R1	20	
1U52505-02	0000075R1	18	(2,0)
Plate, Stiffener Ring	0000076R1	18	
	0000077R1	18	
	0000078R1	18	
	0000111	New	
	0000112	New	
	0000113	New	
	0000114	New	
	0000151	New	
	0000152	New	
	0000153	New	
	0000154	New	

(Flight,Test) Denotes fleet leader status
(Flight,Test)* Denotes fleet leader status of part prior to redesign

Figure 4.2-8. Previous Use History, Stiffener Rings

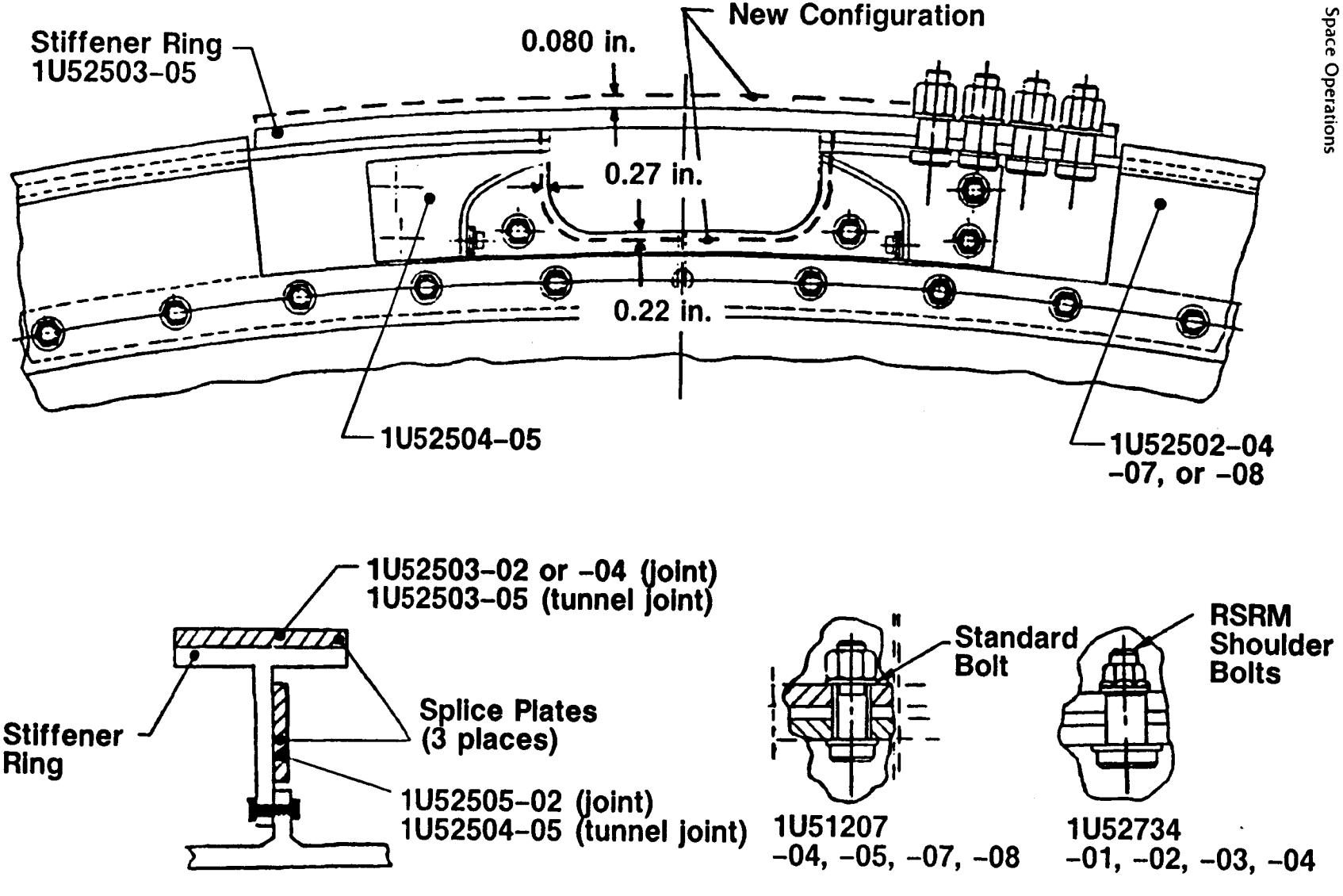

Figure 4.2-9. Previous Use History, Stiffener Rings

001-FRRa-26

- Part No. 1U76034—(nozzle-to-case axial bolt)
  - Parts are identified by lot number
  - Bolts may be reused provided they meet the requirements of STW7-2559
  - All 1U76034 bolts for first flight are new
- Part No. 1U75167 (radial bolt, machine)
  - Parts are identified by lot number
  - Bolts may be reused provided they meet the requirements of STW7-2559
  - First-flight 1U75167 bolts are a mix of new and refurbished
    - Left-hand booster—new
    - Right-hand booster-mixed
      (same lot of used bolts also used on QM-6)
- Part No. 1U51055 (headless straight pin)
  - Parts are identified by lot number
  - Pins may be reused provided they meet the requirements of STW7-2786
  - First-flight 1U51055 pins are a mix of new and refurbished
    (used on static tests motors)

Figure 4.2-10. Previous Use History, Bolts and Pins

Part No.	Serial No.	Remaining Cycles
1U52295-02	0000006	951
	0000007	902

- No constraints for first flight
- A total of 1,160 cycles is allowed
- The Safe&Arm flown on SRM-16B had been cycled 302 times with 858 cycles remaining
- Eight qualification units were cycled a minimum of 2440 times. One unit was cycled 7440 times. All units were functionally operable after conclusion of tests

Figure 4.2-11. Limited Life Items, Safe and Arm Device History for STS-26

Table 4.3-1. 360L001A Sequential Mass Properties

EVENTS/TIMES	WEIGHT (LBS)	CENTER OF GRAVITY LONG.	LAT.	VERT.	MOMENT OF INERTIA PITCH	ROLL	YAW
PRE-LAUNCH TIME = 0.00	1256497.0	1171.351	0.061	0.007	42444.514	879.359	42445.483
LIFT-OFF TIME = 0.23	1255852.4	1171.479	0.061	0.007	42404.640	877.988	42405.609
INTERMEDIATE BURN TIME = 20.00	1011406.5	1208.786	0.075	0.008	30589.436	759.343	30590.403
INTERMEDIATE BURN TIME = 40.00	789554.4	1231.901	0.096	0.011	21578.846	624.150	21579.807
MAX "Q" TIME = 54.00	659619.8	1229.359	0.114	0.013	17919.568	546.909	17920.522
INTERMEDIATE BURN TIME = 60.00	604426.1	1226.778	0.124	0.014	16497.761	509.462	16498.712
INTERMEDIATE BURN TIME = 80.00	411425.5	1215.216	0.181	0.020	11811.641	374.942	11812.580
MAX "G" TIME = 87.00	347625.8	1214.829	0.213	0.024	10441.654	324.415	10442.590
INTERMEDIATE BURN TIME = 100.00	242247.1	1229.124	0.304	0.034	8450.863	235.346	8451.791
WEB BURN TIME = 110.18	173682.6	1267.401	0.422	0.048	7259.128	172.876	7260.047
END OF ACTION TIME TIME = 122.49	144008.2	1313.982	0.507	0.058	6546.684	146.783	6547.598
SEPARATION TIME = 124.72	143340.7	1315.580	0.510	0.058	6517.723	146.307	6518.641
MAX REENTRY "Q" TIME = 309.85	142687.6	1316.203	0.512	0.057	6487.066	145.770	6487.983
NOSE CAP SEPARATION TIME = 334.05	142645.3	1316.188	0.512	0.057	6484.829	145.733	6485.746
DROGUE CHUTE DEPLOYMENT TIME = 342.26	142630.9	1316.183	0.512	0.057	6484.066	145.720	6484.985
FRUSTUM SEPARATION TIME = 351.80	142614.3	1316.177	0.512	0.057	6483.179	145.705	6484.098
MAIN CHUTE 1ST DISREEFING TIME = 356.95	142605.3	1316.174	0.512	0.057	6482.699	145.697	6483.618
MAIN CHUTE 2ND DISREEFING TIME = 363.19	142594.4	1316.170	0.512	0.057	6482.117	145.688	6483.036
MAIN CHUTE DEPLOYMENT TIME = 367.08	142587.6	1316.168	0.512	0.057	6481.753	145.682	6482.672
NOZZLE JETTISIONED TIME = 387.00	140321.4	1305.833	0.510	0.057	6278.363	141.139	6279.215
SPLASHDOWN TIME = 414.00	140275.0	1305.814	0.510	0.057	6275.831	141.098	6276.682

Table 4.3-2. 360L001B Sequential Mass Properties

EVENTS/TIMES	WEIGHT (LBS)	CENTER OF GRAVITY LONG.	LAT.	VERT.	MOMENT OF INERTIA PITCH	ROLL	YAW
PRE-LAUNCH TIME = 0.00	1256381.3	1171.223	0.061	0.007	42447.340	879.276	42448.307
LIFT-OFF TIME = 0.23	1255729.2	1171.327	0.061	0.007	42413.277	877.796	42414.244
INTERMEDIATE BURN TIME = 20.00	1012392.8	1207.917	0.075	0.009	30691.658	760.275	30692.623
INTERMEDIATE BURN TIME = 40.00	791881.5	1231.277	0.096	0.011	21696.378	625.723	21697.337
MAX "Q" TIME = 54.00	662173.0	1229.150	0.114	0.014	18005.182	548.278	18006.134
INTERMEDIATE BURN TIME = 60.00	606924.7	1226.700	0.124	0.015	16592.557	511.841	16593.506
INTERMEDIATE BURN TIME = 80.00	413849.0	1215.368	0.180	0.022	11896.463	376.633	11897.400
MAX "G" TIME = 87.00	349372.3	1214.558	0.213	0.026	10500.727	325.571	10501.660
INTERMEDIATE BURN TIME = 100.00	243655.1	1228.273	0.303	0.037	8489.150	236.375	8490.075
WEB BURN TIME = 110.13	175143.1	1265.431	0.420	0.051	7277.242	174.364	7278.160
END OF ACTION TIME TIME = 123.28	143882.1	1313.852	0.509	0.062	6528.889	146.745	6529.802
SEPARATION TIME = 124.72	143374.8	1315.178	0.511	0.062	6506.164	146.354	6507.080
MAX REENTRY "Q" TIME = 309.85	142593.9	1316.300	0.513	0.062	6468.423	145.714	6469.340
NOSE CAP SEPARATION TIME = 334.05	142551.2	1316.284	0.514	0.062	6466.163	145.677	6467.079
DROGUE CHUTE DEPLOYMENT TIME = 342.26	142536.7	1316.279	0.514	0.062	6465.393	145.664	6466.309
FRUSTUM SEPARATION TIME = 351.80	142519.9	1316.274	0.514	0.062	6464.496	145.649	6465.413
MAIN CHUTE 1ST DISREEFING TIME = 356.95	142510.8	1316.270	0.514	0.062	6464.011	145.641	6464.928
MAIN CHUTE 2ND DISREEFING TIME = 363.19	142499.8	1316.267	0.514	0.062	6463.422	145.631	6464.339
MAIN CHUTE DEPLOYMENT TIME = 367.08	142492.9	1316.264	0.514	0.062	6463.056	145.625	6463.971
NOZZLE JETTISIONED TIME = 384.00	140237.0	1305.922	0.512	0.061	6260.300	141.091	6261.148
SPLASHDOWN TIME = 411.00	140189.8	1305.902	0.512	0.061	6257.729	141.050	6258.578

Table 4.3-3. Sequential Mass Properties Predicted/Actual Comparisons, 360L001A

Event	Weight (lb)				Longitudinal CG (in)			
	Predicted[1]	Actual	Delta[2]	% Error[2]	Predicted[1]	Actual	Delta[2]	% Error[2]
Pre-Ignition	1,256,463	1,256,497	34	0.00	1,171.370	1,171.351	-0.019	0.00
Liftoff	1,255,824	1,255,852	28	0.00	1,171.484	1,171.479	-0.005	0.00
Action Time	142,738	144,008	1,270	0.88	1,310.487	1,313.982	3.495	0.27
Separation[3]	141,963	143,341	1,378	0.96	1,312.686	1,315.580	2.894	0.22
Nose Cap Separation	141,530	142,645	1,115	0.78	1,312.655	1,316.188	3.533	0.27
Drogue Chute Deployment	141,515	142,631	1,116	0.78	1,312.650	1,316.183	3.533	0.27
Main Chute 1st Disreefing	141,489	142,605	1,116	0.78	1,312.640	1,316.174	3.534	0.27
Main Chute 2nd Disreefing	141,478	142,594	1,116	0.78	1,312.636	1,316.170	3.534	0.27
Main Chute Deployment	141,471	142,588	1,117	0.78	1,312.634	1,316.168	3.534	0.27
Nozzle Jettison	139,245	140,321	1,076	0.77	1,302.275	1,305.833	3.558	0.27
Splash Down	139,228	140,275	1,047	0.75	1,302.268	1,305.814	3.546	0.27

Notes:

1. Based on Mass Properties Quarterly Status Report, 5 March 1988 (TWR-10211-86).
2. Difference mainly caused from a slag weight of 650 lbs (predicted) to a slag weight of 1,500 lbs (actual).
3. The separation longitudinal center of gravity of 1,315.580 is 66% of the vehicle length.

Table 4.3-4. Sequential Mass Properties Predicted/Actual Comparisons, 360L001B

Event	Weight (lb)				Longitudinal CG (in)			
	Predicted[1]	Actual	Delta[2]	% Error[2]	Predicted[1]	Actual	Delta[2]	% Error[2]
Pre-Ignition	1,256,463	1,256,381	-82	0.01	1,171.370	1,171.223	-0.147	0.01
Liftoff	1,255,824	1,255,729	-95	0.01	1,171.484	1,171.327	-0.157	0.01
Action Time	142,738	143,882	1,144	0.80	1,310.487	1,313.852	3.365	0.26
Separation[3]	141,963	143,375	1,412	0.98	1,312.686	1,315.178	2.492	0.19
Nose Cap Separation	141,530	142,551	1,021	0.72	1,312.655	1,316.284	3.629	0.28
Drogue Chute Deployment	141,515	142,538	1,023	0.72	1,312.650	1,316.279	3.629	0.28
Main Chute 1st Disreefing	141,489	142,511	1,022	0.72	1,312.640	1,316.270	3.630	0.28
Main Chute 2nd Disreefing	141,478	142,500	1,022	0.72	1,312.636	1,316.267	3.631	0.28
Main Chute Deployment	141,471	142,493	1,022	0.72	1,312.634	1,316.264	3.630	0.28
Nozzle Jettison	139,245	140,237	922	0.71	1,302.275	1,305.922	3.647	0.28
Splash Down	139,228	140,190	962	0.69	1,302.268	1,305.902	3.634	0.28

Notes:

1. Based on Mass Properties Quarterly Status Report, 5 March 1988 (TWR-10211-86).
2. Difference mainly caused from a slag weight of 650 lbs (predicted) to a slag weight of 1,500 lbs (actual).
3. The separation longitudinal center of gravity of 1,315.178 is 66% of the vehicle length.

Properties Quarterly Status Report (TWR-10211-86) for a lightweight case configuration with DFI. Actual STS-26 mass properties may be obtained from Mass Properties History Log Space Shuttle 360L001-LH and 360L001-RH (TWR-17534 and TWR-17335, respectively). Postflight reconstructed data reflect ballistics mass flow data from the 320 samples per sec (sps) measured pressure traces and a predicted slag weight of 1,500 lb. Those mass properties reported after separation reflect delta times from separation and nose cap separation previously used on earlier flights.

CEI Specification Requirements

Tables 4.3.5 and 4.3.6 present CEI specification requirements and predicted and actual weight comparisons. If the earlier predicted slag weight of 650 lb were used, the actual weights would be in close agreement. Mass properties data for both RSRMs comply with the CEI specification requirements.

4.4 SRM PROPULSION PERFORMANCE

This section corresponds to FEWG report Section 2.3.0.

4.4.1 Introduction and Summary

This section contains the propulsion performance data from motors 360L001 which were assigned to the STS-26R launch. The ballistic performance presented in this section was based on the operational flight instrumentation (OFI) 12.5 sps pressure data. The ignition buildup was modeled using the 320 sps DFI data. The DFI data magnitudes were below that of the real-time data (telemetered OFI data); therefore, the left motor DFI data were adjusted up 0.6 percent, and the right motor DFI data were adjusted up 1.2 percent.

The delivered burn rates for both motors were very close to predicted. The delivered burn rates were 0.366 in./sec at 625 psia, and 60°F for both the left and right motors. This was exactly as predicted for the left motor and 0.001 in./sec lower on the right motor. The average of the two motors was only 0.002 in./sec below the target rate of 0.368 in./sec at 625 psia and 60°F. The reconstructed specific impulse values were close to predicted for both motors, although the left motor had a 1.0 (lbf-sec/lbm) lower specific impulse than predicted. The difference in I_{sp} in the left motor indicates

Table 4.3-5. Predicted/Actual Weight Comparisons, 360L001A

Item	Minimum (lb)	Maximum (lb)	Predicted*** (lb)	Actual (lb)	Delta (lb)	Error (%)
Inerts						
Prefire, Controlled*		150,427	148,628	148,831	+203	0.14
Propellant*	1,104,714		1,107,269	1,107,102	-167	0.02
Usable**			1,106,500	1,106,170	-330	0.03
To Lift-Off			539	547	+8	1.46
Lift-Off to Action**			1,105,961	1,105,623	-338	0.03
Unusable			769	932	+163	17.49
Action to Separation			713	602	-111	18.44
After Separation			56	330	+274	83.03
Slag**			650	1,500	+850	56.67

*Requirement per CPW1-3600A, Addendum G, Part I, (RSRM CEI Specification).
**Slag included in usable propellant, lift-off to action.
***Based on Quarterly Status Report (TWR-10211-86), 5 Mar 1988.

Table 4.3-6. Predicted/Actual Weight Comparisons, 360L001B

Item	Minimum (lb)	Maximum (lb)	Predicted*** (lb)	Actual (lb)	Delta (lb)	Error (%)
Inerts						
Prefire, Controlled*		150,427	148,628	148,738	+110	0.07
Propellant*	1,104,714		1,107,269	1,107,077	-192	0.02
Usable**			1,106,500	1,106,181	-319	0.03
To Lift-Off			539	555	+16	2.88
Lift-Off to Action**			1,105,961	1,105,961	-335	0.03
Unusable			769	896	+127	14.17
Action to Separation			713	441	-272	61.68
After Separation			56	455	+399	87.69
Slag**			650	1,500	+850	56.67

*Requirement per CPW1-3600A, Addendum G, Part I, (RSRM CEI Specification).
**Slag included in usable propellant, lift-off to action.
***Based on Quarterly Status Report (TWR-10211-86), 5 Mar 1988.

that the two motors had either different erosion patterns in the nozzle, or that there was a pressure transducer error. The performance of the two motors was very close to the same until about 70 sec, where a slight divergence occurs (Figure 4.4.1).

The data as presented were within expected ranges and met all CEI specification requirements. The impulse gate information has been included and compared to the CEI specification requirements. The data, corrected to 60°F, were well within the variation limits from the high performance motor (HPM) nominal values at a burn rate of 0.368 in./sec at 625 psia and 60°F. The HPM nominal values stated are the average performance data from QM-4, ETM-1A, DM-8, DM-9, QM-6, QM-7, PV-1, RSRM-1, SRM-8 through SRM-24 excluding SRM-9B, SRM-11A, and SRM-20 through SRM-23.

4.4.2 RSRM Propulsion Performance Results

The RSRMs for this flight were designated by Morton Thiokol as 360L001A and 360L001B for the left and right motors respectively, as viewed from the aft end of the vehicle. They were also designated as STS-26A Left and STS-26B Right by NASA. All times shown in this section, unless noted otherwise, are referenced to the SRM ignition command time at 1988:273:11:37:00:009 (EDT).

4.4.2.1 SRM Nominal Performance Requirements

RSRM-1A/RSRM-1B Thrust Time Comparison

The flight motor reconstructed thrust time traces at the delivered temperature of 79°F are shown in Figure 4.4.1. Although thrust measurements are not available for flight sets of motors, the thrust output from each motor can be estimated by using flight pressure measurements with the knowledge of pressure-to-thrust conversions based on the performance of RSRM static tests. Using these tools, a comparison can be made between the predicted thrust and reconstructed thrust for each motor (Figures 4.4.2 and 4.4.3).

The comparison of predicted and measured head end chamber pressure is shown also in Figures 4.4.4 and 4.4.5. The differences in the traces are due to an HPM versus RSRM prediction, small burn rate differences, and a slight

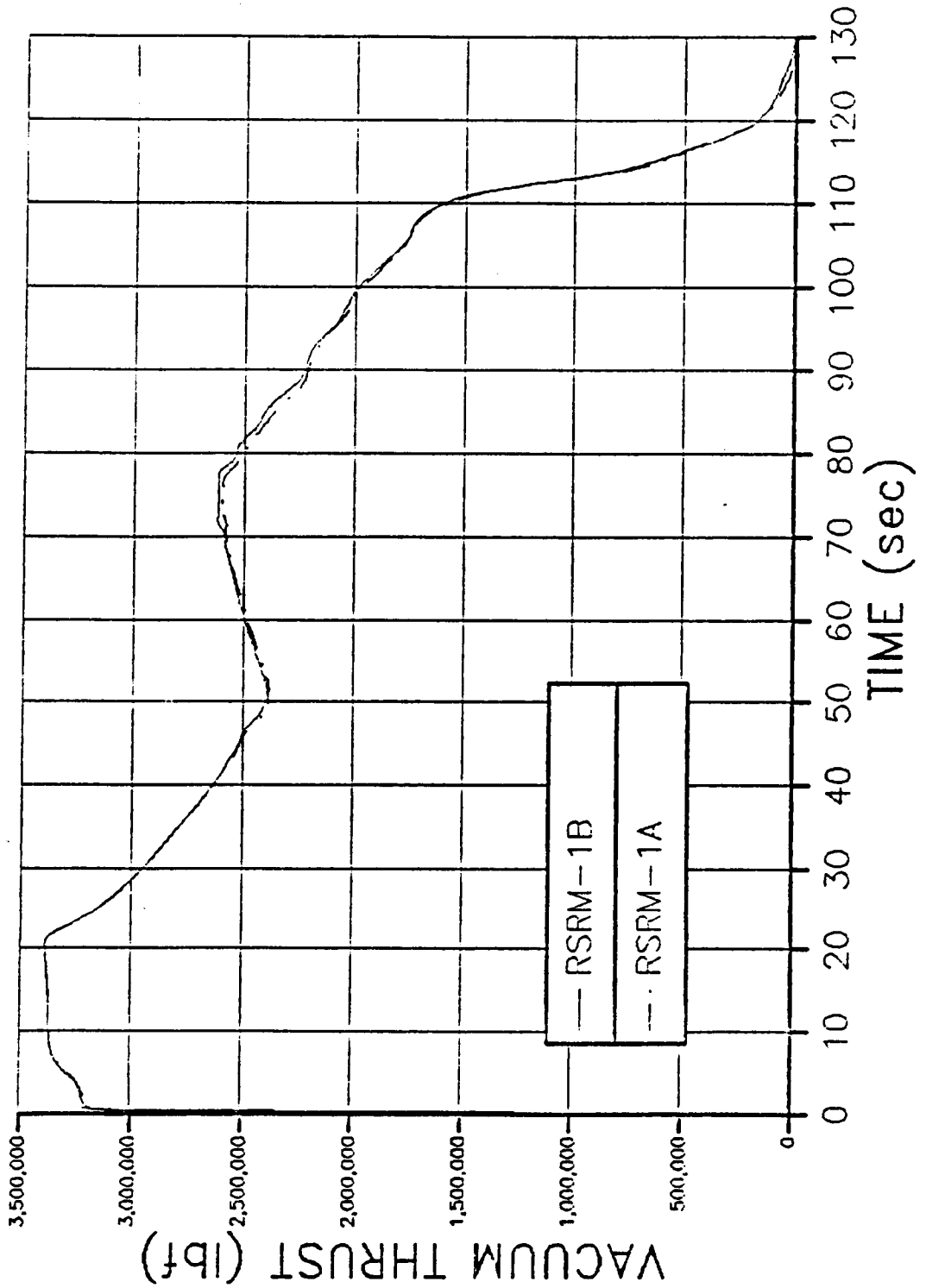

Figure 4.4-1. RSRM-1A and -1B Vacuum Thrust Time Trace at Delivered Conditions

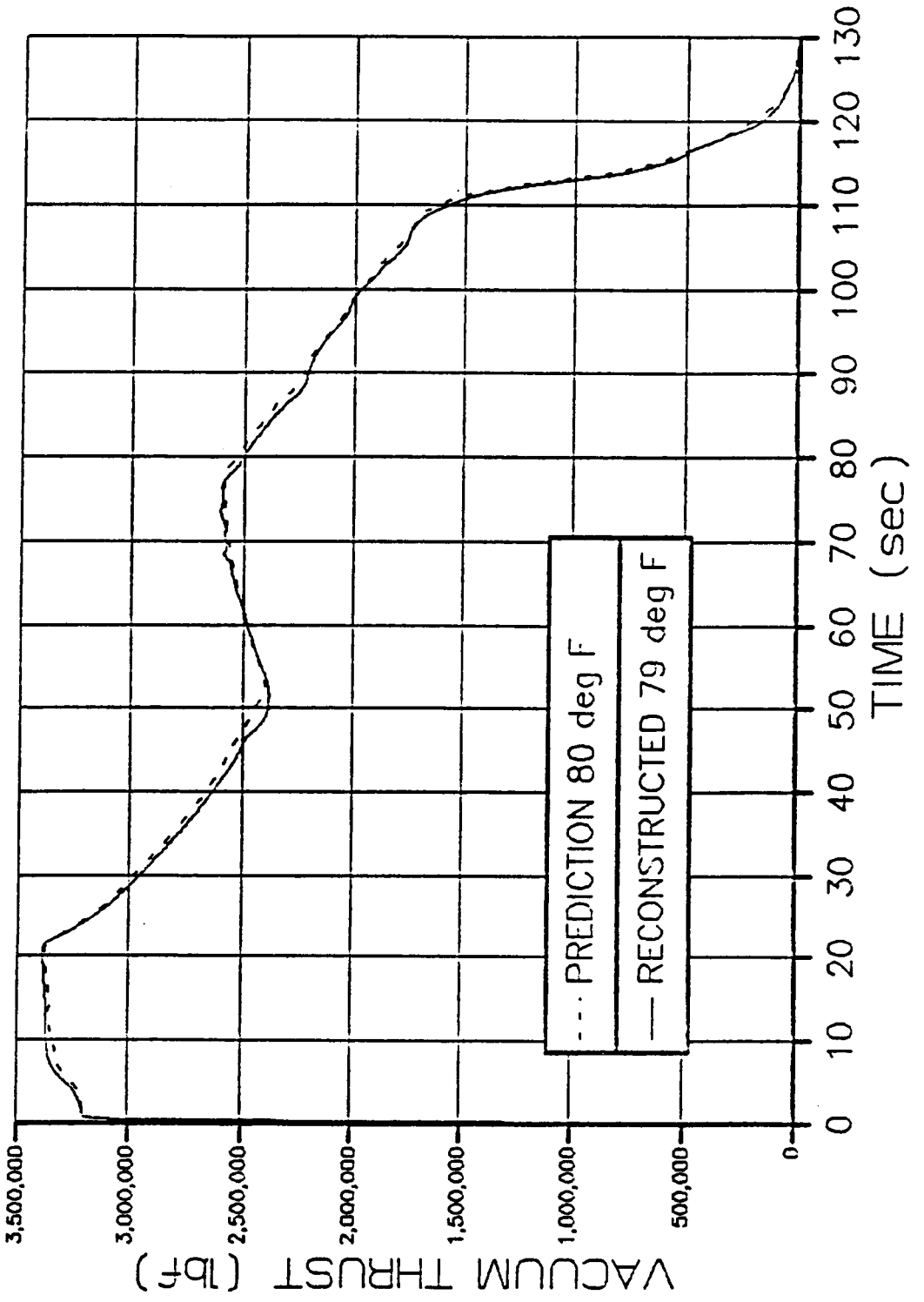

Figure 4.4-2. RSRM-1A Predicted Versus Reconstructed Vacuum Thrust

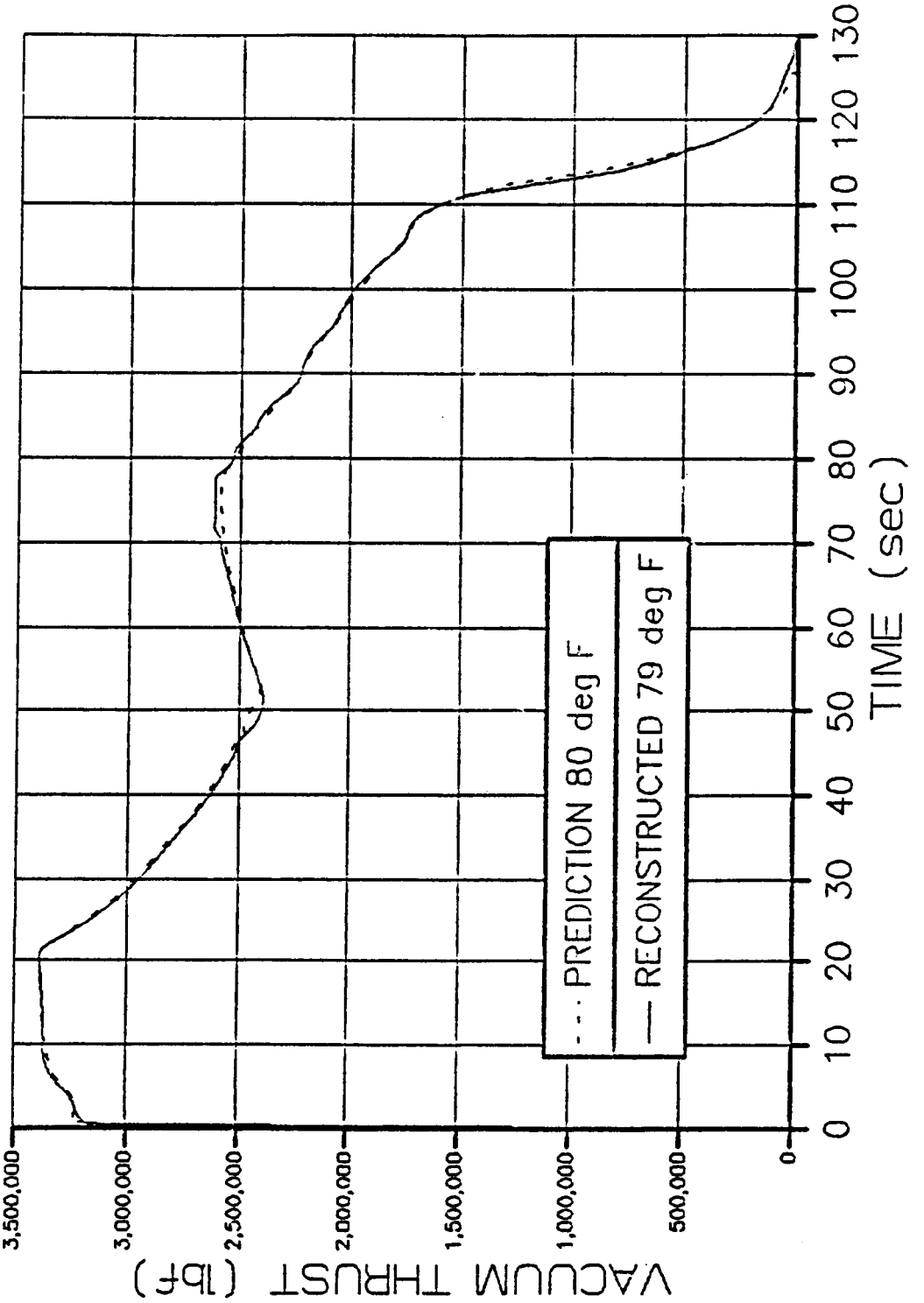

Figure 4.4-3. RSRM-1B Predicted Versus Reconstructed Vacuum Thrust

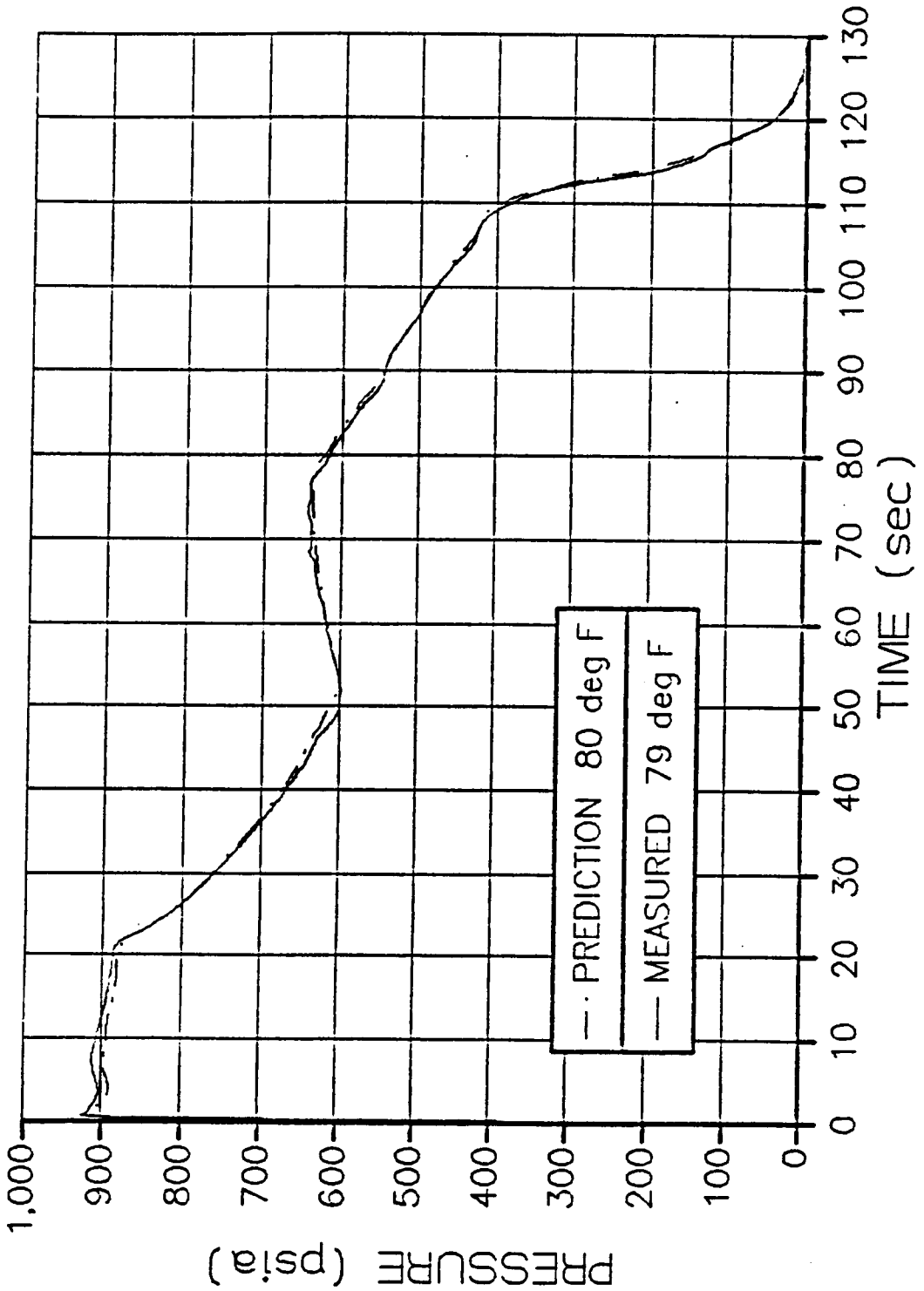

Figure 4.4-4. RSRM-1A Predicted Versus Measured Pressure

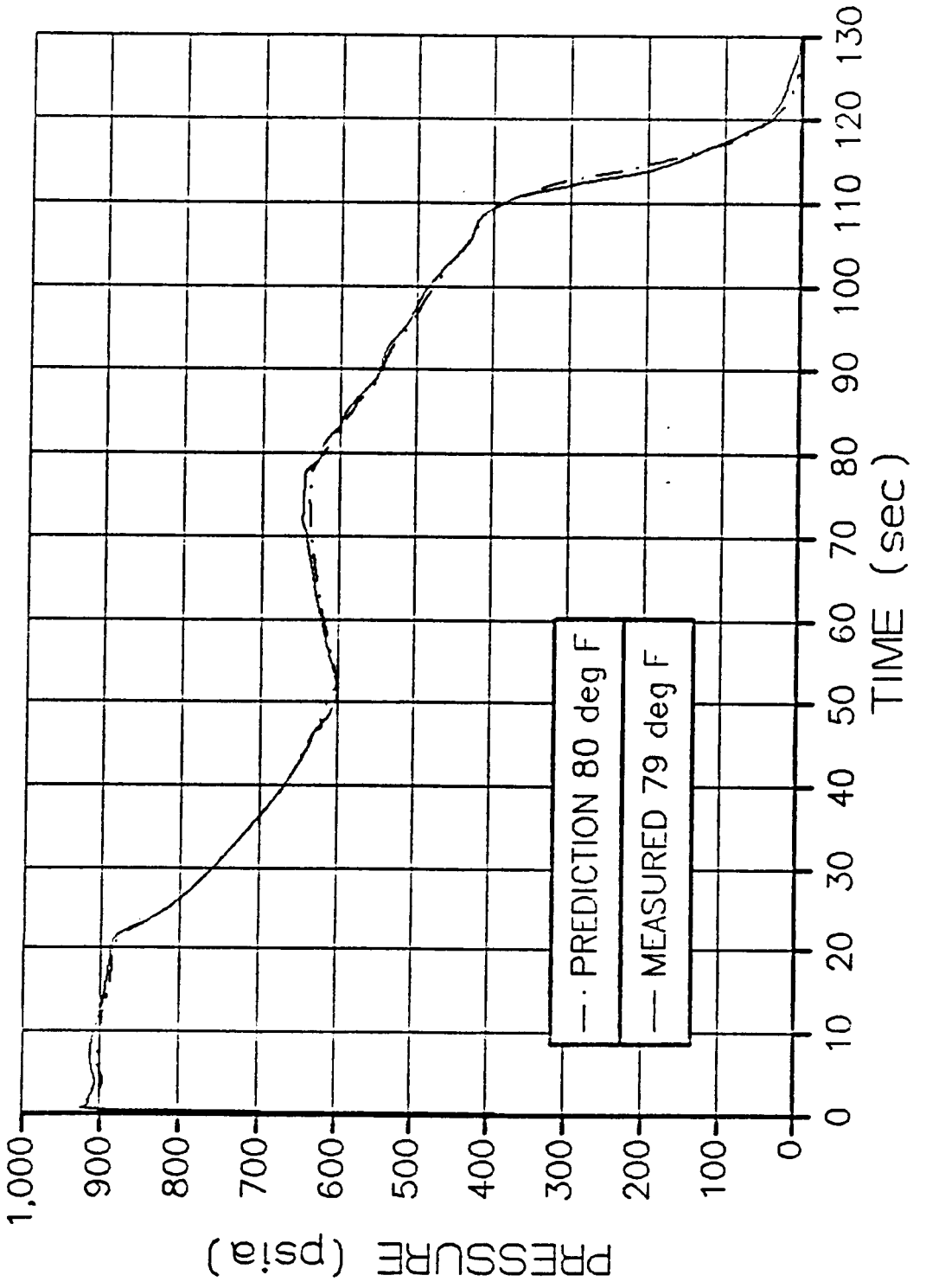

Figure 4.4-5. RSRM-1B Predicted Versus Measured Pressure

temperature difference of one degree. Although no ballistic differences were to have been incorporated into the RSRM design from the HPM design, certain insulation changes have slightly affected the performance of the RSRM. As the propellant burns radially outward to the insulation, small differences are noticed in the chamber pressure measurements from HPM to RSRM. These are best illustrated at the 50-sec point. At this time, the propellant in the aft segment has reached the aft factory joint insulation which was thickened, thereby causing a sudden decrease in propellant surface area and consequently in chamber pressure. Other small differences occur, but the aft factory joint is the most easily recognizable.

The RSRM-1 pressure oscillations encountered were typical of those seen in earlier HPM flight motors. The magnitudes of the thrust oscillation were much smaller than those seen in RSRM static tests. Waterfall plots of the pressure oscillations for STS-26 can be seen in Figures 4.4.6 and 4.4.7.

RSRM Nominal Thrust Time Performance

The nominal RSRM-HPM performance is defined as the average performance of the HPM and RSRM static test and flight motor series at standard conditions. The standard conditions consist of the propellant burn rate of 0.368 in./sec at 625 psia and a PMBT of 60°F.

The flight motor reconstructed thrust time traces are normalized to standard conditions and averaged with the static test data at standard conditions to form the RSRM-HPM population nominal thrust time trace. This RSRM-HPM performance will be continually updated during the shuttle program. It is the current estimate of the total population performance. The nominal performance for the thrust time trace and impulse gate requirements is based on the performance of QM-4, SRM-8A, SRM-8B, SRM-9A, SRM-10A, SRM-10B, SRM-11B through SRM-19B, SRM-24A, SRM-24B, ETM-1A, DM-8, DM-9, QM-6, QM-7, PV-1, and RSRM-1. The delivered RSRM-HPM population nominal performance is compared to the CEI requirements in Figure 4.4.8.

Impulse at Standard Conditions Versus Requirement Gates

The vacuum impulse at standard conditions at each of the gates is compared to the CEI specification requirements below. The population making up the

ORIGINAL PAGE IS
OF POOR QUALITY

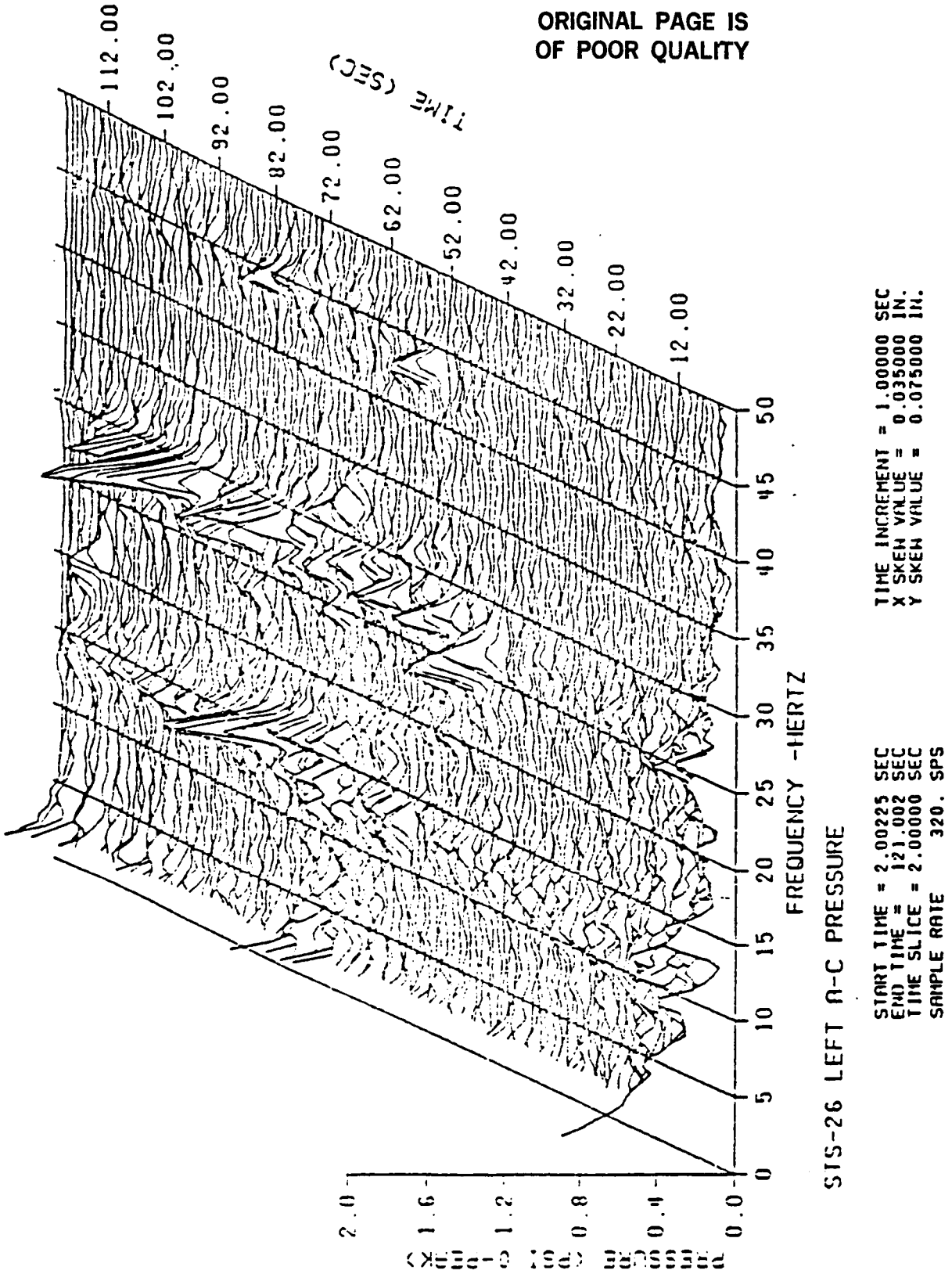

Figure 4.4-6. RSRM-1A Waterfall Pressure Plot

ORIGINAL PAGE IS
OF POOR QUALITY

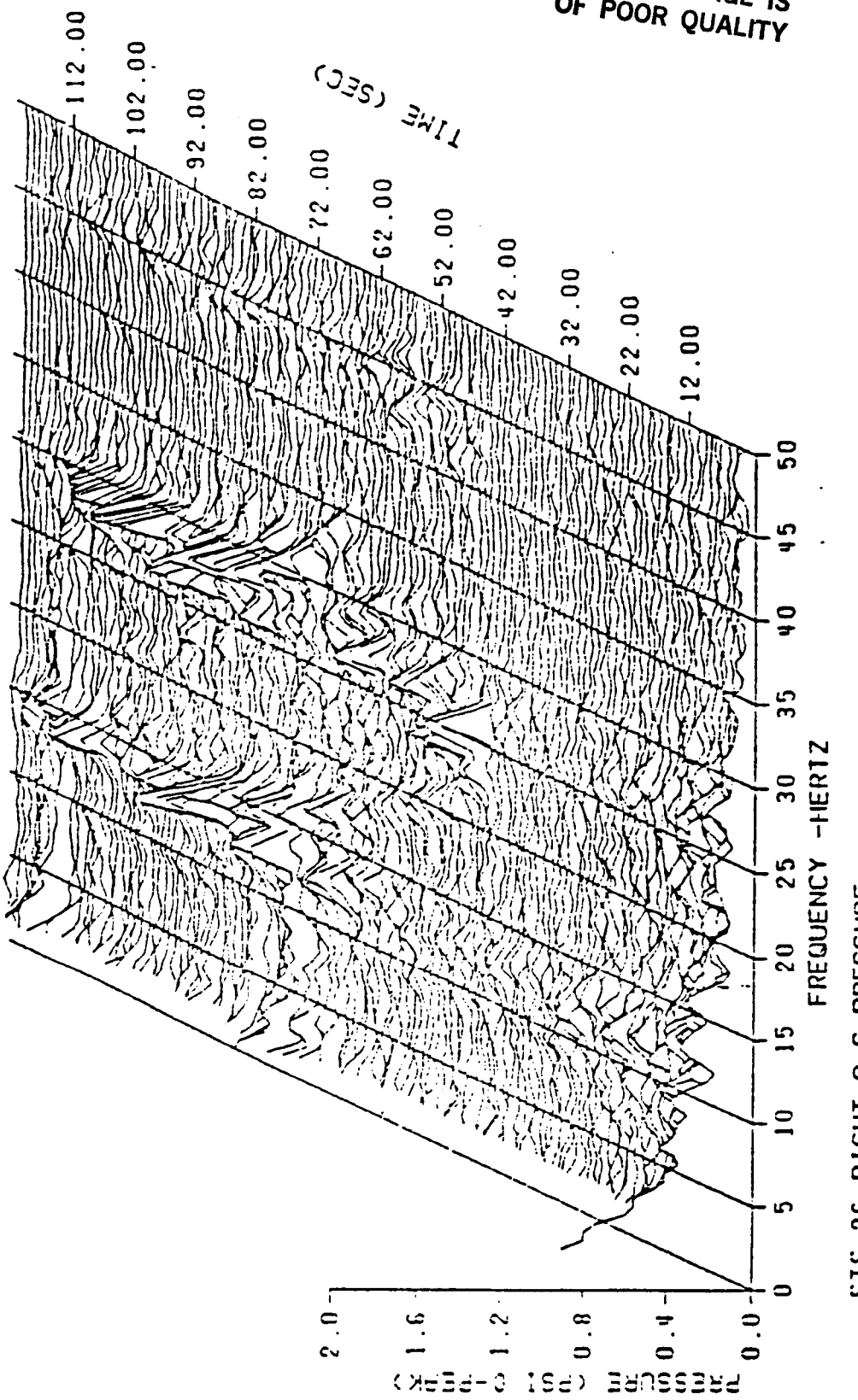

Figure 4.4-7. RSRM-1B Waterfall Pressure Plot

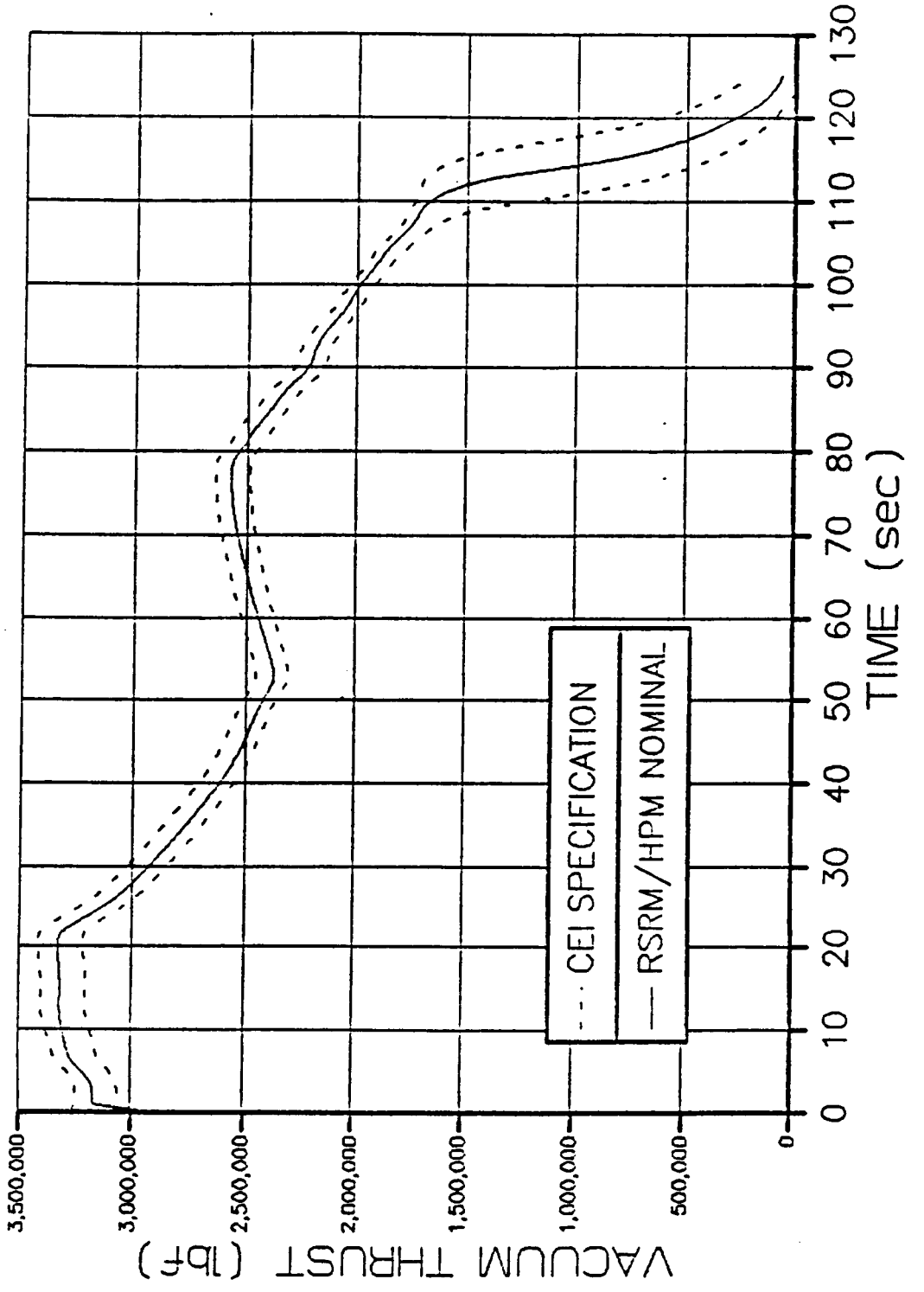

Figure 4.4-8. RSRM-HPM Nominal Thrust Time Trace in CEI Specification Limits

standard nominal for the impulse requirements are the same as those in the nominal thrust time trace (Figure 4.4.8).

RSRM-HPM Population

Impulse	Requirement	Standard Nominal*
I-20 (10^6 lb-sec)	63.1 (minimum)	64.6
I-60 (10^6 lb-sec)	172.9, 178.1(+3%) 171.2(-1%)	172.8
I-Action time (10^6 lb-sec)	293.8 (minimum)	296.6

*Normalized to standard conditions burn rate of 0.368 in./sec. Population is the same as used to compare thrust trace (Figure 4.4.8).

4.4.2.2 SRM Propulsion Performance Comparisons

SRM Predicted Impulse, I_{sp}, Burn Rate, Event Times, Separation, and PMBT Comparison

The reconstructed SRM propulsion performance is compared to the predicted performance in Table 4.4-1. The actual values are very close to the predicted data for both motors with the exception of the following. The actual I_{sp} and action time impulse for RSRM-1A was slightly lower than predicted. An assessment of the pressure trace indicated that the RSRM-1A nozzle eroded slightly differently beginning at 70 sec. Pressure transducer error may also explain the difference.

The pressure rise rates were quite different despite the two motors being matched pairs. A close look at the DFI (320 sps) data showed a slight data dropout at the time of maximum pressure rise rate in the pressure trace of RSRM-1B. The calculated rise rate for RSRM-1B was 80.5 psia/10 ms, while that of RSRM-1A was 99.0 psia/10 ms. It is unclear if this is a valid

Table 4.4-1. RSRM Propulsion Performance

	RSRM-1A		RSRM-1B	
	Predicted	Actual*	Predicted	Actual*
I-20 (10^6 lb-sec)	65.47	65.82	65.87	65.90
I-60 (10^6 lb-sec)	175.19	174.64	175.35	174.94
I-AT (10^6 lb-sec)	297.61	296.18	297.61	297.59
Vac I_{sp} (lb-sec/lbm)	268.82	267.53	268.82	268.81
Burn Rate (in./sec at 60°F and 625 psia)	0.366	0.366	0.367	0.366
Event Times (sec)				
Ignition Interval	0.232	0.230	0.232	0.231
Web Time	110.5	110.3	110.8	110.3
Time of 50 psia Cue	119.8	119.7	119.4	119.7
Action Time	122.1	122.4	121.7	123.2
Separation Command	124.7	124.6	124.3	124.6
PMBT (°F)	80.0	79.0	80.0	79.0
Max Rise Rate (psi/10 ms)	91.8	99.0	91.8	80.5
Decay Time (sec) (59.4 psia to 85k-lb thrust)	3.8	3.2	3.5	4.0

	Predicted	Actual
Tailoff Imbalance Differential (10^3 lbf)	0.82	0.97

*Impulse, I_{sp}, and burn rate parameters are reconstructed values.

calculated rise rate with the data unadjusted to compensate for the data dropout. With the data adjusted, the rise rate would be much closer to the value of RSRM-1A.

A comparison of actual and predicted propellant burn rates to the target burn rate for the flight SRMs at a PMBT of 60°F is shown in Figure 4.4.9.

4.4.2.3 Matched Pair Thrust Differential. The thrust imbalance assessment is shown in Table 4.4-2. Figures 4.4.10 through Figure 4.4.13 show the thrust differential during ignition, steady state, and tailoff. All the thrust differential values were near the nominal values experienced by previous flight SRMs and were well within the CEI specification limits. The thrust values used for the assessment were reconstructed at the delivered conditions of each motor.

4.4.2.4 Performance Tolerances. The parameter variations of the total population of SRMs about a nominal value are constrained by the requirements defined in the SRM CEI specification. A comparison of the RSRM-1A/RSRM-1B calculated and reconstructed parameters at PMBT of 60°F with respect to the nominal values and the SRM CEI specification maximum 3 sigma requirements is shown in Tables 4.4-3 and 4.4-4.

4.4.2.5 Matched Pair Performance Requirements. The CEI specification requires that the performance of a matched pair of motors on a flight set have similar performance according to Table 4.4-5. Flight motors 360L001 were well within the matched pair specification requirements.

4.5 SRM NOZZLE PERFORMANCE

This section corresponds to FEWG report Section 2.4.3.

The SRM nozzle torque was between 1.5×10^6 2.9×10^6 in.-lb, which compares with previous flight torque data and is also comparable to static test nozzle torque data. The char and erosion performance is discussed in Section 4.12.4.

4.6 SRM ASCENT LOADS

This section corresponds to FEWG report Section 2.5.2.

ORIGINAL PAGE IS
OF POOR QUALITY

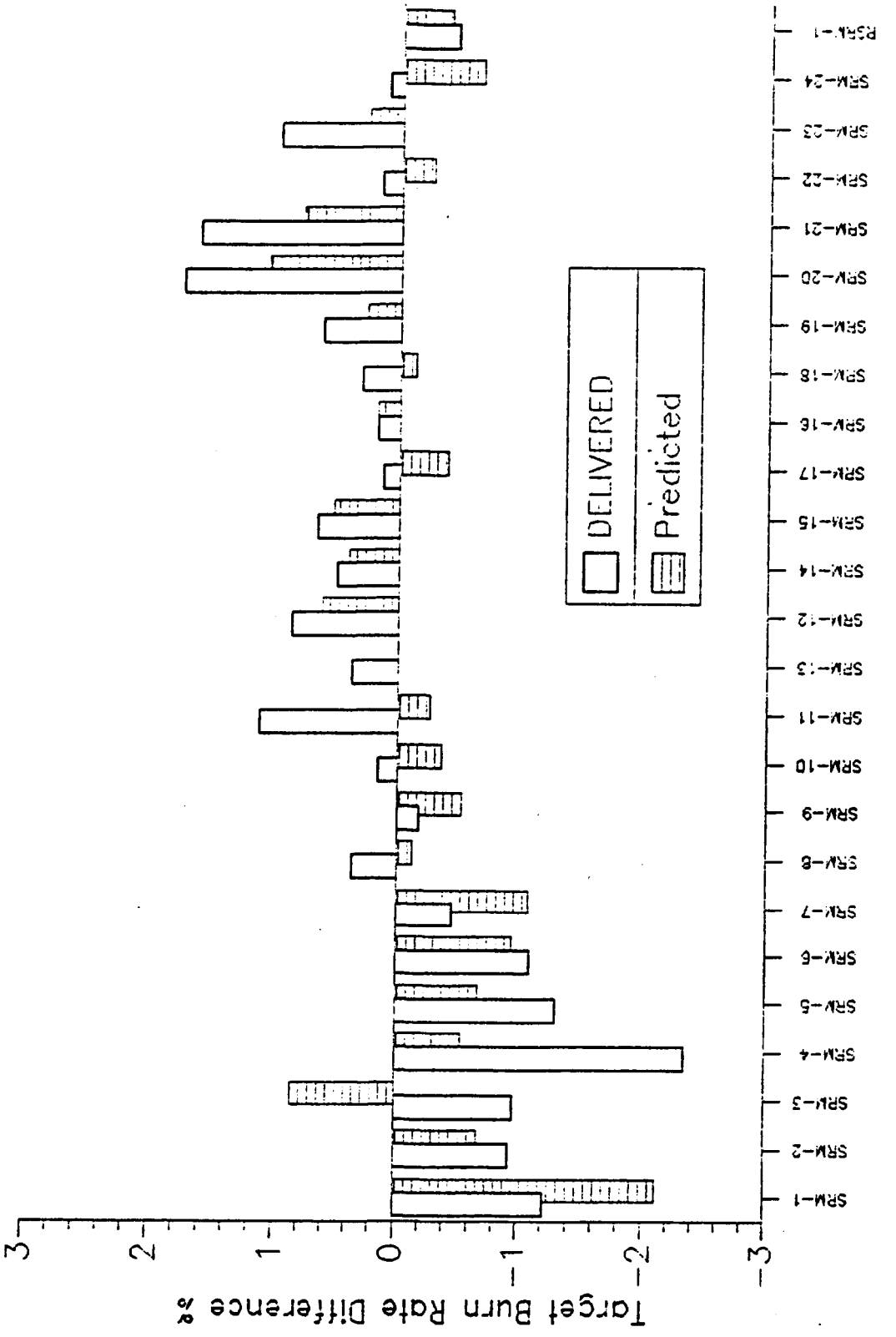

Figure 4.4-9. Comparison of Actual, Predicted, and Target Burn Rates, PMBT = 60°F

Table 4.4-2. RSRM Thrust Imbalance Summary

Event	Spec	Imbalance	Time
Ignition (0 to 1 sec, lbf)	300k	+85.2k	0.160
Steady State (1 sec to first web time -4.5 sec, lbf)	85k	-44.8k	84.0
Transition (first web time -4.5 sec to first web time, lbf)	85 to 268k linear	-25.5k	110.0
Tailoff (first web time to last action time, lbf)	710k	-36.3k	115.0

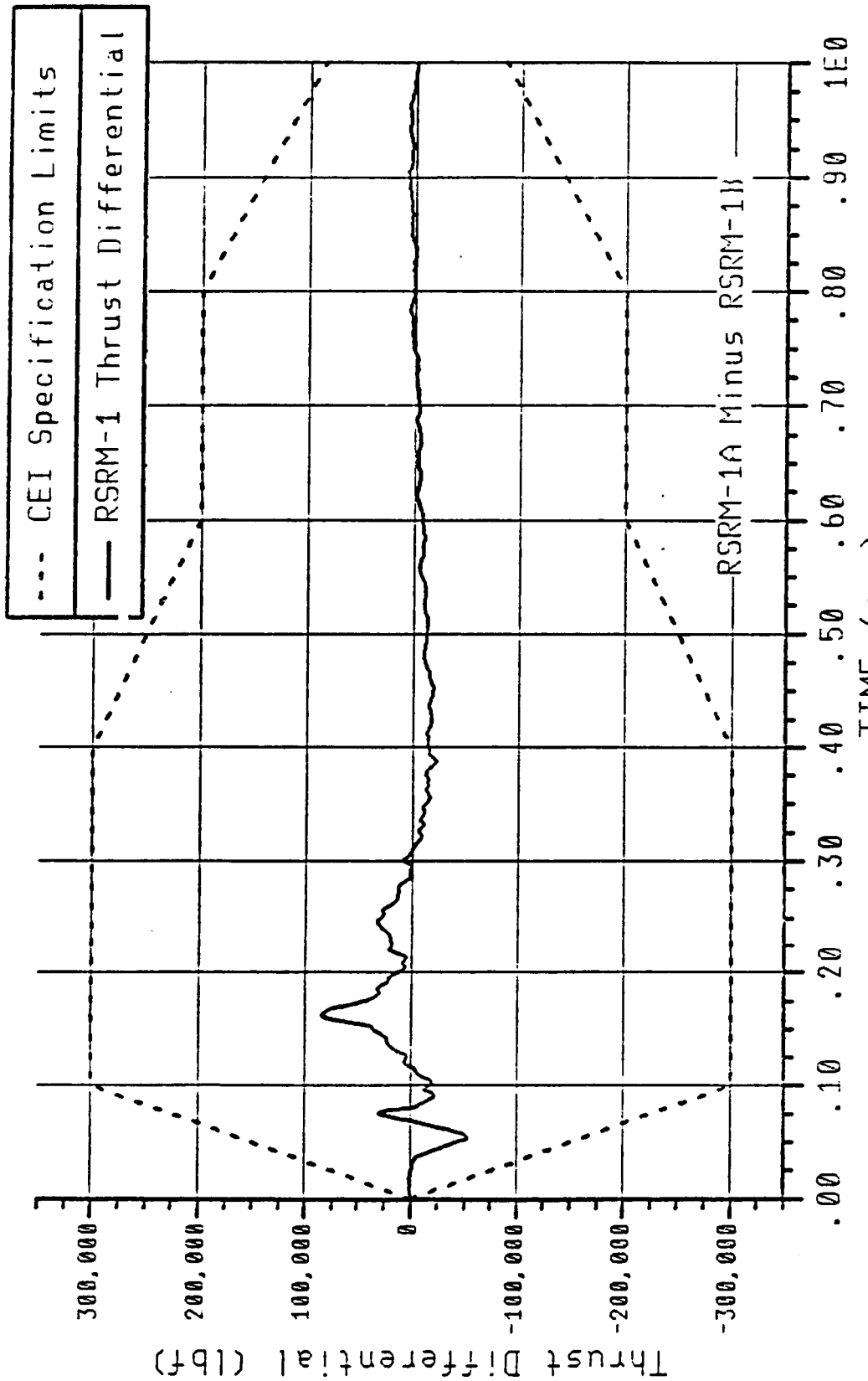

Figure 4.4-10. RSRM-1 Ignition Thrust Imbalance

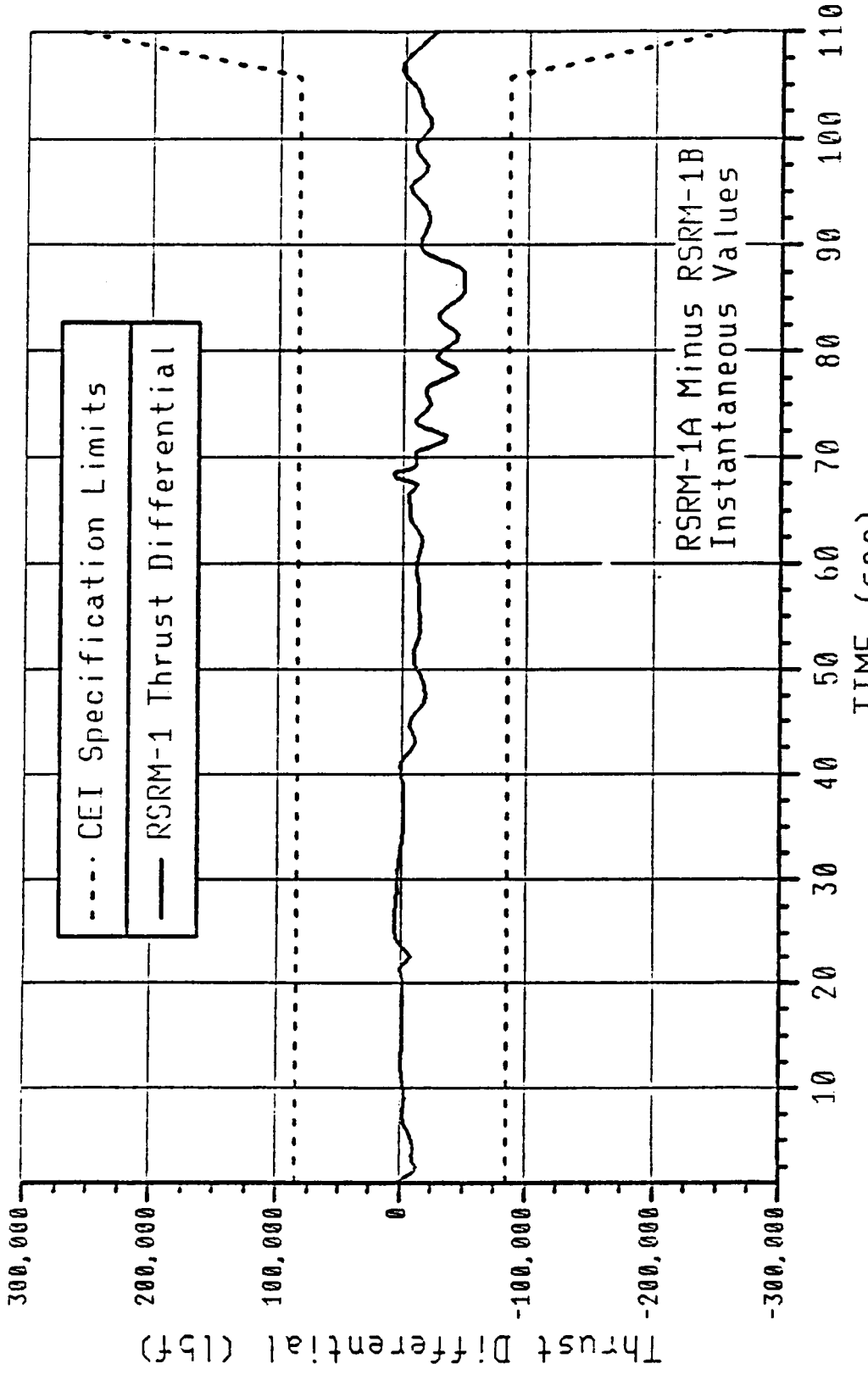

Figure 4.4-11. RSRM-1 Steady State Thrust Imbalance (Instantaneous)

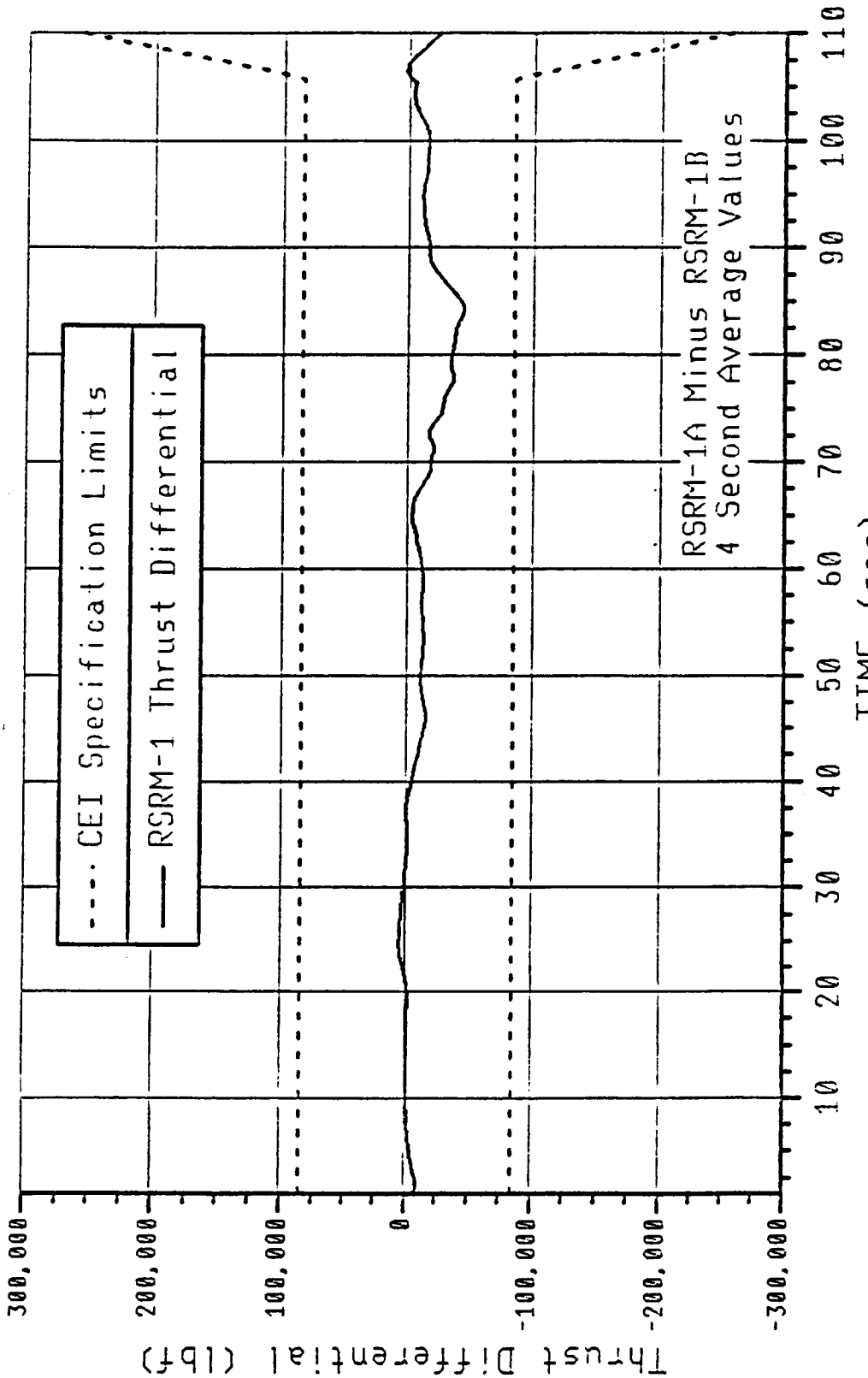

Figure 4.4-12. RSRM-1 Steady State Thrust Imbalance (4-sec Average)

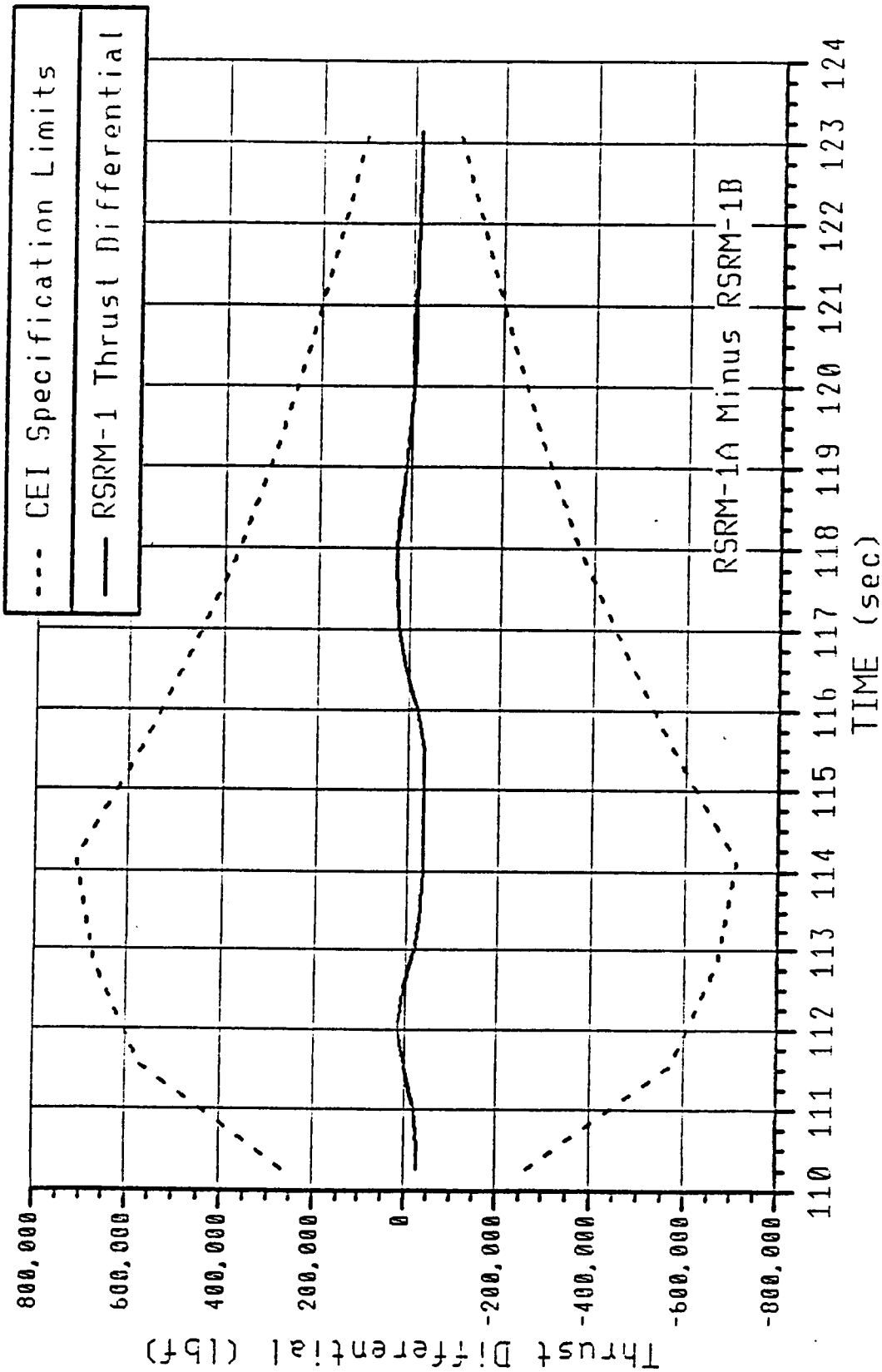

Figure 4.4-13. RSRM-1 Tailoff Thrust Imbalance (Instantaneous)

Table 4.4-3. Comparison of RSRM-1A Variations at PMBT = 60°F About Nominal To CEI Specification Requirements

Parameter	CEI Max 3 Sigma Variation (%)	Nominal Value*	RSRM-1A Value**	RSRM-1A Variation*** (%)
Web Time	±5.0	111.7	112.4	0.63
Action Time	±6.5	123.4	124.8	1.13
Web Time Avg Pressure	±5.3	660.8	656.0	-0.73
Max Pressure	±6.5	918.4	904.4	-1.52
Max Sea Level Trust	±6.2	3.06	3.06	0.00
Web Time Avg Vac Thrust	±5.3	2.59	2.57	-0.77
Vac Del Specific Impulse	±0.7	267.1	267.3	0.07
Web Time Vac Total Impulse	±1.0	288.9	288.5	-0.14
Action Time Vac Total Impulse	±1.0	296.3	295.7	-0.20

Pressure values in psia, thrust values in Mlbf, impulse values in Mlbf-sec

*QM-4 static test and SRM-8A and -8B, SRM-9A, SRM-10A and -10B, SRM-11A, SRM-13A and -13B flight average at standard conditions
**RSRM-1A at PMBT = 60°F
***Variation = ((RSRM-1A - nominal)/nominal) x 100

Table 4.4-4. Comparison of RSRM-1B Variations at PMBT = 60°F About Nominal To CEI Specification Requirements

Parameter	CEI Max 3 Sigma Variation (%)	Nominal Value*	RSRM-1B Value**	RSRM-1B Variation*** (%)
Web Time	±5.0	111.7	112.4	0.63
Action Time	±6.5	123.4	125.4	1.62
Web Time Avg Pressure	±5.3	660.8	659.1	-0.26
Max Pressure	±6.5	918.4	906.6	-1.28
Max Sea Level Trust	±6.2	3.06	3.06	0.00
Web Time Avg Vac Thrust	±5.3	2.59	2.58	-0.39
Vac Del Specific Impulse	±0.7	267.1	268.6	0.56
Web Time Vac Total Impulse	±1.0	288.9	289.7	0.28
Action Time Vac Total Impulse	±1.0	296.3	297.2	0.30

Pressure values in psia, thrust values in Mlbf, impulse values in Mlbf-sec

*QM-4 static test and SRM-8A and -8B, SRM-9A, SRM-10A and -10B, SRM-11A, SRM-13A AND -13B flight average at standard conditions
**RSRM-1A at PMBT = 60°F
***Variation = ((RSRM-1B - nominal)/nominal) x 100

Table 4.4-5. Matched Pair Performance Limits

Parameter	CEI Specification Max Difference (%)	Delivered Difference* (%)
Web Time	±2.0	0.00
Action Time	±3.0	0.48
Web Time Avg Pressure	±2.0	0.47
Max Pressure	NA	0.24
Max Sea Level Thrust	NA	0.00
Web Time Avg Vac Thrust	±2.0	0.39
Vac Del Specific Impulse	±1.0	0.49
Web Time Vac Total Impulse	±1.4	0.42
Action Time Vac Total Impulse	±1.4	0.51

Pressure values in psia, thrust values in Mlbf, impulse values in Mlbf-sec

*Variation = ((RSRM-1B - RSRM-1A)/(RSRM-1 avg) x 100.
Data at PMBT of 60°F.

4.6.1 Introduction

The RSRM set 360L001 (STS-26R), launched 29 Sep 1988, were fully instrumented in order to evaluate motor performance during holddown, lift-off, and ascent through separation. This section details the assessment of the case field joints, factory joints, internal nozzle joints, igniter and S&A joints, nozzle-to-case joint, and case metal components. Comparisons to flight envelopes and previous flights are also presented.

In most cases, actual test data are compared to predicted values for each location. A detailed global model of the RSRM was used to predict joint and case structural responses during STS-26. This finite element model uses super-element techniques to model all components of the RSRM in detail (except for the nozzle-to-case joint, which is in Section 4.6.3.4). Rockwell load case L02044R was chosen to represent typical loading parameters which are imposed upon the RSRM during lift-off. This load case includes a time span from 0 to 10 sec, with SRB ignition occurring at approximately 6.5 sec, and was expected to predict displacement and strain values within an order of magnitude only. A detailed description of the model and analysis techniques used in predicting the structural response of the motor is found in Morton Thiokol document TWR-18212.

The predictions included in the nozzle-to-case tables are ratioed to the 360L001 motor set (STS-26R) pressure. The ratios were determined by multiplying the original prediction by the ratio of the estimated 360L001 (STS-26R) pressure to the prediction pressure. This is done because these predictions were calculated assuming a common pressure, which in most cases is somewhat larger than the actual pressure for the specific location. Therefore, by using the ratio of the predictions to STS-26 values, a comparison can be made. The calculation of the pressure ratio works as follows:

> Maximum radial growth (e.g., girth strain) for a particular location is derived from test data and from the time at which it occurred. The head end pressure at this time is then determined. Also, a predicted pressure drop at this time is found. For set 360L001 (STS-26R), the predicted pressure drops were given in TWR-18766.

Therefore, the pressure ratio is:

$$\frac{\text{Head end pressure - predicted pressure drop}}{\text{Predicted pressure}} = \text{Pressure ratio}$$

The percent difference between analysis and measured data is given by:

$$\left[\frac{\text{Prediction - Measured}}{\text{Measured}}\right] \times 100$$

Biaxial strain gages placed in the aft field joint and ETA ring region and also around the nozzle-to-case joint are used to calculate the corresponding hoop and axial stresses. These stresses illustrate the effects of the ETA ring on the aft field joint and of vectoring on the nozzle-to-case joint. The local stresses are then compared to the predicted values. The maximum measured stress in these areas was found to be hoop stress, and from this stress a safety factor was also determined.

The predictions (not including the nozzle-to-case joint) are the maximum expected values for the first 3 sec of flight. The maximum experienced strain for the duration of the flight was also evaluated.

The strain gages were zeroed after SRB stacking, but before mating with the orbiter and ET, so the strain gages report some initial strain before launch, which is caused by the weight and induced bending of the orbiter and ET. Because of when they were zeroed, the strain gages do not show any strain resulting from the weight of the segments above them. It would be ideal to know the actual strain experienced by the case at every instrumented location for every flight event. After separation and before chute deployment the SRBs are essentially in a load-free state (free fall), with very little if any motor pressure and very small external loads. For this reason, all of the strain gages were adjusted to end at zero at this point. This shifting of the data show, as near as possible, the actual strain level at any point during flight. Because the data are shifted at every time, it also shows the strain caused by the weight of the case segments prior to Space Shuttle main engine (SSME) buildup.

Once this adjustment has been made, the strain values are input into program SLB01, which calculates the stress distribution around the case. The output from this program is put into program SLB06, which calculates bending moment and axial force. These results are presented as a function of time. The results of this program were also plotted with previous flight data as a function of time, and with the envelopes for specific flight events as a function of station.

4.6.2 Summary

The girth gage measurements from field, factory, and nozzle-to-case joints compare closely to pretest predictions and corresponding gages from static tests. The predictions used a typical load case rather than actual loads, so they were only expected to be within an order of magnitude. The highest percentage difference was -17.1 percent on the forward field joint, 17.1 percent on the nozzle-to-case joint, and -5.6 percent on case membrane.

The biaxial gage line/load measurements compared closely with predicted values. The biaxial strain gage data for each station were used to calculate a stress distribution, and this information was used to calculate bending moments and axial force as a function of time. Results show that the maximum bending moment occurred on the left SRB during SSME buildup reaching a maximum value of 290 x 10^6 in.-lb. The axial force initially was not as linear down the motor as expected, and reached a maximum of -13,400 kips at Station 556 on the left motor, occurring at lift-off. The maximum line load was -25 kips/in. and occurred at Station 1466 on the left motor. The flight data were plotted with the flight envelopes, and revealed the data were either within or near the envelope region. The data were also plotted with previous flights and showed good correlation.

4.6.3 Test Results

4.6.3.1 Instrumentation. Instrumentation (girth and biaxial strain gages) was placed on, and close to, the field and nozzle-to-case joints to characterize joint performance. Following is a list of gages used and their function:

Joint Girth Gages	Measure the average hoop strain for the entire 360-deg circumference. From the hoop strain, radial deflections are determined from the product of measured (average) girth strain and the nominal hardware radii at the corresponding gage location.
Biaxial Gages	Measures local rather than average axial and hoop strains incurred in the case during pressurization. From the strains, stress can be calculated.
Pressure Transducer	Installed in the igniter to measure head end chamber pressure.
Thermocouple	Monitors temperature.

4.6.3.2 Case Girth Gage Response

Field Joint Girth Gages

Flight set 360L001 (STS-26R) instrumentation on both the left and right RSRM consisted of six girth gages per field joint. Tables 4.6-1 through 4.6-5 list the girth gage response from 0 to 3 sec, and the maximum strain for 0 to 120 sec for the forward, center, and aft field joints at the time intervals for both the left and right motors. There were an unusually large number of gages that either did not work or gave bad data. No girth gages on the right SRB forward field joint worked properly; therefore, no table for this joint is included. These tables also compare the maximum measured strain and corresponding radial growth with the predicted values for the field joints. The results show a good correlation between analysis and test data. All field joint predictions are within the range of -17.1 to 9.4 percent of measured values. The maximum radial growth was 0.215 in., which occurred at location 6 (Station 857.5) on the left SRB.

Tables 4.6-6 through 4.6-8 compare motor set 360L001 with several static motors. Very good correlation can be seen. Close study of the field joint growth behavior shows the joint is rotating outward. This can be seen from

Table 4.6-1. Left SRM, Forward Field Joint Girth Gages

TEST NAME: STS-26 9-29-88
JOINT: LEFT SRM FWD FIELD
DESCRIPTION: JOINT GIRTH GAGES
JOINT PRESSURE: 862 PSI
THE TIME RANGE IS 0.0 TO 3.0 SECONDS

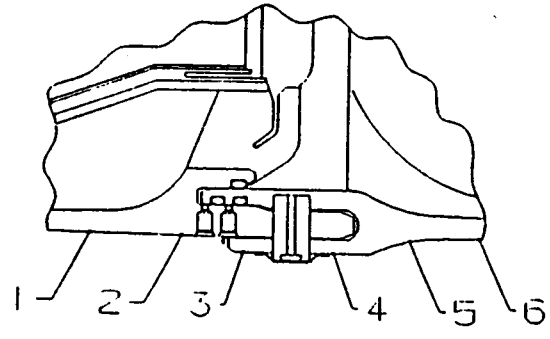

GIRTH GAGE LOCATION	GAGE NUMBER	STATION	RADIUS (IN)	RADIAL GROWTH (IN)	TEST STRAIN (UIN/IN)	ANALYSIS STRAIN (UIN/IN)	ANALYSIS RADIAL GROWTH (IN)	DIFF IN RADIAL GROWTH (% DIFF)	RADIAL GROWTH 0-120s MAX
1	B08G7273	847.0	73.1	0.172	2348	2134	0.156	-9.3	0.175
2	B08G7274	848.5	73.1	ND	ND	2025	0.148	ND	ND
3	B08G7275	850.2	73.5	0.149	2026	1973	0.145	-2.7	0.198
4	B08G7276	852.6	73.5	0.170	2308	1918	0.141	-17.1	0.174
5	B08G7277	855.0	73.1	0.186	2549	2218	0.163	-12.4	0.191
6	B08G7278	857.5	73.1	0.209	2854	2640	0.194	-7.2	0.215

Table 4.6-2. Left SRM, Center Field Joint Girth Gages

TEST NAME: STS-26 9-29-88
JOINT: LEFT SRM CTR FIELD
DESCRIPTION: JOINT GIRTH GAGES
JOINT PRESSURE: 824 PSI
THE TIME RANGE IS 0.0 TO 3.0 SECOND

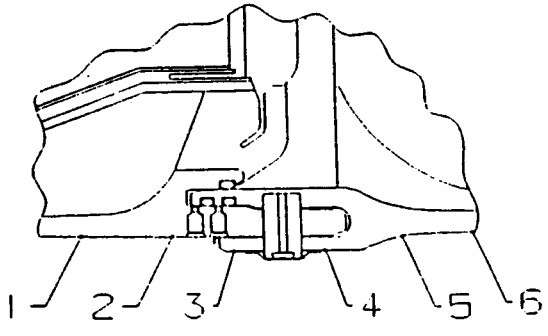

GIRTH GAGE LOCATION	GAGE NUMBER	STATION	RADIUS (IN)	RADIAL GROWTH (IN)	TEST STRAIN (UIN/IN)	ANALYSIS STRAIN (UIN/IN)	ANALYSIS RADIAL GROWTH (IN)	DIFF IN RADIAL GROWTH (% DIFF)	RADIAL GROWTH 0-120s MAX
1	B08G7283	1167.0	73.1	0.170	2332	2120	0.155	-8.8	0.172
2	B08G7284	1168.5	73.1	ND	ND	2052	0.147	ND	ND
3	B08G7285	1170.2	73.5	0.144	1962	1937	0.142	-1.4	0.148
4	B08G7286	1172.6	73.5	ND	ND	1866	0.137	ND	ND
5	B08G7287	1175.0	73.1	ND	ND	2191	0.160	ND	ND
6	B08G7288	1177.5	73.1	0.193	2645	2621	0.192	-0.5	0.205

Table 4.6-3. Left SRM, Aft Field Joint Girth Gages

TEST NAME: STS-26 9-29-88
JOINT: LEFT SRM AFT FIELD
DESCRIPTION: JOINT GIRTH GAGES
JOINT PRESSURE: 780 PSI
THE TIME RANGE IS 0.0 TO 3.0 SECOND

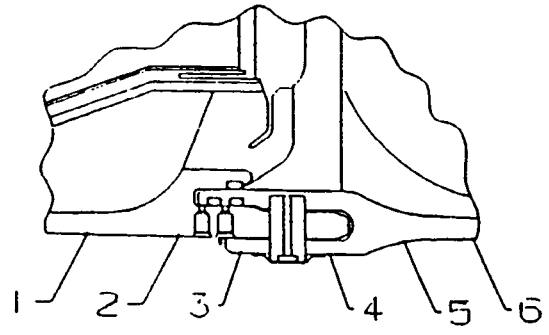

GIRTH GAGE LOCATION	GAGE NUMBER	STATION	RADIUS (IN)	RADIAL GROWTH (IN)	TEST STRAIN (UIN/IN)	ANALYSIS STRAIN (UIN/IN)	ANALYSIS RADIAL GROWTH (IN)	DIFF IN RADIAL GROWTH (% DIFF)	RADIAL GROWTH 0-120s MAX
1	B08G7293	1487.0	73.1	0.185	2525	2153	0.157	-15.1	0.185
2	B08G7294	1488.5	73.1	ND	ND	1995	0.146	ND	ND
3	B08G7295	1490.2	73.5	0.156	2123	1913	0.141	-9.6	0.156
4	B08G7296	1492.6	73.5	0.142	1938	1770	0.130	-8.5	0.153
5	B08G7297	1495.0	73.1	0.166	2275	1995	0.146	-12.0	0.166
6	B08G7298	1497.5	73.1	0.171	2340	2224	0.163	-4.7	0.171

Table 4.6-4. Right SRM, Center Field Joint Girth Gages

TEST NAME: STS-26 9-29-88
JOINT: RIGHT SRM CTR FIELD
DESCRIPTION: JOINT GIRTH GAGES
JOINT PRESSURE: 827.5 PSI
THE TIME RANGE IS 0.0 TO 3.0 SECOND

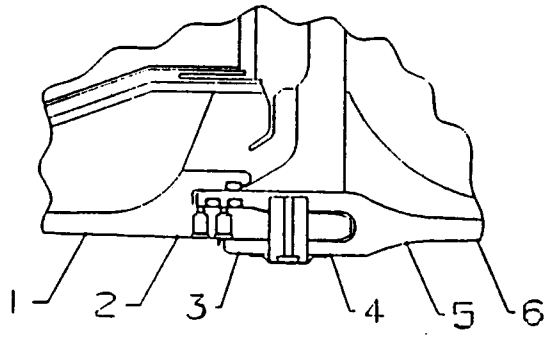

GIRTH GAGE LOCATION	GAGE NUMBER	STATION	RADIUS (IN)	RADIAL GROWTH (IN)	TEST STRAIN (UIN/IN)	ANALYSIS STRAIN (UIN/IN)	ANALYSIS RADIAL GROWTH (IN)	DIFF IN RADIAL GROWTH (% DIFF)	RADIAL GROWTH 0-120s MAX
1	B08G8283	1167.0	73.1	ND	ND	2127	0.155	ND	ND
2	B08G8284	1168.5	73.1	ND	ND	2012	0.147	ND	ND
3	B08G8285	1170.2	73.5	ND	ND	1944	0.143	ND	ND
4	B08G8286	1172.6	73.5	0.157	2139	1872	0.138	-12.1	0.167
5	B08G8287	1175.0	73.1	ND	ND	2199	0.161	ND	ND
6	B08G8288	1177.5	73.1	ND	ND	2630	0.192	ND	ND

Table 4.6-5. Right SRM, Aft Field Joint Girth Gages

TEST NAME: STS-26 9/29/88
JOINT: RIGHT SRM AFT FIELD
DESCRIPTION: JOINT GIRTH GAGES
JOINT PRESSURE: 783 PSI
THE TIME RANGE IS 0.0 TO 3.0 SECOND

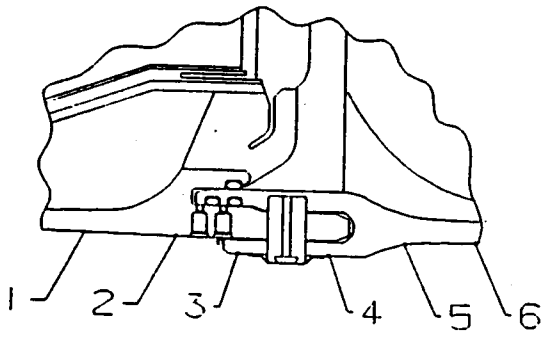

GIRTH GAGE LOCATION	GAGE NUMBER	STATION	RADIUS (IN)	RADIAL GROWTH (IN)	TEST STRAIN (UIN/IN)	ANALYSIS STRAIN (UIN/IN)	ANALYSIS RADIAL GROWTH (IN)	DIFF IN RADIAL GROWTH (% DIFF)	RADIAL GROWTH 0-120s MAX
1	B08G8293	1487.0	73.1	0.162	2211	2162	0.158	-2.5	0.173
2	B08G8294	1488.5	73.1	ND	ND	2003	0.146	ND	ND
3	B08G8295	1490.2	73.5	0.133	1809	1921	0.141	6.0	0.145
4	B08G8296	1492.6	73.5	0.141	1922	1777	0.131	-7.1	0.155
5	B08G8297	1495.0	73.1	ND	ND	2003	0.146	ND	ND
6	B08G8298	1497.5	73.1	0.149	2042	2234	0.163	9.4	0.165

Table 4.6-6. Forward Field Joint Radial Growth Comparisons to 360L001

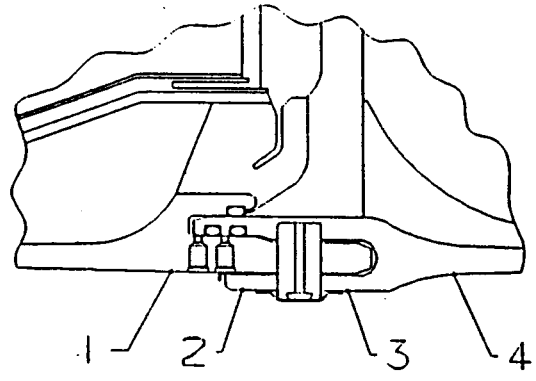

Fwd Field Girths — Joint Pressure 878

LOC.	STS-26 RIGHT	STS-26 LEFT	PV-1	RADIAL GROWTH (Inches) QM-7	QM-6	DM-9	DM-8	PRED
1	ND	ND	ND	0.198	0.161	0.162	0.167	0.163
2	ND	0.198	ND	0.152	0.140	0.155	0.151	0.150
3	ND	0.174	ND	0.171	0.164	ND	0.164	0.153
4	ND	0.191	ND	0.189	0.185	0.177	0.188	0.189

* QM-7, QM-6, and DM-9 Locations are 1/3 Inch Aft of DM-8 Location.
Note: All Test Radial Growths Are Ratios Of STS-26 Test Pressure

C.2

Table 4.6-7. Center Field Joint Radial Growth Comparisons to 360L001

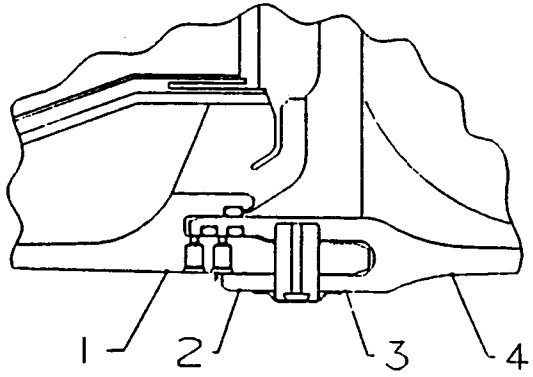

Ctr Field Girths Joint Pressure 853

LOC.	STS-26 RIGHT	STS-26 LEFT	PV-1	QM-7	RADIAL GROWTH (Inches) QM-6	DM-9	DM-8	PRED.
1	ND	ND	ND	ND	ND	0.162	0.168	0.159
2	ND	0.148	ND	0.151	0.140	0.159	0.148	0.146
3	0.167	ND	0.163	0.167	0.159	0.142	0.164	0.148
4	ND	ND	0.182	0.183	0.174	0.170	0.180	0.179

* QM-7, QM-6, and DM-9 Locations are 1/3 Inch Aft of DM-8 Location.
Note: All Test Radial Growths Are Ratios Of STS-26 Test Pressure

Table 4.6-8. Aft Field Joint Radial Growth Comparisons to 360L001

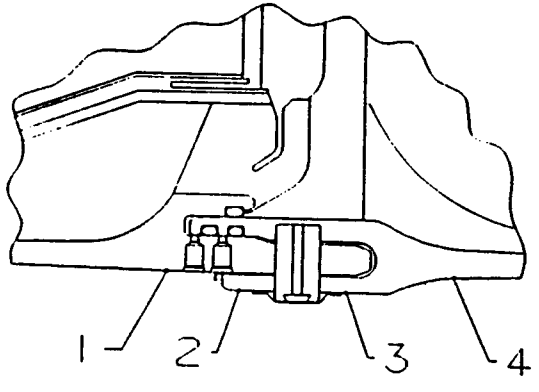

Aft Field Girths — Joint Pressure 828

LOC.	STS-26 RIGHT	STS-26 LEFT	STS-26 PV-1	RADIAL GROWTH (Inches) QM-7	QM-6	DM-9	DM-8	PRED.
1	ND	ND	ND	0.185	0.156	0.158	0.164	0.151
2	0.145	0.156	ND	0.146	0.131	0.138	0.145	0.135
3	0.155	0.153	0.150	0.154	0.148	0.147	0.154	0.134
4	ND	0.166	0.157	0.154	0.156	0.152	0.162	0.147

* QM-7, QM-6, and DM-9 Locations are 1/3 Inch Aft of DM-8 Location.
Note: All Test Radial Growths Are Ratios of STS-26 Test Pressure

the higher radial growth values at the forward and aft ends of each joint, and the lower values closer to the pin centerline.

Case Membrane Girth Gage Response

360L001 (STS-26R) instrumentation on both the left and right RSRM consisted of four girth gages on the case membrane. Tables 4.6-9 and 4.6-10 list the girth gage response from 0 to 3 sec and compares the measured strain and calculated radial growth with predicted values (these predicted values are for the first 3 sec only). Also listed is the maximum radial growth for 0 to 120 sec. Every prediction is within -5.6 percent of the measured test data.

Table 4.6-11 shows the comparison of 360L001 with several static tests, as well as predictions (from 0 to 120 sec). This table shows a good correlation with these tests. The maximum radial growth occurred at location 4 (Station 1091.5) on the right SRB, and has a value of 0.281 inch.

4.6.3.3 Case Biaxial Stresses

Case Line Loads, Aft Field/ETA Joint

360L001 instrumentation consisted of biaxial gages at six locations along the case (4 on Stations 556.50, 876.50, 1196.50, 1466.00, and 1797.00 and eight each on Stations 1493.0 and 1501.00). Tables 4.6-12 and 4.6-13 illustrate case line load and moment biaxials stresses with corresponding predictions for the first 3 sec of flight. These tables show a good correlation between measured and predicted values, with the exception of the axial gages at Station 1493. At this station, due to very localized conditions from case bending (or joint rotation), negative strain values are predicted. Actual readings, however, were positive. One explanation for the discrepancy may be a slight strain gage misplacement, as even a small gage misplacement would move out of the localized area of negative strain into a positive strain region. Instrumentation error is also possible. These explanations are currently being investigated.

Table 4.6-14 lists the maximum hoop and axial stresses measured from biaxial gages for the total 120-sec burn time. These tables do not provide a comparison between test data and analysis. Analysis was performed for the

Table 4.6-9. Left SRM, Case Radial Deflection, Case Girth Gages

TEST NAME: STS-26 9-29-88
JOINT: LEFT SRM CASE RADIAL DEFLECTION
DESCRIPTION: CASE GIRTH GAGES
THE TIME RANGE IS 0.0 TO 3.0 SECOND

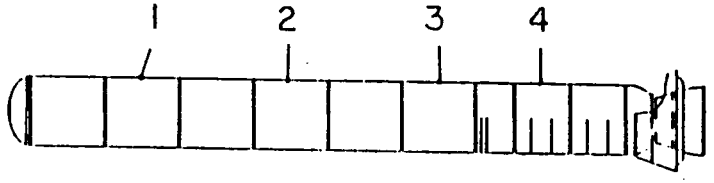

GIRTH GAGE LOCATION	GAGE NUMBER	STATION	RADIUS (IN)	RADIAL GROWTH (IN)	TEST STRAIN (UIN/IN)	ANALYSIS STRAIN (UIN/IN)	ANALYSIS RADIAL GROWTH (IN)	DIFF IN RADIAL GROWTH (% DIFF)	LOCAL CASE PRESS /GAGE	RADIAL GROWTH 0-120s MAX
1	B08G7272	771.5	73.0	0.270	3698	3490	0.255	-5.6	870	0.275
2	B08G7282	1091.5	73.0	0.279	3819	3611	0.264	-5.4	837	0.279
3	B08G7292	1411.5	73.0	ND	ND	3489	0.255	ND	791	ND
4	B08G7301	1637.5	73.0	0.248	3393	3420	0.250	-0.8	784	0.260

Table 4.6-10. Right SRM, Case Radial Deflection, Case Girth Gages

TEST NAME: STS-26 9-29-88
JOINT: RIGHT SRM CASE RADIAL DEFLECTION
DESCRIPTION: CASE GIRTH GAGES
THE TIME RANGE IS 0.0 TO 3.0 SECOND

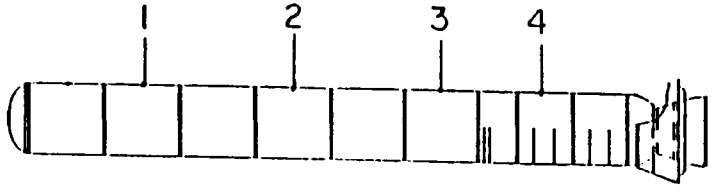

GIRTH GAGE LOCATION	GAGE NUMBER	STATION	RADIUS (IN)	RADIAL GROWTH (IN)	TEST STRAIN (UIN/IN)	ANALYSIS STRAIN (UIN/IN)	ANALYSIS RADIAL GROWTH (IN)	DIFF IN RADIAL GROWTH (% DIFF)	LOCAL CASE PRESS /GAGE	RADIAL GROWTH 0-120s MAX
1	B08G8272	771.5	73.0	ND	ND	3503	0.256	ND	873	ND
2	B08G8282	1091.5	73.0	0.280	3835	3625	0.265	-5.4	840	0.281
3	B08G8292	1411.5	73.0	0.263	3594	3505	0.256	-2.7	794	0.276
4	B08G8301	1637.5	73.0	0.242	3313	3433	0.251	-3.7	787	0.261

Table 4.6-11. Case Membrane Radial Growth Comparisons to 360L001

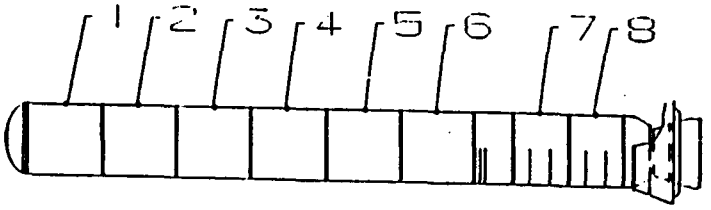

Membrane Girths

Loc.	RIGHT	LEFT	PV-1	QM-7	RADIAL GROWTH (Inches) QM-6	DM-9	DM-8	PRED.	STS-26 Press. psig
1	ND	ND	ND	0.289	0.275	0.268	0.284	0.281	896
2	ND	0.275	ND	0.275	0.262	0.271	0.282	0.278	881
3	ND	ND	ND	0.287	0.279	0.283	0.291	0.278	873
4	0.281	0.279	ND	0.288	0.273	0.279	0.292	0.275	862
5	ND	ND	ND	0.279	0.264	ND	0.285	0.272	850
6	0.276	ND	ND	0.278	0.268	ND	ND	0.268	839
7	0.261	0.260	ND	0.266	0.253	0.253	0.260	0.266	832
8	ND	ND	ND	0.268	0.250	ND	ND	0.268	836

Note: Only The Predictions Are Ratios Of STS-26 Test Pressure

ORIGINAL PAGE IS
OF POOR QUALITY

Table 4.6-12. 360L001A Comparison of Maximum Predicted Versus Measured Biaxial Strain Values (0 - 3 sec), Left RSRM

Station	Degree	Maximum Hoop Strain (micro in/in) Gage	Predicted	Measured	Maximum Axial Strain (micro in/in) Gage	Predicted	Measured
556.5	0.	B08G7319A	3706.	3449.	B08G7318A	799.	528.
"	98.	B08G7321A	3712.	ND	B08G7320A	753.	1514.
"	180.	B08G7323A	3718.	ND	B08G7322A	755.	768.
"	270.	B08G7325A	3724.	ND	B08G7324A	886.	835.
876.5	0.	B08G7327A	3616.	3517.	B08G7326A	1224.	998.
"	98.	B08G7329A	3613.	3485.	B08G7328A	1133.	933.
"	180.	B08G7331A	3668.	3504.	B08G7330A	1014.	810.
"	270.	B08G7333A	3653.	3372.	B08G7332A	930.	829.
1196.5	0.	B08G7335A	3535.	3161.	B08G7334A	1211.	1047.
"	98.	B08G7337A	3506.	ND	B08G7336A	1139.	851.
"	180.	B08G7339A	3610.	3280.	B08G7338A	896.	827.
"	270.	B08G7341A	3587.	3322.	B08G7340A	797.	650.
1466.0	0.	B08G7343A	3387.	3141.	B08G7342A	1286.	1114.
"	98.	B08G7345A	3380.	3313.	B08G7344A	1363.	940.
"	180.	B08G7347A	3491.	3243.	B08G7346A	929.	-1019.
"	270.	B08G7349A	3497.	3454.	B08G7348A	950.	777.
1493.0	0.	B08G7355A	1720.	1946.	B08G7354A	-689.	674.
"	98.	B08G7353A	1634.	1688.	B08G7352A	-680.	927.
"	180.	B08G7351A	1747.	1817.	B08G7350A	-755.	1156.
"	220.	B08G7367A	1769.	1801.	B08G7366A	-768.	778.
"	255.	B08G7365A	1767.	1889.	B08G7364A	-770.	803.
"	270.	B08G7363A	1734.	1777.	B08G7362A	-763.	907.
"	285.	B08G7361A	1704.	1841.	B08G7360A	-752.	766.
"	320.	B08G7357A	1760.	611.	B08G7356A	-716.	939.
1501.0	0.	B08G7391A	1998.	1696.	B08G7390A	1185.	897.
"	98.	B08G7389A	1939.	1833.	B08G7388A	1193.	867.
"	180.	B08G7387A	2062.	1810.	B08G7386A	943.	806.
"	220.	B08G7403A	1978.	1841.	B08G7402A	900.	783.
"	255.	B08G7401A	1994.	1857.	B08G7400A	859.	698.
"	270.	B08G7399A	1984.	1803.	B08G7398A	890.	774.
"	285.	B08G7397A	1885.	1688.	B08G7396A	945.	867.
"	320.	B08G7393A	1872.	1705.	B08G7392A	1162.	851.
1727.0	0.	B08G7405A	3236.	3001.	B08G7404A	1459.	1380.
"	98.	B08G7407A	3402.	3208.	B08G7406A	782.	612.
"	180.	B08G7409A	3333.	ND	B08G7408A	-1173.	-1298.
"	270.	B08G7411A	3453.	ND	B08G7410A	576.	449.

ND = No Data

Table 4.6-13. 360L001B Comparison of Maximum Predicted Versus Measured Biaxial Strain Values (0 - 3 sec), Right RSRM

Station	Degree	Maximum Hoop Strain (micro in/in) Gage	Predicted	Measured	Maximum Axial Strain (micro in/in) Gage	Predicted	Measured
556.5	0.	B0BG8323A	3718.	2790.	B0BG8322A	755.	697.
"	82.	B0BG8321A	3712.	3911.	B0BG8320A	753.	916.
"	180.	B0BG8319A	3706.	3572.	B0BG8318A	799.	ND
"	270.	B0BG8325A	3724.	3216.	B0BG8324A	886.	912.
876.5	0.	B0BG8331A	3668.	ND	B0BG8330A	1014.	1356.
"	82.	B0BG8329A	3613.	3538.	B0BG8328A	1133.	1056.
"	180.	B0BG8327A	3616.	ND	B0BG8326A	1224.	ND
"	270.	B0BG8333A	3653.	ND	B0BG8332A	930.	1496.
1196.5	0.	B0BG8339A	3610.	ND	B0BG8338A	-635.	-677.
"	82.	B0BG8337A	3506.	ND	B0BG8336A	1139.	ND
"	180.	B0BG8335A	3535.	3383.	B0BG8334A	1211.	1066.
"	270.	B0BG8341A	3587.	ND	B0BG8340A	797.	674.
1466.0	0.	B0BG8347A	3491.	3313.	B0BG8346A	-932.	-1006.
"	82.	B0BG8345A	3380.	3128.	B0BG8344A	1363.	853.
"	180.	B0BG8343A	3387.	3097.	B0BG8342A	1286.	1108.
"	270.	B0BG8349A	3497.	3337.	B0BG8348A	950.	674.
1493.0	0.	B0BG8351A	1747.	2010.	B0BG8350A	-755.	594.
"	82.	B0BG8353A	1634.	820.	B0BG8352A	-680.	ND
"	180.	B0BG8355A	1720.	1536.	B0BG8354A	-689.	931.
"	220.	B0BG8357A	1760.	1608.	B0BG8356A	-716.	638.
"	255.	B0BG8361A	1704.	ND	B0BG8360A	-752.	835.
"	270.	B0BG8363A	1734.	ND	B0BG8362A	-763.	654.
"	285.	B0BG8365A	1767.	1897.	B0BG8364A	-770.	626.
"	320.	B0BG8367A	1769.	1906.	B0BG8366A	-768.	558.
1501.0	0.	B0BG8387A	2062.	1915.	B0BG8386A	943.	675.
"	82.	B0BG8389A	1939.	1833.	B0BG8388A	1193.	963.
"	180.	B0BG8391A	1998.	1635.	B0BG8390A	1185.	1121.
"	220.	B0BG8393A	1872.	1737.	B0BG8392A	1162.	831.
"	255.	B0BG8397A	1885.	1745.	B0BG8396A	945.	726.
"	270.	B0BG8399A	1904.	1764.	B0BG8398A	890.	725.
"	285.	B0BG8401A	1994.	1471.	B0BG8400A	859.	498.
"	320.	B0BG8403A	1978.	ND	B0BG8402A	900.	726.
1797.0	0.	B0BG8409A	3333.	3265.	B0BG8408A	-1173.	-1213.
"	82.	B0BG8407A	3402.	3208.	B0BG8406A	782.	580.
"	180.	B0BG8405A	3236.	2919.	B0BG8404A	1459.	1419.
"	270.	B0BG8411A	3453.	3120.	B0BG8410A	576.	511.

ND = No Data

Table 4.6-14. 360L001 Comparison of Maximum Predicted Versus Measured Biaxial Stress Values (0 - 120 sec)

	Left SRB Stress (KSI)			Right SRB Stress (KSI)		
Station	Degree	Max Hoop Measured	Corr. Axial Measured	Degree	Max Hoop Measured	Corr. Axial Measured
556.5	0.	71.6	34.8	0.	102.6	46.3
"	98.	ND	ND	82.	140.2	78.8
"	180.	ND	ND	180.	ND	ND
"	270.	ND	ND	270.	117.1	43.2
876.5	0.	129.3	57.6	0.	ND	ND
"	98.	ND	ND	82.	128.3	67.8
"	180.	124.4	56.3	180.	ND	ND
"	270.	122.1	51.3	270.	ND	ND
1196.5	0.	120.1	54.7	0.	ND	ND
"	98.	78.0	42.8	82.	ND	ND
"	180.	120.3	53.8	180.	126.9	61.9
"	270.	121.0	45.0	270.	ND	ND
1466.0	0.	120.5	53.2	0.	121.7	51.5
"	98.	124.6	56.1	82.	120.0	52.9
"	180.	122.2	51.0	180.	118.2	51.0
"	270.	128.2	54.7	270.	119.7	50.7
1493.0	0.	72.3	40.0	0.	75.9	41.6
"	98.	74.8	43.4	25.	ND	ND
"	180.	75.3	48.0	82.	70.1	43.6
"	220.	73.4	41.9	180.	65.9	28.1
"	255.	74.7	43.2	220.	70.7	31.3
"	270.	72.8	43.1	240.	75.0	38.8
"	285.	70.9	41.7	255.	ND	ND
"	300.	73.5	39.1	270.	ND	ND
"	320.	35.2	38.4	320.	74.6	39.1
1501.0	0.	70.4	40.7	0.	75.0	41.8
"	98.	73.1	43.9	25.	57.6	31.3
"	180.	70.8	45.3	82.	74.2	46.5
"	220.	74.1	45.6	180.	71.5	44.8
"	255.	72.4	38.7	220.	73.5	43.1
"	270.	71.8	42.1	240.	75.1	42.0
"	285.	69.2	43.1	255.	72.2	45.0
"	300.	72.7	43.6	270.	70.1	41.3
"	320.	73.3	43.9	320.	ND	ND
1797.0	0.	122.4	47.7	0.	123.1	49.2
"	98.	120.9	52.1	82.	120.5	51.6
"	180.	ND	ND	180.	119.6	46.5
"	270.	ND	ND	270.	121.4	43.8

ND = No Data

initial 3-sec burn time only, which does not necessarily correspond with maximum stress occurrence.

The maximum measured hoop stress occurred at Station 556.5 on the right SRB at 98 deg, measuring a local stress of 140.2 ksi. The corresponding axial stress occurred at Station 556.5 on the right SRB at 98 deg, measuring a local stress of 78.8 ksi. The ultimate strength of D6AC steel is 214 ksi with biaxial improvement. The maximum measured axial and hoop stress results in a safety factor of 2.72 and 1.53 respectively. The yield strength of D6AC is 180 ksi. Therefore, no local yielding was measured in this area.

4.6.3.4 Nozzle-to-Case Joint Performance

Model Predictions Techniques

360L001 instrumentation on the nozzle-to-case joint consisted of five girth gages, two stations of biaxial gages, and one station of a uniaxial gage (meridional). Test results at these locations are compared to analytical results acquired from a three-dimensional (3-D) finite element analysis. The analysis was performed with the finite element code ANSYS using 1.8-deg model of the nozzle-to-case joint. Near the joint region, the model was 3-D, transforming into two-dimensional (2-D) away from the joint.

The following assumptions and parameters were included in the model:

--Nominal values for material properties and hardware dimensions
--Preload of 140 kips in the axial bolts and 47 kips in the radial bolts
--Internal pressure of 909 psig applied up to the backside of the primary O-ring groove
--Frictionless joint behavior
--Zero vectoring nozzle condition
--Propellant was not modeled

Because the model is cyclic-symmetric, any circumferential variation indicated by the test data will not be taken into account. The analysis was performed at 909 psig, linearly scaled to the estimated nozzle stagnation pressure, which involves approximately five percent error due to the nonlinear analysis. Two sets of tables were run for each gage: the first between the time interval of 18 to 22 sec to show comparisons to predictions

(to exclude the effects of vectoring), and the second between 0 and 120 sec to show the maximum experienced strain for the duration of the test.

Nozzle-to-Case Joint Girth Gages

Radial deflection is an important parameter to characterize, since it is proportional to joint hoop stress. Tables 4.6-15 and 4.6-16 list the girth gage response during the flight for the left and right motors, respectively, and compare the values with analysis. A good correlation with predicted values can be seen. The percent difference ranges from -6.2 to 17.1 percent. These tables also show the maximum radial growth for the duration of the flight. Table 4.6-17 shows a comparison and good correlation between 360L001 and several static test motors.

As expected, calculated radial growths indicated a "prying open" action and outward rotation of the joint. The maximum measured radial growth was 0.108 in. and occurred at location 3 on both the left and right SRBs.

Nozzle-to-Case Joint Biaxial Strain Gages

The nozzle-to-case biaxials measure local rather than average strains. Tables 4.6-18 and 4.6-19 compare the measured and predicted strain values between 18 and 22 sec. This time range was chosen so that the effects of vectoring would be minimal. Some possible reasons for the relatively large discrepancies with the predicted values are discussed below.

Previous static fire tests have shown that the nozzle-to-case joint gages do not compare as well to analytical data as gages on other parts of the motor. The reason for the variation is:

- --Some gages are located in the neck of the fixed housing; the 3-D model grid may not be fine enough to accurately predict circumferential strain
- --Analytical data were linearly scaled to the test data
- --Nozzle stagnation pressure was estimated to be 818 psig, but not measured
- --Nominal materials were used for the finite element model

Tables 4.6-20 and 4.6-21 show the maximum meridional and hoop stress values for the duration of the test (0 to 120 sec). The maximum stress occurs in the hoop direction at location 3, 0 deg on the left SRM, and had a value of 75.1 ksi. This gives a safety factor of 2.85.

Table 4.6-15. Left SRM, Aft Dome Fixed Housing Nozzle Case Girth Gages

TEST NAME: STS-26 9-29-88
JOINT: LEFT SRM AFT DOME, FIXED HOUSING
DESCRIPTION: NOZZLE CASE GIRTH GAGES
MODEL PRESSURE: 920.00 PSIA
THE TIME RANGE IS 18.0 TO 22.0 SECOND

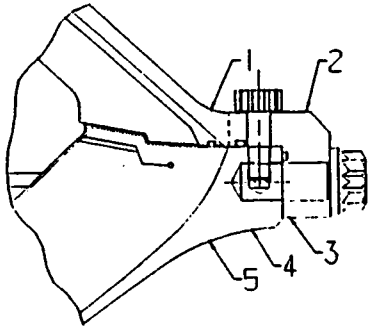

GIRTH GAGE LOCATION	GAGE NUMBER	STATION	RADIUS (IN)	RADIAL GROWTH (IN)	TEST STRAIN (UIN/IN)	ADJUSTED ANALYSIS STRAIN (UIN/IN)	ADJUSTED ANALYSIS RADIAL GROWTH (IN)	DIFF IN RADIAL GROWTH (% DIFF)	RADIAL GROWTH 0-120s MAX
1	B08G7312	1873.0	50.4	0.055	1085	1224	0.062	12.7	0.055
2	B08G7315	1876.0	50.5	0.104	2058	2411	0.122	17.1	0.104
3	B08G7314	1875.5	54.4	0.108	1986	2036	0.111	2.5	0.108
4	B08G7313	1874.0	54.8	0.093	1705	1764	0.097	3.5	0.094
5	B08G7311	1872.5	55.2	0.075	1351	1328	0.073	-1.7	0.075

Table 4.6-16. Right SRM, Aft Dome Fixed Housing Nozzle Case Girth Gages

TEST NAME: STS-26 9-29-88
JOINT: RIGHT SRM AFT DOME, FIXED HOUSING
DESCRIPTION: NOZZLE CASE GIRTH GAGES
JOINT PRESSURE: 856.0 PSIA
THE TIME RANGE IS 18.0 TO 22.0 SECOND

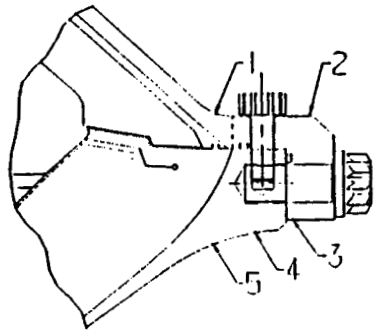

GIRTH GAGE LOCATION	GAGE NUMBER	STATION	RADIUS (IN)	RADIAL GROWTH (IN)	TEST STRAIN (UIN/IN)	ADJUSTED ANALYSIS STRAIN (UIN/IN)	ADJUSTED ANALYSIS RADIAL GROWTH (IN)	DIFF IN RADIAL GROWTH (% DIFF)	RADIAL GROWTH 0-120s MAX
1	B08G8312	1873.0	50.4	ND	ND	1224	0.062	ND	ND
2	B08G8315	1876.0	50.5	0.104	2058	2410	0.122	17.1	0.104
3	B08G8314	1875.5	54.4	0.108	1994	2040	0.111	2.3	0.108
4	B08G8313	1874.0	54.8	0.097	1769	1763	0.097	-0.3	0.097
5	B08G8311	1872.5	55.2	0.078	1415	1327	0.073	-6.2	0.078

Table 4.6-17. Nozzle-to-Case Joint Radial Growth Comparisons to 360L001

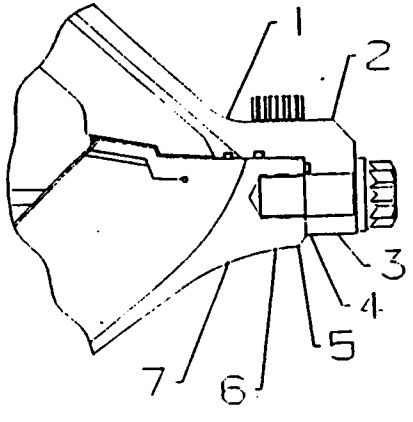

Nozzle/Case Girths — Joint Pressure 847

Loc.	STS-26 RIGHT	STS-26 LEFT	PV-1	QM-7	RADIAL GROWTH (Inches) QM-6	DM-9	DM-8	PRED.
1	ND	0.055	0.096	0.075	0.089	0.080	ND	0.084
2	0.104	0.104	0.142	0.142	0.143	0.128	ND	0.136
3	ND	ND	0.131	0.140	0.138	ND	0.138	0.134
4	0.108	0.108	0.139	0.134	0.131	0.127	ND	0.126
5	ND	ND	0.119	0.121	0.117	0.097	0.122	0.108
6	0.097	0.094	0.111	0.112	0.113	0.114	0.115	0.105
7	0.078	0.075	0.093	0.096	0.094	0.096	0.100	0.086

QM-6 and DM-9 Had Pressure to the Wiper O-ring.
Note: All Test Radial Growths Are Ratios Of STS-26 Test Pressure

Table 4.6-18. Left SRM, Fixed Housing Aft Dome Nozzle/Case Biaxial Gages

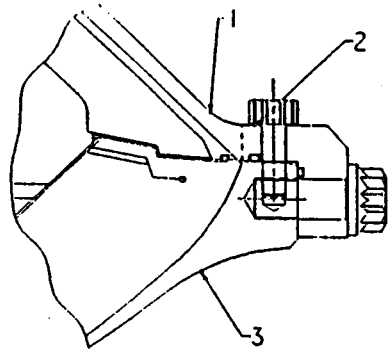

TEST NAME: STS26 9-29-88
JOINT: LEFT SRM FIXED HOUSING, AFT DOME
DESCRIPTION: NOZZLE / CASE BIAXIAL GAGES
THE TIME RANGE IS 18.0 TO 22.0 SECOND

LOCAT	ANGULAR LOCATION	HOOP GAGE	MERID GAGE	MAX HOOP STRESS (KSI)	CORESP MERID STRESS (KSI)	TEST DATA HOOP STRAIN (UIN/IN)	TEST DATA MERID STRAIN (UIN/IN)	ADJUSTED ANALYSIS HOOP STRAIN (UIN/IN)	ADJUSTED ANALYSIS MERID STRAIN (UIN/IN)	ZDIFF HOOP	ZDIFF MERID
1	0.0		B08G7424	ND	ND	ND	-397	ND	-192	ND	-51.2
	90.0		B08G7419	ND	ND	ND	-293	ND	-192	ND	-34.5
	180.0		B08G7414	ND	ND	ND	-401	ND	-192	ND	-52.2
	270.0		B08G7429	ND	ND	ND	ND	ND	-192	ND	-52.2
			AVERAGE:	ND	ND	ND	-364				
2	0.0	B08G7413	B08G7412	46.3	-17.4	1753	-1087	1611	-1426	-9.3	42.7
	90.0	B08G7418	B08G7417	44.1	-20.6	1713	-1172	1611	-1426	-6.8	29.2
	180.0	B08G7423	B08G7422	45.3	-18.4	1722	-1110	1611	-1426	-7.3	34.4
	270.0	B08G7428	B08G7427	ND	ND	ND	ND	1611	-1426	ND	ND
			AVERAGE:	45.2	-18.8	1729	-1123				
3	0.0	B08G7415	B08G7416	73.9	56.2	1889	1100	2085	144	10.4	-86.9
	90.0	B08G7420	B08G7421	67.5	44.4	1801	770	2085	144	15.8	-81.3
	180.0	B08G7425	B08G7426	ND	ND	ND	ND	2085	144	12.3	-81.3
	270.0	B08G7430	B08G7431	71.2	53.5	1825	1043	2085	144	14.2	-86.2
			AVERAGE:	70.9	51.4	1838	971				

Table 4.6-19. Right SRM, Fixed Housing Aft Dome Nozzle/Case Biaxial Gages

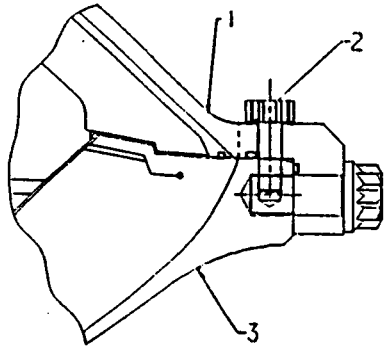

TEST NAME: STS26 9-29-88
JOINT: RIGHT SRM FIXED HOUSING, AFT DOME
DESCRIPTION: NOZZLE / CASE BIAXIAL GAGES
THE TIME RANGE IS 18.0 TO 22.0 SECOND

LOCAT	ANGULAR LOCATION	HOOP GAGE	MERID GAGE	MAX HOOP STRESS (KSI)	CORESP MERID STRESS (KSI)	TEST DATA HOOP STRAIN (UIN/IN)	TEST DATA MERID STRAIN (UIN/IN)	ADJUSTED ANALYSIS HOOP STRAIN (UIN/IN)	ADJUSTED ANALYSIS MERID STRAIN (UIN/IN)	%DIFF HOOP	%DIFF MERID
1	0.0		B08G8424	ND	ND	ND	-357	ND	-192	ND	-46.2
	90.0		B08G8419	ND	ND	ND	-401	ND	-192	ND	-52.2
	180.0		B08G8414	ND	ND	ND	-421	ND	-192	ND	-54.4
	270.0		B08G8429	ND	ND	ND	-357	ND	-192	ND	-46.2
		AVERAGE:		ND	ND	ND	-384				
2	0.0	B08G8423	B08G8422	45.8	-13.9	1696	-963	1611	-1426	-5.0	48.1
	90.0	B08G8418	B08G8417	41.2	-21.5	1624	-1172	1611	-1426	-0.8	21.7
	180.0	B08G8413	B08G8412	40.5	-20.8	1592	-1140	1611	-1426	1.2	25.1
	270.0	B08G8428	B08G8427	46.8	-18.2	1777	-1120	1611	-1426	-9.3	27.4
		AVERAGE:		43.6	-18.6	1672	-1099				
3	0.0	B08G8425	B08G8426	70.0	52.2	1801	1007	2085	144	15.8	-85.7
	90.0	B08G8420	B08G8421	66.3	40.4	1801	650	2085	144	15.8	-77.8
	180.0	B08G8415	B08G8416	67.9	43.5	1825	734	2085	144	14.2	-80.4
	270.0	B08G8430	B08G8431	68.6	49.3	1785	923	2085	144	16.8	-84.4
		AVERAGE:		68.2	46.4	1803	829				

Table 4.6-20. Left SRM, Fixed Housing Aft Dome Nozzle/Case Biaxial Gages

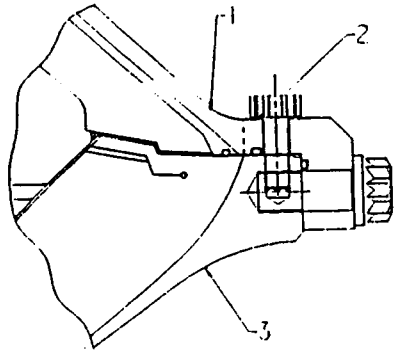

TEST NAME: STS26 9-29-88
JOINT: LEFT SRM FIXED HOUSING, AFT DOME
DESCRIPTION: NOZZLE / CASE BIAXIAL GAGES
THE TIME RANGE IS 0.0 TO 120.0 SECOND

LOCAT	ANGULAR LOCATION	HOOP GAGE	MERID GAGE	MAX HOOP STRESS (KSI)	CORESP MERID STRESS (KSI)	TEST DATA HOOP STRAIN (UIN/IN)	TEST DATA MERID STRAIN (UIN/IN)	ADJUSTED ANALYSIS HOOP STRAIN (UIN/IN)	ADJUSTED ANALYSIS MERID STRAIN (UIN/IN)	%DIFF HOOP	%DIFF MERID
1	0.0		B08G7424	ND	ND	ND	-397	ND	-192	ND	-51.2
	90.0		B08G7419	ND	ND	ND	-293	ND	-192	ND	-34.5
	180.0		B08G7414	ND	ND	ND	-401	ND	-192	ND	-52.2
	270.0		B08G7429	ND	ND	ND	ND	ND	-192	ND	-52.2
			AVERAGE:	ND	ND	ND	-364				
2	0.0	B08G7413	B08G7412	45.0	-14.9	1648	-947	1611	-1426	-2.3	50.
	90.0	B08G7418	B08G7417	48.3	-19.2	1801	-1124	1611	-1426	-10.5	26.
	180.0	B08G7423	B08G7422	41.3	-19.0	1565	-1045	1611	-1426	-254.1	-191.
	270.0	B08G7428	B08G7427	ND	ND	ND	ND	1611	-1426	ND	ND
			AVERAGE:	44.9	17.7	1671	-1039				
3	0.0	B08G7415	B08G7416	75.1	56.5	1938	1132	2085	144	7.6	-87.
	90.0	B08G7420	B08G7421	67.4	42.3	1825	734	2085	144	14.2	-80.
	180.0	B08G7425	B08G7426	ND	ND	ND	ND	2085	144	ND	ND
	270.0	B08G7430	B08G7431	70.6	51.9	1833	1023	2085	144	13.7	-85.
			AVERAGE:	53.3	37.6	1399	72				

Table 4.6-21. Right SRM, Fixed Housing Aft Dome Nozzle/Case Biaxial Gages

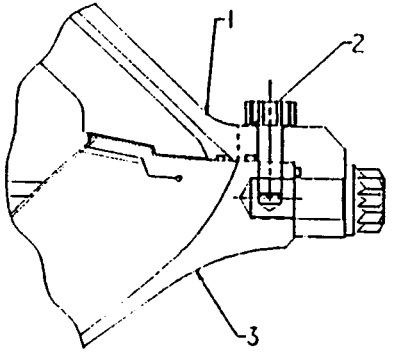

TEST NAME: STS26R 9-29-88
JOINT: RIGHT SRM FIXED HOUSING, AFT DOME
DESCRIPTION: NOZZLE / CASE BIAXIAL GAGES
THE TIME RANGE IS 0.0 TO 120.0 SECOND

LOCAT	ANGULAR LOCATION	HOOP GAGE	MERID GAGE	MAX HOOP STRESS (KSI)	CORESP MERID STRESS (KSI)	TEST DATA HOOP STRAIN (UIN/IN)	TEST DATA MERID STRAIN (UIN/IN)	ADJUSTED ANALYSIS HOOP STRAIN (UIN/IN)	ADJUSTED ANALYSIS MERID STRAIN (UIN/IN)	%DIFF HOOP	%DIFF MERID
1	0.0		B08G8424	ND	ND	ND	-357	ND	-192	ND	-46.2
	90.0		B08G8419	ND	ND	ND	-401	ND	-192	ND	-52.2
	180.0		B08G8414	ND	ND	ND	-421	ND	-192	ND	-54.4
	270.0		B08G8429	ND	ND	ND	-357	ND	-192	ND	-46.2
			AVERAGE:	ND	ND	ND	-348				
2	0.0	B08G8413	B08G8412	39.4	-18.3	1495	-1003	1611	-1426	7.7	42.
	90.0	B08G8418	B08G8417	44.5	-21.2	1696	-1152	1611	-1426	-5.0	23.
	180.0	B08G8423	B08G8422	44.7	-11.2	1600	-819	1611	-1426	0.7	74.
	270.0	B08G8428	B08G8427	50.9	-17.6	1873	-1096	1611	-1426	-14.0	30.
			AVERAGE:	44.9	-17.1	1666	-1018				
3	0.0	B08G8425	B08G8426	71.5	52.5	1857	1035	2085	144	12.3	-86.
	90.0	B08G8420	B08G8421	66.2	38.3	1825	614	2085	144	14.2	-76.
	180.0	B08G8415	B08G8416	69.9	44.0	1889	766	2085	144	10.4	-81.
	270.0	B08G8430	B08G8431	68.3	47.6	1801	903	2085	144	15.8	-84.
			AVERAGE:	69.0	45.6	1843	830				

4.6.3.5 Moment, Shear, and Strut Forces. Six stations along the full length of the SRM contained biaxial strain gages at four locations around the circumference (approximately 90 deg apart). From these a stress plane at each station is generated. From the stress plane the Y and Z axis bending moments and axial loads are computed. These results are compared to both previous flights and predicted loads at all significant operational periods including: lift-off, shuttle roll maneuver, maximum acceleration, maximum dynamic pressure, and separation.

Stations 556 and 876 on the right SRB were determined to have anomalous data because the strain gage data for these stations show a very rapid decrease in strain immediately after lift-off. The main driver for these gages is motor pressure, and since the motor pressure does not decrease nearly as rapidly, there is no reason for this gage behavior. The left and right motor pressure was essentially identical, and the left motor strain gages do not show this behavior. This behavior has not been seen in any previous flights, and is believed to be a data acquisition problem. However, these data were used in the calculations of bending moments and axial force, and plotted to show the difference between the left and right motors.

Bending in the Y-Axis (My)

Figures 4.6.1 through 4.6.6 show the bending about the Y axis for both the left and right motors for Stations 556, 867, 1196, 1466, 1501, and 1797. Initially, the case is seen to be bending in the +Y direction, which is caused by the orbiter weight. The magnitude increases linearly going down the case toward the holddown point. There is an abrupt shift at Station 1501 (Figure 4.6.5) caused by the struts giving added support and the fact that the case is slightly thicker at this point (0.58 in. at Station 1501 as compared to 0.479 in. at other stations).

During SSME buildup, every station experiences a change from positive to negative bending as the SRBs bend over. The maximum value was -290×10^6 in.-lb at Station 1797 on the left SRB (Figure 4.6.6). This value compares well with the design maximum of -304×10^6 in.-lb.

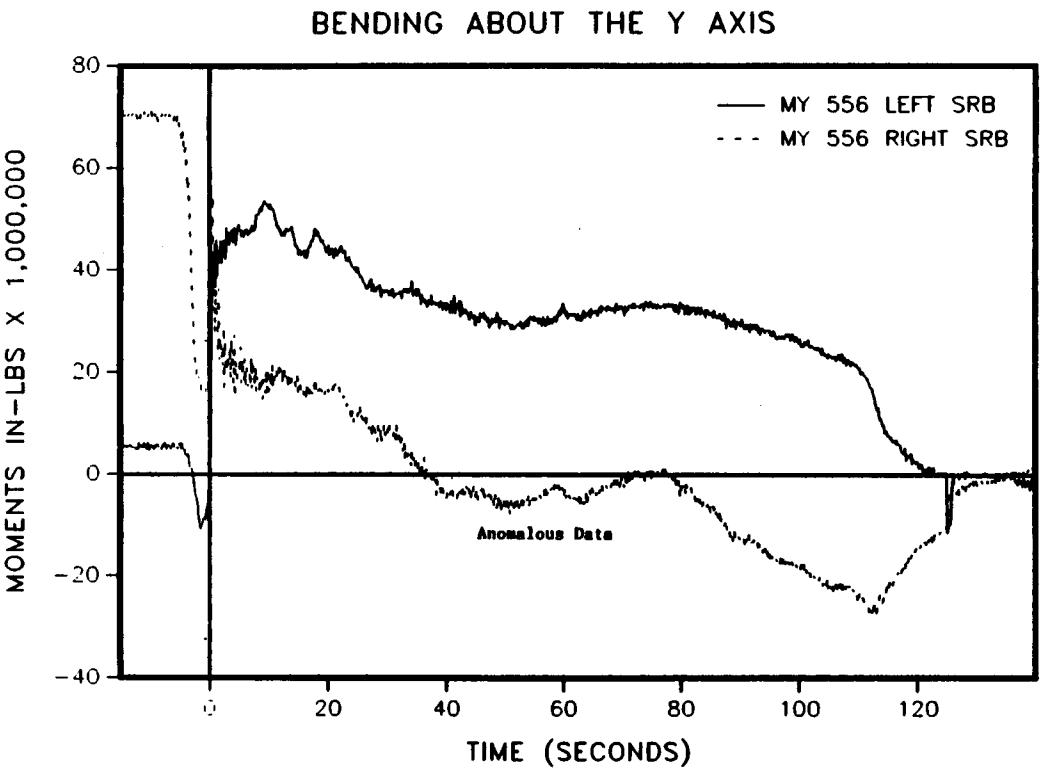

Figure 4.6-1. 360L001 Station 556

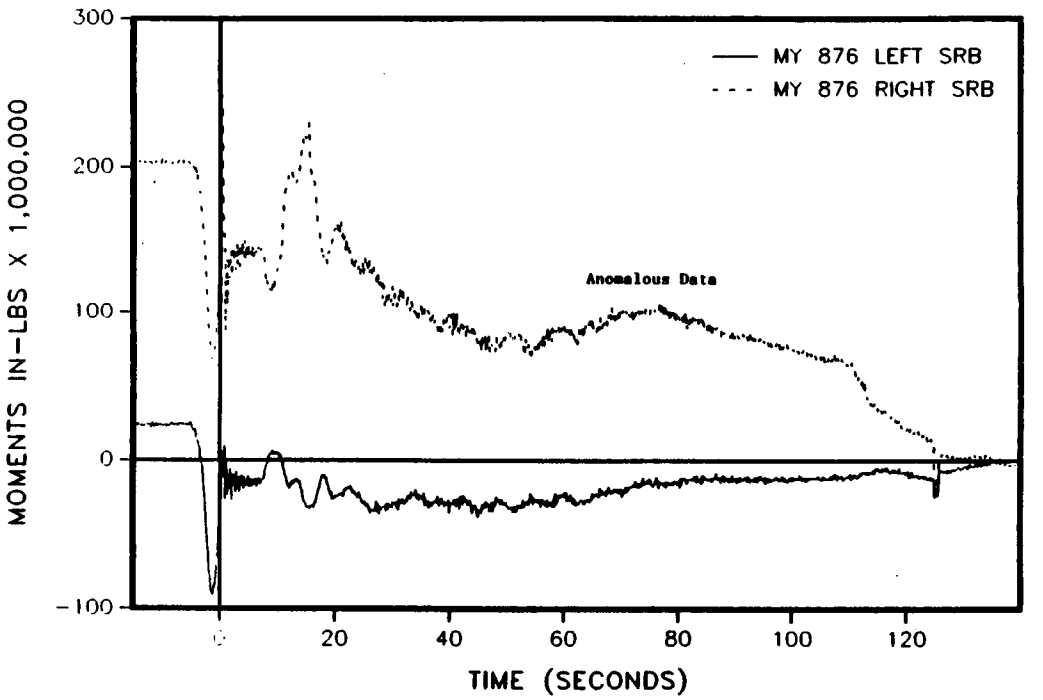

Figure 4.6-2. 360L001 Station 876

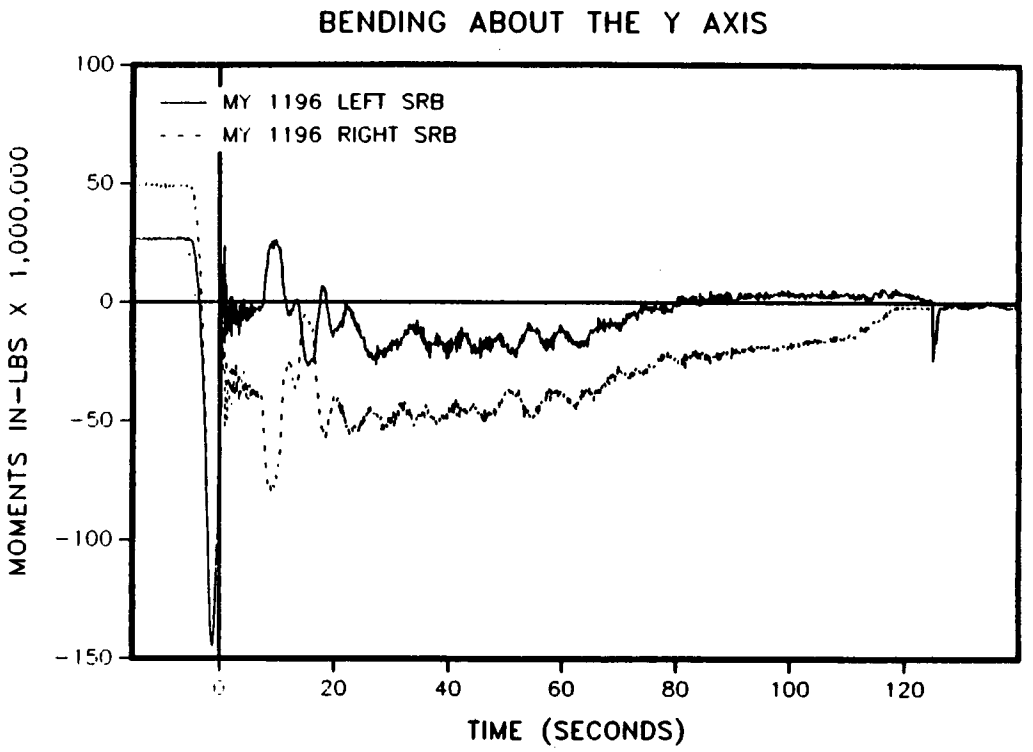

Figure 4.6-3. 360L001 Station 1196

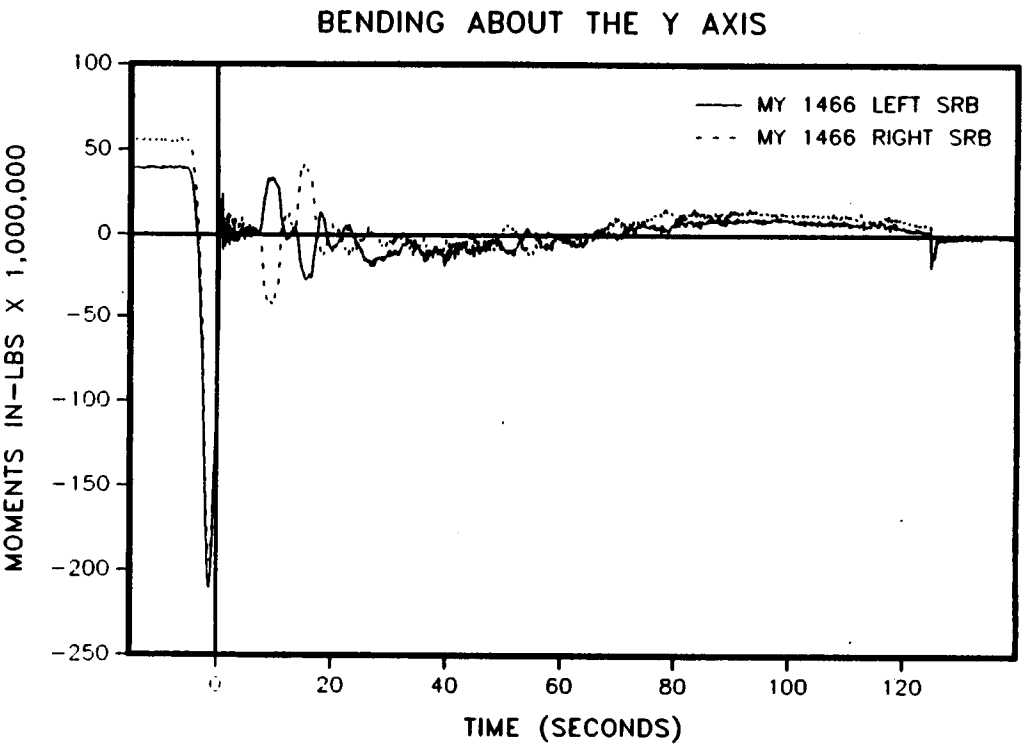

Figure 4.6-4. 360L001 Station 1466

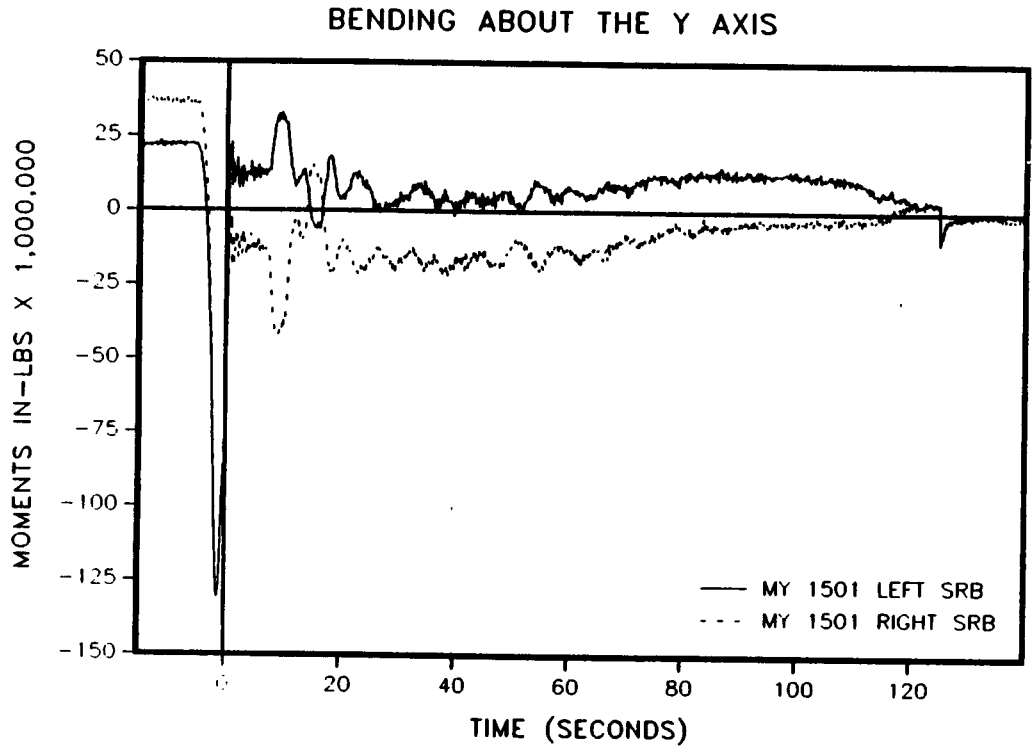

Figure 4.6-5. 360L001 Station 1501

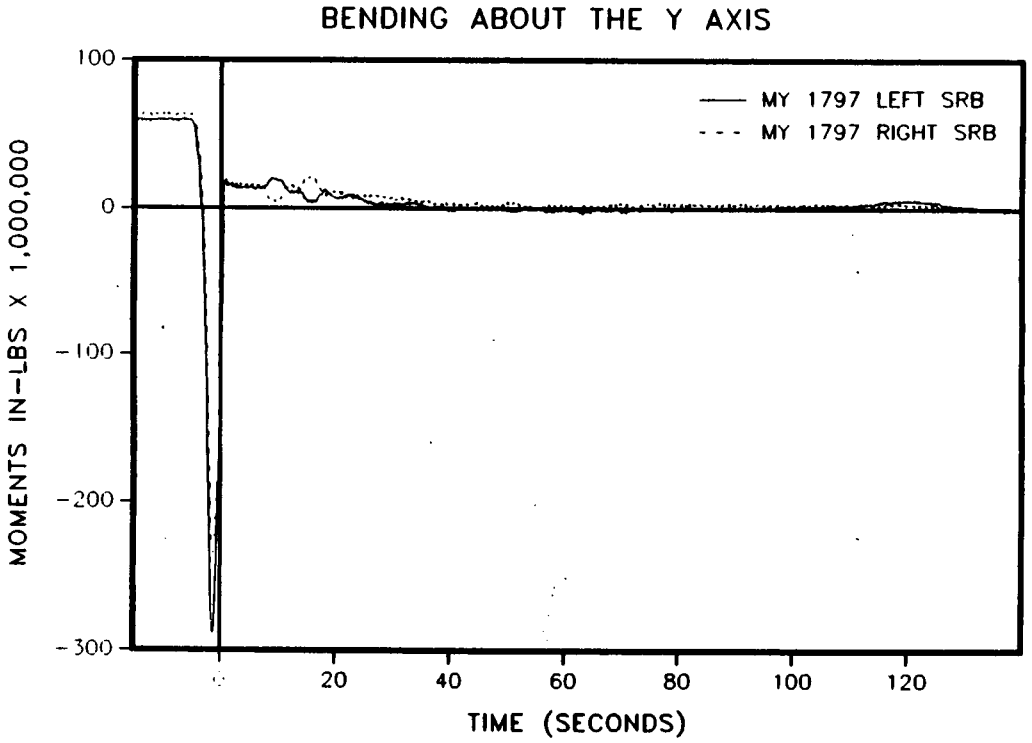

Figure 4.6-6. 360L001 Station 1797

Upon lift-off, the values reduce significantly, coming back to nearly zero for every Station except 556. Station 556 jumps to a positive value at lift-off. During shuttle roll maneuver, the left SRB experiences an increase in bending, while the right SRB experiences a decrease. This is because the nozzles are vectoring to cause the roll, and the SRBs are essentially pivoting about the struts. At the end of the roll, the change for the left and right SRBs is opposite for the reason mentioned previously. No other significant trends occur from this point on, as the data find their way to zero.

Figures 4.6.7 through 4.6.10 are plots of the first three flights, and also include flight set 360L001 (STS-26R). Stations were chosen on 360L001 that were as near as possible to the stations used on these previous flights. The correlation is very good.

Bending in the Z-Axis (Mz)

Figures 4.6.11 through 4.6.16 show the bending about the Z axis for both the left and right motors for Stations 556, 867, 1196, 1466, 1501, and 1797. Initially, the top of the motors is seen to be bending in toward the ET, which is due to the weight of the ET and orbiter. Moving down the motor, the bending becomes less and less, then changes sign between Stations 1196 and 1466 as expected. Upon lift-off, these same effects are seen with a larger magnitude because the SRBs are firing, and the motor is essentially pivoting about the attach points. During roll maneuver, Stations 1196 and 1466 show the same peaks as bending about the Y axis, with the exception that both the left and right motors move in the same direction. This is due to the sign convention. During the first phase of the roll, the left motor is moving away from the ET, and the right motor is moving toward the ET. The opposite is true of the second part of the roll maneuver. Station 1797 is different from the other stations. After lift-off, it follows a more or less linear path back to zero during the flight.

Figures 4.6.17 through 4.6.20 are plots of bending about the Z axis of the first three flights and 360L001 (STS-26R) as a function of time. The overall correlation is very good. At Station 1196, bending about the Z axis of the right motor shows a much higher oscillation during roll maneuver, and

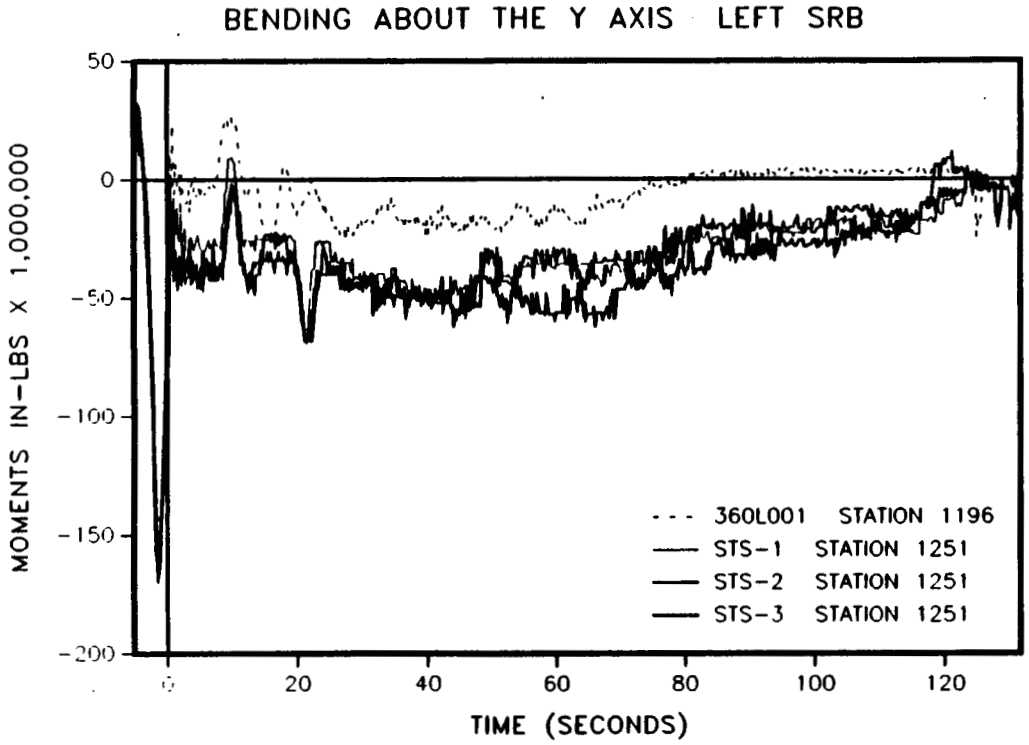

Figure 4.6-7. 360L001 Versus Previous Flights

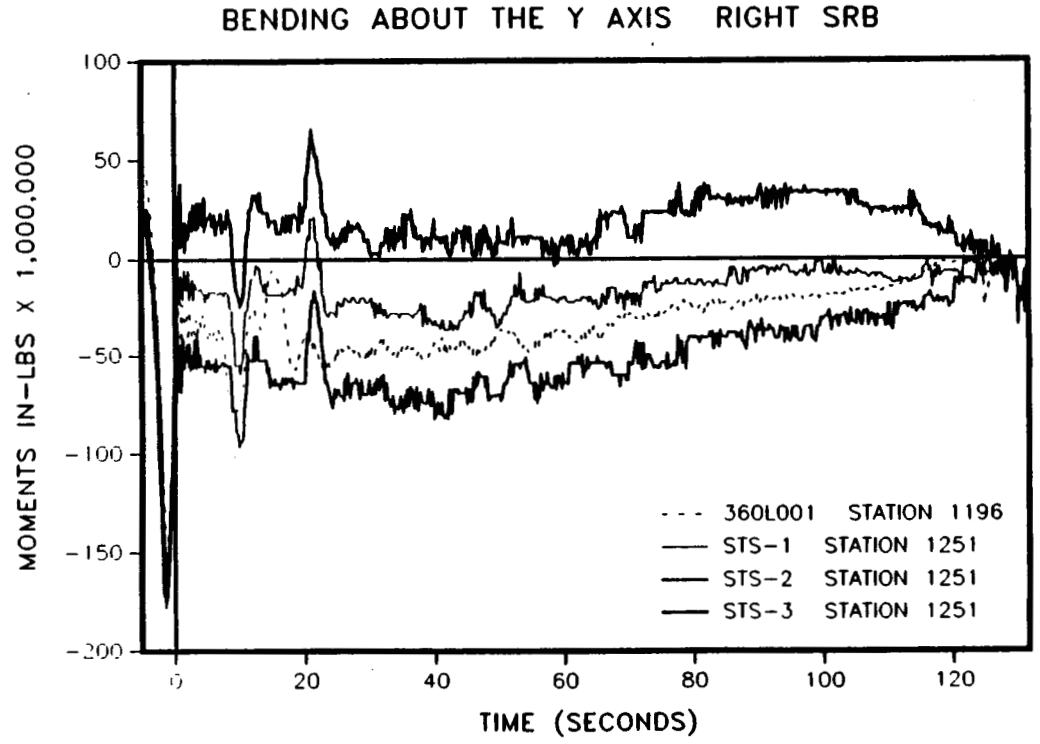

Figure 4.6-8. 360L001 Versus Previous Flights

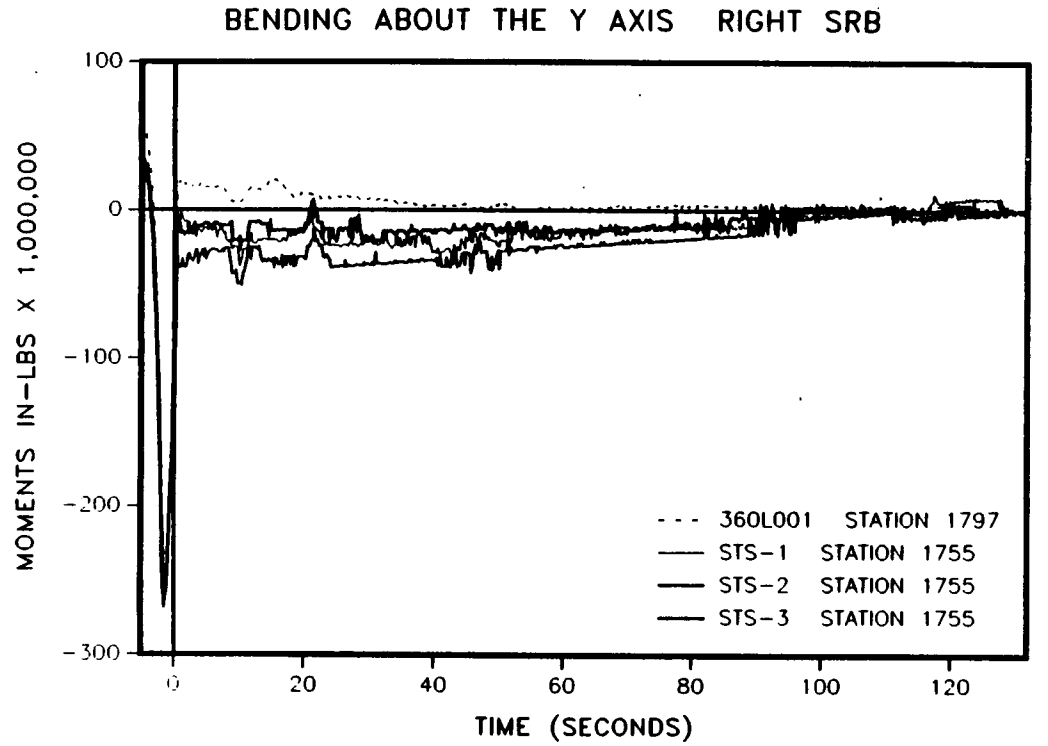

Figure 4.6-9. 360L001 Versus Previous Flights

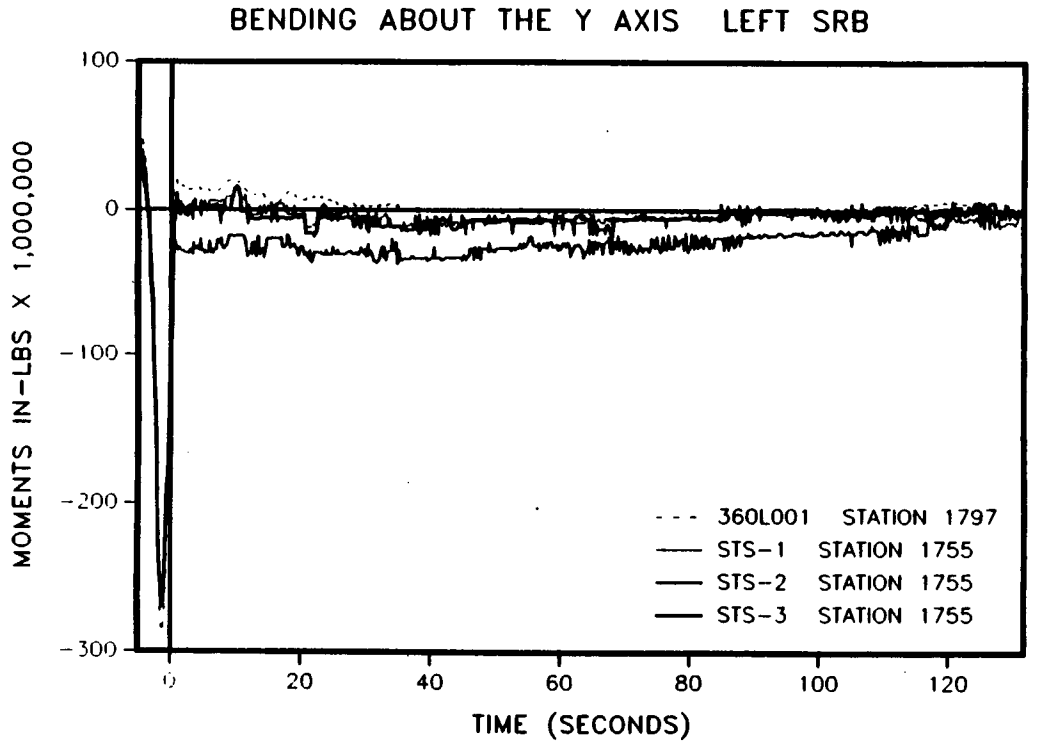

Figure 4.6-10. 360L001 Versus Previous Flights

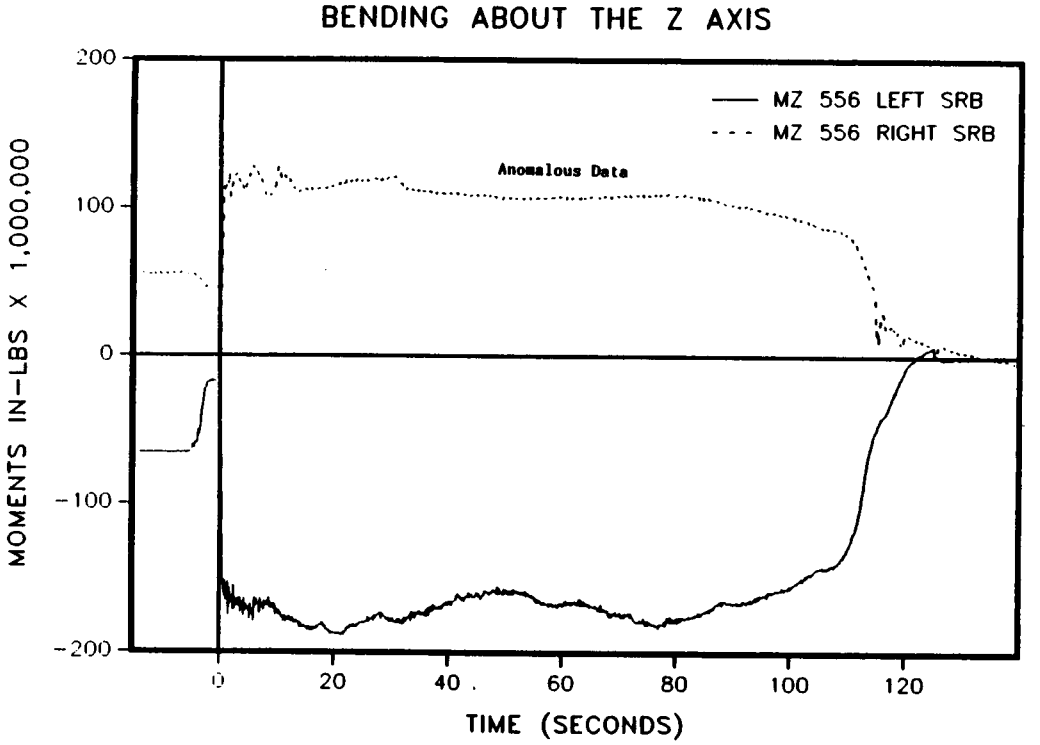

Figure 4.6-11. 360L001 Station 556

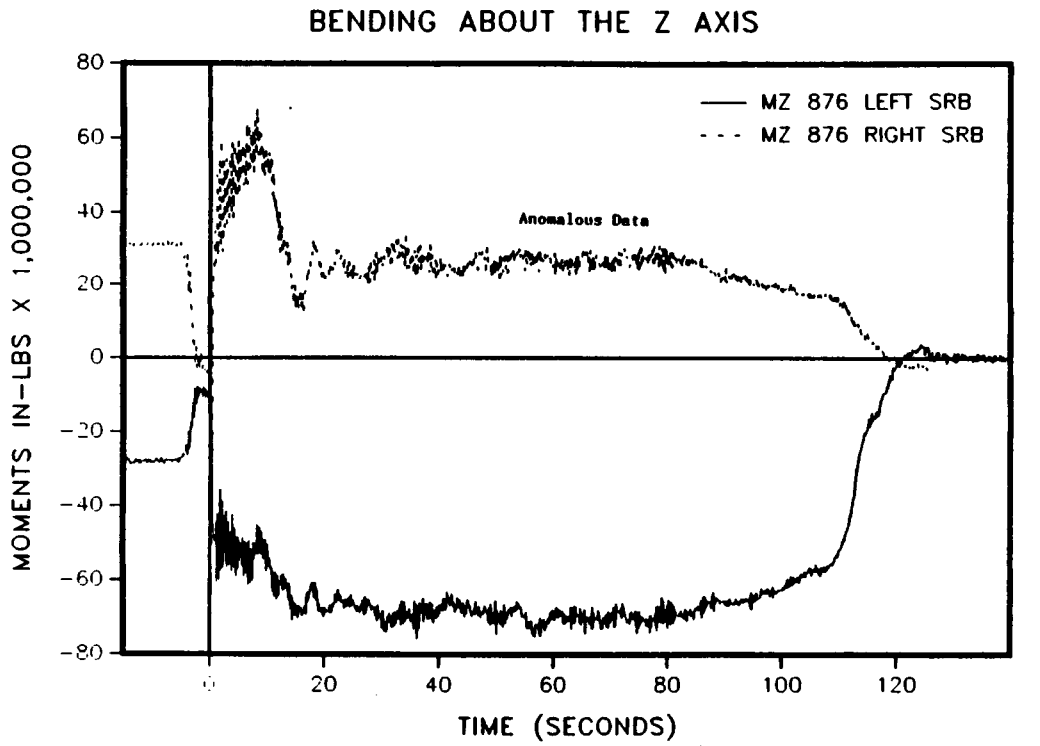

Figure 4.6-12. 360L001 Station 876

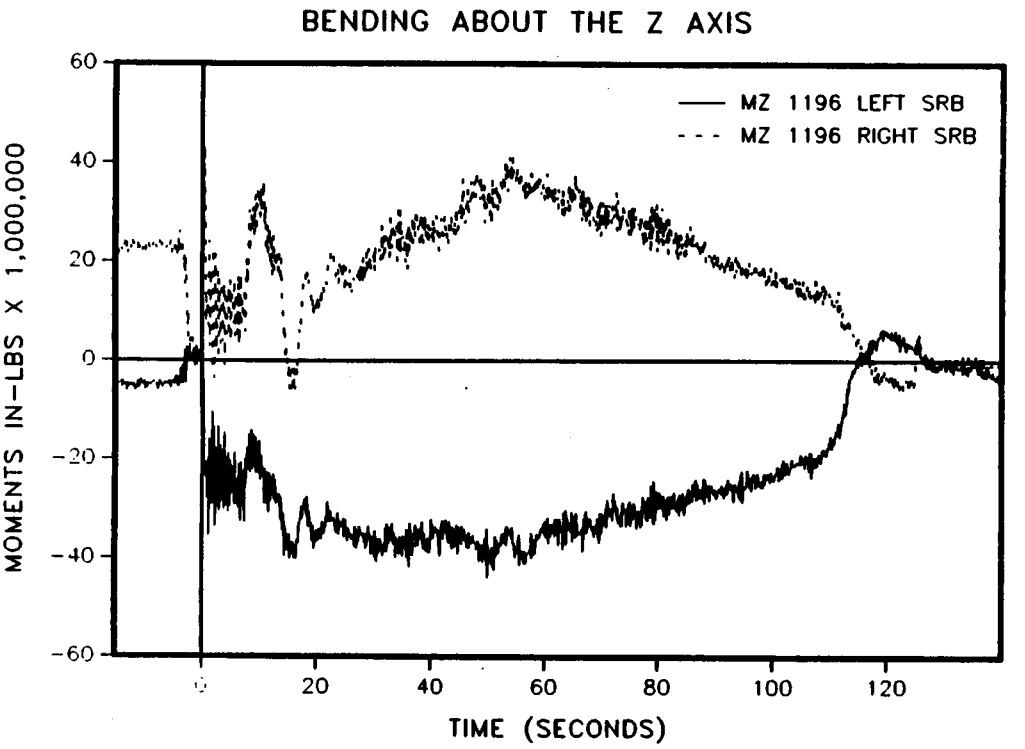

Figure 4.6-13. 360L001 Station 1196

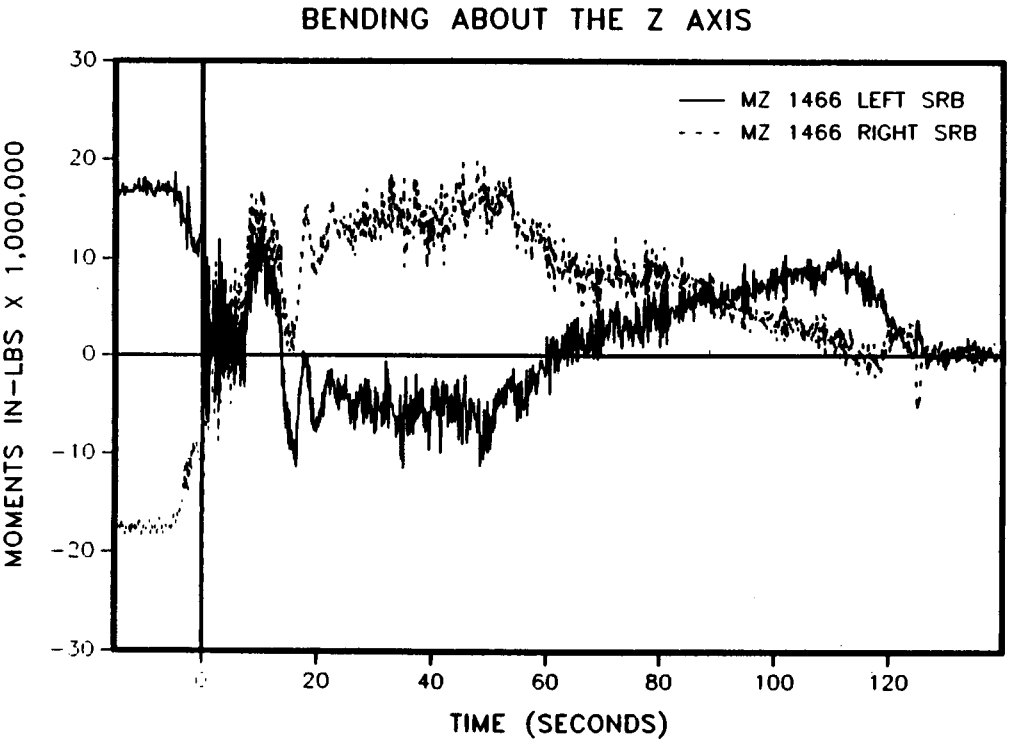

Figure 4.6-14. 360L001 Station 1466

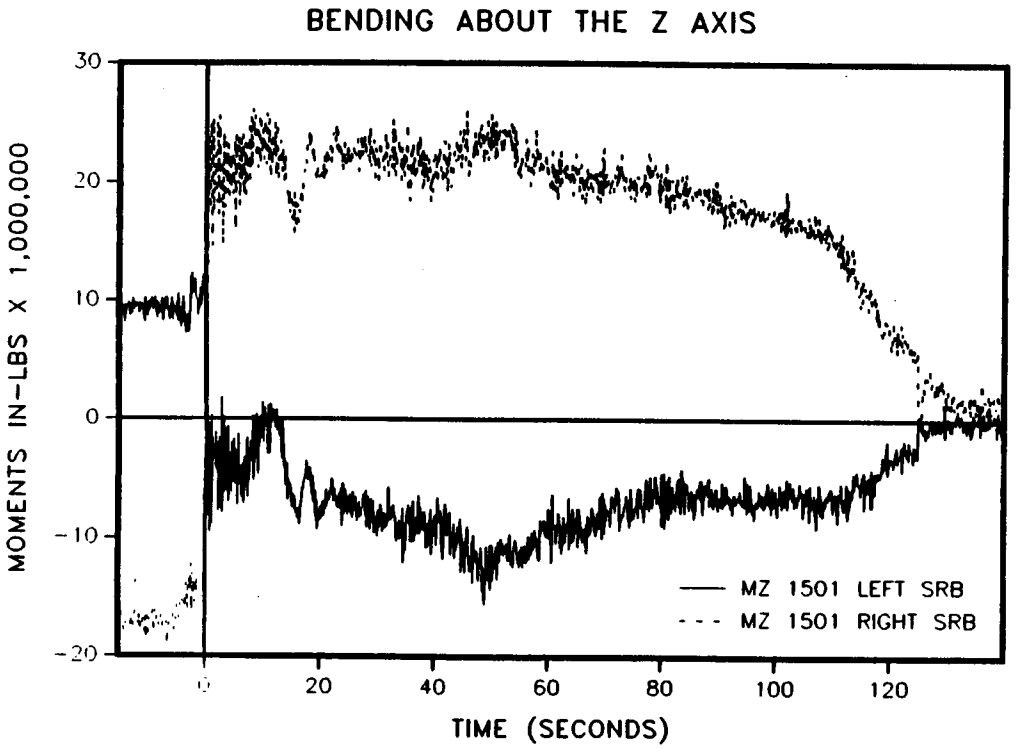

Figure 4.6-15. 360L001 Station 1501

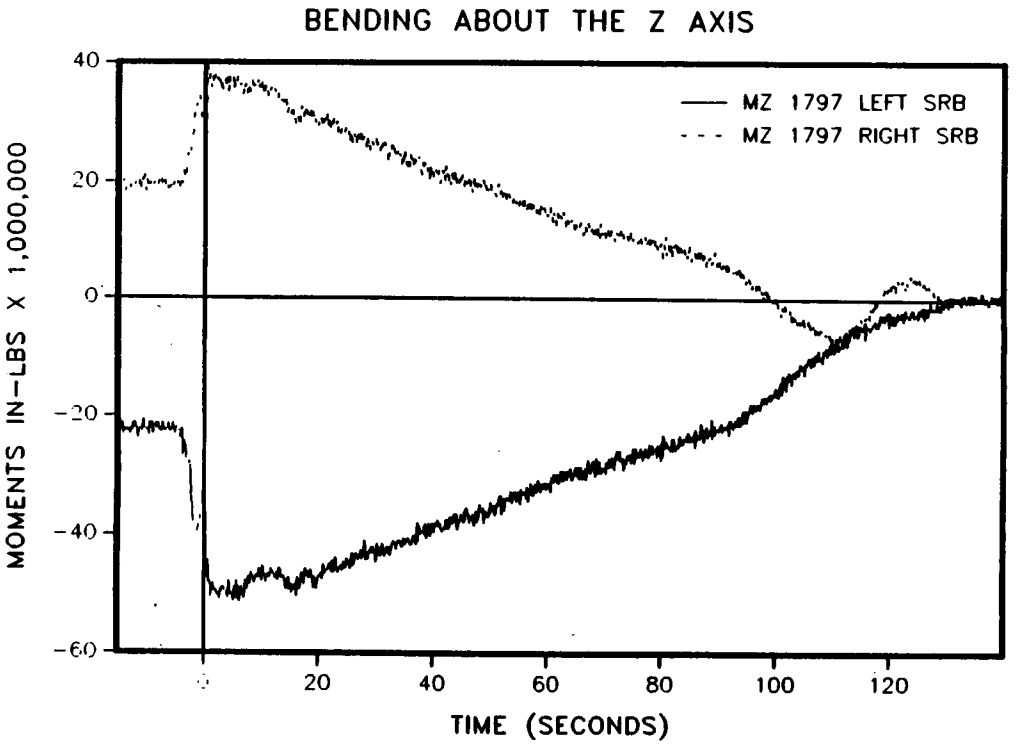

Figure 4.6-16. 360L001 Station 1797

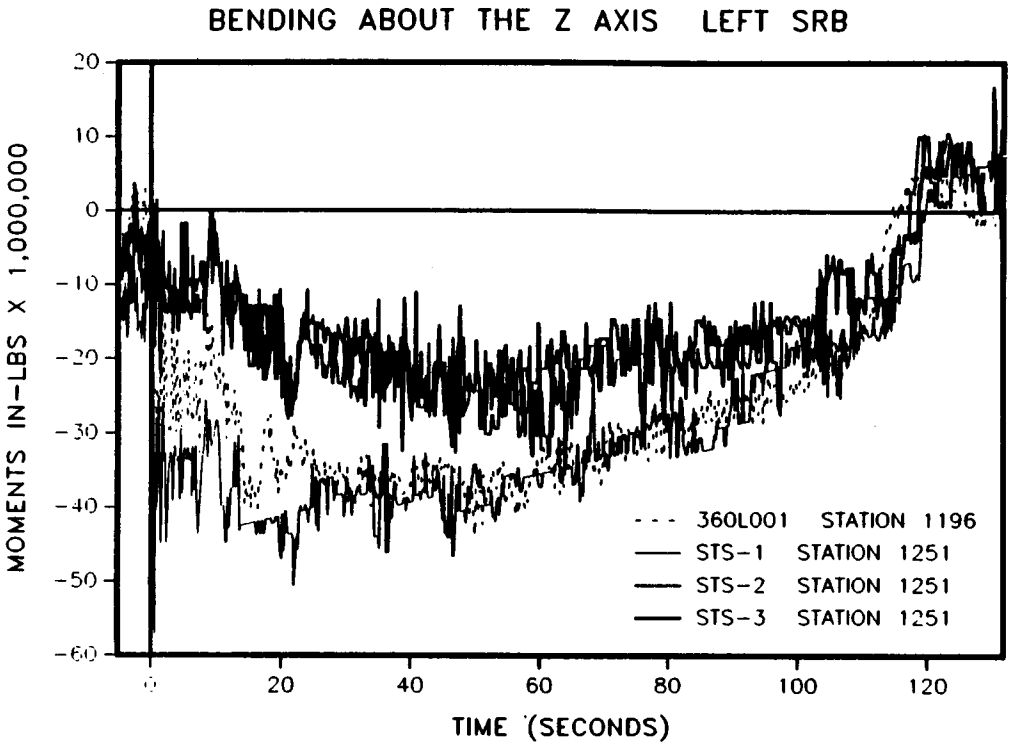

Figure 4.6-17. 360L001 Versus Previous Flights

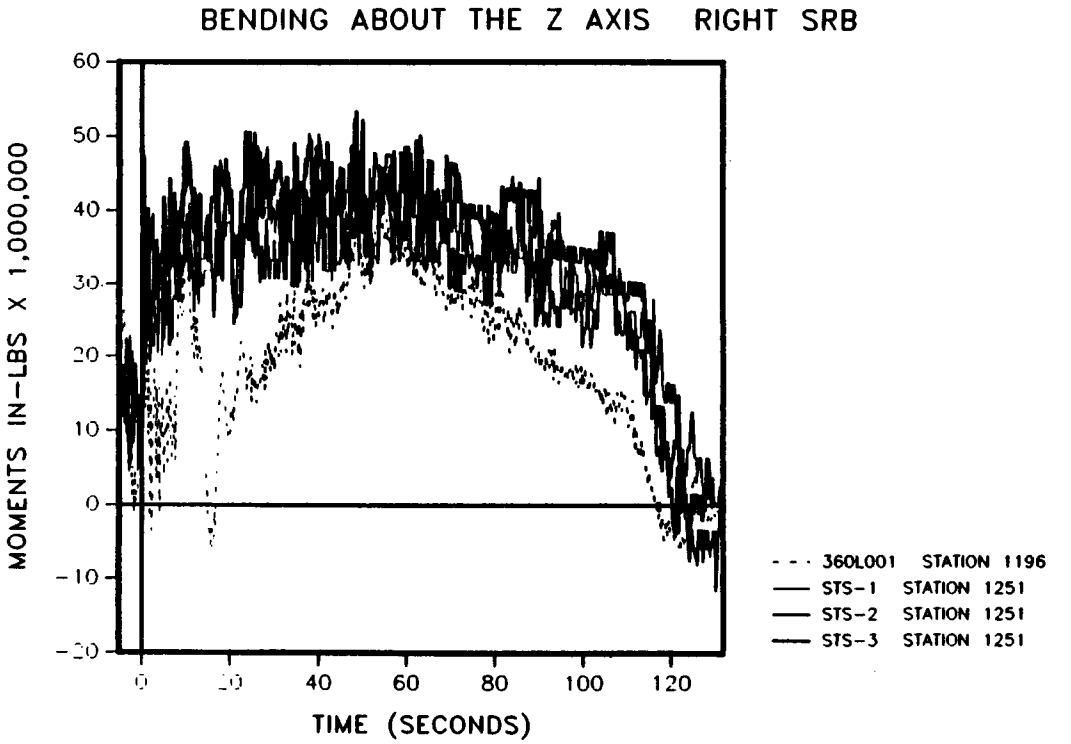

Figure 4.6-18. 360L001 Versus Previous Flights

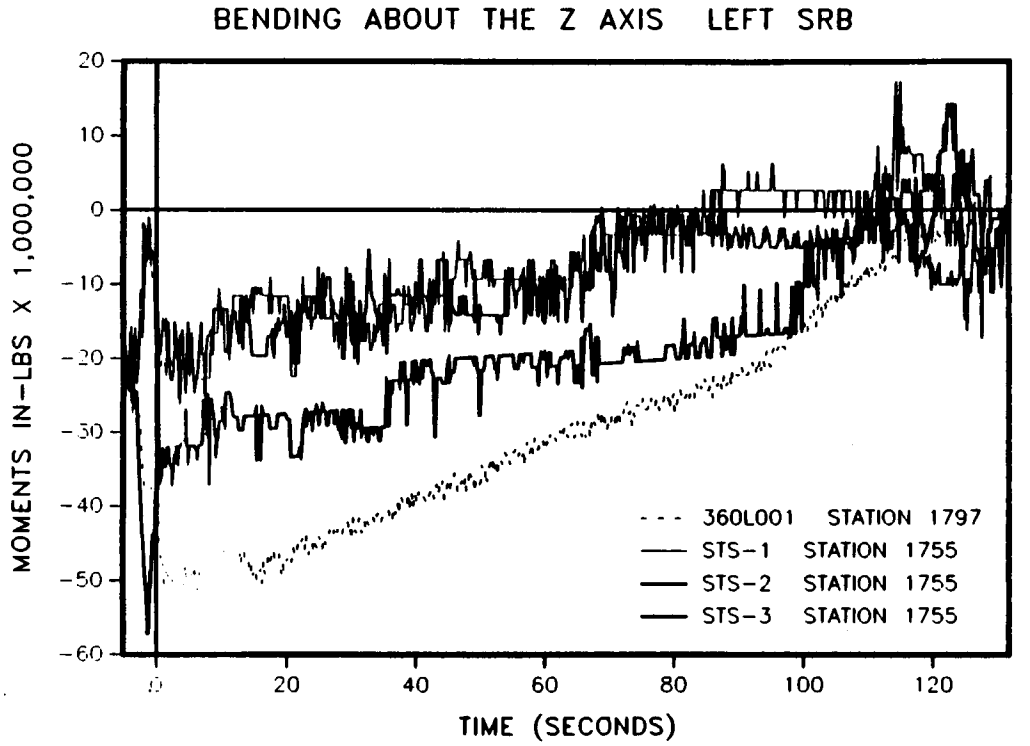

Figure 4.6-19. 360L001 Versus Previous Flights

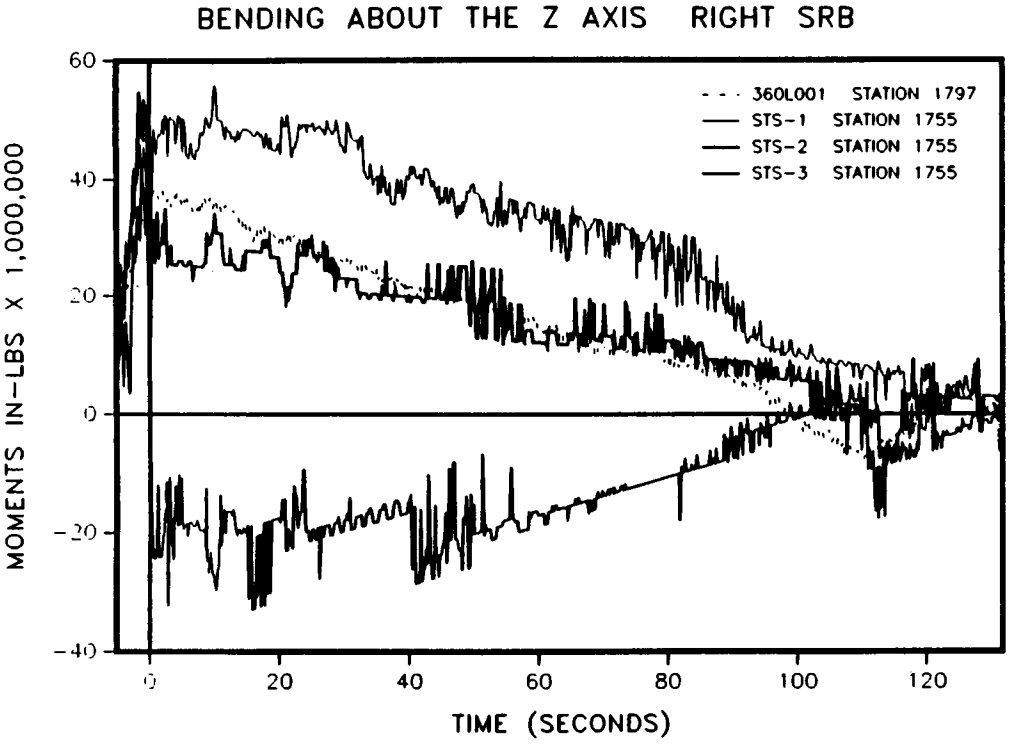

Figure 4.6-20. 360L001 Versus Previous Flights

the overall magnitude is slightly less than STS-1 through STS-3. At Station 1797, bending about the Z axis of the left motor shows a magnitude that is slightly higher than STS-1 through STS-3.

Axial Forces in the X-Axis (Vx)

Figures 4.6.21 through 4.6.26 show the axial force for both the left and right motors for Stations 556, 876, 1196, 1466, 1501, and 1797. A positive value represents a compressive force, and a negative value represents a tensile force. Initially, the axial forces at each station are subjected to the weight of the ET, the orbiter, and the segments above the particular station. Since these are the only forces acting axially, the result should increase linearly proceeding down the case. A comparison of the measured data as compared to the predicted flight envelopes is discussed further in Section 4.6.3.6.

Upon SRB ignition, the cases immediately go into tension as the motors pressurize and lift-off. The maximum value was -13,400 kips and occurred at Station 556 of the left motor. After this point, the shape of the plot looks like the motor pressure plots. There is good agreement between the left and right motors. Some of the differences can be attributed to the fact that the gages were zeroed at the end of the flight, and the actual strain values experienced by the left and right motors, and each station, were probably not exactly zero. This could also account for the nonlinearity before SSME buildup.

Figures 4.6.27 through 4.6.30 compare the axial force of the first three flights and 360L001 (STS-26R). The shape of the curves are very similar. The higher magnitude of 360L001 can be explained by the fact that the redesigned boosters are HPMs, and obtain a higher operating pressure than the older motors.

Line Loads

Using the bending moment and axial force data, the line loads were calculated. The maximum values for each motor and flight event and the station where they occurred are shown in Table 4.6-22.

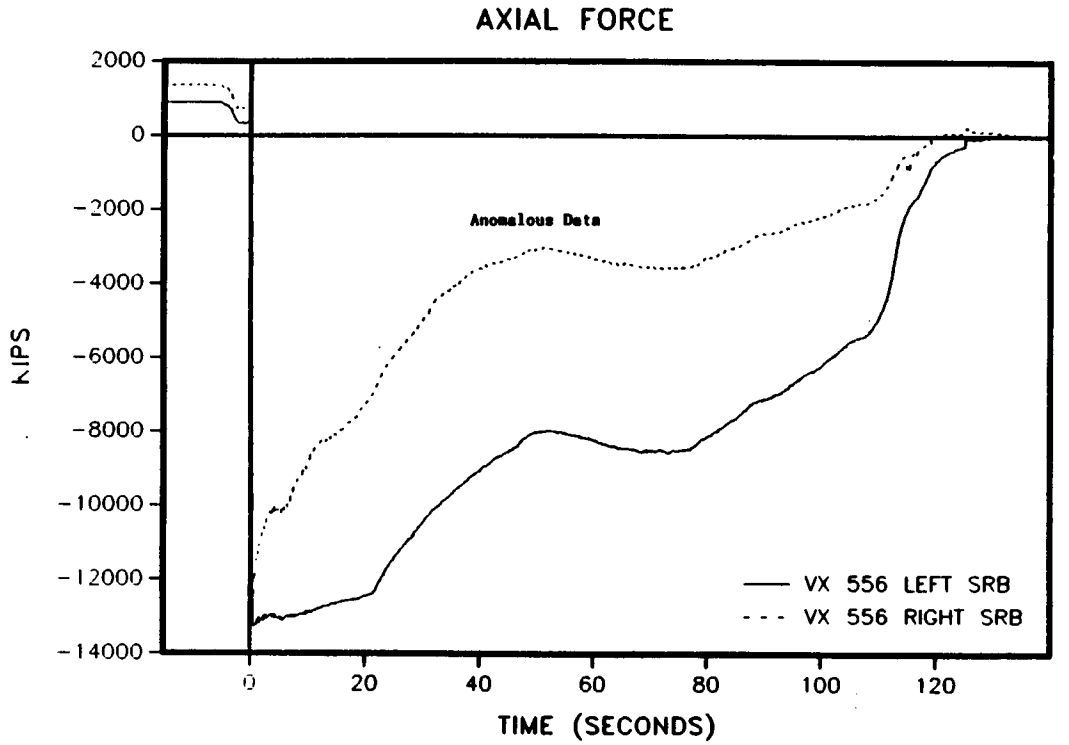

Figure 4.6-21. 360L001 Station 556

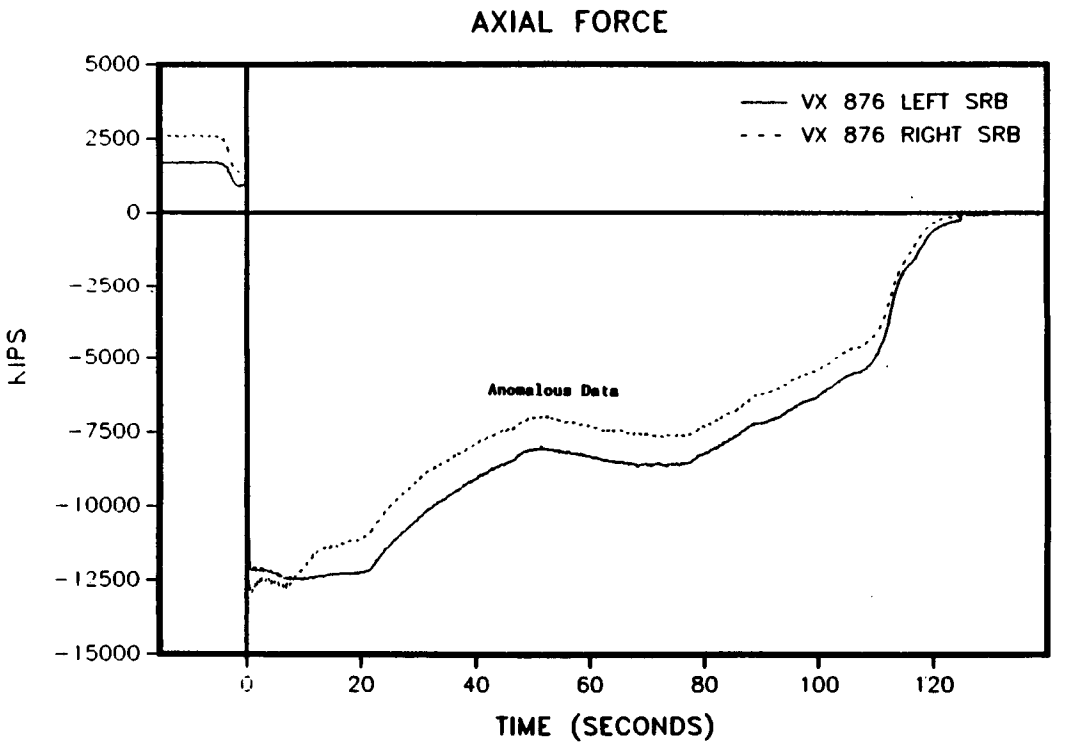

Figure 4.6-22. 360L001 Station 876

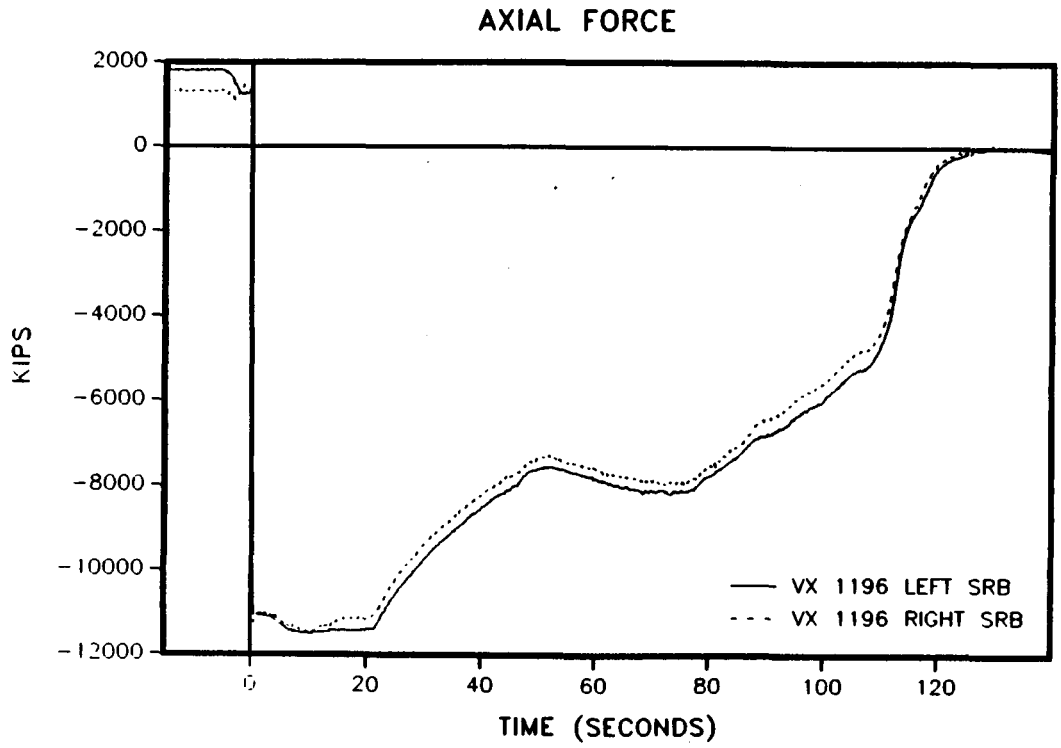

Figure 4.6-23. 360L001 Station 1196

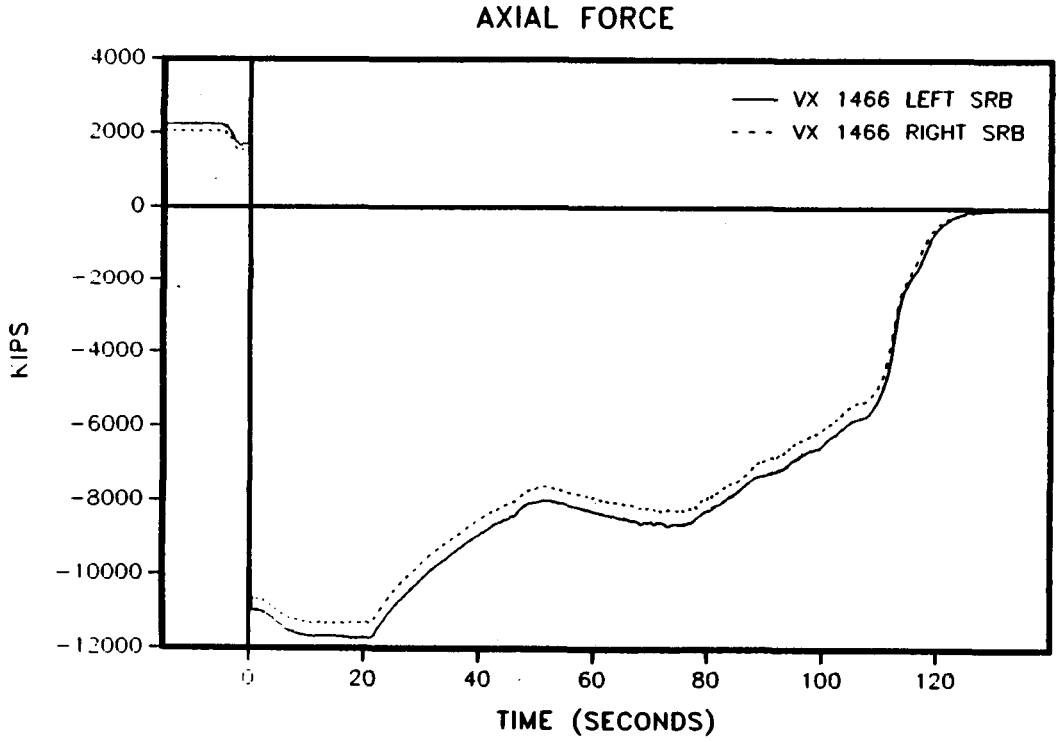

Figure 4.6-24. 360L001 Station 1466

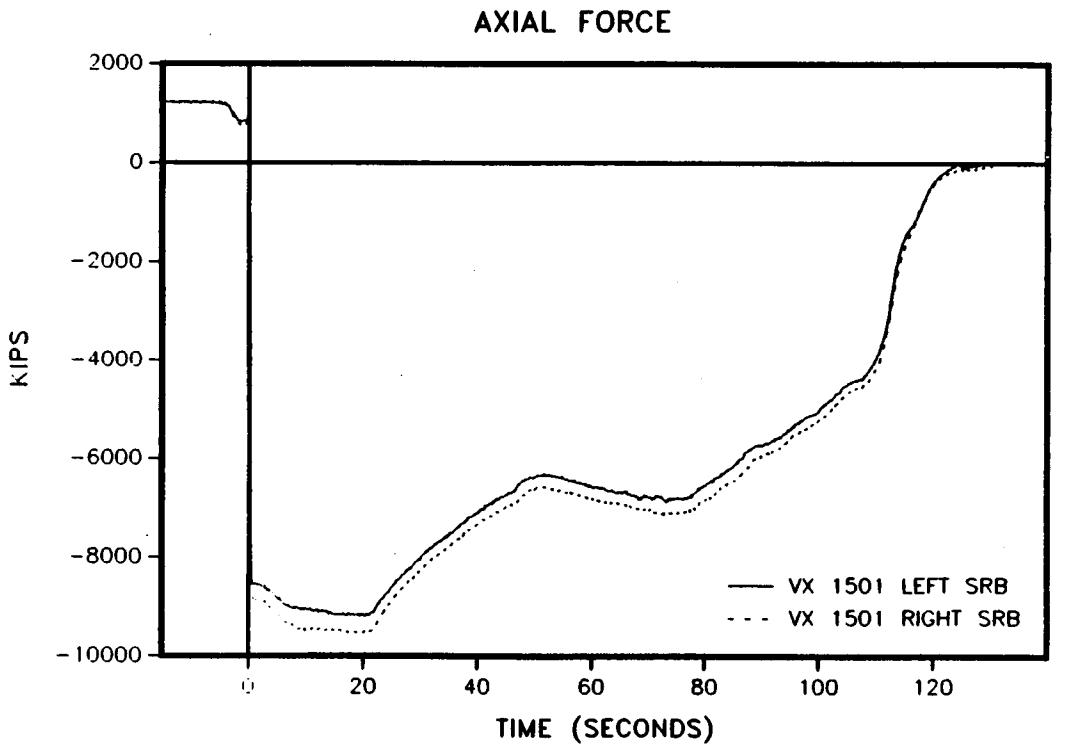

Figure 4.6-25. 360L001 Station 1501

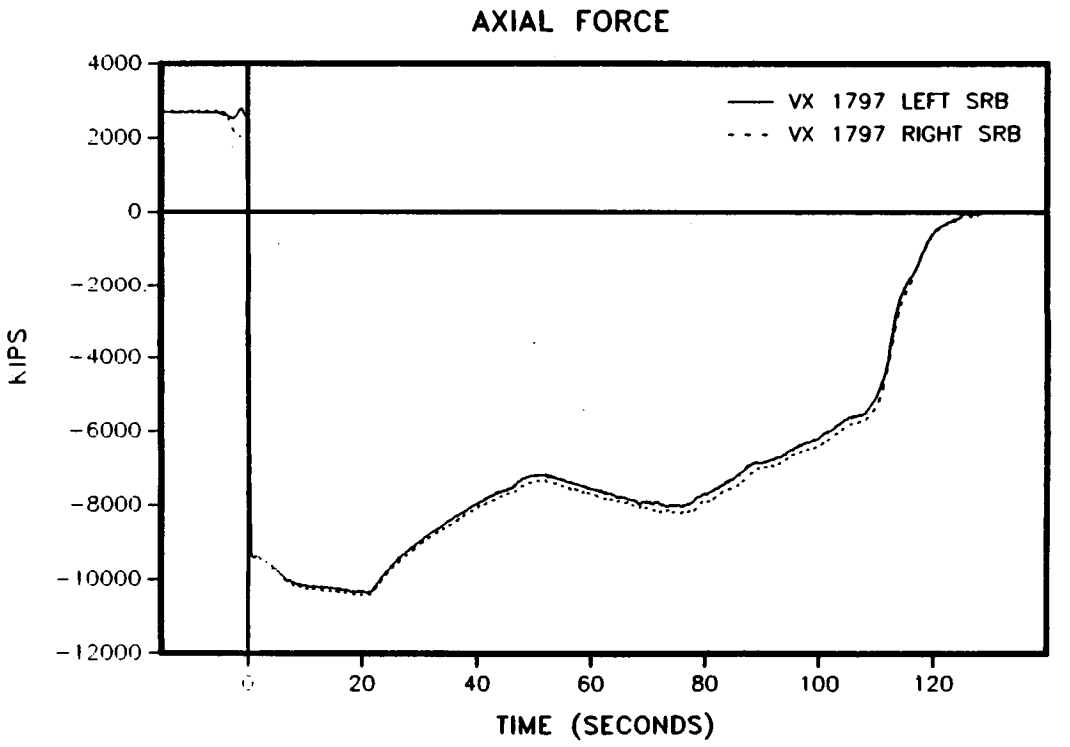

Figure 4.6-26. 360L001 Station 1797

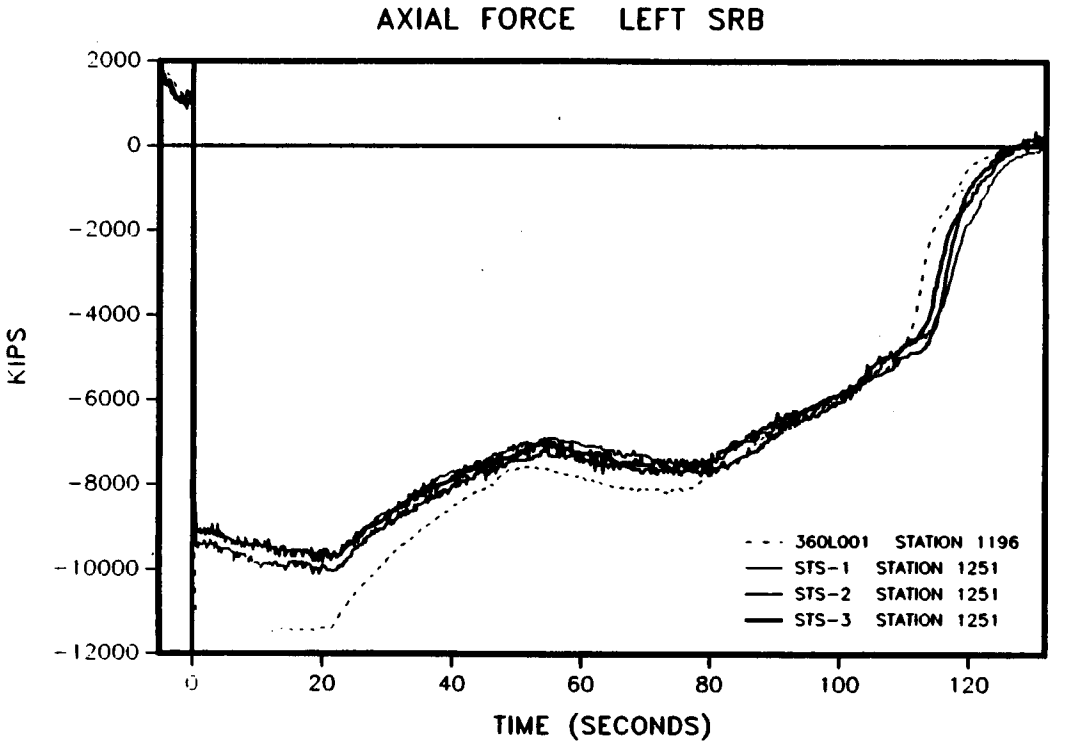

Figure 4.6-27. 360L001 Versus Previous Flights

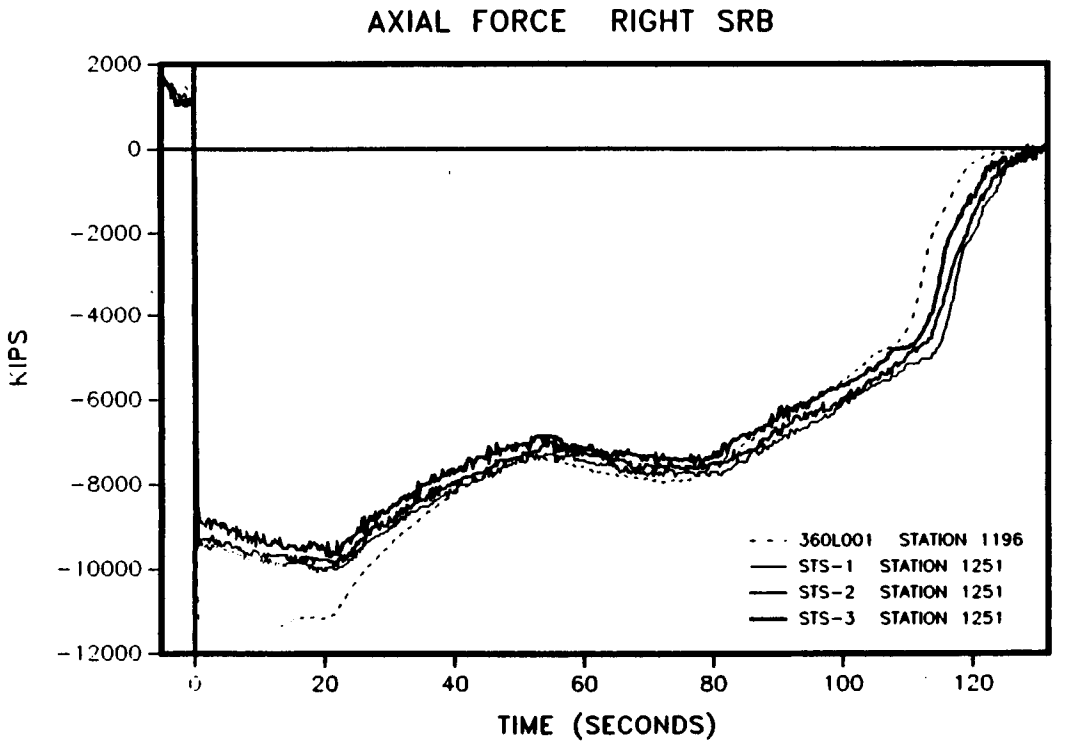

Figure 4.6-28. 360L001 Versus Previous Flights

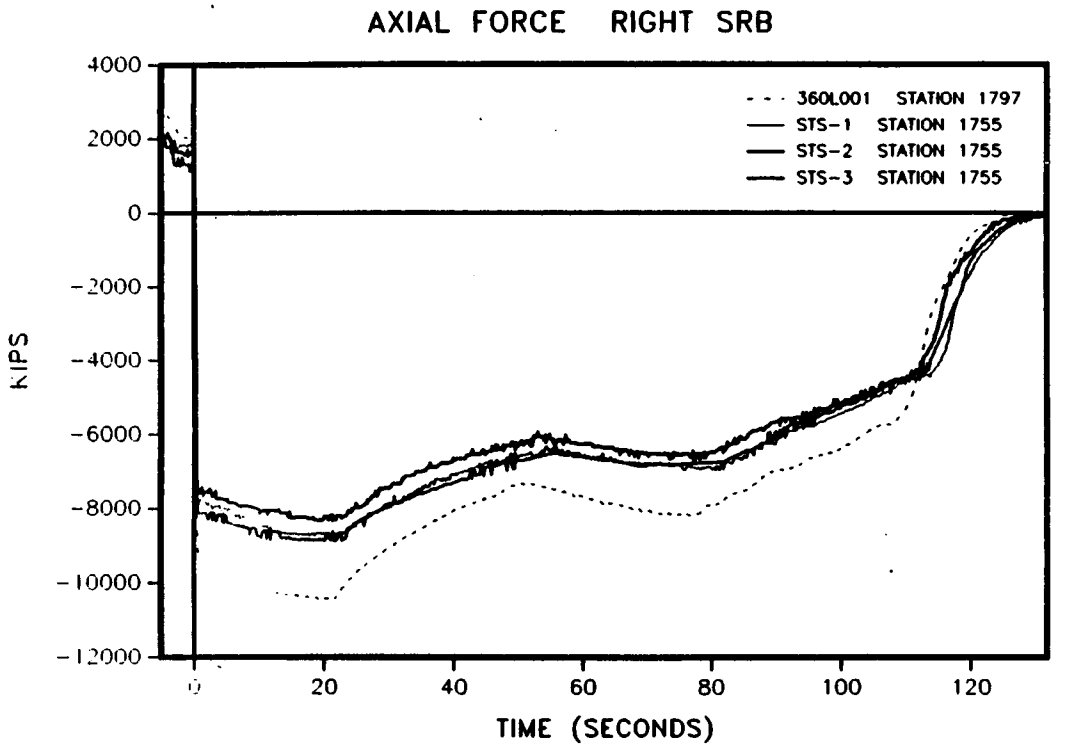

Figure 4.6-29. 360L001 Versus Previous Flights

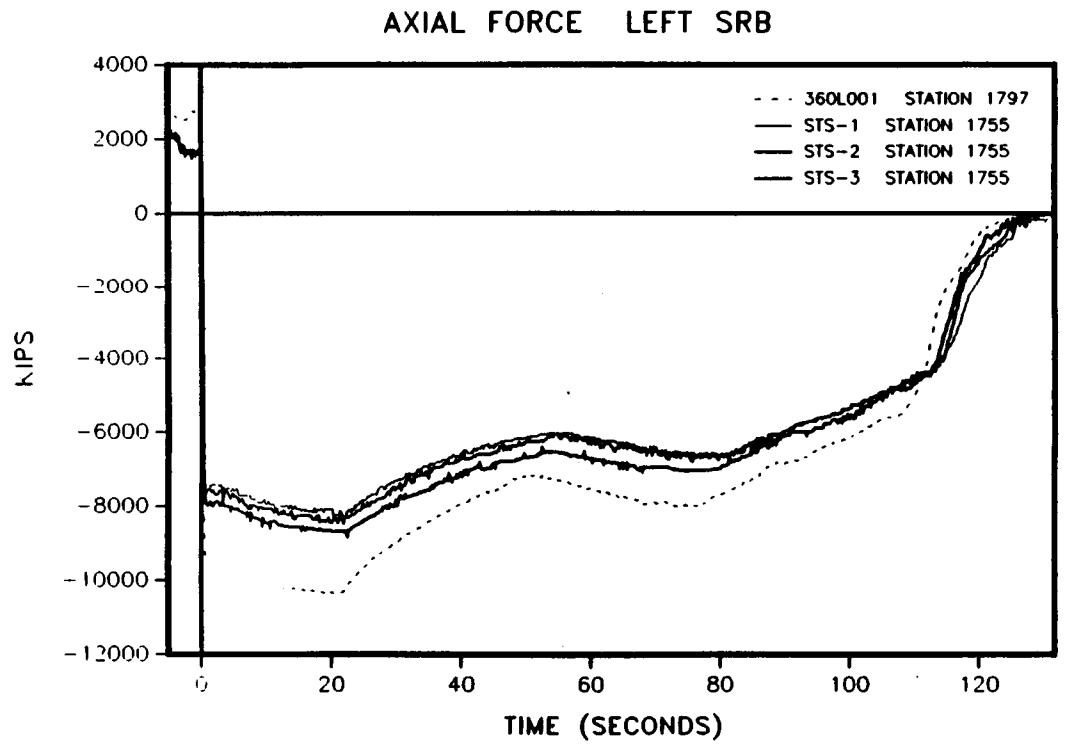

Figure 4.6-30. 360L001 Versus Previous Flights

Table 4.6-22. Maximum Values for Motor and Flight Events

	Right Motor		Left Motor	
Flight Event	Max Line Load (kips/in.)	Station	Max Line Load (kips/in.)	Station
Prelaunch	9.8	1797	10.0	1797
Buildup	23.6	1797	18.8	1797
Lift-Off	-24.3	876	-23.7	1466
Roll	-25.5	1466	-24.4	1466
Max Q	-22.3	1466	-21.5	1466
Max G	-18.9	1466	-17.5	1466
Prestaging	-1.5	1466	-1.6	1797

4.6.3.6 Flight Envelopes. In general, the bending moments and axial force experienced by 360L001 (STS-26R) were either within the envelopes or slightly out. The following are possible reasons why all the loading did not fall within the envelopes:

a. Several strain gages went into the calculation of each load, and every gage has an uncertainty associated with the gage itself, plus some drift in each gage during the flight.

b. Station 1501 is located in an area where the case is slightly thicker than all of the other stations (0.479 in. in the membrane, and 0.58 in. at this station). The programs used will not allow more than one case thickness as an input parameter.

c. Adjusting the strain data to end at zero adds some uncertainty since the exact strain experienced during free fall is not known.

d. The program calculates a linear stress distribution from the strain data, and the case does not necessarily behave linearly during flight. It should be noted that the data compare favorably with the previous flight data, as expected.

The time ranges used to find the maximum and minimum values for each event are defined in Table 4.6-23.

As mentioned previously, Stations 556 and 876 of the right SRB were determined to be bad and were not included in the envelope figures.

Bending About the Y Axis

Figures 4.6.31 through 4.6.44 are plots of the maximum and minimum values for 360L001 and the envelopes for specific flight events. These plots show that the 360L001 maximum and minimum data are consistently too high at Station 556 of the left SRB. Station 1797 of both motors is slightly high, falling just outside the envelopes on several occasions.

Bending about the Z Axis

Figures 4.6.45 through 4.6.58 are plots of the maximum and minimum values for 360L001 and the envelopes for specific flight events. These plots show that the data follow the correct trend, but the magnitude is somewhat inaccurate.

Table 4.6-23. Time Ranges for Flight Events

Flight Event	Time Range (sec)
Prelaunch	-15.0 to -10.0
Buildup	-1.6 to -0.8
Lift-Off	0.5 to 4.0
Roll maneuver	7.0 to 18.0
Max Q	27.0 to 76.0
Max G	72.0 to 90.0
Preseparation	119.0 to 124.0

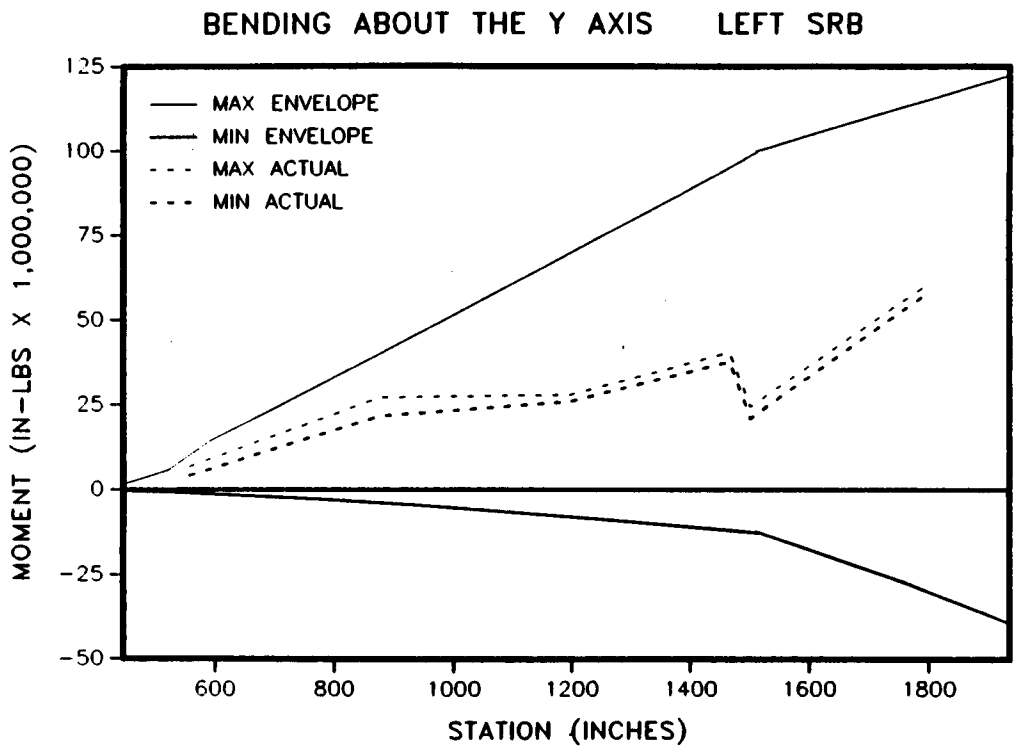

Figure 4.6-31. 360L001 Prelaunch Envelope

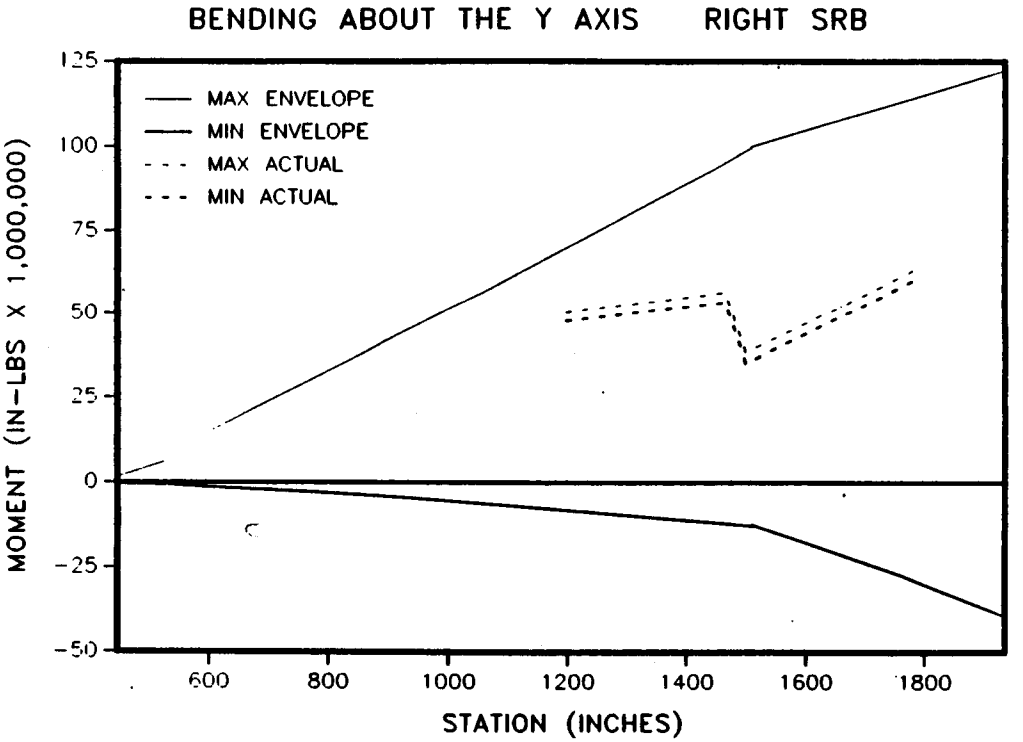

Figure 4.6-32. 360L001 Prelaunch Envelope

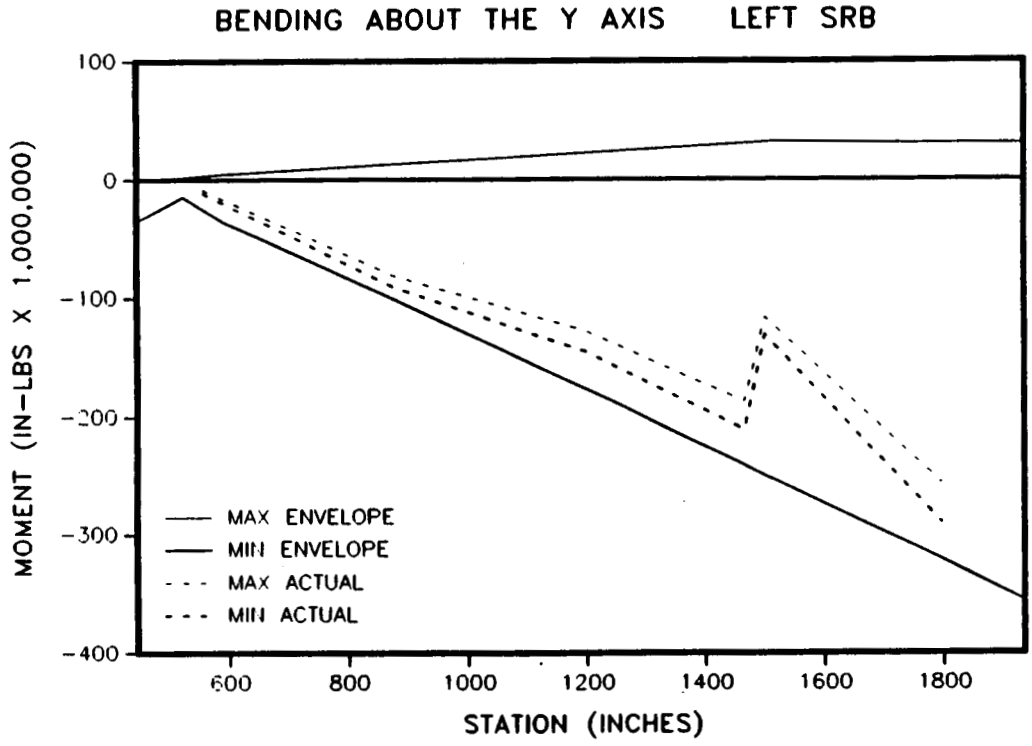

Figure 4.6-33. 360L001 Buildup Envelope

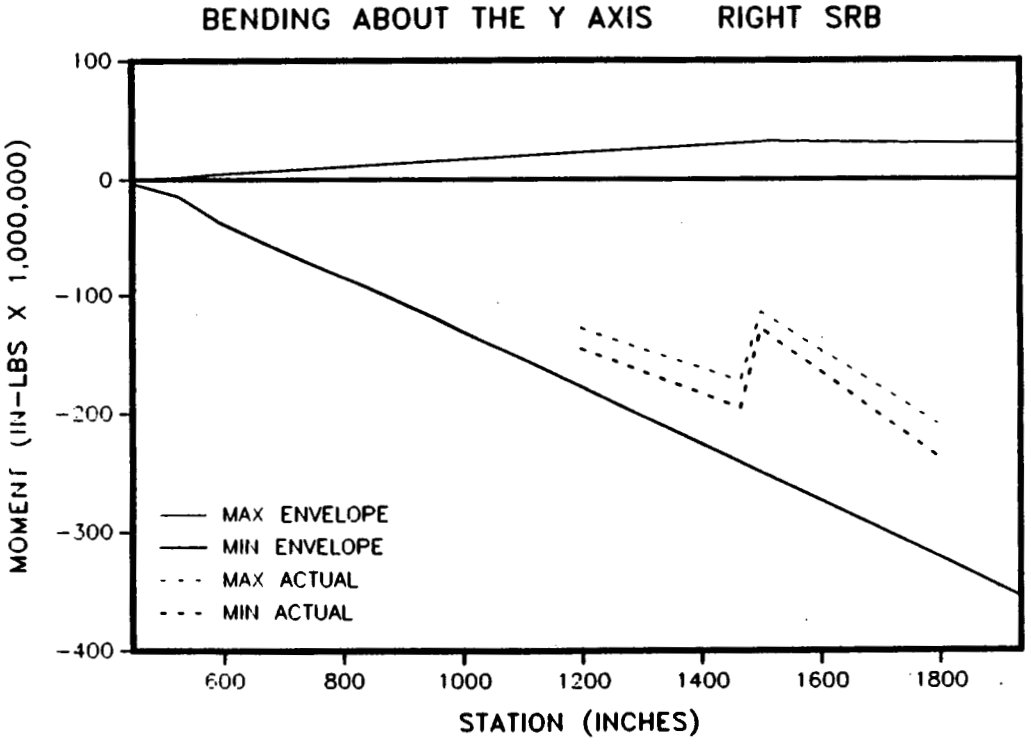

Figure 4.6-34. 360L001 Buildup Envelope

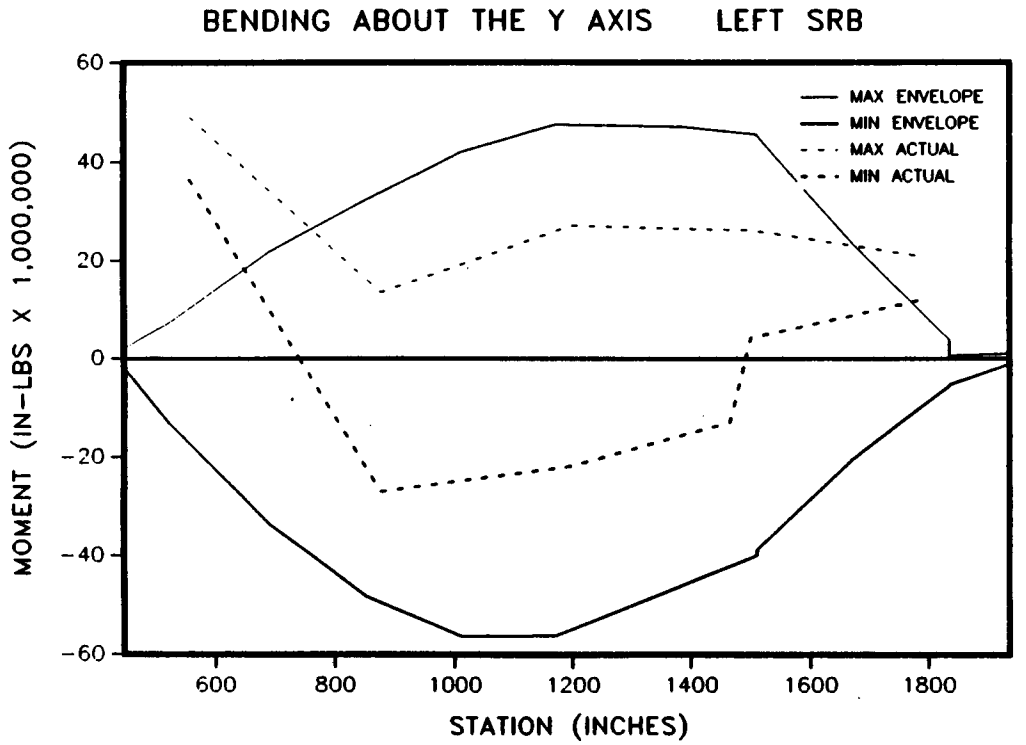

Figure 4.6-35. 360L001 Lift-Off Envelope

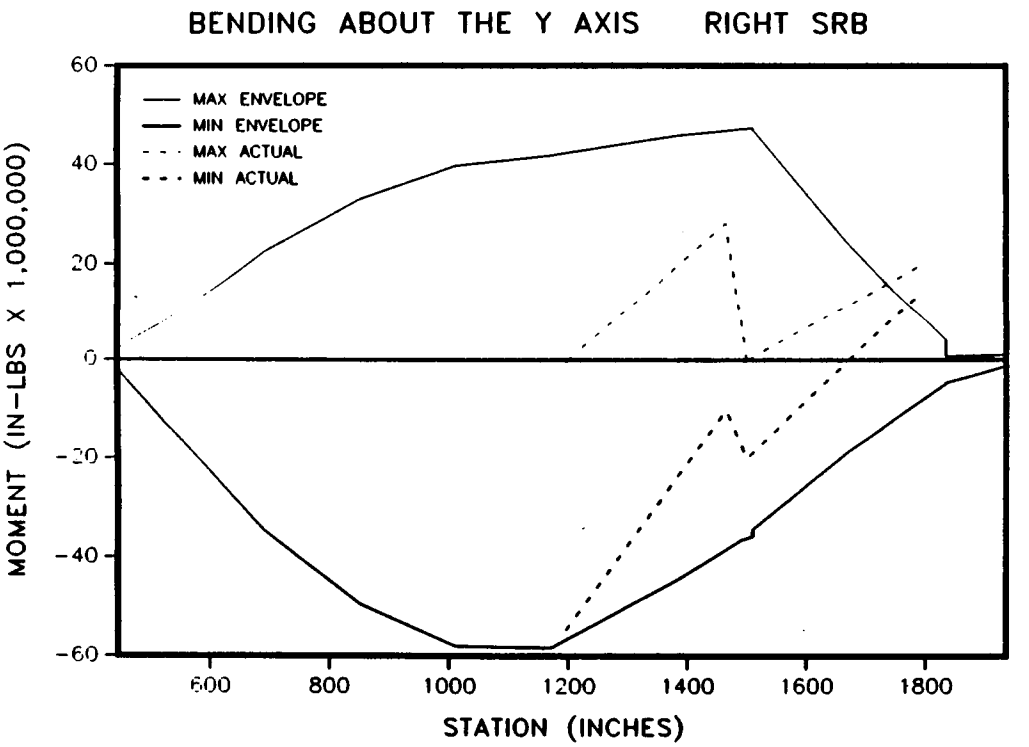

Figure 4.6-36. 360L001 Lift-Off Envelope

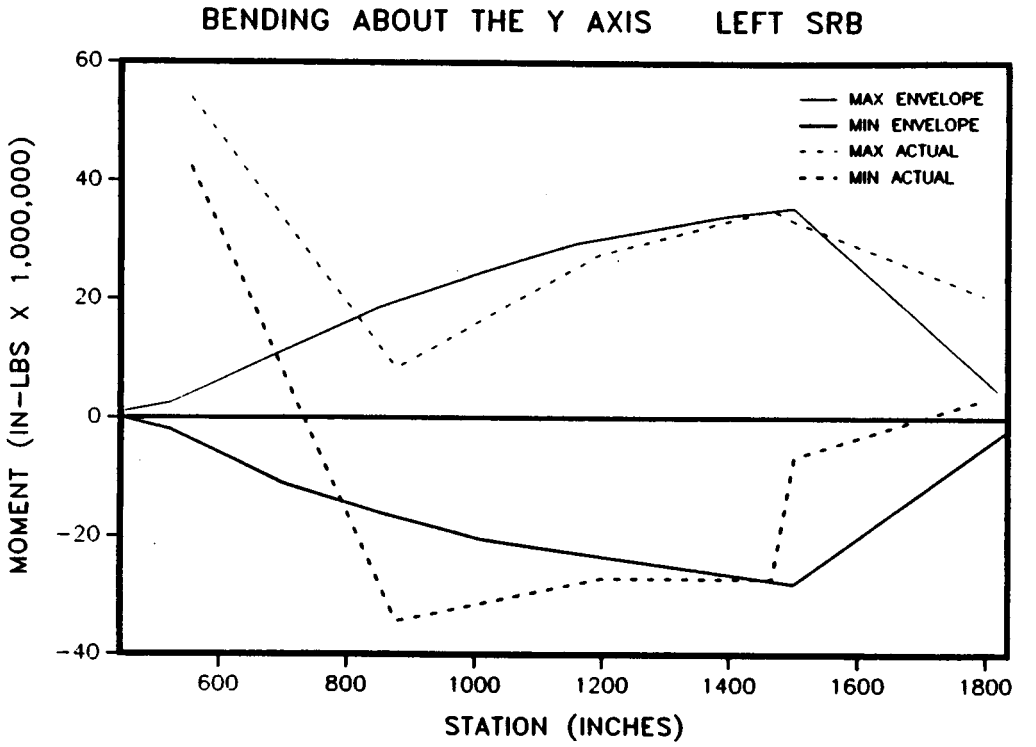

Figure 4.6-37. 360L001 Roll Envelope

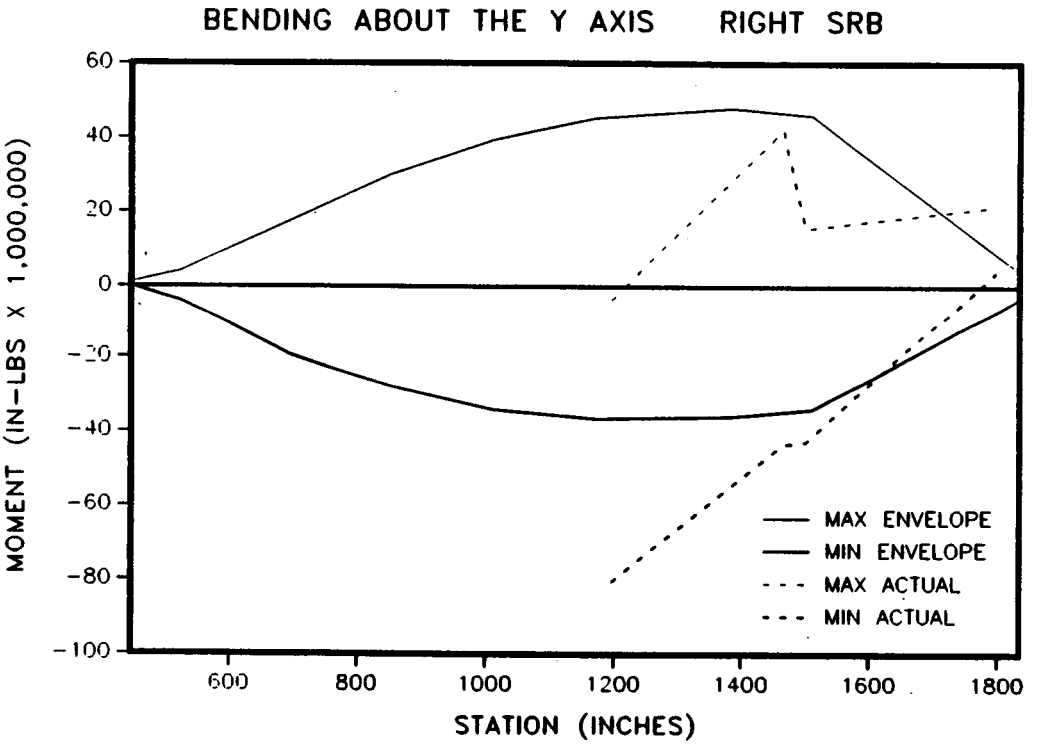

Figure 4.6-38. 360L001 Roll Envelope

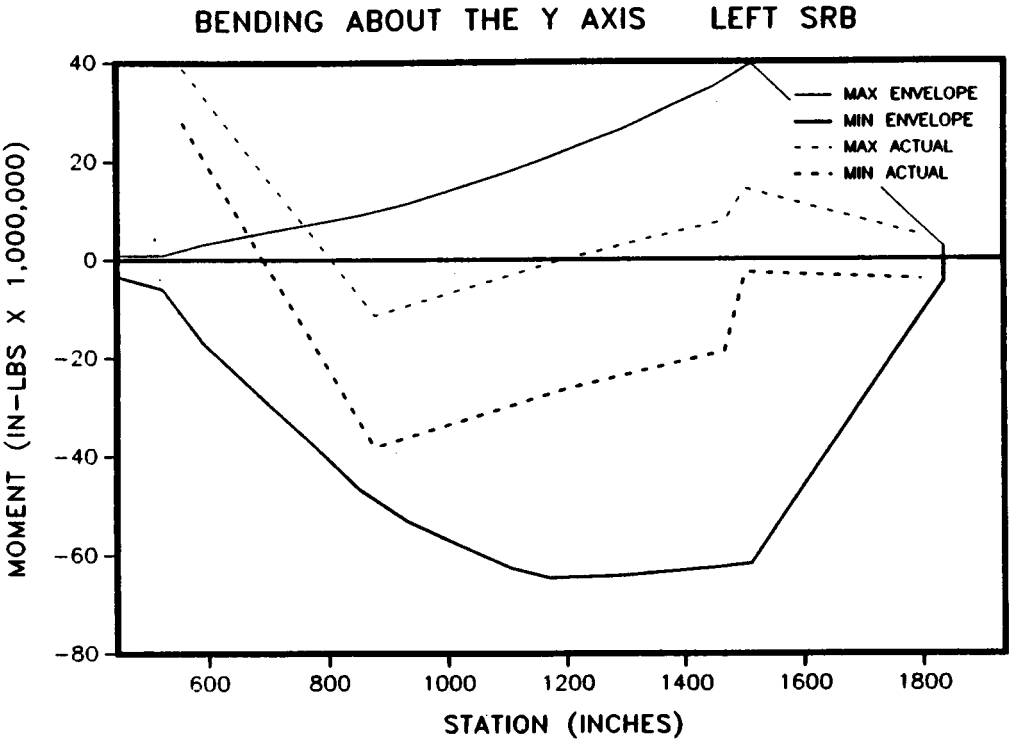

Figure 4.6-39. 360L001 Maximum Q Envelope

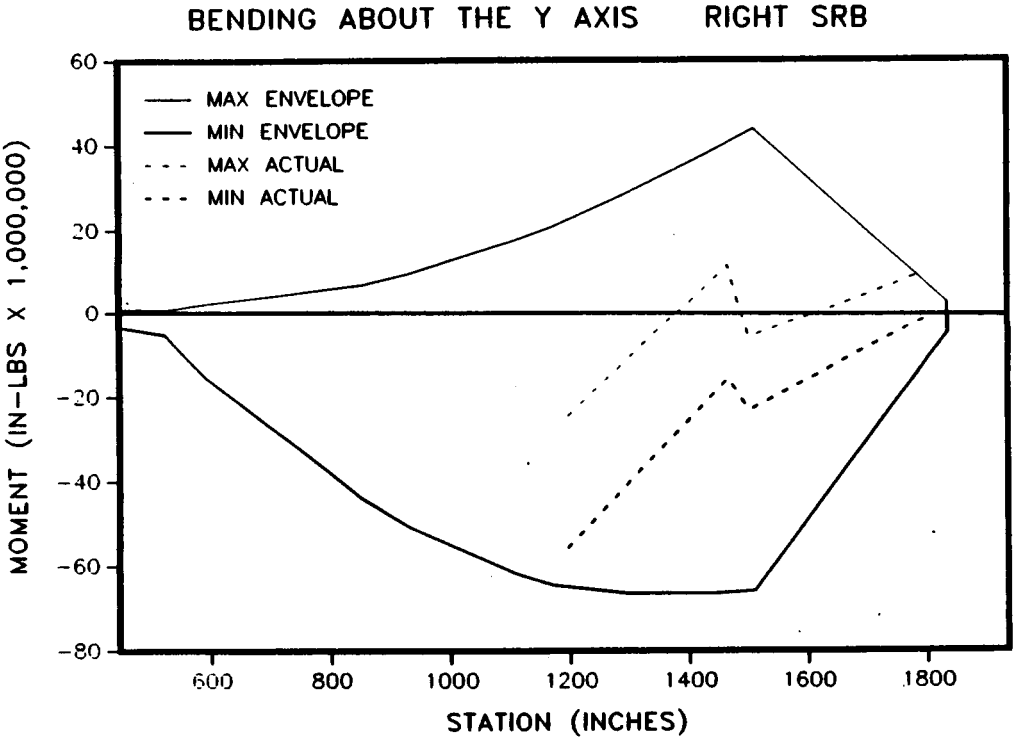

Figure 4.6-40. 360L001 Maximum Q Envelope

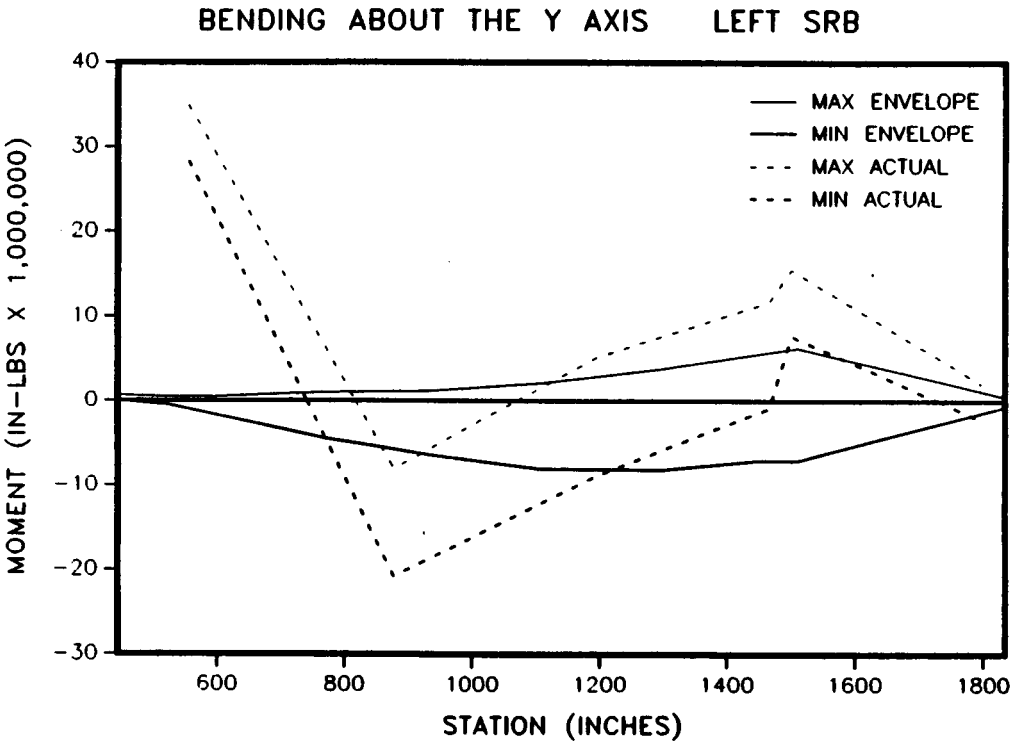

Figure 4.6-41. 360L001 Maximum G Envelope

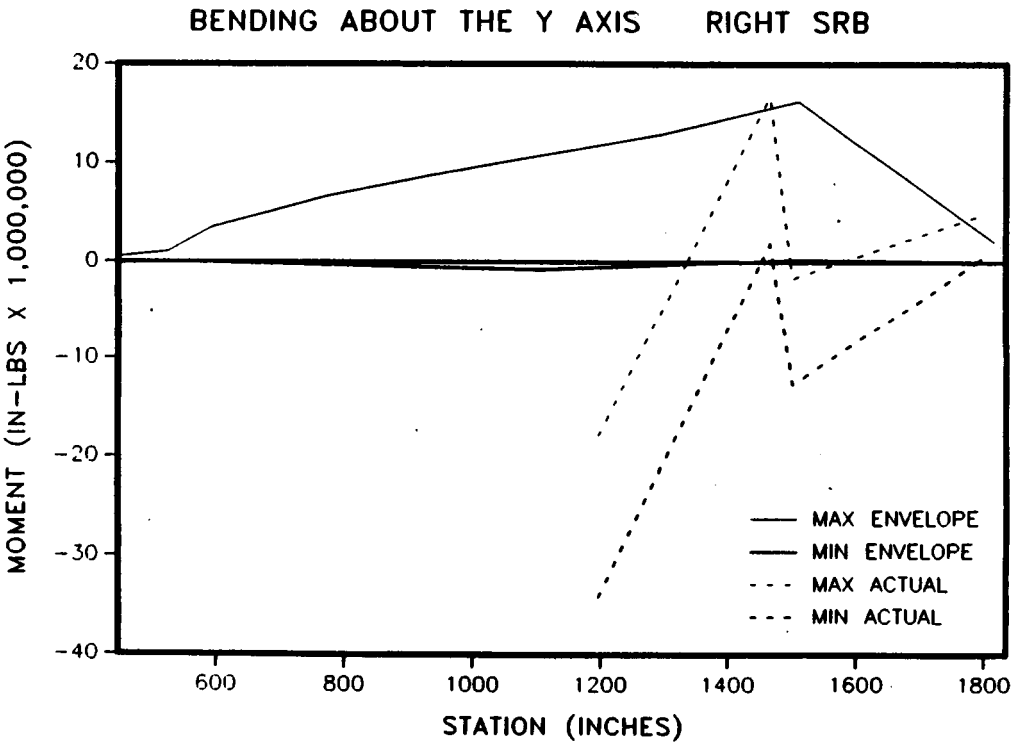

Figure 4.6-42. 360L001 Maximum G Envelope

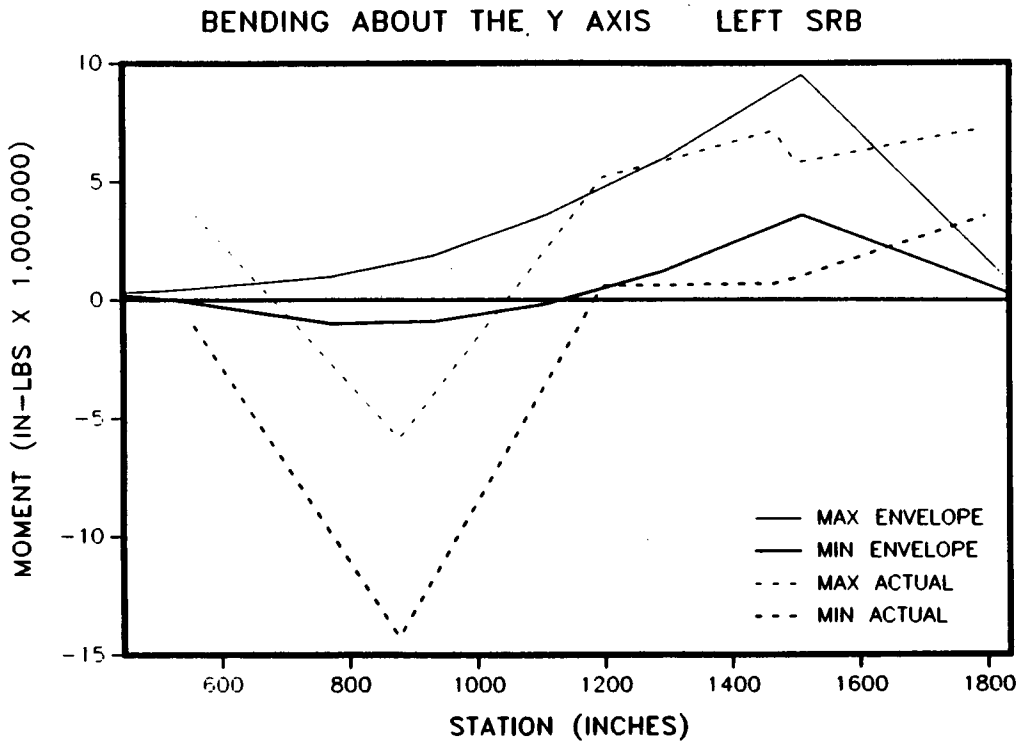

Figure 4.6-43. 360L001 Prestaging Envelope

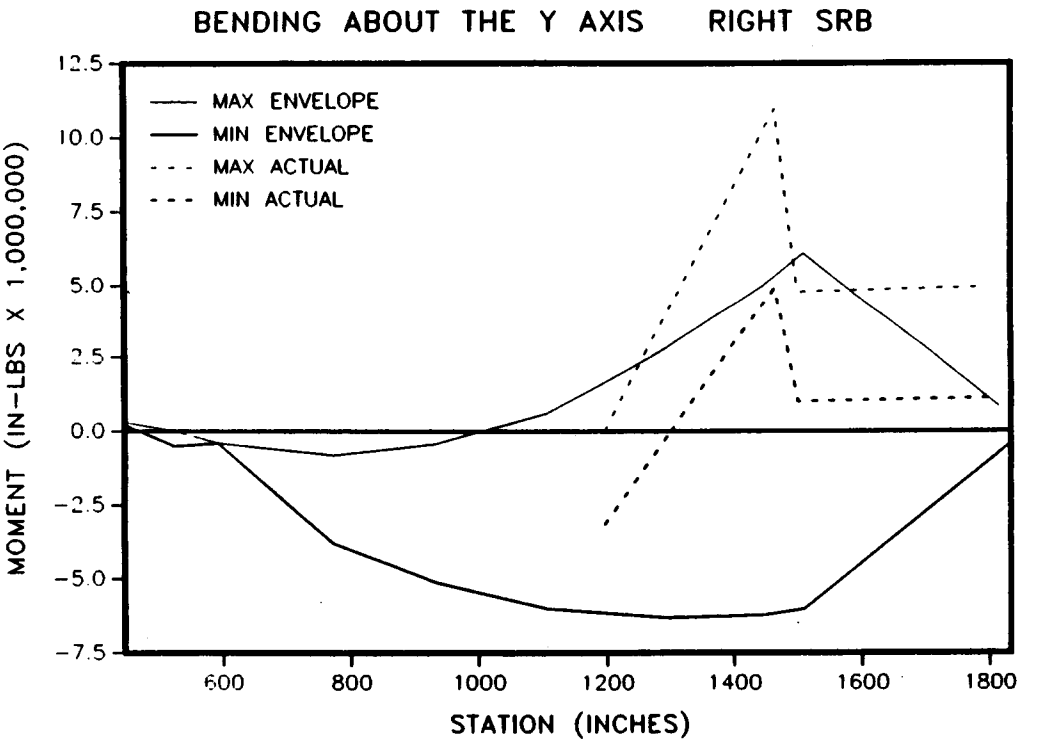

Figure 4.6-44. 360L001 Prestaging Envelope

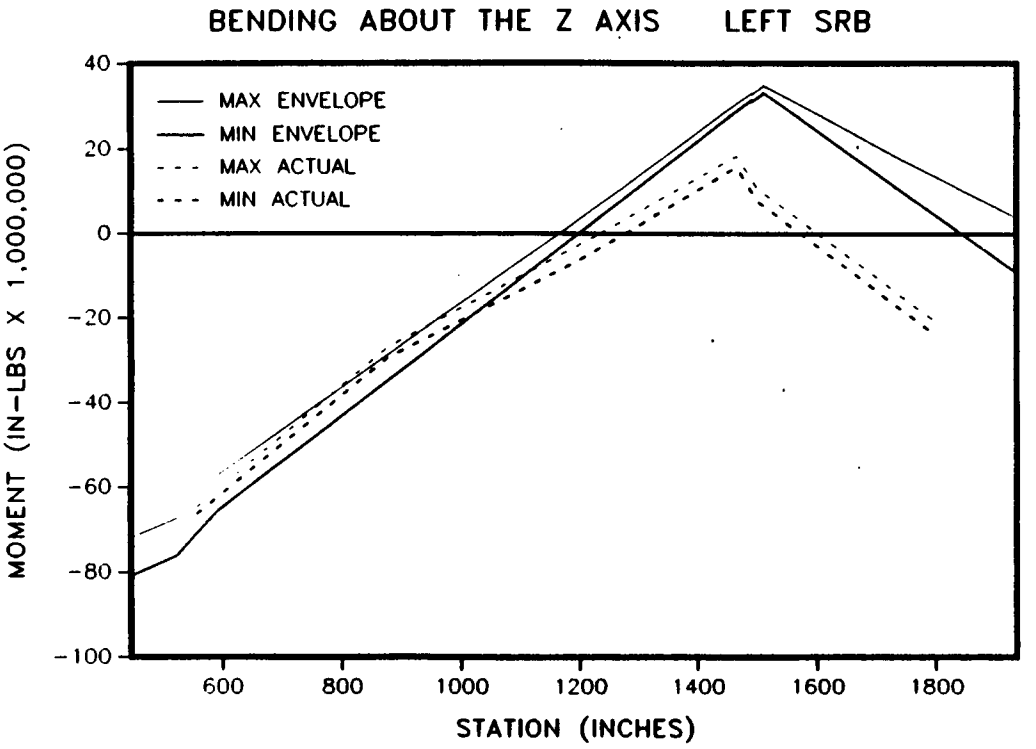

Figure 4.6-45. 360L001 Prelaunch Envelope

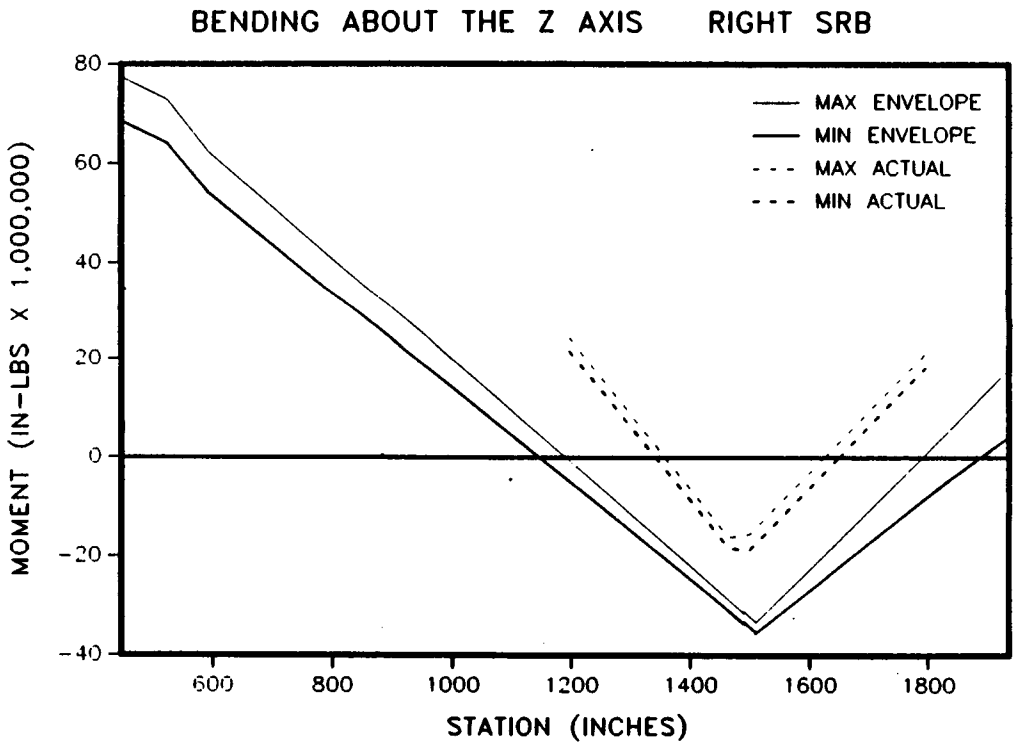

Figure 4.6-46. 360L001 Prelaunch Envelope

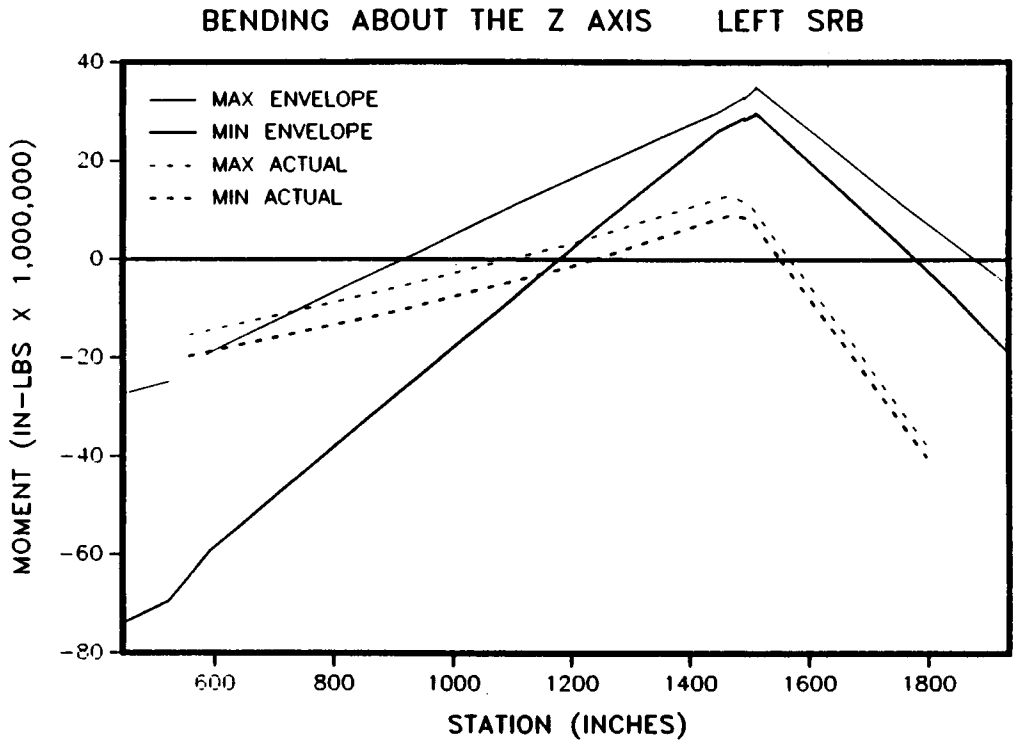

Figure 4.6-47. 360L001 Buildup Envelope

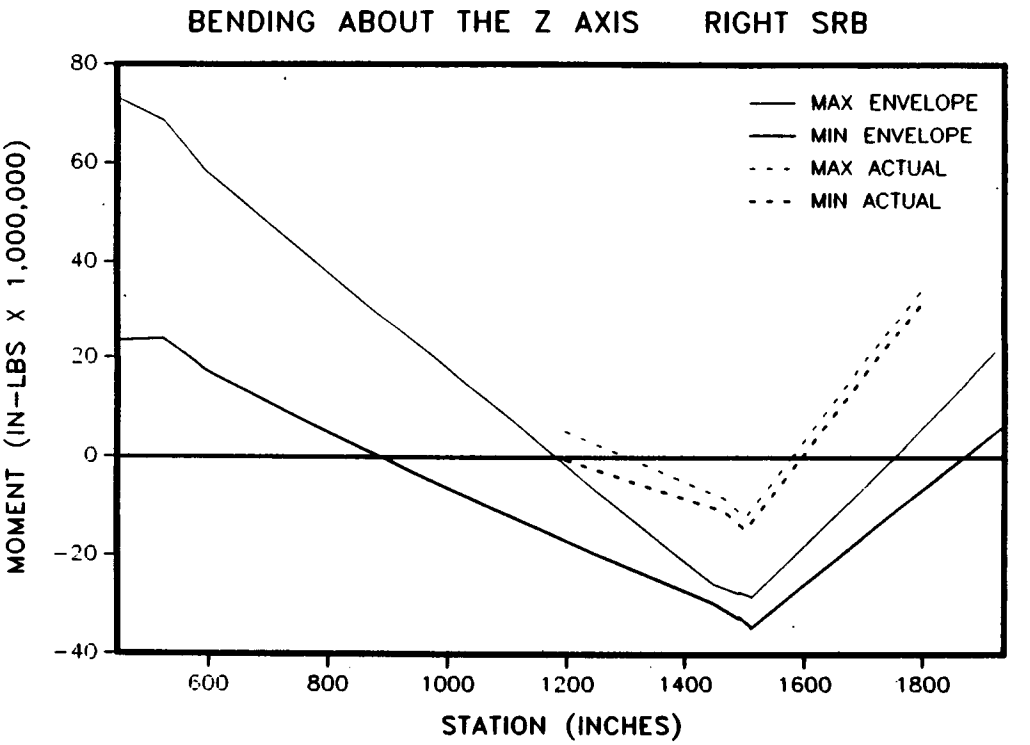

Figure 4.6-48. 360L001 Buildup Envelope

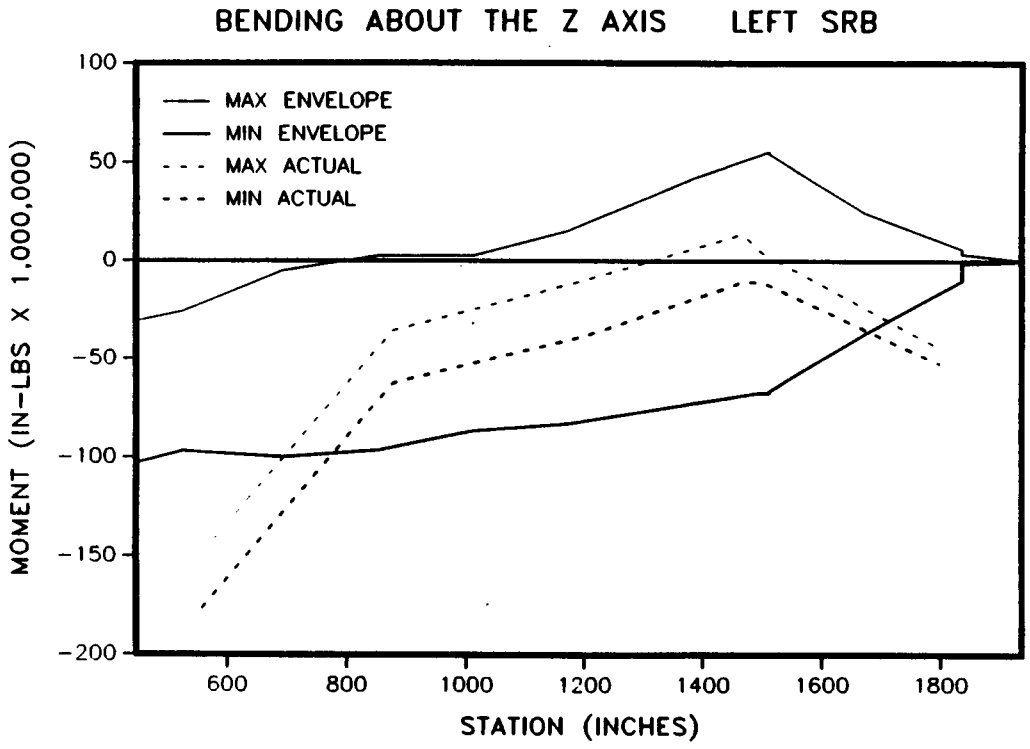

Figure 4.6-49. 360L001 Lift-Off Envelope

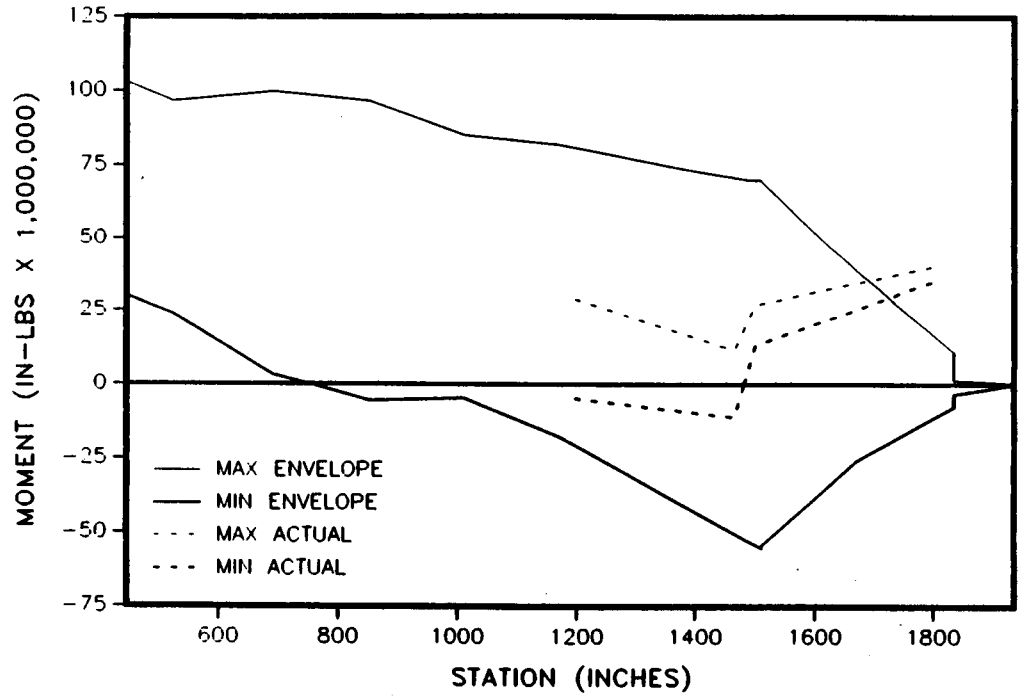

Figure 4.6-50. 360L001 Lift-Off Envelope

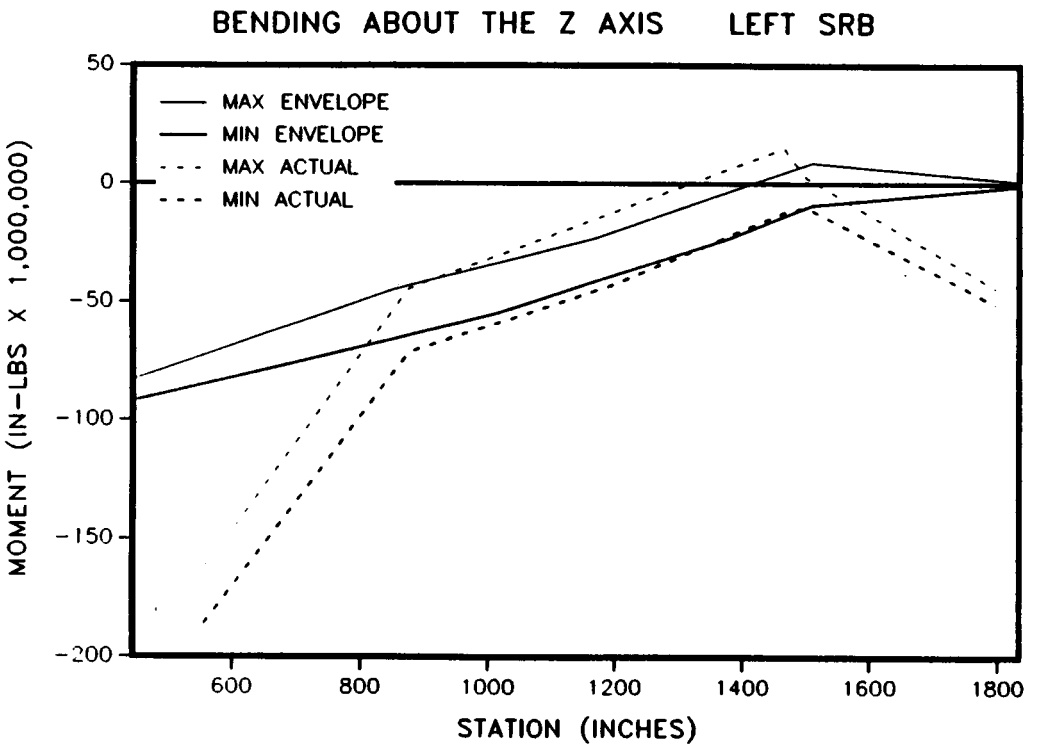

Figure 4.6-51. 360L001 Roll Envelope

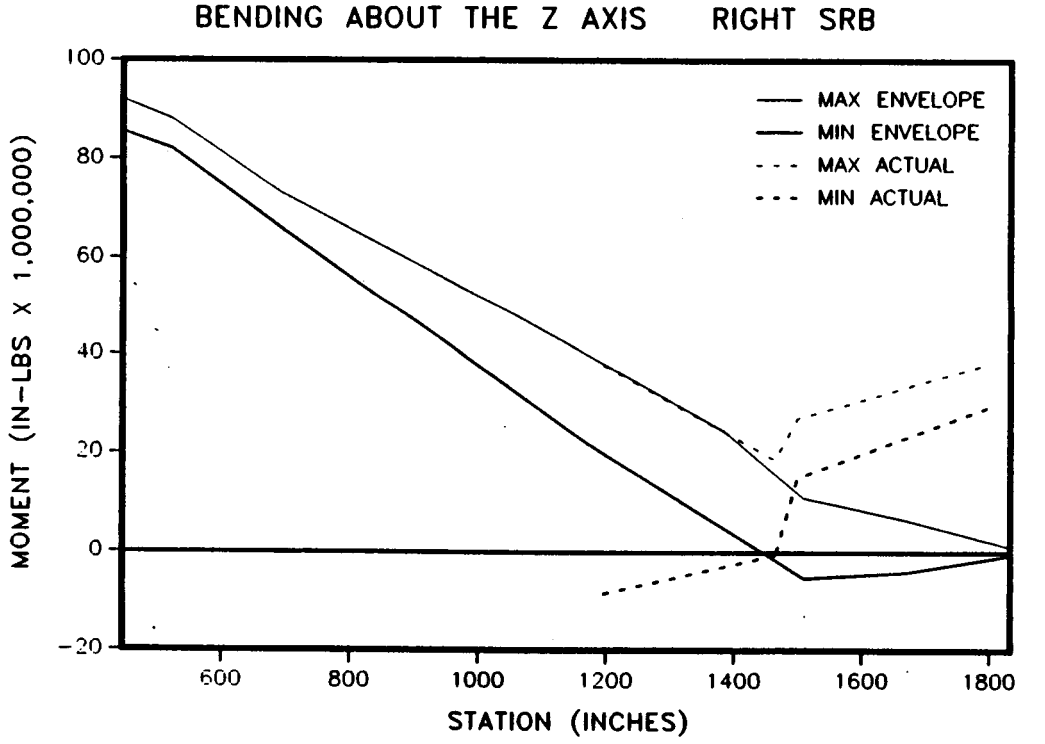

Figure 4.6-52. 360L001 Roll Envelope

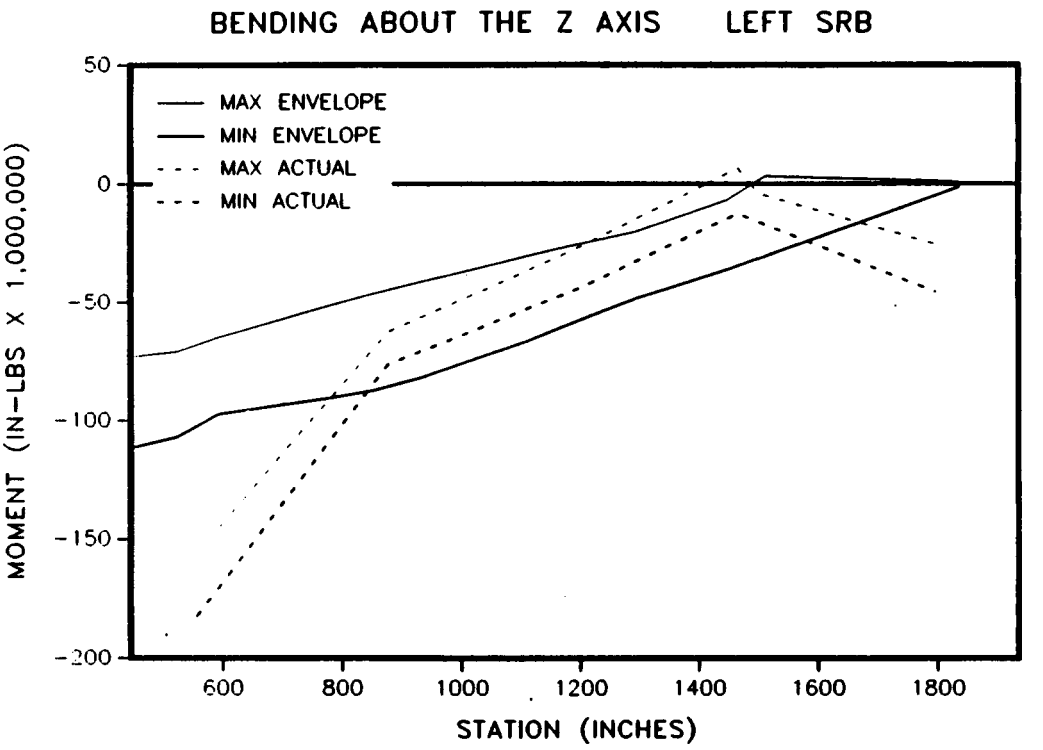

Figure 4.6-53. 360L001 Maximum Q Envelope

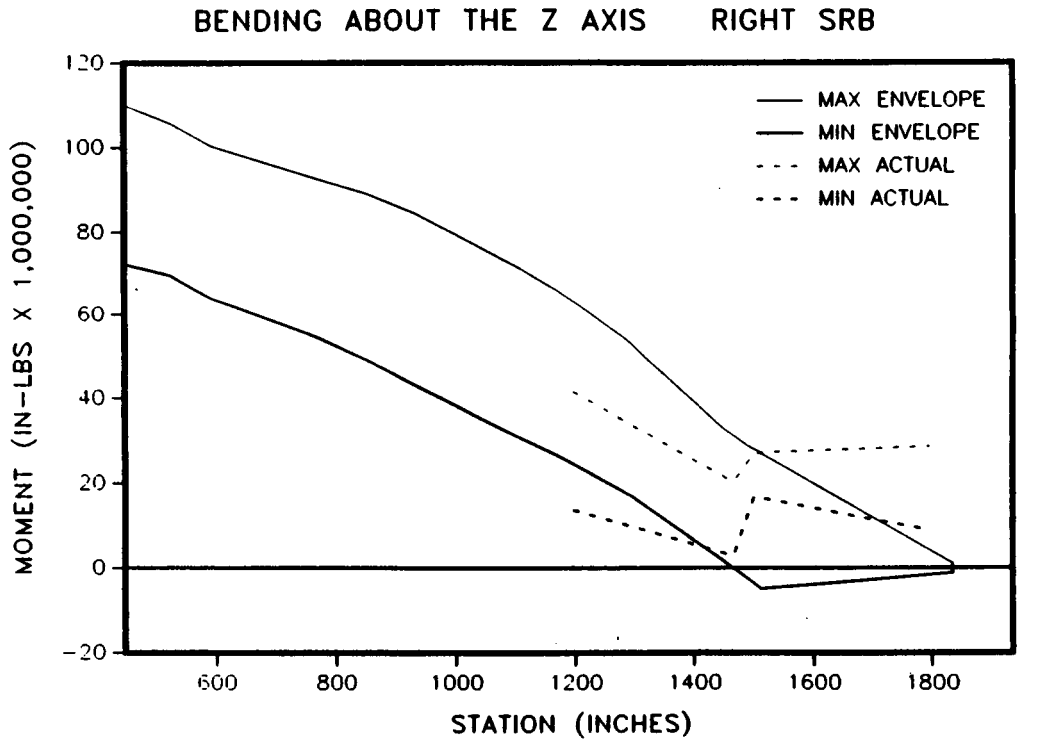

Figure 4.6-54. 360L001 Maximum Q Envelope

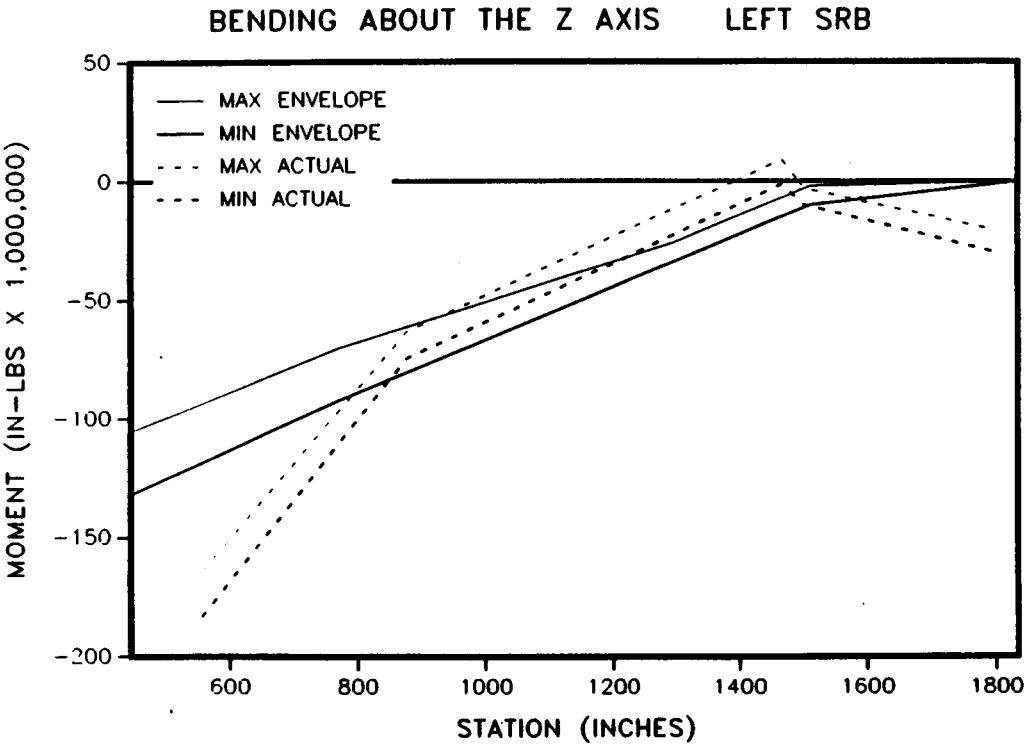

Figure 4.6-55. 360L001 Maximum G Envelope

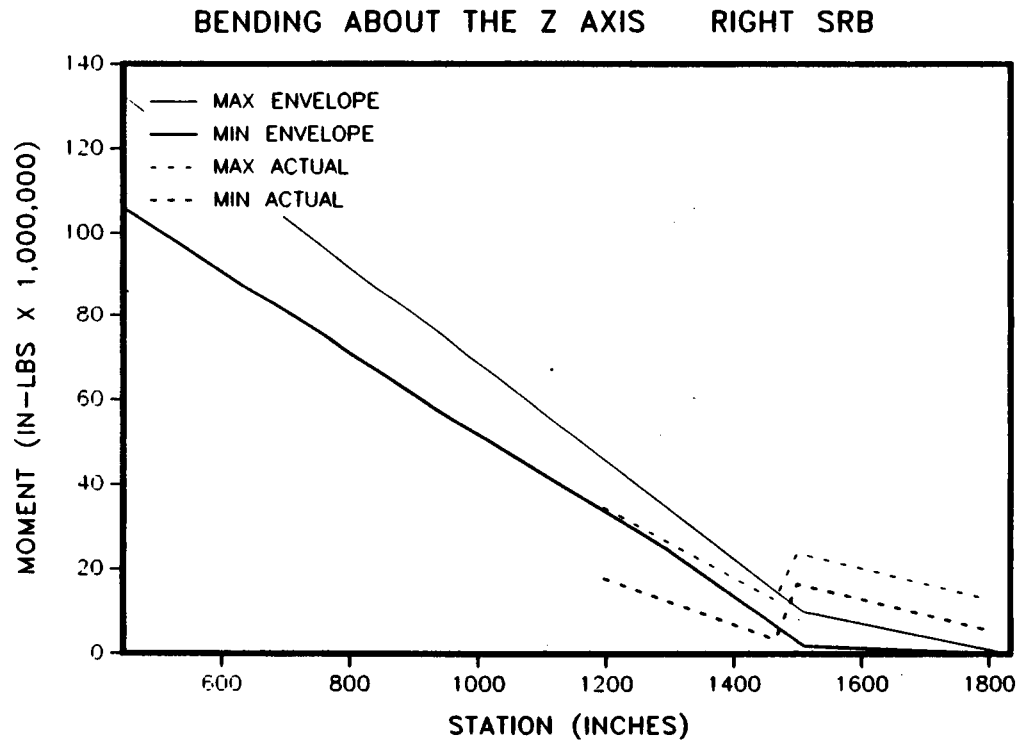

Figure 4.6-56. 360L001 Maximum G Envelope

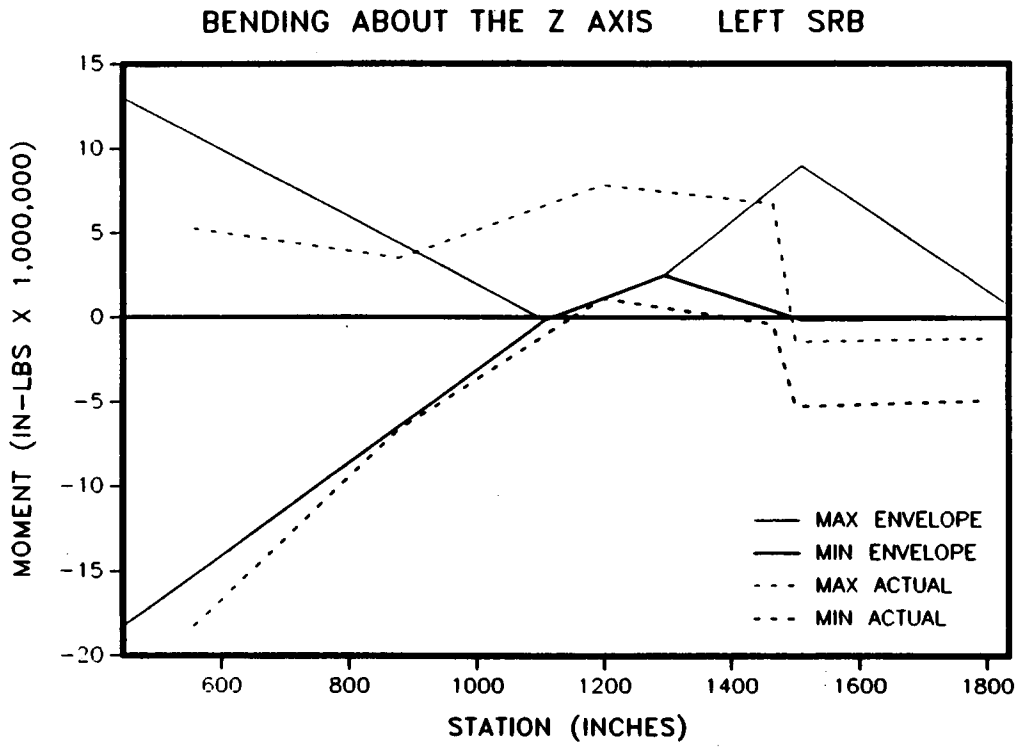

Figure 4.6-57. 360L001 Prestaging Envelope

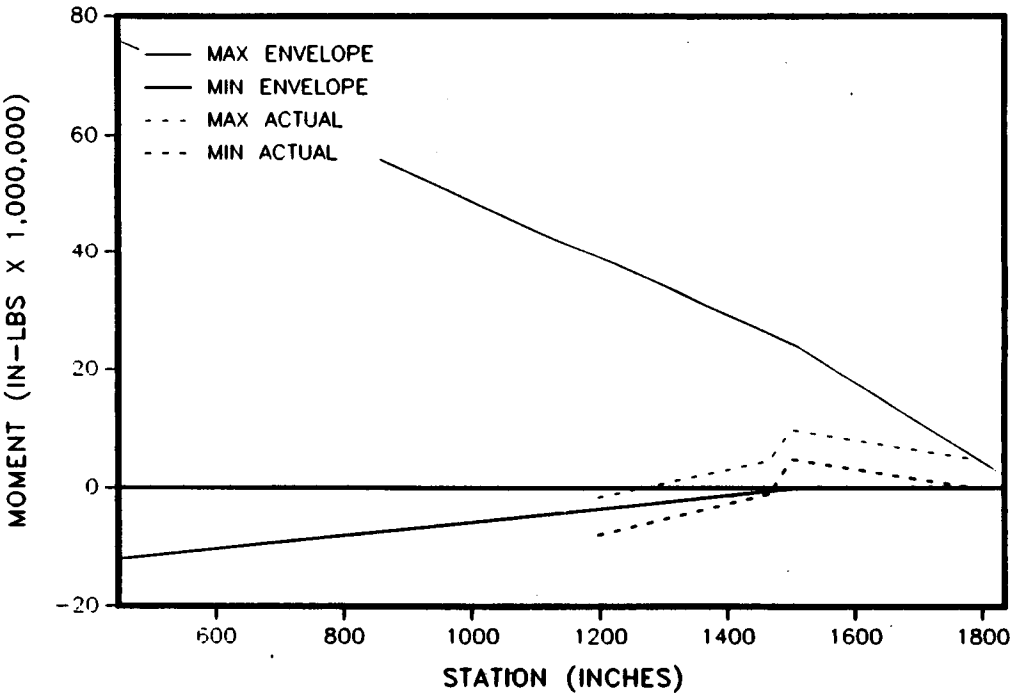

Figure 4.6-58. 360L001 Prestaging Envelope

Axial Force

Figures 4.6.59 through 4.6.72 show the axial force envelopes and the 360L001 data plotted as a function of station. Figure 4.6.59 shows that the loading does increase with progression, but not as linearly as expected. Station 1501 shows a marked decrease in loading (as also seen with the bending about the Y and Z axis) which is due to the increased case thickness in this region. With the exception of prelaunch, buildup, and shuttle roll maneuver, these data are very near the envelopes.

4.6.3.7 Strut Forces. Figures 4.6.73 and 4.6.74 present the resultant strut force in the Y and Z directions, respectively, showing that the data start and end at approximately the same position, and that the resultant Y booster forces are approximately equal and opposite. (The left SRB shows a positive value while the right SRB shows a negative value.) The resultant Z force shows that the right SRB experiences about 900 kips more force than the left SRB. The reason for this has not yet been determined.

4.7 SRM STRUCTURAL DYNAMICS

This section corresponds with FEWG report Section 2.6.2.

4.7.1 Objectives

The objectives of the structural dynamics section were to verify the predicted behavior of the SRM during preflight, lift-off, and flight with respect to accelerations, and to determine if any abnormal vibrations existed. Verification of the analytical techniques utilized for SRM prediction behavior, as well as examination of the SRM random vibration environment were also objectives.

4.7.2 Flight Instrumentation

The specifics of the accelerometers used for data acquisition are summarized as follows:

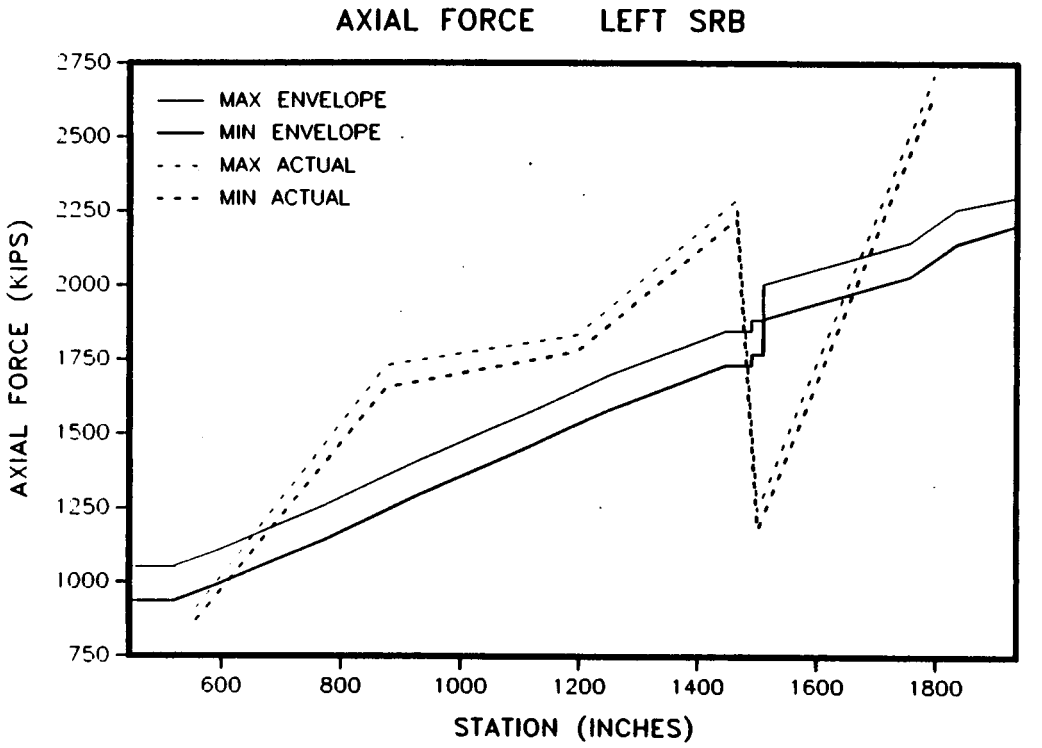

Figure 4.6-59. 360L001 Prelaunch Envelope

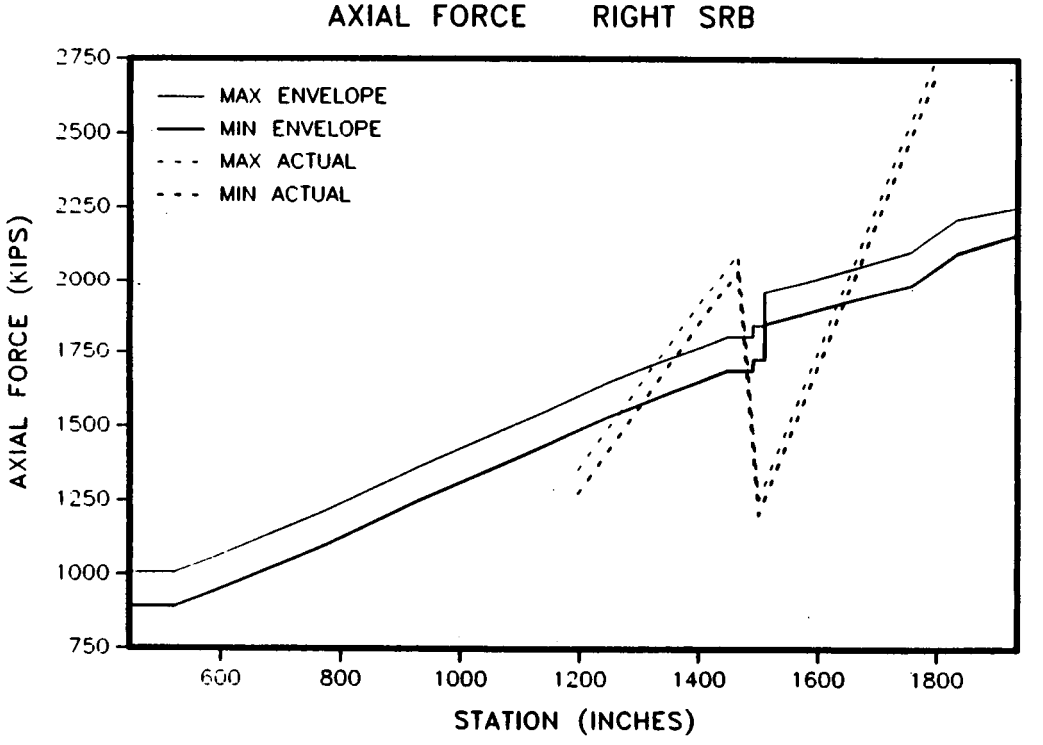

Figure 4.6-60. 360L001 Prelaunch Envelope

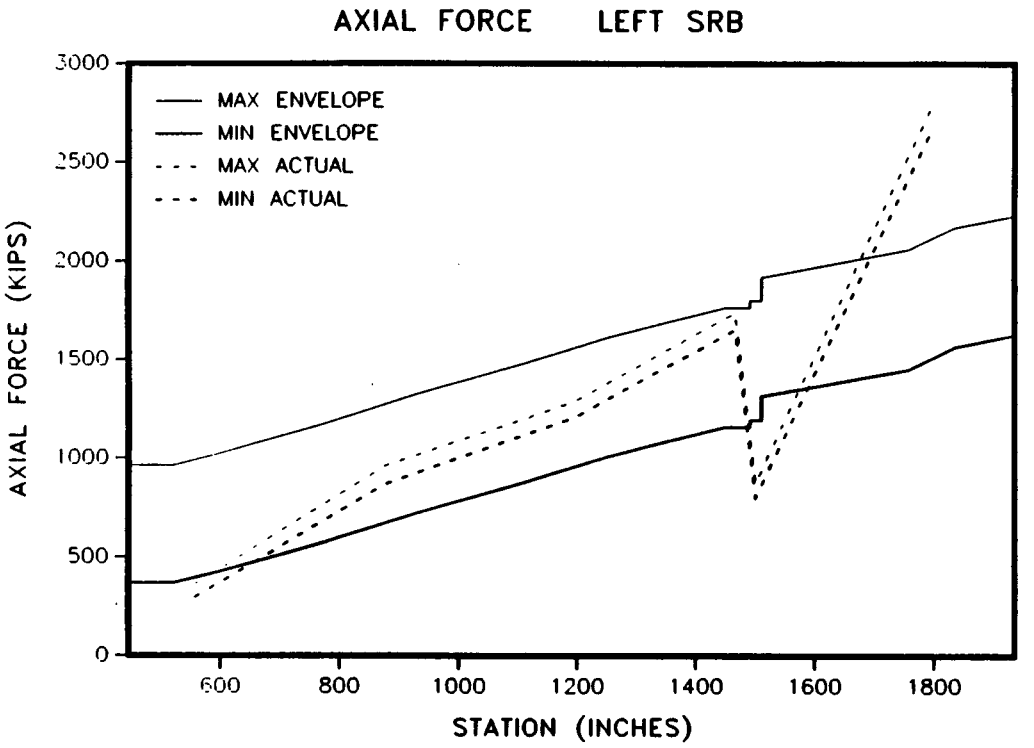

Figure 4.6-61. 360L001 Buildup Envelope

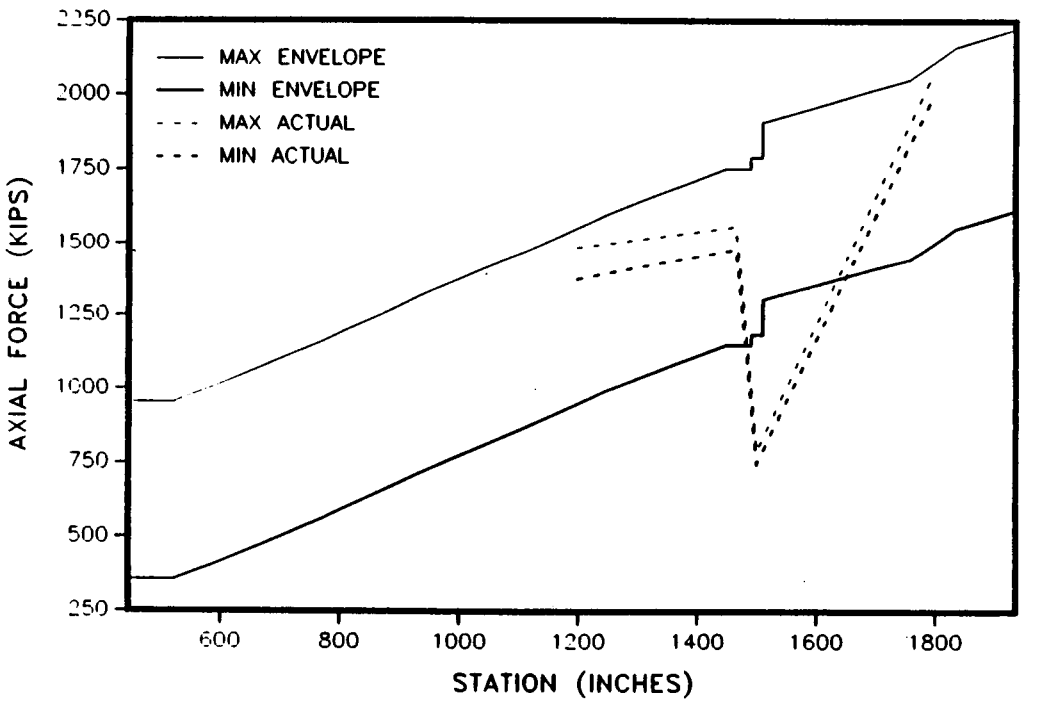

Figure 4.6-62. 360L001 Buildup Envelope

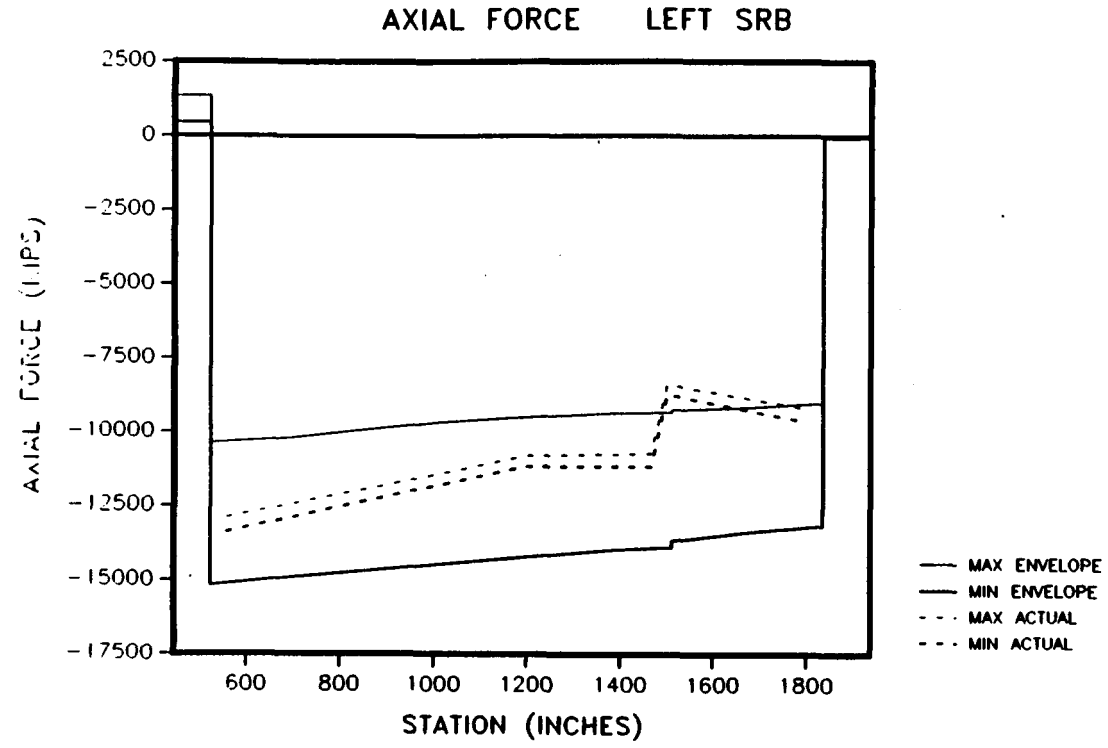

Figure 4.6-63. 360L001 Lift-Off Envelope

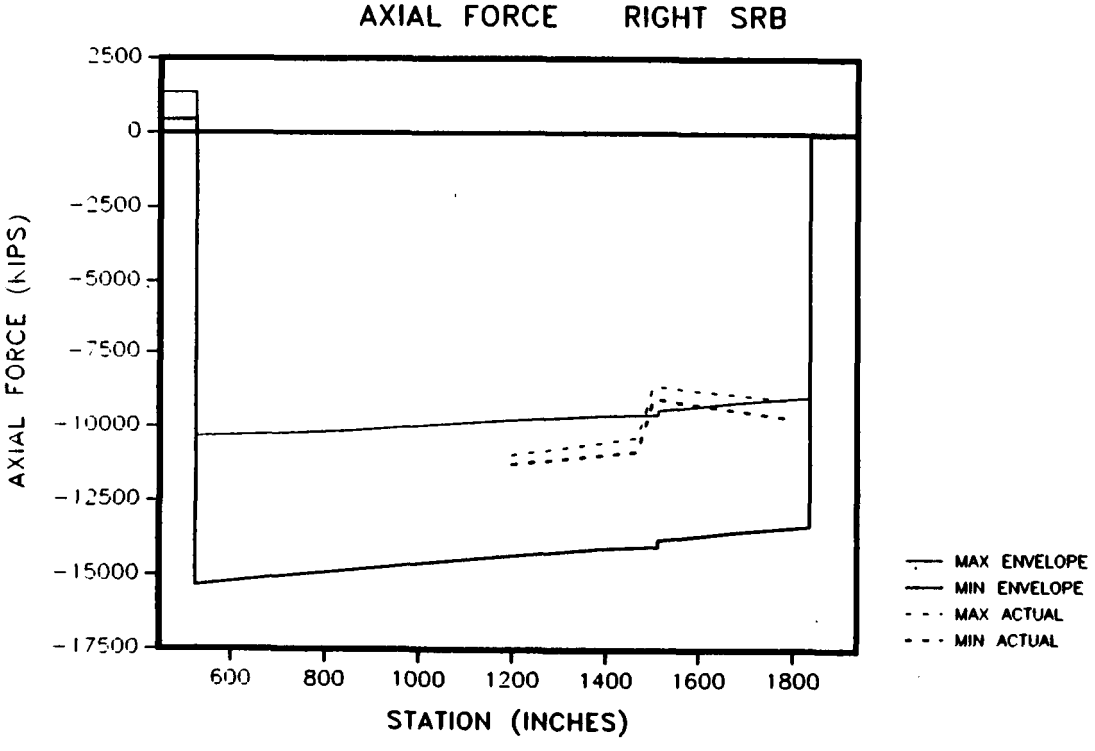

Figure 4.6-64. 360L001 Lift-Off Envelope

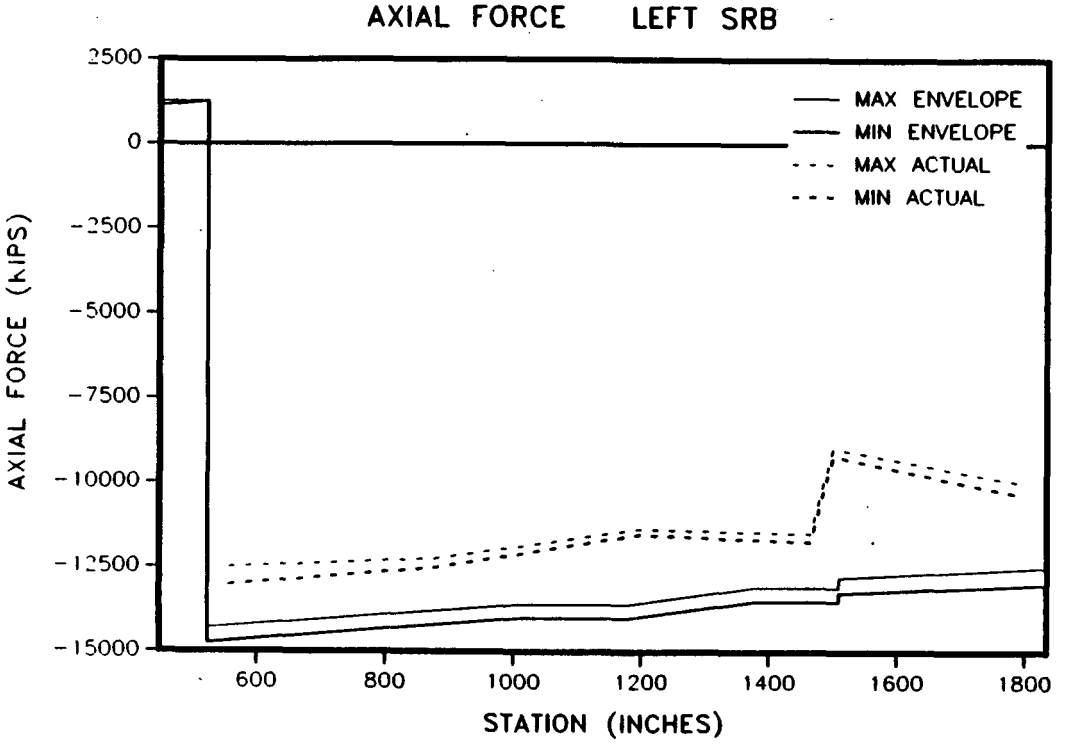

Figure 4.6-65. 360L001 Roll Envelope

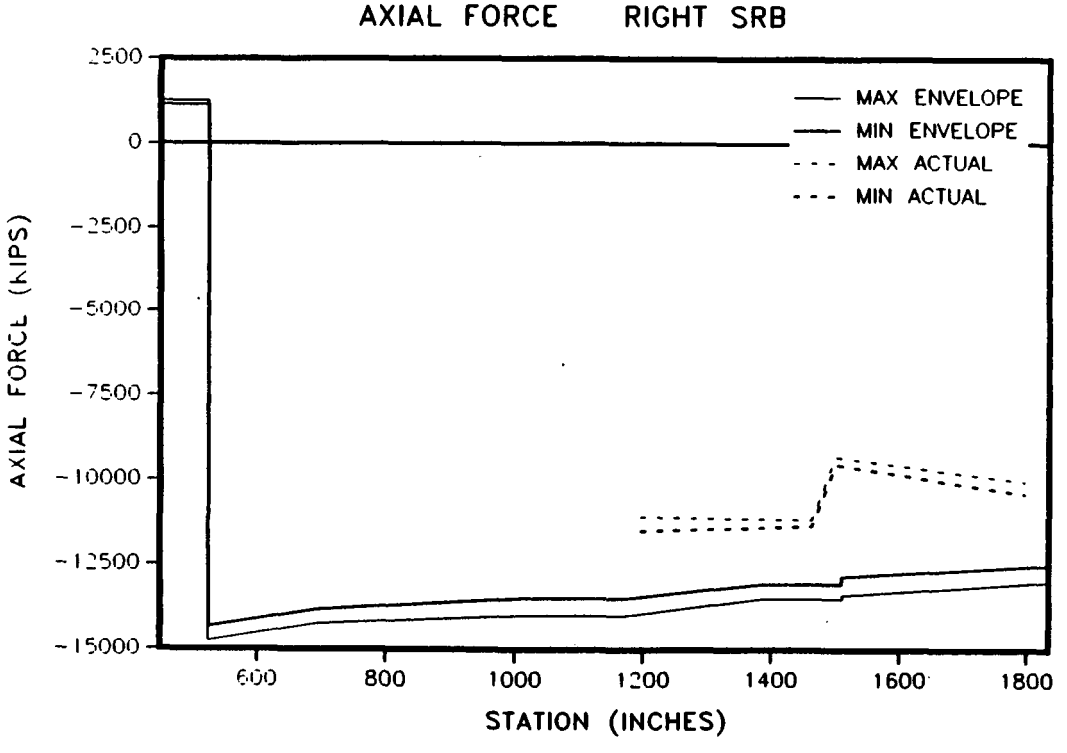

Figure 4.6-66. 360L001 Roll Envelope

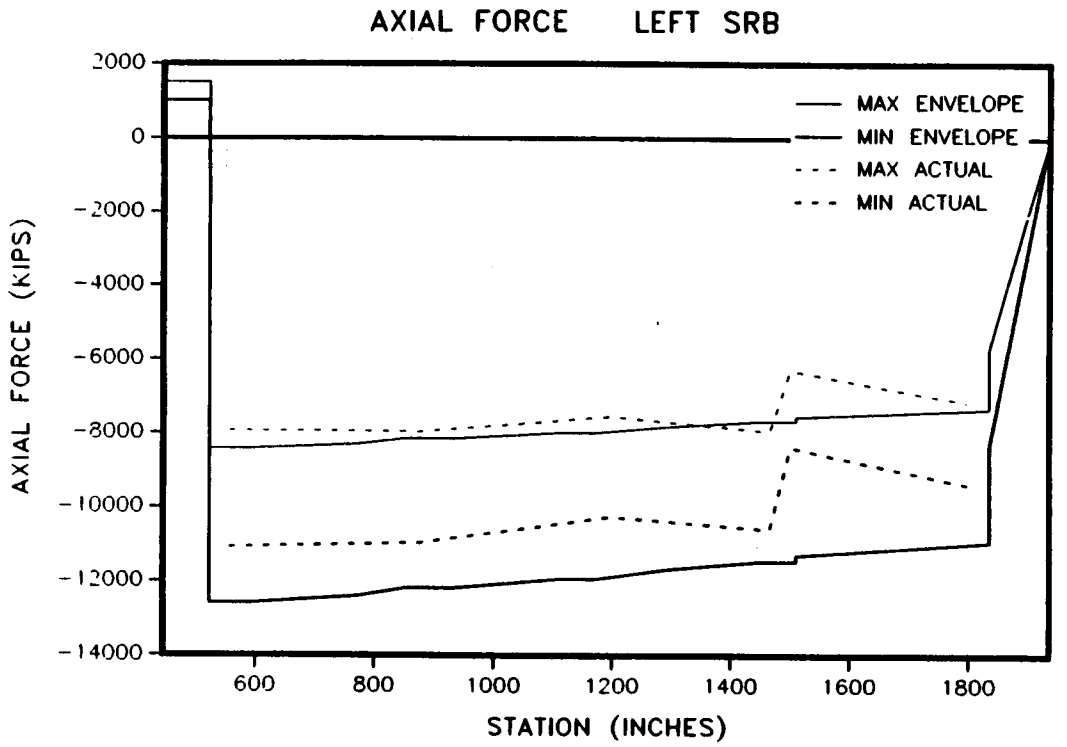

Figure 4.6-67. 360L001 Maximum Q Envelope

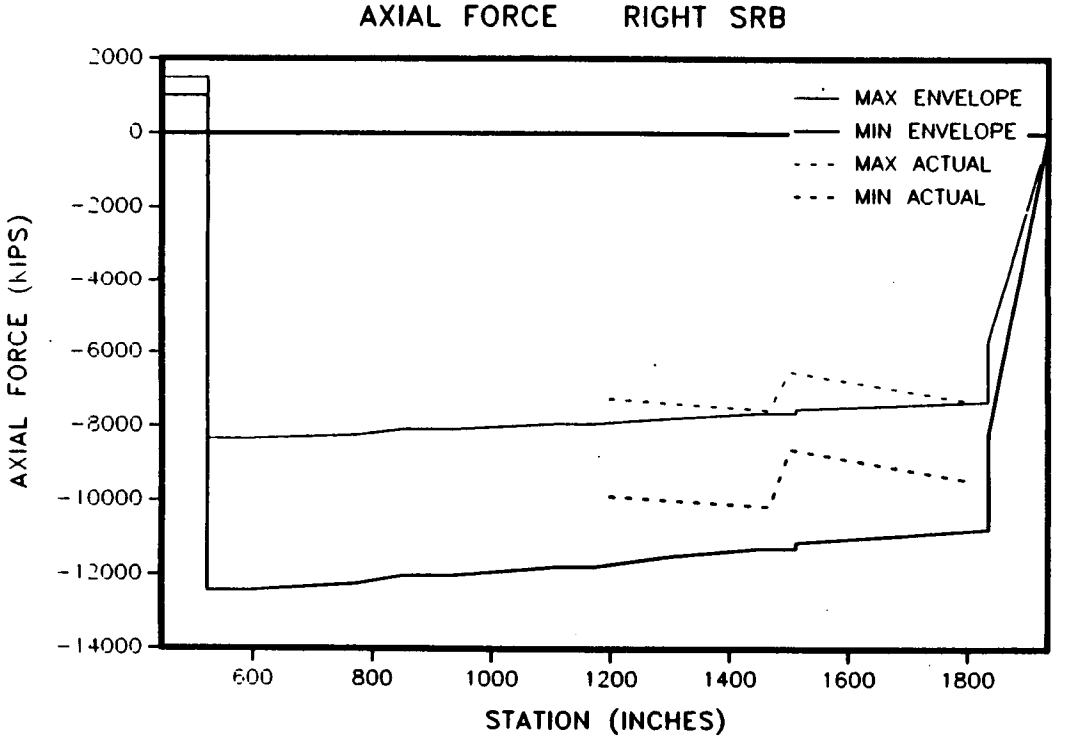

Figure 4.6-68. 360L001 Maximum Q Envelope

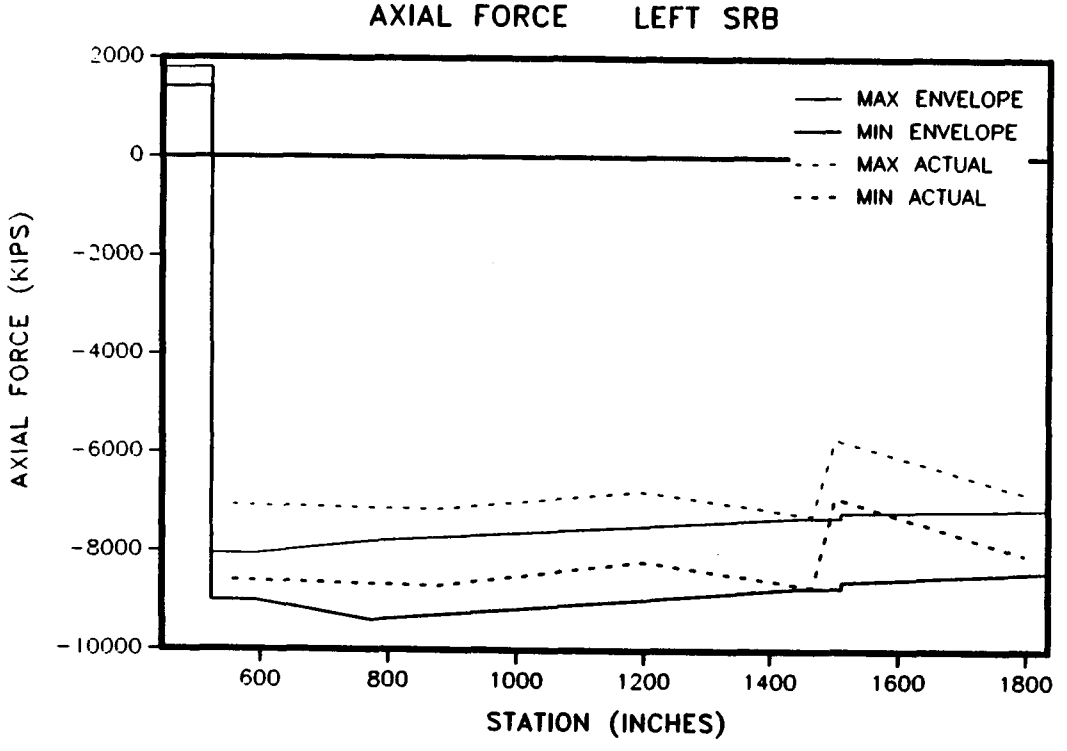

Figure 4.6-69. 360L001 Maximum G Envelope

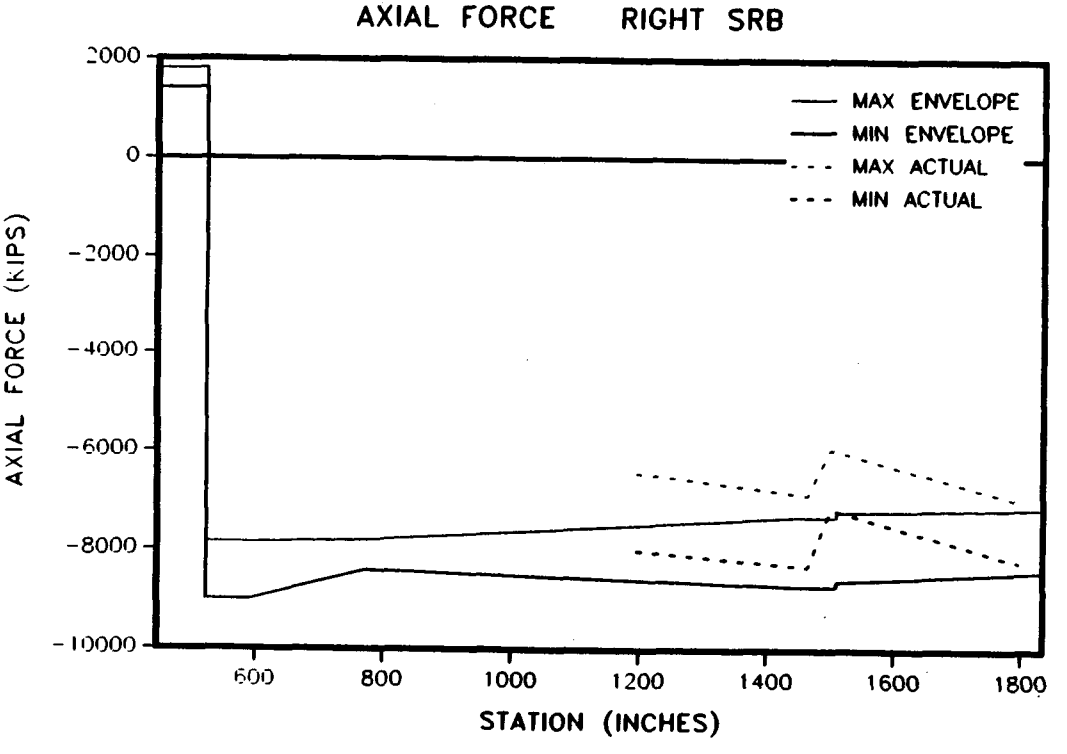

Figure 4.6-70. 360L001 Maximum G Envelope

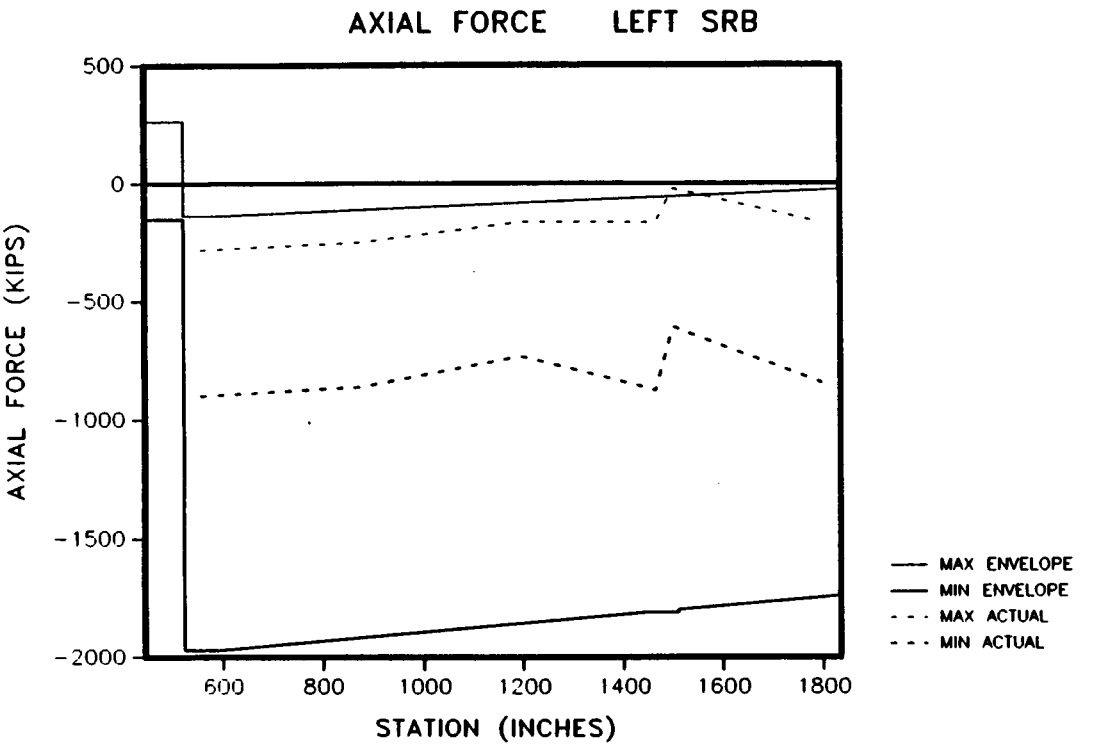

Figure 4.6-71. 360L001 Prestaging Envelope

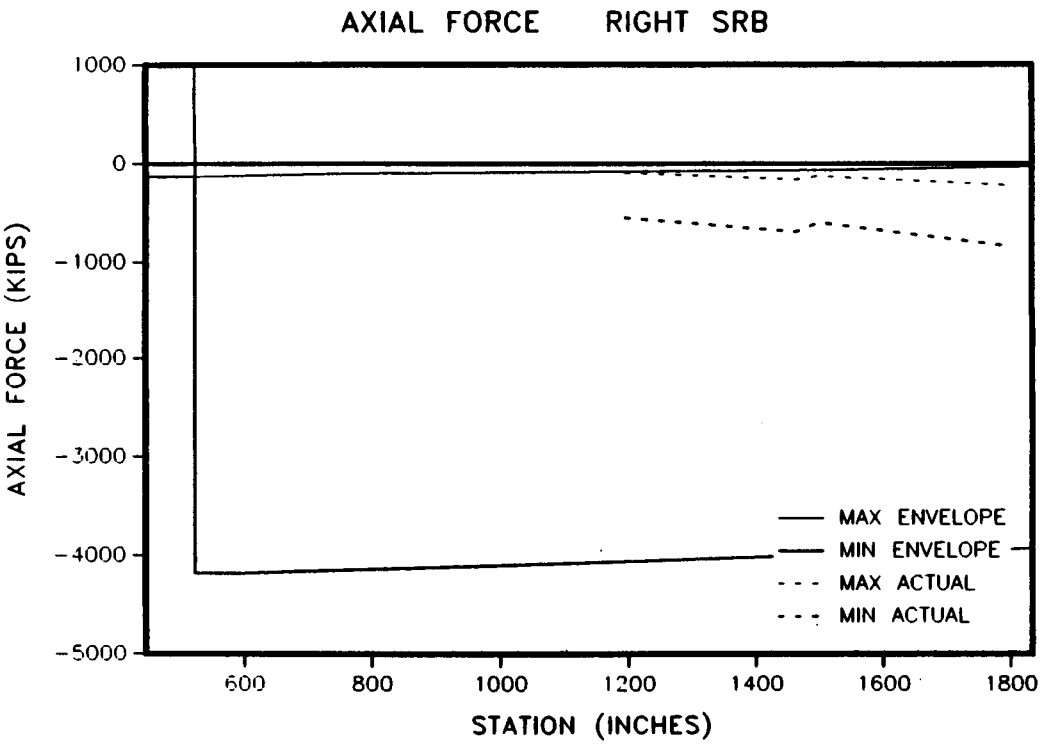

Figure 4.6-72. 360L001 Prestaging Envelope

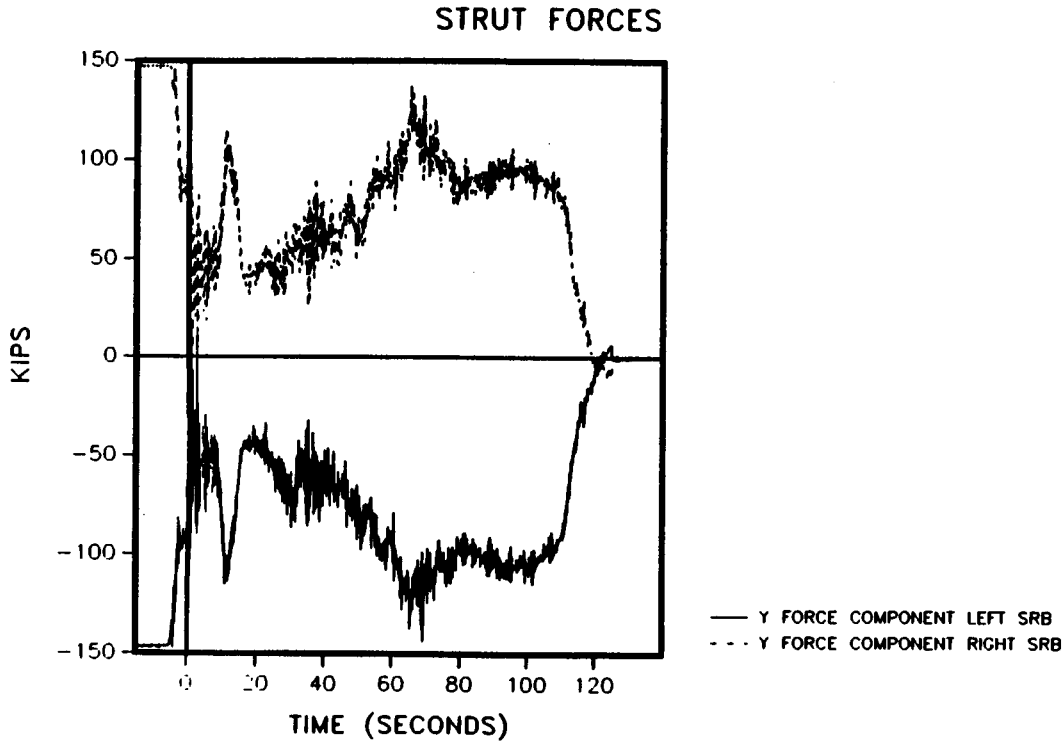

Figure 4.6-73. 360L001 Strut Forces

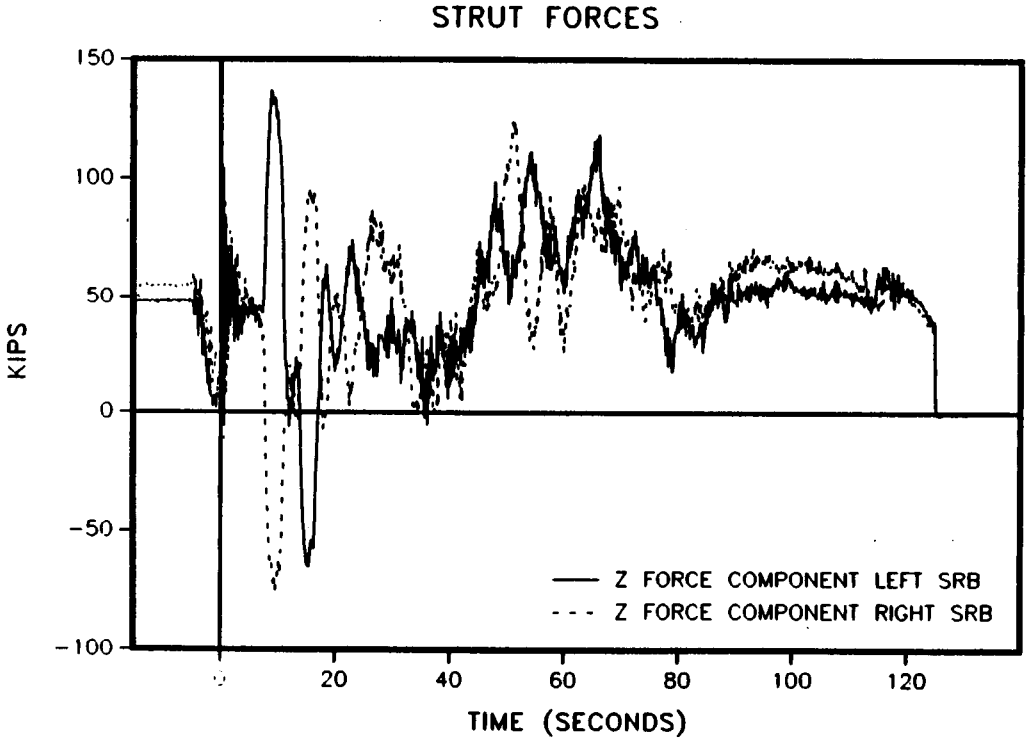

Figure 4.6-74. 360L001 Strut Forces

Instrument No.	Angular Loc (deg)	SRB (L or R)	Direction	Range	FM (Hz)
B08D7160A	0	L	Axial	±10g	5-50
B08D7161A	0	L	Tang.	±10g	5-50
B08D7162A	0	L	Radial	±10g	5-50
B08D8151A	180	R	Axial	±400g	NA
B08D8152A	180	R	Radial	±400g	NA
B08D8153A	180	R	Tang.	±400g	NA
B08D8160A	180	R	Axial	±10g	5-50
B08D8161A	180	R	Tang.	±10g	5-50
B08D8163A	0	R	Tang.	±10g	5-50

4.7.3 Results Discussion

For all the time history plots referenced in this section, the 0.0-sec point is SRB ignition.

Vibration Amplitudes

The time history plots for each channel from 0 to 123 sec are shown in Figures 4.7.1 through 4.7.9. Evaluation indicates that the right-hand SRB has greater vibration in the axial direction than the left-hand SRB. The two tangential direction channels (B08D7161 and B08D8161 located on the left and right SRBs, respectively), which were both located on the orbiter side, show very similar vibration amplitudes (maximum 3g level). Channel B08D8163, however, which was located on the outboard side of the right SRB in the tangential direction, showed very significant strong vibration levels of up to 12g. The rigid body acceleration in the axial direction can not be seen from either channel B08D7160 (left SRB axial) or channel B08D8160 (right SRB axial). The reason (for not detecting the axial acceleration) may occur because the frequency of rigid body acceleration is so low that it is outside the accelerometer detection range.

Channels B08D8151 through B08D8153, which are axial, radial, and tangential gages on the right SRB, detected only noise. One possible reason for this is that the vibration range of those three channels is so high (±400g) that they cannot detect the actual vibration environment of ±10g.

ORIGINAL PAGE IS
OF POOR QUALITY

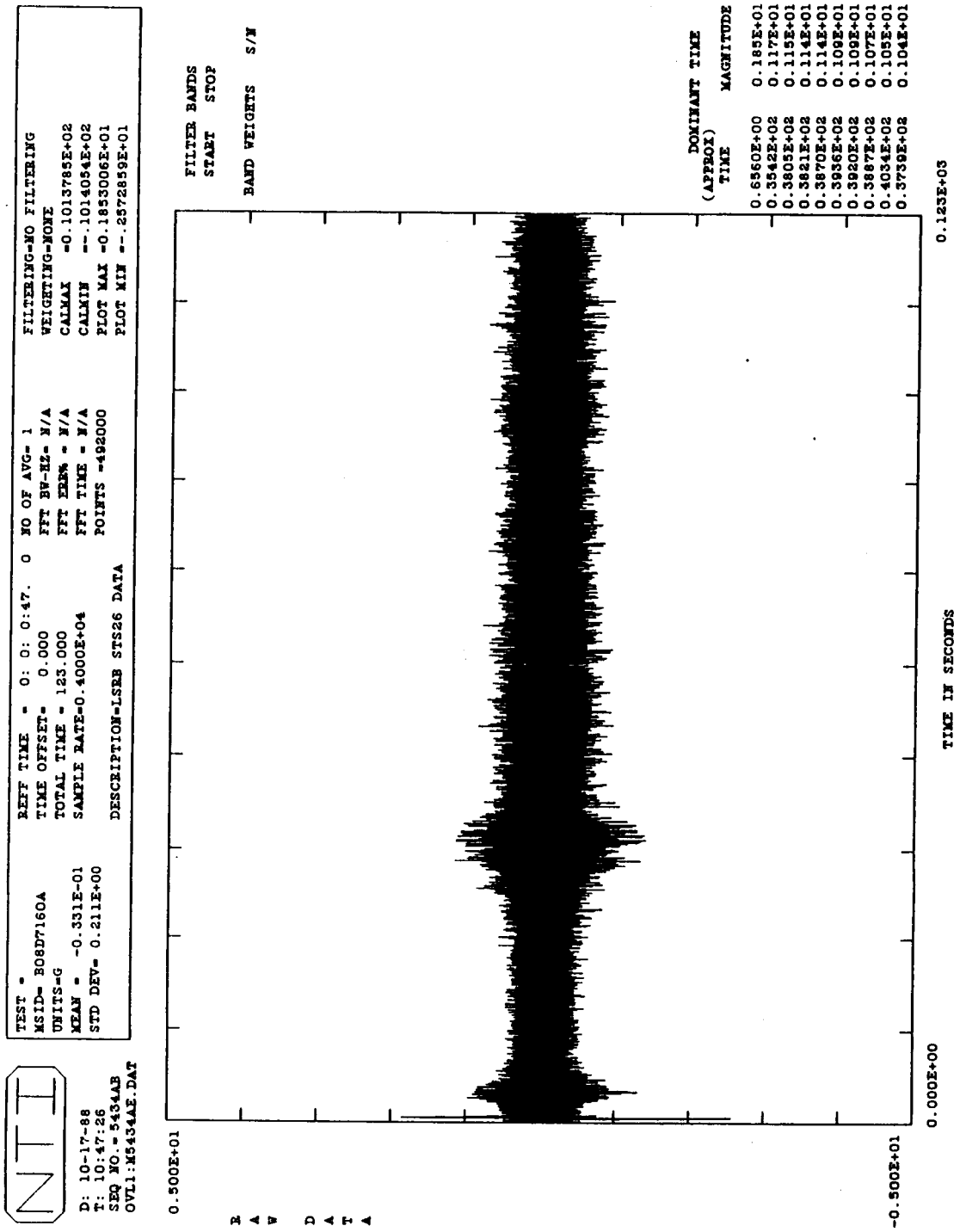

Figure 4.7-1. Time History of B08D7160

ORIGINAL PAGE IS
OF POOR QUALITY

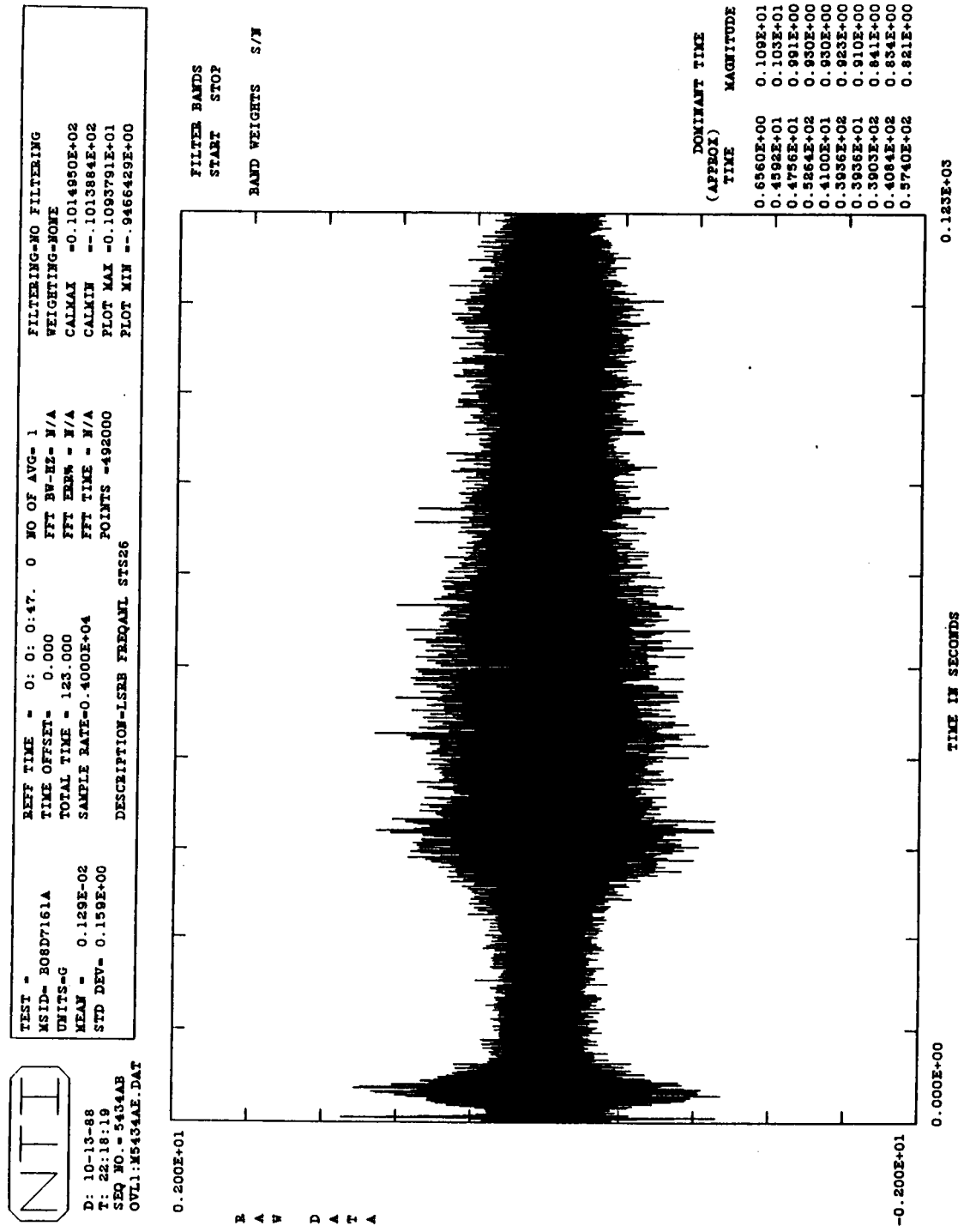

Figure 4.7-2. Time History of B08D7161

ORIGINAL PAGE IS
OF POOR QUALITY

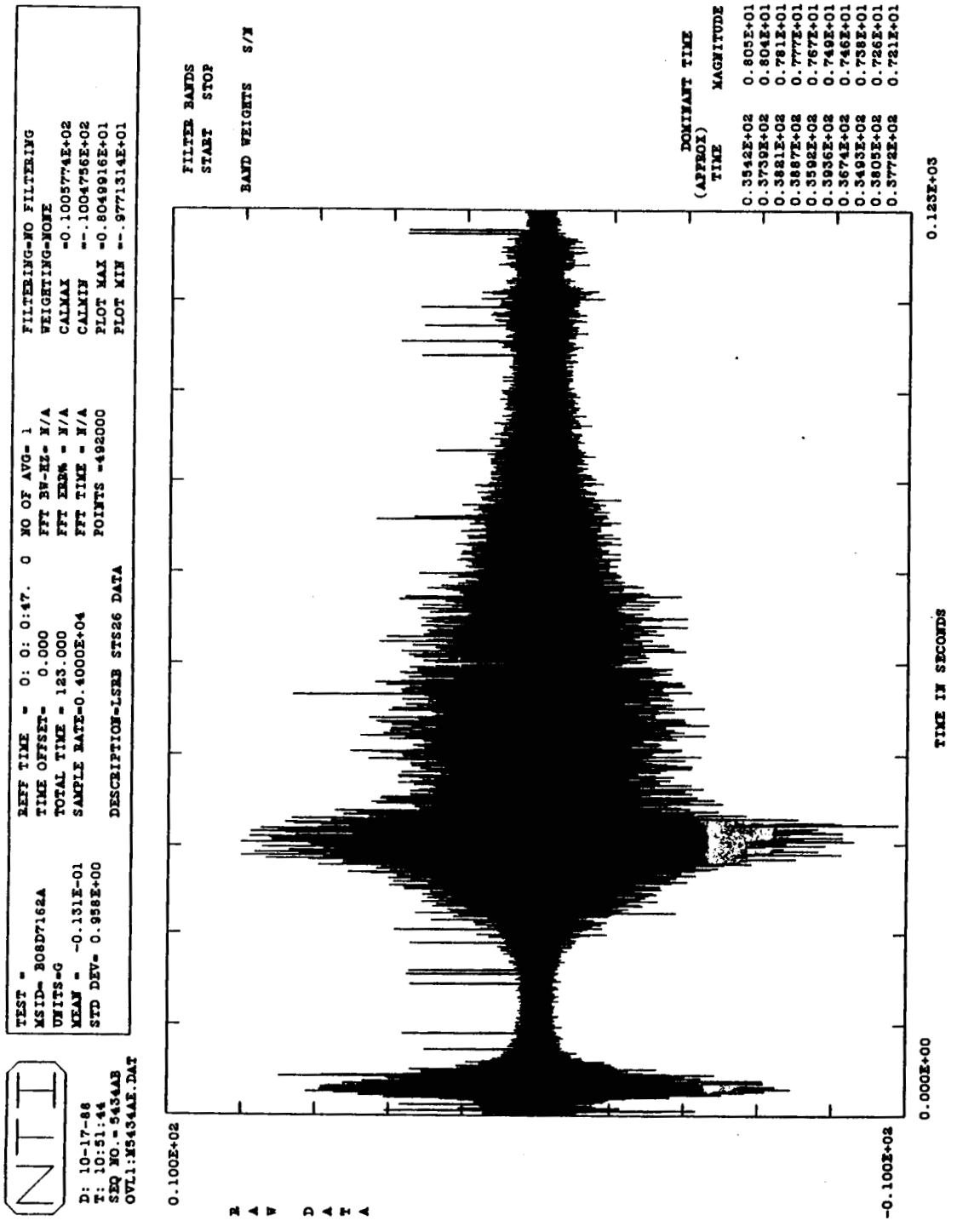

Figure 4.7-3. Time History of B08D7162

ORIGINAL PAGE IS
OF POOR QUALITY

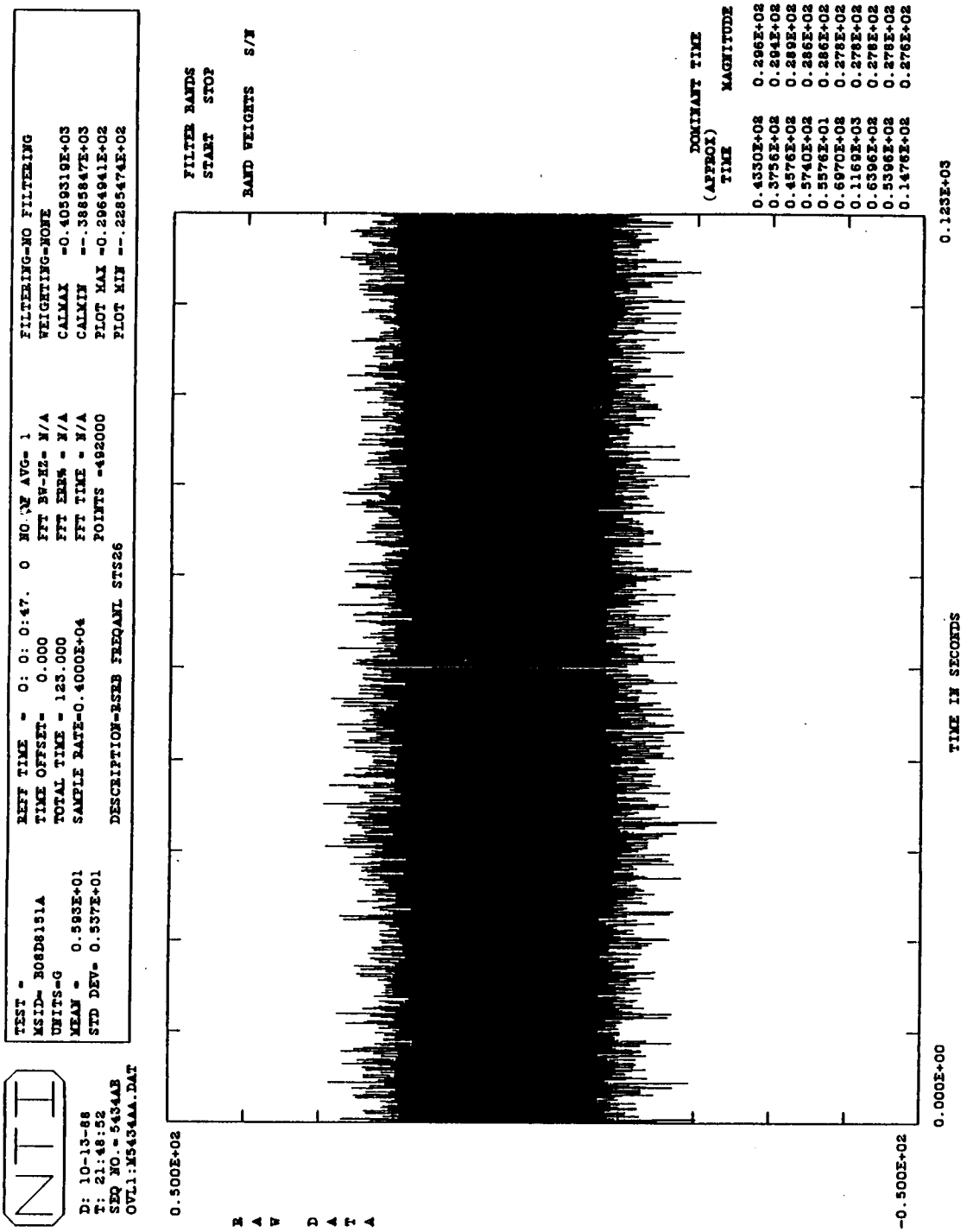

Figure 4.7-4. Time History of B08D8151

ORIGINAL PAGE IS
OF POOR QUALITY

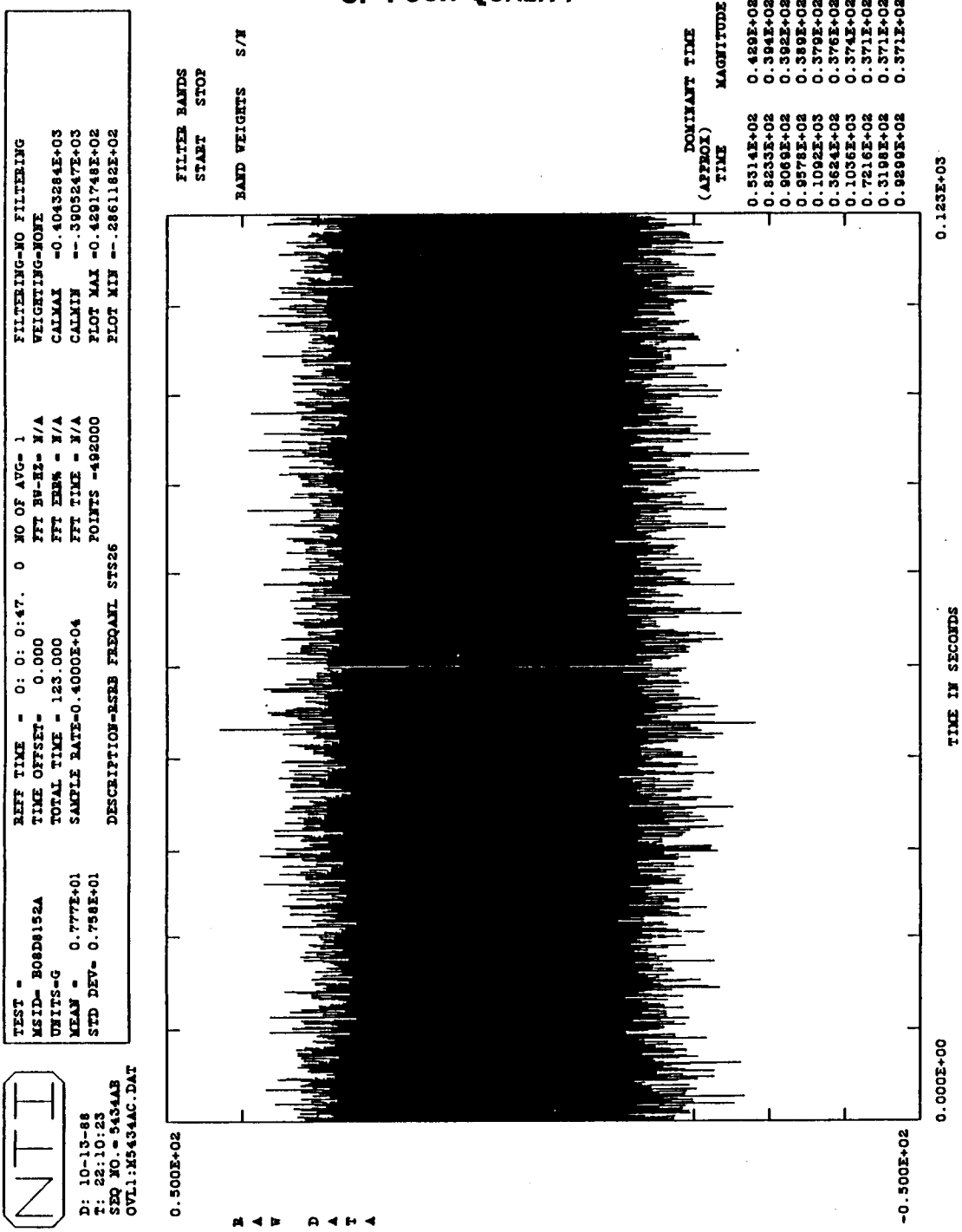

Figure 4.7-5. Time History of B08D8152

ORIGINAL PAGE IS
OF POOR QUALITY

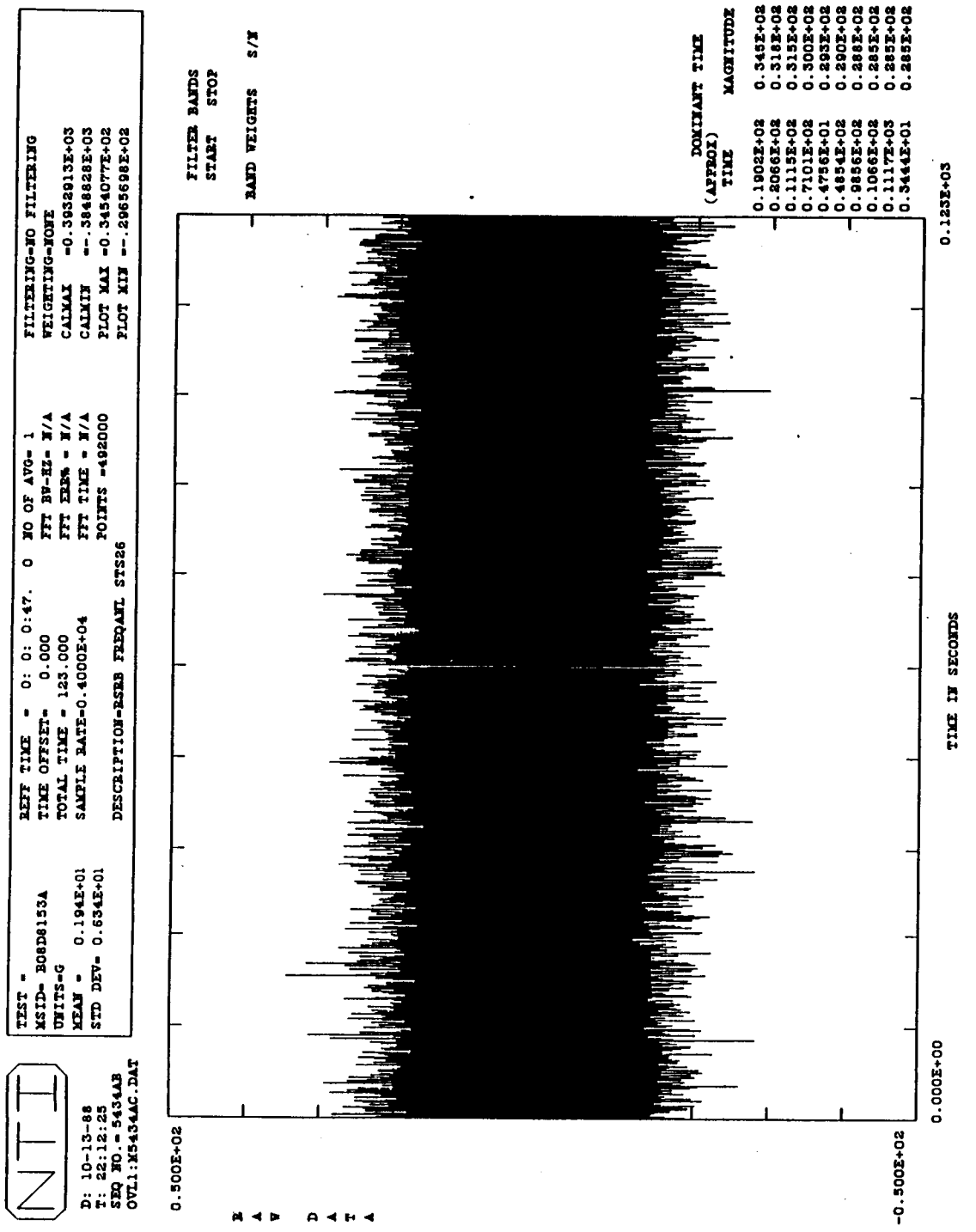

Figure 4.7-6. Time History of B08D8153

ORIGINAL PAGE IS
OF POOR QUALITY

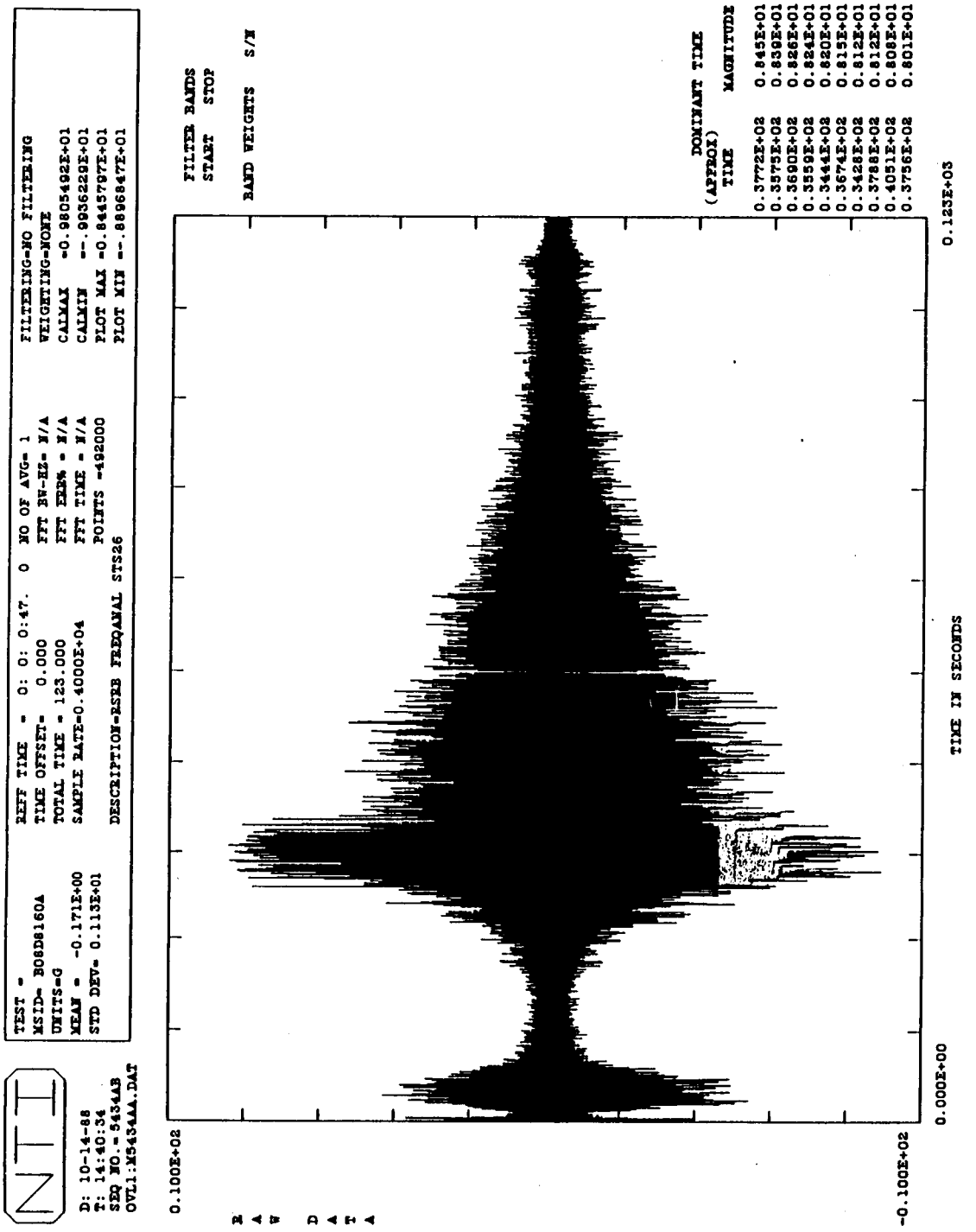

Figure 4.7-7. Time History of B08D8160

ORIGINAL PAGE IS
OF POOR QUALITY

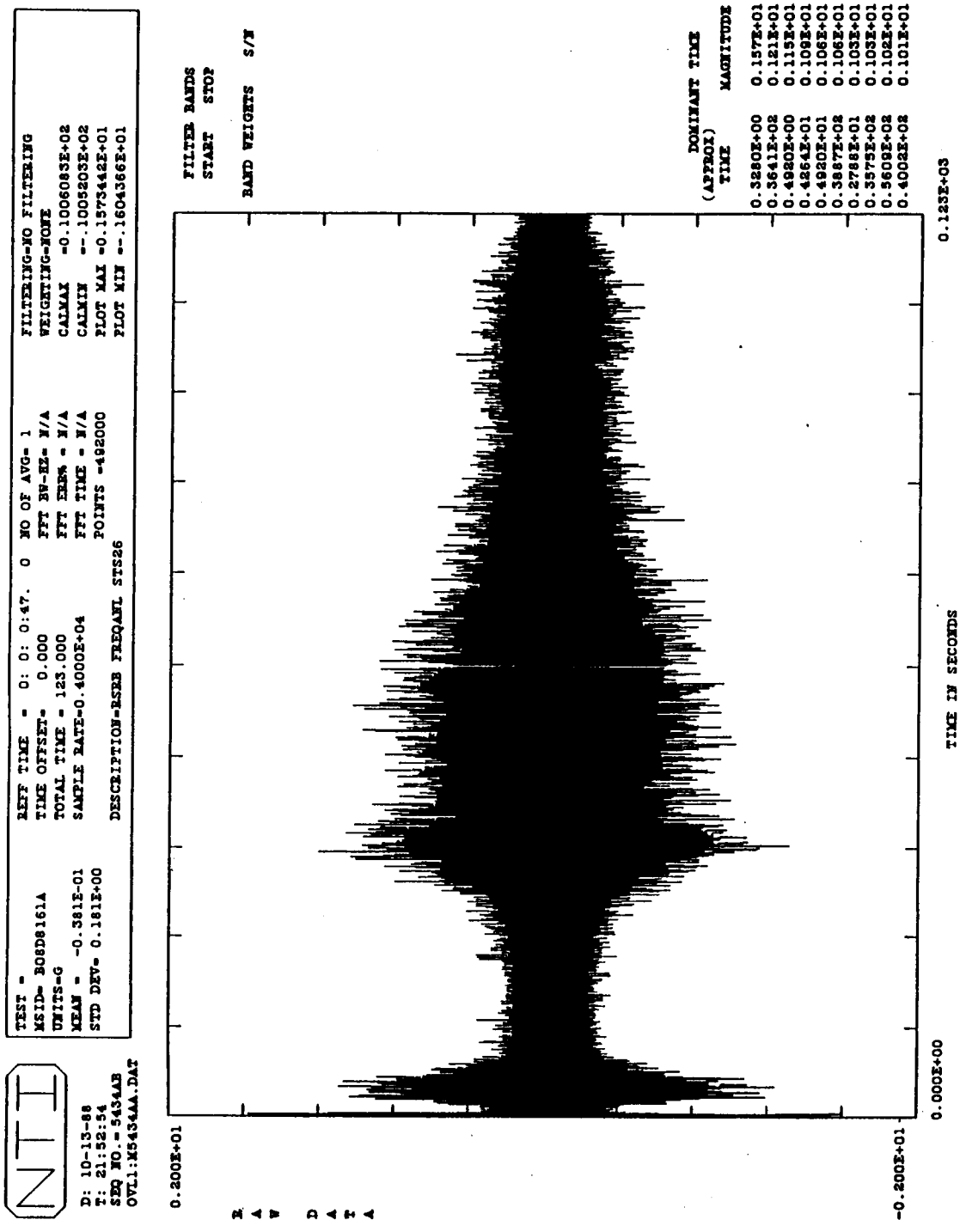

Figure 4.7-8. Time History of B08D8161

ORIGINAL PAGE IS
OF POOR QUALITY

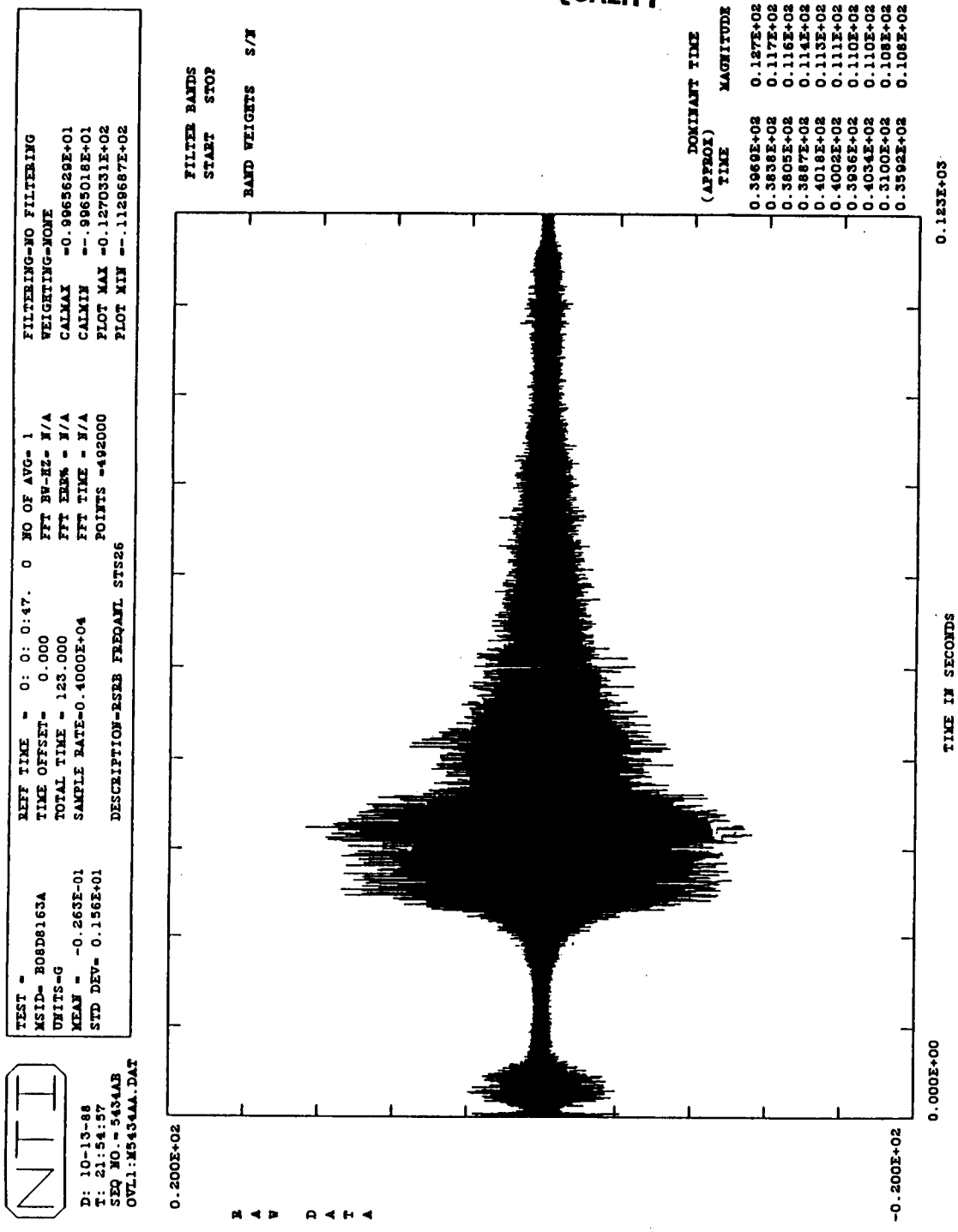

Figure 4.7-9. Time History of B08D8163

Predicted and Actual Results

To compare to predicted results, the data from -5 to 5 sec were selected and filtered using a low-pass 15 Hz filter, which is the maximum frequency used in the analytical model. The results are shown in Figures 4.7.10 through 4.7.15. The comparison of peak values between predicted and measured results are given in Table 4.7-1.

From Table 4.7-1 it can be seen that the predicted peaks in the tangential direction are not very close. The reason for the poor correlation may be that the frequency used in the NASTRAN model is only valid up to 15 Hz. If the dominant modes of vibration in the tangential direction do not occur below 15 Hz, the measured values would vary from the predicted results. Another reason for the variation is that the load case used for predictions is the Rockwell Load Case RI-L02044, which is not the actual load case during the STS-26 flight. It is predicted that the post-test correlation, which will use the modal frequency up to 40 Hz and the actual STS-26 flight loads, will decrease the difference between actual and predicted values.

Modal Frequencies

Modal frequencies representing the structural modes of vibration can be identified by using waterfall plots. Waterfall plots for each channel are shown in Figures 4.7.16 through 4.7.24. It can be seen from the figures that the first axial mode, which starts at about 20 Hz and ends about 39 Hz, dominates the axial mode of vibration. Since the NASTRAN analytical model only forecasts up to 15 Hz, this axial made was not predicted. The tangential direction channels, B08D7161 and B08D8161, have very similar waterfall plots, and are consistent with the time history data.

The torsional vibration mode, starting at about 14 Hz and ending about 32 Hz, dominated the tangential direction of vibration. Figures 4.7.19 through 4.7.21 show that the waterfall plots for the three tangential channels (B08D7161, B08D8161, and B08D8163) are constant with the flight time data. This again indicates that these three channels contain only noise, which is consistent with the previous vibration level observation.

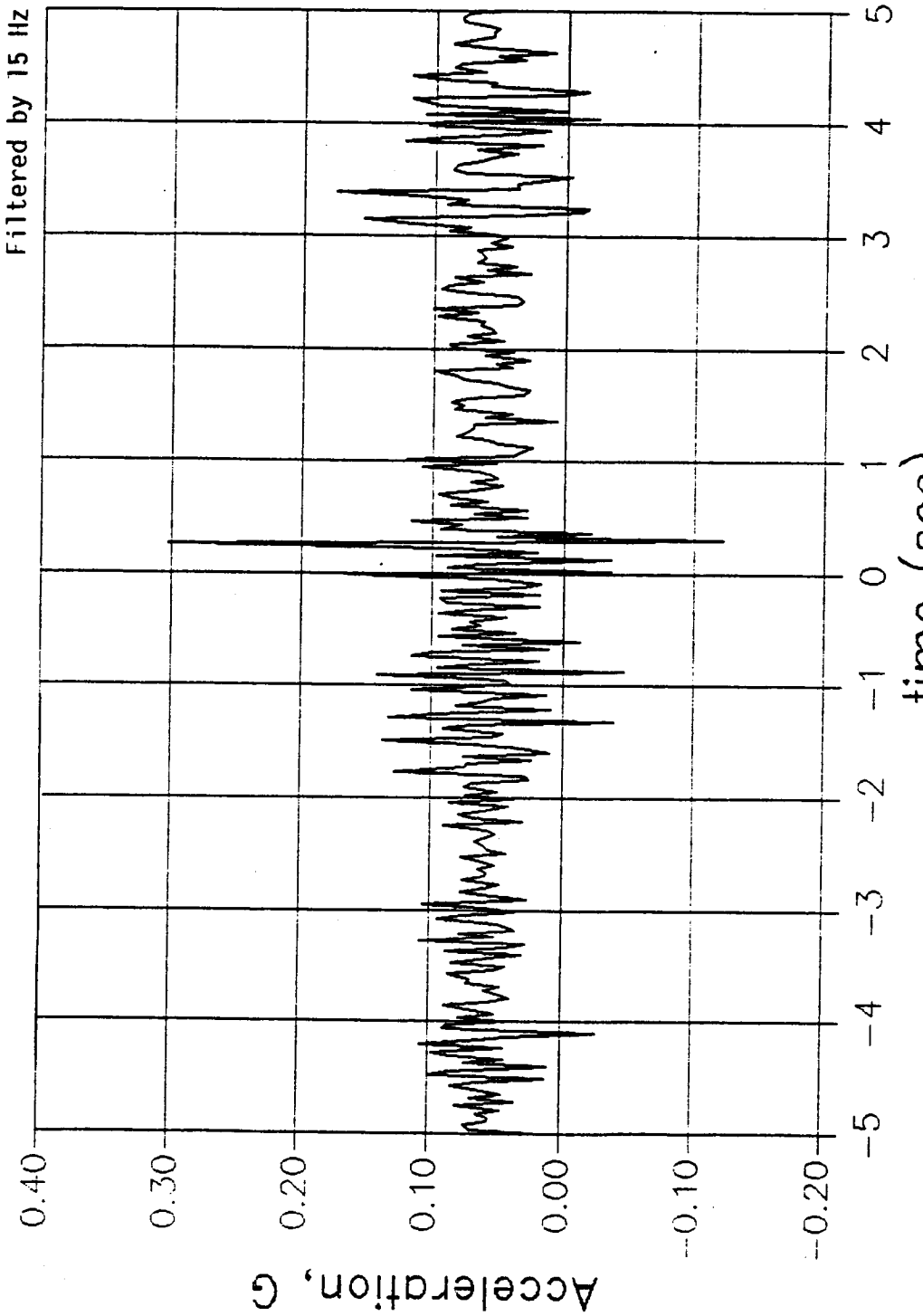

Figure 4.7-10. Time History of B08D7160 (Axial)

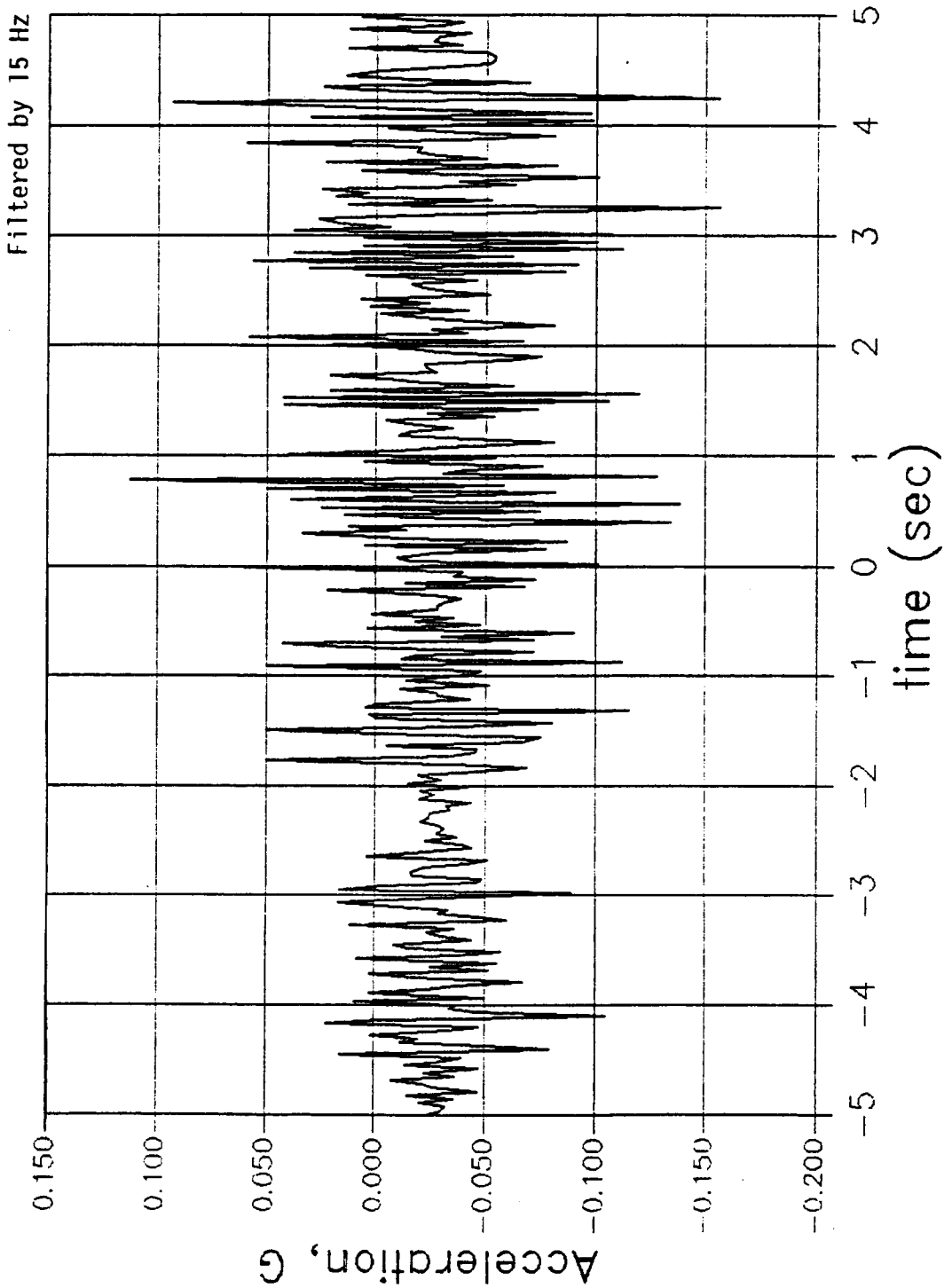

Figure 4.7-11. Time History of B08D7161 (Tangential)

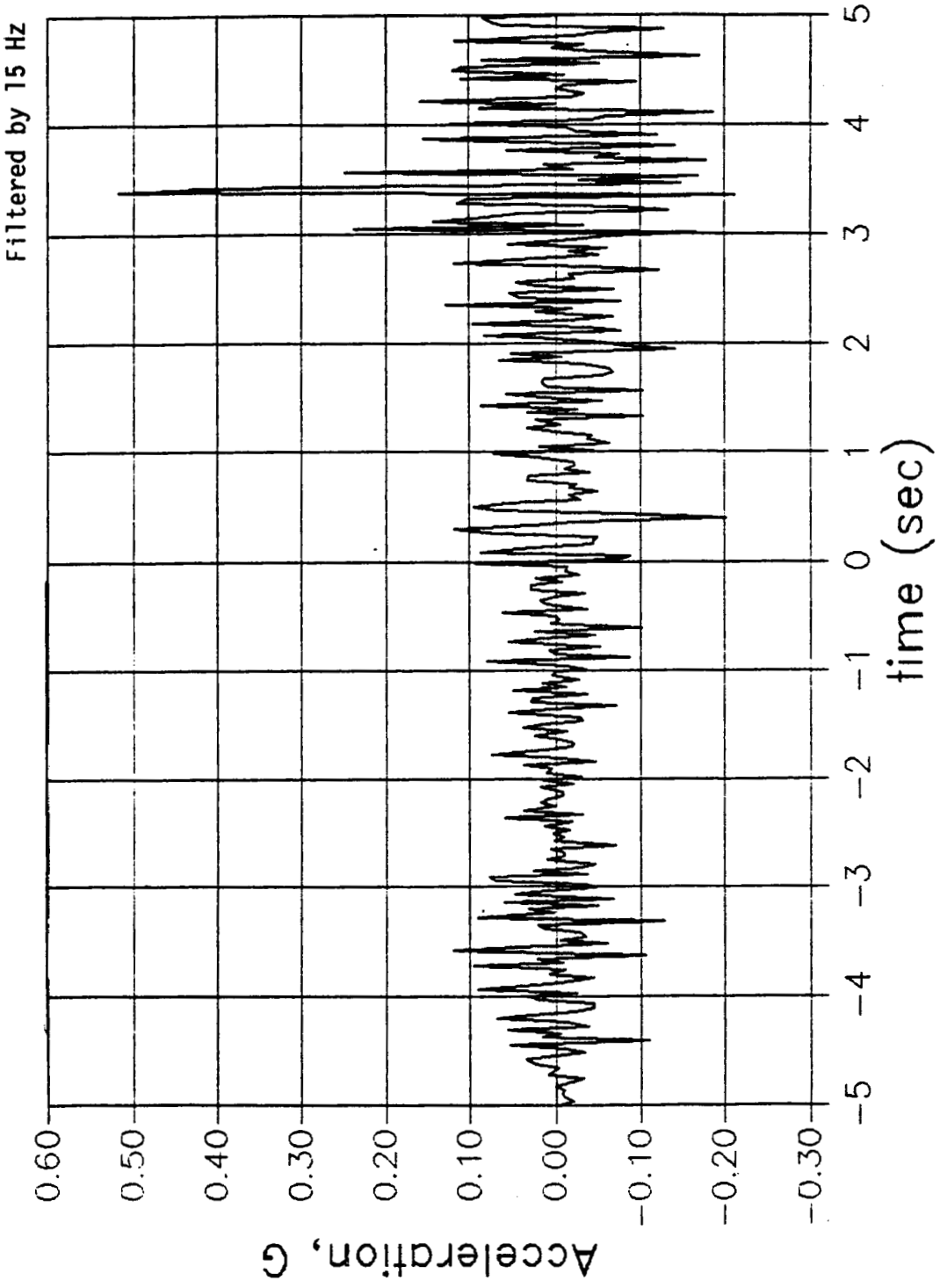

Figure 4.7-12. Time History of B08D7162 (Radial)

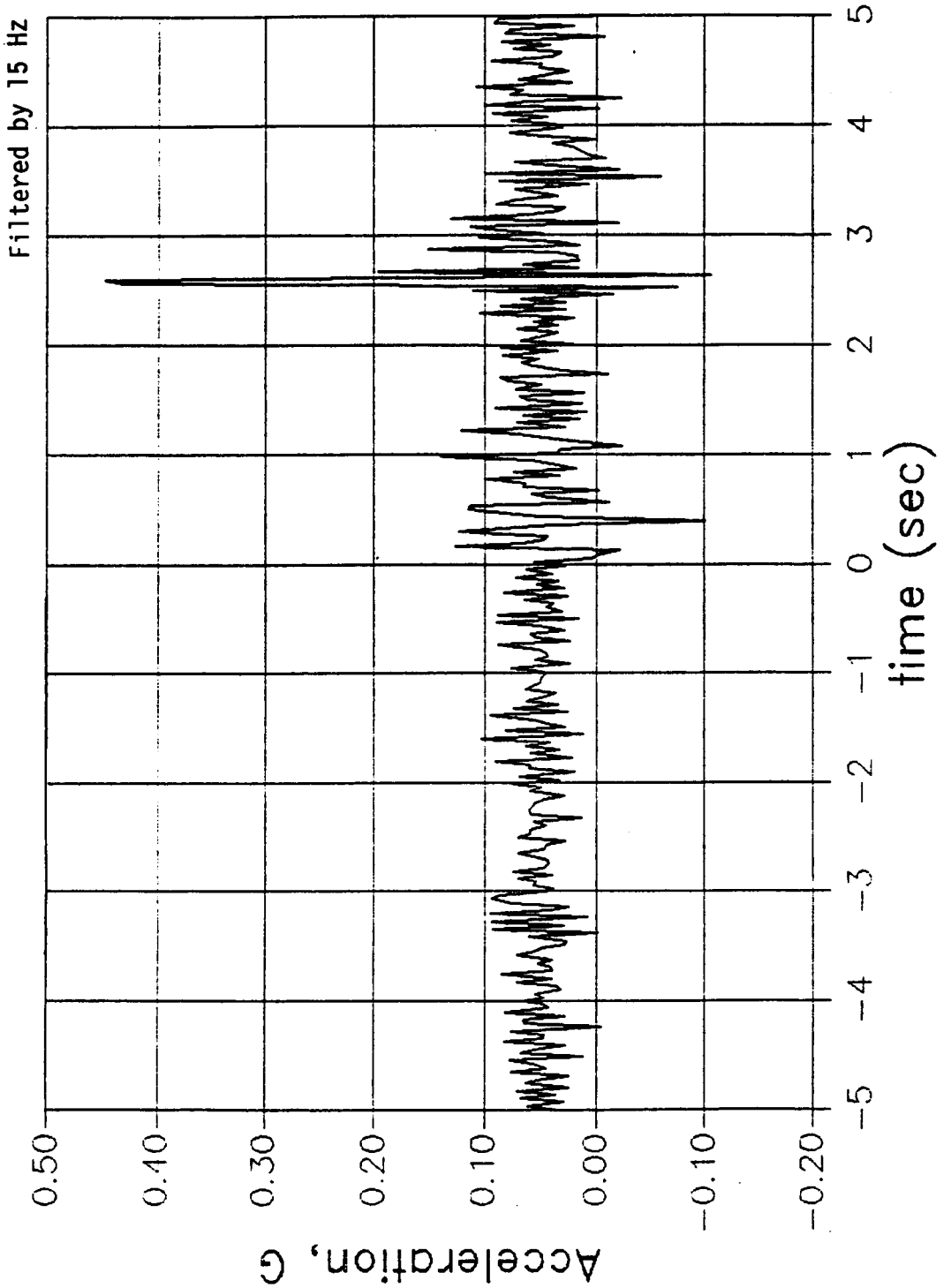

Figure 4.7-13. Time History of B08D8160 (Axial)

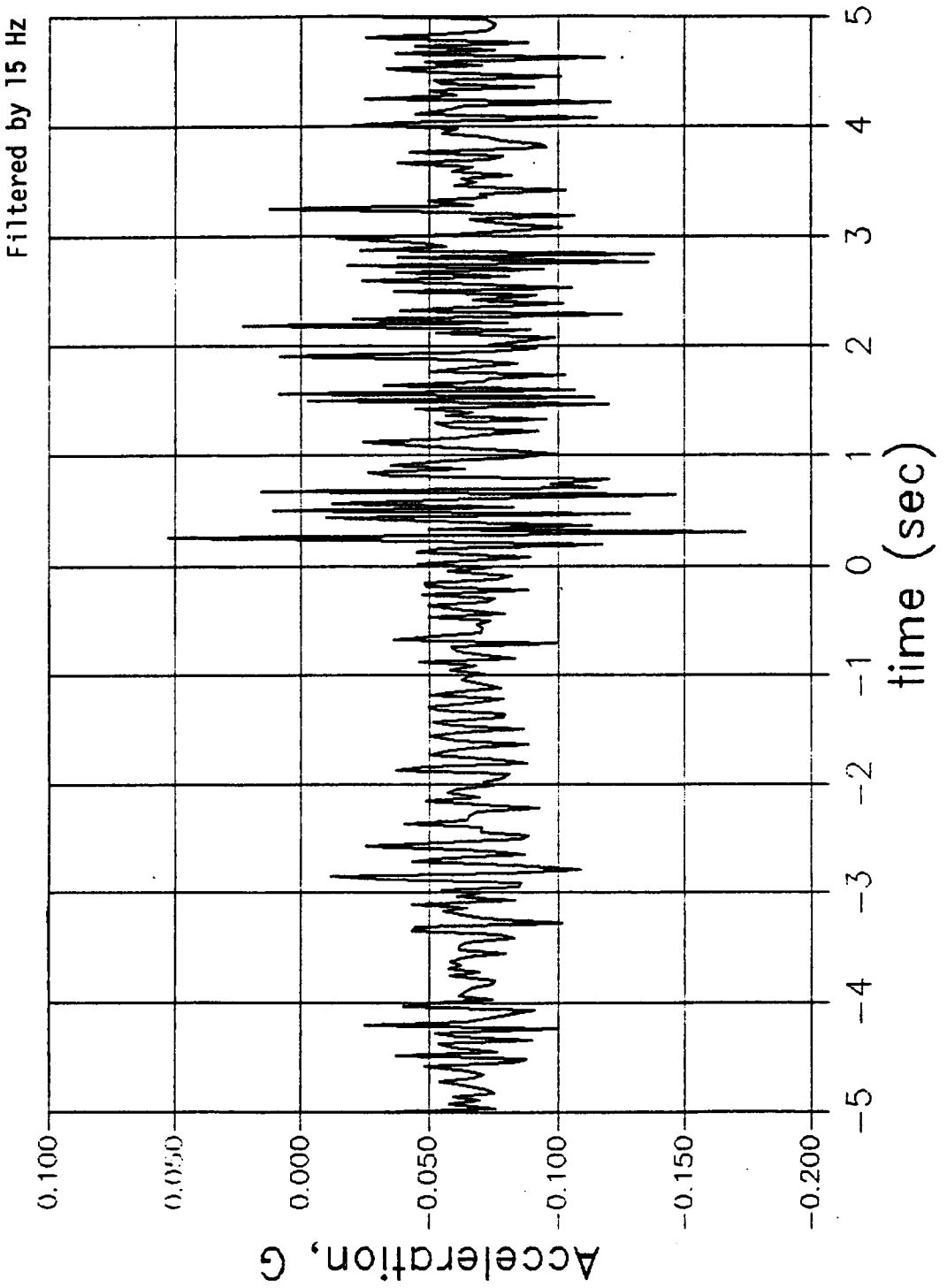

Figure 4.7-14. Time History of B08D8161 (Tangential)

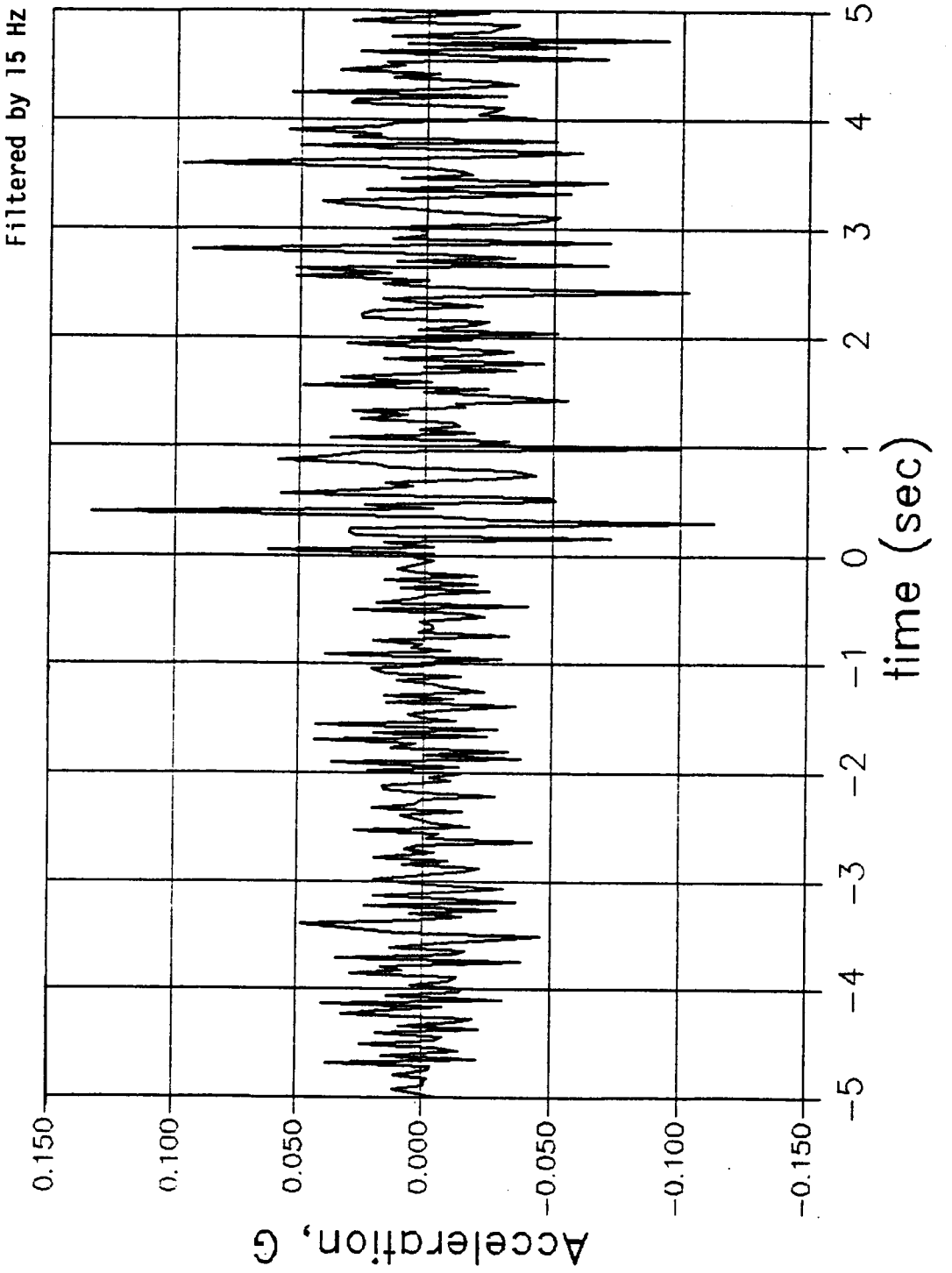

Figure 4.7-15. Time History of B08D8163 (Tangential)

Table 4.7-1. Peak Accelerations Comparisons

Gage	Direction	Predicted (g)	Measured (STS-26) (g)
B08D7160	Axial	0.6	0.3
B08D7161	Tangential	1.2	0.1
B08D7162	Radial	0.5	0.5
B08D8160	Axial	0.6	0.45
B08D8161	Tangential	1.2	0.05
B08D8163	Tangential	1.3	0.15

ORIGINAL PAGE IS
OF POOR QUALITY

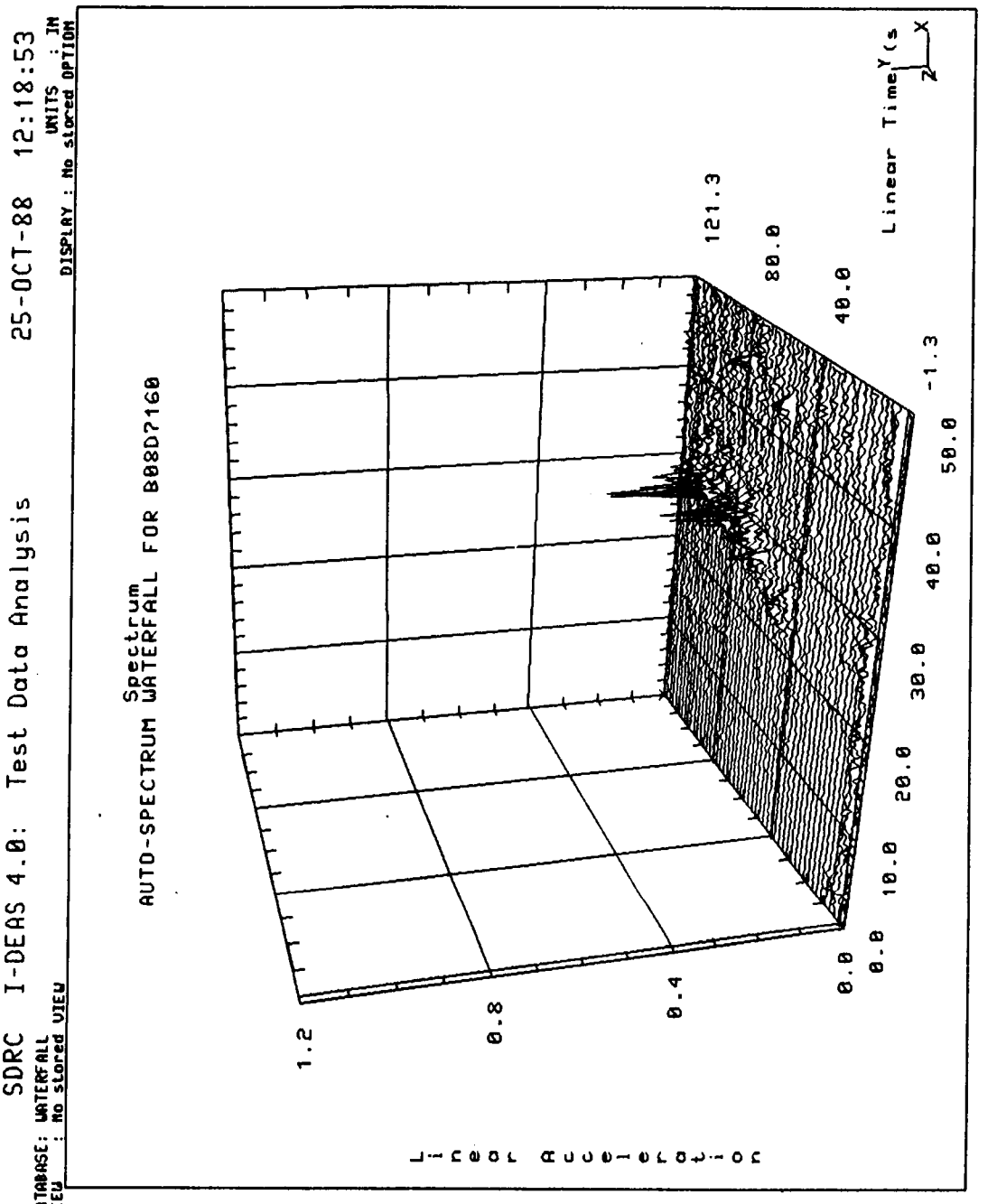

Figure 4.7-16. Autospectrum Waterfall for B08D7160

ORIGINAL PAGE IS
OF POOR QUALITY

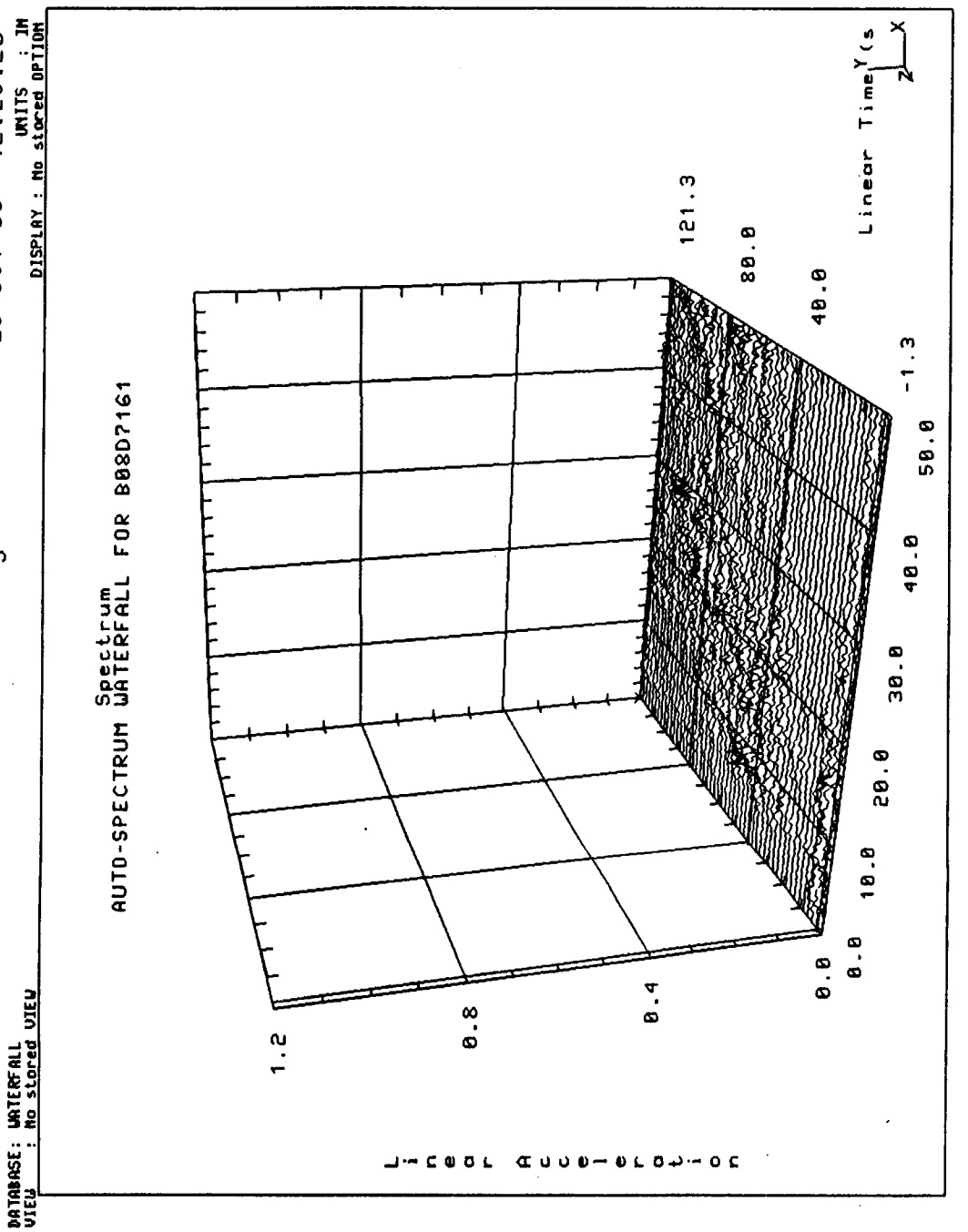

Figure 4.7-17. Autospectrum Waterfall for B08D7161

ORIGINAL PAGE IS
OF POOR QUALITY

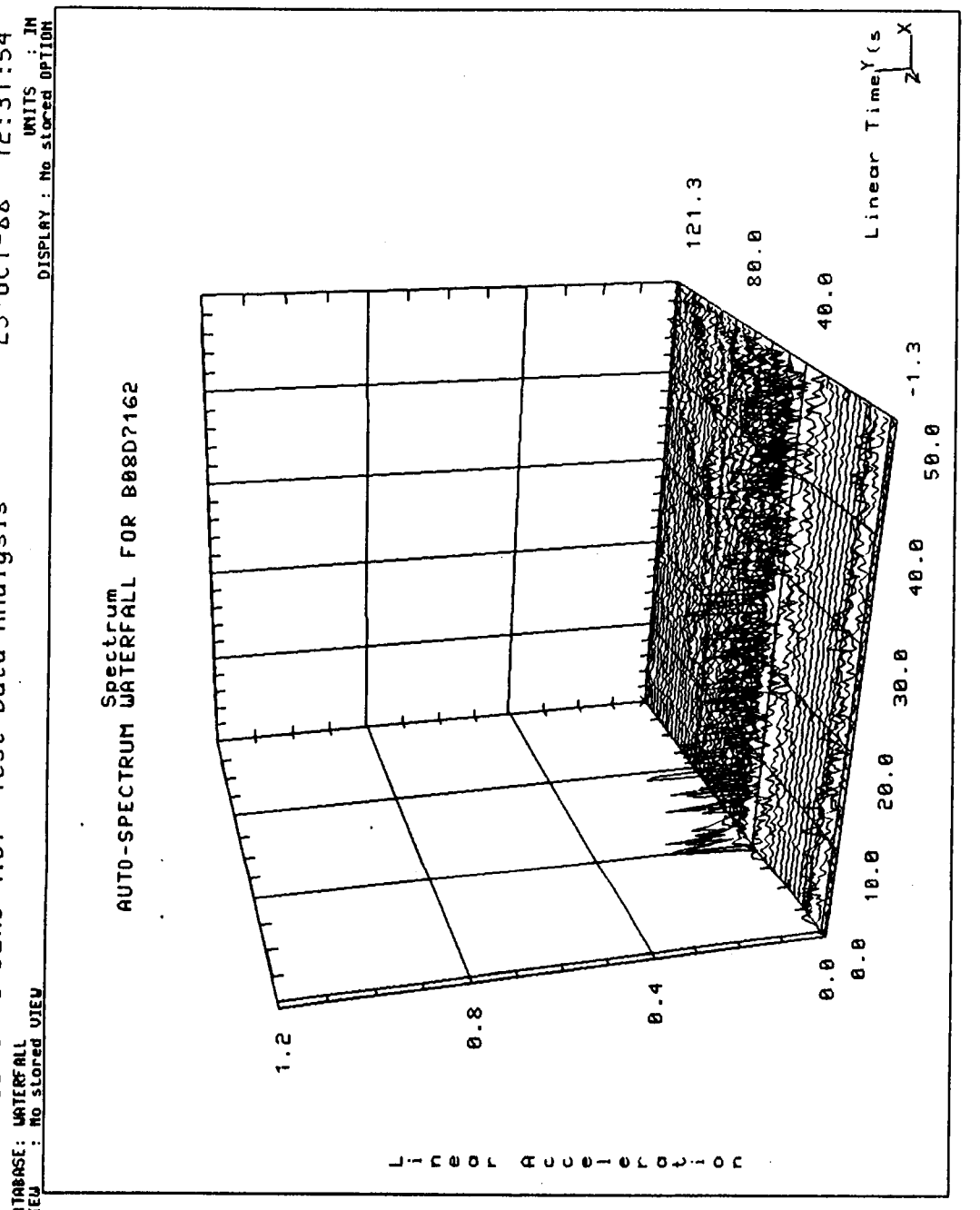

Figure 4.7-18. Autospectrum Waterfall for B08D7162

ORIGINAL PAGE IS
OF POOR QUALITY

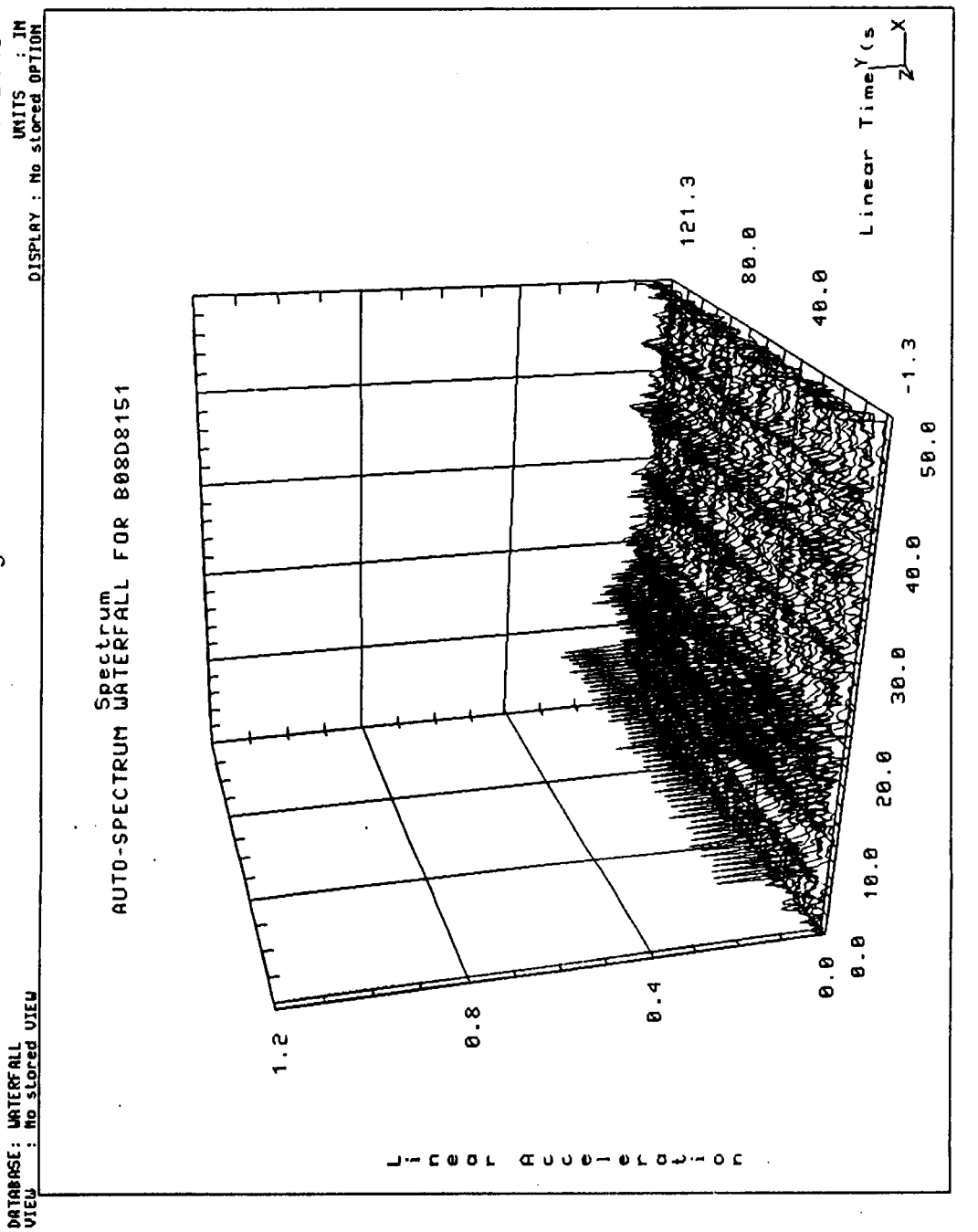

Figure 4.7-19. Autospectrum Waterfall for B08D8151

ORIGINAL PAGE IS
OF POOR QUALITY

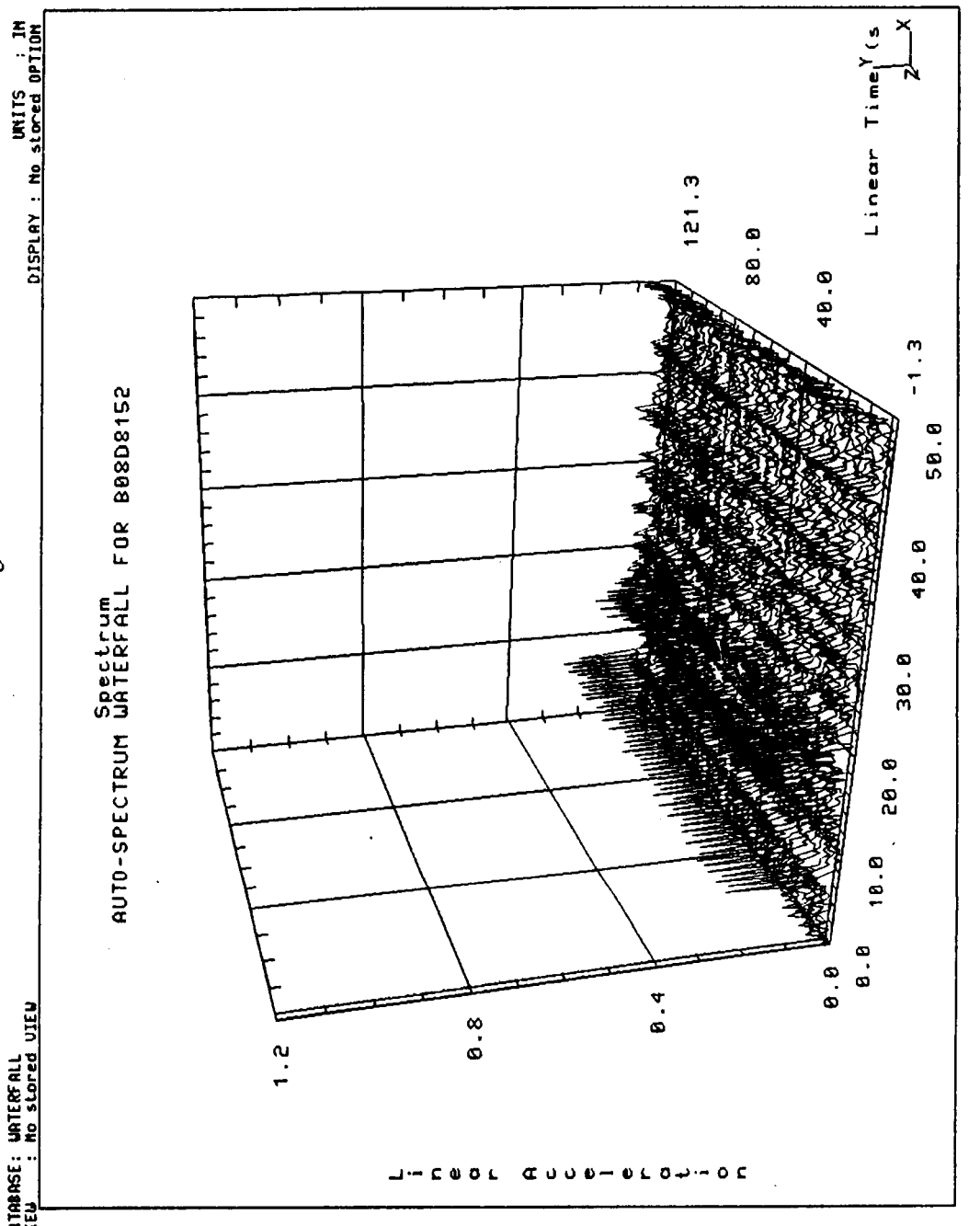

Figure 4.7-20. Autospectrum Waterfall for B08D8152

ORIGINAL PAGE IS
OF POOR QUALITY

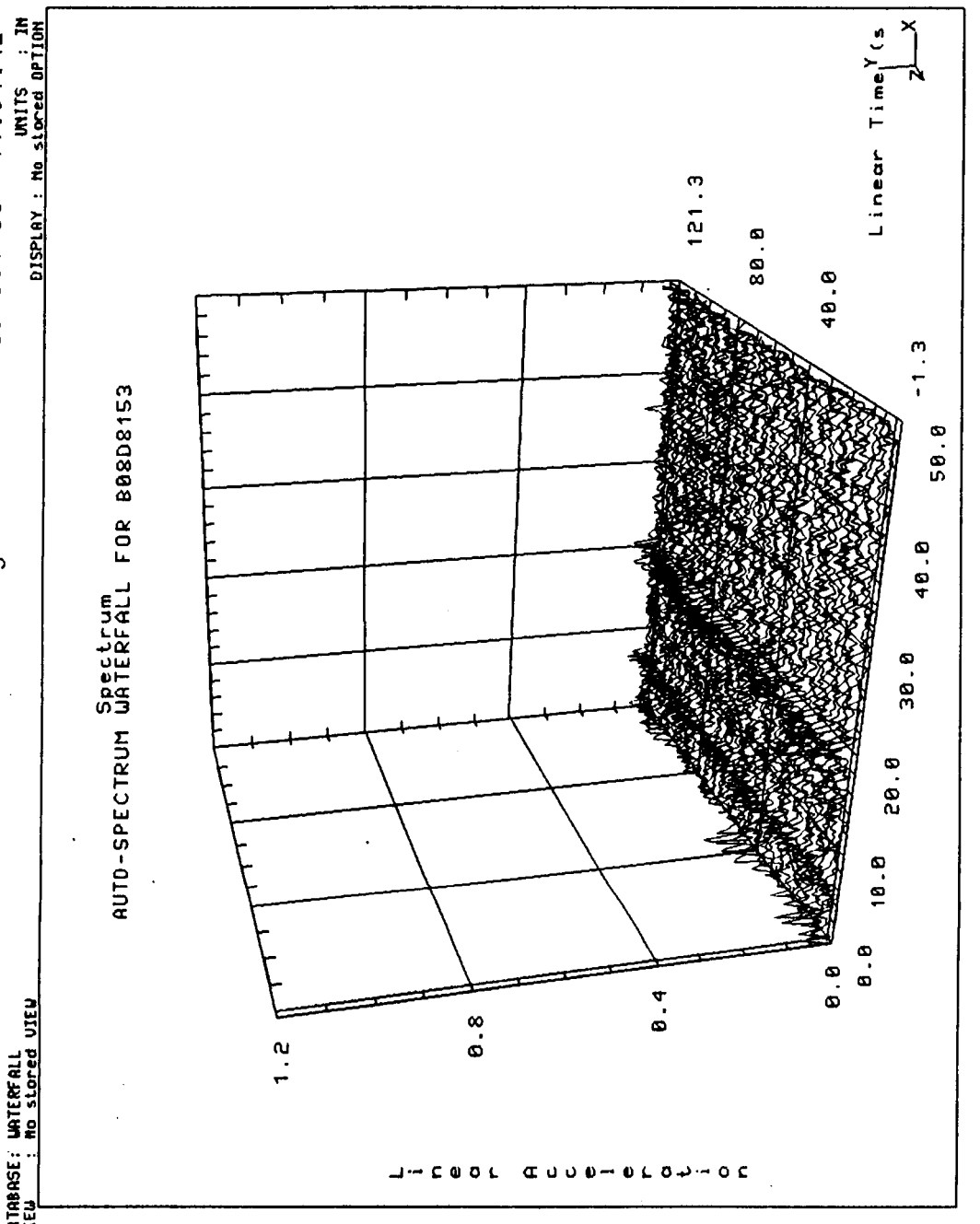

Figure 4.7-21. Autospectrum Waterfall for B08D8153

ORIGINAL PAGE IS
OF POOR QUALITY

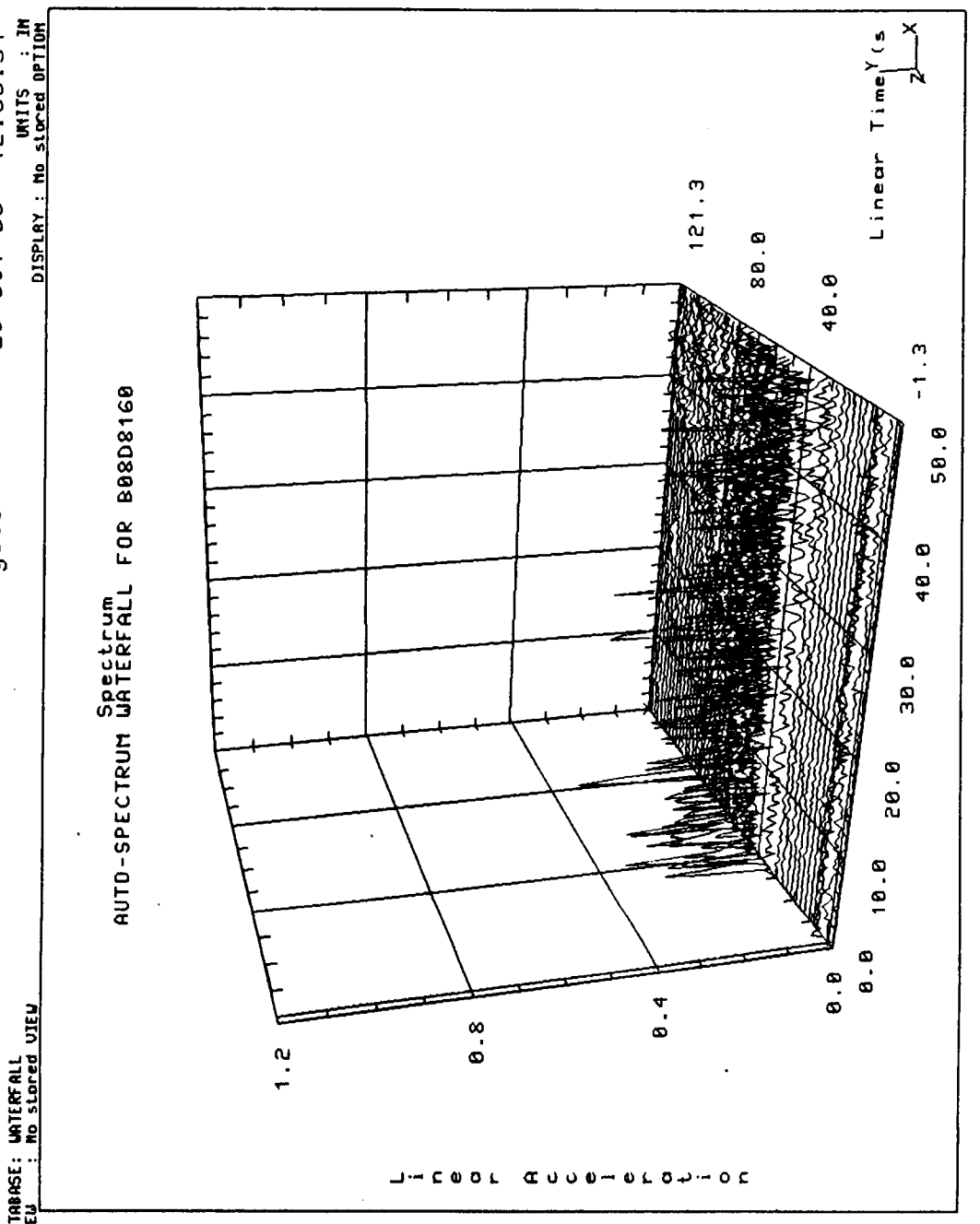

Figure 4.7-22. Autospectrum Waterfall for B08D8160

ORIGINAL PAGE IS
OF POOR QUALITY

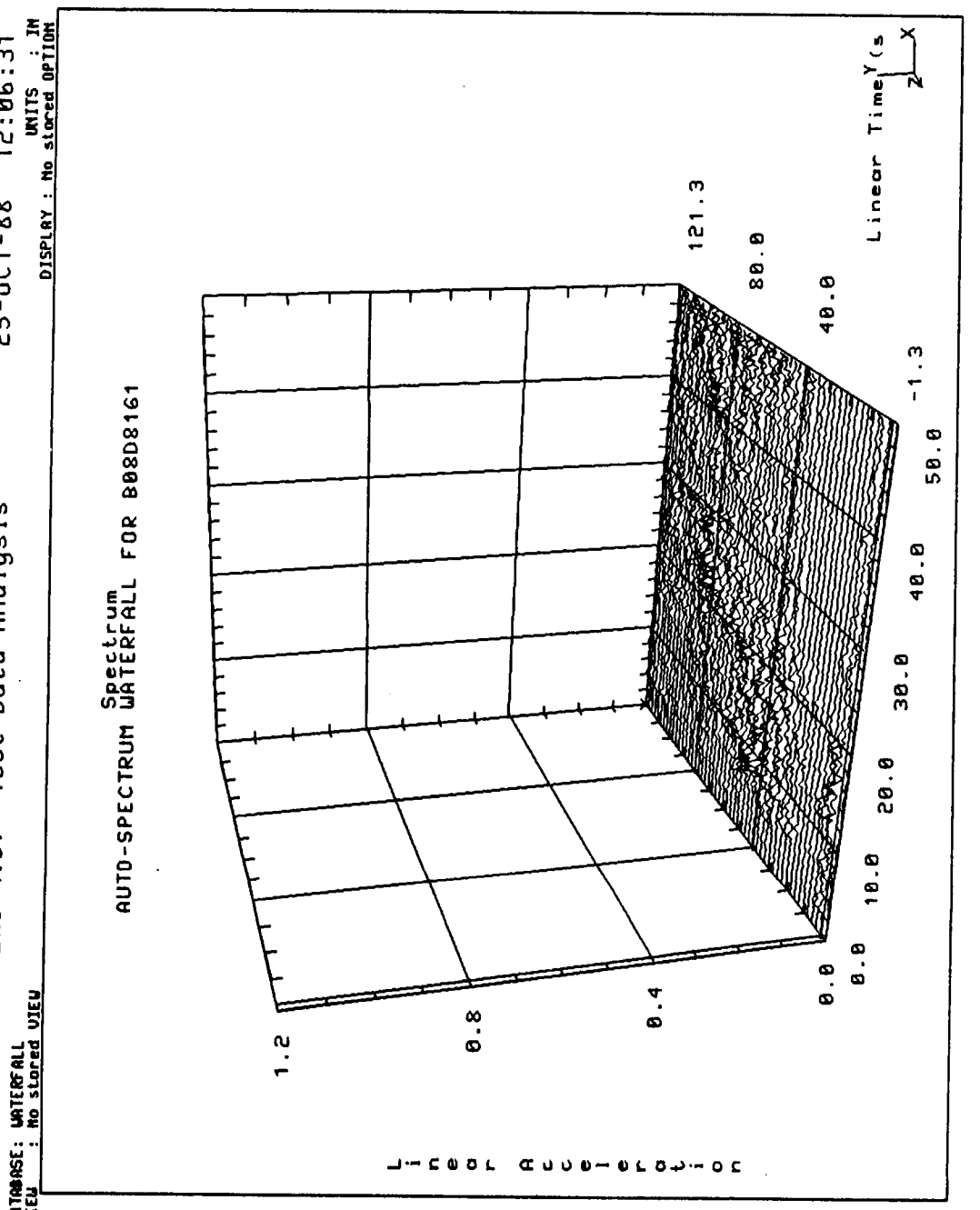

Figure 4.7-23. Autospectrum Waterfall for B08D8161

ORIGINAL PAGE IS
OF POOR QUALITY

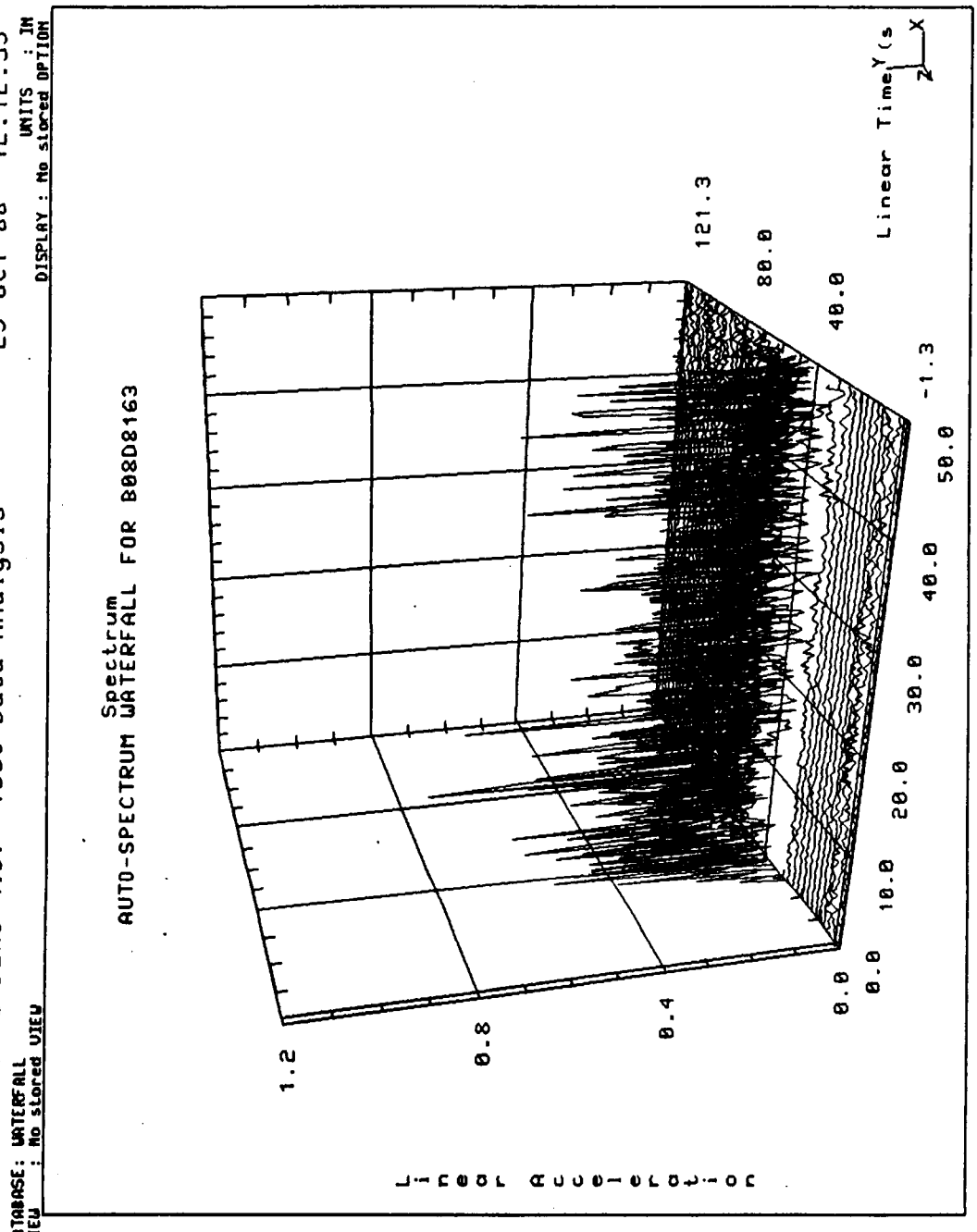

Figure 4.7-24. Autospectrum Waterfall for B08D8163

The predicted and measured modal frequencies are listed as follows in Table 4.7-2. To obtain more detail on the actual flight frequencies and modes, additional accelerometers would be required.

Table 4.7-2. Predicted and Measured Modal Frequencies

Direction	Predicted	Measured (STS-26)
Axial	Not applicable, modes limited to 15 Hz	Started at 20 Hz Ended at about 39 Hz
Torsional	Started at 14.9 Hz	Started at about 14 Hz Ended at about 32 Hz

The random vibration criterion cannot be checked adequately since the available sample rate (320 sps) is too low (NASA SE-019-049-2H criterion required up to 2,000 Hz).

4.8 SRM AEROHEATING ENVIRONMENT

This section corresponds to FEWG report Section 2.7.0.

4.8.1 Introduction

Component design analyses due to current flight-induced thermal loads were performed during the redesign effort and will be documented in the SRB Thermal Design Data Book, SE-019-068-2H. Thermal response estimates for DFI locations were inferred from these analyses and summarized together with actual STS-26R DFI response (Table 4.9-2 in Section 4.9.2).

The current design loads were developed for a conservative trajectory (Table 4.9-7 in Section 4.9.3.1). This trajectory (IVBC-3) is presently not included in planned flight trajectories. Since thermal loads data were not available for the trajectory of STS-26R, there was no direct correlation possible with actual DFI data. However, actual DFI data were used to determine whether design predictions were exceeded.

4.8.2 Summary and Conclusion

Primarily, all DFI data were within design estimates (Table 4.9-2 in Section 4.9.2). The only exception was the measured data on the SRM nozzle

fixed housing flange within the SRB aft skirt base region. These data exceeded design estimates. This was attributed to a possible adhesive failure, causing gage detachment from the hardware. No insulation was used to cover these gages on STS-26R. The high readings are explainable, assuming slight gage detachment, due to the direct exposure of these gages to the hot environment (reentry nozzle flame and aerodynamic heating) following thermal curtain breakup.

This assessment will be confirmed with STS-27 and subsequent developmental flight sets, where the gages will be directly insulated from the environment with a minimal amount of K5NA, and should better follow hardware response. If not confirmed, SRB reentry environments and/or SRM aft end thermal modeling will need to be considered and appropriately modified.

Further details concerning DFI thermal SRM assessments and flight-induced problems can be found in Section 4.9.

4.9 SRM TEMPERATURE AND TPS PERFORMANCE

This section corresponds to FEWG report Section 2.8.2.

4.9.1 Introduction

STS-26R thermal performance of the SRM external components and TPS has been evaluated. This section documents the assessments of postflight hardware inspection and DFI/GEI/joint heater sensor/thermal imaging data.

Performance of internal components (insulation, case metal components, and seals) is reported in Section 4.12.

4.9.2 Summary

a. Postflight inspection data revealed no anomalies or unexpected problems. The condition of both SRMs was similar to that of previous flight motors. Table 4.9-1 provides an overall summary of SRM TPS condition.

b. DFI thermal data were for the most part well within the estimated values derived from design trajectory analyses. The only exception was that the measured data on the SRM nozzle fixed housing flange within the SRB aft skirt base region exceeded design estimates (Section 4.9.3). Table 4.9-2 details flight design trajectory temperature estimates versus actual

Table 4.9-1. SRM External Performance Summary
(Left and Right Motors)

Component	TPS Material	Performance	Recovered Hardware Performance Assessment
Field Joints	Cork	Typical	All field joints in excellent condition; slight paint blistering.
Factory Joints	EPDM	Typical	All factory joints in very good condition; slight ablation of EPDM on aft segment joints on inboard side of both motors (approximately 220 to 320 deg).
Systems Tunnel	Cork	Typical	Cork TPS adjacent to tunnel floor plate in excellent condition; very little paint discoloration and no measurable cork ablation.
Stiffener Rings	EPDM	Typical	Normal thermally, only significant ablation was on stub tips and leading edge of "t" sections on inboard side of motors; stiffener rings on RH motor were fractured at approximately 160 deg due to water impact.
DFI, Cables	Cork, silica phenolic	Typical	Generally in good condition with slight paint blistering; several pieces of cap cork missing on DFI cable runs.
Nozzle Exit Cone	Cork	Typical	Normal, based on temperature sensor data.
Motor Case	NA	Typical	No hot spots or discoloration of the motor case paint due to external or internal heating; intermittent paint blistering on either side of forward stubs.

Table 4.9-2. Flight Design Trajectory Estimates Versus Actual STS-26R Ascent and Reentry DFI Data

Component and Location	Axial Station (in.)	Angular Location (deg)	Maximum Temperature (°F) Design Estimate	Measured Ascent	Measured Reentry
Igniter Adapter	486				
RH		191	200	80	96
LH		191	200	73	85
Fwd Field Joint	846.3				
RH		180	120	95	97
		60	120	95	97
		300	120	89	91
LH		0	120	92	95
		120	120	95	96
		240	120	89	92
Aft Field Joint	1486.3				
RH		180	132	99	104
		60	125	99	100
		300	128	92	95
LH		0	132	95	100
		120	125	99	100
		240	128	94	96
Nozzle/Case Joint	1877.5				
RH		180	150	88	--*
		90	150	85	260**
		0	150	91	--*
		270	150	90	--*
LH		0	150	87	143
		90	150	87	255**
		180	150	87	186**
		270	150	87	220**
Nozzle Aft Exit Cone, Aluminum	1905				
RH		0	290	85	200
LH		180	290	84	185
Nozzle Exit, Under Cork	1996.5				
RH		300	350	98	230
LH		240	350	90	243

*Data were lost following thermal curtain breakup at ≃290 sec.
**Gage response exceeded design estimates. This was attributed to possible adhesive failure, causing gage detachment from the hardware. No insulation was used to cover these gages on STS-26R. The high readings are explainable, assuming slight gage detachment, due to the direct exposure of these gages to the hot environment following thermal curtain breakup. This assessment will be confirmed with STS-27 and subsequent developmental flight sets, where the gages will be directly insulated from the environment with a minimal amount of K5NA and should better follow hardware response.

ascent and reentry DFI data. Figures 4.9.1 through 4.9.4 show locations for DFI on igniter adapter, field joints, nozzle-to-case joint, and aft exit cone, respectively.

c. SRM local environment on-pad due to September historical predictions suggested as much as a 2°F temperature suppression while the ET was loaded. After assessing GEI data, there was no apparent evidence of temperature depression due to ET cooling effects.

d. Ambient environment on-pad data were in good agreement with September historical data except during the early morning hours of the final day when ambient temperature fell to 70°F and remained at that level through the night (Table 4.9-3).

e. Launch commit criteria were not violated (Table 4.9-4). The SRM field joint heaters performed adequately and as expected. The SRB aft skirt conditioning system performed adequately, but not as expected. The conditioning operation was not in accordance with the operational maintenance requirements specification.

f. GEI data were in relatively good agreement with on-pad thermal predictions for both September historical and pre-T-6 hr real-time assessments (Tables 4.9-3 and 4.9-4, respectively). Figures 4.9.5 and 4.9.6 show locations for GEI and joint heater sensors, respectively.

g. Infrared temperature measurements (IR gun) were available for both L-24 hr and T-3 hr time frames. Measurements were as expected and comparable with GEI data, when considering the accuracy associated with present measurement techniques. Table 4.9-5 details infrared on-pad temperature measurements versus actual GEI and joint heater sensor data.

4.9.3 Results Discussion

4.9.3.1 Postflight Hardware Inspection. Following the recovery of the STS-26 SRBs, a postflight inspection of the external hardware was conducted at the SRB disassembly facility (Hangar AF). The TPS performance was considered to be excellent in all areas, with external heating and recession effect less than predicted (Table 4.9-6). Predictions due to the design trajectory environments in Table 4.9-7 will be documented in the SRB Thermal Design Data Book, SE-019-068-2H. The condition of both motors appeared to be

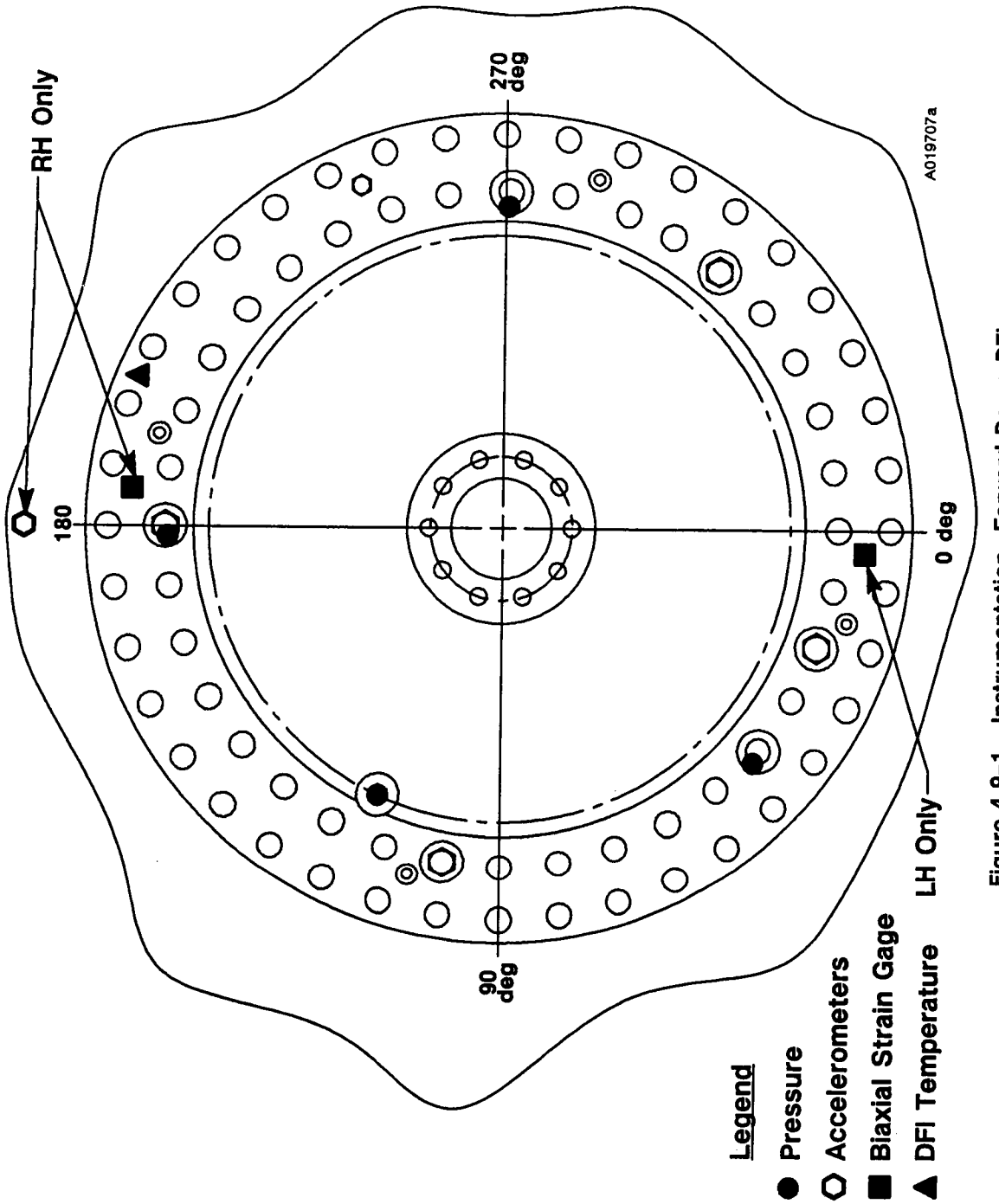

Figure 4.9-1. Instrumentation—Forward Dome DFI

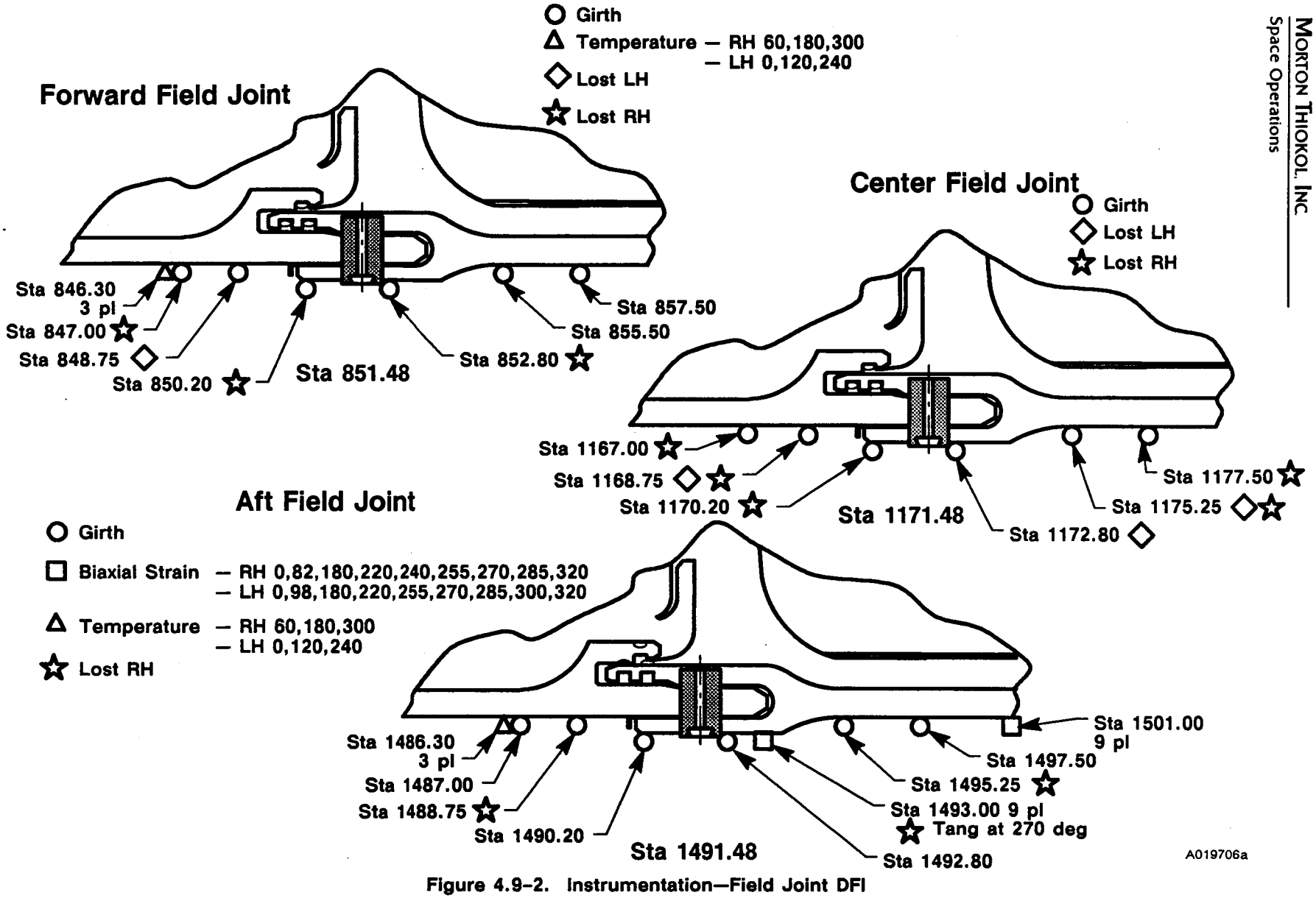

Figure 4.9-2. Instrumentation—Field Joint DFI

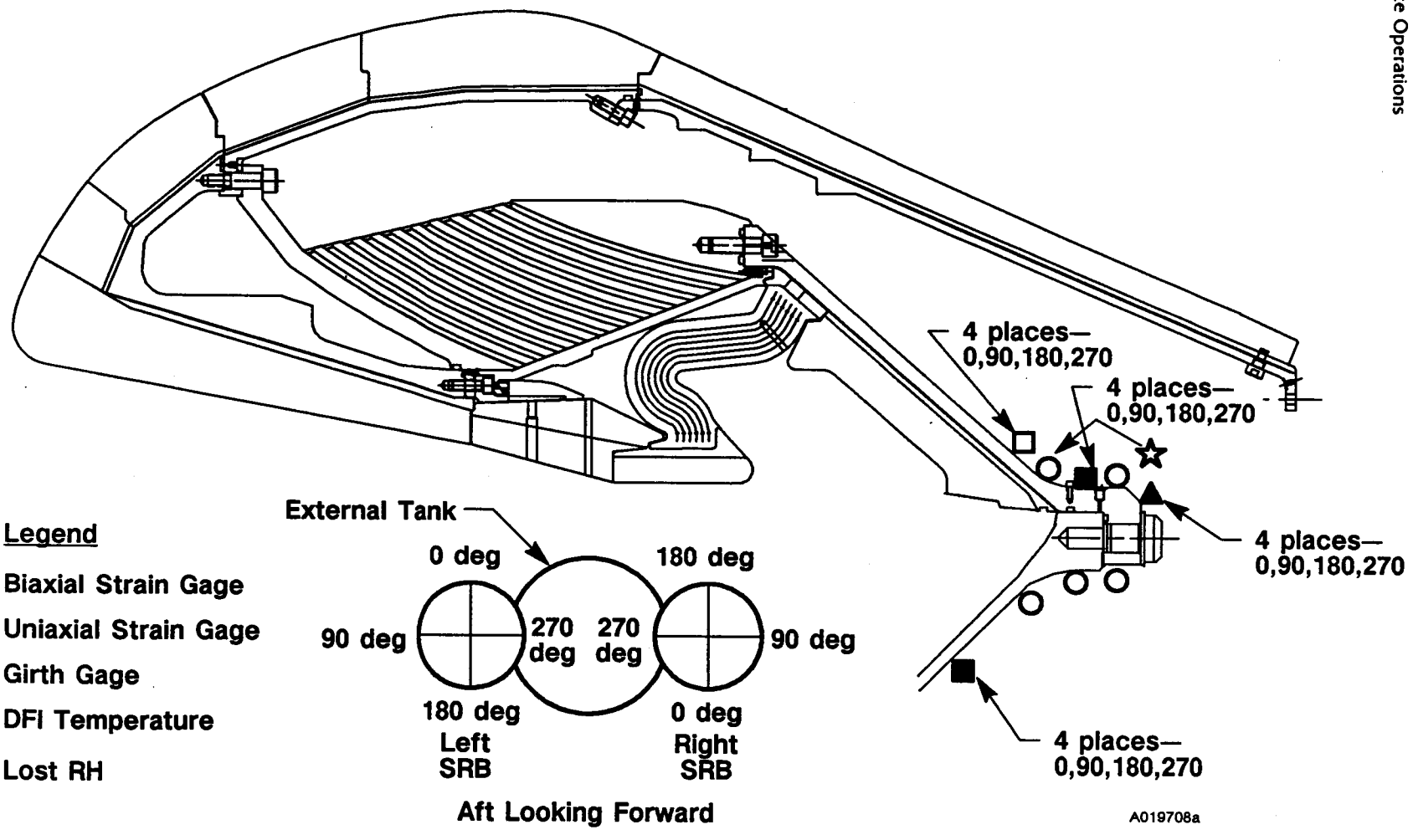

Figure 4.9-3. Instrumentation—Nozzle DFI

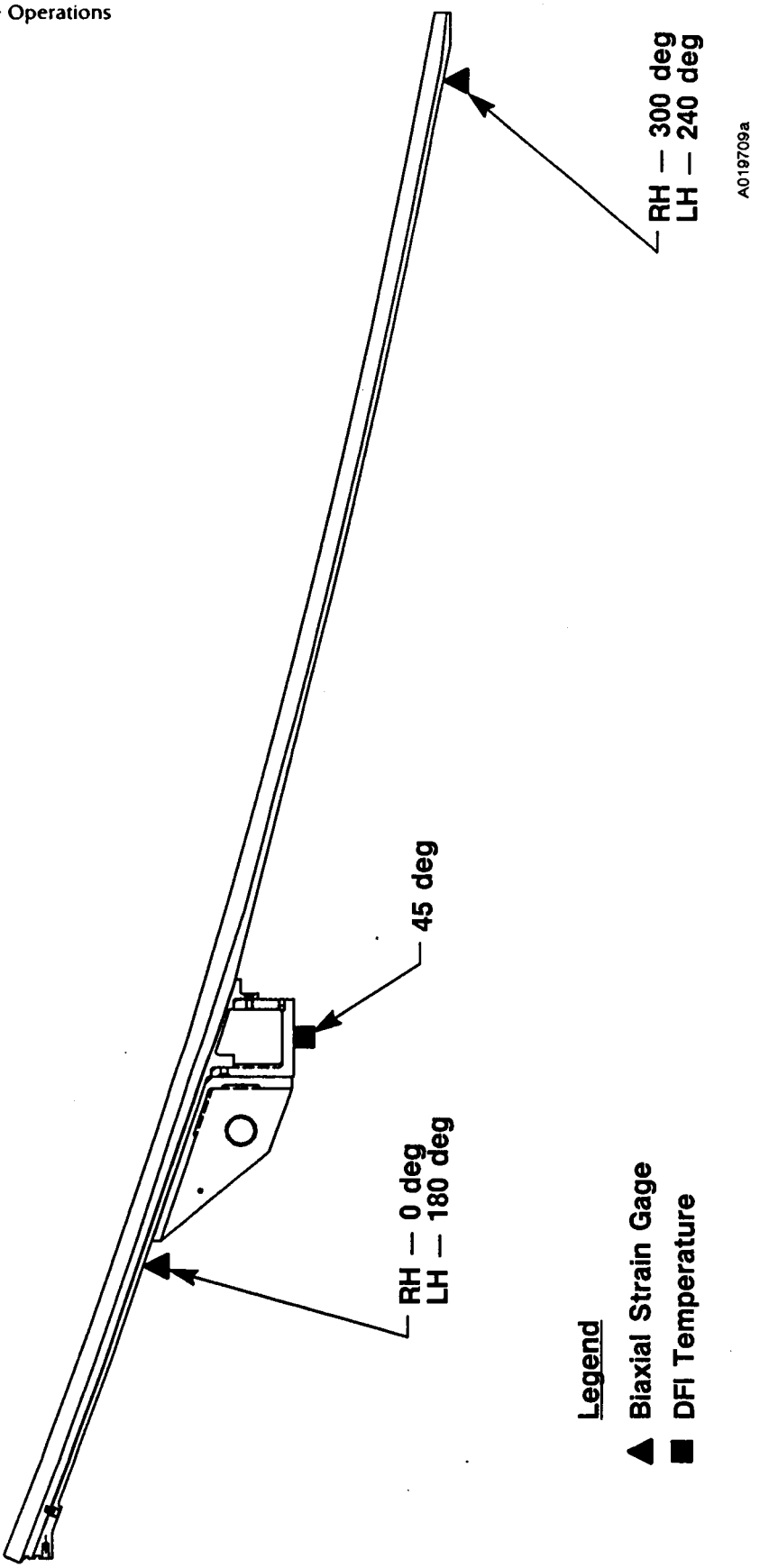

Figure 4.9-4. Instrumentation—Aft Exit Cone DFI

Table 4.9-3. September Historical On-Pad Temperature Predictions Versus Actual GEI/Joint Heater Sensor Data (°F)

Component	Daily Cycling		T-6 Hr to T-5 Min		T-5 Min	
	Histor	Actual	Histor	Actual	Histor	Actual
Igniter/Case Joint						
RH	86-88	85-89	86-87	83-86	87	86
LH	86-88	83-87	86-87	82-85	87	83
Field Joint						
RH Fwd	72-101	83-97	97-112	94-107	97-112	96-107
LH Fwd	73-98	83-90	97-105	95-104	98-105	96
RH Ctr	72-99	83-96	97-112	96-111	97-112	98-109
LH Ctr	73-97	83-88	97-105	94-101	99-103	98-100
RH Aft	72-100	80-86	97-112	94-105	98-112	96-104
LH Aft	73-95	82-87	97-105	94-101	100-105	98-101
Nozzle/Case Joint						
RH	76-78	75-82	88-95	82-90	94	83-90
LH	76-78	80-82	88-95	86-90	94	86-88
Flex Bearing*						
RH	76-78	82-83	81-87	88-91	87	90-91
LH	76-78	82-85	81-87	88-91	87	90-91
Case Acreage (deg)						
RH 45	72-90	78-90	72-88	74-88	88	83-88
270	75-94	76-83	75-90	74-80	90	78-80
266 ETA	75-92	80-83	92-97	79-82	97	82
90 Tunnel	75-83	75-91	75-80	72-88	80	88
LH 45**	73-98	66-82	73-88	62-82	88	67-82
270	75-93	74-85	75-90	72-80	90	78-80
274 ETA	75-92	82-85	90-98	77-82	98	83
90 Tunnel	75-83	80-86	75-78	77-82	77	82
Local Environment						
Temperature	74-86	74-86	74-84	70-84	84	83
Wind Speed (K)	9	2-18	9	3-9	9	9
Wind Direction***	NE	NE	NE	NW-NE	NE	NE
Cloud Cover		Broken		Scattered		Scattered

*Nozzle flex bearing aft end ring
**Actual readings were low due to bad sensor on aft segment
***Predominant direction

Table 4.9-4. Pre-T-6 Hr On-Pad Temperature Predictions Versus Actual GEI/Joint Heater Sensor Data (°F)

Component	T-6 Hr to T-5 Min		T-5 Min	
	Pre-T-6	Actual	LCC	Actual
Igniter/Case Joint				
RH	84-87	83-86	66-123	86
LH	82-85	82-85	66-123	83
Field Joint				
RH Fwd	96-106	94-107	85-122	96-107
LH Fwd	96-102	95-104	85-122	96
RH Ctr	96-106	96-111	85-122	98-109
LH Ctr	96-102	94-101	85-122	98-100
RH Aft	96-102	94-105	85-122	96-104
LH Aft	96-102	94-101	85-122	98-101
Nozzle/Case Joint				
RH	88-94	82-90	75-115	83-90
LH	88-94	86-90	75-115	86-88
Flex Bearing*				
RH	88-94	88-91	NA-115	90-91
LH	88-94	88-91	NA-115	90-91
Case Acreage (deg)				
RH 45	78-87	74-88	35-NA	83-88
270	75-83	74-80	35-NA	78-80
266 ETA	--	79-82	35-NA	82
90 Tunnel	--	72-88	35-NA	88
LH 45**	77-85	62-82	35-NA	67-82
270	75-83	72-80	35-NA	78-80
274 ETA	--	82-83	35-NA	83
90 Tunnel	--	77-82	35-NA	82
Local Environment				
Temperature	77-81	70-84	38-99	83
Wind Speed (K)	9	2-18	24	9
Wind Direction***	NE	NE	NE	NE
Cloud Cover		Scattered		Scattered

*Nozzle flex bearing aft end ring
**Actual readings were low due to bad sensor on aft segment
***Predominant direction

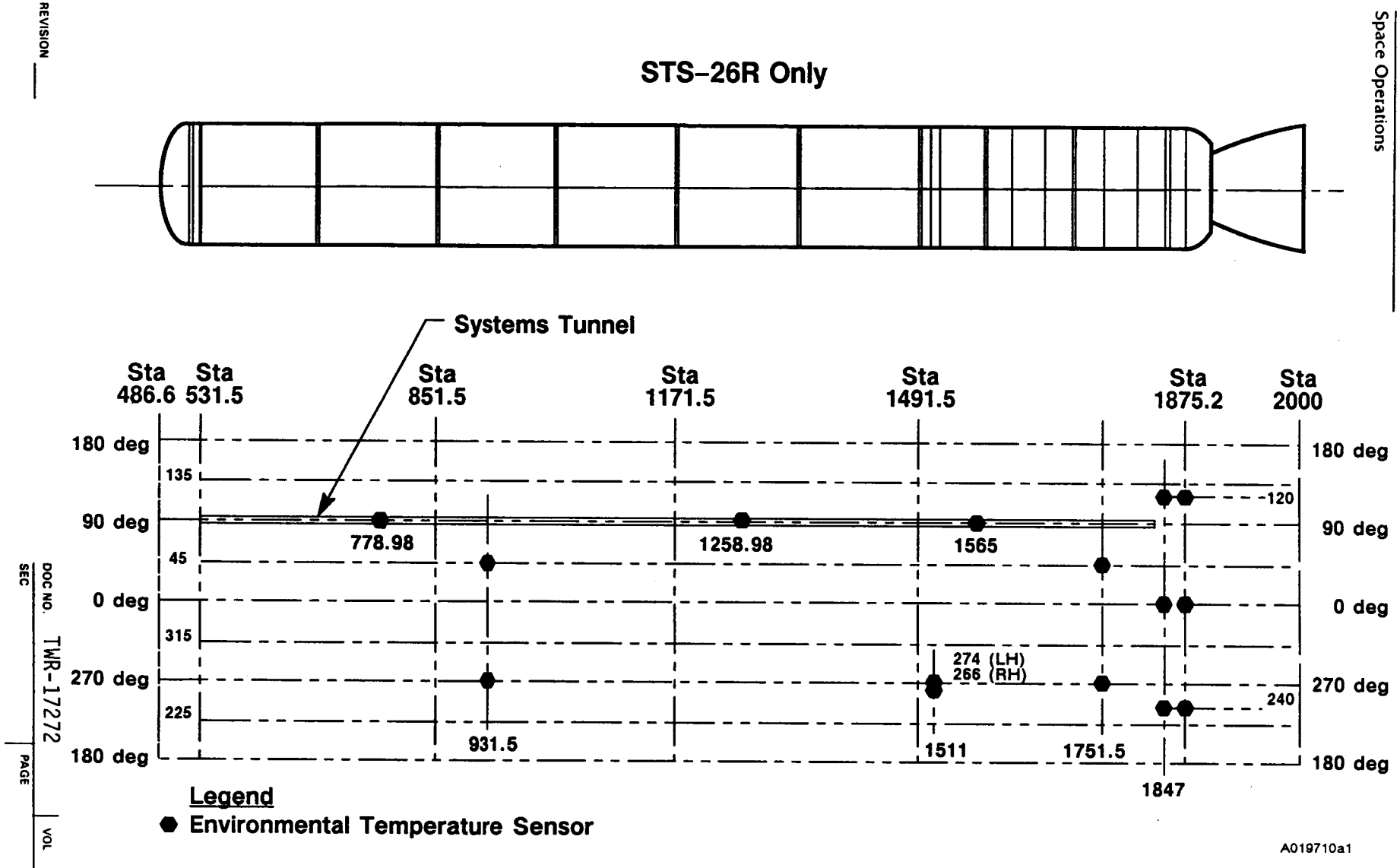

Figure 4.9-5. Instrumentation—Case Ground Environmental Instrumentation

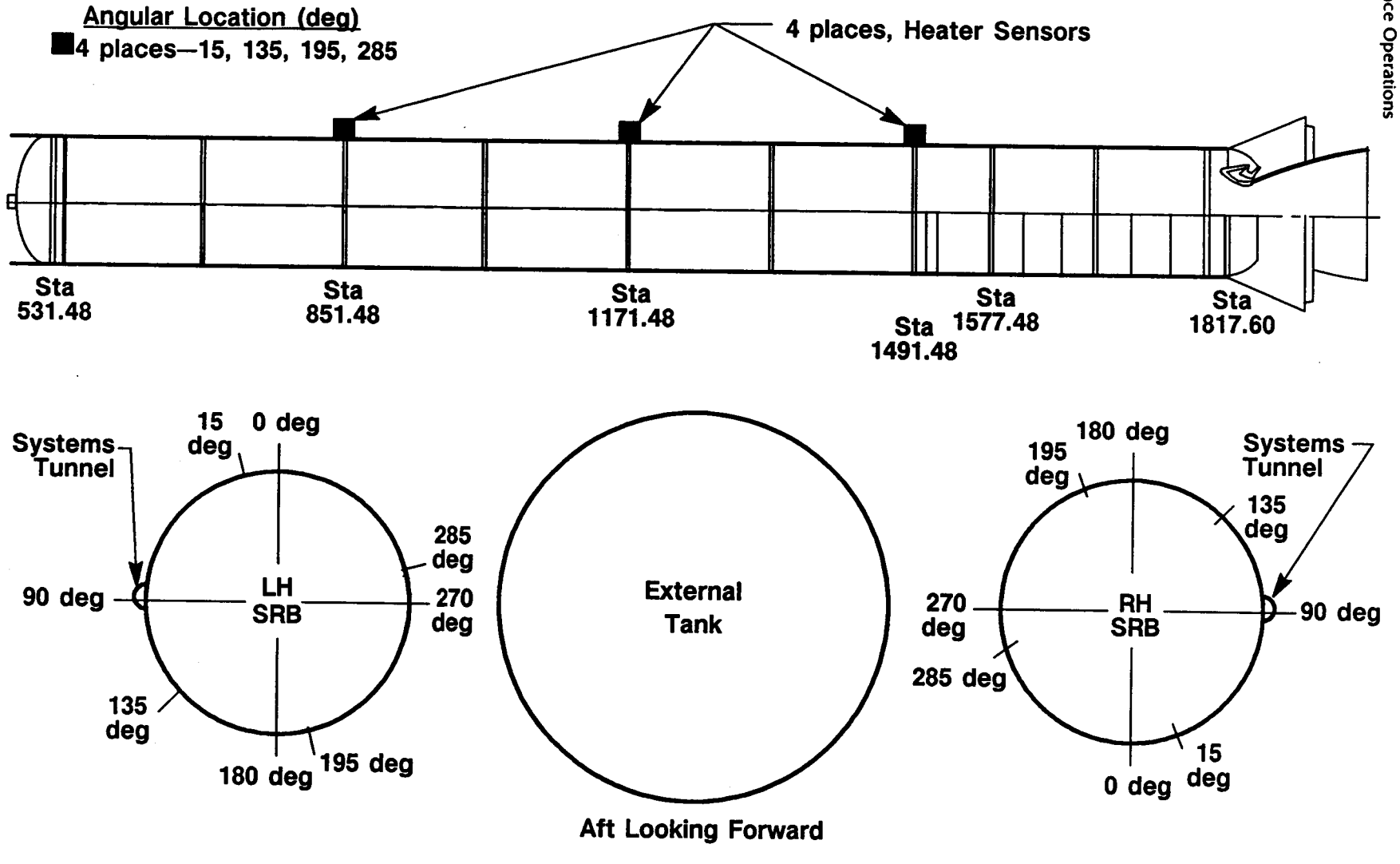

Figure 4.9-6. Instrumentation Field Joint Heater Temperature Sensors

A019070a

Table 4.9-5. Infrared On-Pad Measurements Versus Actual GEI/Joint Heater Sensor Data at 1000 Hr on 28 Sep 1988

Component	Infrared Location (deg)	Infrared Temp (°F)	Actual GEI Location (deg)	Actual GEI Temp (°F)
Field Joint				
LH Aft	0	81	345	84
	90	81	45	84
	180	80	165	83
	270	81	255	85
LH Ctr	0	80	15	84
	90	81	135	85
	180	79	195	84
RH Aft	0	82	15	81
	90	84	135	83
	180	83	195	83
	270	81	285	84
RH Ctr	0	80	15	83
	90	90	135	90
	180	90	195	83
Case Acreage				
LH Aft*	45	81	45	67
	270	82	270	75
LH Fwd**	45	75	45	78
RH Aft	45	81	45	80
	270	81	270	80
RH Fwd**	45	77	45	86

*Actual readings at 45 deg aft were low due to bad sensor. Actual readings at 270 deg have been up to 6°F low.
**Infrared gun measurements taken at a steep angle have always read low and are questionable.

Table 4.9-6. SRM External Performance Summary (TPS Erosion), Left and Right Motors

Component	TPS Material	Maximum Erosion (in.) Predicted	Measured
Field Joints	Cork	0.003	None
Factory Joints	EPDM	0.014	Immeasurable*
Systems Tunnel	Cork	0.014	None
Stiffener Rings	EPDM	0.009	Immeasurable*
DFI, Cables	Cork	0.036	Immeasurable*
	Silica Phenolic	0.000	None
Nozzle Exit Cone	Cork	0.104	NA**

*All evidences of erosion were apparent only on the inboard region of the aft segment, where flight-induced thermal environments are most severe.
**Nozzle exit cones are not recovered.

Table 4.9-7. SRB Flight-Induced Thermal Environments

Ascent Heating	Document No. STS 84-0575, dated 24 May 1985
	Change Notice 2, SE-698-D, dated 30 Apr 87
	Data on computer tapes No. DN 4044 and DN 9068
	Change Notice 3, SE-698-D, dated 30 Oct 1987 Tape No. DP 5309
Base Recirculation Heating	Document No. STS 84-0259, dated Oct 1984
	Change Notice 1, SE-698-D, dated 30 Sep 1987
SSME and SRB Plume Radiation	Document No. STS 84-0259, dated Oct 1984
	Change Notice 1, SE-698-D, dated 30 Sep 1987
SSME Plume Impingement After SRB Separation	Document No. STS 84-0259, dated Oct 1984
	Change Notice 1, SE-698-D, dated 30 Sep 1987
Reentry Heating	Document No. SE-0119-053-2H, Rev. D, dated Aug 1984, and Rev. E, dated 12 Nov 1985

similar to previous flight motors, with most of the heat effects seen on the aft segments on the inboard side of the SRBs. The aft segment inboard regions facing the ET experience high aerodynamic heating normal to protuberance components. They also receive the highest plume radiation and recirculation heating, induced from the adjacent SRB and SSMEs, to aft facing surfaces. There was slight ablation in this area to the TPS over the factory joints, the stiffener rings and stubs, and DFI runs. A concise summary of hardware condition is shown in Table 4.9-1.

a. Field Joints

1. Field Joint Cork. All of the cork on all field joints was in place with no pieces or parts of pieces missing. None of the ablative compound was missing. No debonds were found.

The paint on the aft surface of the joint protection system (JPS) thermal insulation showed sporadic pitting. This was apparently caused by debris on water impact, as the adjacent area of the motor case contained streaks made by debris traveling up the case during impact. Also, the aft joints of both motors which are protected on splashdown by the ETA ring had no pitting of the paint.

The paint on the field joints was slightly darkened and blistered. The amount of blistering and darkening was greater in some areas in others.

A bubble containing water was found in the cork insulation at 150 deg on the right motor center field joint. This was removed and examined. The cork-to-case bondline was intact. A small void apparently developed in the cork during manufacturing and during ascent. The air in this void expanded, generating the bubble.

2. Field Joint Moisture Seals. All six moisture seals were opened and found to contain water. The 12 vent valves were hand removed and evaluated. Five were open and a sixth one had been damaged by the water laser prior to hand removal, so it could not be evaluated. The vent valves appear to have permitted the water to enter the joints.

The forward field JPS on the right motor was removed by hand. The sealing surfaces on both edges of the moisture seal were

inspected. The seals were still in place and properly bonded to the motor. In many areas the paint on the motor came up with the moisture seal as it was removed, providing evidence of a secure bond.

3. Field Joint Heater and Sensors. The heater and sensor assemblies showed no signs of overheating, discoloration, or delamination.

b. Factory Joints. The factory joints on each of the motors were in very good condition. The only signs of ablation experienced on the factory joints were located on the aft segments of each motor. There was only slight ablation or charring that occurred on the inboard regions of the aft segment factory joints. This occurred approximately between 220 and 320 deg circumferentially on each motor. Again, this is a normal occurrence that has been observed consistently on previous flight motors.

c. Systems Tunnel. The cork TPS adjacent to the systems tunnel floor plate was in excellent condition. There was very little paint discoloration and no measurable cork ablation.

d. Stiffener Rings. The stiffener ring TPS was generally in very good condition with only slight thermal degradation. The ablation was again experienced in the 220- to 320-deg sector, with the ethylene propylene diene monomer (EPDM) on the outer flange showing signs of heat effect. This region was subjected to aeroheating along the outboard tip forward face, and the aft face experienced radiant heating. The K5NA TPS on the forward side of the stubs was also slightly charred in the same regions, with intermittent pitting around the entire circumference. The three stiffener rings on the right-hand SRB were fractured during water impact, typically at about the 160-deg location, but the TPS was in good condition.

e. DFI and Cables. The cork TPS covering the DFI and cableways was generally in good condition. There was very little heat effect observed, with only slight paint discoloration and blistering. Several DFI cable runs had small areas of missing cap cork at intermittent regions. The largest sections missing were sections of cap cork, full width (2.5 in.) by about 8 in. long. These sections were located at Station 1180 on the

left-hand motor at 0, 20, 40, and 270 deg. The largest sections on the right-hand motor were located at Station 930 at 140, 150, and 190 deg.

This was apparently the result of poor bonding, as the adhesive appeared completely gone in these areas. Based on the shape of the cork fracture edges and the lack of heat effect, it appeared that most of the cork was removed late in reentry or at water impact.

f. Nozzle (External). The external appearance of the nozzles was typical, as observed in other flights. Internal nozzle assessment is found in Section 2.11.2

4.9.3.2 DFI Thermal Sensor Assessments. The STS-26R flight trajectory was a lofted trajectory as compared to the IVBC-3 design trajectory. Consequently, the flight aerodynamic heating and plume heating pulses would be lower than the corresponding heat pulses for the design trajectory. Therefore, the measured DFI thermal data, barring some unforeseen circumstances, would be lower than the analytically predicted data. The predicted data are based on the results of computer-aided thermal analysis using the thermal environments provided by MSFC (Table 4.9-7).

The DFI was installed on both the right and left SRM on the igniter adapter, the forward and aft field joints, the nozzle fixed housing flange, the nozzle aft exit cone aluminum supporting structure, and the aft exit cone near the exit plane under the cork (Figures 4.9.1 through 4.9.4). Most of the instrumentation was installed to detect any possible leakage of combustion gases through the igniter joint, the field joints, and the nozzle-to-case joint. Furthermore, the DFI were to record the time of certain events, such as the severance of the aft exit cone and the blowing away of the thermal curtain which protects the equipment in the base region. It may be stated here that the predicted temperatures do not consider the leakage of combustion gases.

Table 4.9-2 presents the list of DFI thermal gages, their locations, the maximum predicted temperatures, and the actual maximum temperatures recorded at the time of SRB separation and later during reentry. Figures 4.9.7 through 4.9.32 detail actual DFI thermal histories. The following general comments are observations and concerns:

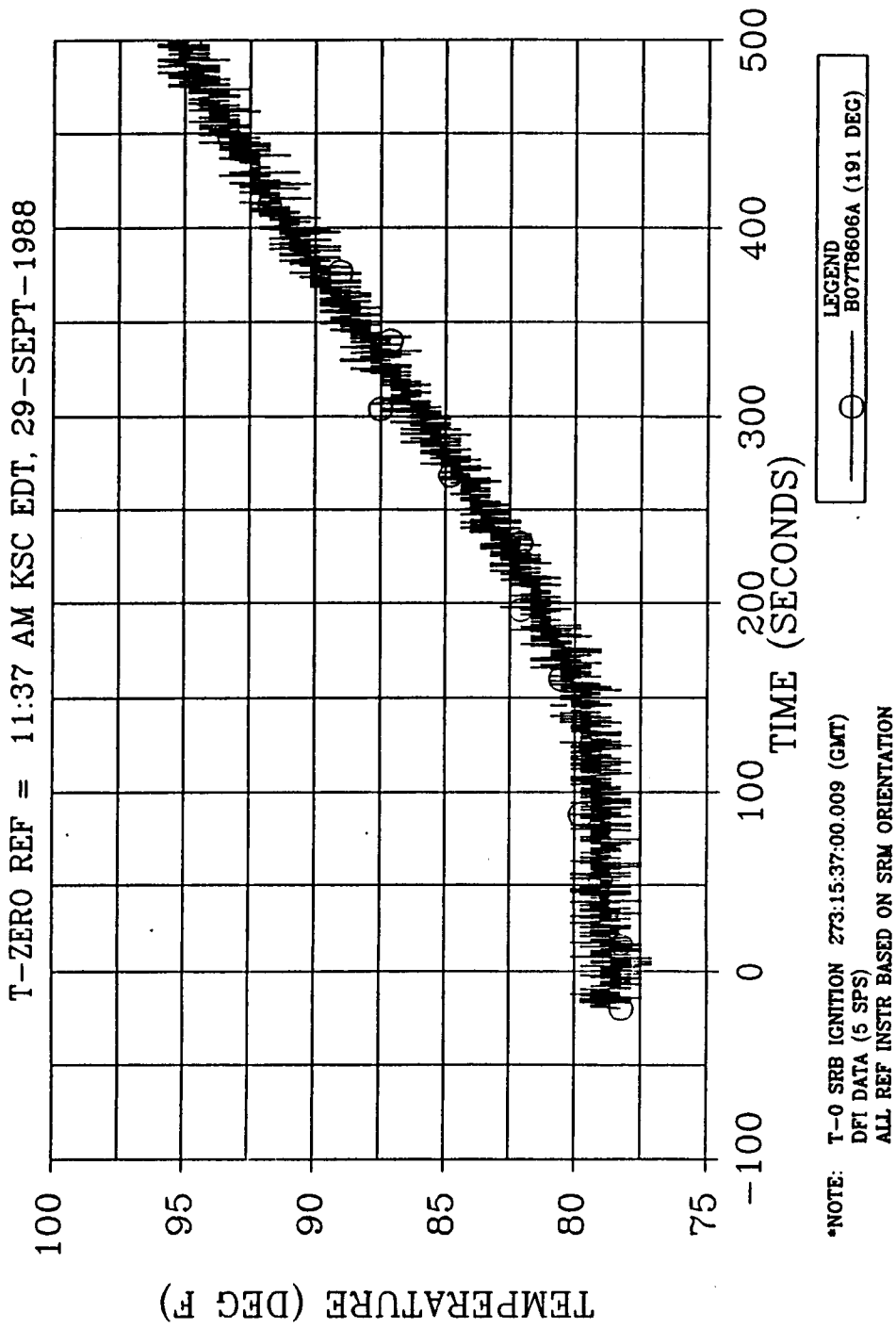

Figure 4.9-7. 360L001 Right SRM Igniter Adapter Temperature, Station 486.40

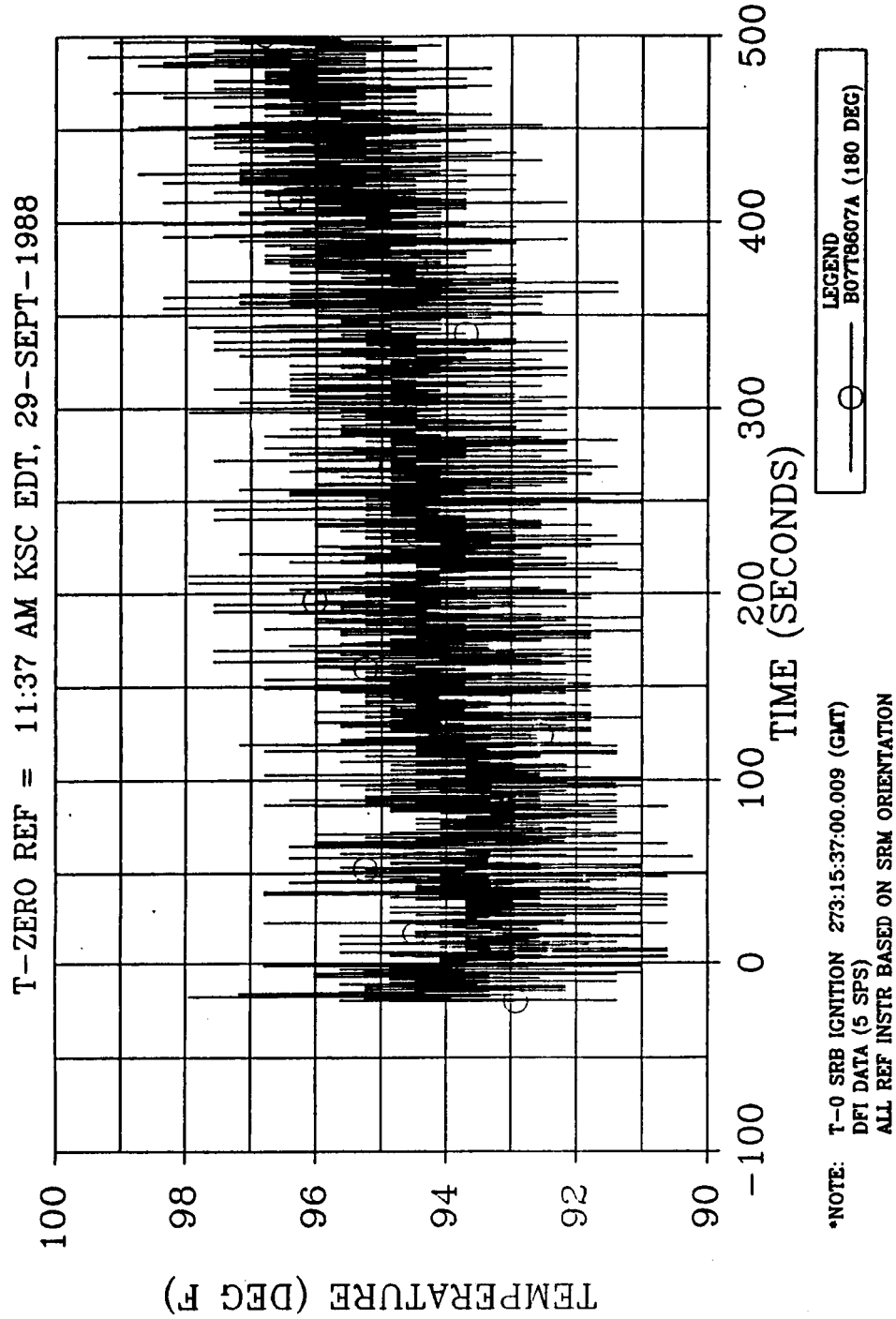

Figure 4.9-8. 360L001 Right SRM Forward Field Joint Temperature, Station 846.30

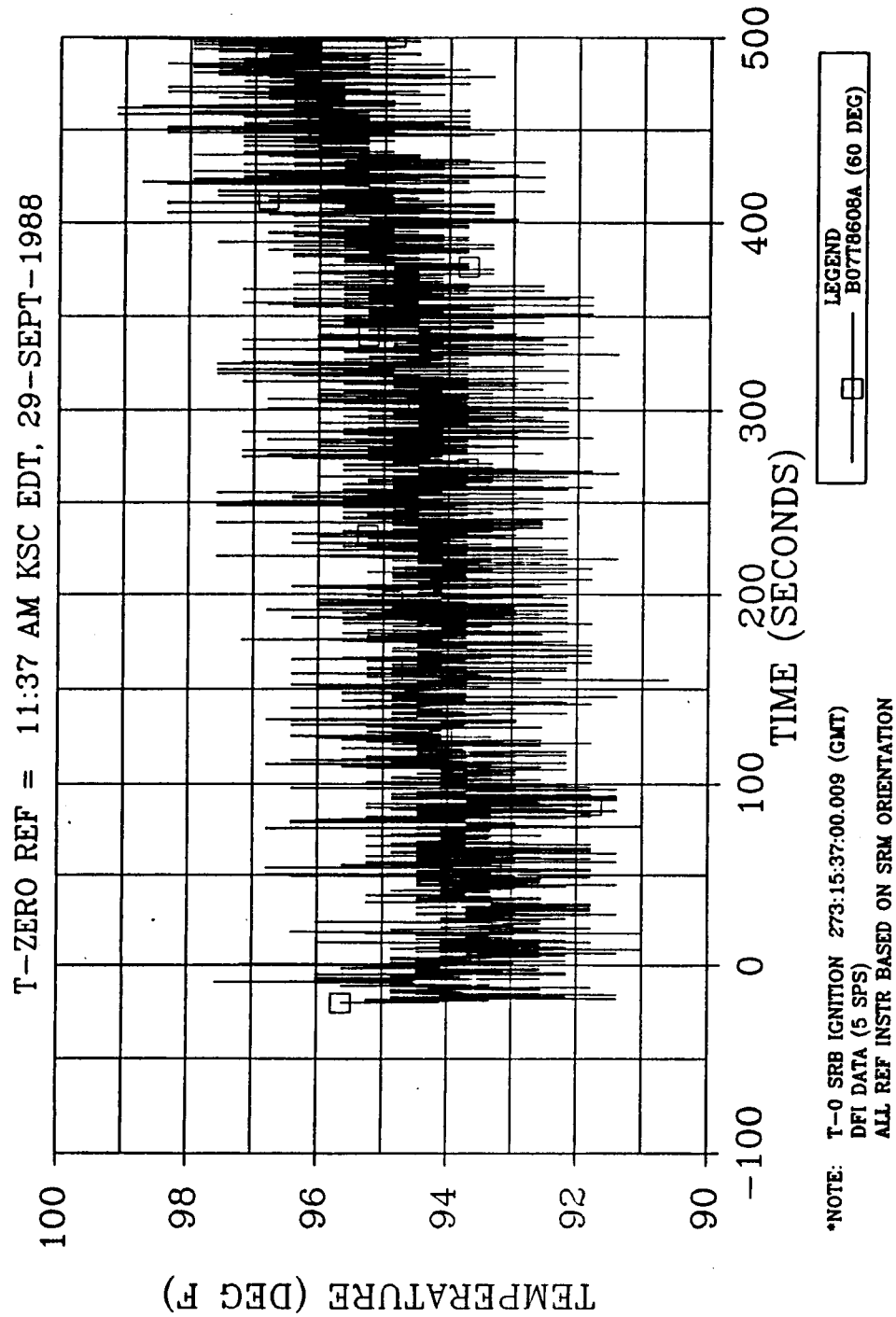

Figure 4.9-9. 360L001 Right SRM Forward Field Joint Temperature, Station 846.30

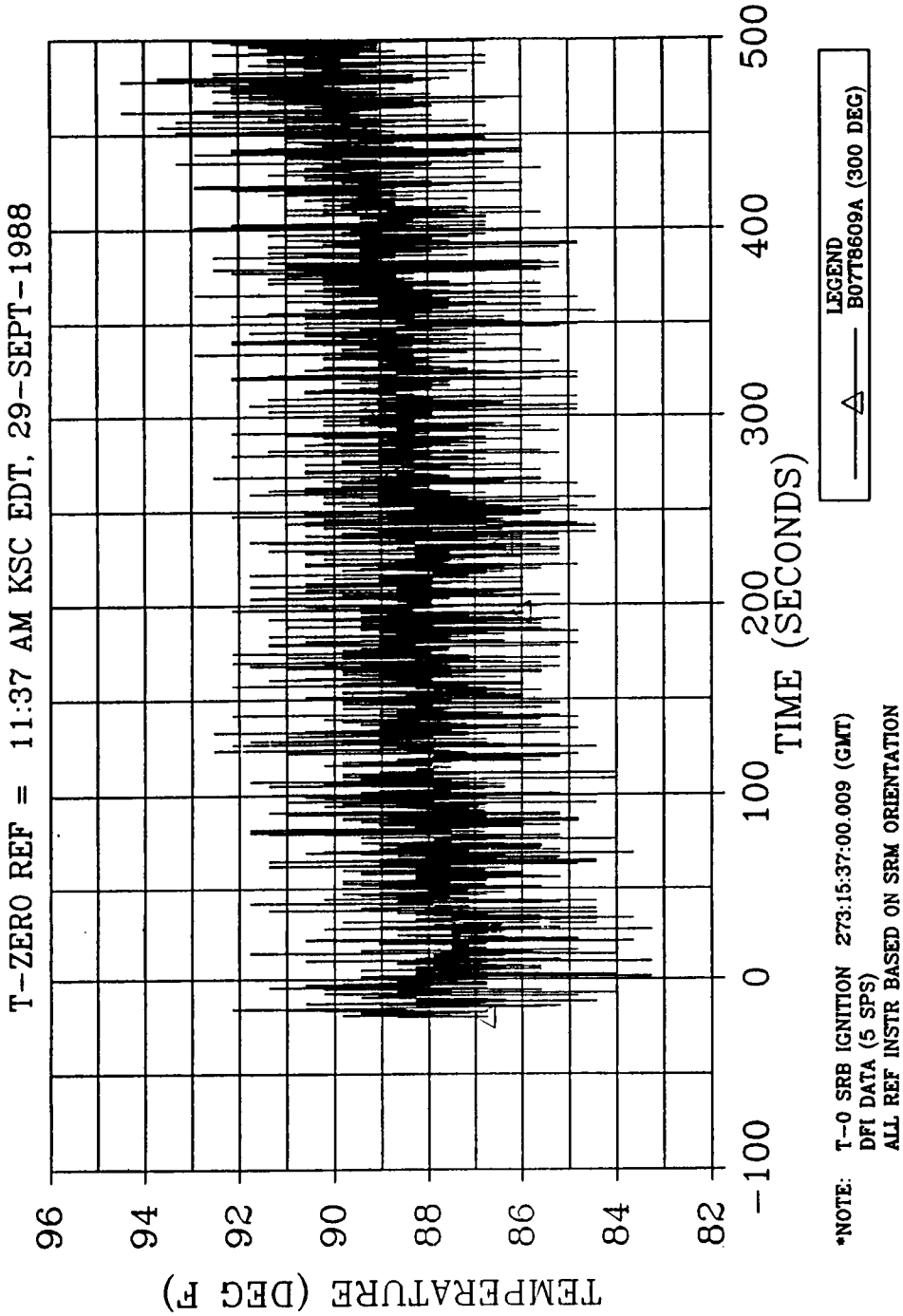

Figure 4.9-10. 360L001 Right SRM Forward Field Joint Temperature, Station 846.30

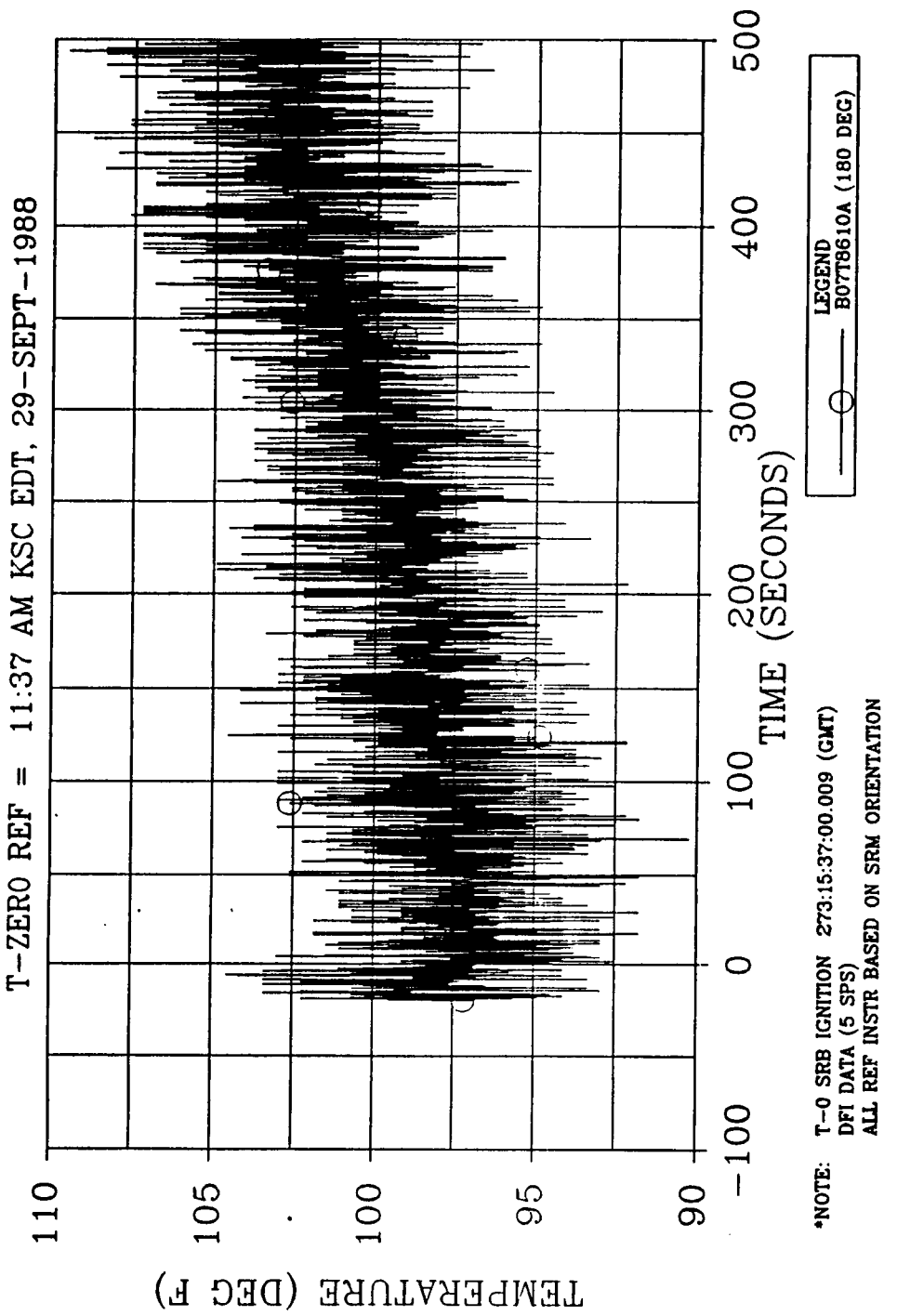

Figure 4.9-11. 360L001 Right SRM Aft Field Joint Temperature, Station 1486.30

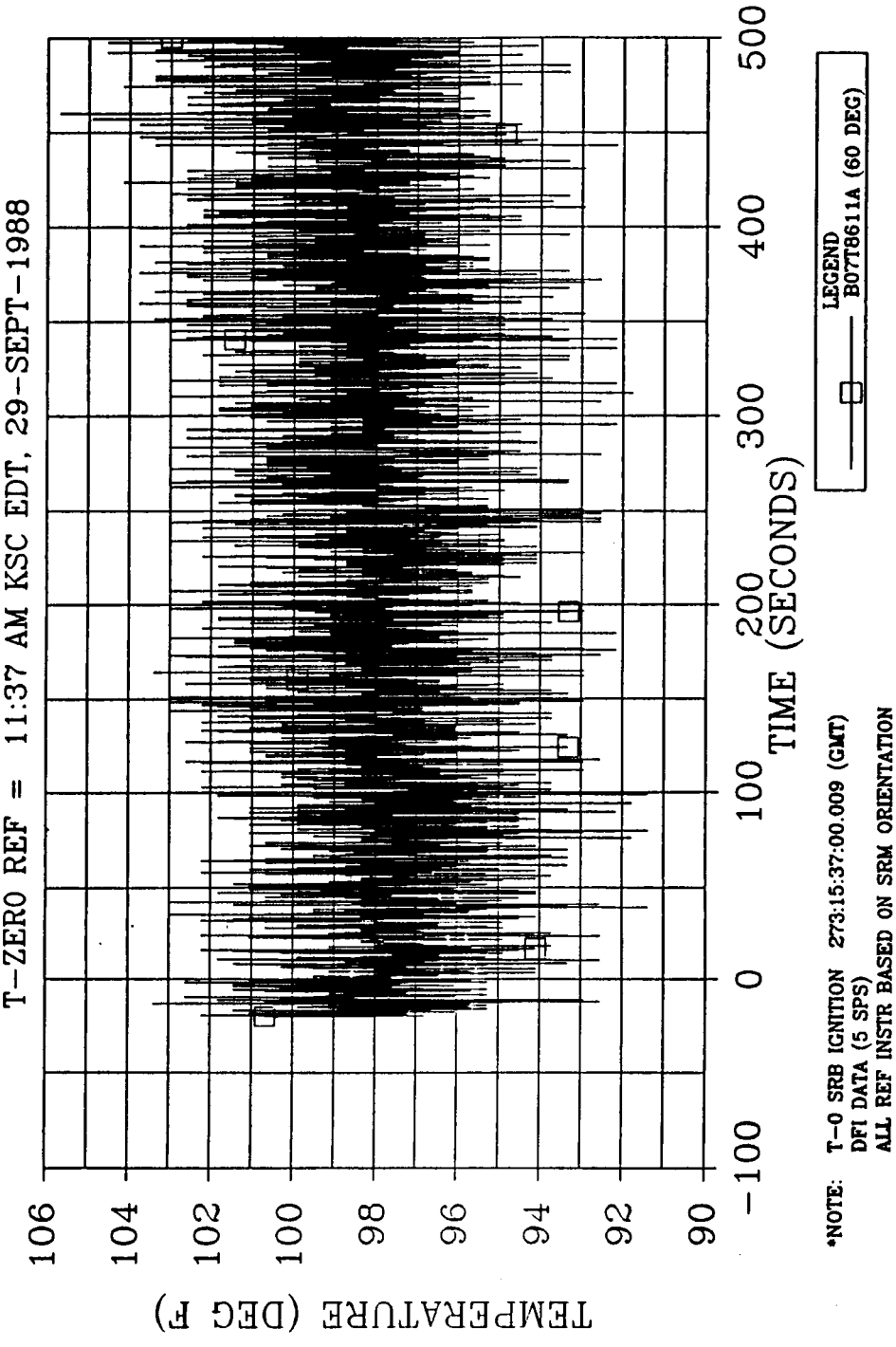

Figure 4.9-12. 360L001 Right SRM Aft Field Joint Temperature, Station 1486.30

ORIGINAL PAGE IS
OF POOR QUALITY

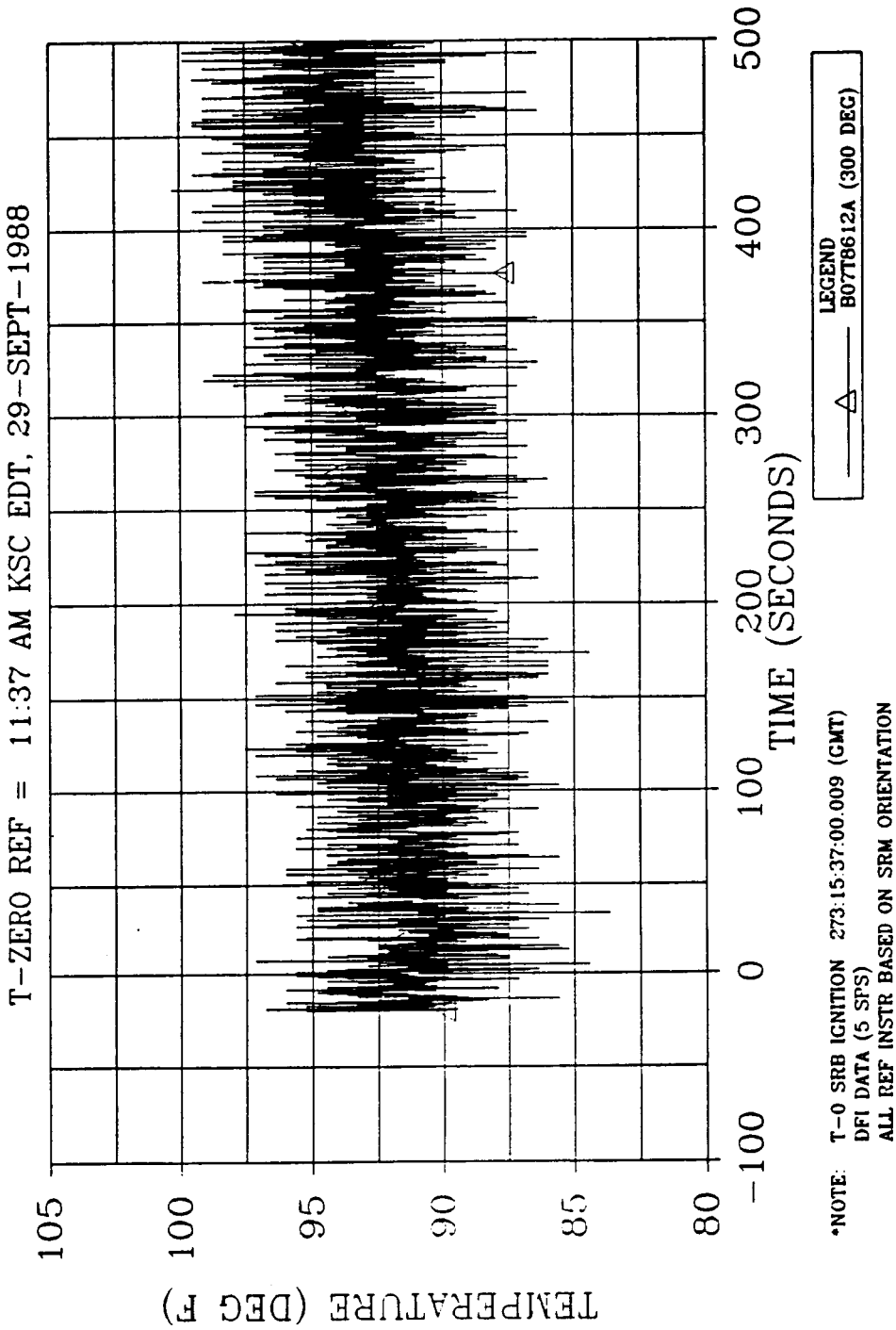

Figure 4.9-13. 360L001 Right SRM Aft Field Joint Temperature, Station 1486.30

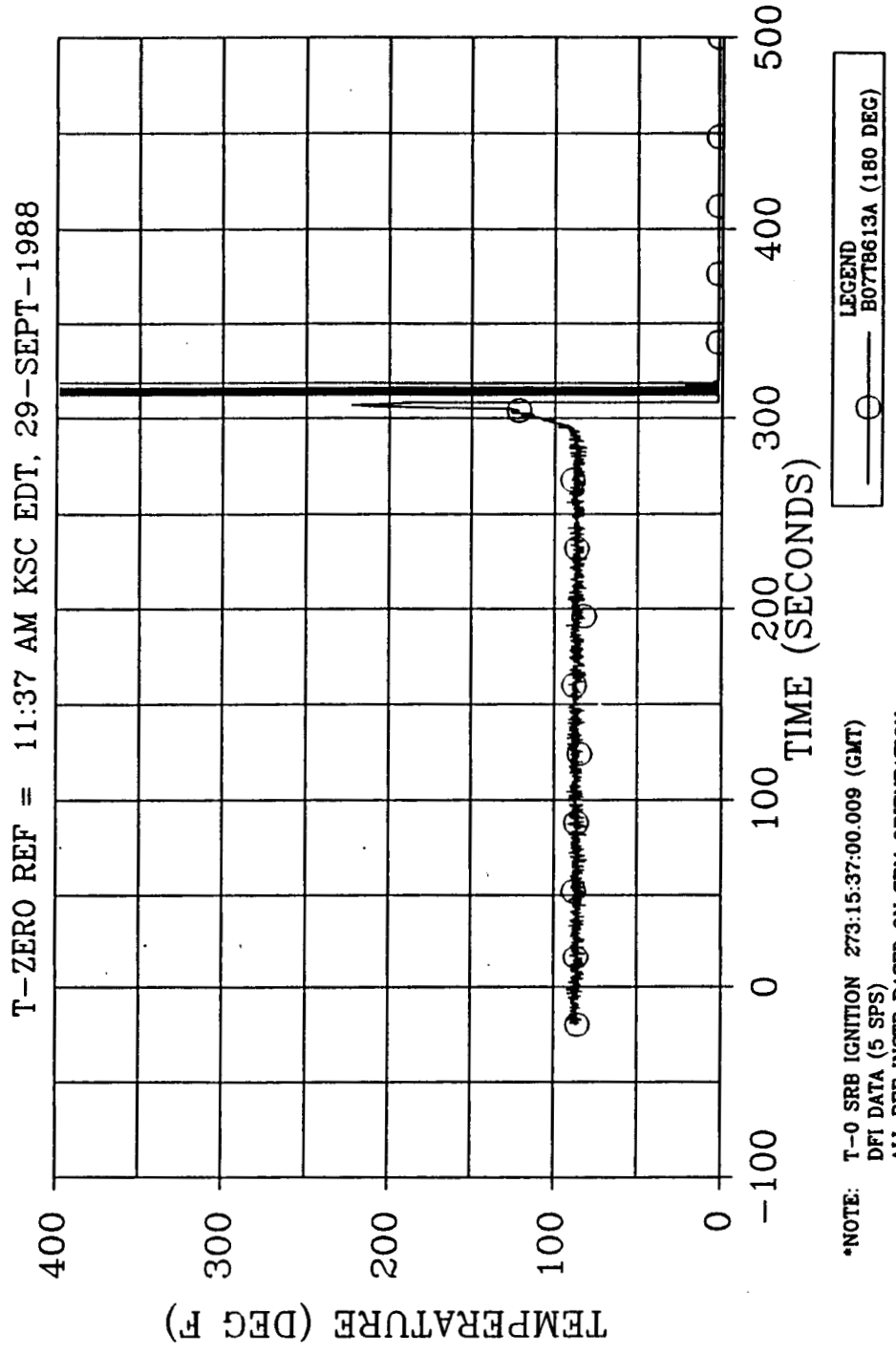

Figure 4.9-14. 360L001 Right SRM Nozzle Housing Temperature, Station 1877.50

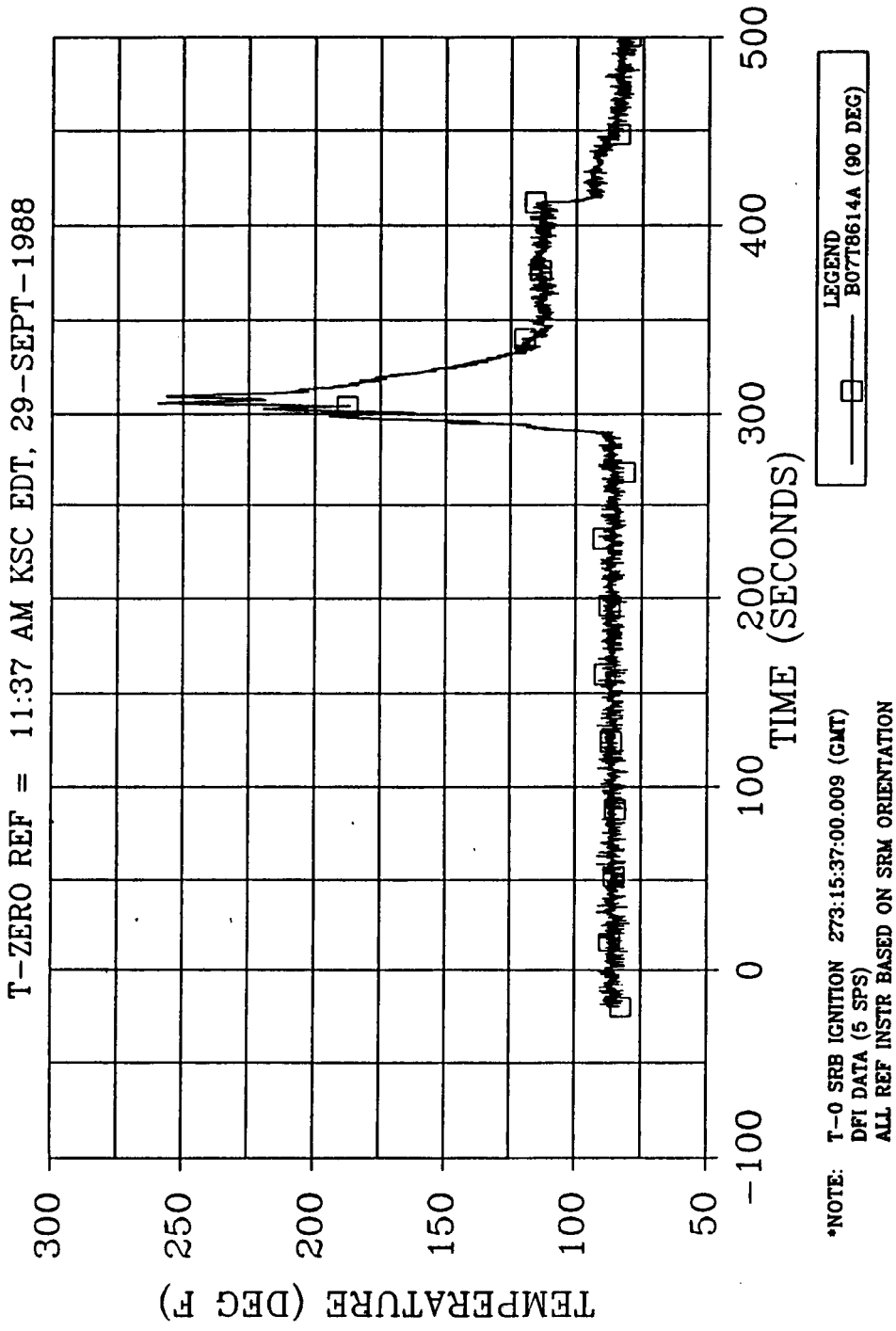

Figure 4.9-15. 360L001 Right SRM Nozzle Housing Temperature, Station 1877.50

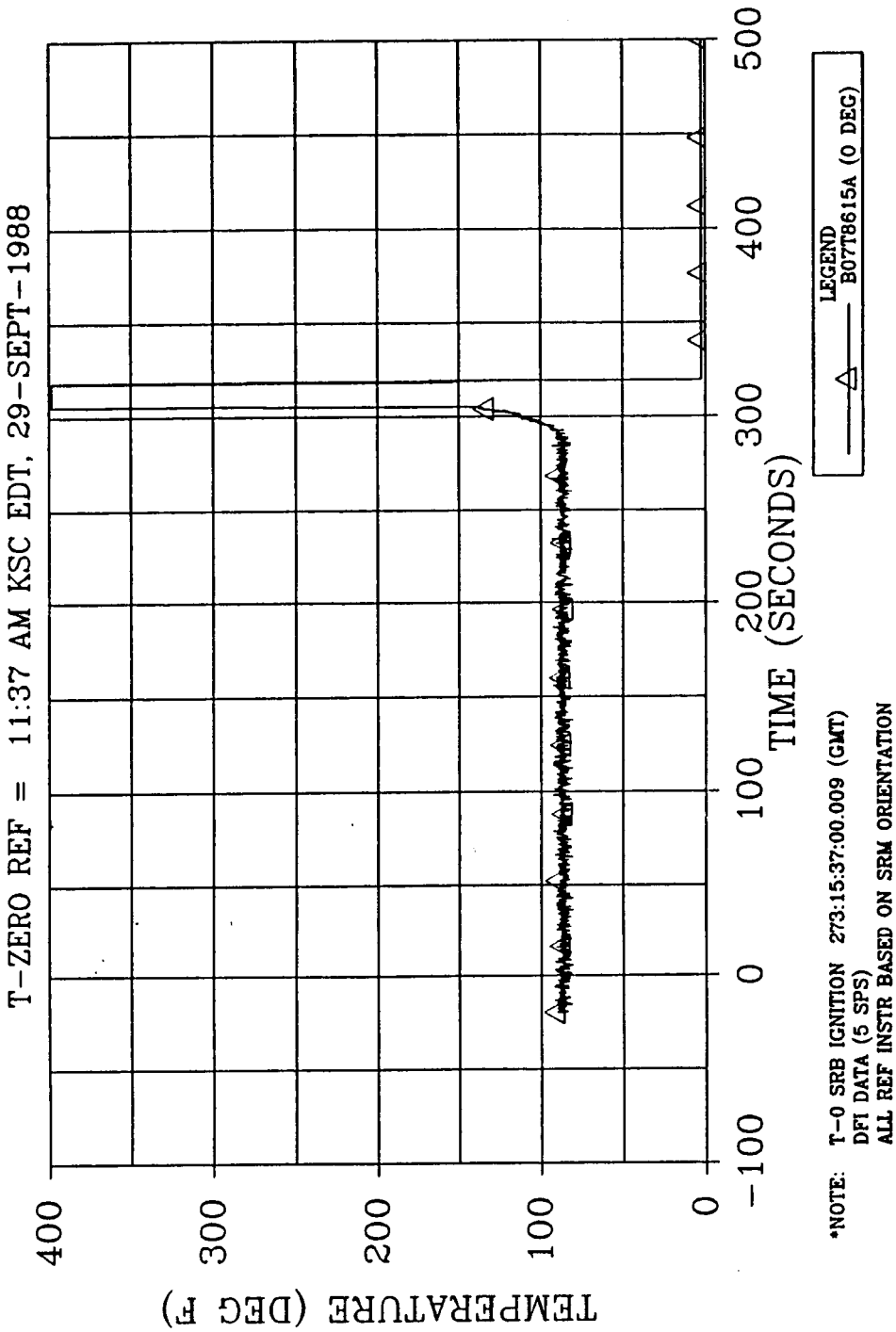

Figure 4.9-16. 360L001 Right SRM Nozzle Housing Temperature, Station 1877.50

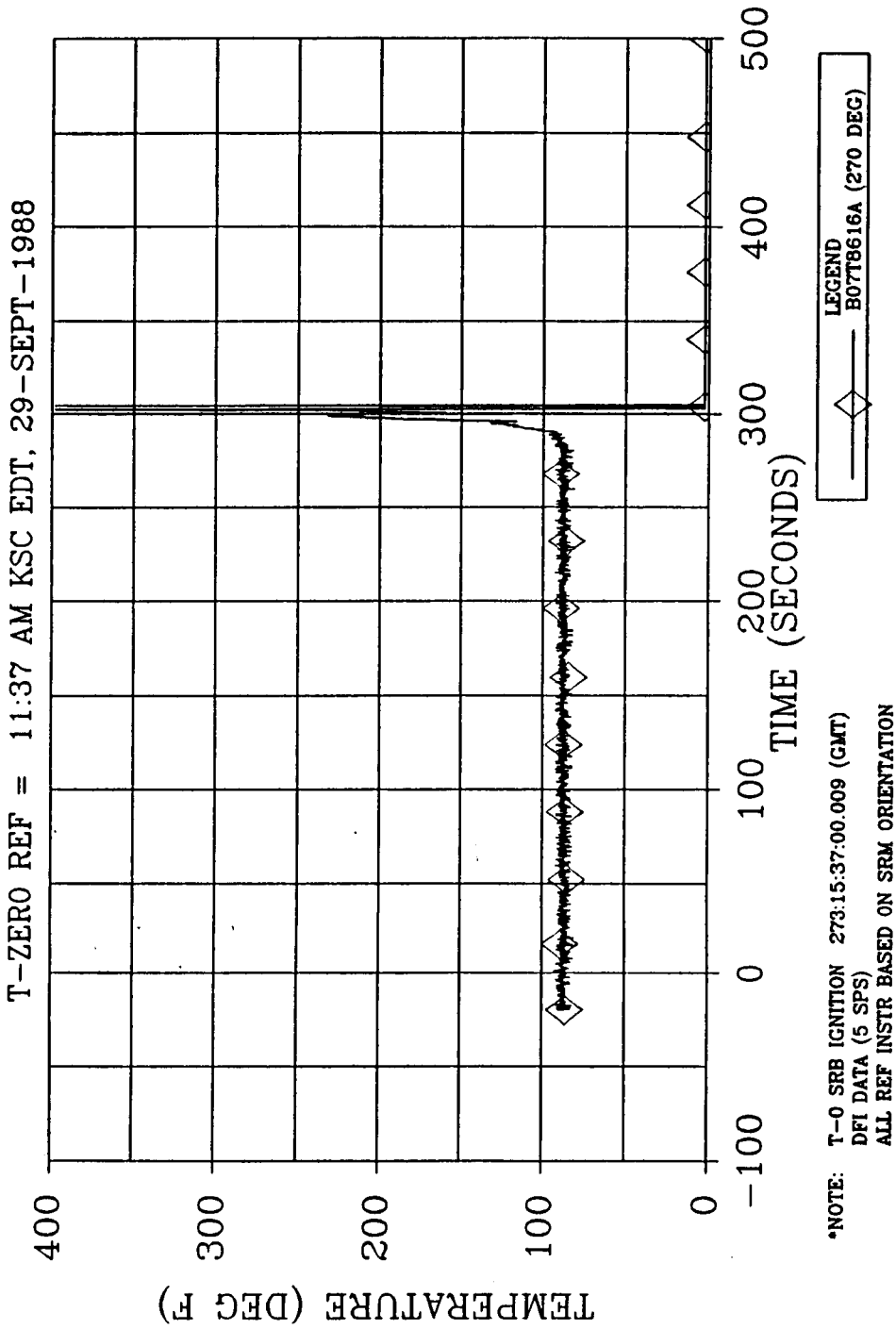

Figure 4.9-17. 360L001 Right SRM Nozzle Housing Temperature, Station 1877.50

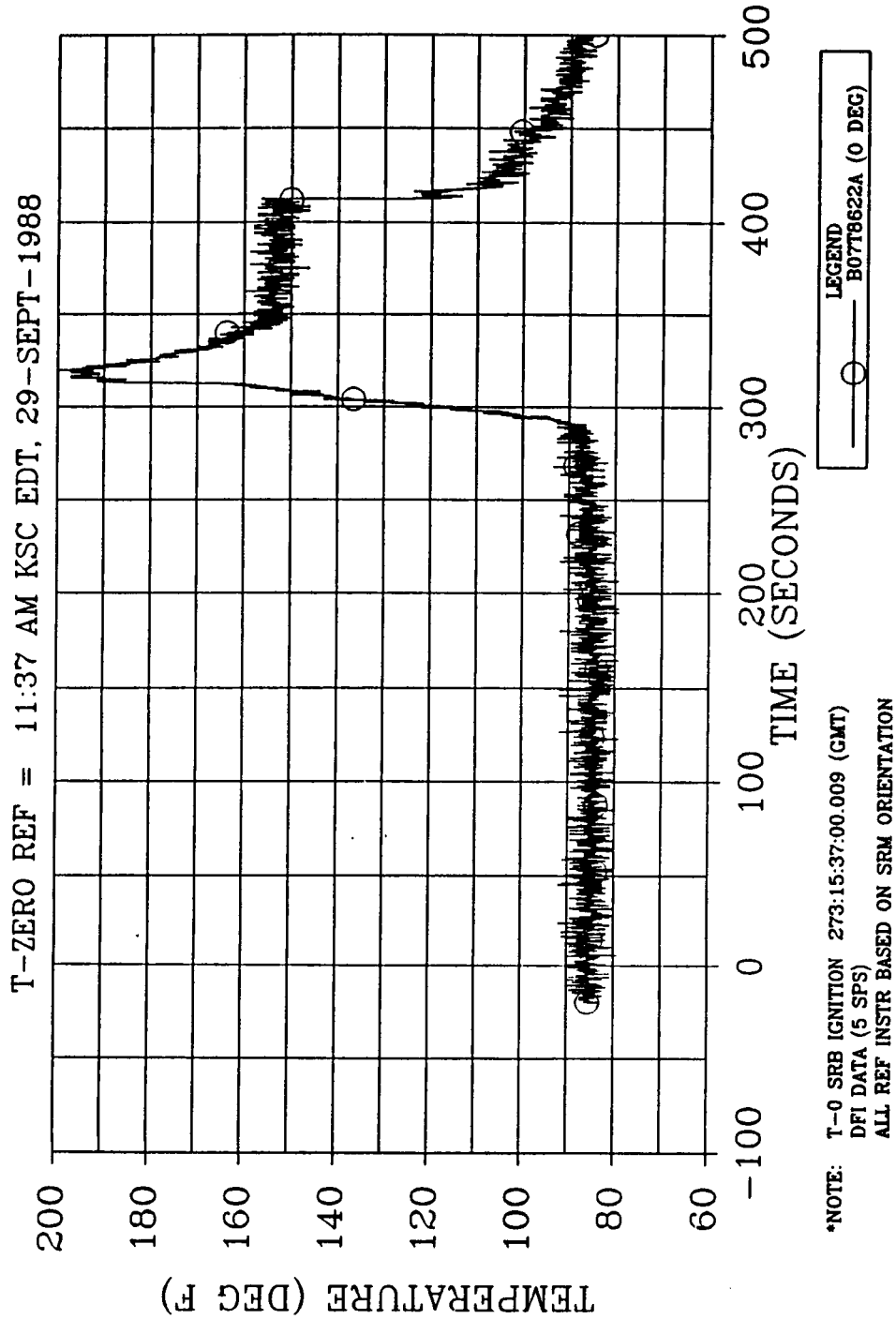

Figure 4.9-18. 360L001 Right SRM Nozzle Exit Cone Temperature, Station 1905.00

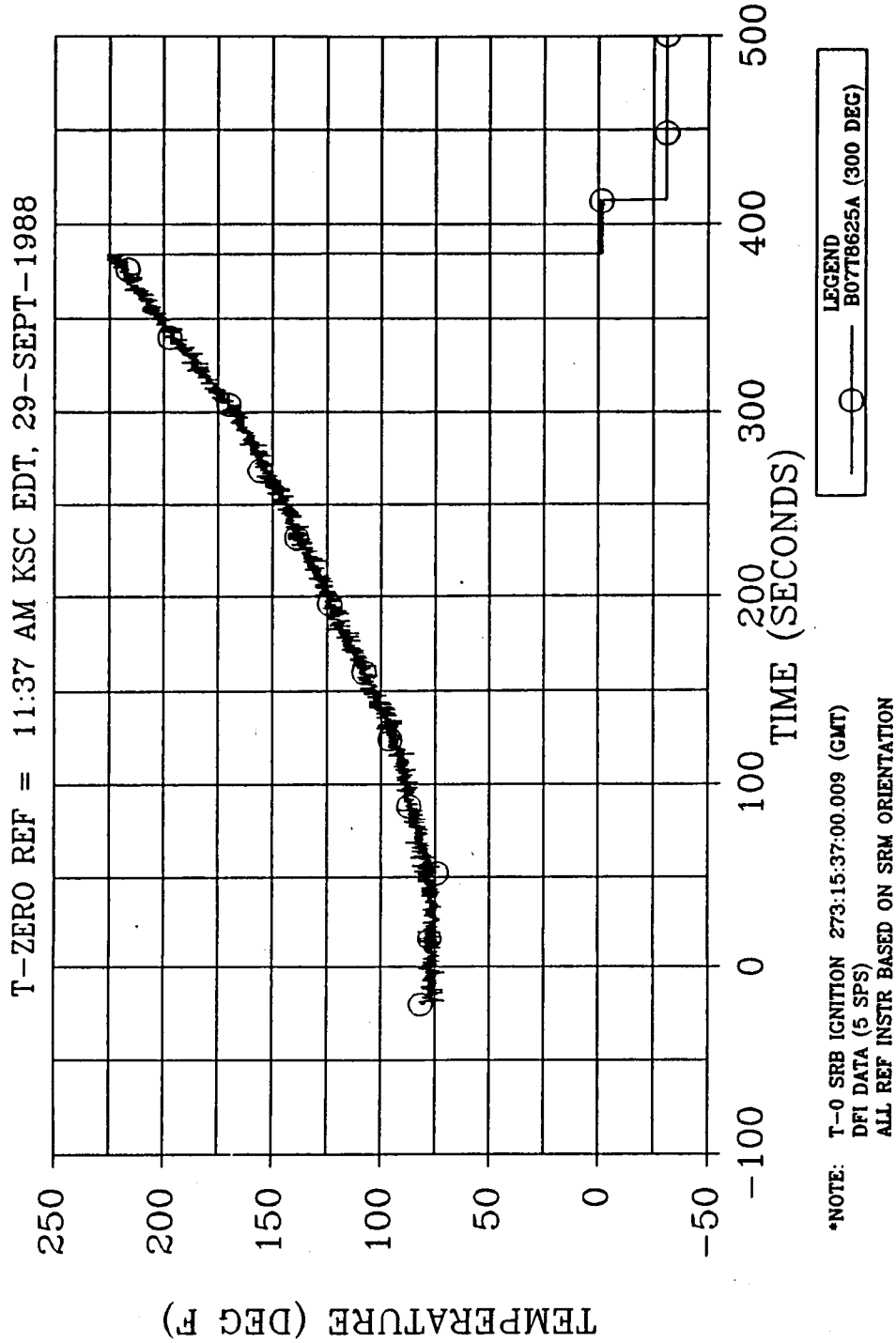

Figure 4.9-19. 360L001 Right SRM Nozzle Exit Cone Temperature, Station 1996.50

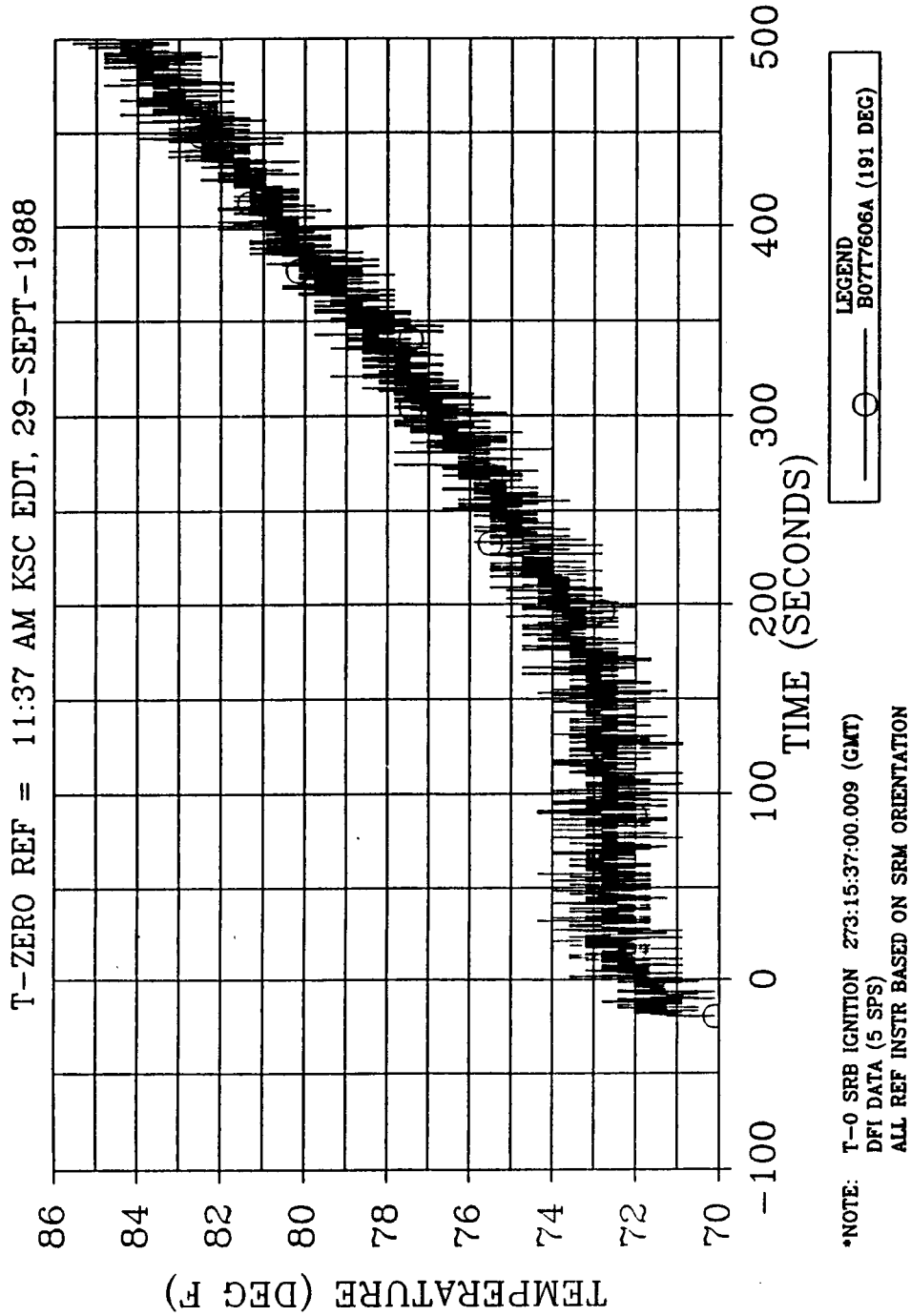

Figure 4.9-20. 360L001 Left SRM Igniter Adapter Temperature, Station 486.40

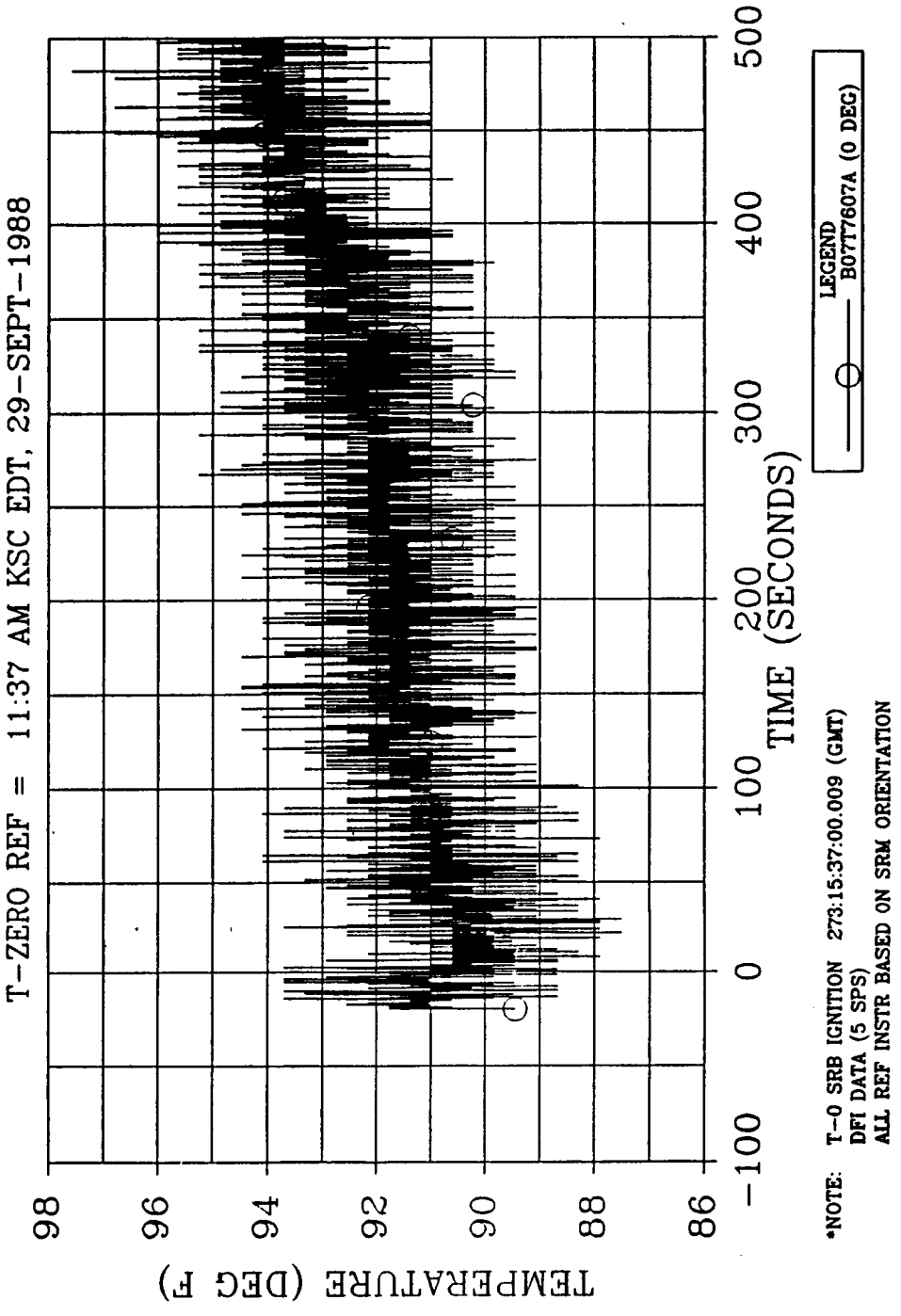

Figure 4.9-21. 360L001 Left SRM Forward Field Joint, Station 846.30

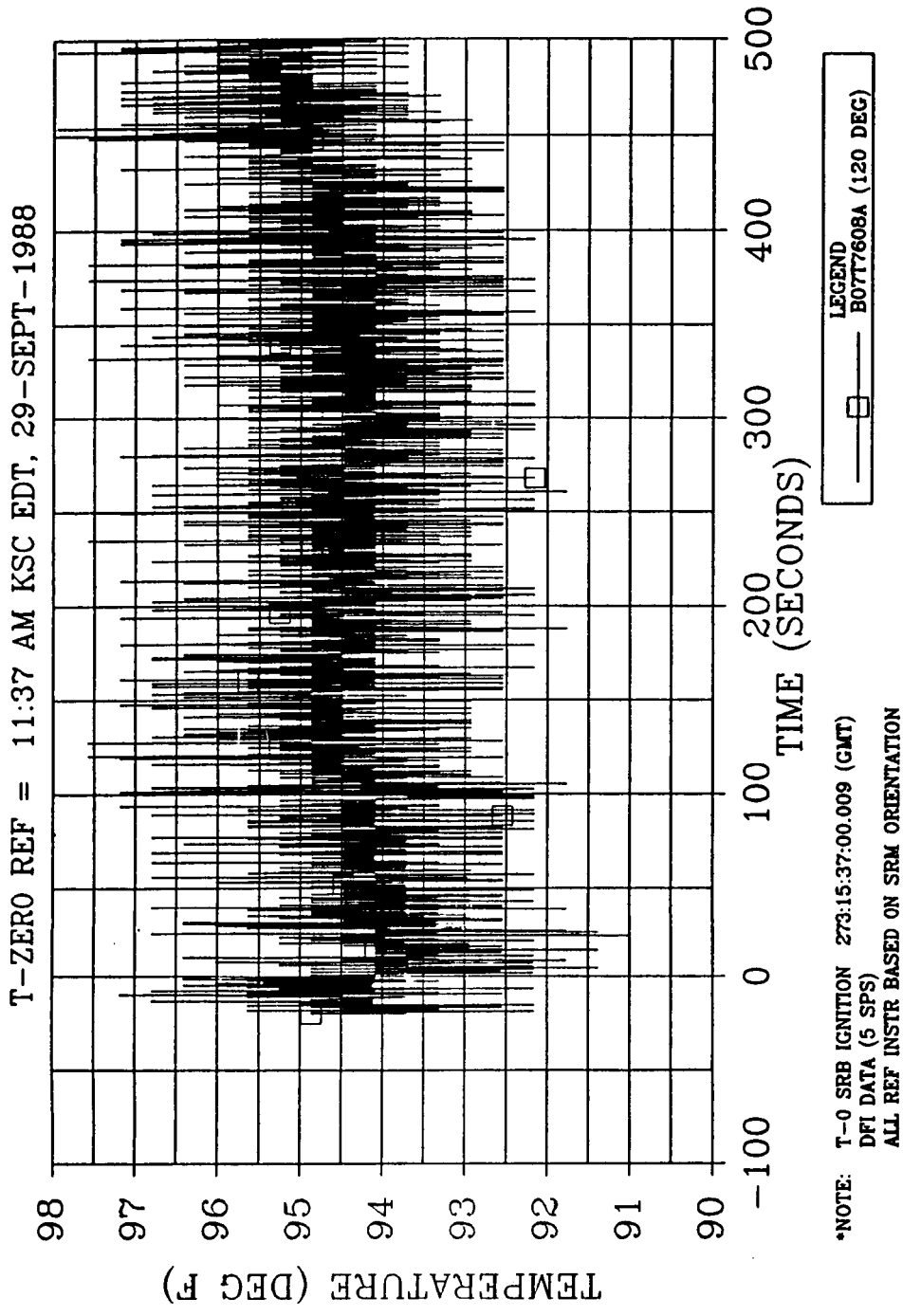

Figure 4.9-22. 360L001 Left SRM Forward Field Joint, Station 846.30

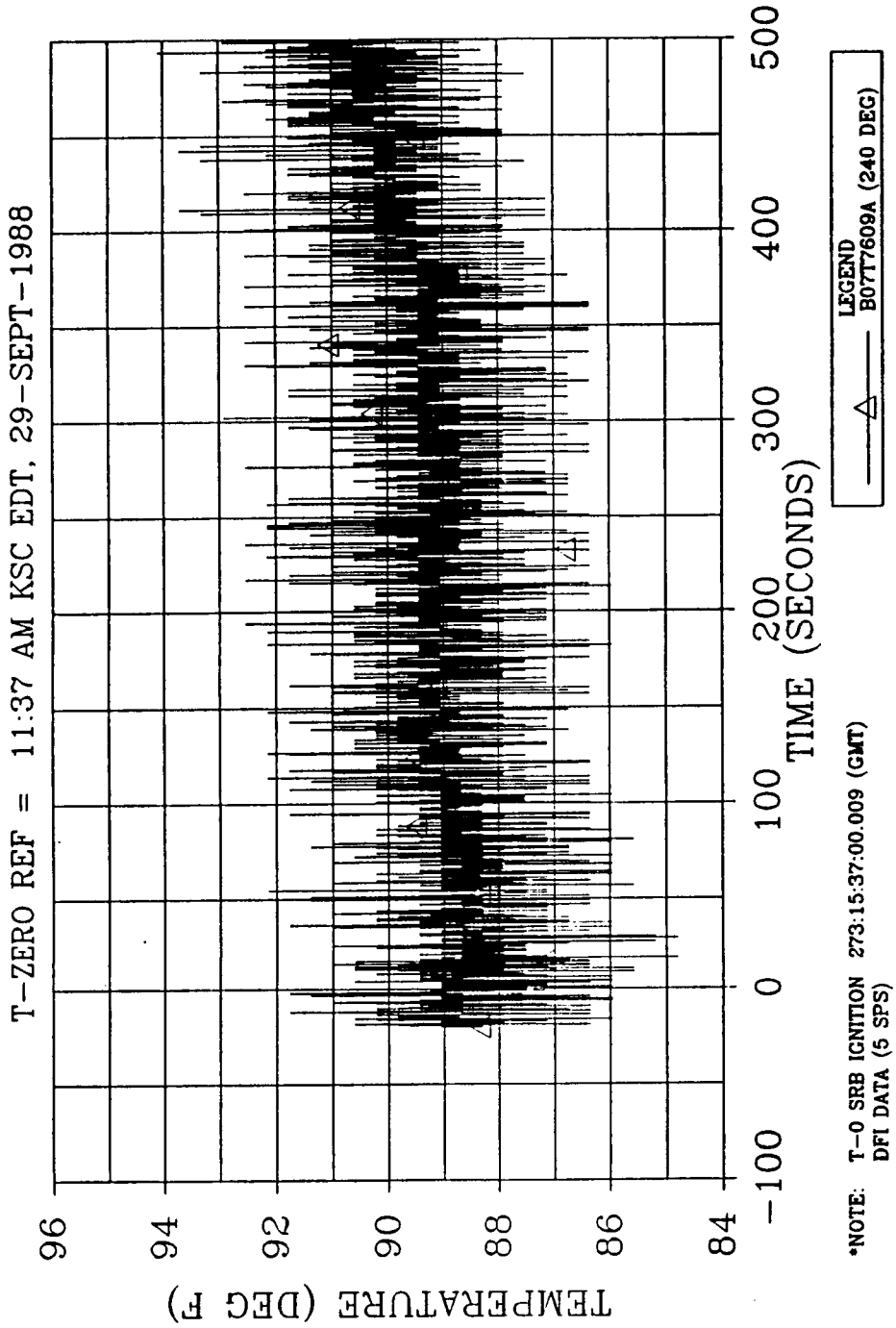

Figure 4.9-23. 360L001 Left SRM Forward Field Joint, Station 846.30

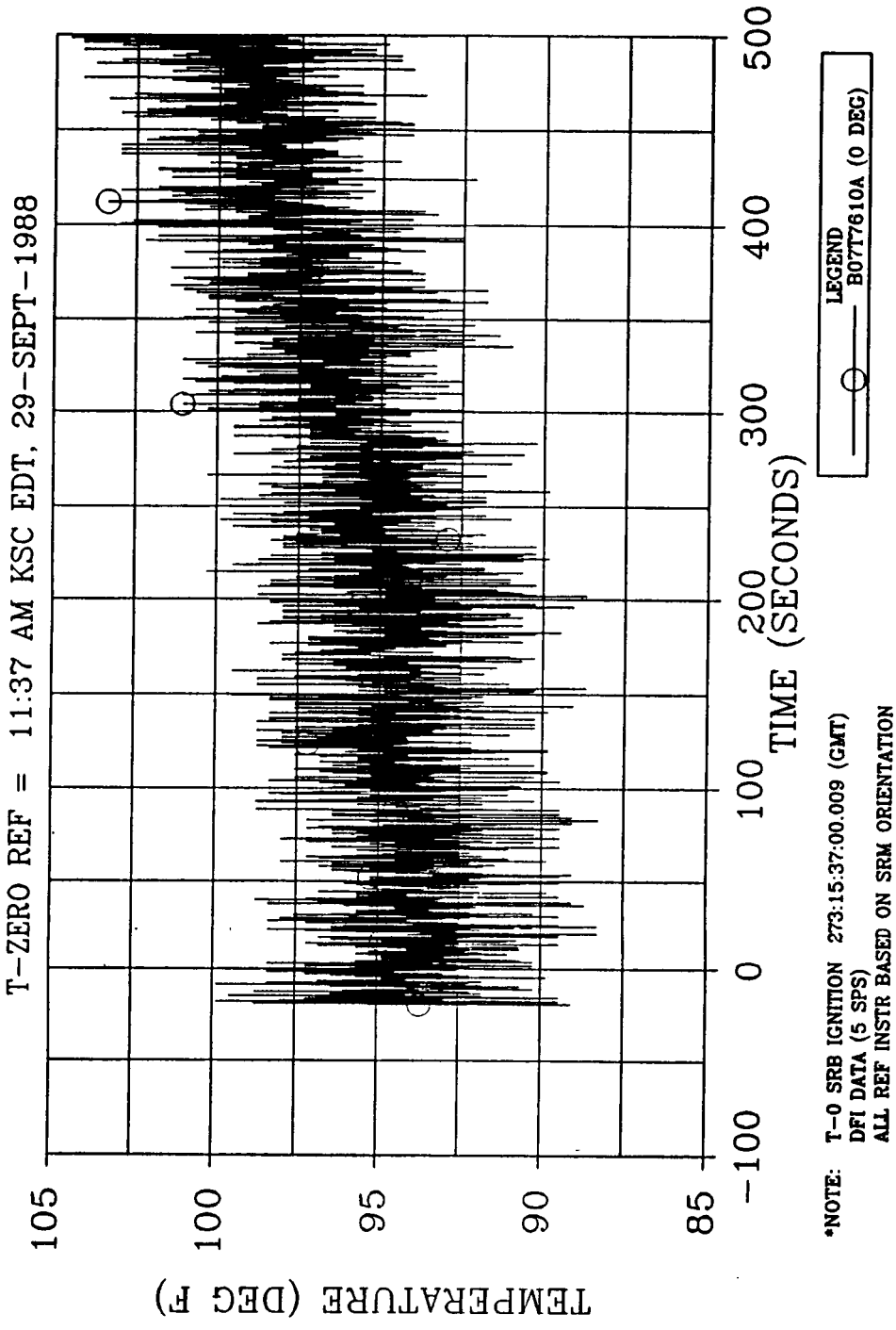

Figure 4.9-24. 360L001 Left SRM Aft Field Joint Temperature, Station 1486.30

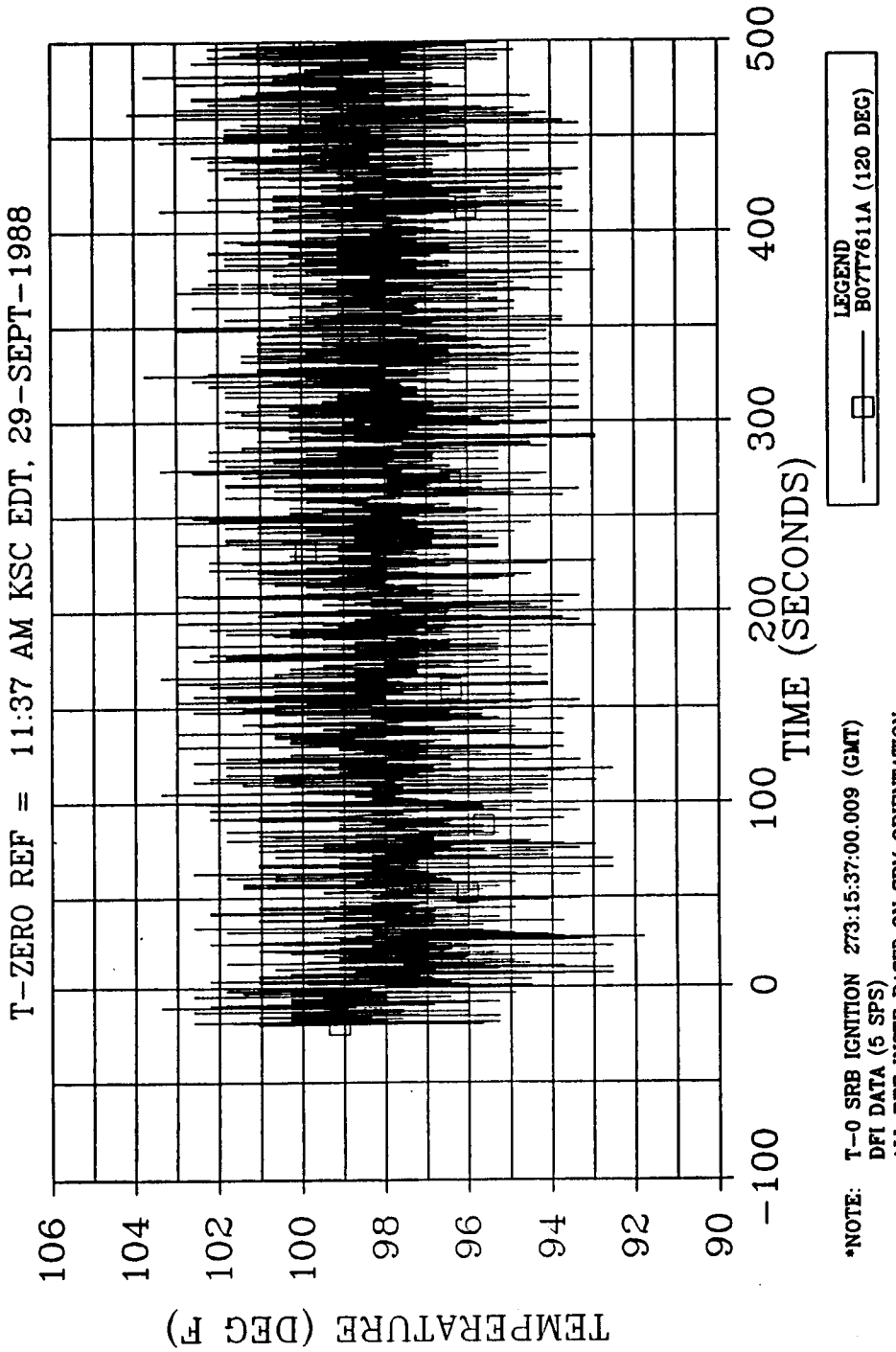

Figure 4.9-25. 360L001 Left SRM Aft Field Joint Temperature, Station 1486.30

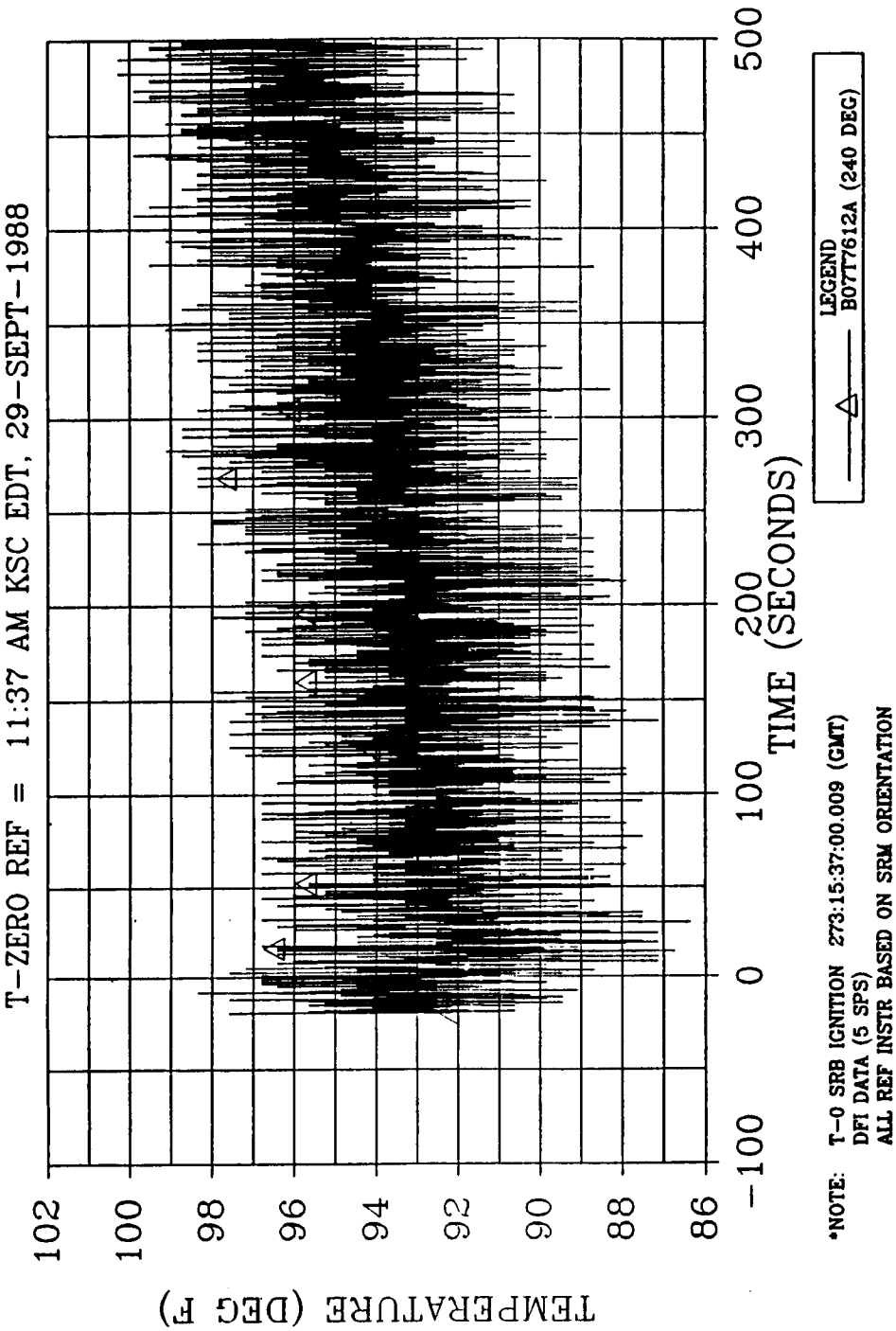

Figure 4.9-26. 360L001 Left SRM Aft Field Joint Temperature, Station 1486.30

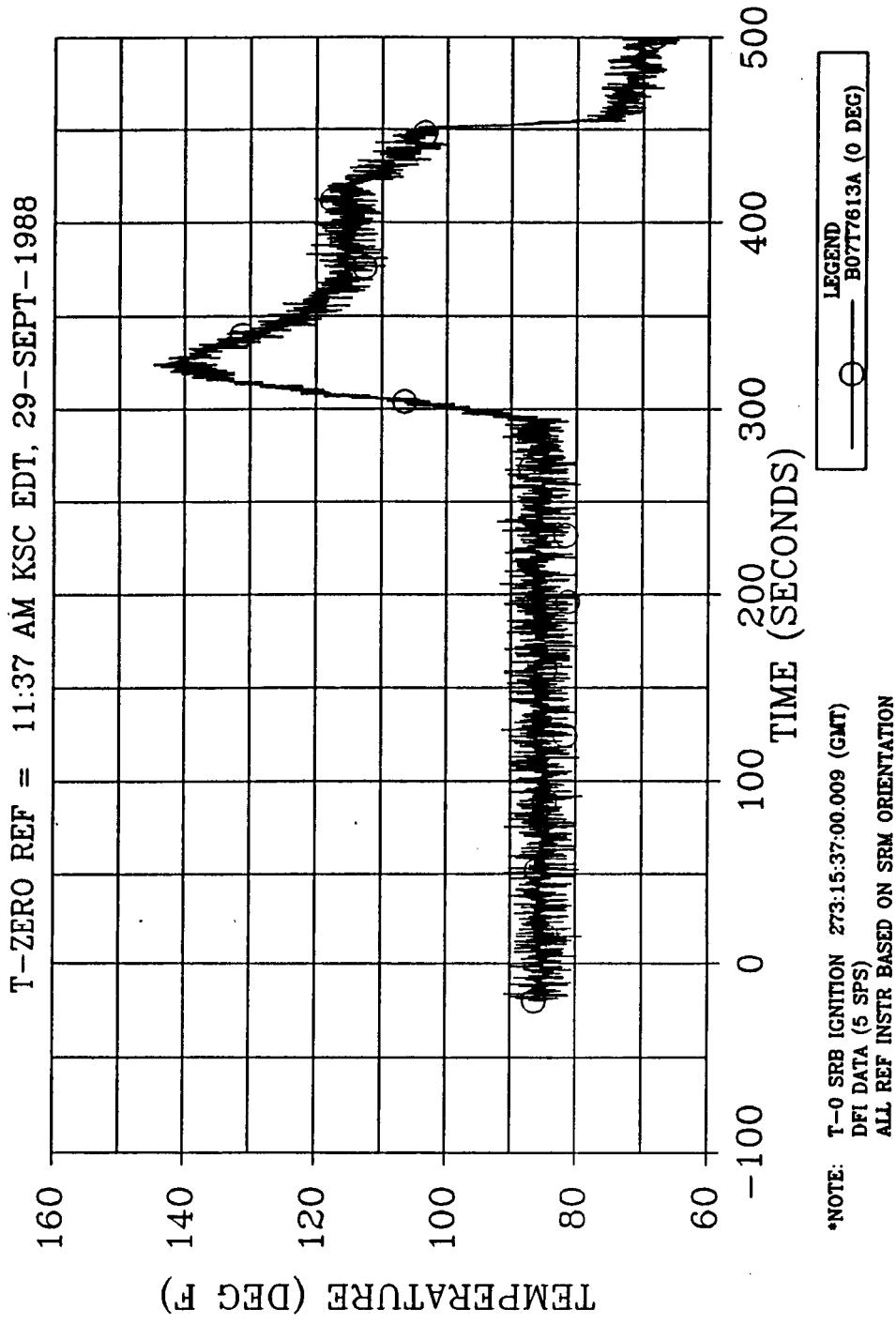

Figure 4.9-27. 360L001 Left SRM Nozzle Housing Temperature, Station 1877.50

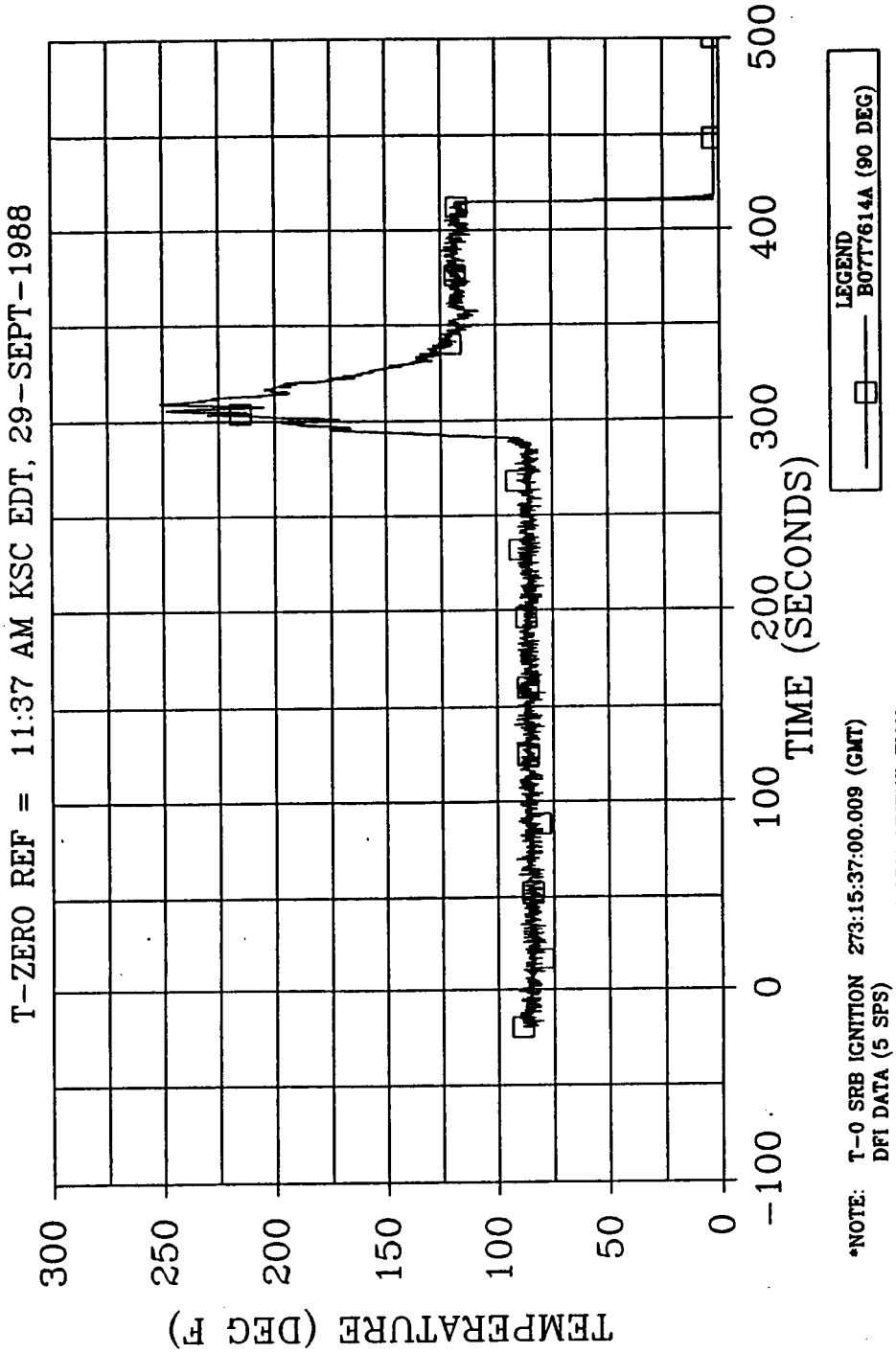

Figure 4.9-28. 360L001 Left SRM Nozzle Housing Temperature, Station 1877.50

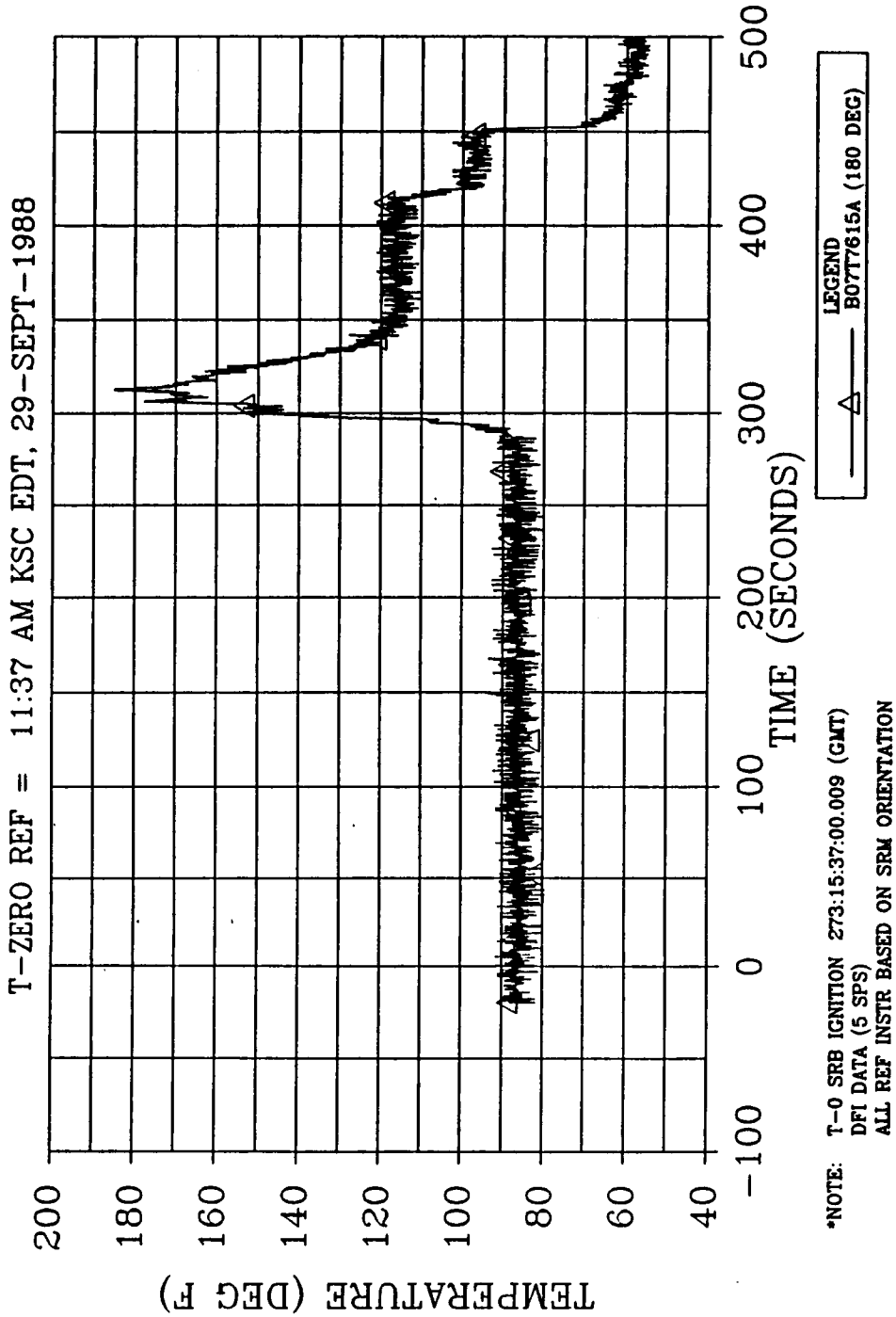

Figure 4.9-29. 360L001 Left SRM Nozzle Housing Temperature, Station 1877.50

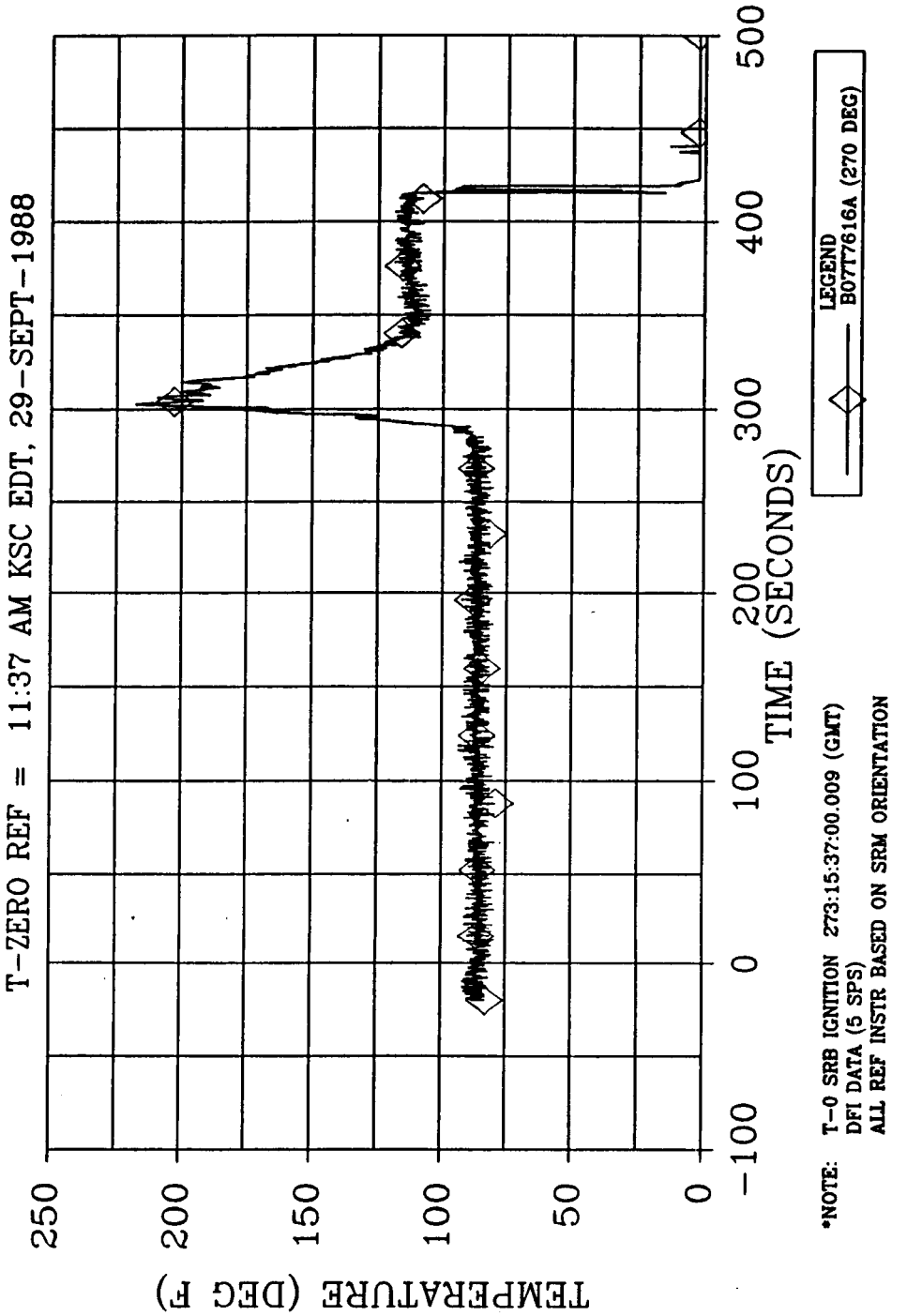

Figure 4.9-30. 360L001 Left SRM Nozzle Housing Temperature, Station 1877.50

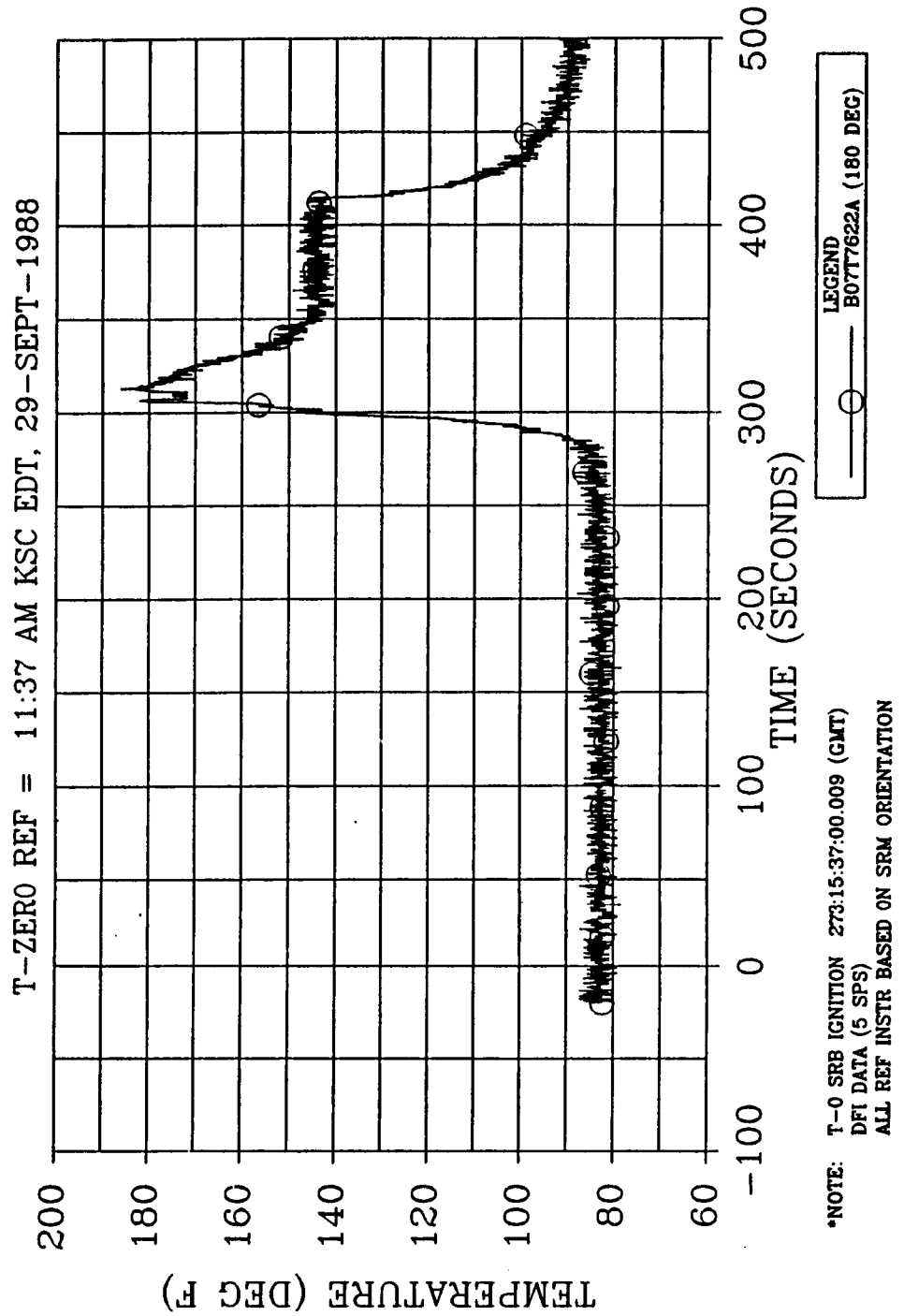

Figure 4.9-31. 360L001 Left SRM Nozzle Exit Cone Temperature, Station 1905.00

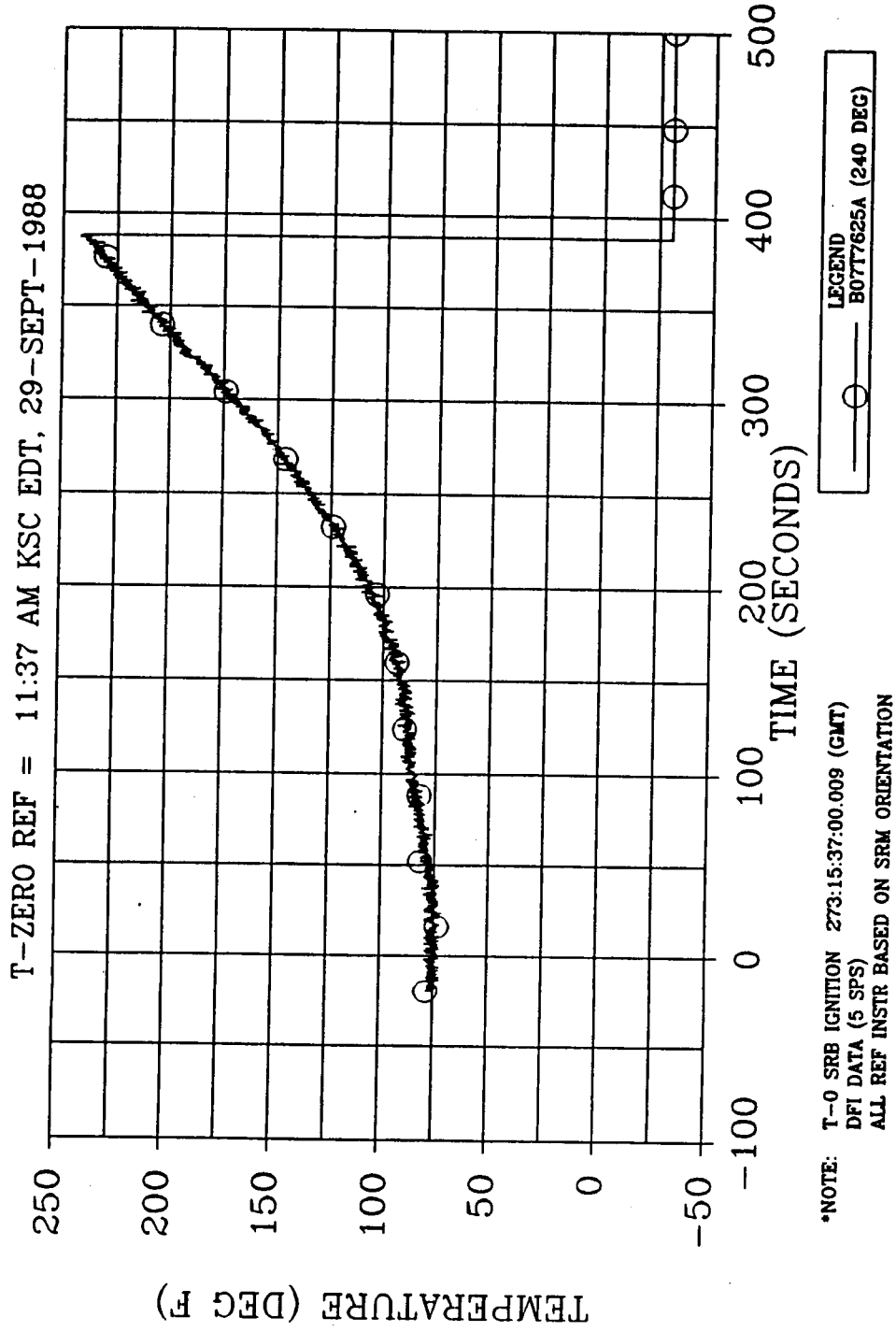

Figure 4.9-32. 360L001 Left SRM Nozzle Exit Cone Temperature, Station 1996.50

a. All the measured data showed oscillations around the mean values indicating that the DFI thermal gages were picking up stray signals from vibrations or a problem may exist in the data acquisition system.

b. All of the measured data registered normal temperatures during the ascent of the STS, indicating that there was no leakage around the field joints or the nozzle-to-case joint.

c. All the DFI thermal gages in the base region were protected from the external thermal environments by the thermal curtain and showed normal measured temperatures up to the flight time of about 290 to 295 sec. After this time frame their recorded temperatures suddenly rose, indicating that they had lost the protection of the thermal curtain. Therefore, it is surmised that the thermal curtain broke up and blew away at about 290 sec into flight.

d. The DFI on the aft exit cone near the exit plane stopped recording data at about 385 sec after lift-off. This suggests that the aft exit cone was severed from the SRBs at about 385 sec into flight.

e. Three DFI thermal gages on the nozzle fixed housing flange on the left SRM and one gage at the same location on the right SRM measured much higher temperatures than the predicted values. The measured data further showed that three gages on the right SRM went off scale and apparently lost their recording capability following the breakup of the thermal curtain at 290 sec. This might be attributed to a thermal curtain debris problem. All these gages were bonded to massive chunks of steel and should have indicated normal steel temperatures, within the predicted values, as was done by gage B07T7613A on the left SRM.

However, the data from the four gages which exceeded the estimates are attributed to possible adhesive failure, causing gage detachment from the hardware. No insulation was used to cover the gages on STS-26R. The high readings are explainable, assuming slight gage detachment, due to the direct exposure of these gages to the hot environment (reentry nozzle flame and aerodynamic heating) following thermal curtain breakup.

This assessment will be confirmed with STS-27 and subsequent flights, where the gages will be directly insulated from the environment with a minimal amount of K5NA, and should better follow hardware response. If not confirmed, SRB reentry environments and/or SRM aft end thermal modeling will need to be considered and appropriately modified.

Apart from the anomalies explained previously in item e, it can reasonably be stated that the majority of the DFI thermal gages recorded temperature data well within the predicted data. Upon comparing the data (prediction versus actual measurements), it appears that the thermal environments presented in Table 4.9-7 are overly conservative.

4.9.3.3 PMBT and Flex Bearing Predictions

Temperature predictions (°F), performed at various times with respect to flight, are summarized as follows:

	Historical	L-2 Days	L-24 Hr	Postflight
PMBT	78	80	--	-79
Flex Bearing Bulk	81	--	83	TBD

Postflight flex bearing bulk temperature predictions will be calculated pending acquisition of aft skirt conditioning data (actual GN_2 temperature and set point histories).

4.9.3.4 SRM Local Environment Predictions

September historical flow/thermal predictions suggested a local induced environment due to ET cooling. The prediction was as much as a 2°F temperature suppression with increased heat transfer while the ET was loaded.

4.9.3.5 Ambient Environment Assessments

Data correlations (September historical-versus-actual STS-26R data) suggest good agreement. The only major deviation was during the early morning hours of the final day when ambient temperature fell to 70°F and remained at that level through the night (Table 4.9-3 and Figure 4.9.85 in Section 4.9.3.6).

4.9.3.6 GEI and Joint Heater Sensor Assessments. There were no LCC violations or new sensor anomalies during T-6 hr to T-5 min (Table 4.9-4).

Figures 4.9.33 through 4.9.62 present September historical predictions. These predictions are based upon event sequencing as specified in Table 4.9-8. Figures 4.9.63 through 4.9.97 present actual STS-26R countdown data.

Data correlations, predictions versus actual, suggest relatively good agreement (Tables 4.9-3 and 4.9-4). However, modeling considerations (environment and detail) need to be looked at closely. Future modeling will check these and incorporate updates as solutions are found. Significant observations and modeling considerations are discussed as follows.

Igniter/Case Joint

The igniter GEI remained consistently above average ambient temperature. This is due to the storage of heat in the forward end of the motor during the summer to fall/winter cooling trend. The opposite effect, to a limited extent, should be evident during the winter-to-spring/summer warming trend.

Data correlations suggest good agreement between historical predictions and actual GEI response, except that the right SRM response was consistently above that of the left SRM. If GEI data are accurate, this would suggest a greater amount of stored heat than the predicted environments allow.

Field Joint and Heaters

Joint heater operation was satisfactory and as expected. However, there still seems to be a minor problem with maintaining the lower set point range. Actual data during LCC heater operation reached as low as 94°F, while the accepted set point range was 98 ±2°F.

During countdown it was learned that joint heater activation time had been changed. Operations and maintenance requirements and specification document (OMRSD) guidelines now require that the heaters be activated at L-24 hr in place of the previous requirement of T-24 hr.

Data correlations suggest that actual daily cycling amplitude of the sensors during nonheater operation is considerably less than predicted. More detailed modeling of this region will be considered for subsequent flights.

ORIGINAL PAGE IS
OF POOR QUALITY

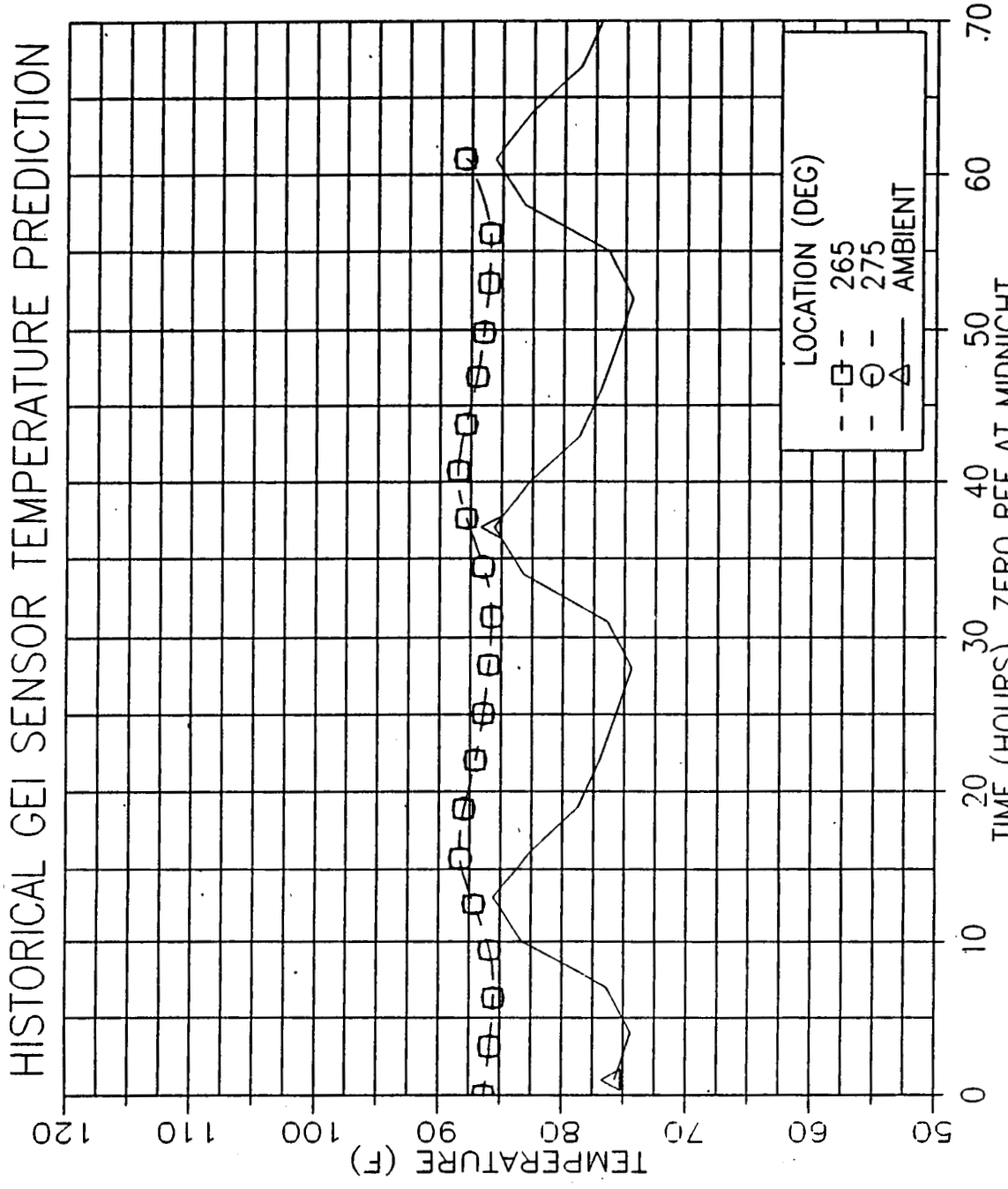

Figure 4.9-33. Right SRM Igniter/Case Joint (September)

ORIGINAL PAGE IS
OF POOR QUALITY

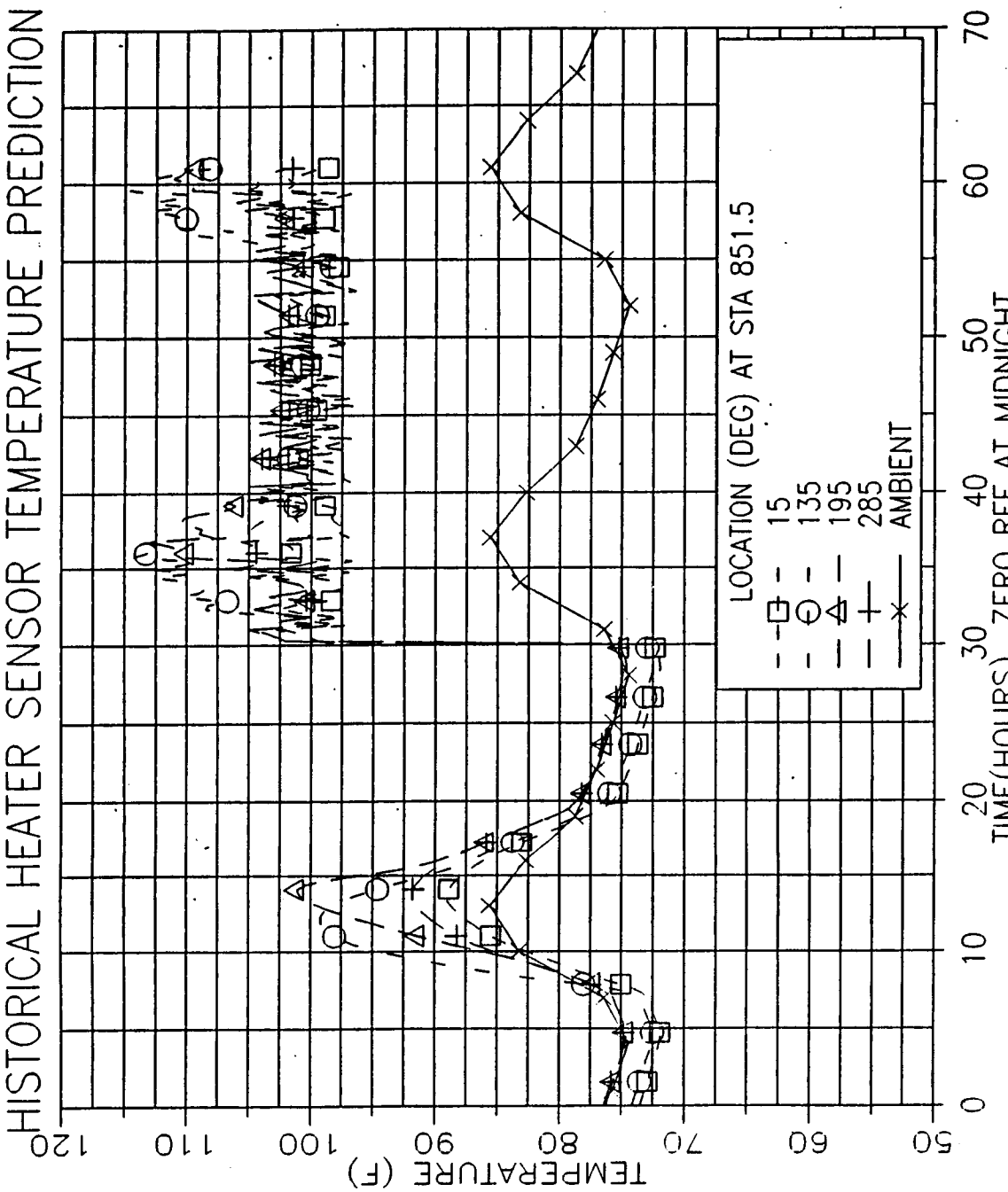

Figure 4.9-34. Right SRM Forward Field Joint (September)

ORIGINAL PAGE IS
OF POOR QUALITY

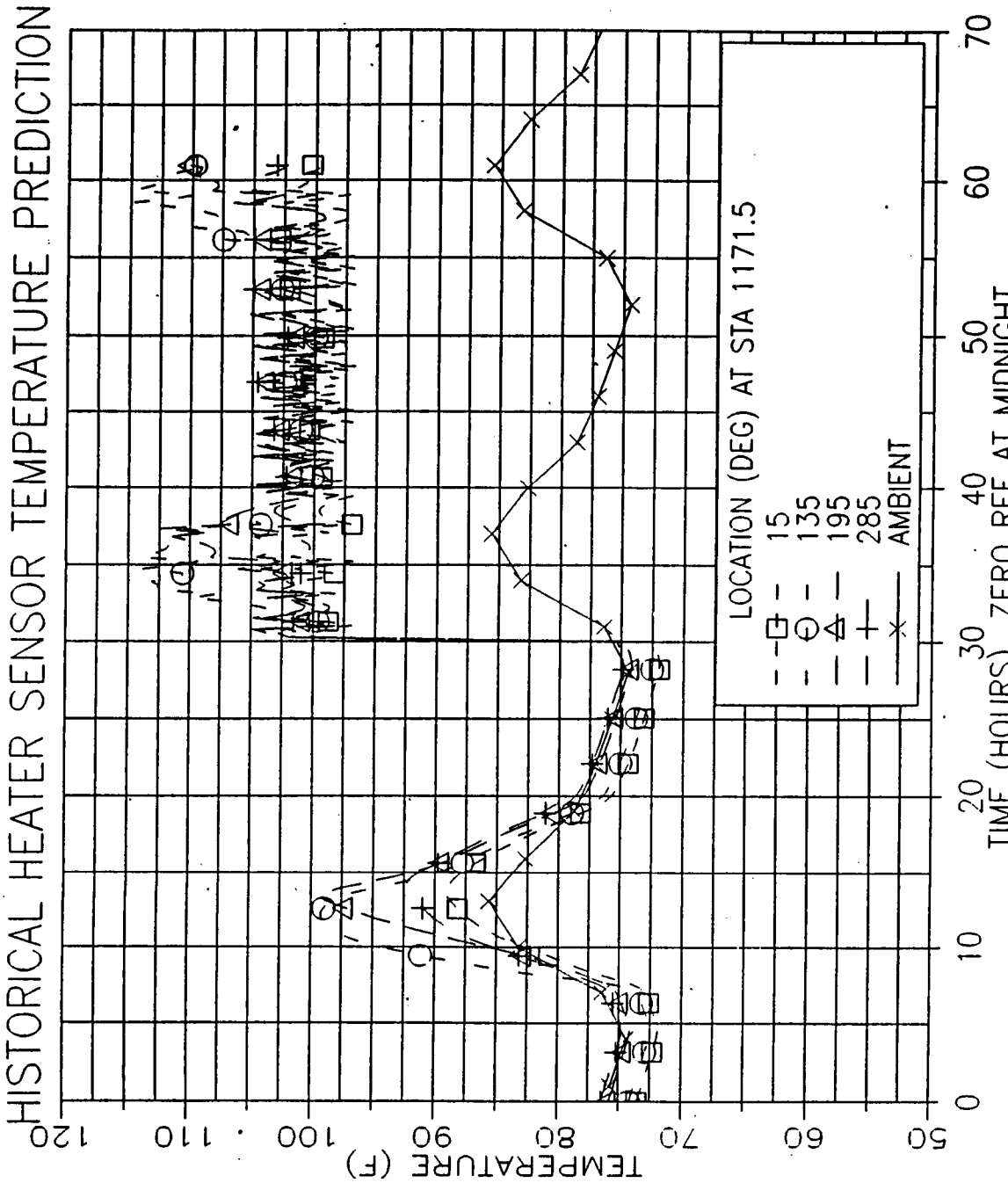

Figure 4.9-35. Right SRM Center Field Joint (September)

ORIGINAL PAGE IS
OF POOR QUALITY

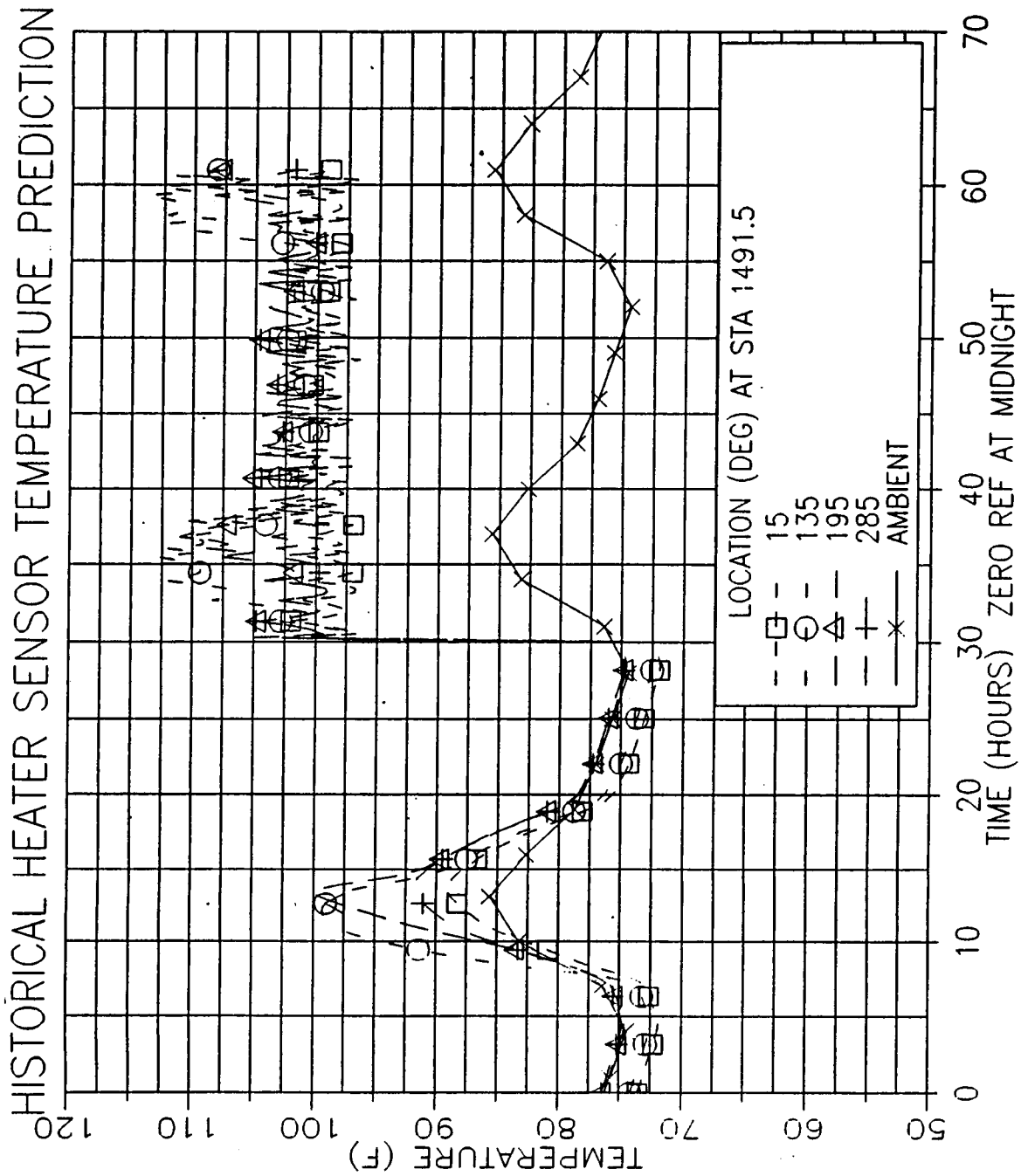

Figure 4.9-36. Right SRM Aft Field Joint (September)

ORIGINAL PAGE IS
OF POOR QUALITY

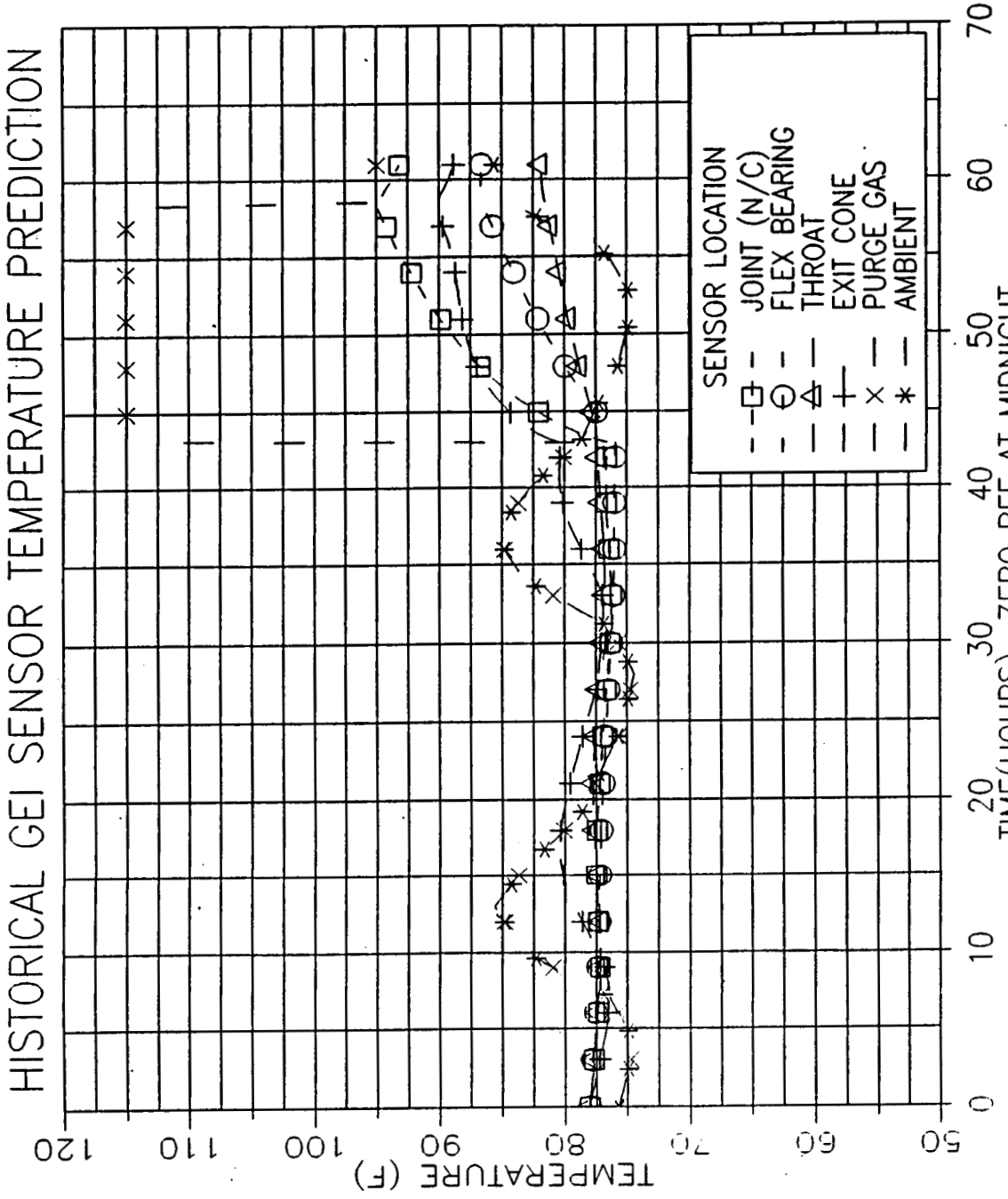

Figure 4.9-37. Right SRM Aft End Region (September)

ORIGINAL PAGE IS
OF POOR QUALITY

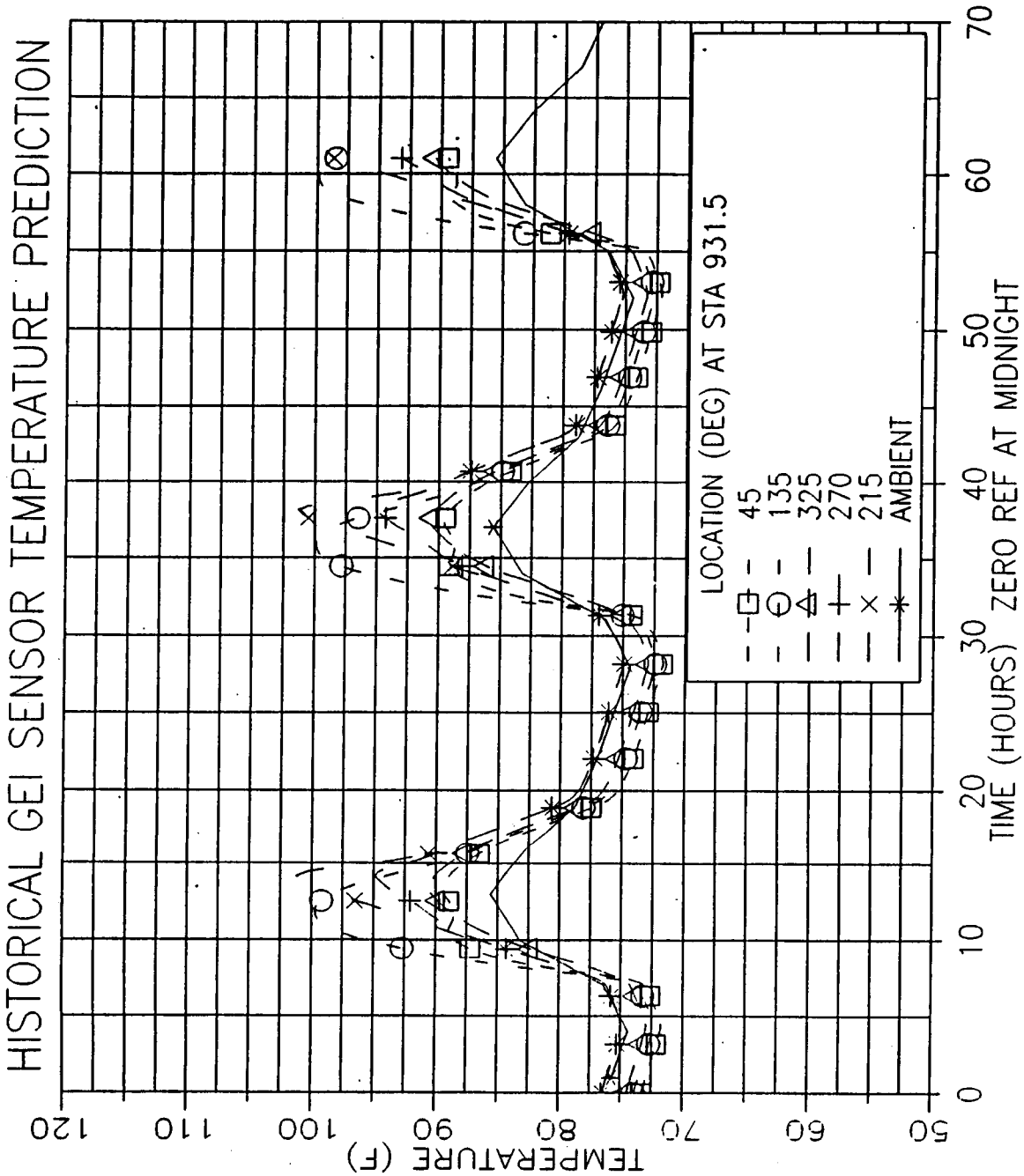

Figure 4.9-38. Right SRM Forward Case Acreage (September)

ORIGINAL PAGE IS
OF POOR QUALITY

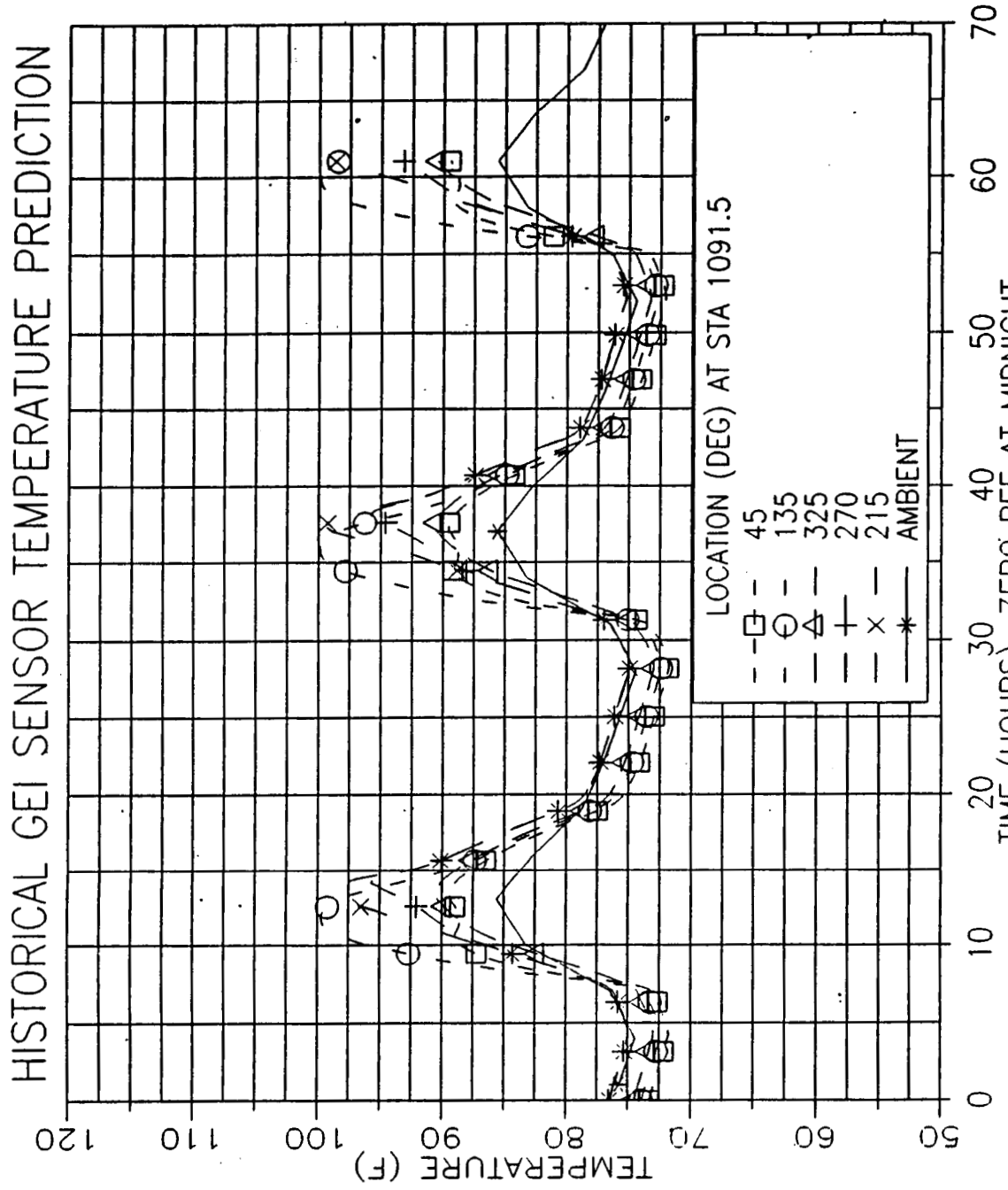

Figure 4.9-39. Right SRM Forward Center Case Acreage (September)

ORIGINAL PAGE IS
OF POOR QUALITY

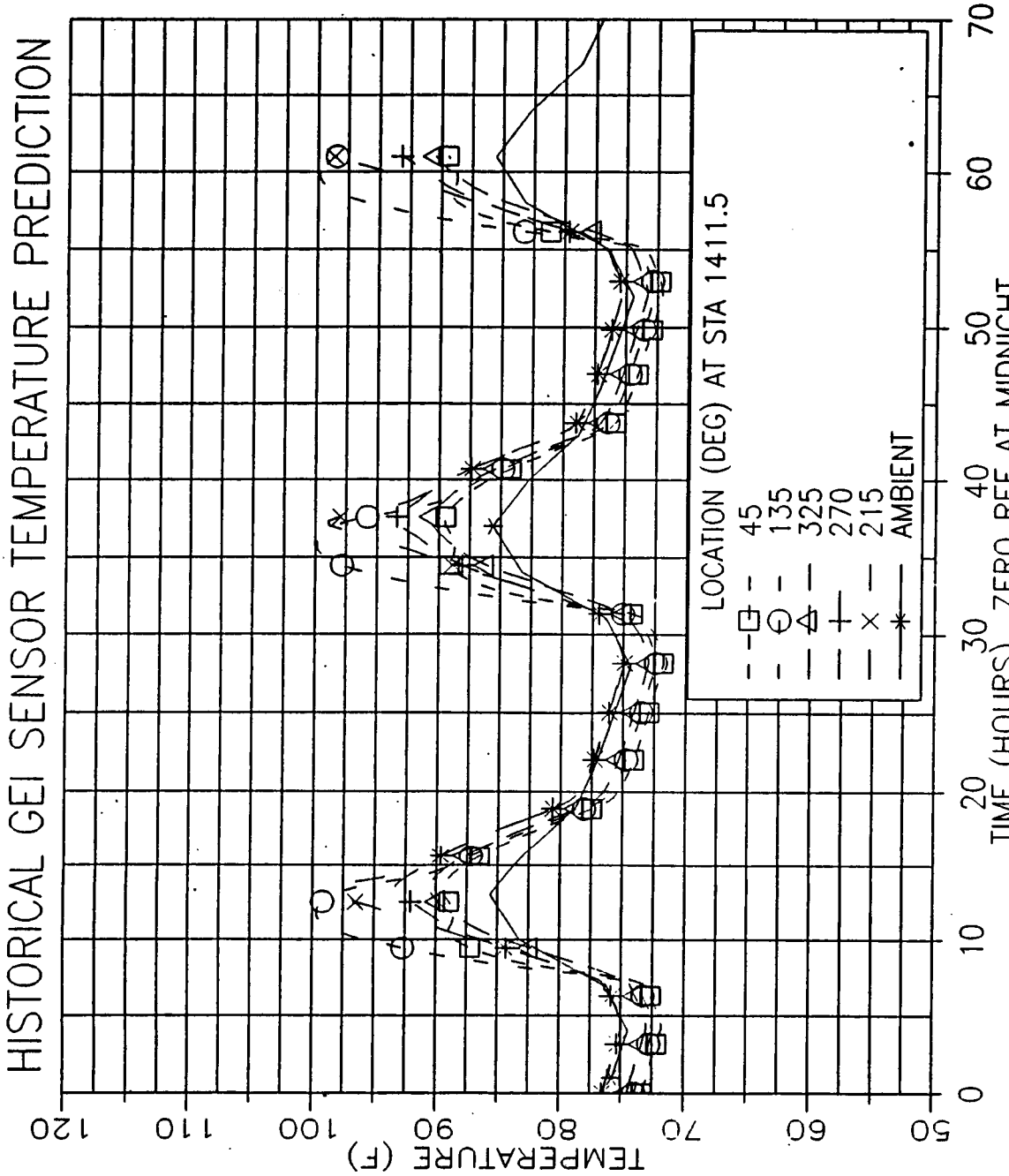

Figure 4.9-40. Right SRM Aft Center Case Acreage (September)

ORIGINAL PAGE IS
OF POOR QUALITY

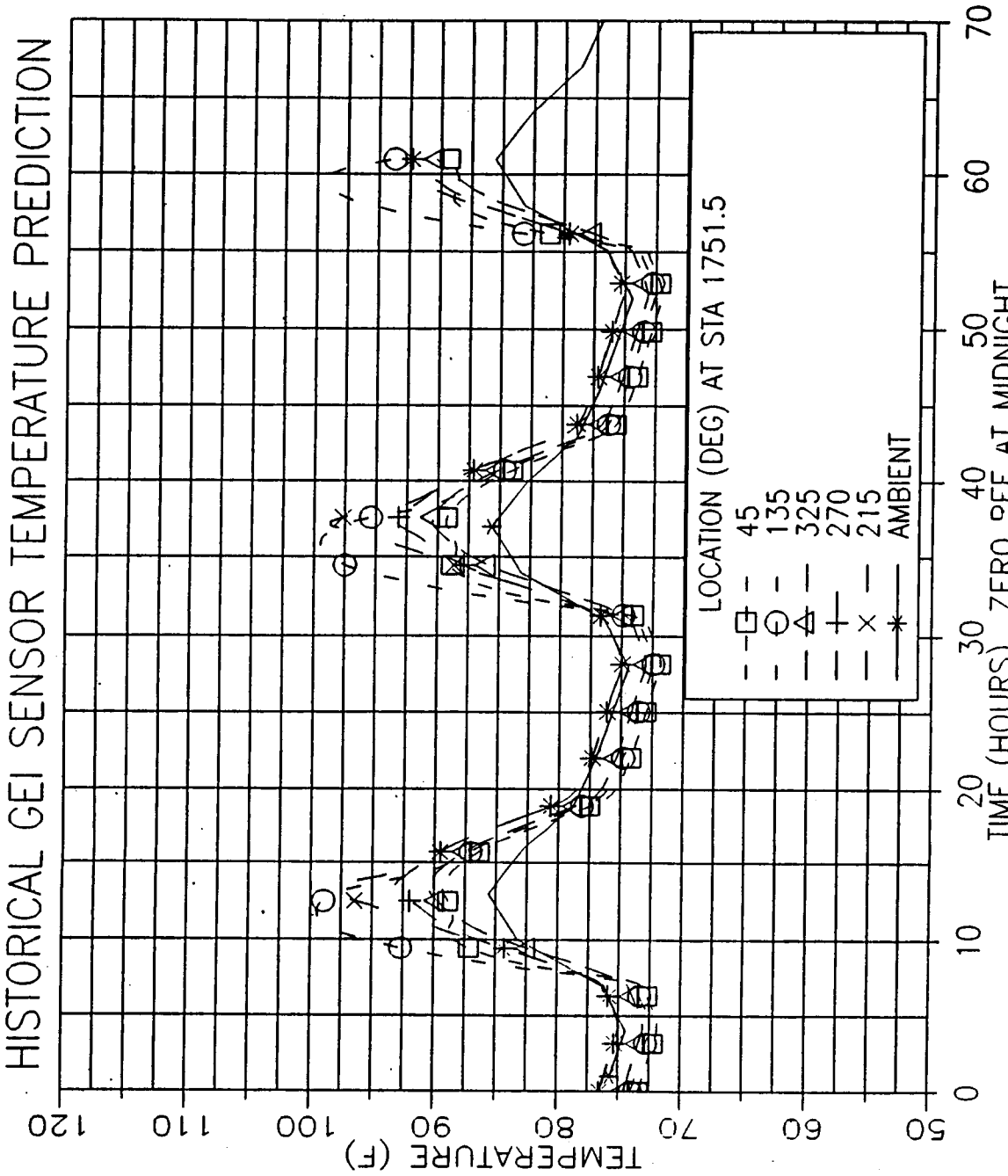

Figure 4.9-41. Right SRM Aft Case Acreage (September)

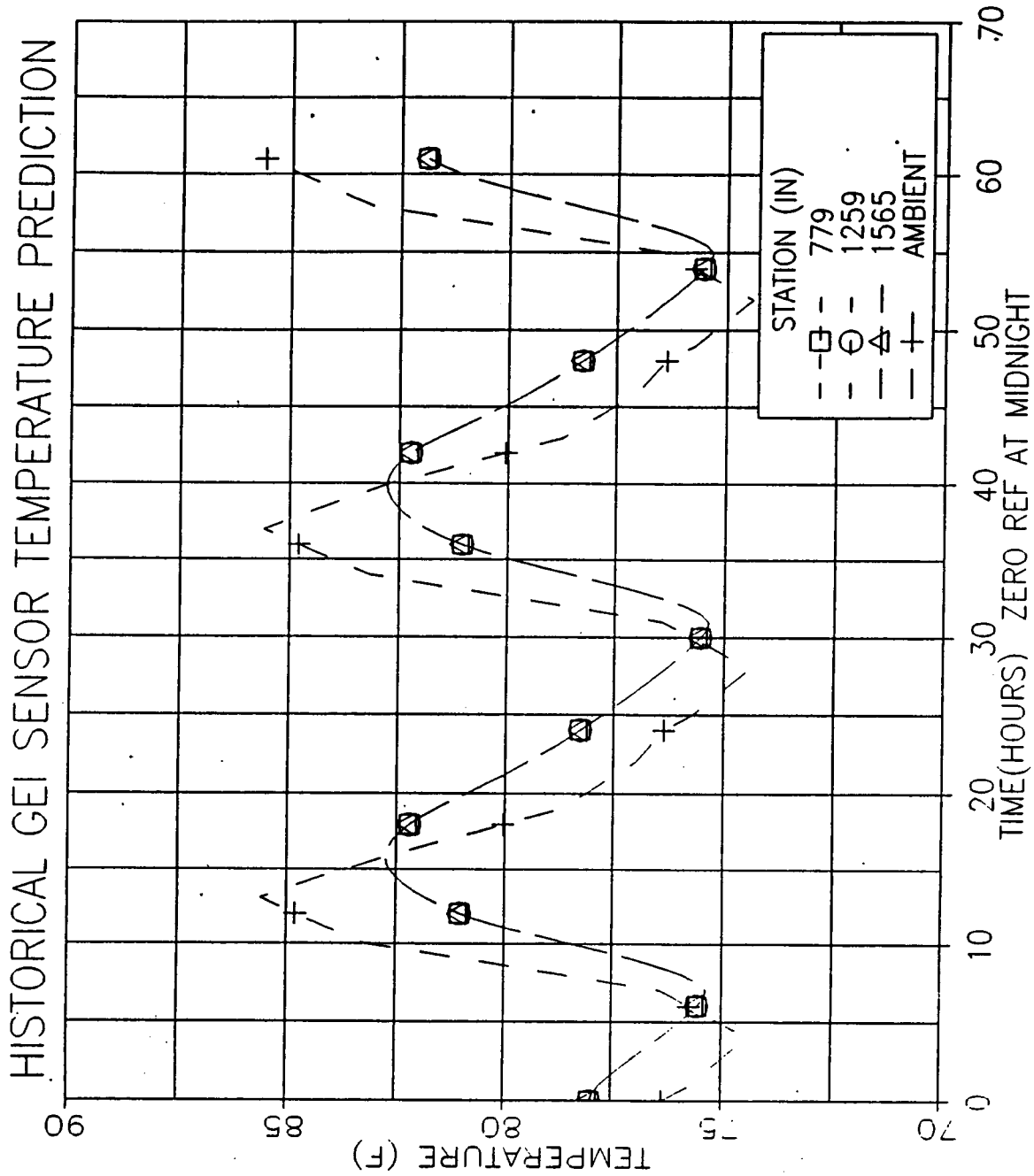

Figure 4.9-42. Right SRM Tunnel Bondline (September)

ORIGINAL PAGE IS
OF POOR QUALITY

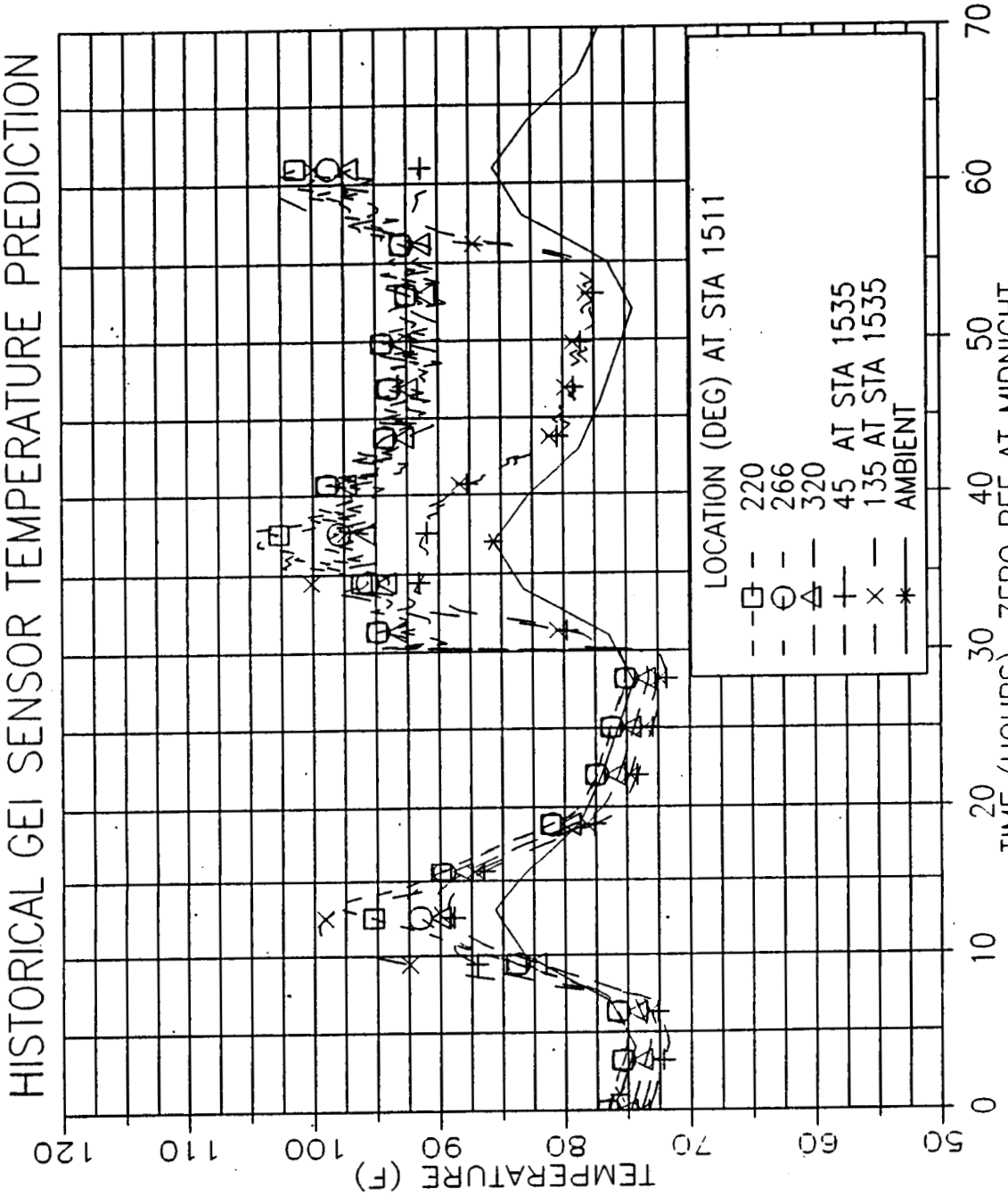

Figure 4.9-43. Right SRM ETA Region (September)

ORIGINAL PAGE IS
OF POOR QUALITY

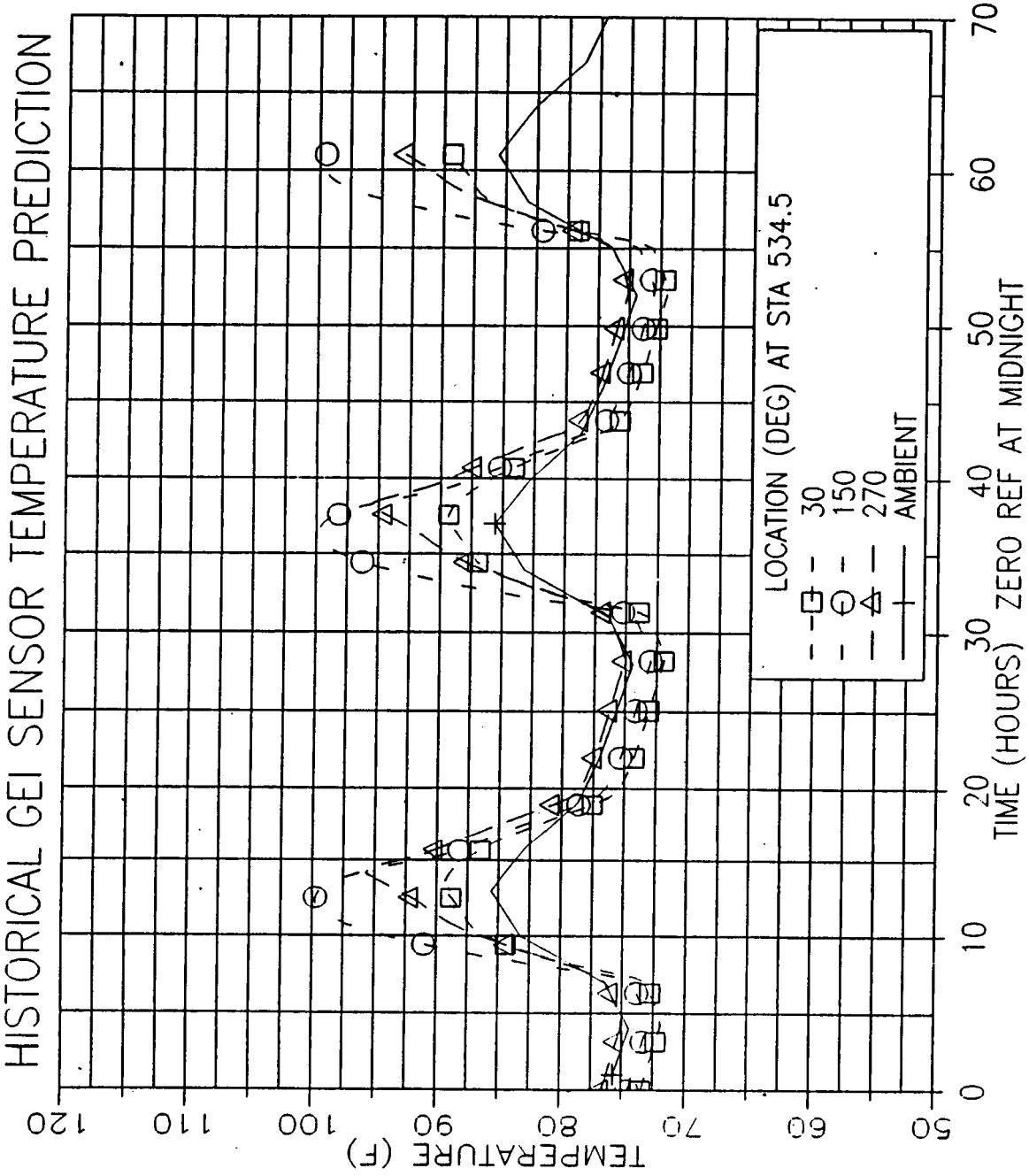

Figure 4.9-44. Right SRM Forward Dome Factory Joint (September)

ORIGINAL PAGE IS
OF POOR QUALITY

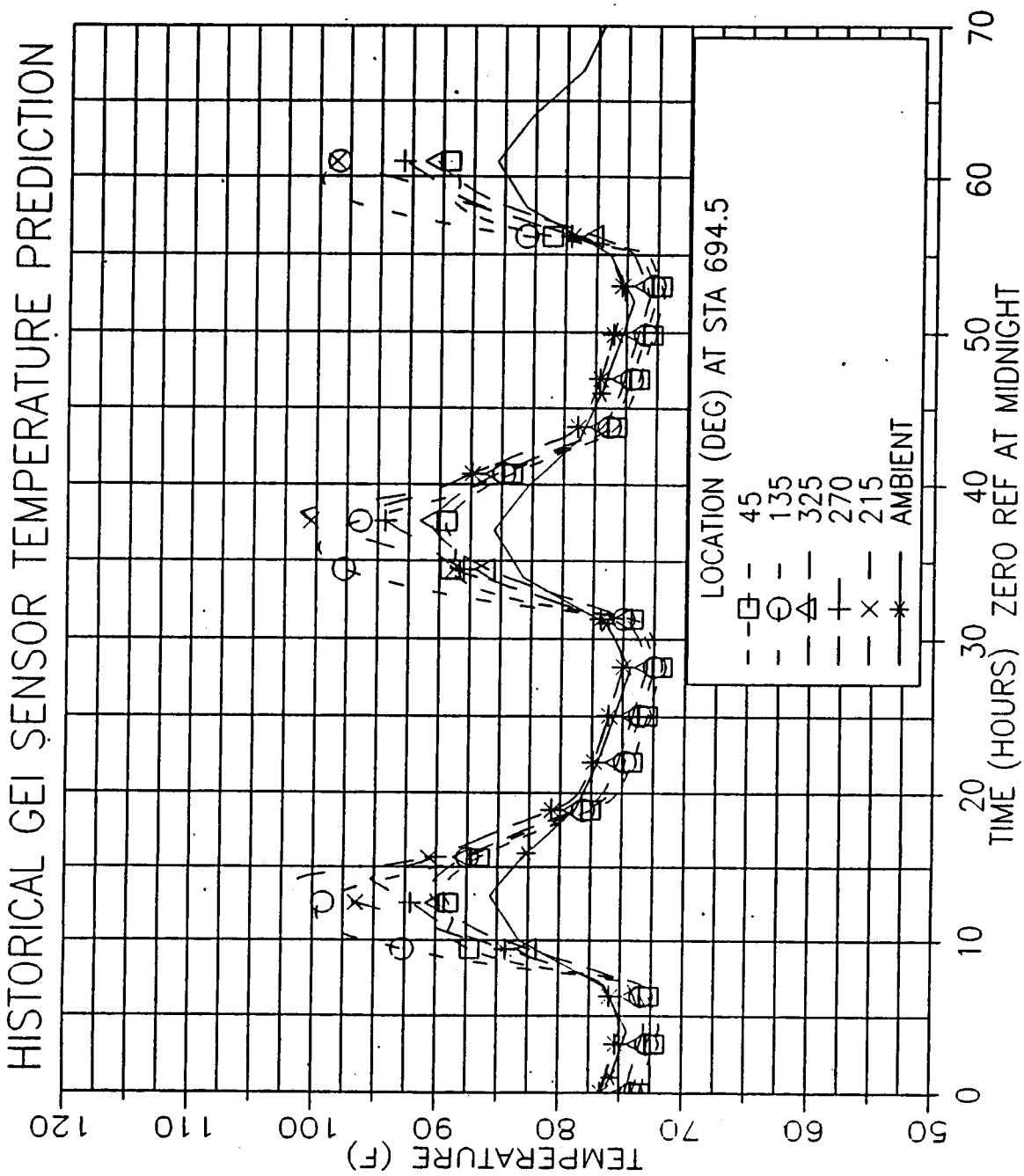

Figure 4.9-45. Right SRM Forward Factory Joint (September)

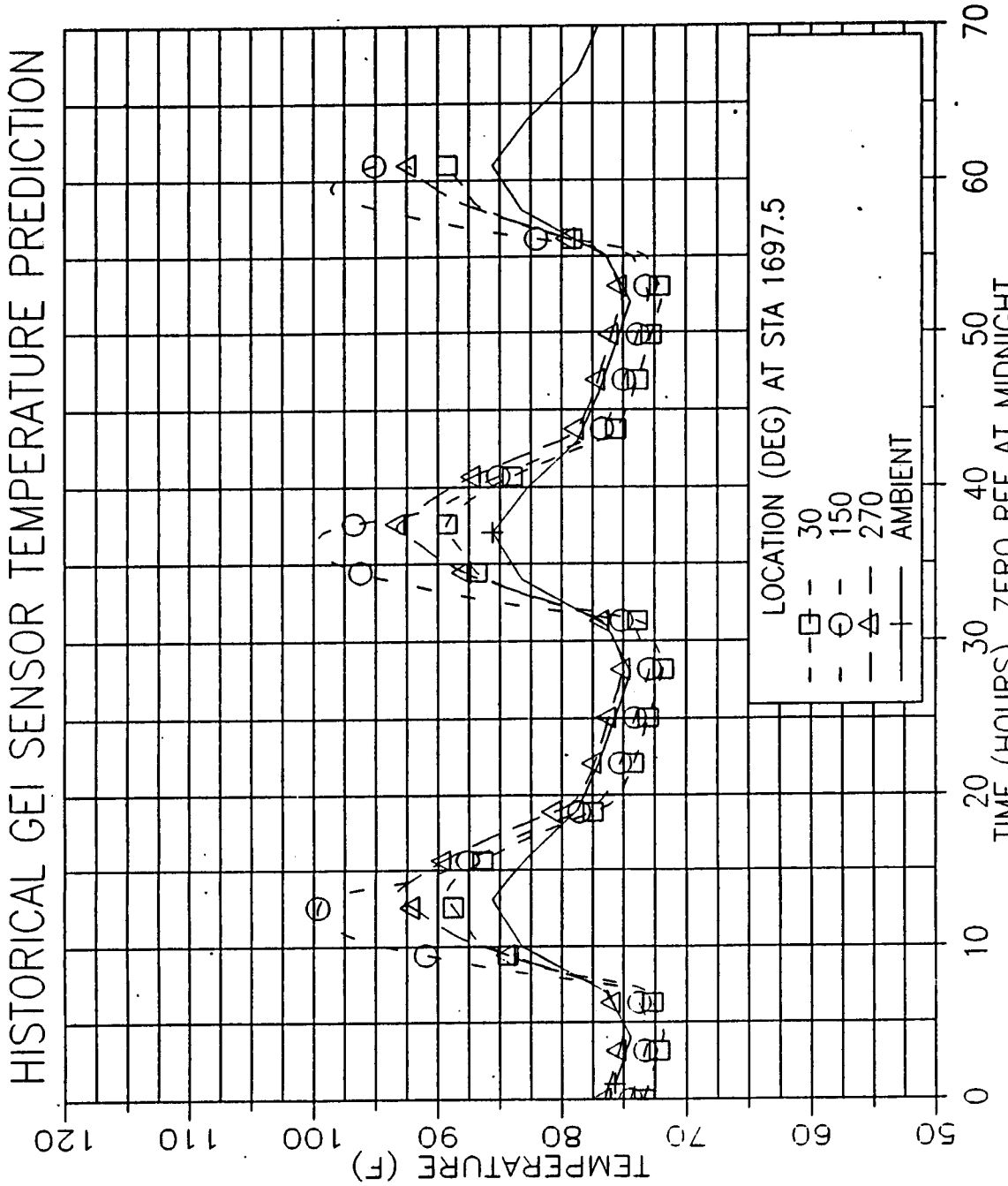

Figure 4.9-46. Right SRM Aft Factory Joint (September)

ORIGINAL PAGE IS
OF POOR QUALITY

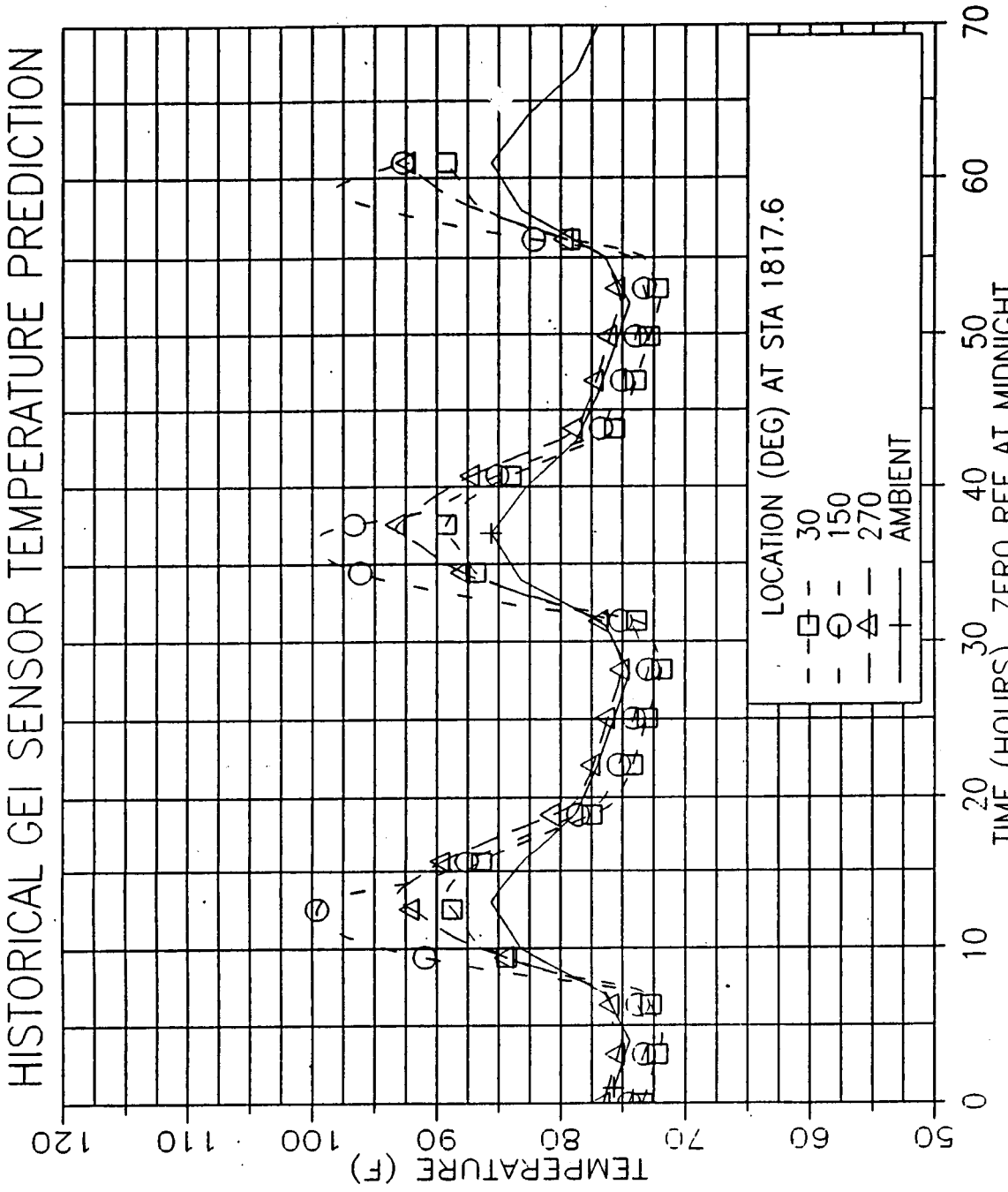

Figure 4.9-47. Right SRM Aft Dome Factory Joint (September)

ORIGINAL PAGE IS
OF POOR QUALITY

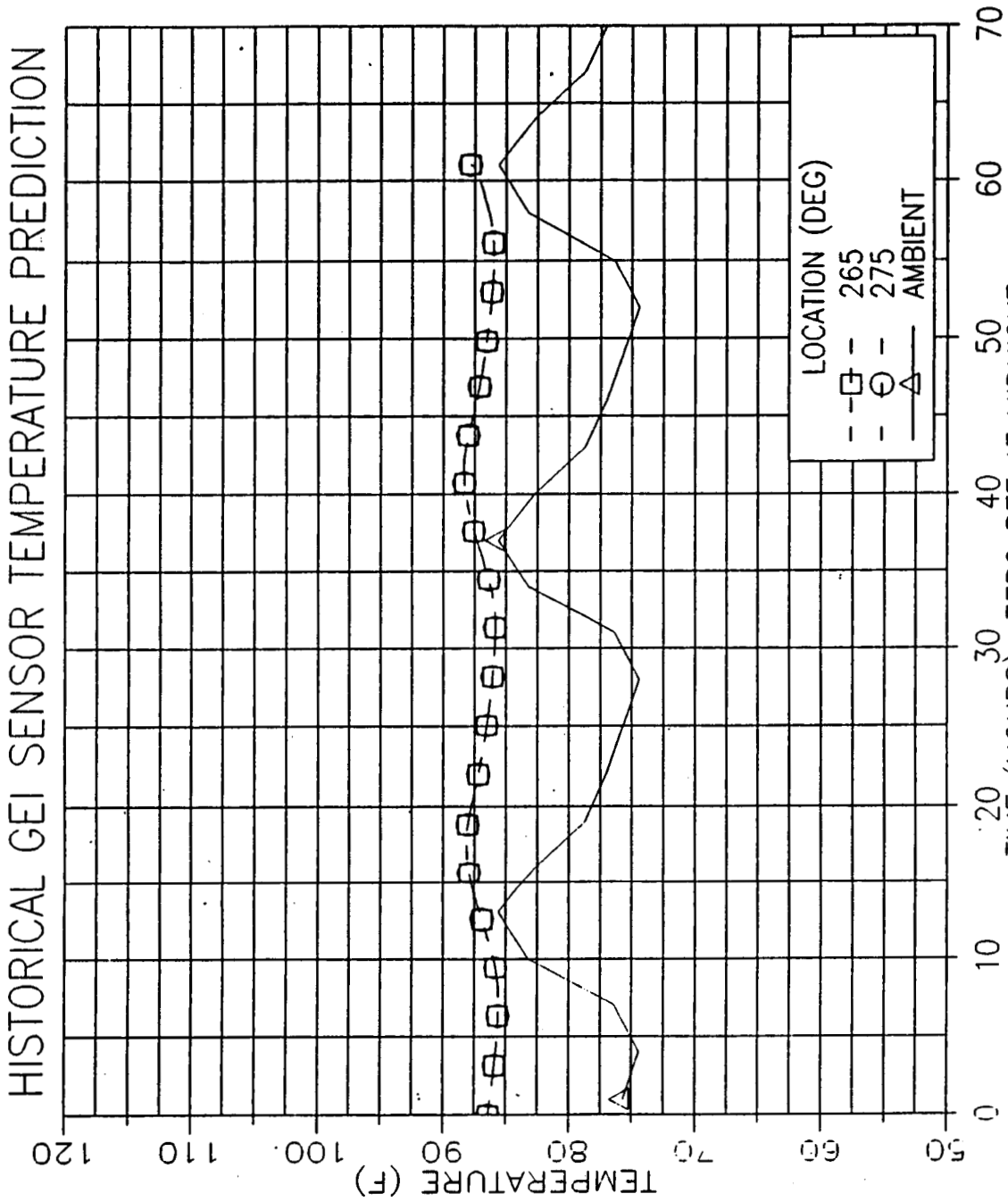

Figure 4.9-48. Left SRM Igniter/Case Joint (September)

ORIGINAL PAGE IS
OF POOR QUALITY

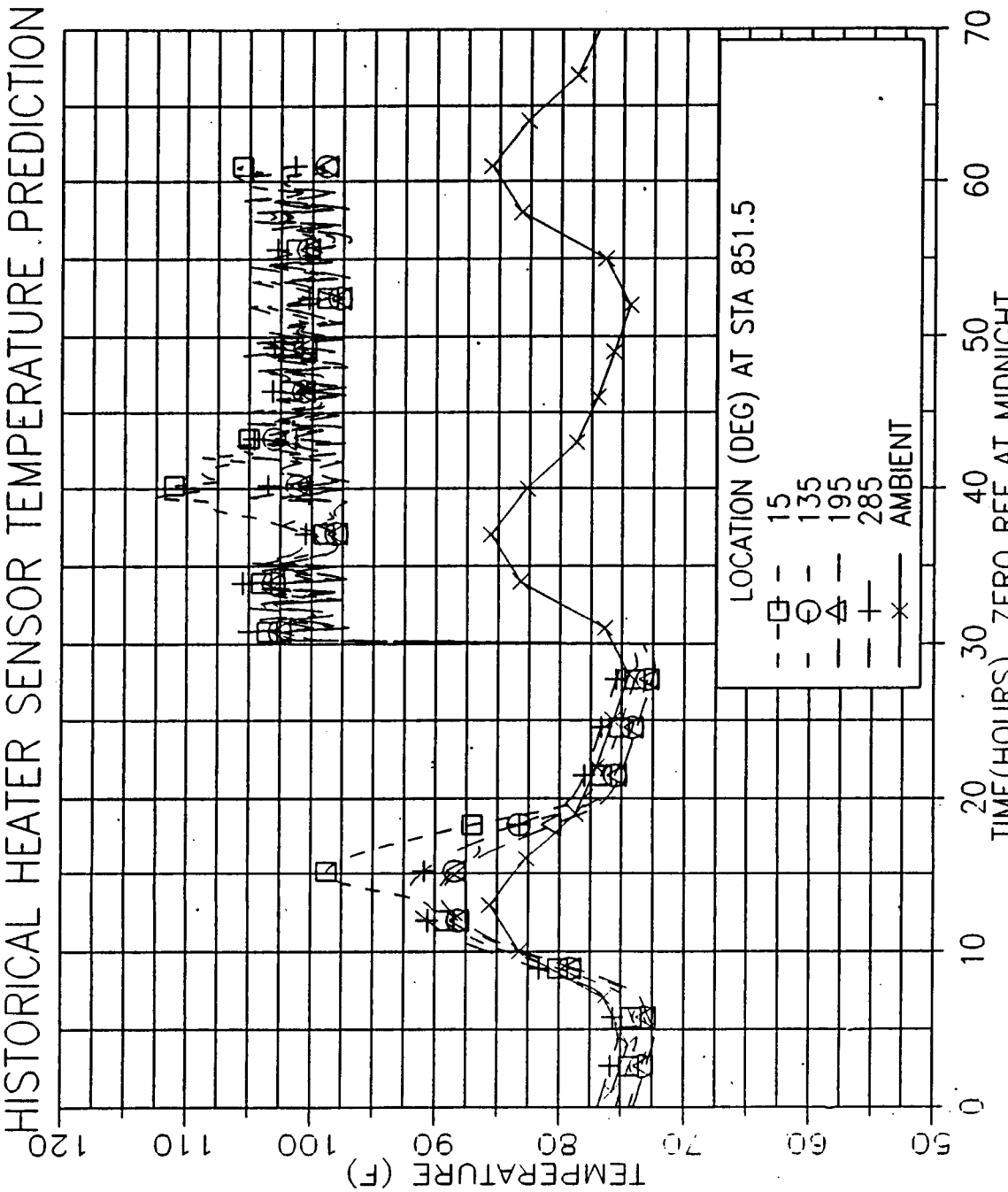

Figure 4.9-49. Left SRM Forward Field Joint (September)

ORIGINAL PAGE IS
OF POOR QUALITY

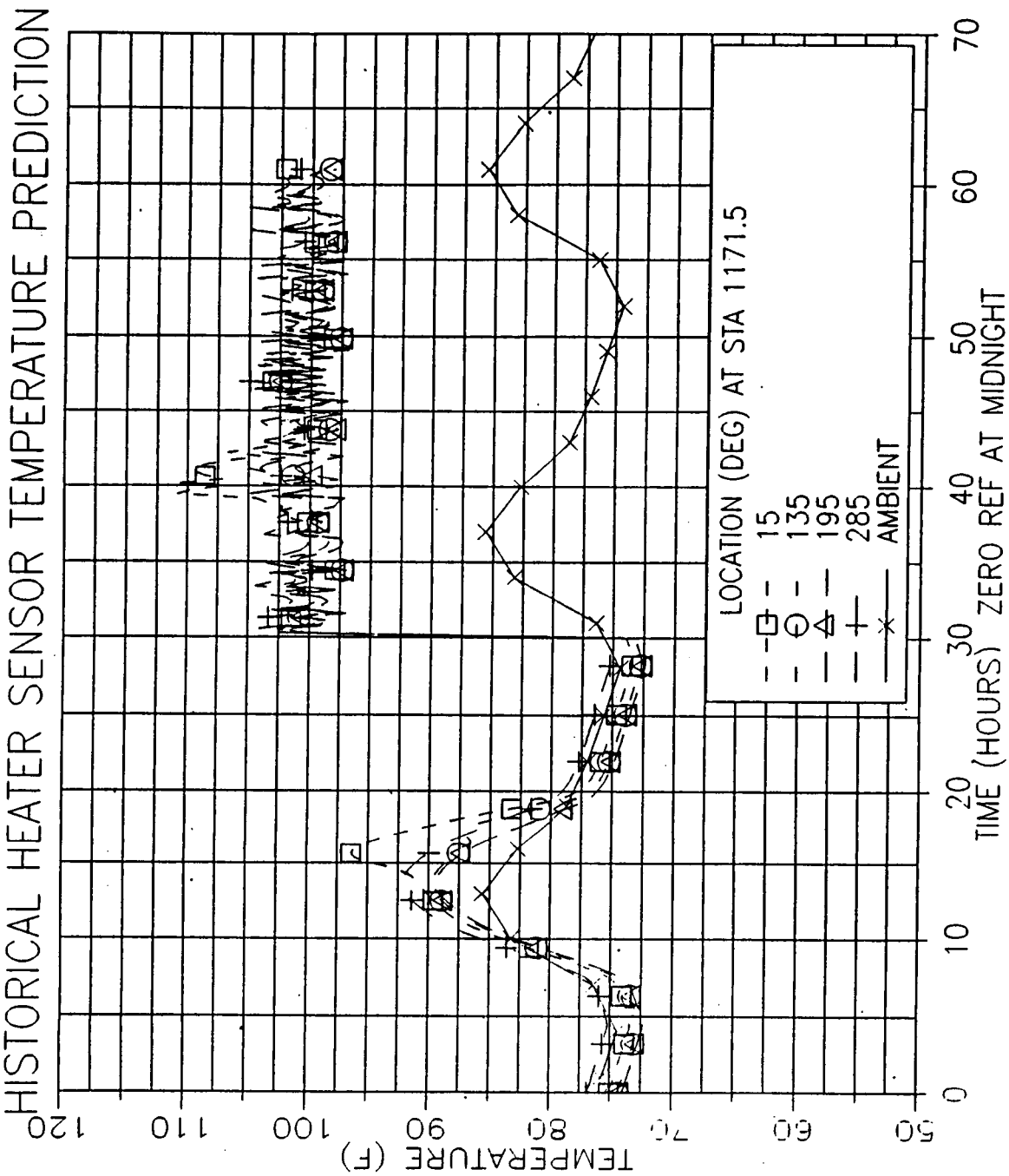

Figure 4.9-50. Left SRM Center Field Joint (September)

ORIGINAL PAGE IS
OF POOR QUALITY

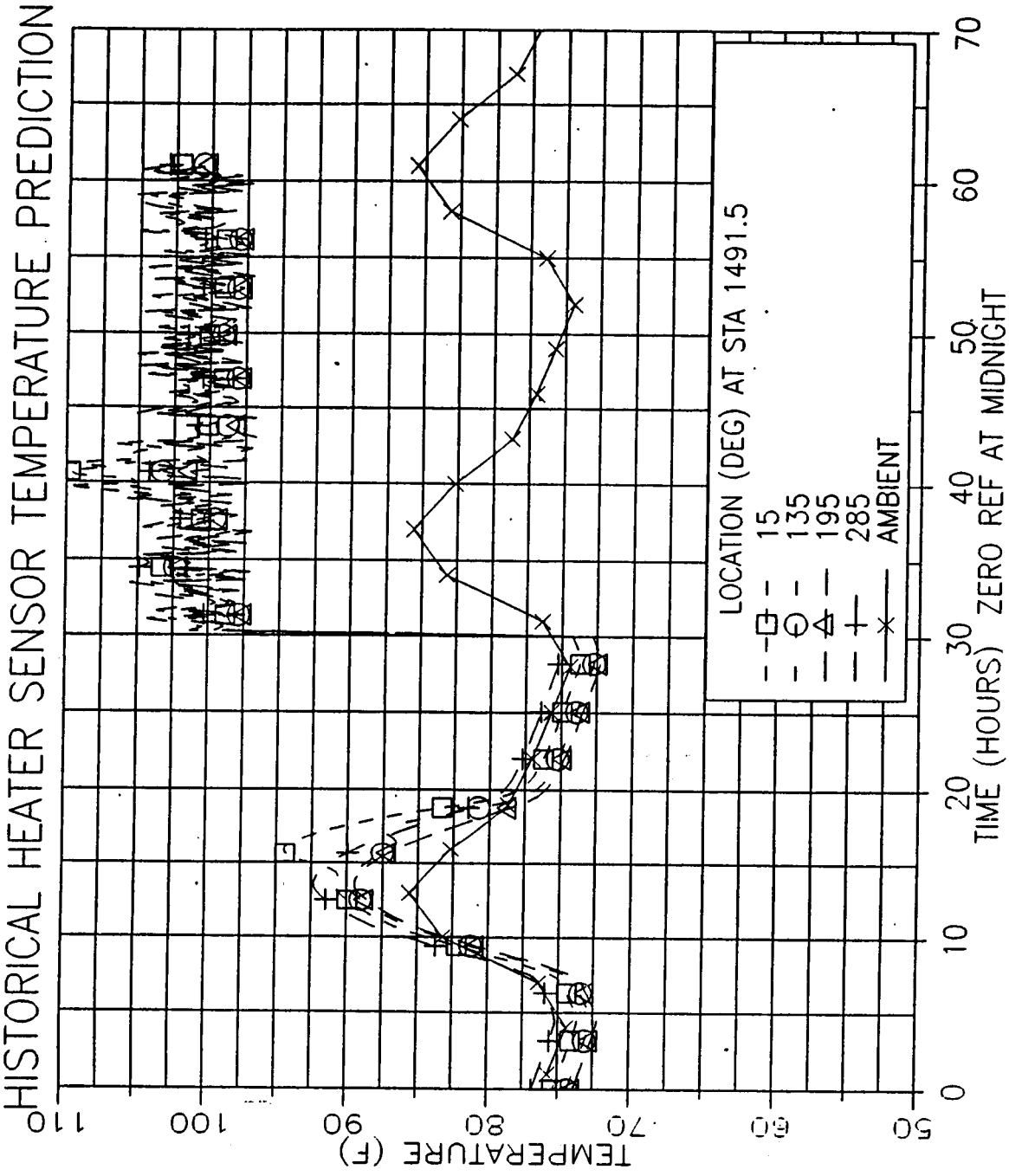

Figure 4.9-51. Left SRM Aft Field Joint (September)

ORIGINAL PAGE IS
OF POOR QUALITY

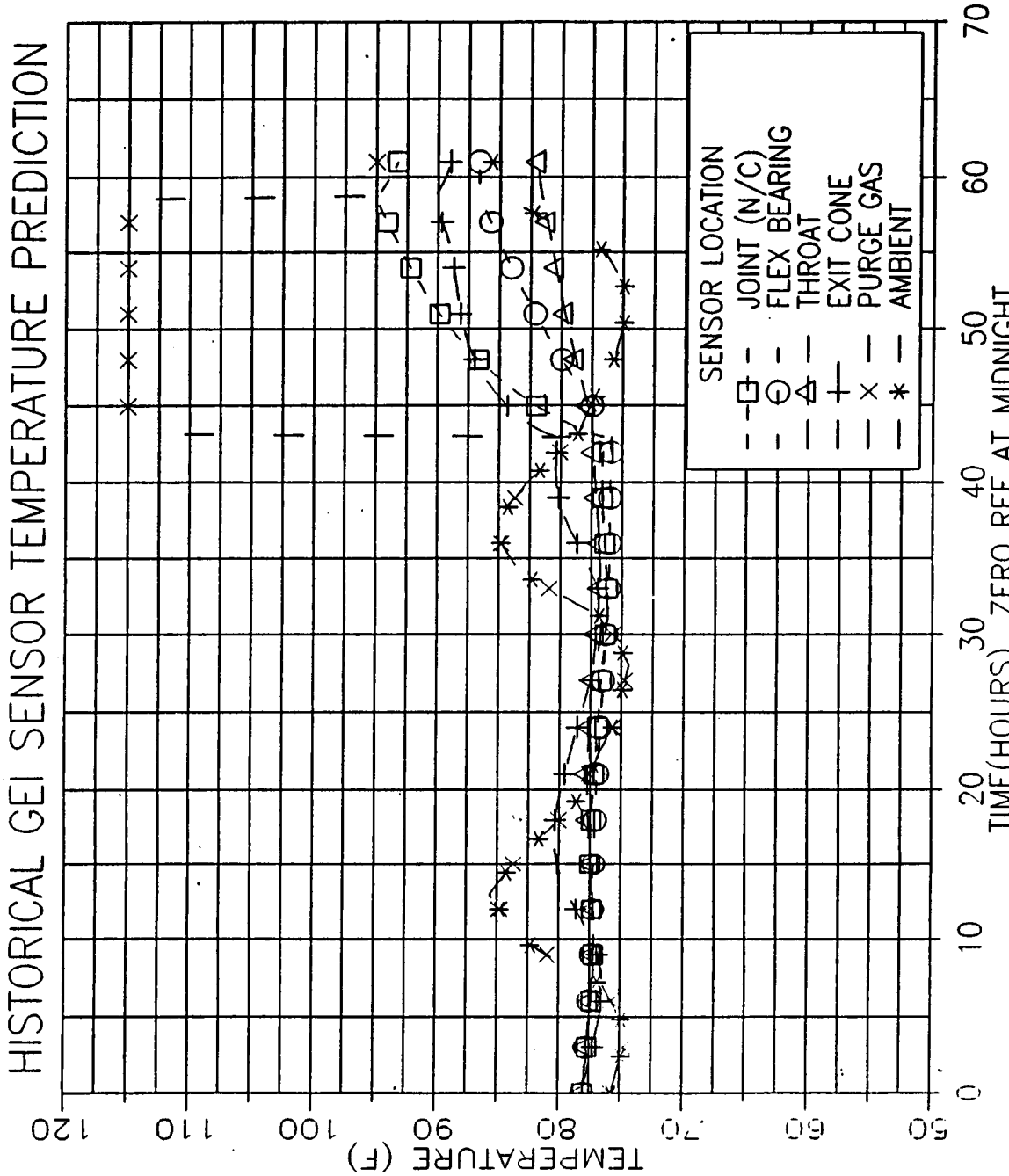

Figure 4.9-52. Left SRM Aft Region (September)

ORIGINAL PAGE IS
OF POOR QUALITY

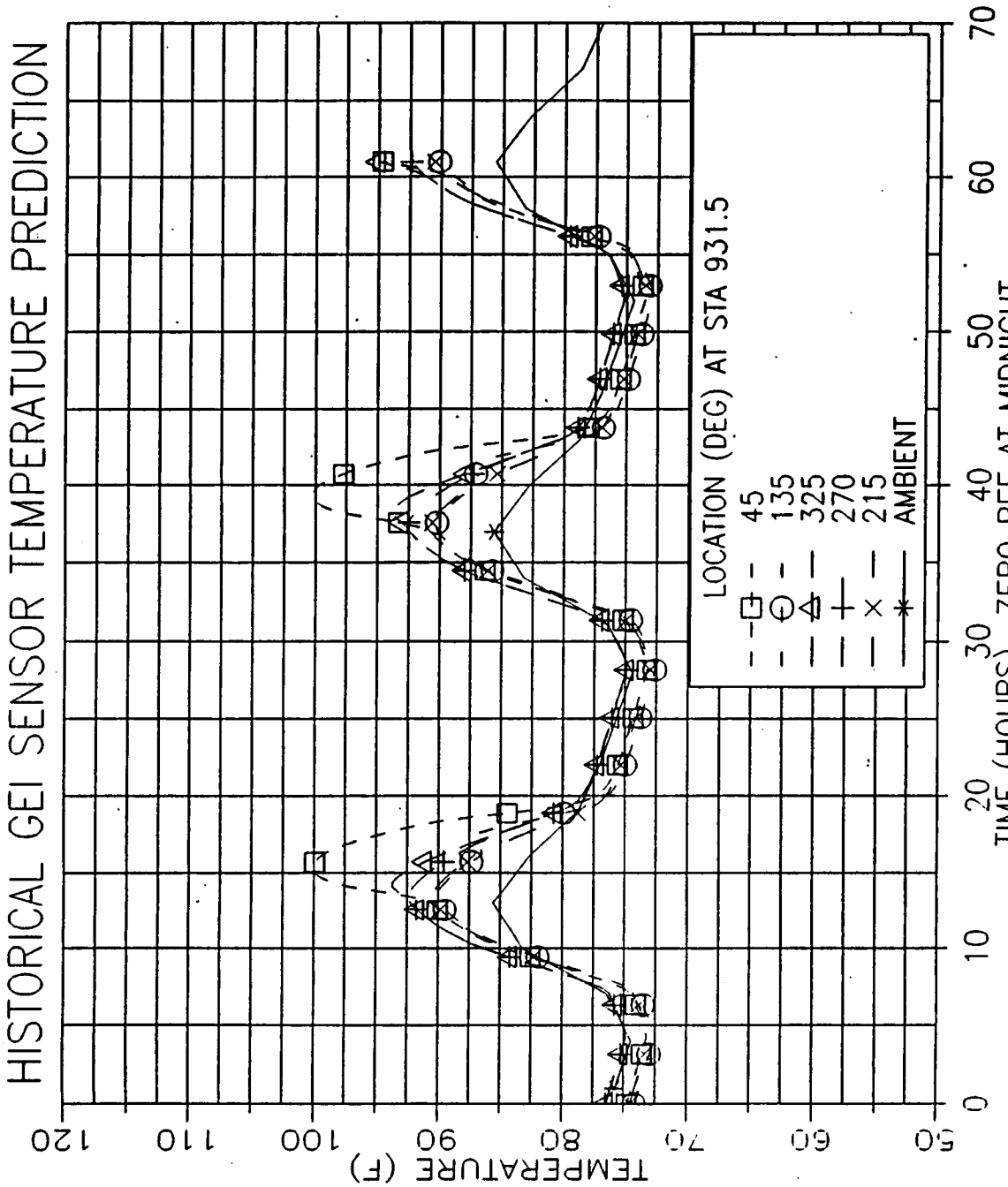

Figure 4.9-53. Left SRM Forward Case Acreage (September)

ORIGINAL PAGE IS
OF POOR QUALITY

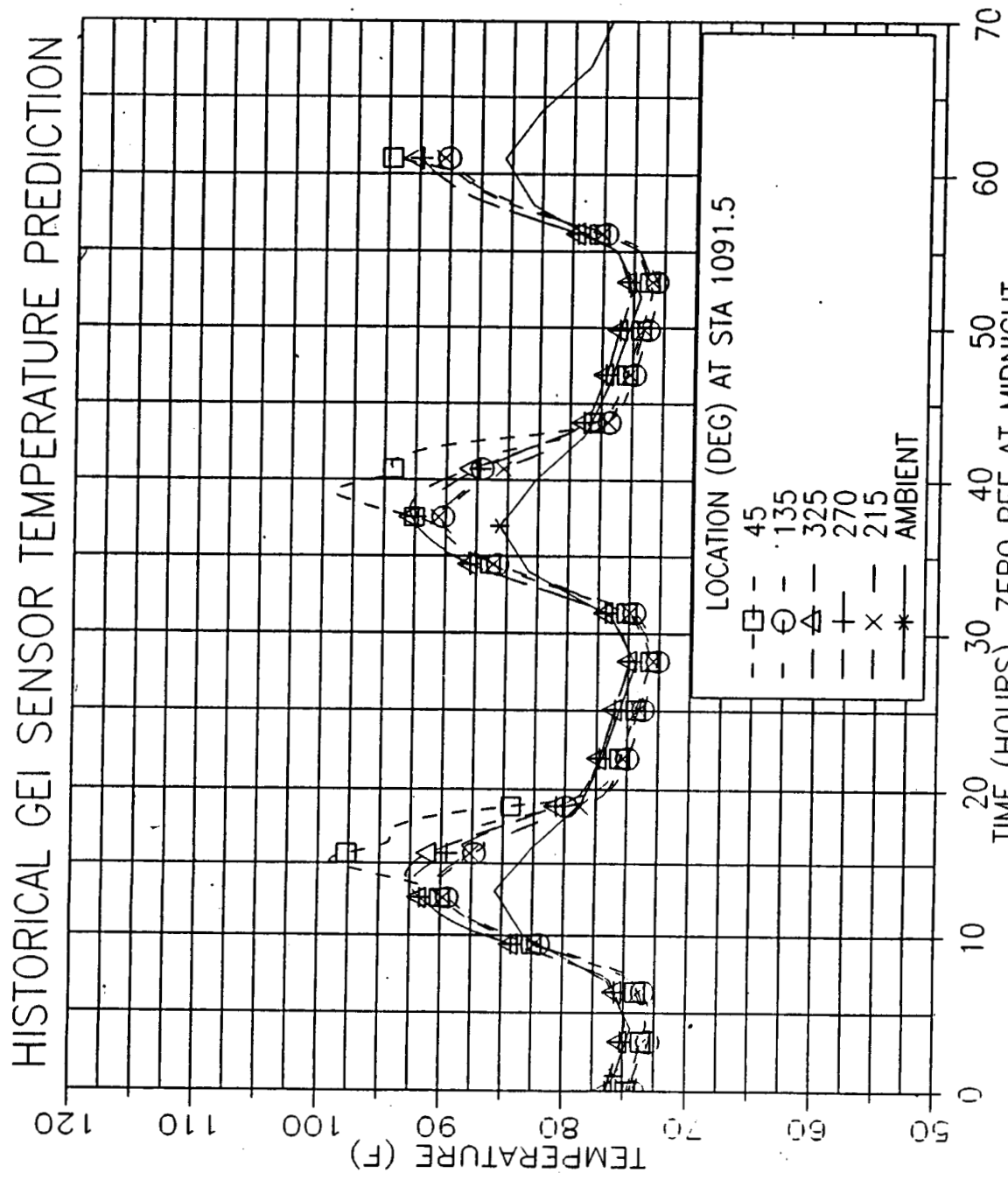

Figure 4.9-54. Left SRM Forward Center Case Acreage (September)

ORIGINAL PAGE IS
OF POOR QUALITY

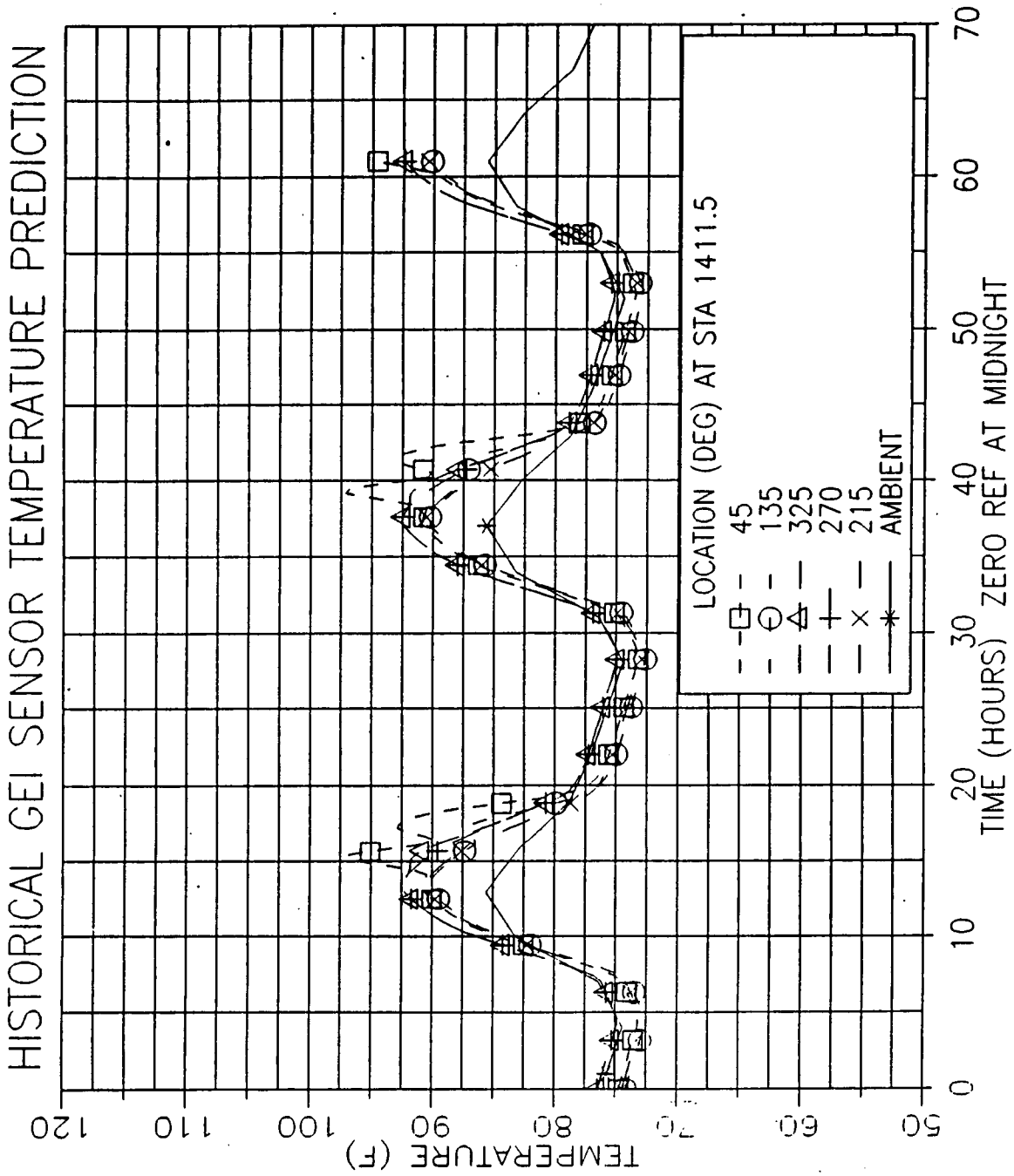

Figure 4.9-55. Left SRM Aft Center Case Acreage (September)

ORIGINAL PAGE IS
OF POOR QUALITY

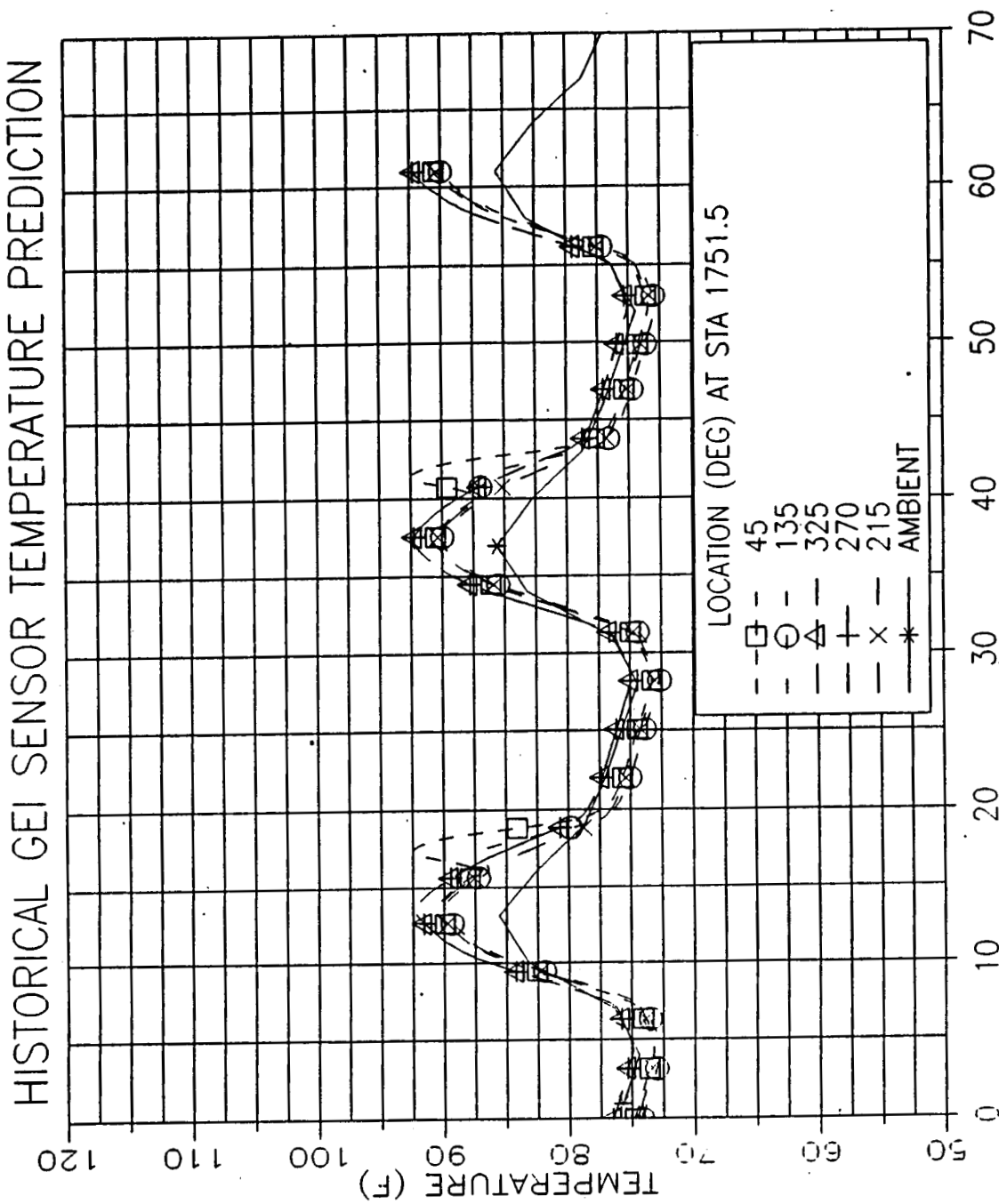

Figure 4.9-56. Left SRM Aft Case Acreage (September)

ORIGINAL PAGE IS
OF POOR QUALITY

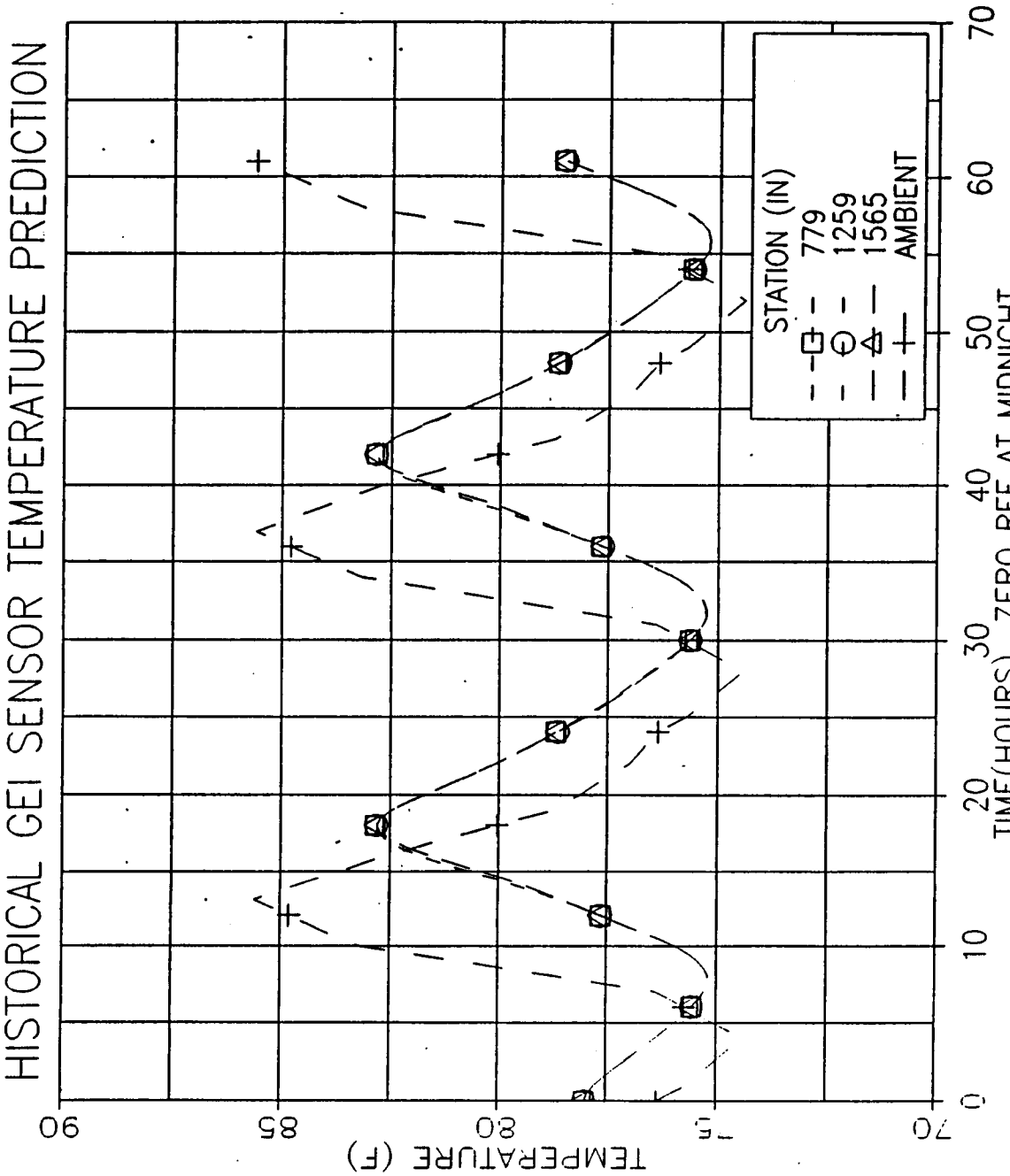

Figure 4.9-57. Left SRM Tunnel Bondline (September)

ORIGINAL PAGE IS
OF POOR QUALITY

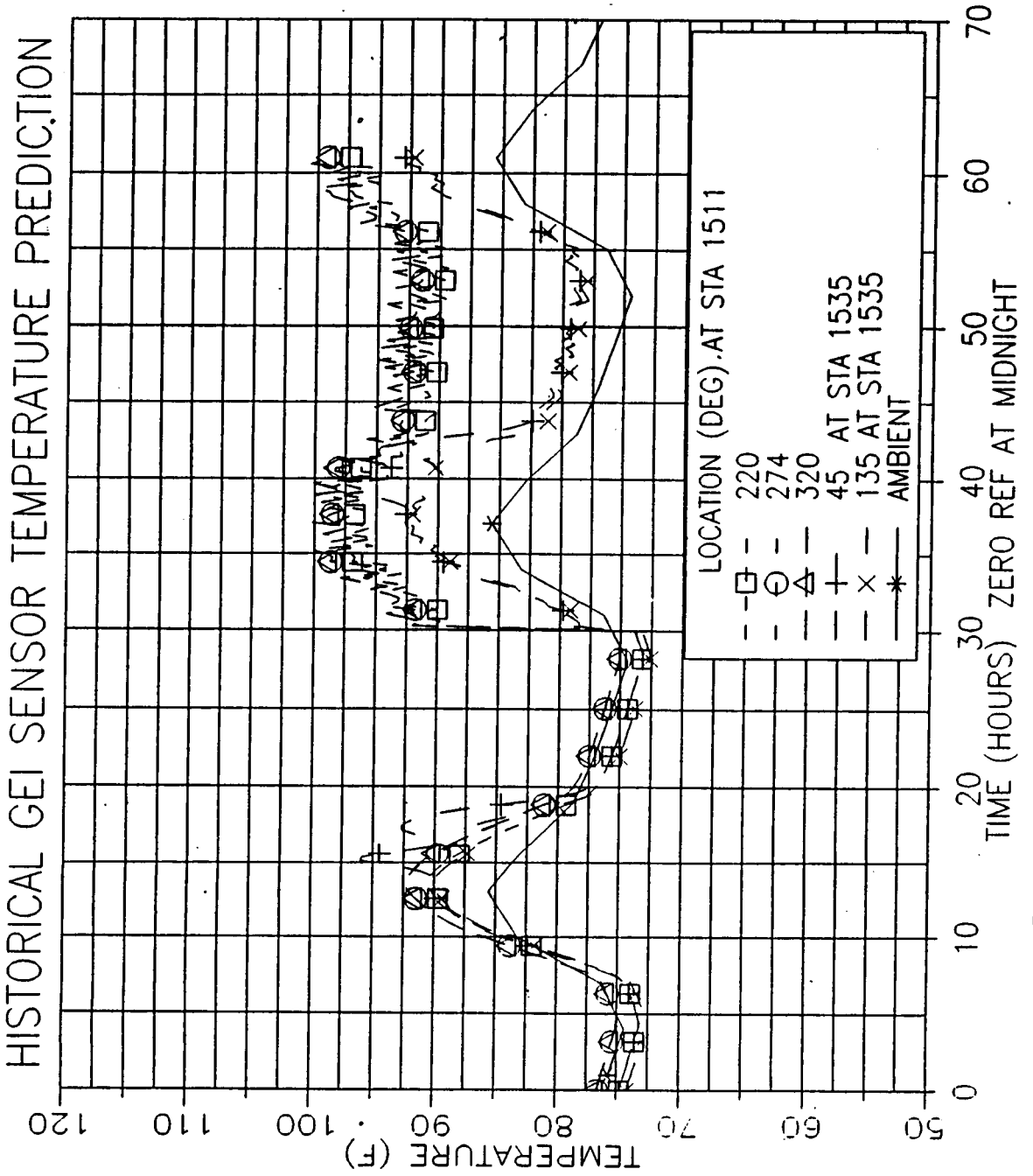

Figure 4.9-58. Left SRM ETA Region (September)

ORIGINAL PAGE IS
OF POOR QUALITY

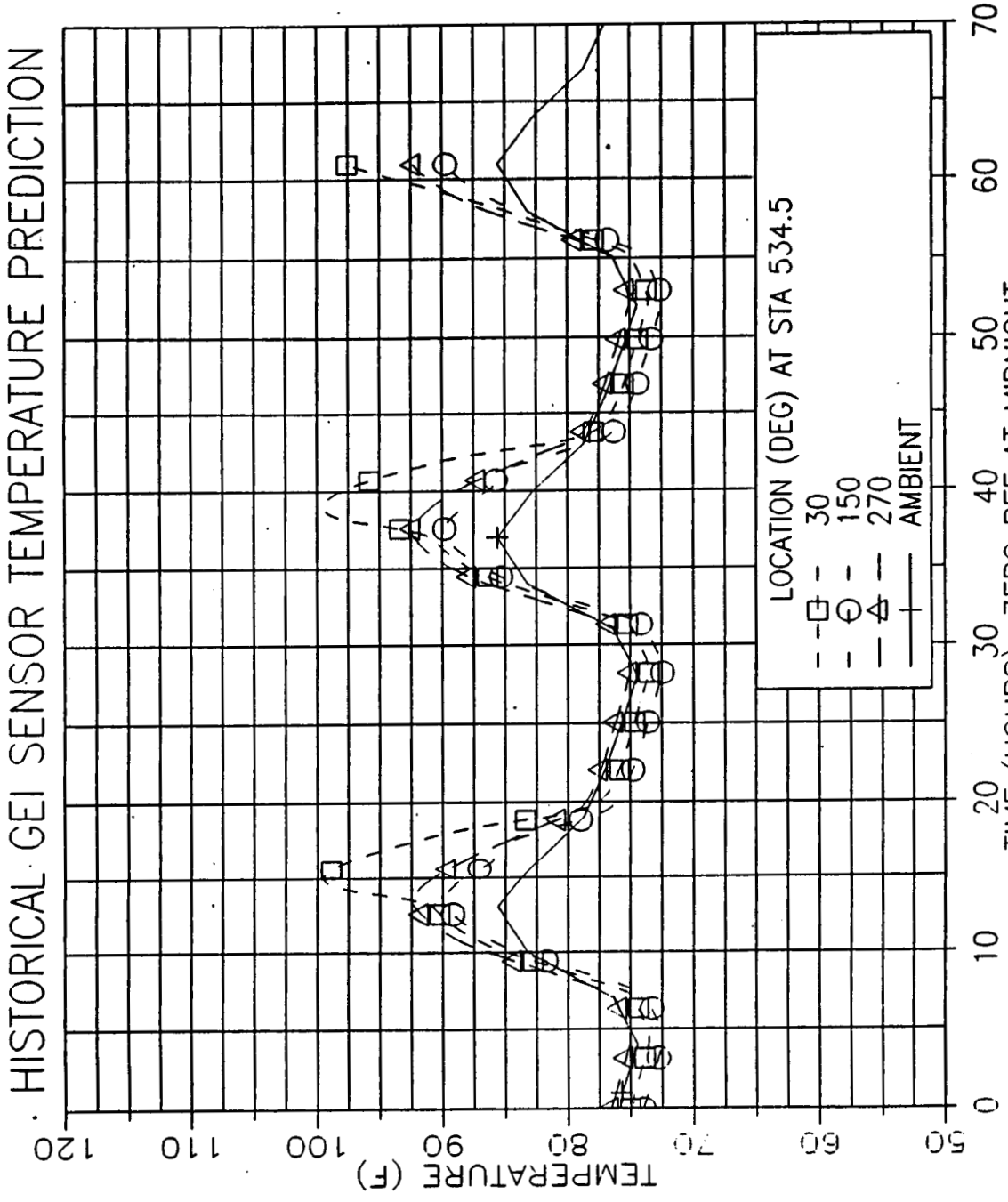

Figure 4.9-59. Left SRM Forward Dome Factory Joint (September)

ORIGINAL PAGE IS
OF POOR QUALITY

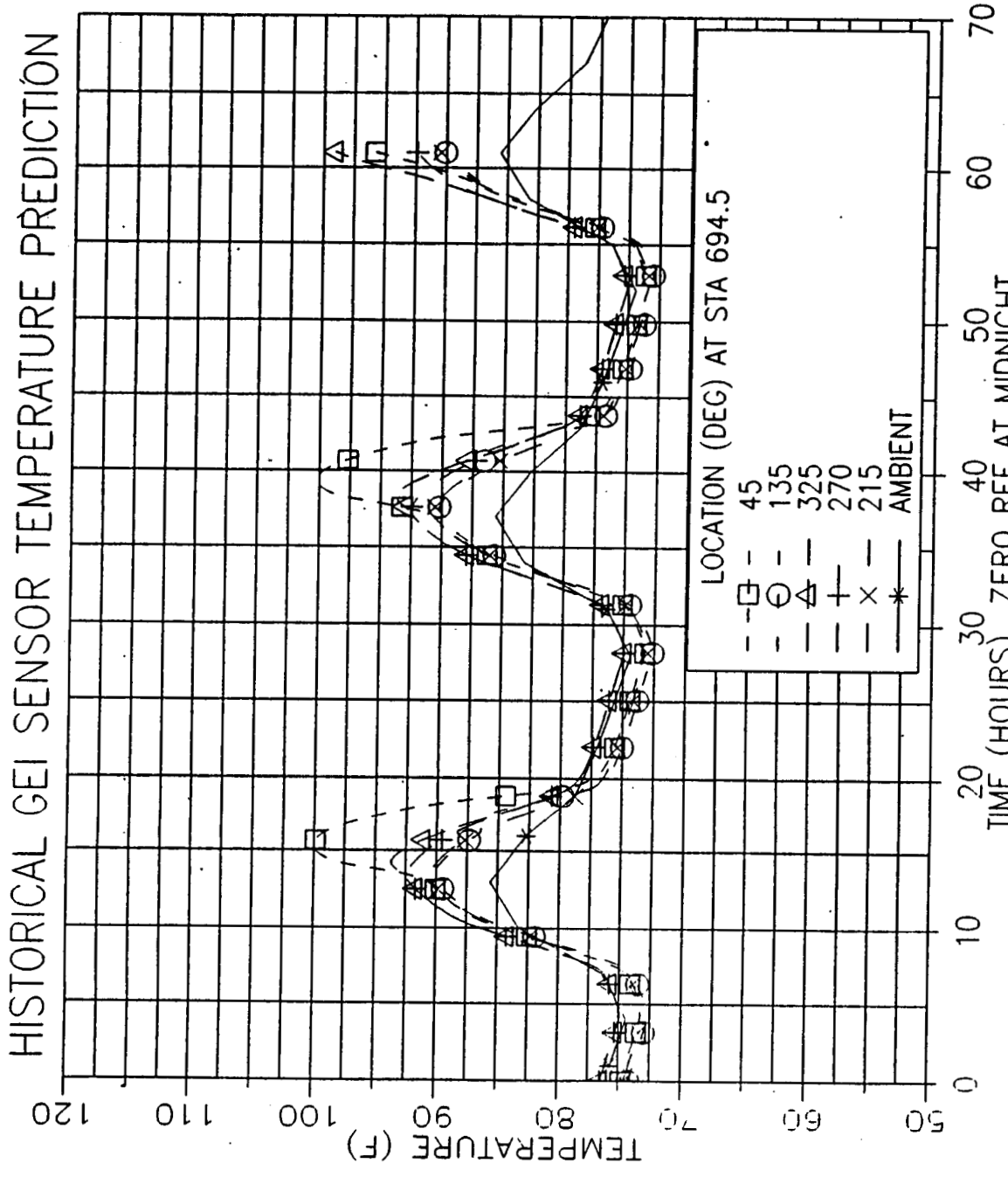

Figure 4.9-60. Left SRM Forward Factory Joint (September)

ORIGINAL PAGE IS
OF POOR QUALITY

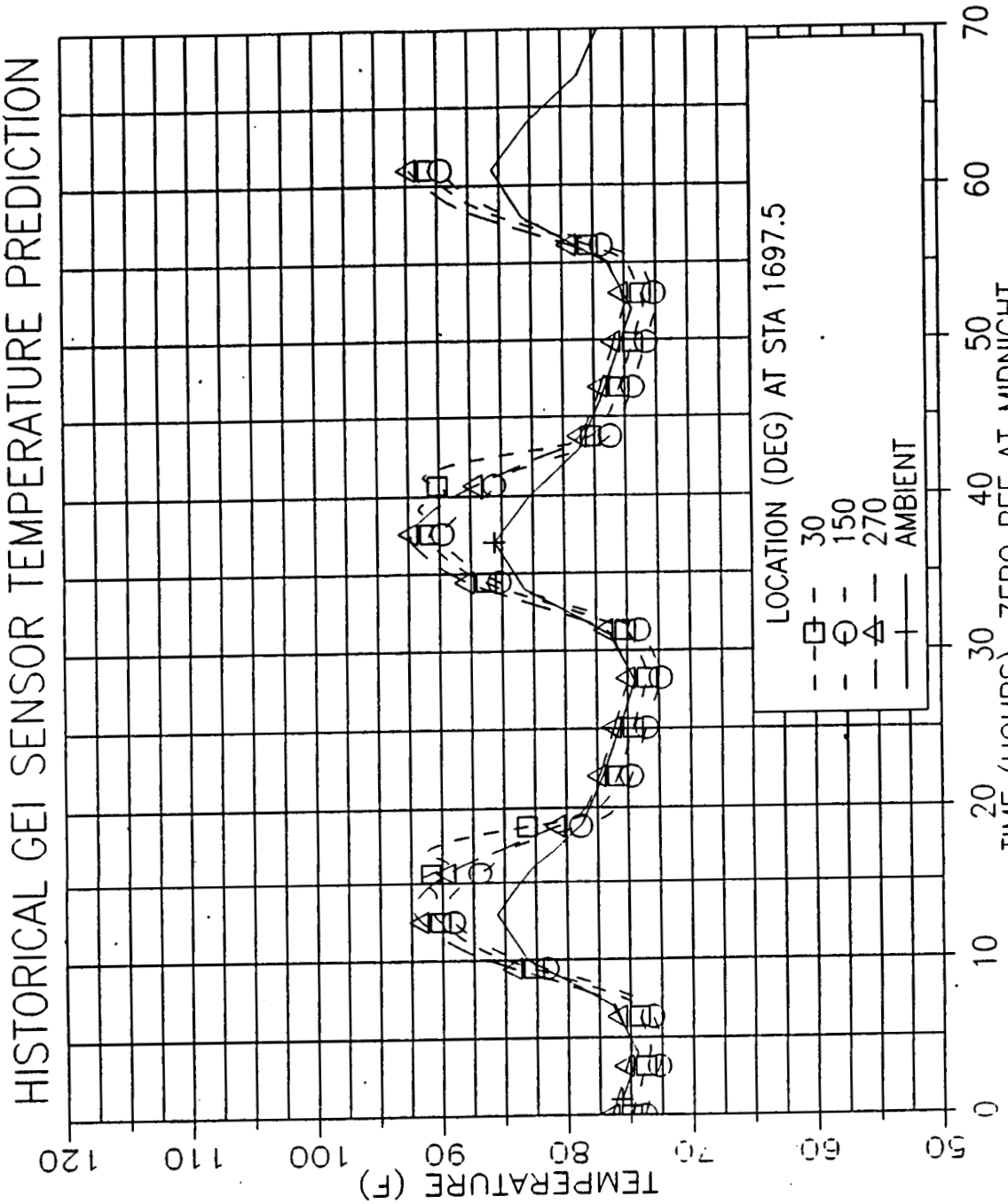

Figure 4.9-61. Left SRM Aft Factory Joint (September)

ORIGINAL PAGE IS
OF POOR QUALITY

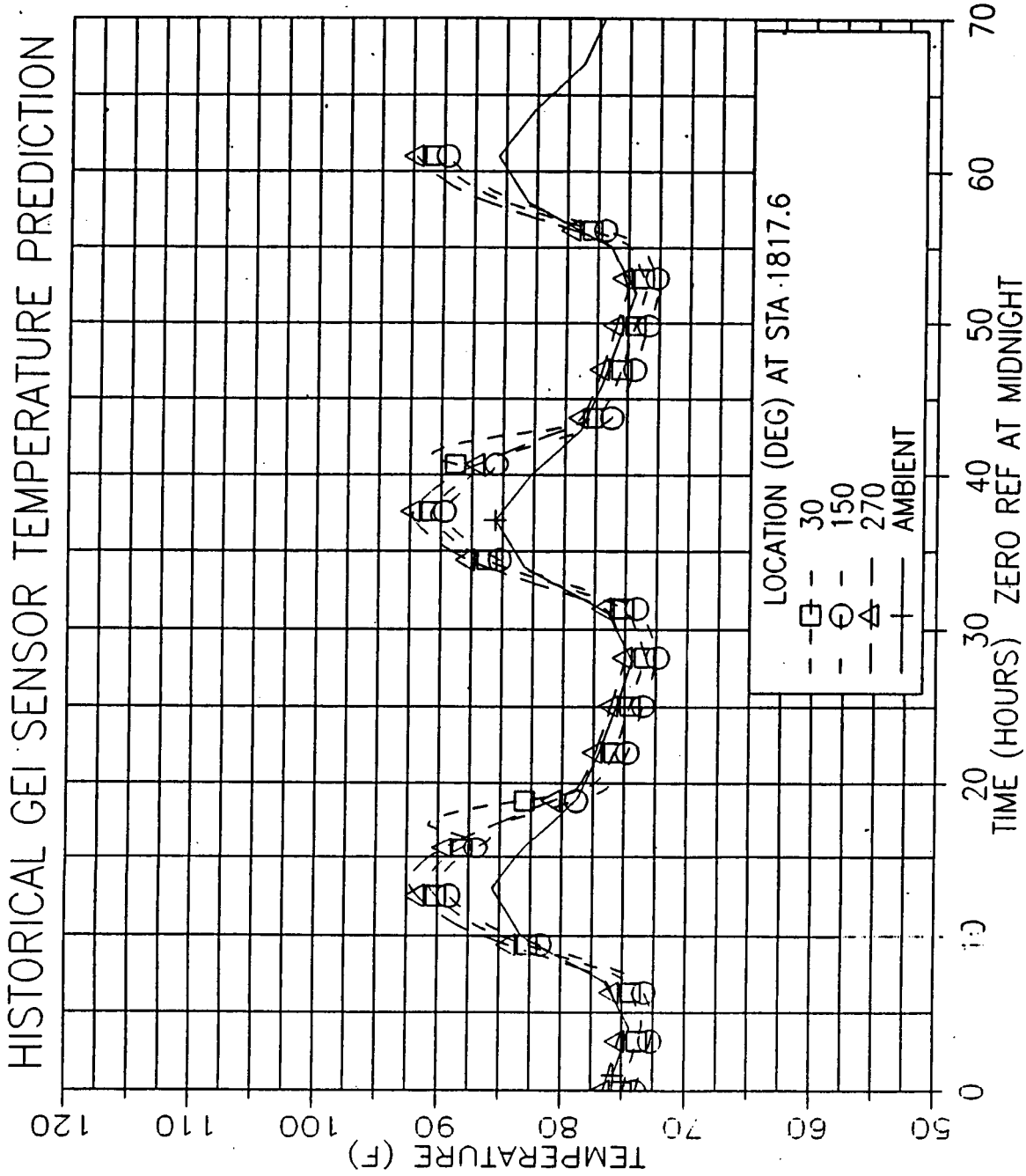

Figure 4.9-62. Left SRM Aft Dome Factory Joint (September)

Table 4.9-8. Analytical Time Frames For Estimating Event Sequencing of September Historical Joint Heater and GEI Sensor Predictions

Time (hr)	Countdown Events in Analysis
0	Midnight KSC EDT (28 Sep 1988)
30	Joint heater operation begins at 0600 hr KSC EDT (28 Sep 1988) (T-24 hr + 4 hr for holds)
43	Aft skirt conditioning operation begins at 1900 hr KSC EDT (28 Sep 1988) (T-12 hr + 3 hr for holds)
48	Induced environments due to ET refrigeration effect begins at midnight (29 Sep 1988) (T-6 hr + 4 hr for ET loading and holds) Note: Induced environments not available for these predictions; figures will be updated when they are available.
58	Time of launch (0959 hr, 29 Sep 1988)
61	Up to a 1300 hr launch 29 Sep 1988 (allowing for a 3-hr delay)

Note: Figures 2.8.2-35 through 2.8.2-64 consist of a 2-day + 13-hr scenario.

ORIGINAL PAGE IS
OF POOR QUALITY

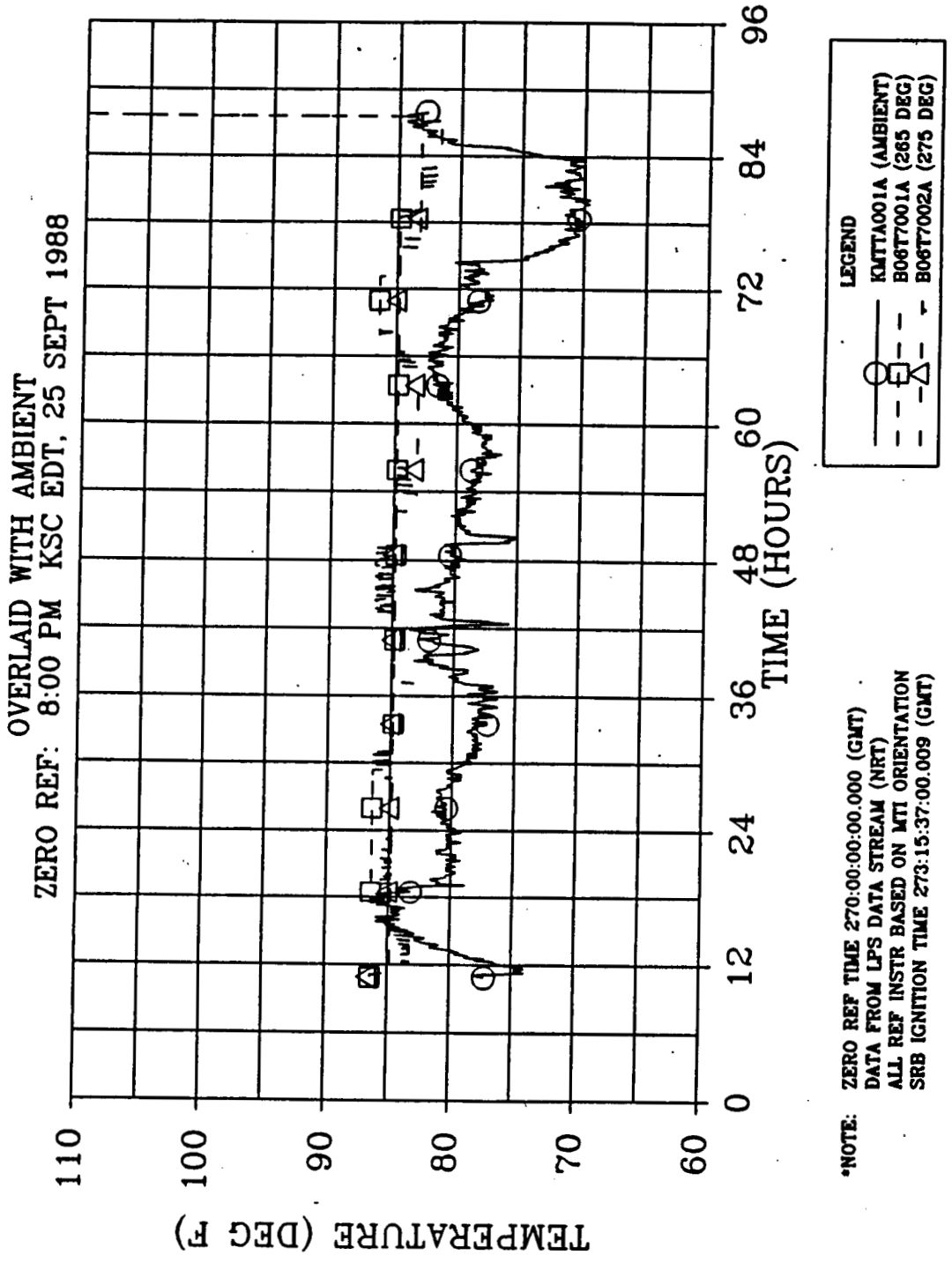

Figure 4.9-63. 360L001 Prelaunch Left SRM Igniter Joint Temperature

ORIGINAL PAGE IS
OF POOR QUALITY

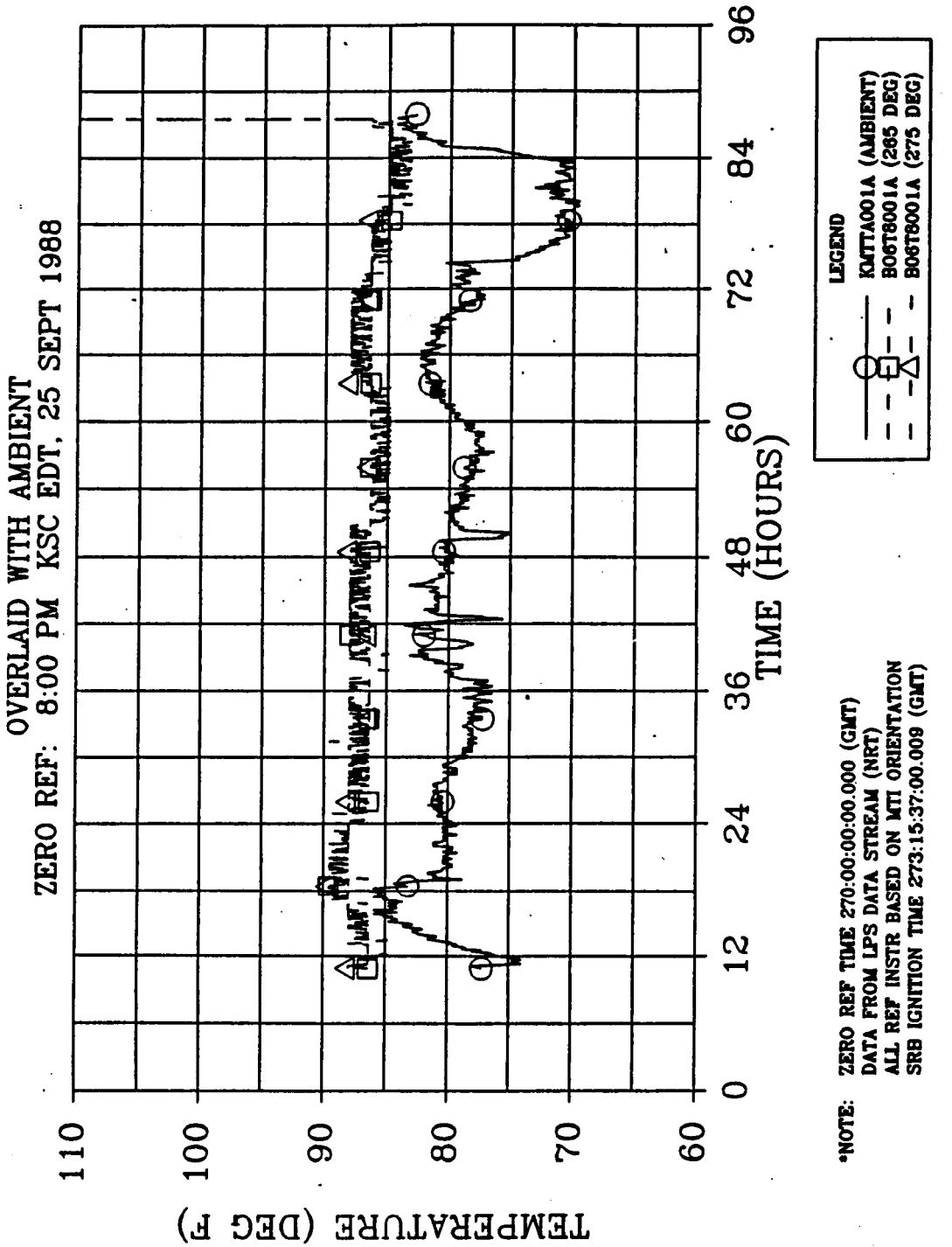

Figure 4.9-64. 360L001 Prelaunch Right SRM Igniter Joint Temperature

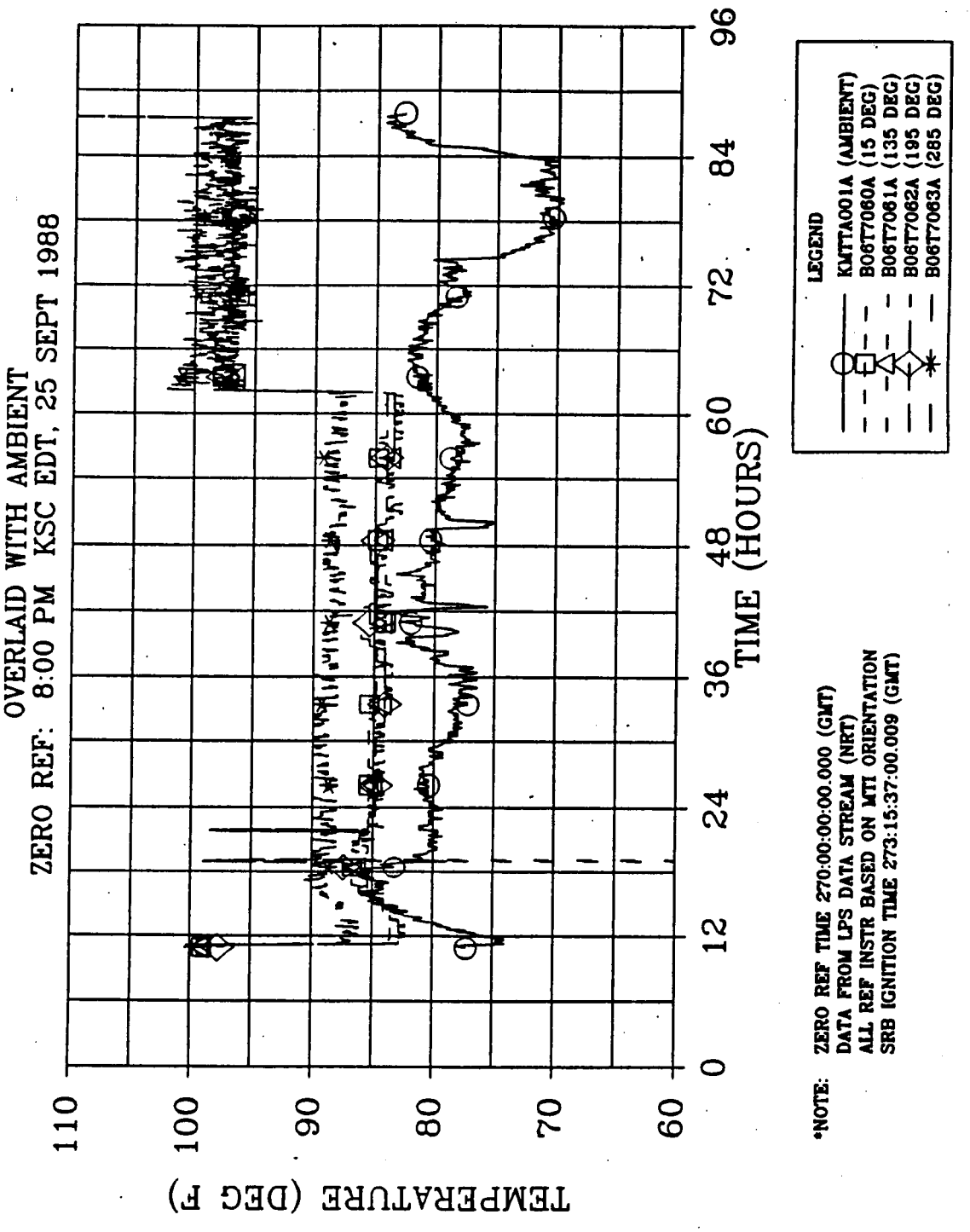

Figure 4.9-65. 360L001 Prelaunch Left SRM Forward Field Joint Temperature

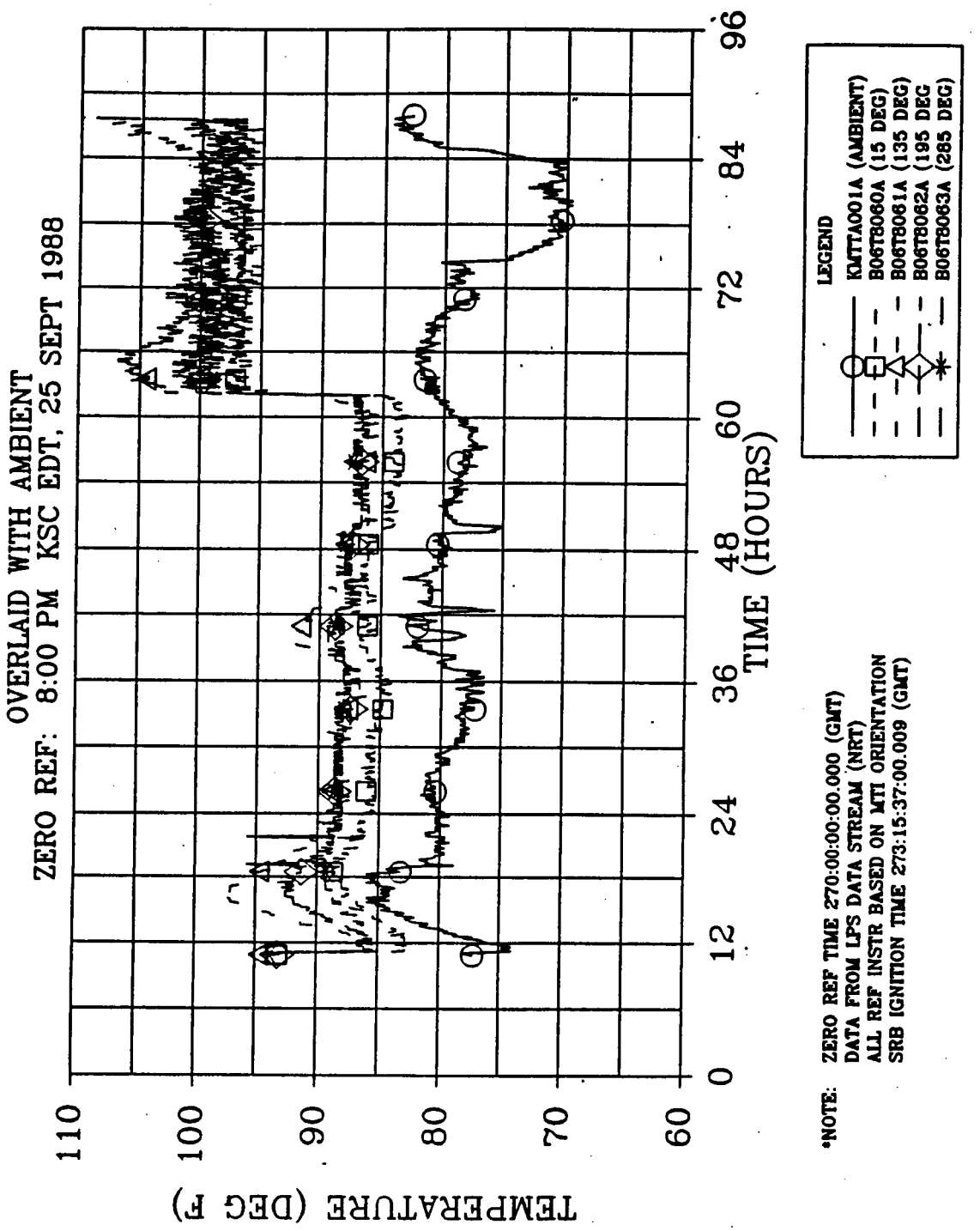

Figure 4.9-66. 360L001 Prelaunch Right SRM Forward Field Joint Temperature

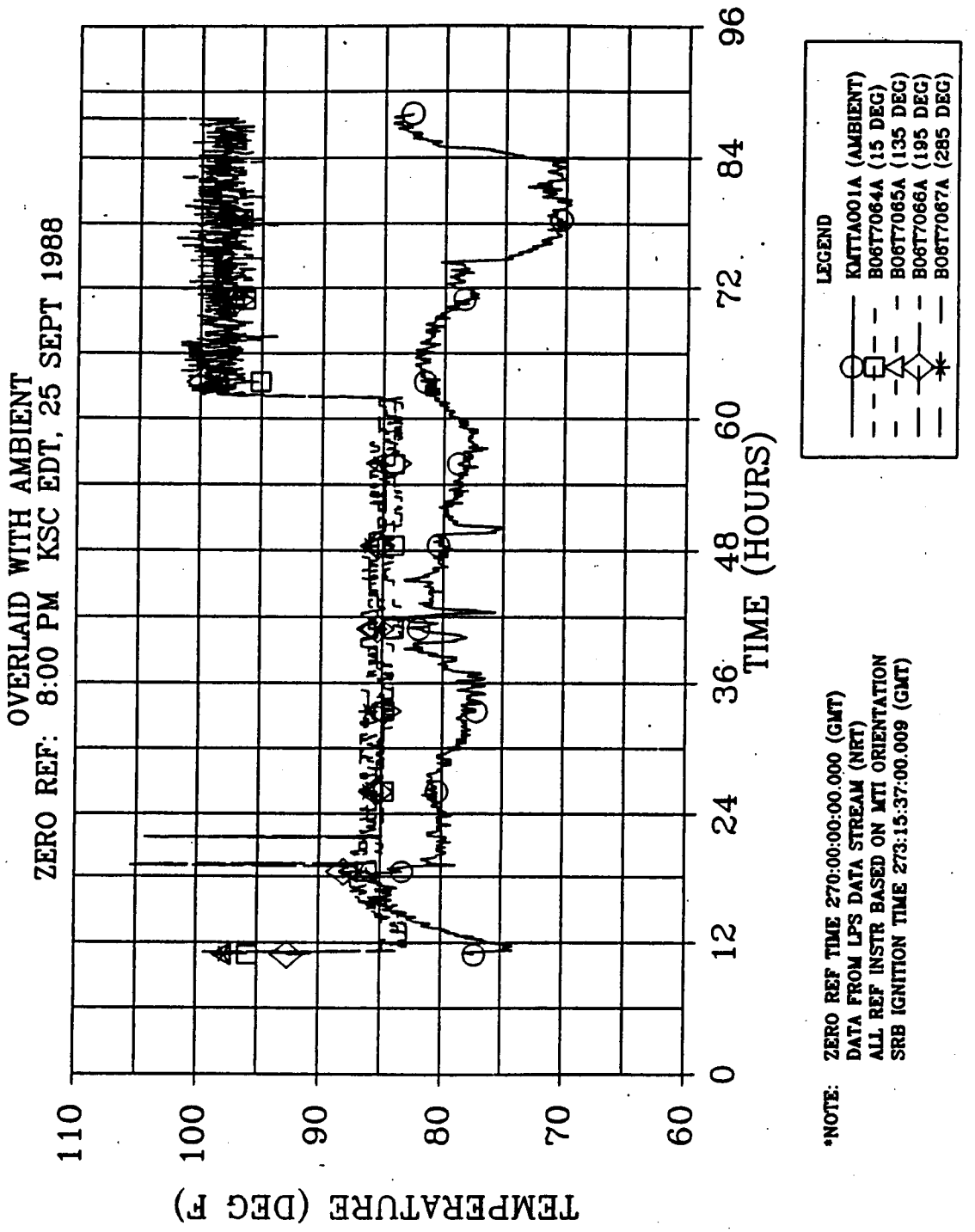

Figure 4.9-67. 360L001 Prelaunch Left SRM Center Field Joint Temperature

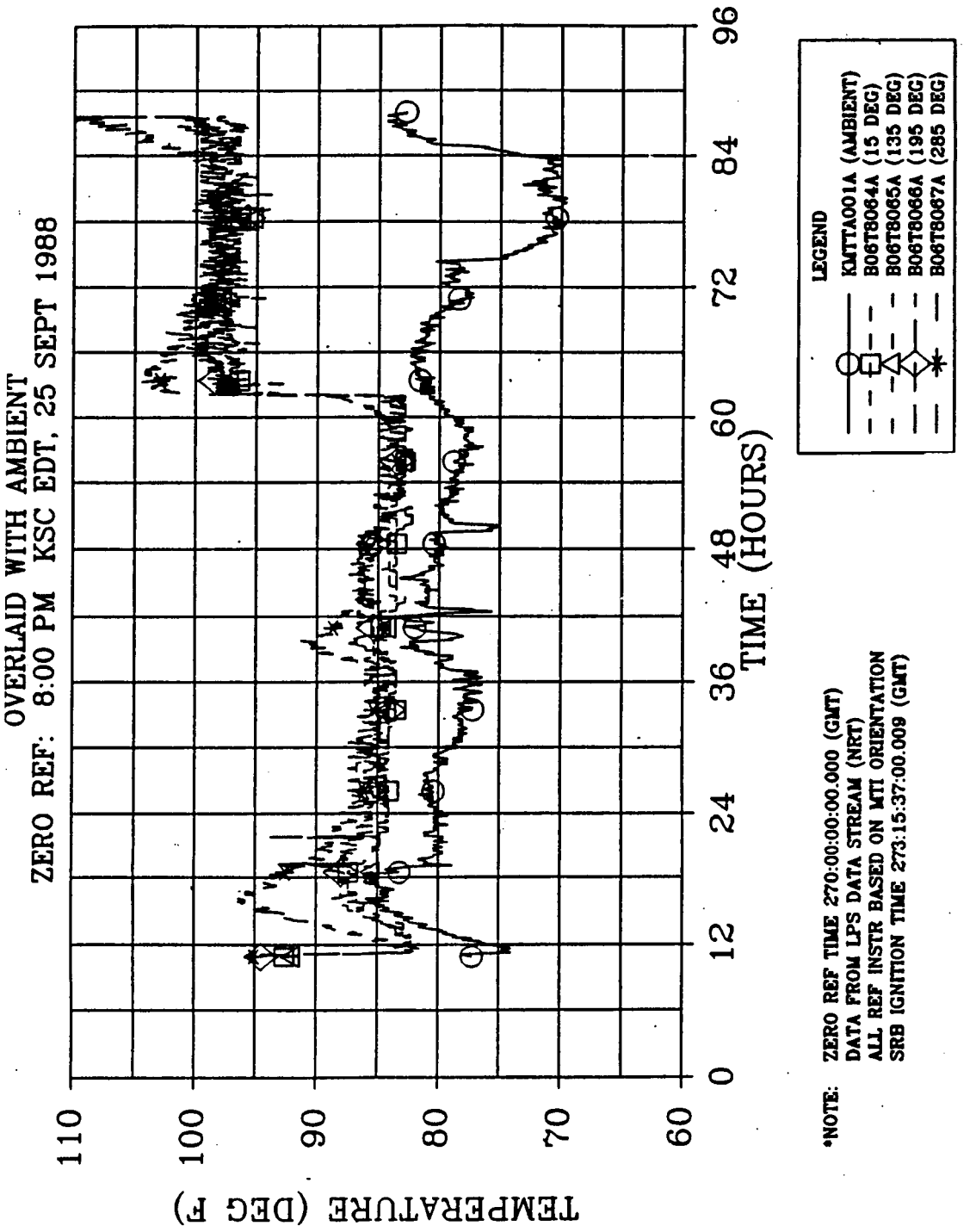

Figure 4.9-68. 360L001 Prelaunch Right SRM Center Field Joint Temperature

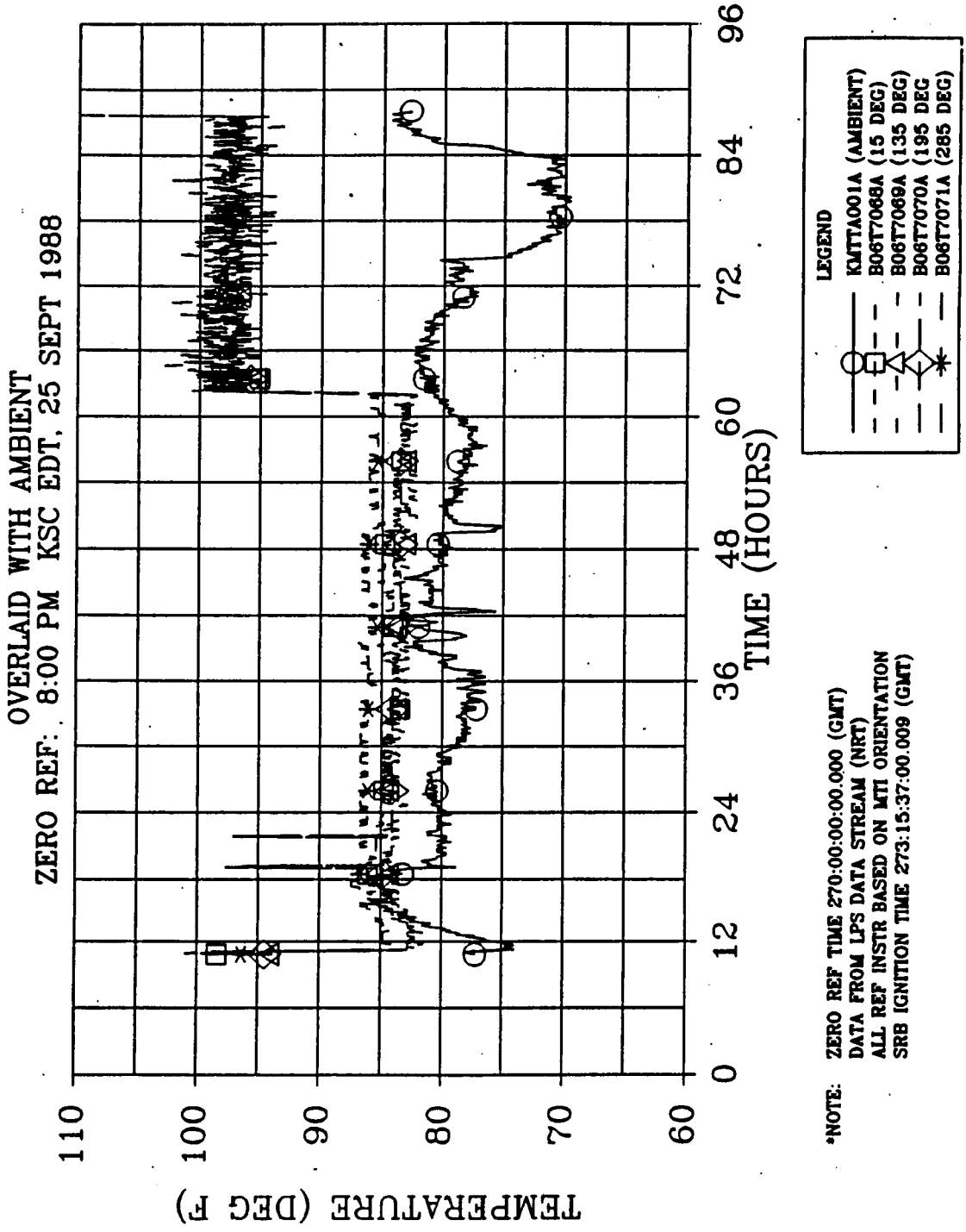

Figure 4.9-69. 360L001 Prelaunch Left SRM Aft Field Joint Temperature

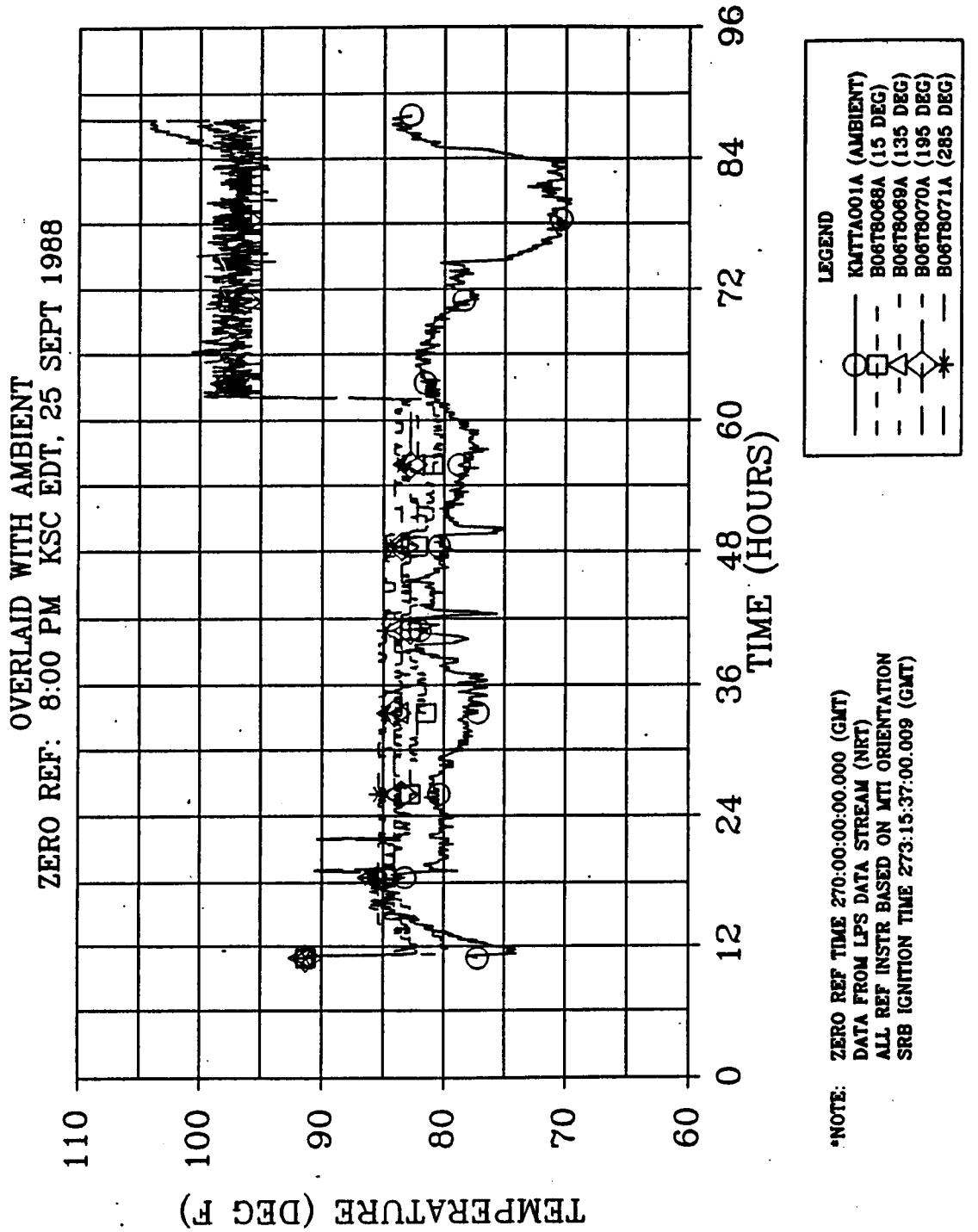

Figure 4.9-70. 360L001 Prelaunch Right SRM Aft Field Joint Temperature

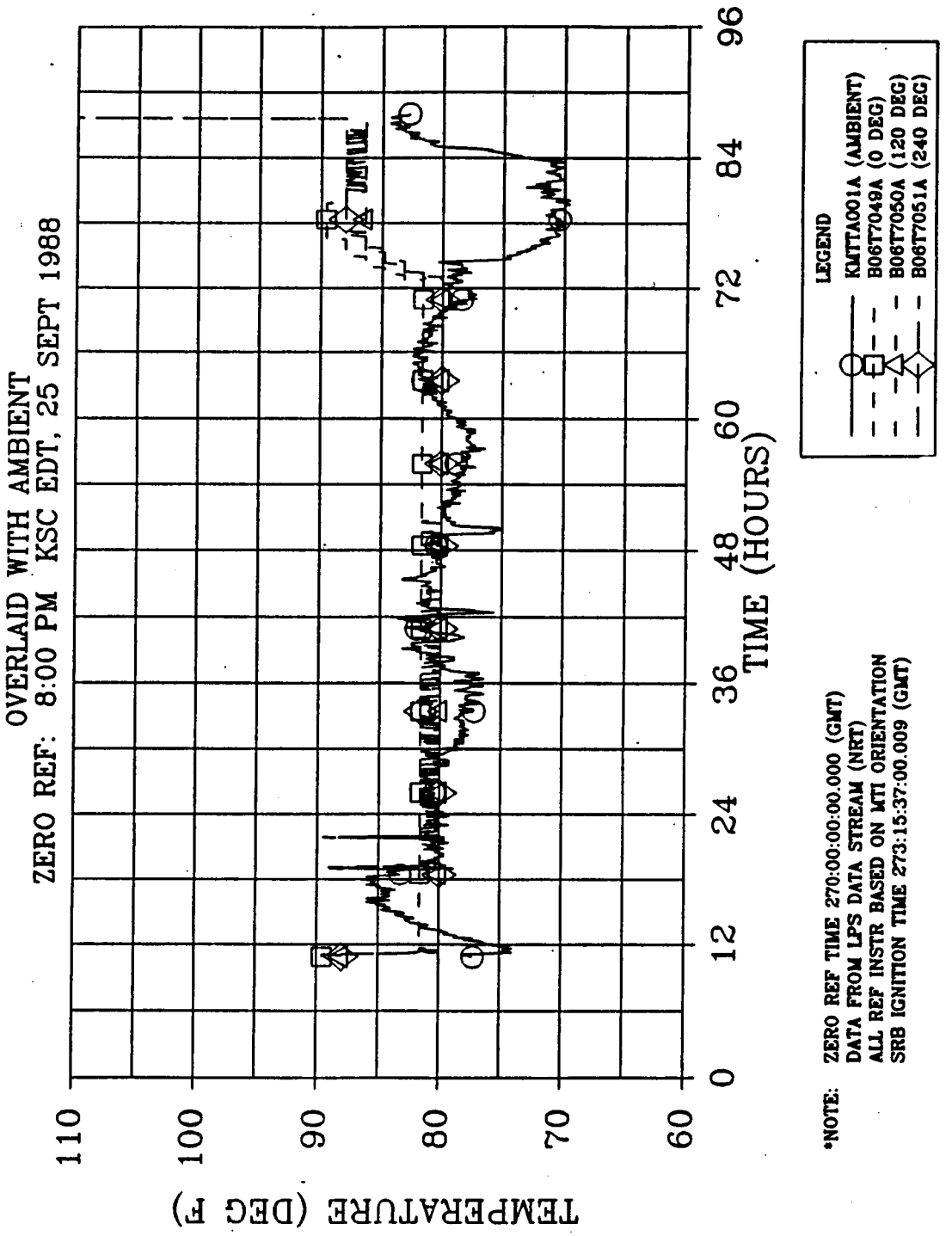

Figure 4.9-71. 360L001 Prelaunch Left SRM Nozzle/Case Joint Temperature

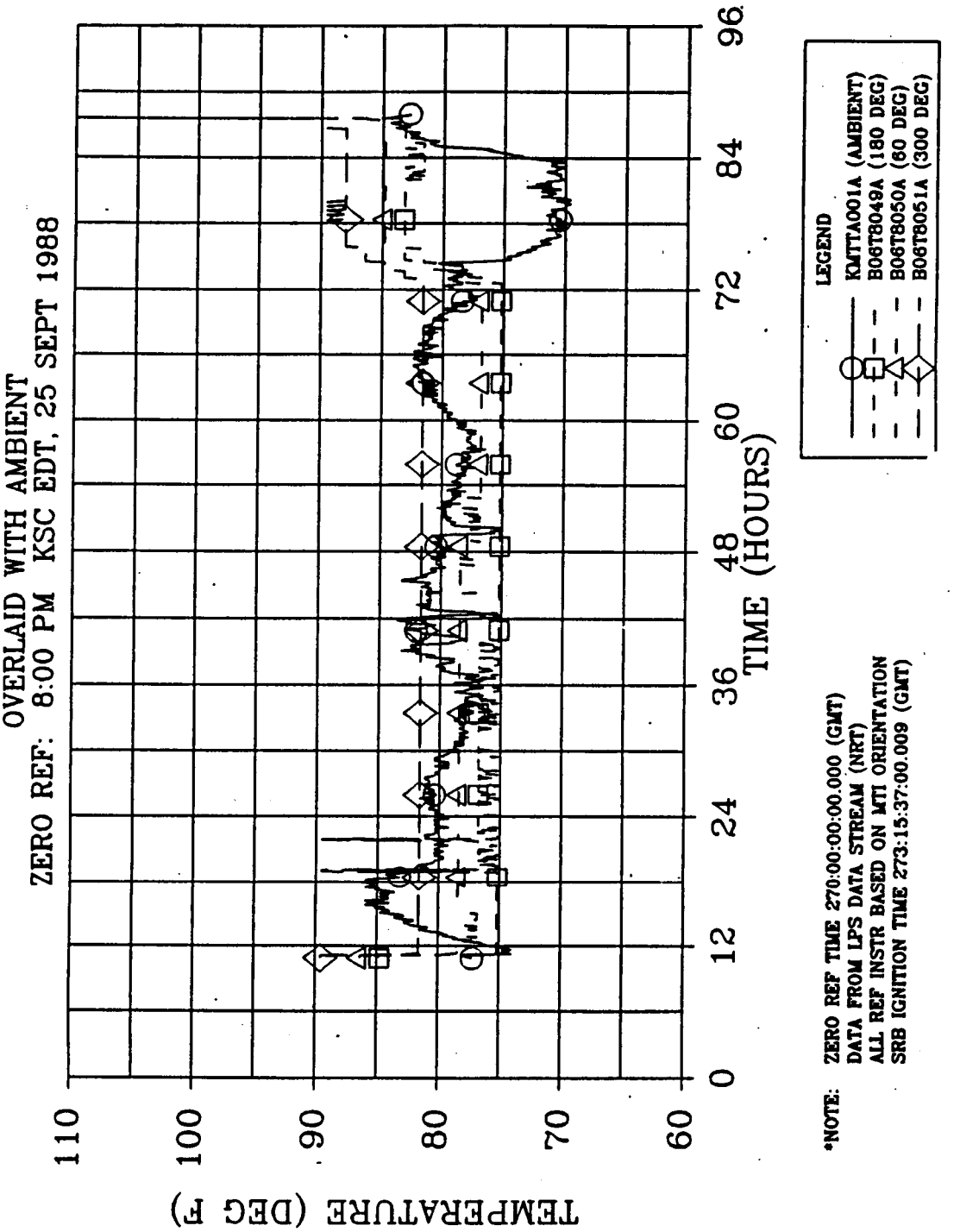

Figure 4.9-72. 360L001 Prelaunch Right SRM Nozzle/Case Joint Temperature

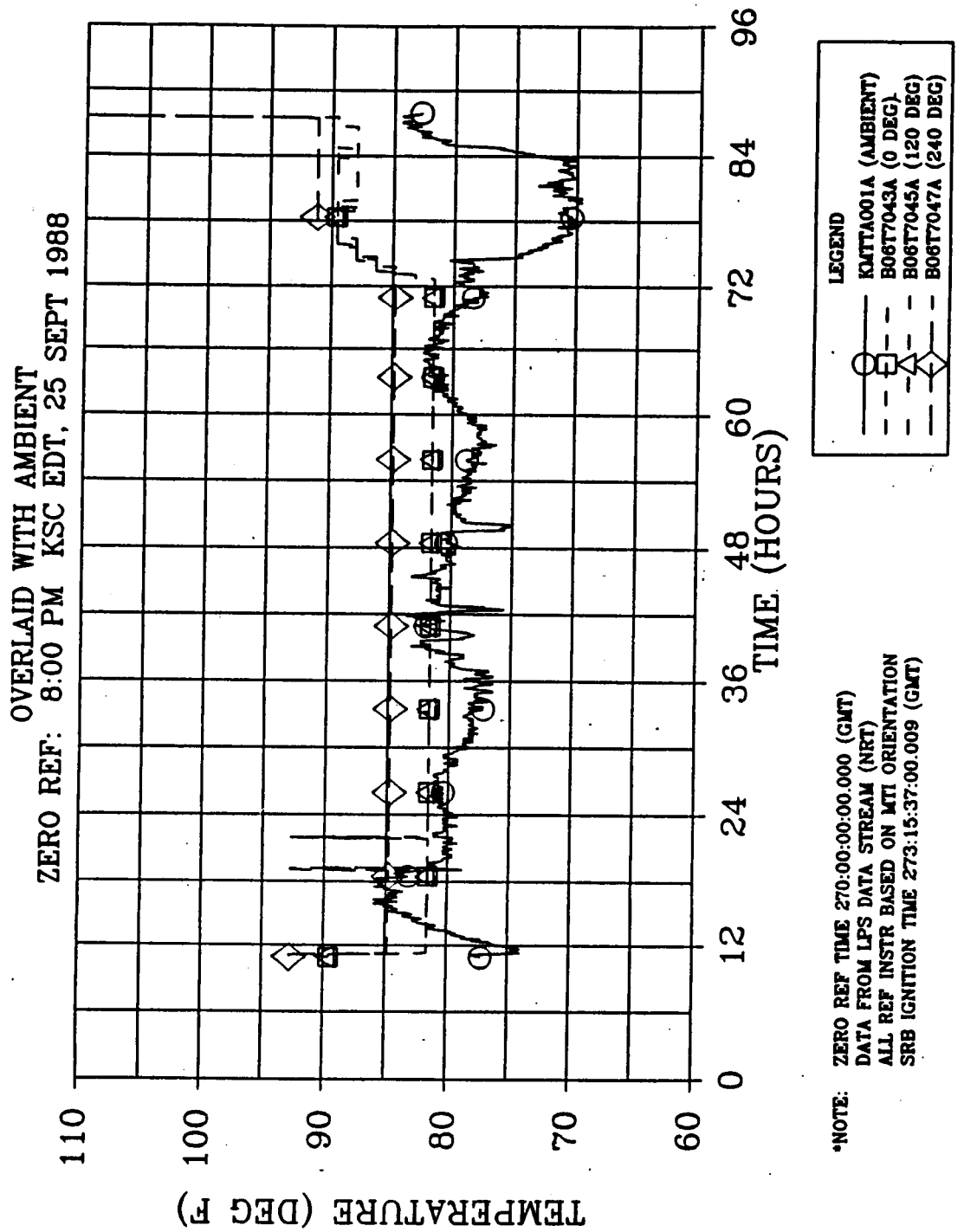

Figure 4.9-73. 360L001 Prelaunch Left SRM Flex Bearing Aft End Ring Temperature

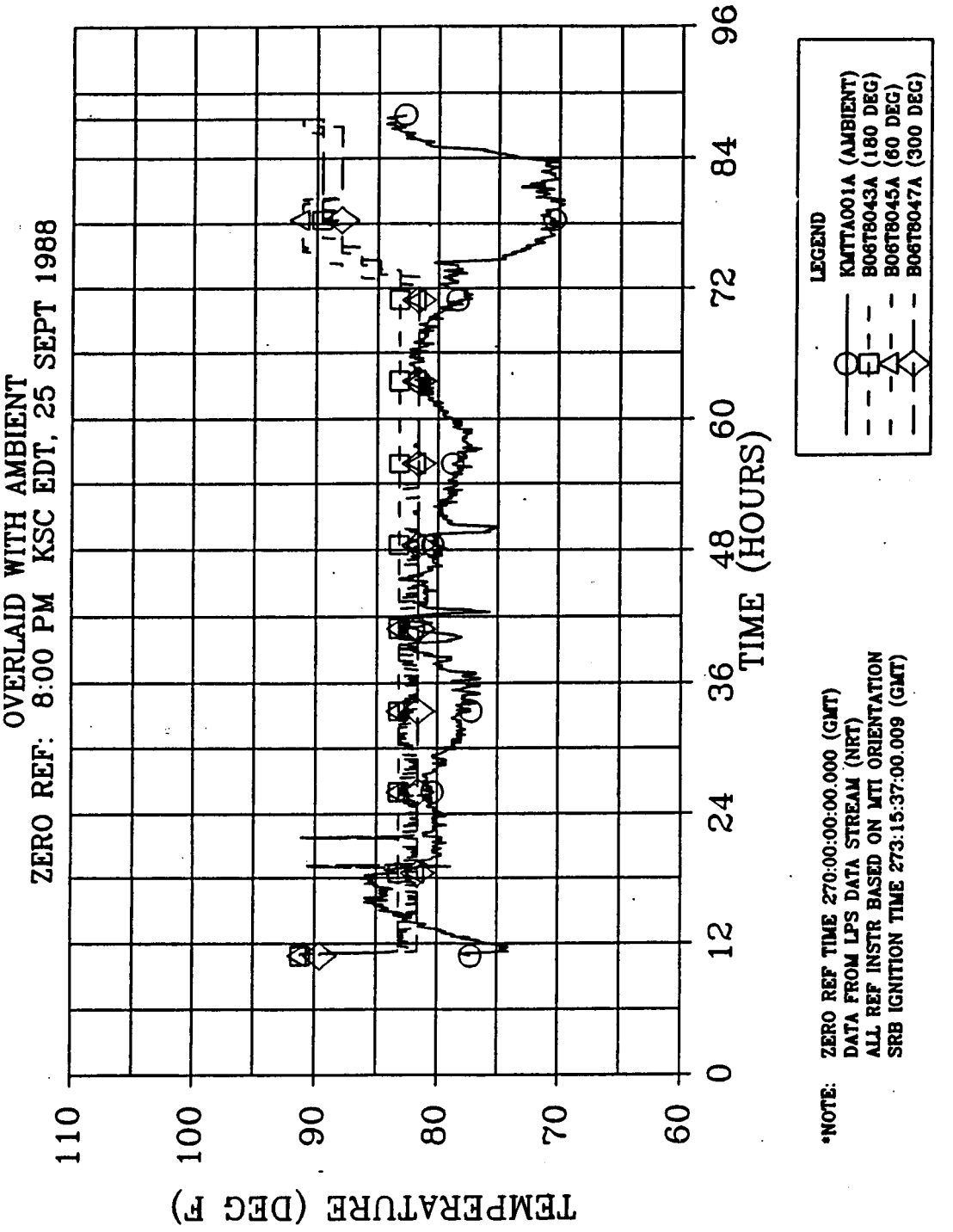

Figure 4.9-74. 360L001 Prelaunch Right SRM Flex Bearing Aft End Ring Temperature

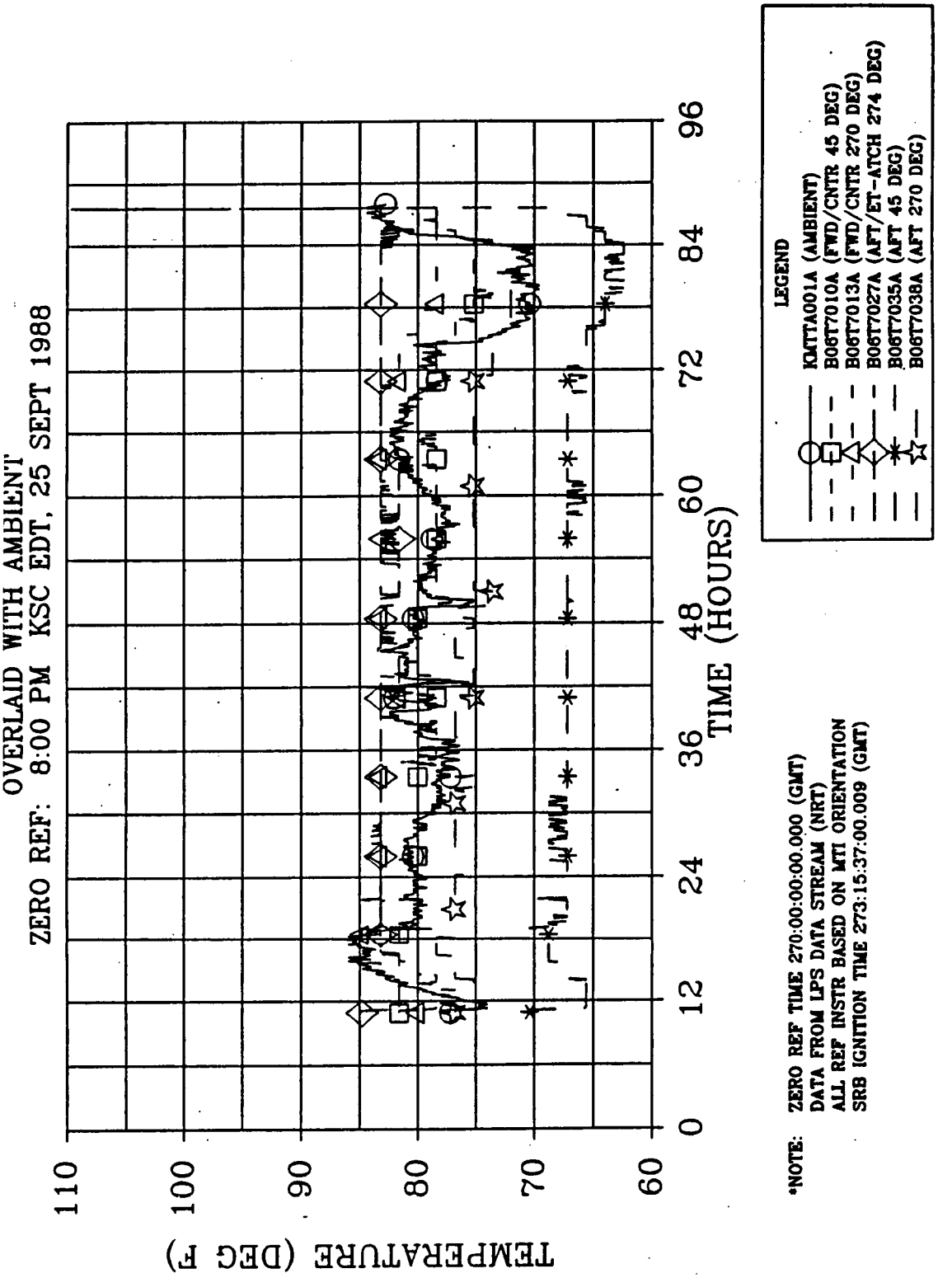

Figure 4.9-75. 360L001 Prelaunch Left SRM Case Acreage Temperature

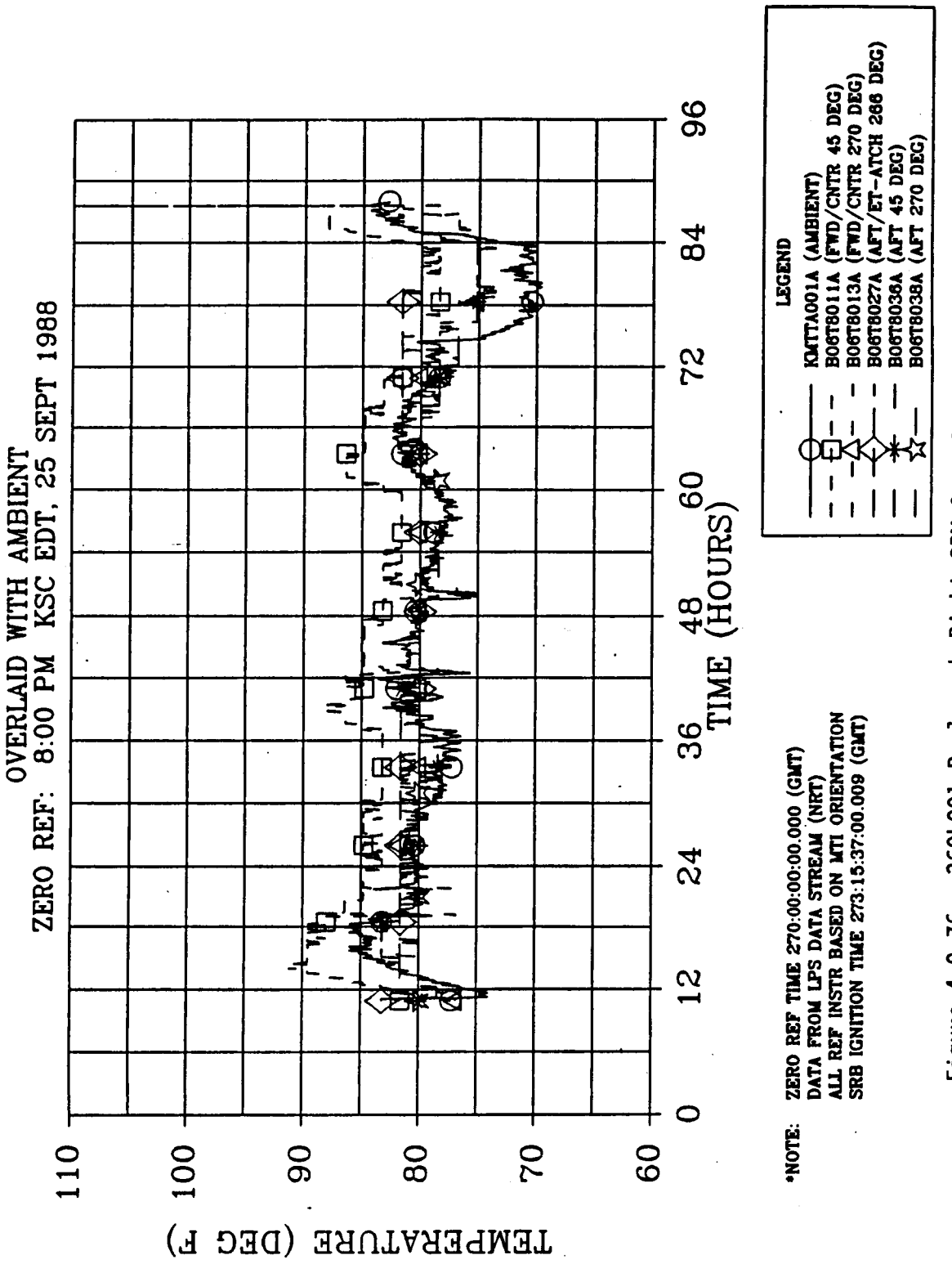

Figure 4.9-76. 360L001 Prelaunch Right SRM Case Acreage Temperature

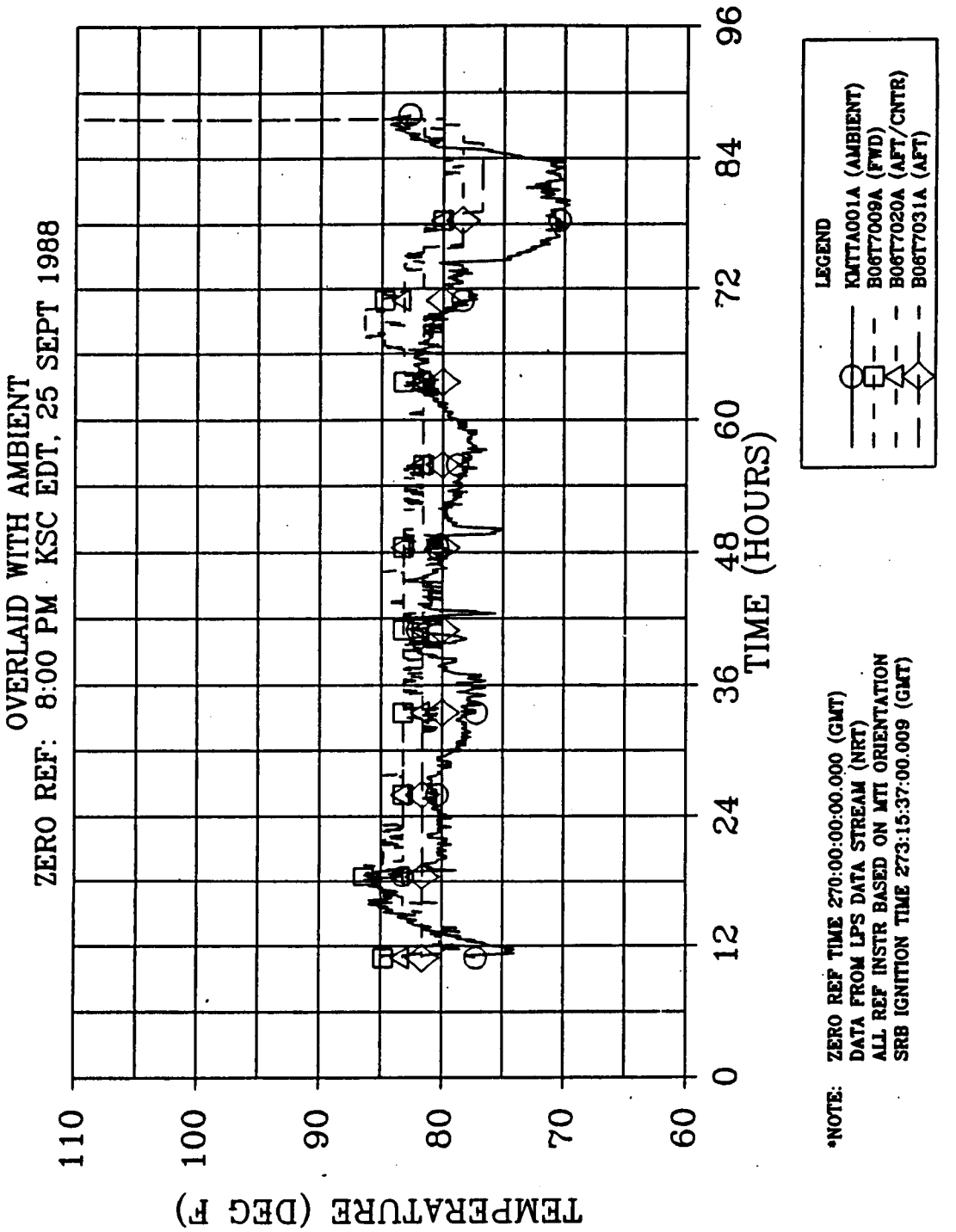

Figure 4.9-77. 360L001 Prelaunch Left SRM Tunnel Bondline Temperature

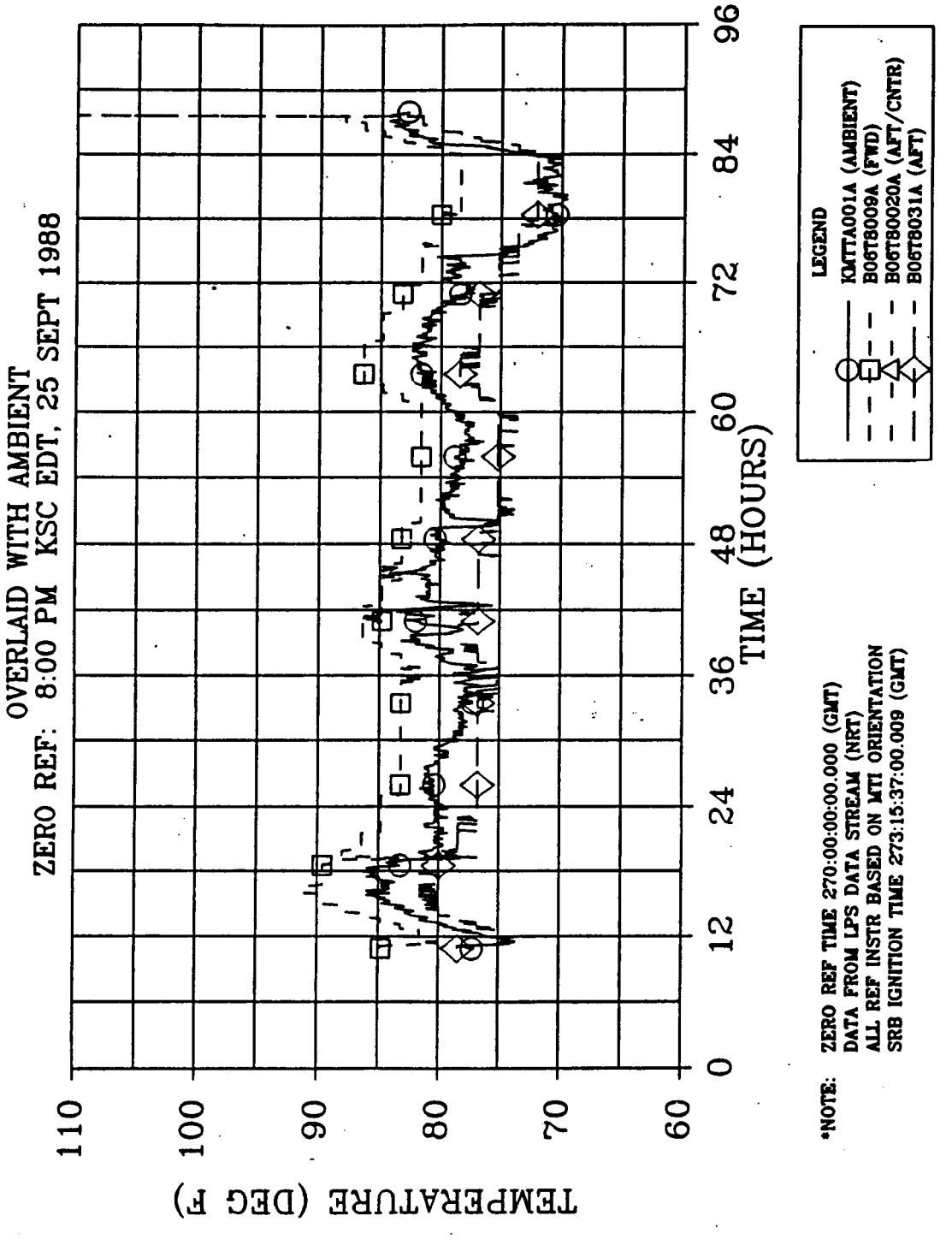

Figure 4.9-78. 360L001 Prelaunch Right SRM Tunnel Bondline Temperature

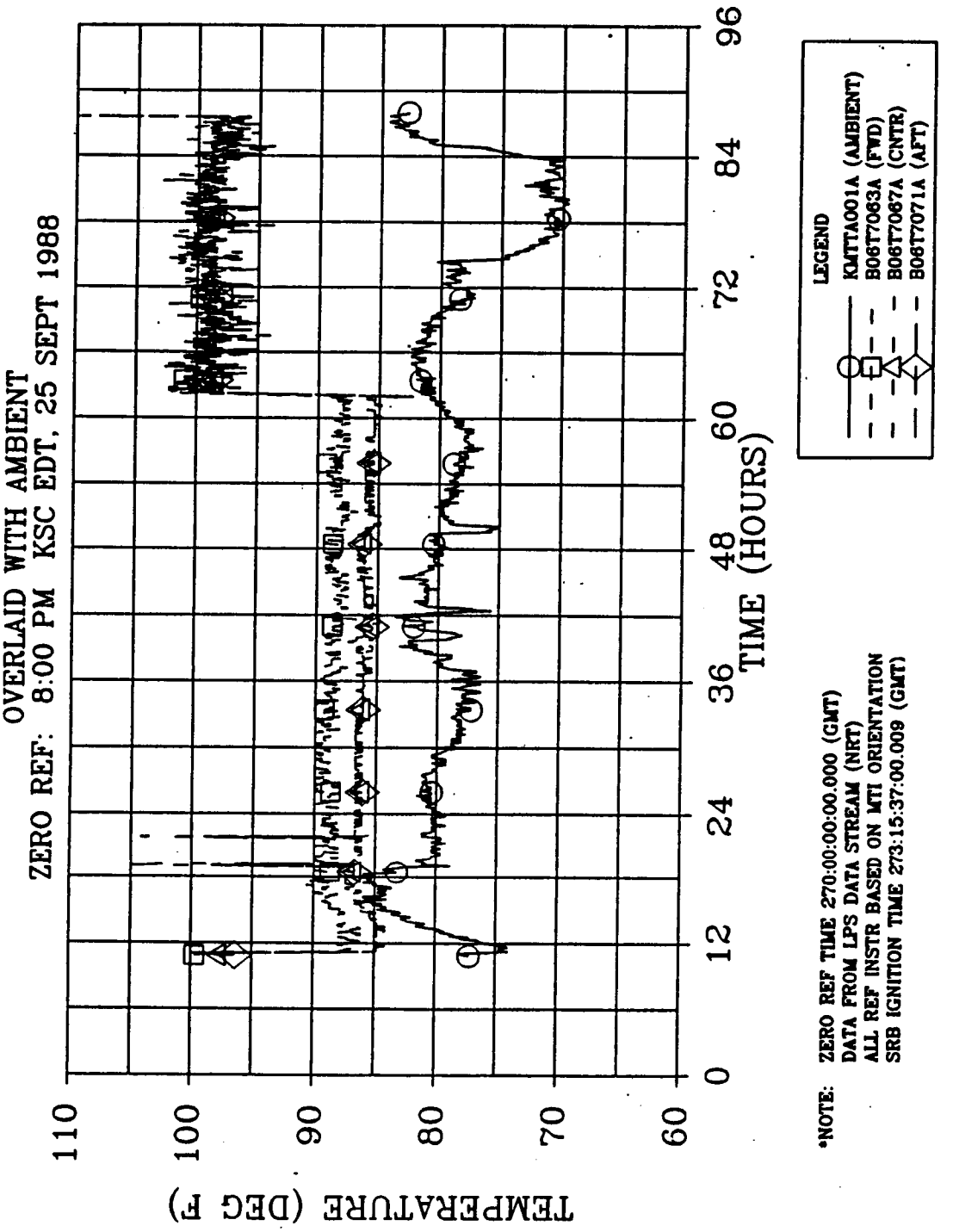

Figure 4.9-79. 360L001 Prelaunch Left SRM Field Joint Temperature at 285-deg Location

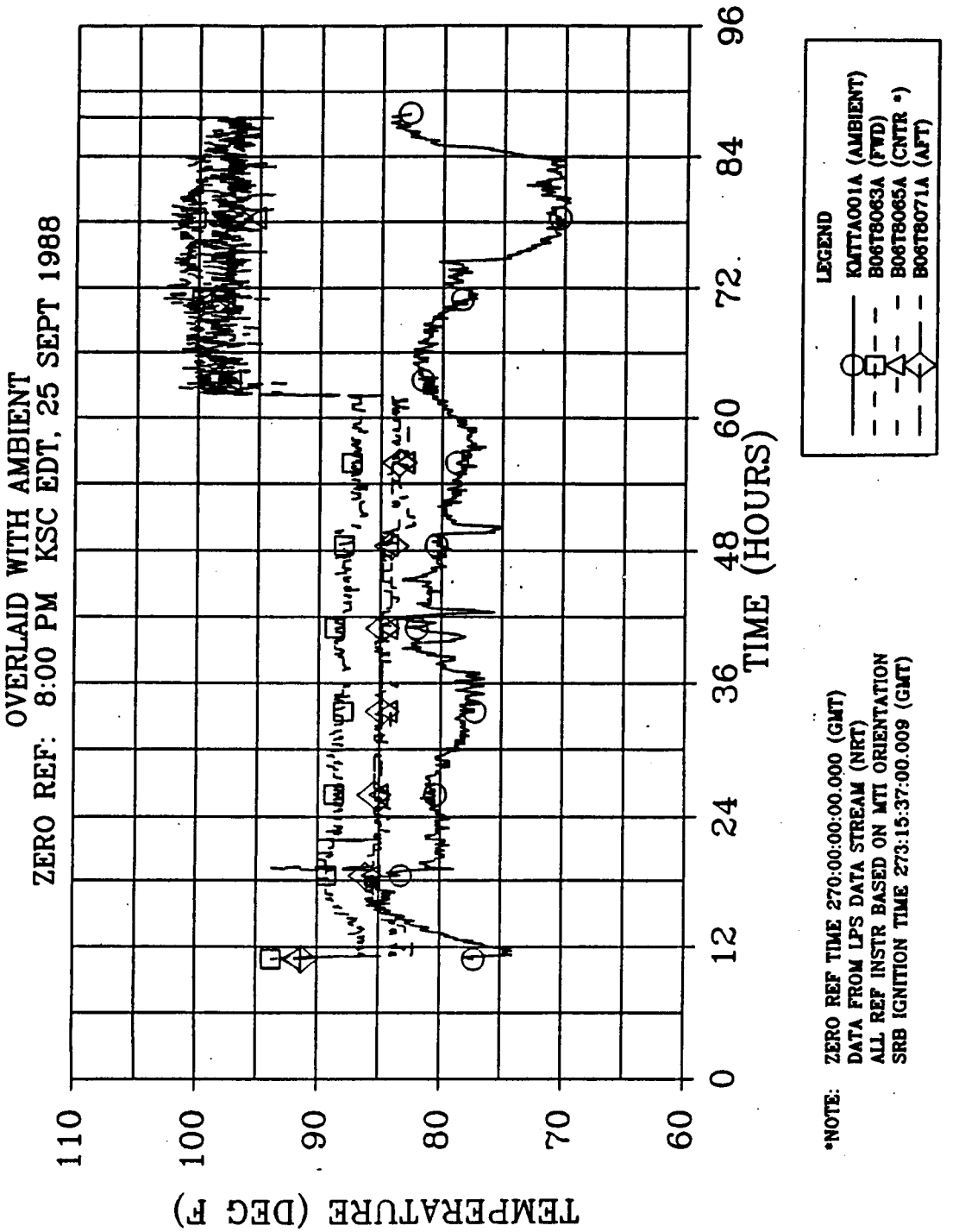

Figure 4.9-80. 360L001 Prelaunch Right SRM Field Joint Temperature at 285-deg Location

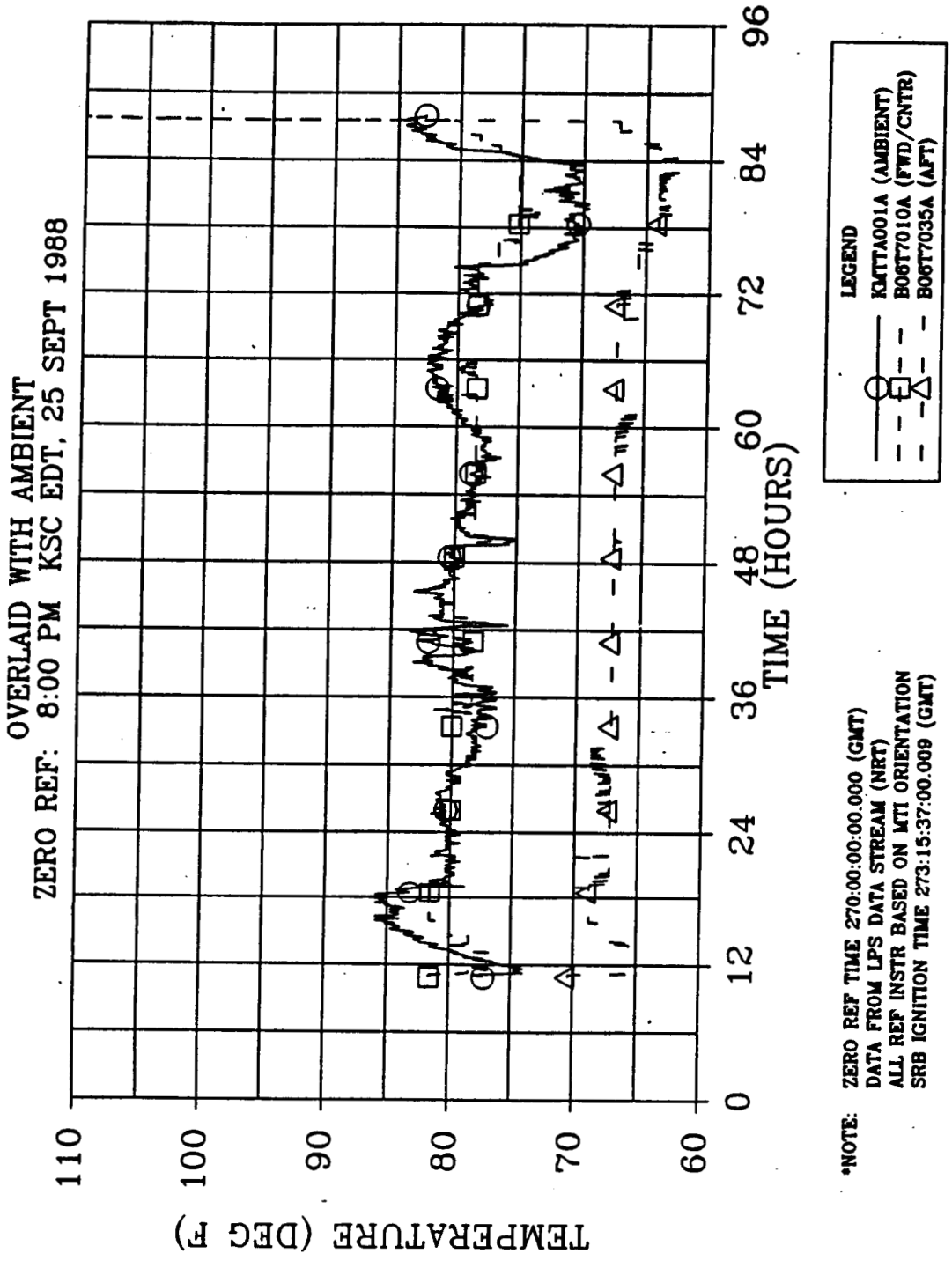

Figure 4.9-81. 360L001 Prelaunch Left SRM Case Acreage Temperature at 45-deg Location

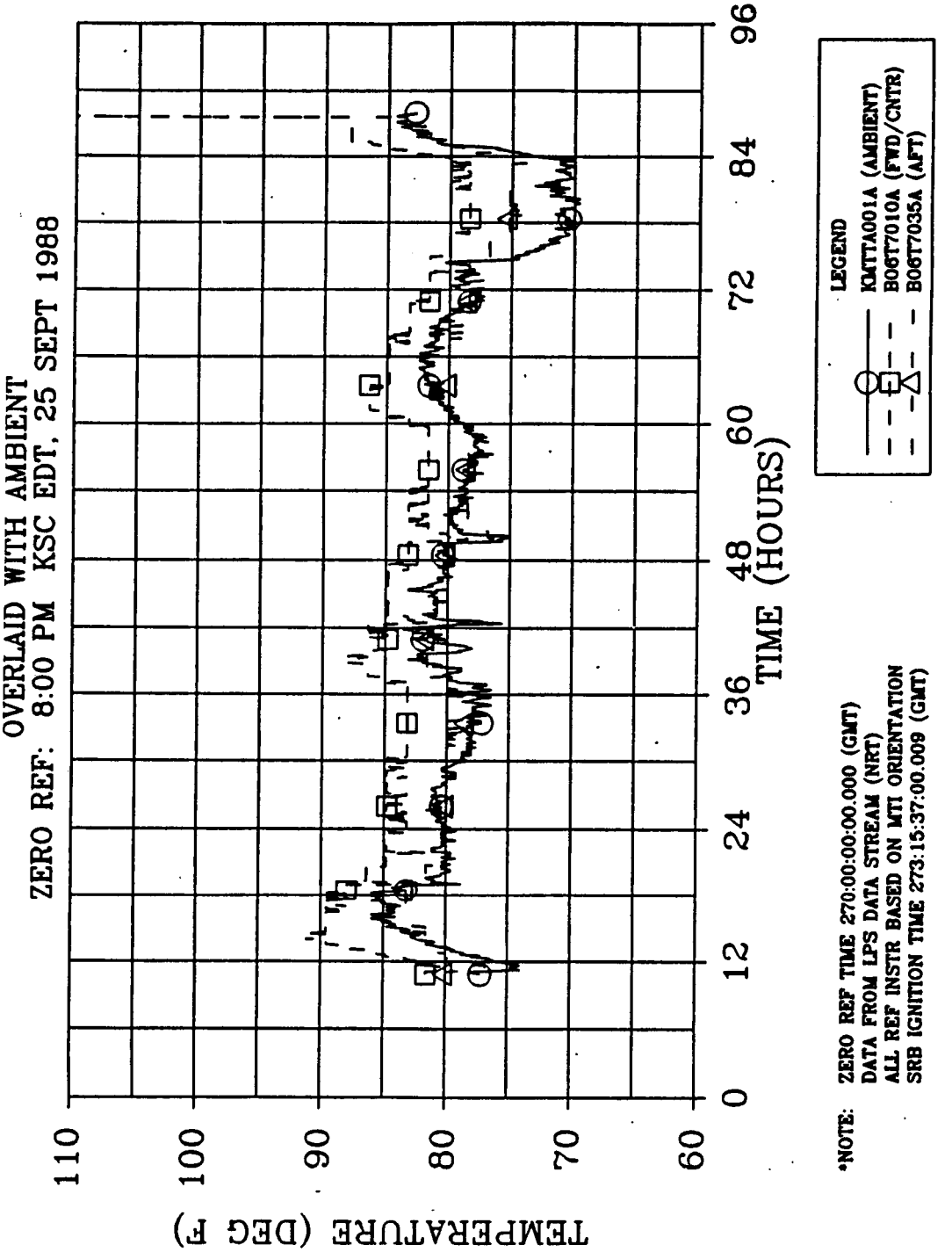

Figure 4.9-82. 360L001 Prelaunch Right SRM Case Acreage Temperature at 45-deg Location

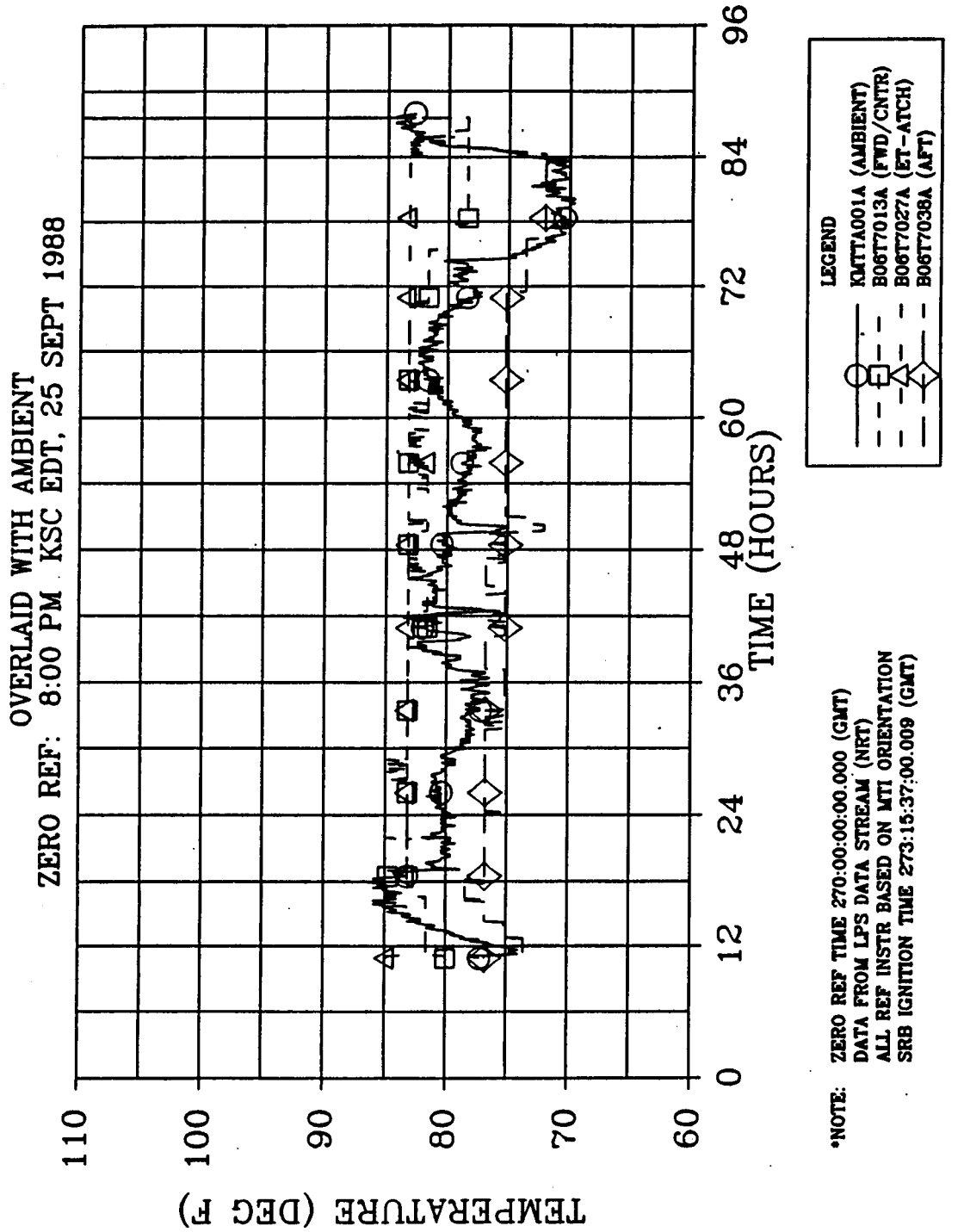

Figure 4.9-83. 360L001 Prelaunch Left SRM Case Acreage Temperature at 270-deg Location

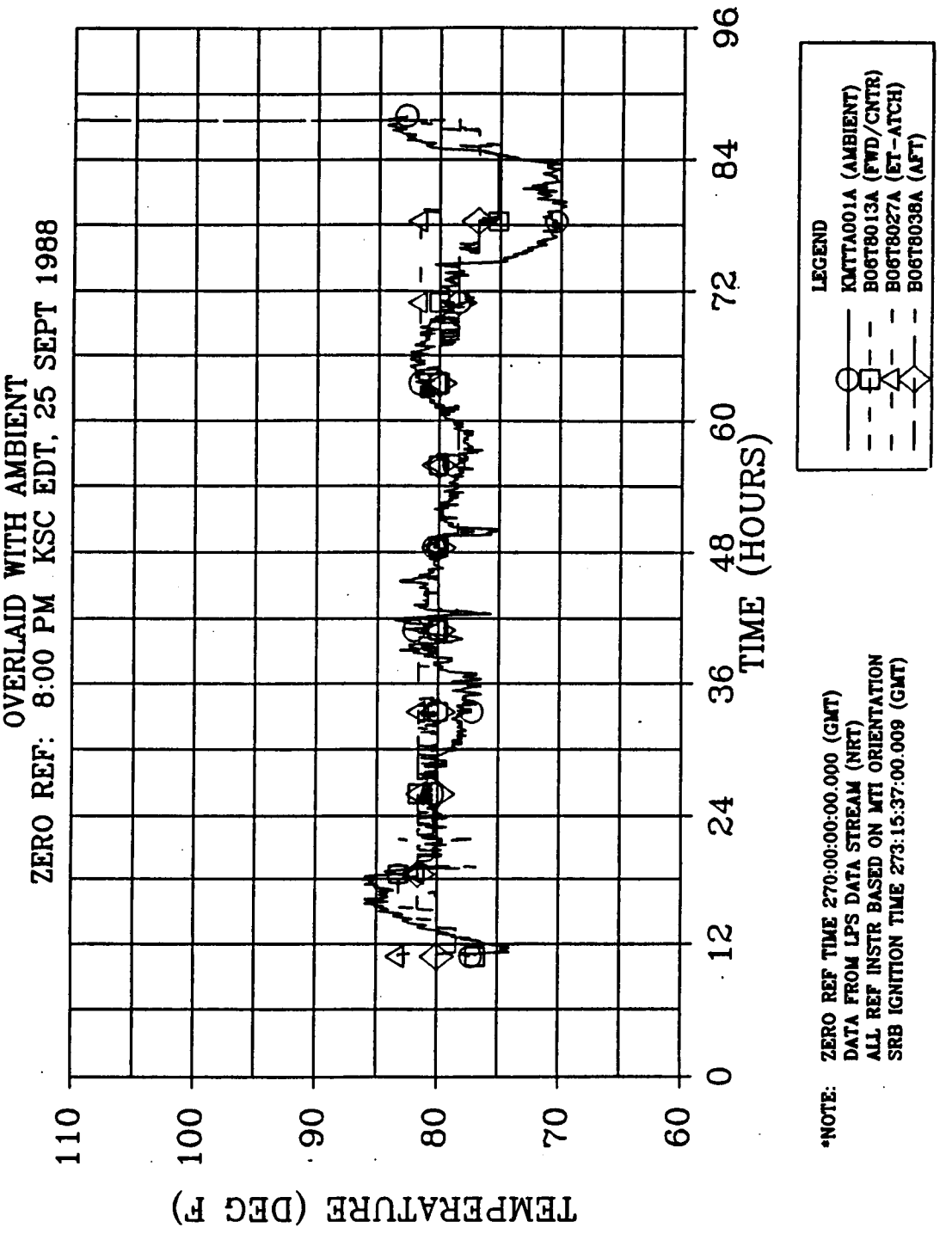

Figure 4.9-84. 360L001 Prelaunch Right SRM Case Acreage Temperature at 270-deg Location

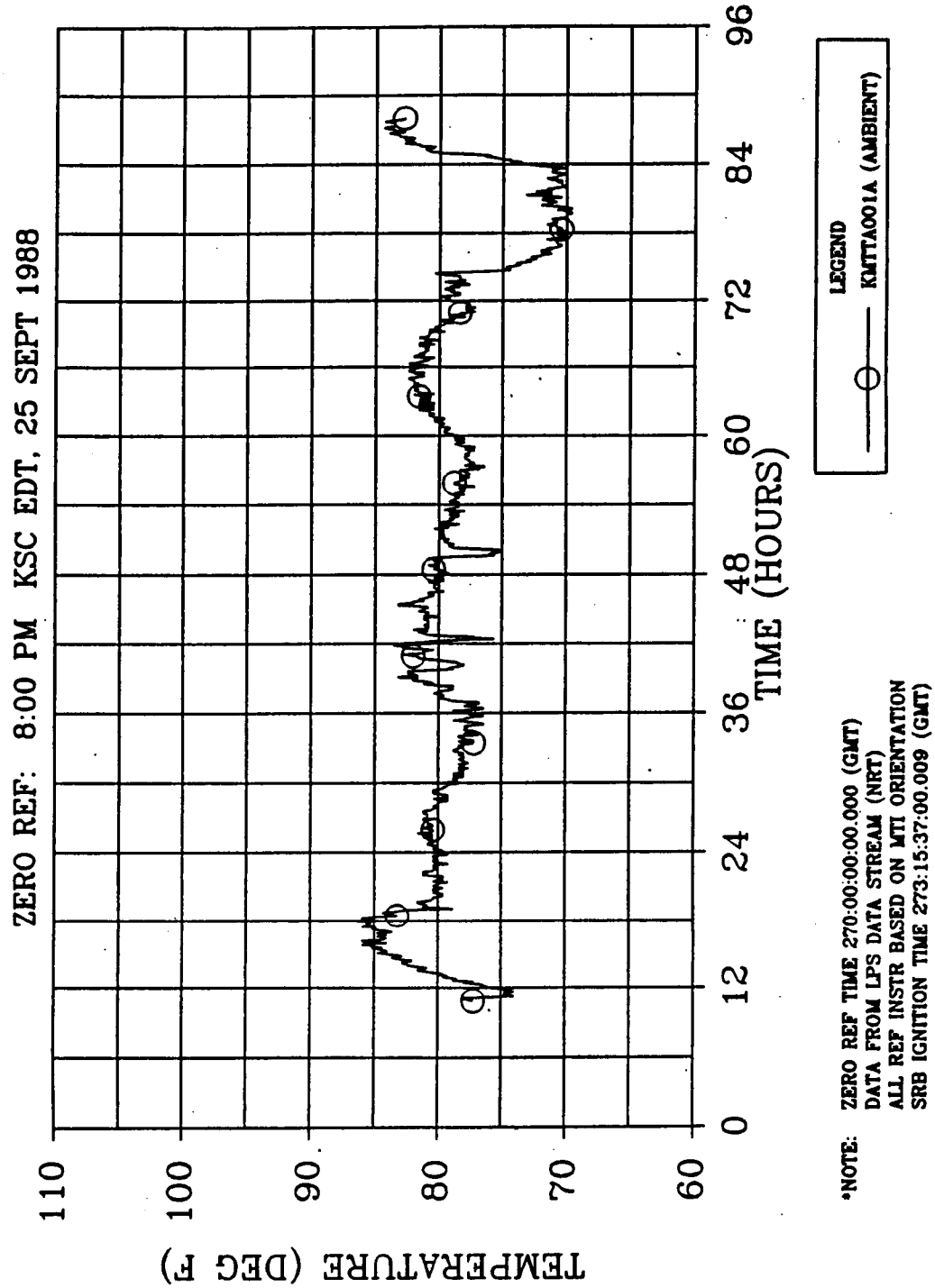

Figure 4.9-85. 360L001 Prelaunch Ambient Temperature at Camera Site No. 3

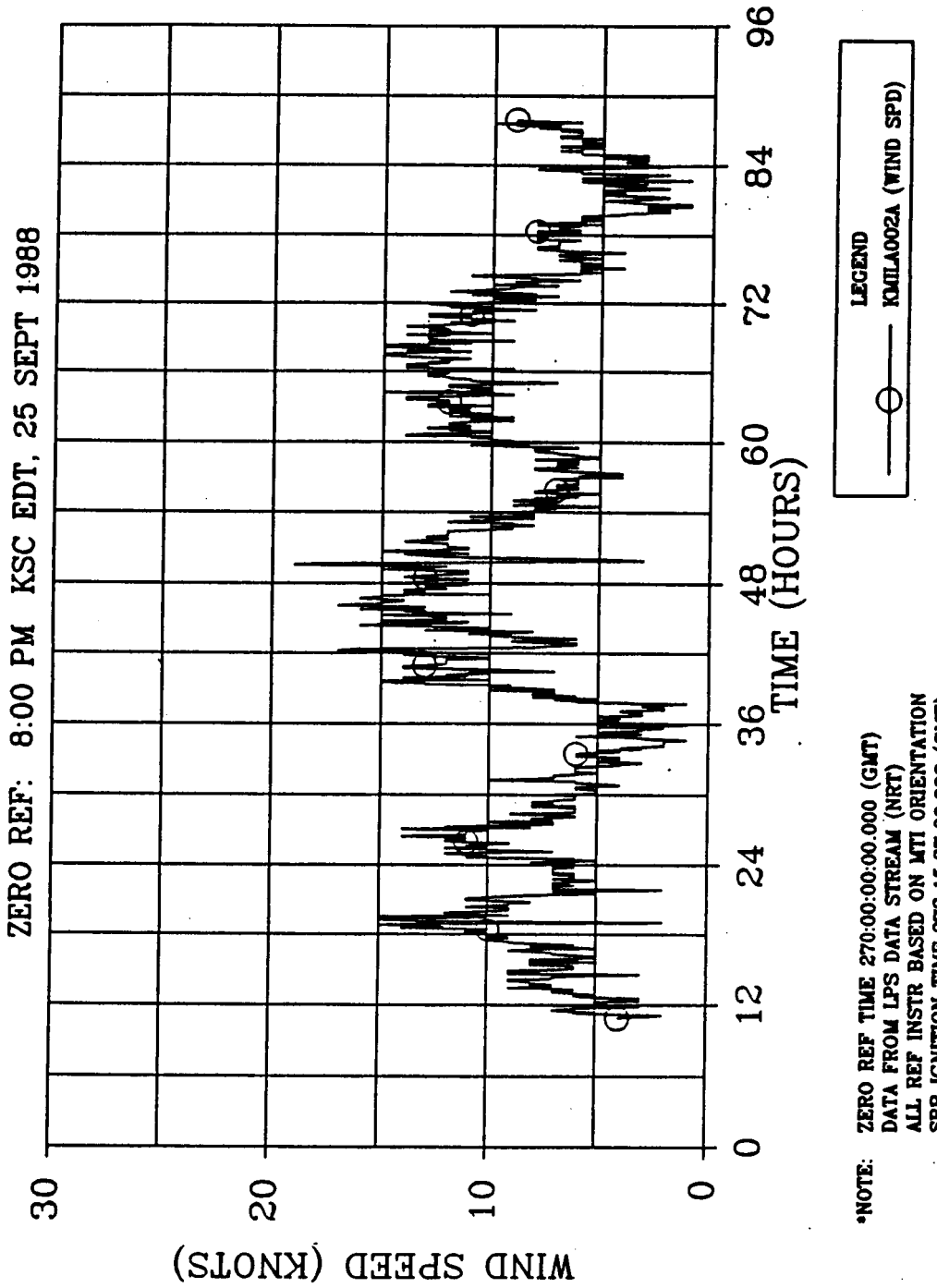

Figure 4.9-86. 360L001 Prelaunch Wind Speed at Camera Site No. 3

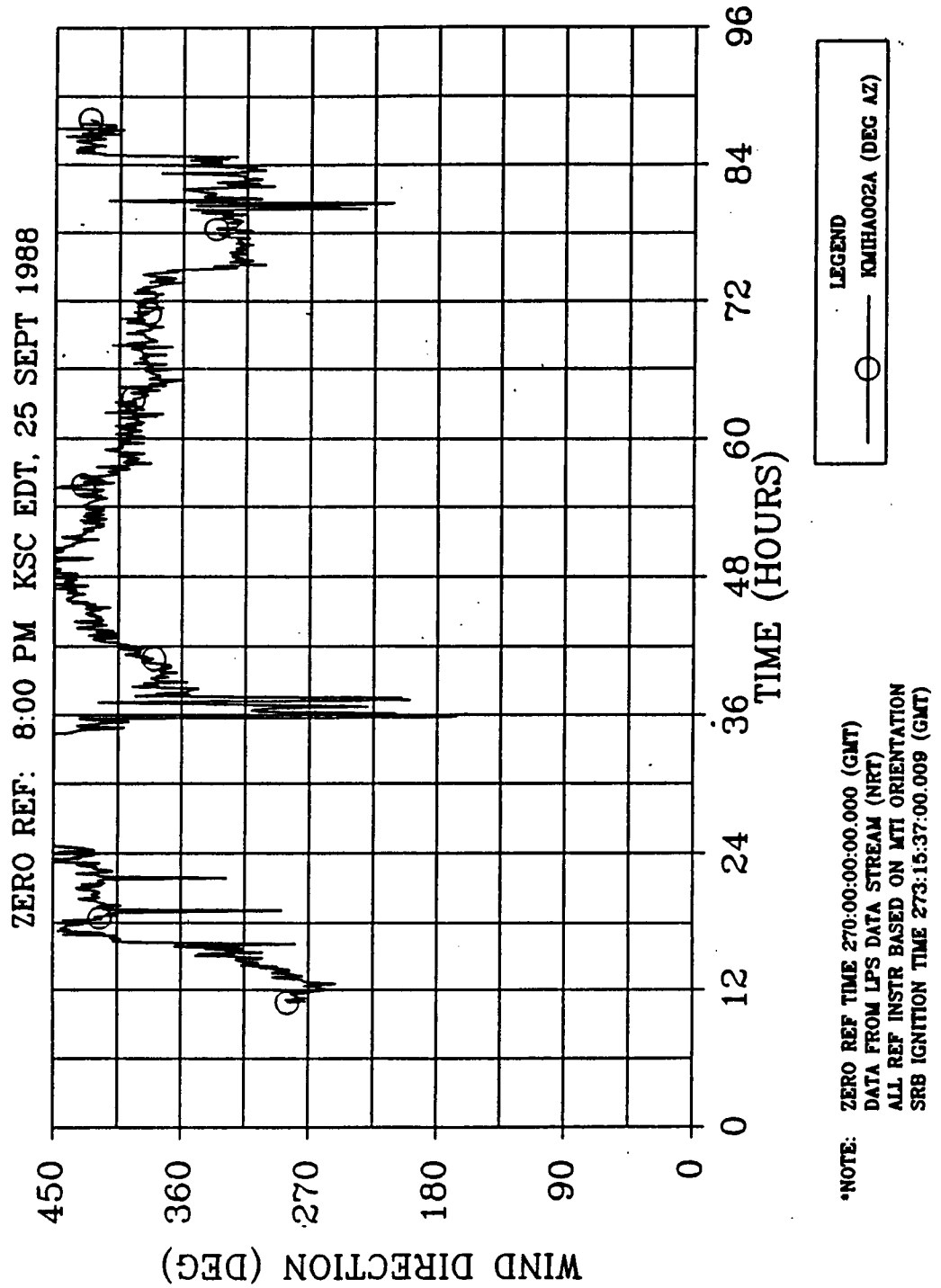

Figure 4.9-87. 360L001 Prelaunch Wind Direction at Camera Site No. 3

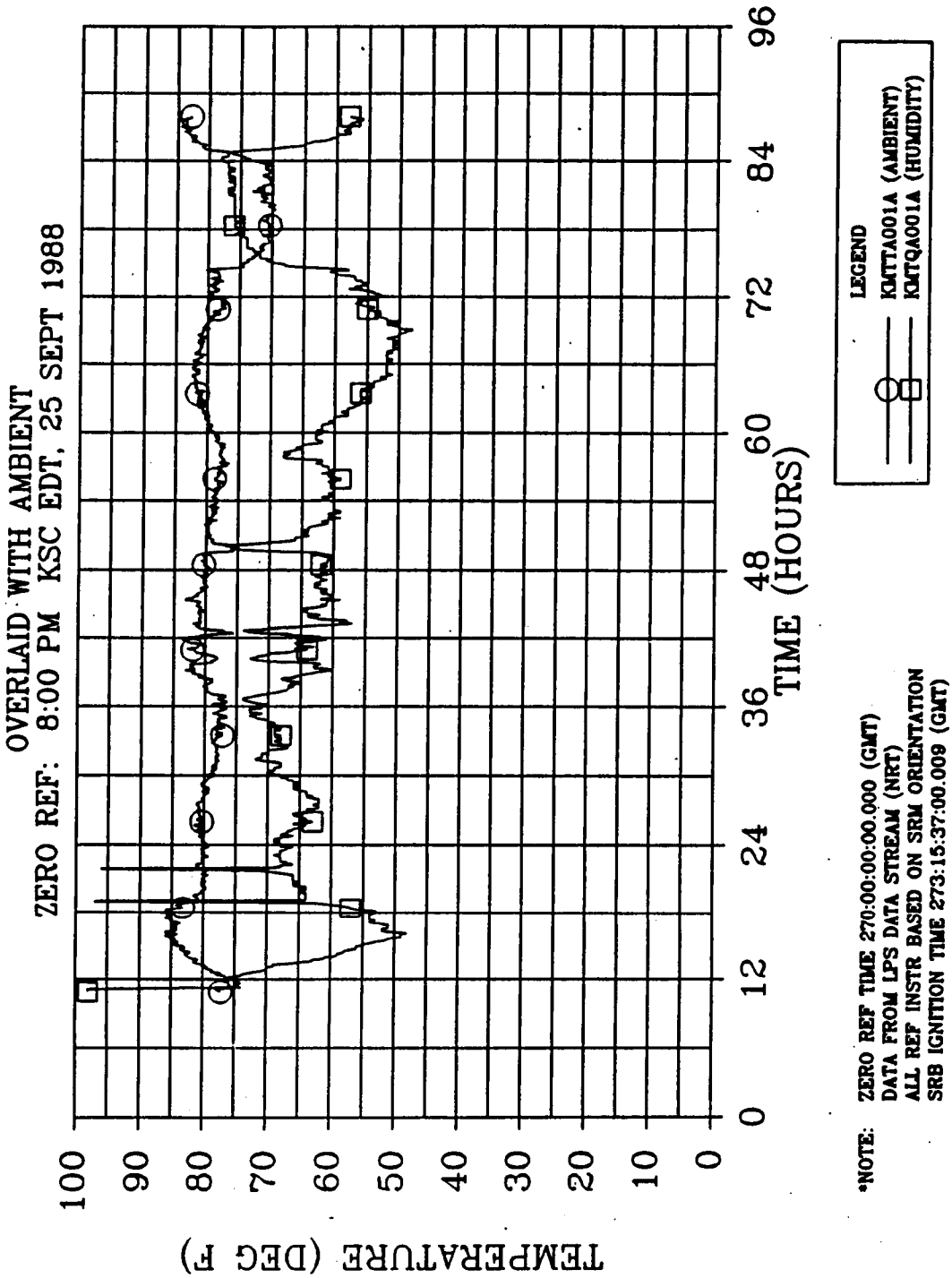

Figure 4.9-88. 360L001 Prelaunch Humidity Camera Site No. 3

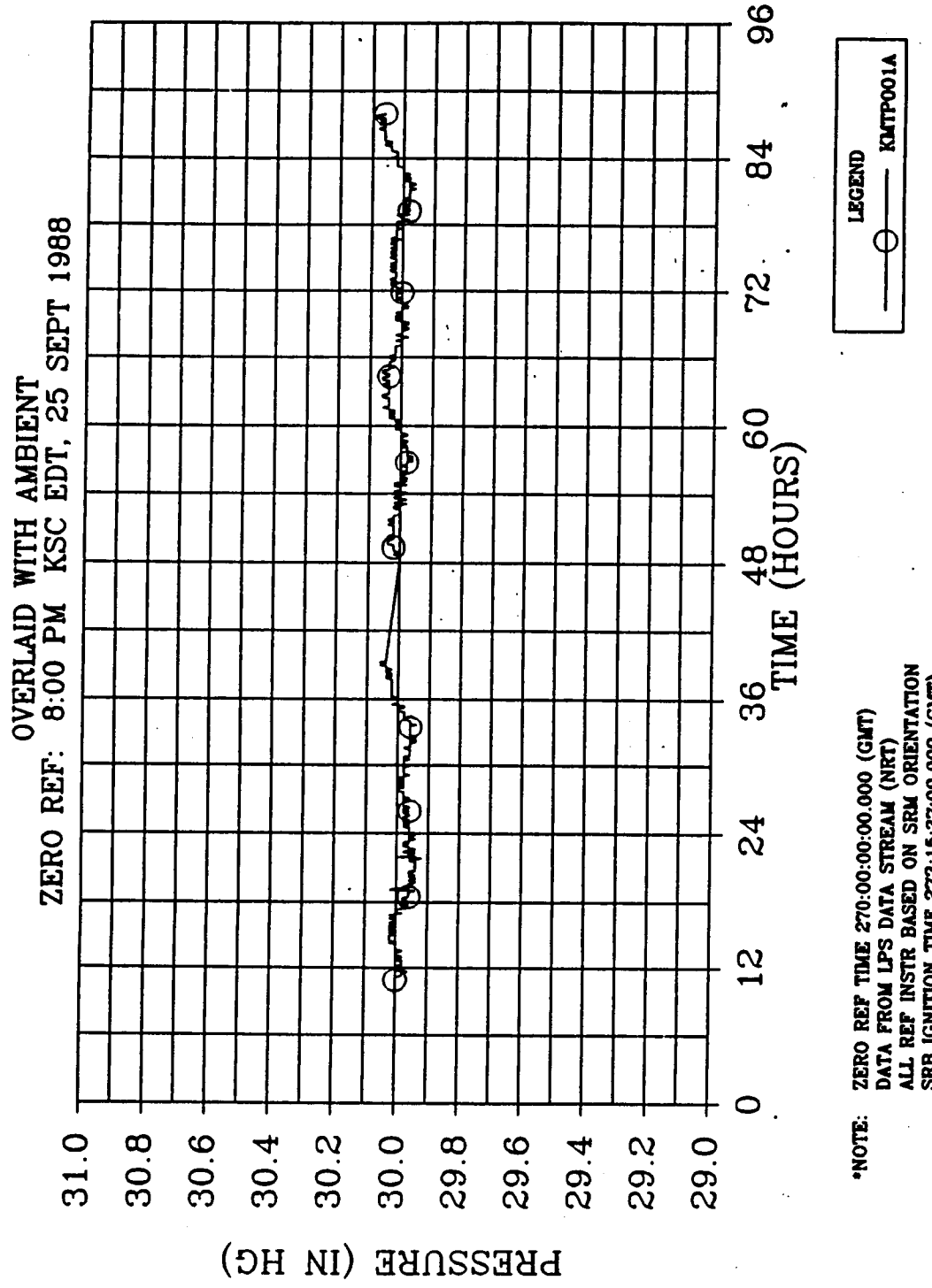

Figure 4.9-89. 360L001 Prelaunch Barometric Pressure Camera Site No. 3

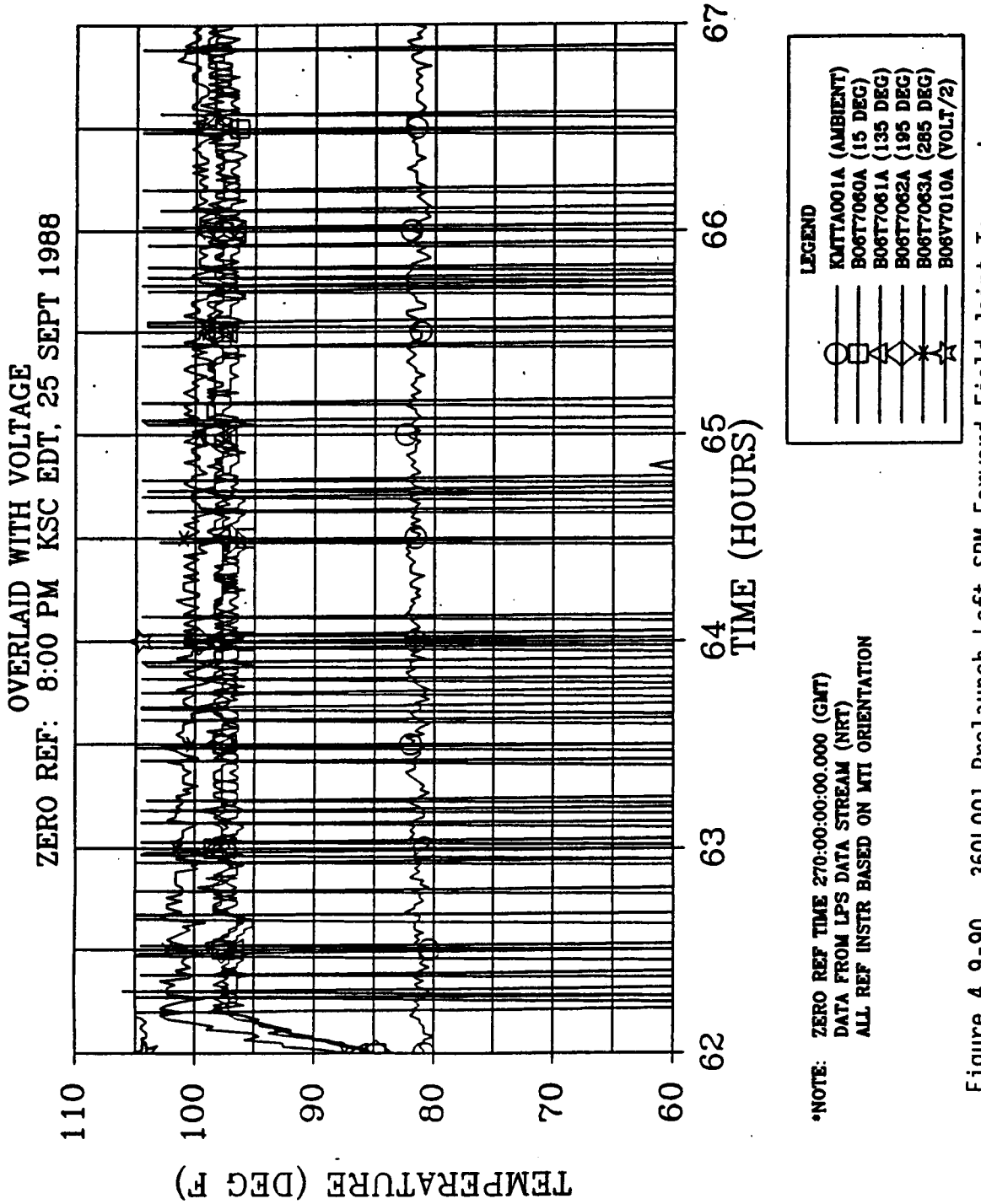

Figure 4.9-90. 360L001 Prelaunch Left SRM Forward Field Joint Temperature

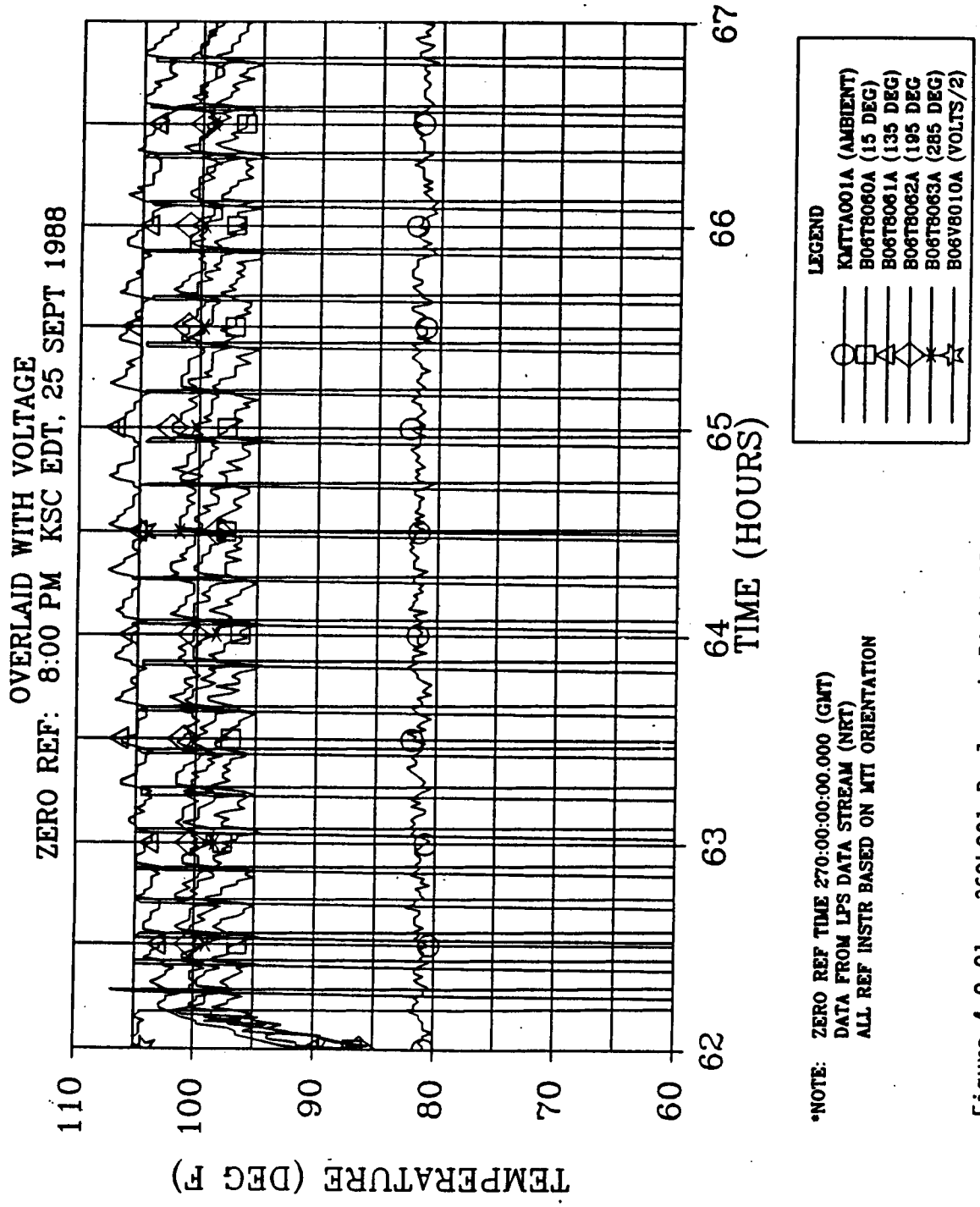

*NOTE: ZERO REF TIME 270:00:00:00.000 (GMT)
DATA FROM LPS DATA STREAM (NRT)
ALL REF INSTR BASED ON MTI ORIENTATION

Figure 4.9-91. 360L001 Prelaunch Right SRM Forward Field Joint Temperature

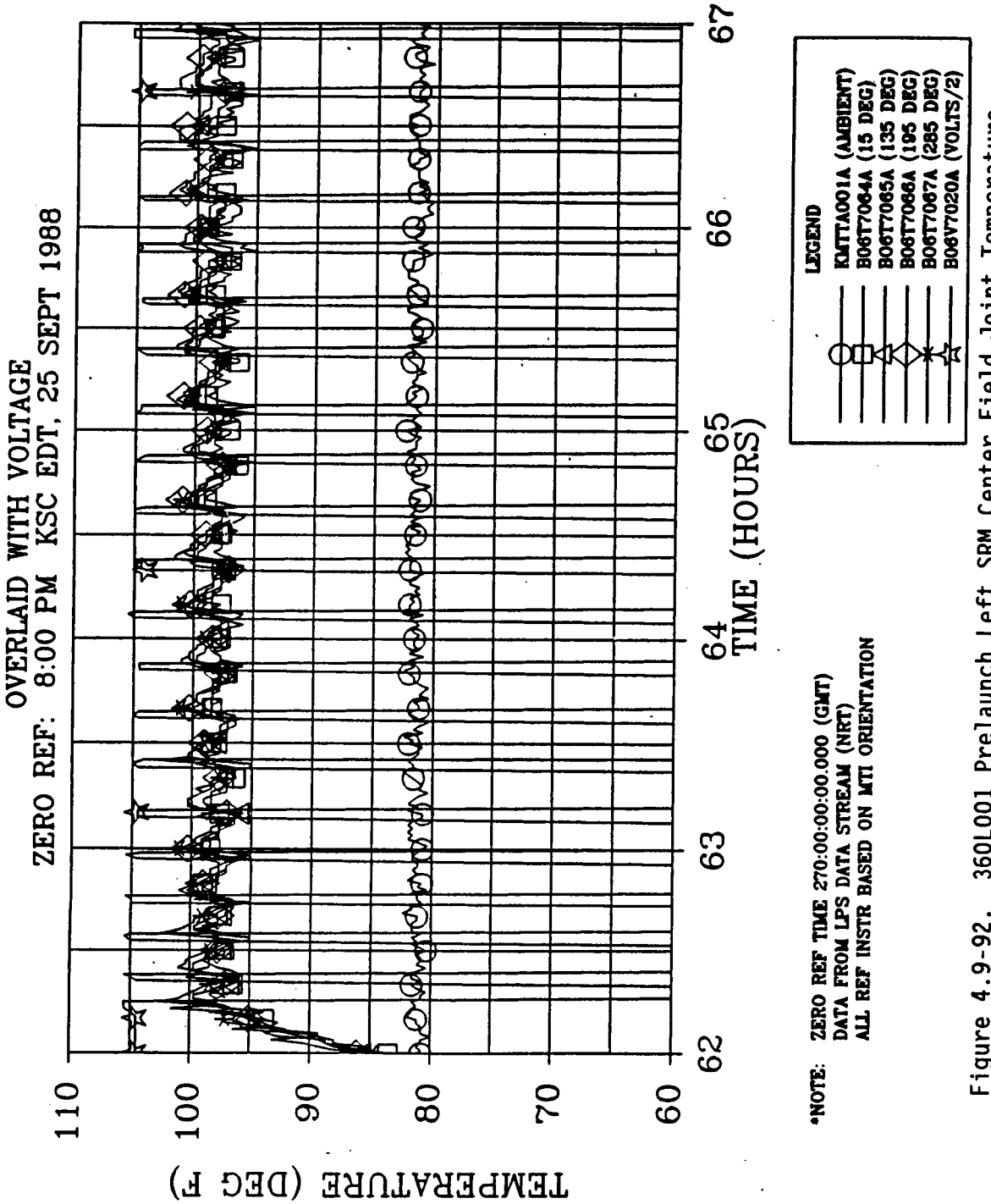

Figure 4.9-92. 360L001 Prelaunch Left SRM Center Field Joint Temperature

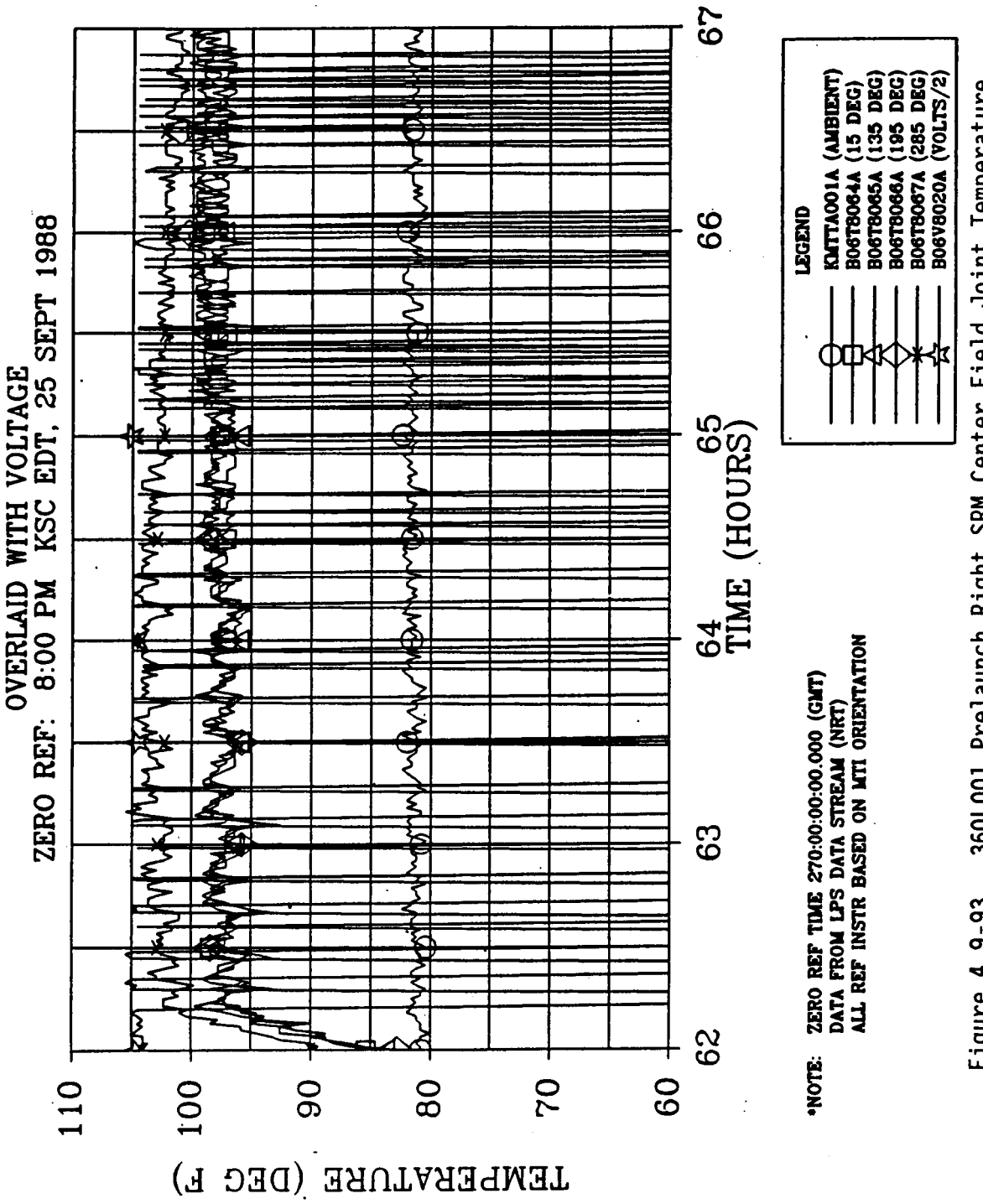

Figure 4.9-93. 360L001 Prelaunch Right SRM Center Field Joint Temperature

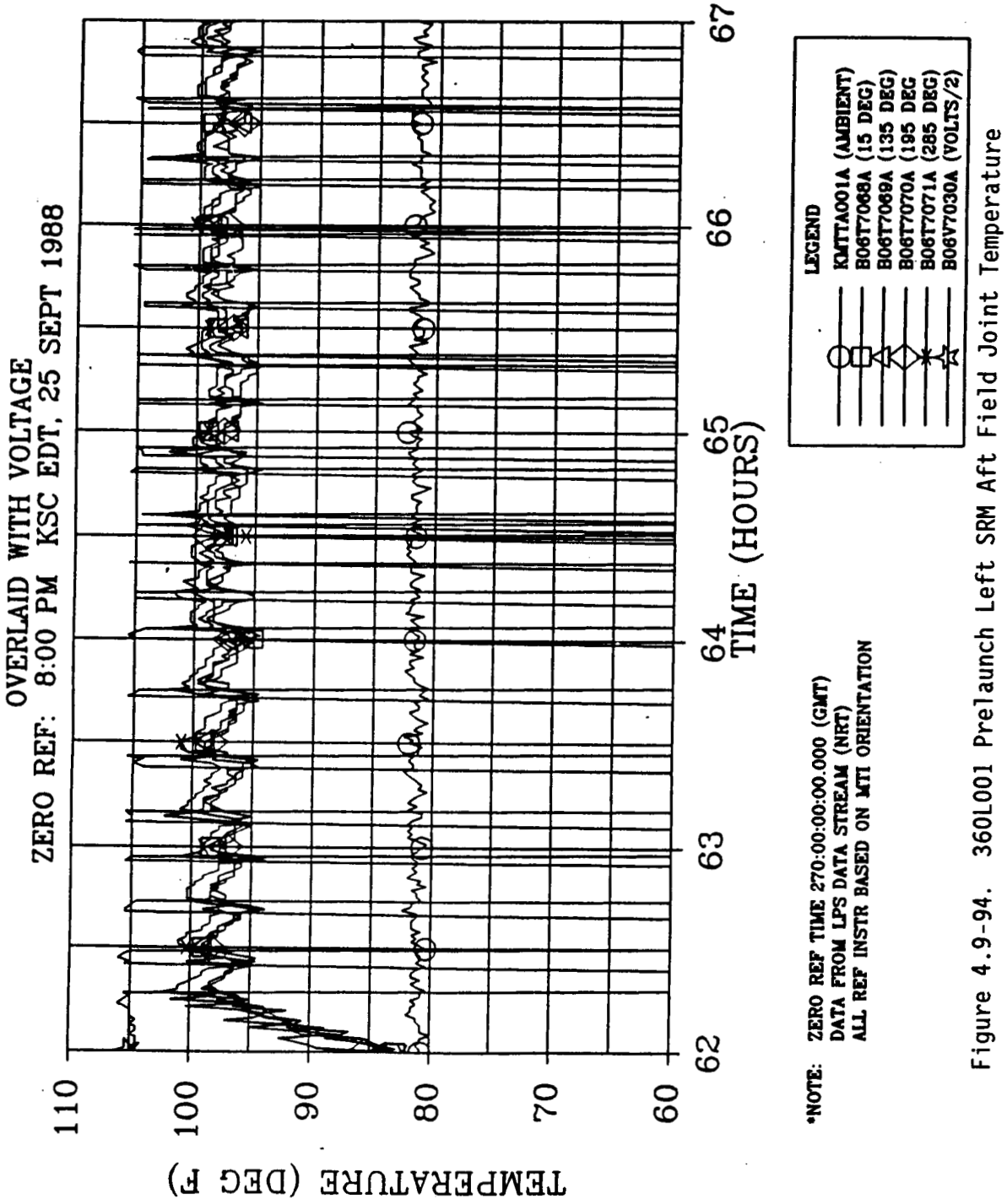

Figure 4.9-94. 360L001 Prelaunch Left SRM Aft Field Joint Temperature

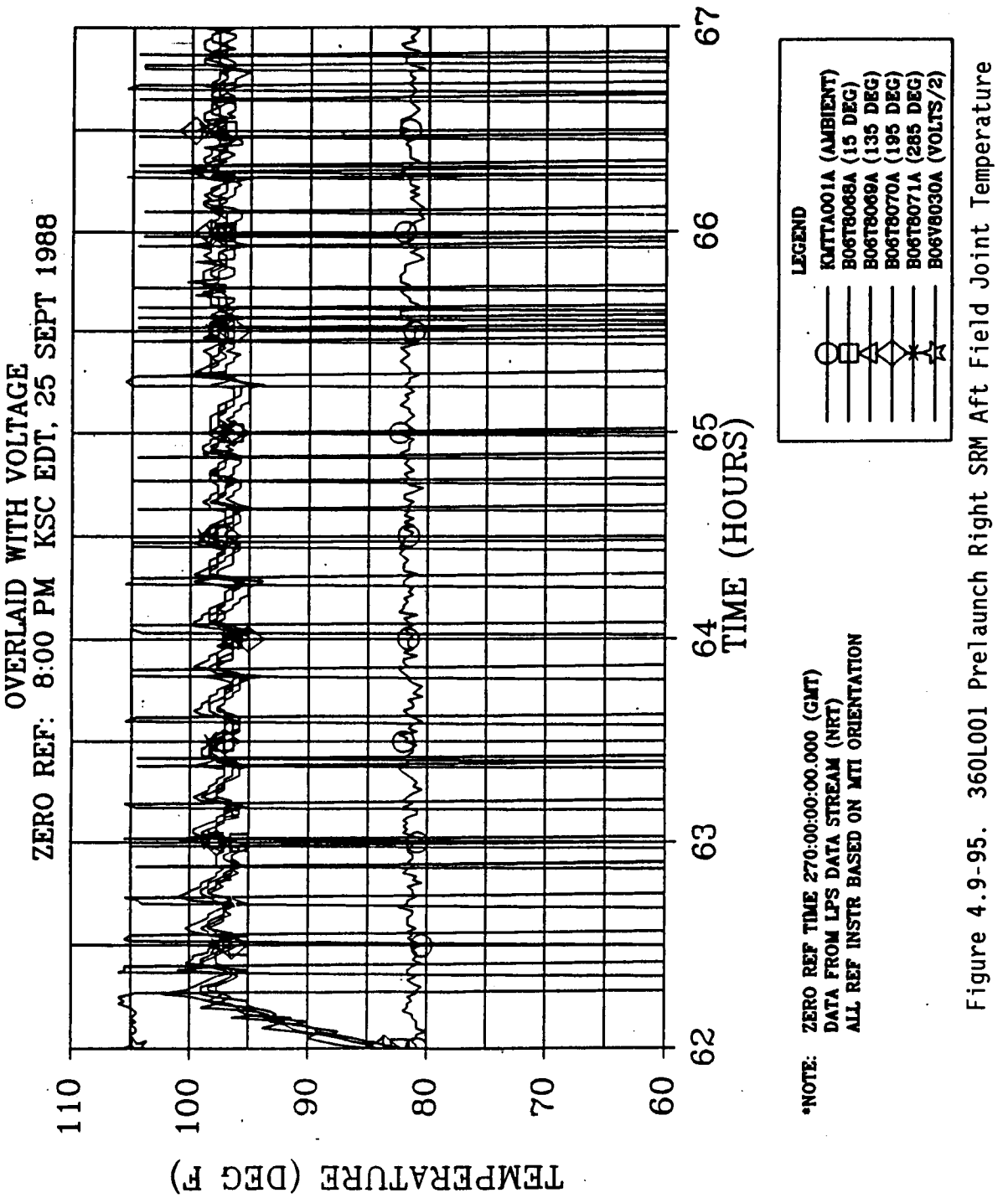

Figure 4.9-95. 360L001 Prelaunch Right SRM Aft Field Joint Temperature

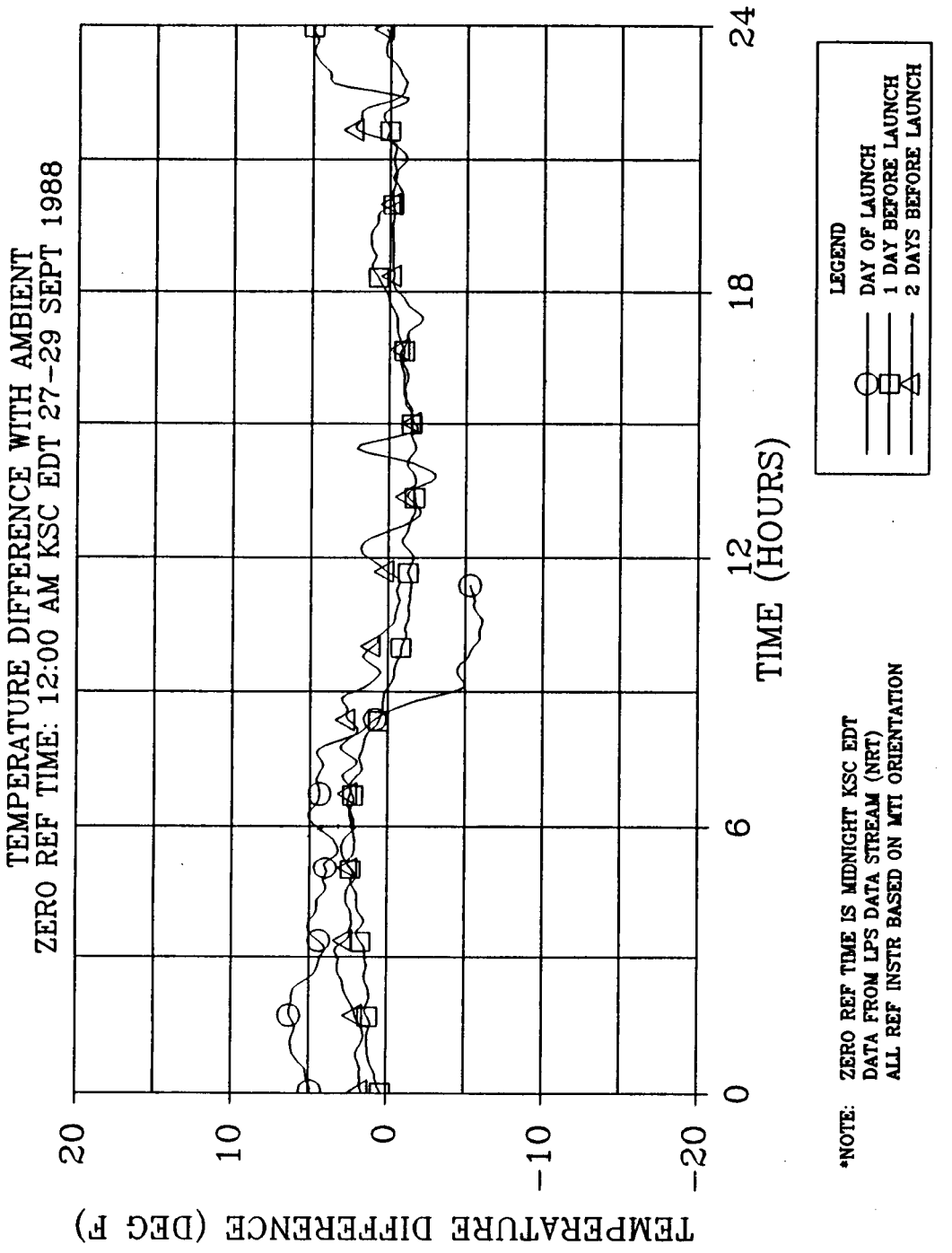

Figure 4.9-96. 360L001 Prelaunch Right SRM Forward/Center Case Acreage Temperature at 270-deg Location

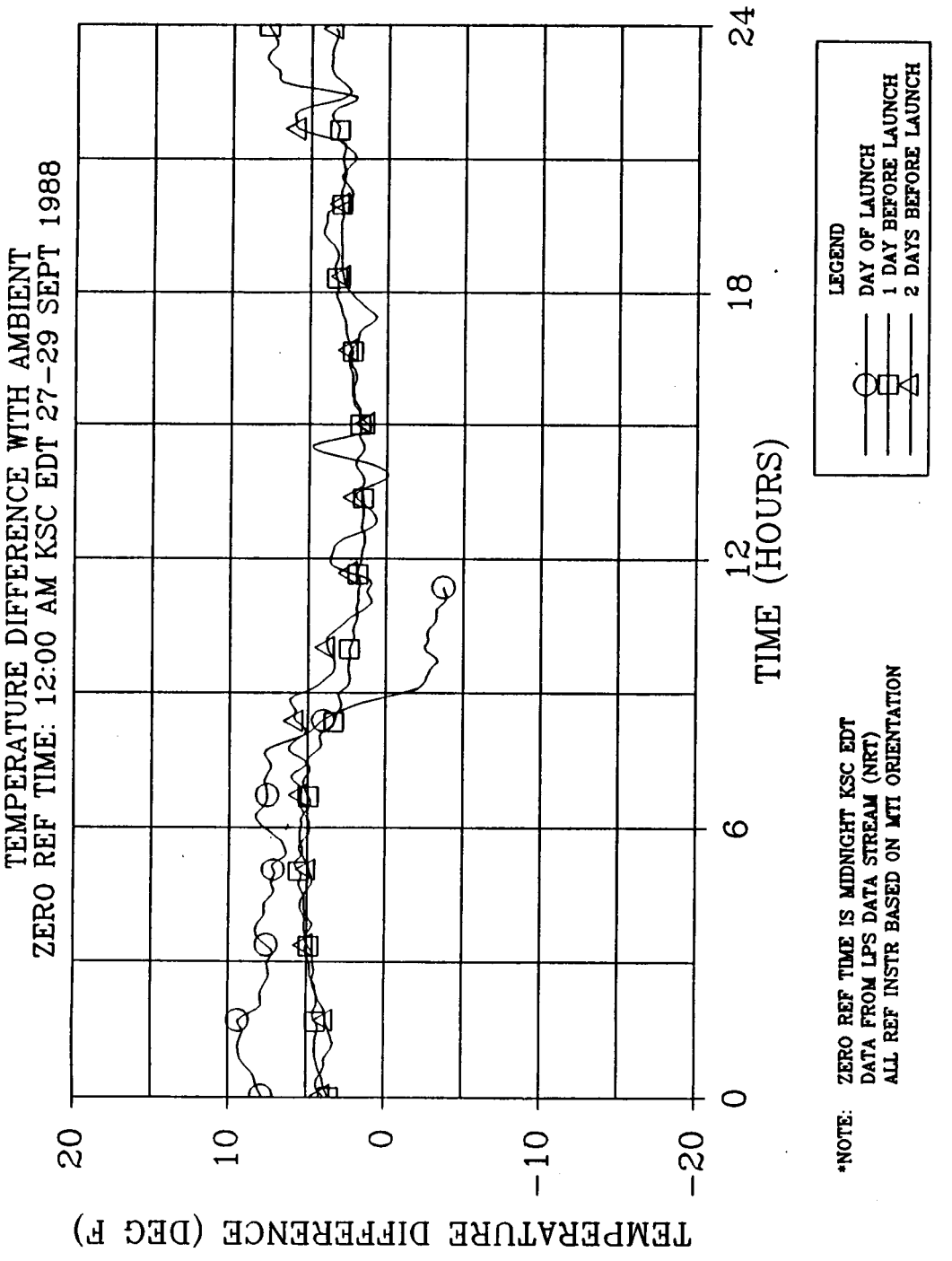

Figure 4.9-97. 360L001 Prelaunch Left SRM Forward/Center Case Acreage Temperature at 270-deg Location

Aft End Region and Conditioning

The aft skirt conditioning operation was satisfactory, but not as expected. Operation in accordance with OMRSD requirements was not followed. It seems that the required operation will only be followed when there is an apparent need. This assessment will need to be confirmed.

Data correlations at this time are limited due to the absence of GN2 temperature and set point histories. Higher GEI response on the flex bearing aft end ring, with respect to the nozzle/case joint, is attributed to the storage of heat in the aft end of the motor during the summer-to-fall/winter cooling trend. The opposite effect, to a limited extent, should be evident during the winter-to-spring/summer warming trend.

Case Acreage

Case GEI responded to the ambient conditions as expected. There was no apparent evidence of temperature depression due to ET cooling effects.

When considering thermal modeling, data correlations suggest that the historical predictions for the inboard quadrant of both SRMs around 270 deg and the left SRM forward center 45-deg location were higher than actual GEI response. The difference is attributed to inconsistencies (orientation and accuracy) of radiation interchange effects and solar heating, respectively.

Sensor Anomalies

Thermal instrumentation problems have been identified. These problems are: 1) a nonfunctional sensor on the right SRM tunnel bondline (B06T8020A), 2) an incorrect sensor reading on the left SRM aft segment at the 45-deg location (B06T7035A consistently reading 10°F low), 3) improper heater sensor strip placement on the left SRM aft field joint, and 4) improper connection of heater sensors on the right SRM center field joint.

Also, the left center field joint sensor at the 195-deg location (B06T7066A) had been reading up to 5°F higher than other sensors at the time of pad validation. During the wet countdown demonstration test (WCDDT) and the aborted flight readiness firing (FRF) this value appeared to be within the expected range (similar to that of other sensors on the same joint).

At the time of the successful FRF, this sensor was reading 4°F lower than the other sensors on the same joint and it was always the controlling sensor. During the terminal countdown demonstration test (TCDDT) this sensor was reading 10°F warmer than the other sensors. However, there was no apparent problem with this sensor during the final STS-26R countdown. Either the problem had been fixed as recommended after the TCDDT or by coincidence it was once again within the expected range.

The placement of the joint heater sensors on the left aft field joint was improperly performed. The actual and correct locations are listed as follows for each sensor:

Sensor	Correct Location (deg)	Actual Location (deg)
B06T7068A	15	45
B06T7069A	135	165
B06T7070A	195	255
B06T7071A	285	345

Two concerns were a result of this incorrect placement. First, the sensor which was to be located at the 135-deg location was supposed to measure the lower temperature which would occur at the heater gap/pressure port cutout. This was determined as a nonproblem because the LCC redline temperature assumes a possible failure at that location. Therefore, no further adjustment was necessary. Second, it was necessary to have a sensor between the ET and SRB (285-deg location) to be able to take into account the local ET cooling effects. However, another sensor was available at the 255-deg location, which is also an acceptable location for measuring ET cooling effects. No intervention was needed to modify this situation with regard to heater control set points and redline values.

The sensors on the right-hand center field joint did not respond as expected to the early morning solar radiation. The sensor located at 285 deg, which was shaded from solar radiation, responded to solar radiation as would be expected of the sensor at 135 deg. It was believed that the jiffy connections at the tunnel were improperly mated. However, it was

possible that the gage identification numbers were mixed up. The best estimation of actual locations are listed as follows for each sensor on the right center joint:

Sensor	Correct Location (deg)	Actual Location (deg)
B06T8064A	15	15
B06T8065A	135	285
B06T8066A	195	195
B06T8067A	285	135

Because the sensor strips were properly installed, there is no required intervention as temperatures at the correct locations are being recorded (there is only confusion as to which is which).

4.9.3.7 Infrared Measurement Assessments. Thermal support was provided to the KSC ice/debris team during the STS-26R launch countdown activities. A pad prelaunch walkdown was completed the day prior to the launch to assess any debris or temperature concerns. Infrared (IR gun) measurements taken during the walkdown showed case acreage temperatures between 75° and 85°F, with field joint temperatures recorded between 80° and 90°F. The higher temperatures were measured on the aft region of the right-hand SRB between angular locations of 90 and 180 deg, as this area was receiving direct solar radiation while other areas were shaded.

Table 4.9-5 gives a comparison of IR measurements and GEI readings at 1000 hr the day before launch, near the time of joint heater activation. It should be noted that the angular locations of field joint sensors do not correspond with those of IR measurements. Sensor response to a change in ambient is slower than for IR measured locations adjacent to the JPS. With these given differences, along with the inherent built-in measurement errors, the temperatures seem reasonably close.

IR data taken for the T-3 hr launch report showed temperatures between 71° and 75°F on the left-hand SRB and between 72° and 75°F on the right-hand SRB. No comparison is given for the T-3 hr IR measurements as no specific locations were identified; only ranges were provided. The surface temperature of SRB field joints was reported to be at an average of 82°F.

This is a believable temperature, realizing that a gradient exists between the sensor locations and the measured locations.

4.9.4 Conclusions and Recommendations

Cork Debris Problem

Based on the quick-look external inspection, the SRM TPS performed adequately on STS-26R. The only concern was the missing regions of TPS from the cork caps covering the instrumentation cables.

This problem could be alleviated by one of two avenues. The first would be to ensure better cork bonds by requiring that adhesive be applied to both adherents. This should also include the use of a vacuum bag cure on all bonds. The second alternative would be to remove the cork cap completely and rely on the K5NA filler to insulate the instrumentation cables.

These cables have a temperature limit of 500°F. Based on design trajectory (IVBC-3) aerodynamic and plume heating, a thermal analysis was conducted to determine the K5NA thickness required to keep the temperature of the instrumentation cables below 500°F. It should be mentioned that STS-26R flew a lofted trajectory which would present lower heating environments than the design trajectory.

The results of the analysis indicated that it would be feasible to remove the cork cap over the cables and maintain a cable jacket temperature below 500°F, provided the minimum thickness of K5NA over the cable jacket is 0.1 in. for the forward and center segments, and 0.15 in. for the aft segment.

It should also be mentioned that from a thermal perspective, the side strips of cork are unnecessary along these runs of cable. One inch of K5NA on both sides of the cables would suffice. However, removing the side strips would possibly create other problems from a structural and installation point of view.

DFI Measurement Problem

The DFI thermal nozzle-to-case joint data, which exceeded the design estimates, are attributed to possible adhesive failure, causing gage

detachment from the hardware. No insulation was used to cover these gages on STS-26R. The high readings are explainable, assuming slight gage detachment, due to the direct exposure of these gages to the hot environment (reentry nozzle flame and aerodynamic heating) following thermal curtain breakup.

This assessment will be confirmed with data from STS-27 and subsequent developmental flight sets, where the gages will be directly insulated from the environment with a minimal amount of K5NA, and should better follow hardware response. If not confirmed, SRB reentry environments and/or SRM aft end thermal modeling will need to be considered and appropriately modified.

GEI Prediction Problem

Data correlations, predictions versus actual, suggest relatively good agreement. However, modeling considerations (environment and detail) should be looked at closely. Future modeling should check the observations and suggested modeling improvements discussed in the results section and incorporate updates as solutions are found.

Field Joint Heater Sensor Placement Problem

It is recommended that sensor strip installation and jiffy connection procedures be reviewed and possibly changed to avoid the reoccurrence of these situations. This action should be taken before the STS-27 flight.

Aft Skirt Conditioning Problem

In the aft skirt region, a possible error range in instrumentation of ±1 percent suggests a potential of up to an 8°F disparity between gages. This creates problems in ascertaining circumferential temperature differences between gages. Actual flow model verification can not be made without proper instrumentation on the hardware (SRM, aft skirt, and thermal curtain) and adjacent to the hardware in the gas stream and at the orifice. It is doubtful that data correlations and flow modeling of the benign STS-26R situation will be of any value, based on the above observations and concerns. It is essentially impossible for any practical extrapolation to be made of a worst-case cold environment.

It is recommended that the on-pad system be tested in a worst-case, on-pad cold environment prior to a cold weather launch. This will qualify aft region components to on-pad specification requirements.

If the actual on-pad system cannot be tested, a suitable alternative should be found. This could possibly be accomplished with a fully instrumented mockup and/or QM-8 testing. Testing of the conditioning system in a cold environment should include simulated convective cooling on the aft skirt and exit cone because of wind effects. Aft skirt and conditioning system hardware should be as close to flight configuration as possible.

GEI Accuracy Problem

It is recommended that the GEI data collection accuracy be increased by reducing the gage range and increasing the digital word length.

Infrared Measurement Problem

It is recommended that future field joint measurements be taken at locations corresponding to joint heater sensor angular locations so that better correlations can be made. Also, it is recommended that measurements be taken prior to joint heater activation.

Real-Time Data Acquisition Problem

It is recommended that aft skirt conditioning system data (GN2 temperature and pressure) be built into and be accessible from the HOSC data network system. These data are necessary for aft end data correlations and postflight flex bearing predictions.

It is also recommended that near real-time on-pad GEI and environmental data be available to Morton Thiokol after pad validation. These data, collected hourly, need to be transmitted electronically at weekly intervals until two weeks prior to scheduled launch dates. From this point until launch, daily transmittals are necessary. These data are necessary to help meet the requirement of PMBT updates prior to launch and to aid in predicting the local SRM environment by building a variable conditions data base.

4.9.5 Thermal Prediction Methodology

Methodology will be presented for PMBT, GEI, and component predictions due to on-pad natural and induced environments. Also, methodology will be presented for DFI and component predictions, including TPS recession, due to flight-induced environments.

Flight-Induced DFI and Component Predictions

Component design analyses due to current flight-induced thermal loads were performed during the redesign effort and will be documented in the SRB Thermal Design Data Book, SE-019-068-2H. Estimates for DFI locations were inferred from these analyses and summarized.

The current design loads were developed for a conservative trajectory which is not included in presently planned flight trajectories. Since thermal loads data were not available for the trajectory of STS-26R, there will be no direct correlation possible with actual DFI data.

Actual DFI data were used to determine if design predictions were exceeded. If they were exceeded, the design analyses and environments were to be readdressed to identify problem areas and to update and/or modify analytical models.

On-Pad PMBT and Flex Bearing Predictions

PMBT and flex bearing predictions were performed using on-pad environmental and GEI measurements. However, these data were limited due to availability and access problems.

From these data, boundary conditions were derived for a coarse three-dimensional (3-D) global thermal model in predicting PMBT and for a two-dimensional (2-D) axisymmetric model of the aft end in predicting flex bearing temperatures.

Two possible methods were considered in making the predictions. The first involved using the environmental data (convecting to the ambient and adding solar heating where appropriate). The predicted surface temperatures from this method could then be compared to the case acreage GEI in an attempt

to perfect modeling techniques. The second method was to apply the GEI data directly to the model as imposed surface temperatures. However, the first method was the only one performed due to limited data.

On-Pad GEI and Component Predictions

Four methods were considered. Three of the four are concerned with predicting boundary conditions using September historical data. Results from these three were applied to a coarse 3-D SINDA global thermal model of the SRM for predicting case acreage GEI and joint heater sensor response. For other regions such as the systems tunnel and the aft end components, 2-D axisymmetric and planar models were used. The fourth was an estimation based upon near real-time GEI and environmental data, and this method was used to supplement and update the results of the other three during HOSC support. The four methods are detailed as follows:

a. Historical Ambient Correlations - Natural Environments. This method is used to predict historical average monthly boundary conditions for the month of September based upon solar heating, predominant wind speeds, and ambient temperature cycling.

   Monthly averaged heat transfer coefficients were calculated using the NASA large cylinder correlation for every hour of the day. Solar heating input was calculated using the methods described in standard solar heating texts for a single, monthly averaged daily insolation profile to represent all days of the month. Shading aspects were also considered through experimental use of a model representing the STS on the MLP with service structures. This model was mounted on a heliodon, and shading factors were visually estimated.

b. 3-D Flow/Thermal Modeling - Natural/Induced Environments. This method is used to predict boundary conditions due to the ET cooling effect (local air temperatures and heat transfer coefficients) during final countdown while the ET was loaded. The geometry used consisted of the STS on the MLP, the orbiter support structure, the concrete hardstand, and the flame trenches. It can be used for modeling winds originating from

the north, northeast, east, southeast, and south. Historically, September-October winds are predominantly from the northeast, and this was considered for STS-26R.

c. Experimental With Near Real-Time Data - Natural and Induced. This method is used to experimentally predict local heat transfer coefficients at GEI locations during preflight activities, and at IR locations during post-flight activities. This task has not been accomplished at this time, but will be considered in future correlations in an attempt to data base heat transfer coefficients for a given wind direction, wind speed, and ambient temperature. The task consists of the following:

1. Local heat transfer coefficients will be calculated by measuring the change in skin and ambient air temperature over a period of time. This will be correlated to the average weather conditions existing over this time period (wind speed, wind direction, and ambient air temperature). It would also be advantageous to correlate it with the internal bore temperature. Response due to solar heat flux to the surface will be taken into consideration. A calculated solar component will be removed from the measured value.

2. For future efforts after development flights, a data base of overall local heat transfer coefficients could be generated for a spectrum of wind speeds, wind directions, and ambient air temperatures. Heat transfer models will access and extrapolate from this data base. These coefficients will also take into account the complex air flow pattern around the motors, the specific locations on the motors, radiation interchange with the surrounding surfaces, and radiation to the sky.

d. Estimates from Near Real-Time and Projected Weather Data. This method is used to estimate GEI response at the time of launch by interpreting previously collected (prior week) GEI and environmental data and projecting with day-of-launch weather predictions.

This determination was based upon having a near real-time update available prior to HOSC support. This update was at two intervals:

a week's data before leaving Morton Thiokol for the HOSC, and then a data supplement with T-36 to T-6 hr data at the HOSC. Results from the previously discussed methods and projected weather data were taken into consideration. This effort provided the final T-6 hr to T-5 min predictions.

4.10 MEASUREMENT SYSTEM PERFORMANCE (DFI)

This section corresponds to FEWG report Section 2.9.6.

A total of 310 SRM DFI measurements were on the 360L001 motors. Of the total SRM DFI measurements, 264 (80 percent) performed properly throughout their respective mission phases. Those gages that were inoperative before flight, those that failed during flight, and those that produced questionable readings are listed in Table 4.10.1.

4.11 MEASUREMENT SYSTEM PERFORMANCE (GEI)

This section corresponds to FEWG report Section 2.9.8.

A total of 33 GEI measurements were on the STS-26 RSRMs. Sensor B06T8020A, located at 90 deg at Station 1258.98 on the right-hand SRM became inoperative during stacking. Sensor number B06T7035A, which is a case acreage sensor located at 45 deg at Station 1751.5 on the left-hand SRM, consistently read 10°F below ambient. Due to the constant low reading of this sensor, it was felt that reliable thermal data could be obtained by shifting the reading 10°F higher. Therefore, of the total GEI measurements, 32 (97 percent) performed properly throughout their respective mission phases. Table 4.11.1 provides a GEI list.

4.12 SRM HARDWARE ASSESSMENT

This section corresponds to FEWG report Section 2.11.2.

4.12.1 Insulation Performance

4.12.1.1 Summary and Conclusions. The entire insulation system of flight motors 360L001A and 360L001B performed in an excellent manner. Insulation Design Engineering performed a postflight evaluation of all case field

Table 4.10-1. Development Flight Instrumentation, 360L001

AST= ALL SYSTEM TEST CDDT= COUNT DOWN DEMONSTRATION TEST VAB= VEHICAL ASSY BLDG

INST.NO	ANG LOC	STA LOC	MEAS DIR	RANGE	REQ ACC	FM (HZ)	DIG (SPS)	REMARKS	CONDITION
			DFI LEFT HAND SRM (LOOKING FORWARD)						
B08G7274A	N/A	848.75	HOOP	+6K,-2K	+/- 2%		160	STRAIN, GIRTH	SHORTED DURING HEATER INSTALLATION
B08G7284A	N/A	1168.75	HOOP	+6K,-2K	+/- 2%		160	STRAIN, GIRTH	SHORTED DURING HEATER INSTALLATION
B08G7286A	N/A	1172.80	HOOP	+6K,-2K	+/- 2%		160	STRAIN, GIRTH	SHORTED DURING HEATER INSTALLATION
B08G7287A	N/A	1175.25	HOOP	+6K,-2K	+/- 2%		160	STRAIN, GIRTH	OPEN AT FINAL ASSY
B08G7292A	N/A	1411.80	HOOP	+6K,-2K	+/- 2%		80	STRAIN, GIRTH	OPEN AT FINAL ASSY
B08G7294A	N/A	1488.75	HOOP	+6K,-2K	+/- 2%		160	STRAIN, GIRTH	INTERMITTENT AT AST
B08G7299A	N/A	1574.75	HOOP	+6K,-2K	+/- 2%		160	STRAIN, GIRTH	SHORTED IN PLANT
B08G7305A	N/A	1834.75	HOOP	+6K,-2K	+/- 2%		160	STRAIN, GIRTH	BAD AT FLIGHT
B08G7306A	N/A	1836.20	HOOP	+6K,-2K	+/- 2%		160	STRAIN, GIRTH	QUESTIONABLE
B08G7312A	N/A	1873.50	HOOP	+6K,-2K	+/- 2%		80	STRAIN, GIRTH	LOST AT 300 SEC
B08G7324A	270.0	556.50	AXIAL	+/-2K	+/- 2%		80	STRAIN, BIAX	QUESTIONABLE
B08G7336A	98.0	1196.50	AXIAL	+/-2K	+/- 2%		80	STRAIN, BIAX	SWITCHED WITH B08G7337A
B08G7337A	98.0	1196.50	TANG.	+6K,-2K	+/- 2%		80	STRAIN, BIAX	SWITCHED WITH B08G7336A
B08G7357A	320.0	1493.00	TANG.	+6K,-2K	+/- 2%		80	STRAIN, BIAX	QUESTIONABLE
B08G7386A	180.0	1501.00	AXIAL	+/-2K	+/- 2%		160	STRAIN, BIAX	SWITCHED WITH B08G7387A
B08G7387A	180.0	1501.00	TANG.	+6K,-2K	+/- 2%		160	STRAIN, BIAX	SWITCHED WITH B08G7386A
B08G7409A	180.0	1797.00	TANG.	+6K,-2K	+/- 2%		160	STRAIN, BIAX	BAD AT FLIGHT
B08G7410A	270.0	1797.00	AXIAL	+/-2K	+/- 2%		80	STRAIN, BIAX	SWITCHED WITH B08G7411A BAD
B08G7411A	270.0	1797.00	TANG.	+6K,-2K	+/- 2%		80	STRAIN, BIAX	SWITCHED WITH B08G7410A
B08G7412A	0.0	1875.00	AXIAL	+/-2K	+/- 2%		160	STRAIN, BIAX	SWITCHED WITH B08G7417A REVERSED
B08G7417A	90.0	1875.00	AXIAL	+/-2K	+/- 2%		80	STRAIN, BIAX	SWITCHED WITH B08G7412A REVERSED
B08G7422A	180.0	1875.00	AXIAL	+/-2K	+/- 2%		160	STRAIN, BIAX	SWITCHED WITH B0867423A
B08G7423A	180.0	1875.00	TANG.	+6K,-2K	+/- 2%		160	STRAIN, BIAX	SWITCHED WITH B08G7422A
B08G7426A	180.0	1868.00	AXIAL	+/-2K	+/- 2%		160	STRAIN, BIAX	SHORT
B08G7427A	270.0	1875.00	AXIAL	+/-2K	+/- 2%		80	STRAIN, BIAX	OPEN

Table 4.10-1. Development Flight Instrumentation, 360L001 (Cont)

AST= ALL SYSTEM TEST CDDT= COUNT DOWN DEMONSTRATION TEST VAB= VEHICAL ASSY BLDG

INST.NO	ANG LOC	STA LOC	MEAS DIR	RANGE	REQ' ACC	FM (HZ)	DIG (SPS)	REMARKS	CONDITION
B08G7428A	270.0	1875.00	TANG.	+6K,-2K	+/- 2%		160	STRAIN, BIAX	OPEN
B08G7429A	270.0	1871.00	AXIAL	+/-2K	+/- 2%		160	STRAIN, UNIAX	OPEN
B07T7613A	0.0	1877.50		0-400 deg	+/-1%		10	TEMP. SRM	LOST AT 300 SEC
B07T7615A	180.0	1877.50		0-400 deg	+/-1%		10	TEMP. SRM	LOST AT 300 SEC
B07T7616A	270.0	1877.50		0-400 deg	+/-1%		10	TEMP. SRM	LOST AT 300 SEC
B47P1301A		487.00		0-1000 psia	+/- 2%		320	OPT	7% NOISE AT CDDT
			DFI RIGHT	HAND SRM					
B08G8272A	N/A	771.50		+6K,-2K	+/-2%		80	STRAIN, GIRTH	OPEN
B08G8273A	N/A	847.00		+6K,-2K	+/-2%		160	STRAIN, GIRTH	SHORTED DURING HTR INST
B08G8274A	N/A	848.75		+6K,-2K	+/-2%		160	STRAIN, GIRTH	BAD RANGE AT LAUNCH PAD
B08G8275A	N/A	850.20		+6K,-2K	+/-2%		160	STRAIN, GIRTH	OPEN DURING HTR INST
B08G8276A	N/A	852.80		+6K,-2K	+/-2%		160	STRAIN, GIRTH	OPEN DURING HTR INST
B08G8277A	N/A	855.50		+6K,-2K	+/-2%		160	STRAIN, GIRTH	RANGE BAD
B08G8278A	N/A	857.50		+6K,-2K	+/-2%		160	STRAIN, GIRTH	QUESTIONABLE
B08G8283A	N/A	1167.00		+6K,-2K	+/-2%		160	STRAIN, GIRTH	OPEN DURING HTR INST
B08G8284A	N/A	1168.75		+6K,-2K	+/-2%		160	STRAIN, GIRTH	QUESTIONABLE
B08G8285A	N/A	1170.20		+6K,-2K	+/-2%		160	STRAIN, GIRTH	SHORTED DURING HTR INST
B08G8287A	N/A	1175.25		+6K,-2K	+/-2%		160	STRAIN, GIRTH	OPEN
B08G8288A	N/A	1177.50		+6K,-2K	+/-2%		160	STRAIN, GIRTH	SHORTED
B08G8294A	N/A	1488.75		+6K,-2K	+/-2%		160	STRAIN, GIRTH	SHORTED DURING HTR INST
B08G8297A	N/A	1495.25		+6K,-2K	+/-2%		160	STRAIN, GIRTH	OPEN
B08G8300A	N/A	1576.40		+6K,-2K	+/-2%		160	STRAIN, GIRTH	BAD RANGE AT LAUNCH PAD
B08G8306A	N/A	1836.20		+6K,-2K	+/-2%		160	STRAIN, GIRTH	BAD AT FLIGHT
B08G8312A	N/A	1873.50		+6K,-2K	+/-2%		80	STRAIN, GIRTH	SHORT
B08G8314A	N/A	1876.00		+6K,-2K	+/-2%		160	STRAIN, GIRTH	LOST AT 300 SEC

Table 4.10-1. Development Flight Instrumentation, 360L001 (Cont)

AST= ALL SYSTEM TEST CDDT= COUNT DOWN DEMONSTRATION TEST VAB= VEHICAL ASSY BLDG

INST.NO	ANG LOC	STA LOC	MEAS DIR	RANGE	REQ ACC	FM (HZ)	DIG (SPS)	REMARKS	CONDITION
B08G8315A	N/A	1876.30		+6K,-2K	+/-2%		160	STRAIN, GIRTH	LOST AT 300 SEC
B08G8316A	185.0	486.40	AXIAL	+/-2k	+/-2%		160	STRAIN, BIAX	OPEN AT AST
B08G8317A	185.0	486.40	TANG.	+6K,-2K	+/-2%		160	STRAIN, BIAX	SHORTED AT AST
B08G8318A	180.0	556.50	AXIAL	+/-2k	+/-2%		160	STRAIN, BIAX	BAD AT FLIGHT
B08G8323A	0.0	556.50	TANG.	+6K,-2K	+/-2%		160	STRAIN, BIAX	QUESTIONABLE
B08G8324A	270.0	556.50	AXIAL	+/-2k	+/-2%		80	STRAIN, BIAX	QUESTIONABLE
B08G8325A	270.0	556.50	TANG.	+6K,-2K	+/-2%		80	STRAIN, BIAX	QUESTIONABLE
B08G8326A	180.0	876.50	AXIAL	+/-2k	+/-2%		160	STRAIN, BIAX	QUESTIONABLE
B08G8327A	180.0	876.50	TANG.	+6K,-2K	+/-2%		160	STRAIN, BIAX	QUESTIONABLE
B08G8331A	0.0	876.50	TANG.	+6K,-2K	+/-2%		160	STRAIN, BIAX	QUESTIONABLE
B08G8332A	270.0	876.50	AXIAL	+/-2k	+/-2%		80	STRAIN, BIAX	QUESTIONABLE
B08G8333A	270.0	876.50	TANG.	+6K,-2K	+/-2%		80	STRAIN, BIAX	QUESTIONABLE
B08G8336A	82.0	1196.50	AXIAL	+/-2k	+/-2%		80	STRAIN, BIAX	BAD RANGE AT LAUNCH PAD
B08G8337A	82.0	1196.50	TANG.	+6K,-2K	+/-2%		80	STRAIN, BIAX	BAD AT FLIGHT
B08G8339A	0.0	1196.50	TANG.	+6K,-2K	+/-2%		160	STRAIN, BIAX	SHORTED AT AST
B08G8341A	270.0	1196.50	TANG.	+6K,-2K	+/-2%		80	STRAIN, BIAX	BAD AT FLIGHT
B08G8352A	82.0	1493.00	AXIAL	+/-2k	+/-2%		80	STRAIN, BIAX	SWITCHED WITH B08G8353A
B08G8353A	82.0	1493.00	TANG.	+6K,-2K	+/-2%		80	STRAIN, BIAX	SWITCHED WITH B08G8352A
B08G8361A	255.0	1493.00	TANG.	+6K,-2K	+/-2%		80	STRAIN, BIAX	BAD AT FLIGHT
B08G8363A	270.0	1493.00	TANG.	+6K,-2K	+/-2%		160	STRAIN, BIAX	SHORTED IN VAB
B08G8403A	320.0	1501.00	TANG.	+6K,-2K	+/-2%		160	STRAIN, BIAX	OPEN
B08G8440A	45.0	1922.00	AXIAL	+/-2k	+/-2%		160	STRAIN, BIAX	BAD AT FLIGHT
B07T8615A	0.0	1877.50		0-400 deg	+/- 1%		10	TEMP. SRM	LOST AT 300 SEC
B07T8616A	270.0	1877.50		0-400 deg	+/- 1%		10	TEMP. SRM	LOST AT 310 SEC
B47P2301A		487.00		0-1000 psia	+/- 2%		320	OPT	7% NOISE AT CDDT

Table 4.11-1. Ground Environmental Instrumentation, 360L001

INST. NO.	ANG. LOC.	STATION	RANGE	REQ. ACC.	DIG. (spm)	REMARKS	FLT. NO.	NOTES
B06T7009A	90	778.98	0-200 deg	+/- 1%	1	RTD	1-6	
B06T7010A	45	931.5	0-200 deg	+/- 1%	1	RTD	1-6	
B06T7013A	270	931.5	0-200 deg	+/- 1%	1	RTD	1-6	
B06T7020A	90	1258.98	0-200 deg	+/- 1%	1	RTD	1-6	
B06T7027A	274	1511	0-200 deg	+/- 1%	1	RTD	1-6	
B06T7031A	90	1565	0-200 deg	+/- 1%	1	RTD	1-6	
B06T7035A	45	1751.5	0-200 deg	+/- 1%	1	RTD	1-6	QUESTIONABLE - READS CONSTANT 10 DEF F LOW
B06T7038A	270	1751.5	0-200 deg	+/- 1%	1	RTD	1-6	
B06T7043A	0	1847	0-200 deg	+/- 1%	1	RTD	1-6	
B06T7045A	120	1847	0-200 deg	+/- 1%	1	RTD	1-6	
B06T7047A	240	1847	0-200 deg	+/- 1%	1	RTD	1-6	
B06T7049A	0	1876.6	0-200 deg	+/- 1%	1	RTD	1-6	
B06T7050A	120	1876.6	0-200 deg	+/- 1%	1	RTD	1-6	
B06T7051A	240	1876.6	0-200 deg	+/- 1%	1	RTD	1-6	
B06T7081A	265	486.4	0-200 deg	+/- 1%	1	RTD	1-6	
B06T7082A	275	486.4	0-200 deg	+/- 1%	1	RTD	1-6	
B06T8009A	90	778.98	0-200 deg	+/- 1%	1	RTD	1-6	
B06T8011A	45	931.5	0-200 deg	+/- 1%	1	RTD	1-6	
B06T8013A	270	931.5	0-200 deg	+/- 1%	1	RTD	1-6	
B06T8020A	90	1258.98	0-200 deg	+/- 1%	1	RTD	1-6	LOST DURING STACKING
B06T8027A	266	1511	0-200 deg	+/- 1%	1	RTD	1-6	
B06T8031A	90	1565	0-200 deg	+/- 1%	1	RTD	1-6	
B06T8036A	45	1751.5	0-200 deg	+/- 1%	1	RTD	1-6	
B06T8038A	270	1751.5	0-200 deg	+/- 1%	1	RTD	1-6	
B06T8043A	180	1847	0-200 deg	+/- 1%	1	RTD	1-6	
B06T8045A	60	1847	0-200 deg	+/- 1%	1	RTD	1-6	
B06T8047A	300	1847	0-200 deg	+/- 1%	1	RTD	1-6	
B06T8049A	180	1876.6	0-200 deg	+/- 1%	1	RTD	1-6	
B06T8050A	60	1876.6	0-200 deg	+/- 1%	1	RTD	1-6	
B06T8051A	300	1876.6	0-200 deg	+/- 1%	1	RTD	1-6	
B06T8081A	265	486.4	0-200 deg	+/- 1%	1	RTD	1-6	
B06T8082A	275	486.4	0-200 deg	+/- 1%	1	RTD	1-6	

joints, nozzle-to-case joints, the igniter-to-case joints, internal acreage insulation, and external factory joint weather seals. Complete detailed results and final insulation evaluation is found in Volume III of this report.

4.12.1.2 Field Joints. No anomalous conditions were identified in any of the six field joints. J-leg tip contact was evident over the full circumference at each joint. Soot deposits extending down the bondline into the start of the radius were noted on both forward field joints. This soot may have been from chamber gas leakage into the joint bondline; however, the soot was readily removable with solvent. This sooting occurrence is believed to be related to the postflight phenomena that generates the nitrile butadiene rubber (NBR) inhibitor stub radial tears. This phenomena is discussed further in Volume III, Section 6.1.10.

Axial growth of clevis edge separations occurred in five of the six segments. The maximum axial growth identified during preliminary evaluation was 0.20 inch. This growth may indicate a cohesive failure of the NBR, or adhesive failure of the insulation-to-case bondline. Initial evaluation indicates adhesive failure.

4.12.1.3 Nozzle-to-Case Joints. Based on visual evaluation, both nozzle-to-case joints performed exceptionally well. No gas paths through the polysulfide adhesive or any other anomalies were identified. The polysulfide adhesive had numerous small voids (4 on 360L001A and 20 on 360L001B) around the circumference. All of the observed voids were less than 1.03 in. axially and 0.34 in. circumferentially in size. These voids are typical of RSRM nozzle-to-case joint polysulfide adhesive voids seen in the past, and none of the voids were as large as those previously observed on other static test motors.

4.12.1.4 Internal Acreage

Factory Joints

Evaluation of the internal factory joint insulation identified no anomalies. No evidence of gas paths through the insulation or severe erosion was identified. The depth of the remaining insulation over each factory joint

was measured using a "Fletcher" needle depth gage. Preliminary measurements show that all factory joints met the minimum required safety factory of 2.0. Based on these measurements, a minimum of three virgin insulation plies remained over each factory joint.

Internal System (Inhibitors, Flaps, and Acreage Insulation)

Numerous radial tears (17 on 360L001A and 11 on 360L001B greater than 3 in. radially) were noted in the forward center segment NBR inhibitor stubs. Some of the tears extended radially outward to approximately 5 in. inboard from the clevis inside diameter (ID). The edges of the tears appeared rough and matched when placed back together, demonstrating no material loss or erosion, and indicating the tears occurred after motor burn. Tears were also noted in the 360L001A aft center segment inhibitor stub. The radial extent and amount of all tears identified in the inhibitor stubs are within the range of tears noted on past flight motors.

The stress relief flap including the castable inhibitor slot was present for the full circumference with no significant erosion on either forward segment. The castable inhibitor was completely missing full circumference including the material normally present in the castable inhibitor slot. Numerous axial tears (46 in 360L001A and 75 on 360L001B) were identified on the remaining flap. The edges of the tears appeared rough, and matched when placed together demonstrating no material loss or erosion; this also indicated that the tears occurred after motor burn. This condition, however, has not been documented on any previous flight motors.

4.12.1.5 External Insulation. The stiffener ring and stub insulation, factory joint insulation (weatherseal), and exterior motor case appeared to be in good condition. A small area (approximately 1 by 3 in.) of missing EPDM insulation was noted on 360L001A aft center factory joint weatherseal at approximately 190 deg. An axial streak mark on the case aft of the mission material indicates that the weatherseal was probably hit by nozzle debris at severance or splashdown. No evidence of moisture under the weatherseal on any of the factory joints was identified. During the hydrolase process for TPS removal, a gouge was accidentally cut through the insulation weatherseal in the 360L001A aft dome factory joint.

4.12.2 Case Component Performance

4.12.2.1 Summary. From the steel case standpoint, the hardware performed as expected during flight. All case joints, including the newly redesigned field joints and nozzle-to-case joints, provided a good seal with no indications of hot gas leakage. Only during splashdown, and possibly during disassembly did any structural damage occur. These effects are discussed in further detail by component.

4.12.2.2 Inspection Results

Right-Hand Booster Stiffener Damage

The damage most apparent on this booster was on the stiffener ring, caused by splashdown. Video footage showed that this booster hit the calm ocean water at a slight angle, and immediately lay down on top of the water without ever submerging completely. Foam on aft sides of the stiffener and ETA rings was missing in an arc that ranged from 120 deg to around 180 deg. Cracks were noted in the stiffener webs during the initial walk-around inspection. After stiffener ring removal the following characteristics were identified:

Forward Stiffener: ring web buckling occurred in the area of 120 to 130 deg and 178 to 198 deg. The web was cracked radially to the flange at 160 deg and then extended 5 in. circumferentially along the web near the flange. Raised metal was noted in the attach boltholes near the crack. The raised area was radially inward and toward the crack. No case stub damage was noted except for some possible raised metal in some of the boltholes. In the region between web buckles, 38 bolts were broken or missing.

Center Stiffener: ring web buckling occurred at 140 and 176 deg. The web was cracked radially at 158 deg and extended 7.5 in. circumferentially near the flange. Raised metal occurred as in the forward ring. The case stub had two adjacent boltholes with outboard cracks at 186 and 188 deg. Thirty attach bolts were broken or missing between ring web buckles.

Aft Stiffener: ring web buckling occurred at 145 and 183 deg. The web was cracked radially at 160 deg and extended 7.5 in. circumferentially

near the flange. The ring bolthole at 144 deg was also cracked in an inboard direction, and in a circumferential direction about 1 in. in length. Raised metal occurred as in the forward ring. The case stub had a bolthole with an outboard crack at 142 deg. Twenty attach bolts were broken or missing between ring web buckles.

Left-Hand Booster Stiffeners

This booster hit the water in a near vertical position, completely submerged, bobbed up, and lay over on its side. Although cavity collapse potential was extremely high with this type of entry, no damage was found on either the rings or stubs. There was foam missing from about 120 to 180 deg on all the stiffener and ET rings.

Field Joint Interference Surface Damage

Axially-oriented gouges were found on the clevis inner leg ID (capture feature O-ring sealing surface) on two field joints of each motor. The joints affected were left-hand center, left-hand aft, right-hand center, and right-hand forward. By far the worst affected was the left-hand center joint. The number of gouges for each joint are as follows:

--Left-hand center - 99 (90 in a 90-deg arc)
--Left-hand aft - 2
--Right-hand center - 21
--Right-hand forward - 21

The length of the gouges was the same for all: approximately 0.375 inch. They extended from the ID chamfer back towards the insulation, ending in somewhat of a pit. The pits were up to 4 or 5 mil deep. The scratches were about 1 mil deep.

There are spots on the face of the interference surface of the capture feature which seem to correspond in circumferential location to many of the clevis gouges. Most of these spots seem to be raised, as if something is deposited there.

It is difficult to determine when these gouges occurred, possibly at the disassembly operation. But assembly, flight, and transporting have not been ruled out as contributors to this damage.

Paint Blistering and Corrosion

During the initial walk-around inspection of the boosters, paint blistering or debonds were evident just fore and aft of the unstiffened forward stubs of both motors. They seemed to be lightly heat affected. But the painted surfaces were suspected of inadequate preparation. Surface corrosion had set in immediately.

The outer clevis leg outside diameter (OD) surfaces of the field joints also exhibited extensive paint debonding and subsequent surface corrosion. The center field joint of the left-hand booster was left devoid of almost all paint on the referred surface.

The nozzle-to-case joints of both boosters appeared in excellent condition with only a minimum of very light surface corrosion on nonsealing surfaces.

4.12.3 Seals Performance

4.12.3.1 Summary. Postflight inspection of both motors showed the seals component to be in excellent condition. There was no hot gas or soot past the J-leg on the six field joints or past the polysulfide adhesive on the two nozzle-to-case joints. The igniter joints had no hot gas or soot past the primary seals. There was no soot to the nozzle aft exit cone primary seals, as it is questionable weather hot gas ever reached these seals. Inspection of all O-rings and gasket seals revealed no damage.

4.12.3.2 Results

Igniter

The igniter joints had no hot gas or soot past the primary seals. The inspection of the O-rings and Gask-O-Seal® seals revealed no damage.

Field Joints

There was light to heavy corrosion on most of the joints; however, there was none on the sealing surfaces. The corrosion was typical of what was seen on the pre-51-L motors. The vent valve plugs (in the field joint weather seals) all leaked water into the joints. In some areas the grease application was a little light, but overall the grease was nominal. In some of the corroded areas of the joint it was evident that the grease had not been rubbed into the metal thoroughly. It is recommended that the KSC grease application personnel be more consistent in applying the grease to the joints.

Nozzle-to-Case Joint

The radial bolthole plugs were used in the nozzle-to-case disassembly to prevent damage to the wiper O-ring. There was no O-ring damage; however, 49 plugs on the right motor were damaged, ranging from slight plug edge wrinkling to the entire plug head being sheared off. It appeared that the majority of these plugs were installed incorrectly. When the left motor nozzle-to-case joint was disassembled, no plugs were damaged.

Aft Exit Cone

There was no evidence of hot gas or soot past the primary seals on either aft exit cone joint, as it is questionable whether hot gas ever reached these primary seals. There was aluminum oxidation found between the primary and secondary seals on both exit cone joints. During disassembly both exit cones dropped slightly, breaking the Teflon® tip off the guide pins and smashing the guide pin ends. On the left motor one guide pin slid across the forward exit cone sealing surface, scratching it at 90 deg (3.375 in. long by 0.375 in. wide).

Vent Port Plugs

There was damage to seven vent port plug primary O-rings. This damage occurred during assembly and is inherent in the design. These O-rings are packing seals and would have maintained a seal if pressurized. The damage is within our data base from the certification program; in fact, more severe damage has been seen in the certification motors. The secondary O-ring of

the right nozzle-to-case joint vent port plug was also damaged. Preliminary investigation indicates a discrepant vent porthole. This problem is still under investigation.

4.12.4 Nozzle Performance

4.12.4.1 Summary. The CCP on the exit cone was either fractured or completely missing from linear-shaped charge (LSC) and water impact, exposing the GCP insulator. The GCP was delaminated from water impact,but showed no signs of heat effect. The internal parts of the nozzle also had the appearance of previous postflight hardware. There were intermittent impact marks located circumferentially around both of the nozzles. There were a few instances of charred CCP popping up and postfire wedgeouts which have been observed on previous postfired nozzles. A map of postfire quick-look observations for the right-hand and left-hand nozzles are depicted in Figures 4.12-1 and 4.12-2, respectively.

4.12.4.2 Left-Hand Nozzle

Aft Exit Cone

The STS-26 left-hand aft exit cone showed missing CCP liner 360-deg circumferentially. GCP plies exposed by the missing liner is a typical postflight observation, and occurs at splashdown. The aft exit cone forward end showed no separations within the GCP insulator.

The polysulfide groove fill on the forward end of the aft exit cone showed no separations. Postflight measurements of the polysulfide groove radial width showed that the GCP insulator did not pull away from the aluminum shell during cooldown. The polysulfide appeared to shrink axially aft up to 0.12 inch.

Forward Exit Cone Assembly

The forward exit cone showed missing CCP liner over the center portion of the cone. Liner remained bonded on the forward 11 in. and on the aft 8 in., 360 deg circumferentially. The GCP insulator exposed by the missing liner showed no signs of heat effect. The missing CCP liner is a typical postflight observation and occurs at splashdown and during detailed operating

Aft Exit Cone

All CCP liner missing
Exposed GCP insulator showed no signs of heat effect
GCP insulator delaminated from LSC and splashdown

Throat Inlet Assembly (Throat Inlet Ring and Throat Ring)

Intermittent impact marks located circumferentially (throat ring)
Smooth erosion
Forward 1.5 in. of throat ring showed popped-up, charred CCP material intermittently around the circumference
Postburn wedgeout on forward ≈0.5 in. of throat inlet ring (355 to 5, 28 to 40, 95 to 105 deg)

Nose/Inlet Assembly (503, 504 Rings and Nose Cap)

Smooth erosion; slag deposits observed on nose cap wedgeout
503 ring raised above nose cap ≈0.08 in. from 155 to 165 deg
Intermittent impact marks located circumferentially
Popped-up, charred CCP material and wedgeouts on aft 2 to 3 in. of nose cap intermittently around the circumference
Radial depth = 0.5 in. at cowl interface

Cowl Ring

Typical erratic erosion on cowl; intermittent wash areas between ventholes around the circumference
Ventholes plugged
Wedgeout on aft ≈3.5 in. from 120 to 137 deg with ≈max radial depth = 0.6 in.; slag exposed on plies

Outer Boot Ring

Smooth erosion
Intermittent popped-up, charred CCP material around circumference on forward 1.8 in.
No missing material on forward 1.8 in.
Wash areas on forward 1.5 in. of OBR; wash areas extended from cowl to OBR ≈ 0.15 in. deep radially

Fixed Housing Assembly

Smooth erosion
No bondline separations (aft end)

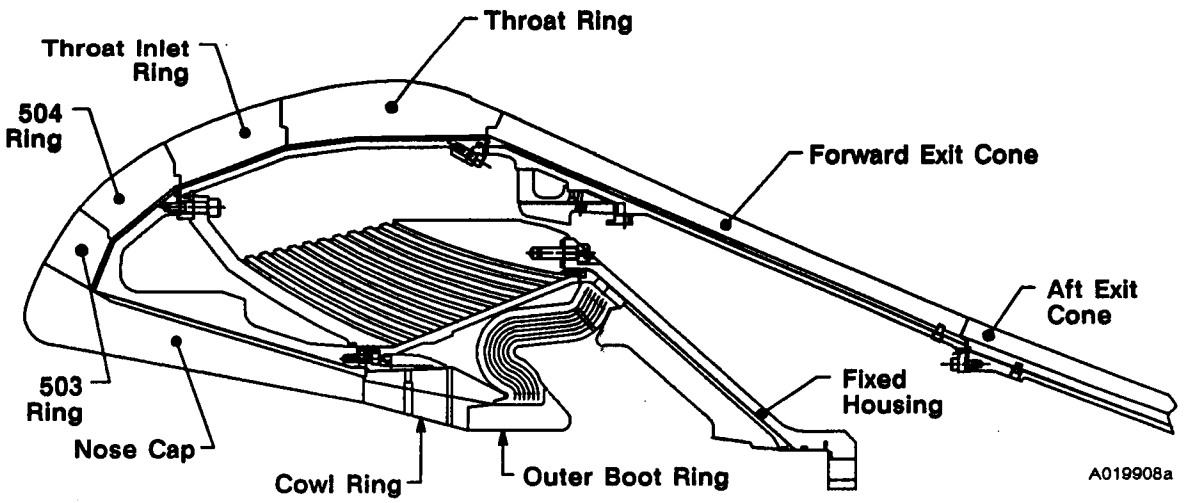

Figure 4.12-1. Map of Nozzle Erosion for Right-Hand Motor

Aft Exit Cone

All CCP liner missing
Exposed GCP insulator showed no signs of heat effect
GCP insulator delaminated from LSC and splashdown

Throat Inlet Assembly (Throat Inlet Ring and Throat Ring)

Intermittent impact marks located circumferentially
Smooth erosion
Typical dimpled erosion on aft 6 in. of throat ring
Forward 1.5 in. of throat ring showed popped-up, charred CCP material at 345 deg ≈5.0 in. circumferentially, 285 deg ≈5.0 in. circumferentially, 210 deg ≈2.0 in. circumferentially, 70 deg ≈2.0 in. circumferentially, and 10 deg ≈2.0 in. circumferentially

Forward Exit Cone Assembly

Exposed GCP insulator showed no signs of heat effect

Nose/Inlet Assembly (503, 504 Rings and Nose Cap)

Smooth erosion
Popped-up, charred CCP material on aft 2 to 3 in. at 137, 280, 310, and 332 deg
Aft 2 to 3 in. showed wedgeouts from 14 to 26, 40 to 93, 110 to 122, 156 to 172, and 248 to 265 deg
Radial depth = 0.5 in. at cowl interface

Cowl Ring

Typical erratic erosion on cowl; appeared to erode 0.15 in.
Ventholes plugged; no wedgeouts

Outer Boot Ring

Smooth erosion; no wedgeouts

Fixed Housing Assembly

Smooth erosion
Forward 2 in. showed intermittent wedgeouts of 0.5-in. maximum radial depth
No bondline separations (aft end)

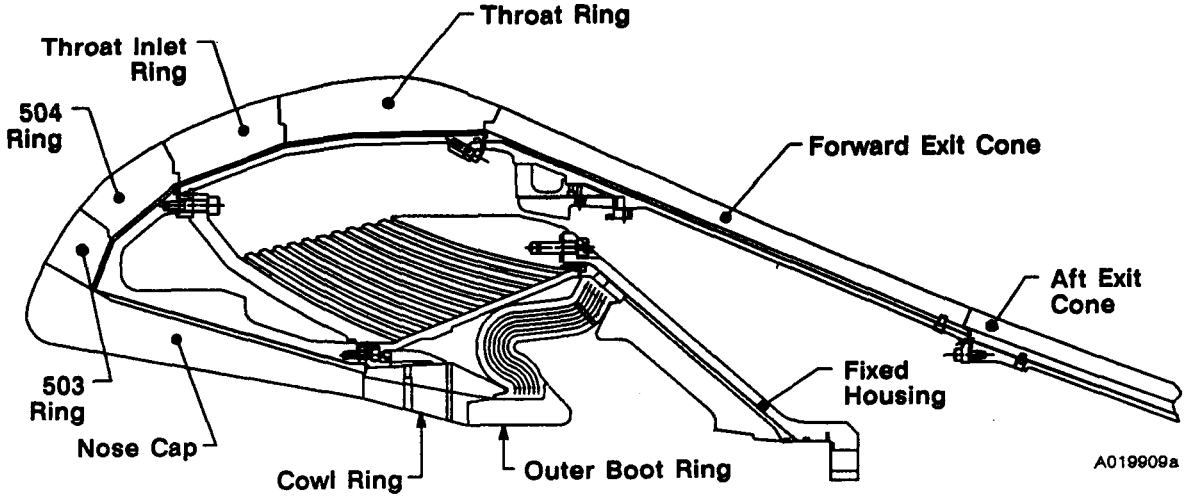

Figure 4.12-2. Map of Nozzle Erosion for Left-Hand Motor

procedures (DOP) insertion. The aft 8 in. of the liner showed the typical dimpled erosion pattern that has occurred on all flight and static test forward exit cones. The maximum radial depth of the dimpled erosion was 0.15 inch.

The aft end of the forward exit cone showed separations between the EA946 adhesive and the steel housing from 30 to 60 deg and from 124 to 148 deg. The maximum radial width of the separations was 0.025 inch. There were no separations within the GCP insulator or at the GCP/CCP interface. The aft flange was scratched at the 90-deg location by a guide pin during aft exit cone demate. The scratch was approximately 0.002-in. deep axially, 3.5 in. long circumferentially, and 0.375-in. wide radially.

Throat Assembly

Erosion of the throat and throat inlet rings was smooth and uniform, with no wedgeouts observed. Popped-up, charred CCP material was observed on the forward 1.5 in. of the throat ring at 10, 70, 210, 285, and 345 deg. Sharp edges indicate that the popped-up material occurred after motor operation. Typical dimpled erosion was observed on the aft 6 in. of the throat ring. Impact marks were also noted on the aft end intermittently and on 0.08 in. of the throat inlet rings. This is typical of past static test and flight nozzles.

Impact marks were evident on the throat inlet ring intermittently around the circumference. The largest was located at 130 deg and measured 1 in. circumferentially by 0.5 in. axially by 0.25 in. radially.

Forward Nose (-503) and Aft Inlet (-504) Rings

The forward nose and aft inlet rings showed smooth erosion with no pockets, wash areas, or wedgeouts. The ply angle of the -503 ring was checked and found to be of the RSRM design. The flow surface bondline gap between the -503 and -504 rings was 0.15 inch. The flow surface bondline gap between the -503 ring and the nose cap was 0.05 inch. These postfired measurements are typical of past static test and flight nozzles. Impact marks occurring after motor operation were observed on both rings intermittently around the circumference. These marks most likely resulted from the loose aft and forward exit cone CCP material at splashdown.

Nose Cap

The nose cap showed smooth erosion with no pockets or major washes observed. The nose cap aft 2 to 3 in. showed popped-up, charred CCP material at 137, 280, 310, and 332 deg. Sharp edges indicate that this occurred after motor operation. Typical postburn wedgeouts on the aft 2 to 3 in. were noted from 14 to 26, 40 to 93, 110 to 122, 156 to 172, and 248 to 265 deg. The maximum radial depth was 0.5 in. at the cowl interface. No wedgeouts were observed on the forward end of the nose cap.

Cowl Ring

Typical erratic erosion was observed intermittently around the cowl circumference. The forward portion of the ring eroded a maximum of 0.15 in. greater than on the aft portion of the ring. This erratic erosion is a result of the low ply angle of the cowl ring and has been observed on the majority of flight and static test nozzles. There were no wedgeouts observed on the cowl ring. All cowl ventholes appeared plugged with slag on the OD of the ring.

Outer Boot Ring

The outer boot ring (OBR) showed smooth erosion with no pockets, major washes, or wedgeouts. Delaminations in the charred CCP of the aft tip were observed 360 deg circumferentially. Charred CCP material on the aft tip fractured and popped up over a majority of the circumference. A large impact mark was located on the aft end of the OBR at 190 deg, and measured 6 in. circumferentially. Sharp edges on the surfaces indicated that this occurred after motor operation. This may have been due to the loose CCP material in the motor after splashdown. The flow surface bondline gap between the OBR and cowl ring was 0.18 in., which is typical of past static test and flight nozzles.

Fixed Housing Assembly

The fixed housing insulation erosion was smooth and uniform. Postburn wedgeouts of charred CCP material were observed on the forward 2 in.

intermittently around the circumference. The maximum radial depth was 0.5 inch. There were no bondline separations observed on the aft end, and the GCP was not heat affected.

Aft Exit Cone Field Joint Observations

The backfilled room temperature vulcanization (RTV) extended below the joint char line 360 deg circumferentially except at the 266.2-deg location. RTV completely filled the radial ID portion of the joint except at 236.2, 266.2, 292.8, and 296.6 deg where unfilled void areas were located. The backfill also reached the high pressure side of the primary O-ring from 38 to 185 and 314.4 to 356.2 deg.

One blowpath 0.10-in. wide circumferentially was observed at the 266.2-deg unfilled void area. The primary O-ring saw pressure, but showed no signs of blowby, erosion, or heat effect.

Examination of the joint showed a black residue and white corrosion appearing between the primary and secondary O-rings, and outboard of the secondary O-ring intermittently around the circumference. The black residue was heaviest from 131 to 270 to 0 deg. The white corrosion was heaviest from 0 to 90 to 131 deg. There was no pitting observed. Samples have been taken for laboratory analysis. It is believed that the black residue is the beginning stage of the white corrosion.

4.12.4.3 Right-Hand Nozzle

Aft Exit Cone

The STS-26 right-hand aft exit cone showed missing CCP liner 360 deg circumferentially. GCP plies exposed by the missing liner showed no signs of heat effect. The missing CCP liner is a typical postflight observation and occurs at splashdown. There were no separations observed within the GCP insulator on the forward end of the aft exit cone.

The polysulfide groove fill on the forward end of the aft exit cone showed one separation between the polysulfide and the GCP insulator. The separation was located at 211 deg and measured 0.02 in. wide radially, 0.04 in. deep axially, and 1.3 in. long circumferentially. The polysulfide

also appeared to shrink axially up to 0.10 inch. Postflight measurements of the polysulfide groove radial width showed that the GCP insulator did not pull away from the aluminum shell during cooldown.

Forward Exit Cone

The forward exit cone showed missing CCP liner over the center portion of the cone. Liner remained on the forward 11 in. and on the aft 9 in. at 360 deg circumferentially. The GCP insulator exposed by the missing liner showed no signs of heat effect. The missing CCP liner is a typical postflight observation and occurs at splashdown and during DOP insertion. The aft 9 in. of the liner showed the typical dimpled erosion pattern that has occurred on all flight and static test forward exit cones. The maximum radial depth of the dimpled erosion was 0.15 inch.

The forward exit cone aft end showed no separations at the bondline or CCP/GCP interface, or within the GCP insulator. One through hole on the forward exit cone housing aft flange was "dinged" by a guide pin during aft exit cone demate. The ding was approximately 0.02 in. deep at the 97.5-deg hole location.

Throat Assembly

The throat and throat inlet rings eroded smoothly with no pockets or major washes observed. The throat inlet ring forward end showed postburn wedgeouts of charred CCP material from 28 to 40, 95 to 105 and 355 to 0 to 5 deg. The maximum axial width of the wedgeouts was 0.75 in. at the 28- to 40-deg location. Postburn wedgeouts of the throat inlet ring forward end have been observed on previous postflight nozzles. The flow surface bondline gap between the throat and throat inlet ring was 0.10 in. and is typical of past static test and flight nozzles.

Impact marks resulting from DOP insertion were observed on the throat ring intermittently around the circumference. The throat ring forward 1.5 in. also showed popped-up, charred CCP material intermittently around the circumference. Sharp edges indicate the popped-up material occurred after motor operation.

Forward Nose (-503) and Aft Inlet (-504) Rings

The forward nose and aft inlet rings showed smooth erosion with no pockets or major washes observed. The ply angle of the -503 ring was found to be of the RSRM design. The flow surface bondline gap between the -503 and -504 rings was 0.18 inch. The flow surface bondline gap between the -503 ring and nose cap was 0.05 inch. These postfire measurements are typical of past static test and flight nozzles. The -503 ring showed popped-up CCP material at the nose cap interface from 155 to 165 deg. The popped up material was 0.08 in. wide axially and occurred after motor operation. Impact marks occurring after motor operation were observed on both rings intermittently around the circumference. The marks most likely resulted from the loose aft and forward exit cone CCP material at splashdown.

Nose Cap

The nose cap showed smooth erosion with no pockets or major washes observed. The aft 2.0 to 3.5 in. of the nose cap showed wedgeouts intermittently around the circumference. The wedgeout location from 5 to 20 deg showed slag covering exposed CCP material. Sectioning is required to determine the occurrence time of this wedgeout. Postburn wedgeouts on the aft end of flight and static test nozzles are commonly observed.

Cowl Ring

The cowl ring showed erratic erosion intermittently around the part circumference. The forward portion of the ring appeared to erode a maximum of 0.15 in. greater than the aft portion of the ring. This erratic erosion is a result of the low ply angle of the cowl ring and has been observed on the majority of flight and static test nozzles. One wedgeout was observed on the aft 3.5 in. of the cowl ring from 120 to 137 deg. The maximum radial depth of the wedgeout was 0.6 in. at the OBR interface. Slag coated the exposed CCP material at the wedgeout location. Sectioning is required to determine the occurrence time of this wedgeout.

Outer Boot Ring

The OBR showed smooth erosion with no pockets or major washes observed. Minor wash areas extended from the cowl to the forward 1.5 in. of the OBR

from 120 to 130, 130 to 140, and 150 to 158 deg. The maximum radial depth of the wash areas was 0.2 inch. These wash areas have occurred on the majority of flight and static test nozzles. Popped-up, charred CCP material was also observed on the forward 1.8 in. of the OBR intermittently around the circumference. The popped-up material is a common observation and occurs after motor operation. Delaminations in the charred CCP of the aft tip were observed 360 deg circumferentially. Charred CCP material on the aft tip fractured and popped up over a majority of the circumference. All cowl ventholes appeared plugged with slag on the OD of the ring. The flow surface bondline gap between the OBR and cowl ring was 0.20 in. and is typical of past static test and flight nozzles.

Fixed Housing Assembly

The fixed housing insulation showed smooth erosion with no pockets or major washing observed. Postburn wedgeouts were observed on the forward 2.0 in. of the fixed housing insulation from 30 to 65, 135 to 145, and 165 to 180 deg. The wedgeouts were a maximum of 0.5 in. deep radially.

Aft Exit Cone Field Joint Observations

The backfilled RTV extended below the joint char line 360 deg circumferentially. RTV completely filled the radial ID portion of the joint except at 103 deg where an unfilled void area approximately 1.0 in. wide circumferentially was located. The backfill also extended to the high-pressure side of the primary O-ring from 0 to 81, 82 to 101, 103 to 123, 154 to 178, 182 to 237, 243 to 251, 258 to 265, and 268 to 360 deg.

There were no blowpaths observed in the joint and the primary O-ring saw no pressure.

Examination of the joint showed a black residue and white corrosion appearing between the primary and secondary O-rings, and outboard of the secondary O-ring intermittently around the circumference. The white corrosion was heaviest from 112.6 to 143.2 deg. There was no pitting observed. Samples have been taken for laboratory analysis. It is believed that the black residue is the beginning stage of the white corrosion.

Char was observed on the RTV in the axial portion of the joint at 237 deg. The RTV was not eroded or heat affected at the charred location. It is believed that the char penetrated the joint at splashdown.

DISTRIBUTION

Recipient	No. of Copies	Mail Stop
C. Saderholm	1	E16
R. Riley	1	E16
L. Bailey	1	L10
D. Roth	1	L10
P. Petty	1	L10
B. MacBeth	1	L10
J. Sutton	1	L10
S. Morris	1	L10
D. Campbell	1	L10
J. Detrio	1	L10
J. Seiler	1	L10
C. Ralston	1	L10
G. Lasley	1	L10
T. Gregory	1	L10
D. Wagoner	1	L10
B. McQuivey	1	L10
S. Medrano	1	L10
T. Morgan	1	L10
J. Kapp	1	L20
H. Huppi	1	L21
B. Laubacher	1	L21
C. Richards	1	L21
S. Hicken	1	L21
R. George	1	L23
V. Call	1	L22
D. Gurney	1	L22D
R. Mackley	1	L22
M. Cox	1	L30
M. Williams	1	L36
C. Bacon	1	L34
B. Baugh	1	L36
N. Black	1	L36
S. Henderson	1	L36
G. Ricks	3	L36
Print Crib	5	K23B1
Data Management	5	L23E
F. Call	15	E05